Benjamin A. Stickler · Ewald Schachinger

Basic Concepts in Computational Physics

Springer

Basic Concepts in Computational Physics

Benjamin A. Stickler · Ewald Schachinger

Basic Concepts in Computational Physics

Springer

Benjamin A. Stickler
Faculty of Physics
University of Duisburg-Essen
Duisburg
Germany

Ewald Schachinger
Institute of Theoretical and Computational Physics
Graz University of Technology
Graz
Austria

ISBN 978-3-319-02434-9 ISBN 978-3-319-02435-6 (eBook)
DOI 10.1007/978-3-319-02435-6
Springer Cham Heidelberg New York Dordrecht London

Library of Congress Control Number: 2013949666

Printed on acid-free paper

Springer is part of Springer Science+Business Media (www.springer.com)

Preface

Traditionally physics was divided into two fields of activities: theoretical and experimental. As a consequence of the stunning increase in computer power and of the development of more powerful numerical techniques, a new branch of physics was established over the last decades: Computational Physics. This new branch introduced as a spin-off what nowadays is commonly called *computer simulations*, which play an increasingly important role in physics and in related sciences as well as in industrial applications. They serve two purposes

- Direct simulation of physical processes (*theoretical-experimental-physics*) such as for instance
  - molecular dynamics or
  - Monte Carlo simulation of physical processes.
- Solution of complex mathematical problems such as
  - differential equations,
  - minimization problems as well as
  - high dimensional integrals or sums.

This book addresses all these scenarios on a very basic level. It is addressed to lecturers who will have to teach a basic course/basic courses in Computational Physics or Numerical Methods and to students as a companion in their first steps into the realm of this fascinating field of modern research. Following these intentions, this book was divided into two parts. Part I deals with deterministic methods in Computational Physics. We discuss, in particular, numerical differentiation and integration, the treatment of ordinary differential equations, and we present some notes on the numerics of partial differential equations. Each chapter within this part of the book is complemented by numerous applications. Part II of this book provides an introduction to stochastic methods in Computational Physics. In particular, we will examine how to generate random numbers following a given distribution, summarize the basics of stochastics in order to establish the necessary background to understand techniques like MARKOV-Chain Monte Carlo. Finally, algorithms of stochastic optimization are discussed. Again, numerous examples out of physics like diffusion processes or the POTTS model are investigated exhaustively. Finally, this book contains an Appendix that augments the main parts of the book with a detailed discussion of supplementary topics.

This book is not meant to be just a collection of algorithms which can immediately be applied to various problems which may arise in Computational Physics. On the contrary, the scope of this book is to provide the reader with a mathematically well founded glance behind the scene of Computational Physics. Thus, particular emphasis is on a clear mathematical analysis of the various topics and to even provide, in some cases, the necessary mathematical means to understand the very background of these methods. Although there is a barely comprehensible amount of excellent literature on Computational Physics, most of these books seem to concentrate either on deterministic methods or on stochastic methods. It is not our goal to compete with these rather specific works. On the contrary, it is the particular focus of this book to discuss deterministic methods on a par with stochastic methods.

Nevertheless, a certain overlap with existing literature was unavoidable and we apologize if we were not able to cite appropriately all existing works which are of importance and which influenced this book. However, we believe that by putting the emphasis on an exact mathematical analysis of both the deterministic as well as the stochastic methods we created a stimulating presentation of the basic concepts applied in Computational Physics.

If we assume two basic courses in Computational Physics to be part of the curriculum, nick-named here: *Computational Physics 101* and *Computational Physics 102*, then we would like to suggest to present/study the various topics of this book according to the following syllabus:

- Computational Physics 101:
  - Chapter 1: Some Basic Remarks.
  - Chapter 2: Numerical Differentiation.
  - Chapter 3: Numerical Integration.
  - Chapter 4: The Kepler Problem.
  - Chapter 5: Ordinary Differential Equations: Initial Value Problems.
  - (Chapter 6: The Double Pendulum).
  - Chapter 7: Molecular Dynamics.
  - Chapter 8: Numerics of Ordinary Differential Equations: Boundary Value Problems.
  - (Chapter 9: The One-Dimensional Stationary Heat Equation).
  - Chapter 10: The One-Dimensional Stationary Schrödinger Equation.
  - Chapter 12: Pseudo Random Number Generators.
- Computational Physics 102:
  - Chapter 11: Partial Differential Equations.
  - Chapter 13: Random Sampling Methods.
  - Chapter 14: A Brief Introduction to Monte-Carlo Methods.
  - Chapter 15: The Ising Model.

- Chapter 16: Some Basics of Stochastic Processes.
- Chapter 17: The Random Walk and Diffusion Theory.
- Chapter 18: Markov-Chain Monte Carlo and the Potts Model.
- Chapter 19: Data Analysis.
- Chapter 20: Stochastic Optimization.

The various chapters are augmented by problems of medium complexity which help to understand better the numerical part of the topics discussed within this book.

Although the manuscript has been carefully checked several times, we cannot exclude that some errors escaped our scrutiny. We apologize in advance and would highly appreciate reports of potential mistakes or typos to Benjamin A. Stickler (benjamin.stickler@uni-due.de).

Throughout the book SI-units are used except stated otherwise.

Graz, July 2013

Benjamin A. Stickler
Ewald Schachinger

Acknowledgments

The Authors are grateful to Prof. Dr. C. Gattringer (Karl-Franzens Universität, Graz), to Profs. Dr. W. von der Linden, Dr. H.-G. Evertz, and Dr. H. Sormann (Graz University of Technology, Austria). They inspired this book with their lectures on various topics of Computational Physics, computer simulation, and numerical analysis. Last but not least the Authors thank Dr. Chris Theis (CERN) for meticulously reading the manuscript, for pointing out inconsistencies, and for suggestions to improve the text.

Contents

1 **Some Basic Remarks** 1
1.1 Motivation 1
1.2 Rounding Errors 6
1.3 Methodological Errors 8
1.4 Stability 9
1.5 Concluding Remarks 12
References 13

Part I Deterministic Methods

2 **Numerical Differentiation** 17
2.1 Introduction 17
2.2 Finite Differences 18
2.3 Finite Difference Derivatives 20
2.4 A Systematic Approach: The Operator Technique 22
2.5 Concluding Discussion 25
Summary 27
Problems 28
References 28

3 **Numerical Integration** 29
3.1 Introduction 29
3.2 Rectangular Rule 30
3.3 Trapezoidal Rule 33
3.4 The SIMPSON Rule 35
3.5 General Formulation: The NEWTON-COTES Rules 36
3.6 GAUSS-LEGENDRE Quadrature 38
3.7 An Example 44
3.8 Concluding Discussion 45
Summary 47
Problems 48
References 49

4 The Kepler Problem . . . 51
4.1 Introduction . . . 51
4.2 The Problem . . . 52
4.3 Numerical Treatment . . . 54
Summary . . . 59
References . . . 59

5 Ordinary Differential Equations: Initial Value Problems . . . 61
5.1 Introduction . . . 61
5.2 Simple Integrators . . . 62
5.3 Runge-Kutta Methods . . . 66
5.4 Hamiltonian Systems: Symplectic Integrators . . . 71
5.5 An Example: The Kepler Problem, Revisited . . . 73
Summary . . . 78
Problems . . . 79
References . . . 79

6 The Double Pendulum . . . 81
6.1 Hamilton's Equations . . . 81
6.2 Numerical Solution . . . 85
6.3 Numerical Analysis of Chaos . . . 88
Summary . . . 95
Problems . . . 95
References . . . 96

7 Molecular Dynamics . . . 97
7.1 Introduction . . . 97
7.2 Classical Molecular Dynamics . . . 97
7.3 Numerical Implementation . . . 102
Summary . . . 107
Problems . . . 108
References . . . 109

8 Numerics of Ordinary Differential Equations: Boundary Value Problems . . . 111
8.1 Introduction . . . 111
8.2 Finite Difference Approach . . . 113
8.3 Shooting Methods . . . 118
Summary . . . 121
References . . . 122

9 The One-Dimensional Stationary Heat Equation . . . 123
9.1 Introduction . . . 123
9.2 Finite Differences . . . 124

9.3 A Second Scenario 126
Summary 128
Problems 129
Reference 129

10 The One-Dimensional Stationary SCHRÖDINGER Equation 131
10.1 Introduction 131
10.2 A Simple Example: The Particle in a Box 134
10.3 Numerical Solution 139
10.4 Another Case 142
Summary 145
Problems 146
References 146

11 Partial Differential Equations 147
11.1 Introduction 147
11.2 The POISSON Equation 148
11.3 The Time-Dependent Heat Equation 151
11.4 The Wave Equation 157
11.5 The Time-Dependent SCHRÖDINGER Equation 160
Summary 167
Problems 167
References 168

Part II Stochastic Methods

12 Pseudo Random Number Generators 171
12.1 Introduction 171
12.2 Different Approaches 174
12.3 Quality Tests 178
Summary 182
Problems 182
References 183

13 Random Sampling Methods 185
13.1 Introduction 185
13.2 Inverse Transformation Method 187
13.3 Rejection Method 190
13.4 Probability Mixing 193
Summary 195
Problems 195

14 A Brief Introduction to Monte-Carlo Methods 197
14.1 Introduction 197
14.2 Monte-Carlo Integration 198
14.3 The Metropolis Algorithm: An Introduction 205
Summary 208
References 208

15 The Ising Model 209
15.1 The Model 209
15.2 Numerics 218
15.3 Selected Results 223
Summary 227
Problems 228
References 228

16 Some Basics of Stochastic Processes 229
16.1 Introduction 229
16.2 Stochastic Processes 230
16.3 Markov Processes 233
16.4 Markov-Chains 241
16.5 Continuous-Time Markov-Chains 247
Summary 249
Problems 250
References 250

17 The Random Walk and Diffusion Theory 251
17.1 Introduction 251
17.2 The Random Walk 253
17.3 The Wiener Process and Brownian Motion 259
17.4 Generalized Diffusion Models 265
Summary 272
Problems 272
References 273

18 Markov-Chain Monte Carlo and the Potts Model 275
18.1 Introduction 275
18.2 Markov-Chain Monte Carlo Methods 276
18.3 The Potts Model 279
18.4 Advanced Algorithms for the Potts Model 284
Summary 285
Problems 286
References 286

19 Data Analysis 287
19.1 Introduction 287
19.2 Calculation of Errors 287
19.3 Auto-Correlations 291
19.4 The Histogram Technique 295
Summary 296
Problems 297
Reference 297

20 Stochastic Optimization 299
20.1 Introduction 299
20.2 Hill Climbing 301
20.3 Simulated Annealing 303
20.4 Genetic Algorithms 310
20.5 Some Further Methods 312
Summary 313
Problems 314
References 314

Appendix A: The Two-Body Problem 315

Appendix B: Solving Non-Linear Equations: The NEWTON Method . . . 321

Appendix C: Numerical Solution of Linear Systems of Equations 323

Appendix D: Basics of Probability Theory 331

Appendix E: Phase Transitions 345

Appendix F: Fractional Integrals and Derivatives in 1D 349

Appendix G: Least Squares Fit 351

Appendix H: Deterministic Optimization 357

Index 369

Acronyms

cdf	Cumulative distribution function
CFL	Courant-Friedrichs-Lewy condition
e-RK-4	Explicit Runge-Kutta four stage method
n. n.	Nearest neighbors
pdf	Probability density function

Chapter 1
Some Basic Remarks

1.1 Motivation

Let us introduce the basic concepts and notations: Computational physics aims at solving physical problems by means of numerical methods developed in the field of numerical analysis. According to I. Jacques and C. Judd [1], numerical analysis is defined as, quote: "*Numerical analysis is concerned with the development and analysis of methods for the numerical solution of practical problems.*" Although the term *practical problems* remained unspecified in this definition, it is certainly necessary to reflect on ways to find approximate solutions to complex problems which occur regularly in natural sciences. In fact, in most cases it is not possible to find analytic solutions and one must rely on good approximations. Let us give some examples.

Consider the definite integral

$$\int_a^b \mathrm{d}x \exp\left(-x^2\right), \tag{1.1}$$

which, for instance, may occur when it is required to calculate the probability that an event following a normal distribution takes on a value within the interval $[a, b]$, where $a, b \in \mathbb{R}$. In contrast to the much simpler integral

$$\int_a^b \mathrm{d}x \exp(x) = \exp(b) - \exp(a), \tag{1.2}$$

the integral (1.1) cannot be solved analytically because there is no elementary function which differentiates to $\exp\left(-x^2\right)$. Hence, we have to approximate this integral in such a way that the approximation is accurate enough for our purpose. This example illustrates that even mathematical expressions which appear quite simple at the first

B. A. Stickler and E. Schachinger, *Basic Concepts in Computational Physics*,
DOI: 10.1007/978-3-319-02435-6_1, © Springer International Publishing Switzerland 2014

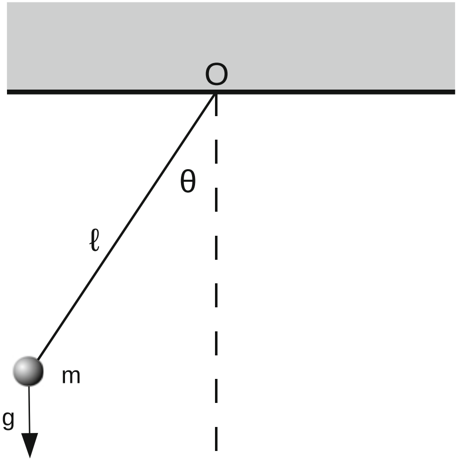

Fig. 1.1 Schematic illustration of the pendulum

glance may need a closer inspection when a numerical estimate for the expression is required. In fact, most numerical methods we will encounter within this book have been designed before the invention of modern computers or calculators. However, the applicability of these methods has increased and is still increasing drastically with the development of even more powerful machines. We give another example, namely the oscillation of a pendulum. From basic mechanics [2] we know that the time evolution of a frictionless pendulum of mass m and length ℓ in a gravitational field is defined by the differential equation

$$\ddot{\theta} + \frac{g}{\ell} \sin(\theta) = 0. \tag{1.3}$$

The solution of this equation describes the oscillatory motion of the pendulum around the origin O within a two-dimensional plane (Fig. 1.1). Here θ is the angular displacement and g is the acceleration due to gravity. Furthermore, we restrict the discussion to initial conditions of the form

$$\begin{cases} \theta(0) = \theta_0, \\ \dot{\theta}(0) = 0. \end{cases} \tag{1.4}$$

In the small angle approximation Eq. (1.3) is readily solved: For $\theta \ll 1$, in particular, $\theta_0 \ll 1$, we set $\sin(\theta) \approx \theta$ and obtain the differential equation of the harmonic oscillator:

$$\ddot{\theta} + \frac{g}{\ell}\theta = 0. \tag{1.5}$$

Together with the initial conditions (1.4) we arrive at the solution

$$\theta(t) = \theta_0 \cos(\omega t), \tag{1.6}$$

with

$$\omega = \sqrt{\frac{g}{\ell}}\,. \tag{1.7}$$

The period τ of the pendulum follows immediately:

$$\tau = 2\pi\sqrt{\frac{g}{\ell}}\,. \tag{1.8}$$

However, if the approximation of a small angular displacement $\theta_0 \ll 1$ is not applicable, expressions (1.6) and (1.8) will not be valid. Thus, it is advisable to apply energy conservation in order to arrive at analytic results. The energy is given by:

$$E = \frac{1}{2}mv^2 + mg\ell\left[1-\cos\left(\theta\right)\right] = \frac{1}{2}mv_0^2 + mg\ell\left[1-\cos\left(\theta_0\right)\right]. \tag{1.9}$$

Here v is the velocity of the point mass m and v_0 and θ_0 are defined by the initial conditions (1.4). Since $\dot{\theta}(0) = 0$ we have

$$\begin{aligned} E &= mg\ell\left[1-\cos\left(\theta_0\right)\right] \\ &= 2mg\ell\sin^2\left(\frac{\theta_0}{2}\right), \end{aligned} \tag{1.10}$$

where we made use of:

$$1-\cos(x) = 2\sin^2\left(\frac{x}{2}\right). \tag{1.11}$$

We use this result in Eq. (1.9) and arrive at:

$$\frac{1}{2}v^2 = 2g\ell\left[\sin^2\left(\frac{\theta_0}{2}\right) - \sin^2\left(\frac{\theta}{2}\right)\right]. \tag{1.12}$$

Since $v^2 = \ell^2\dot{\theta}^2$ we have

$$\dot{\theta} = 2\sqrt{\frac{g}{\ell}}\sqrt{\sin^2\left(\frac{\theta_0}{2}\right) - \sin^2\left(\frac{\theta}{2}\right)}. \tag{1.13}$$

Separation of variables yields

$$\sqrt{\frac{g}{\ell}}t = \frac{1}{2k}\int\limits_0^\theta \frac{\mathrm{d}\varphi}{\sqrt{1-\frac{1}{k^2}\sin^2\left(\frac{\varphi}{2}\right)}}, \tag{1.14}$$

with $k = \sin\left(\theta_0/2\right)$. For $t = \tau$ we have $\theta = \theta_0$ and we obtain for the period

$$\tau = \frac{2}{k}\sqrt{\frac{\ell}{g}}\int\limits_0^{\theta_0}\frac{\mathrm{d}\varphi}{\sqrt{1-\frac{1}{k^2}\sin^2\left(\frac{\varphi}{2}\right)}}, \tag{1.15}$$

where we defined the limits of integration as $\theta \in [-\theta_0, \theta_0]$. Let us transform the above integral into a more convenient form with help of the substitution $k\sin(\alpha) = \sin(\varphi/2)$. Thus, $\alpha \in [0, \pi/2]$ and a straightforward calculation yields:

$$\begin{aligned}\tau &= 4\sqrt{\frac{\ell}{g}}\int\limits_0^{\frac{\pi}{2}}\frac{\mathrm{d}\alpha}{\sqrt{1-k^2\sin^2(\alpha)}} \\ &= 4\sqrt{\frac{\ell}{g}}K_1(k).\end{aligned} \tag{1.16}$$

The function $K_1(k)$ introduced in (1.16) for $k \in \mathbb{R}$ is referred to as the complete elliptic integral of the first kind. All these manipulations did not really result in a simplification of the problem at hand because we are still confronted with the integral in Eq. (1.16) which cannot be evaluated without the use of additional approximations which will, in the end, result in a numerical solution of the problem. A natural way to proceed would be to expand the complete elliptic integral in a power series up to order N, where N is chosen in such a way that the *truncation error* $R_N(k)$ becomes negligible. We can find the desired expression in any text on special functions [3–5]. It reads

$$\begin{aligned}K_1(k) &= \frac{\pi}{2}\sum_{n=0}^{\infty}\left[\frac{(2n)!}{2^{2n}(n!)^2}\right]^2 k^{2n} \\ &= \frac{\pi}{2}\sum_{n=0}^{N}\left[\frac{(2n)!}{2^{2n}(n!)^2}\right]^2 k^{2n} + R_N(k).\end{aligned} \tag{1.17}$$

Furthermore, imagine the inverse problem: the period τ is given and the initial angle θ_0 is unknown. Again, we could expand the integrand in a power series and solve the corresponding polynomial for θ_0. However, such an approach would be very inefficient due to two reasons: first of all, we are confronted with the impossibility of finding analytically the roots of a polynomial of order $N > 4$ and, secondly, at which value of N should we truncate the power series if θ_0 is unknown? A glance in a book on special functions might give us a better, i.e. more convenient, alternative. Indeed, the inverse functions of the incomplete elliptic integral $F(a, b)$ with respect to a are referred to as JACOBI elliptic functions [3–5]. Given the equation

$$u = F(a, b), \tag{1.18}$$

the quantity of interest b can be expressed in terms of the JACOBI amplitude $\mathrm{am}(u, b)$, where

$$\mathrm{am}(u, a) = b. \tag{1.19}$$

Series expansions of $\mathrm{am}(u, a)$ have been developed, such that we can approximate θ_0 by truncating the respective series. These two examples illustrated that we have to depend on numerical approximations of definite expressions in a multitude of cases. Even if an approximate solution has been found for a particular problem it will be adamant to check quite carefully if the approach was (i) justified within the required accuracy, and (ii) if it allowed to improve the induced error of the result. The second point is known as the *stability* of a routine. We will discuss this topic in more detail in Sect. 1.4.

Throughout this book we will be confronted with numerous methods which will allow approximate solutions of problems similar to the two examples illustrated above. First of all, we would like to specify the properties we expect these methods to have. Primarily, the method is to be formulated as an unambiguous mathematical recipe which can be applied to the set of problems it was designed for. Its applicability should be well defined and it should allow to determine an estimate for the error. Moreover, infinite repetition of the procedure should approximate the exact result to arbitrary accuracy. In other words, we want the method to be well defined in *algorithmic* form. Consequently, let us define an algorithm as *a sequence of logical and arithmetic operations (addition, subtraction, multiplication or division) which allows to approximate the solution of the problem under consideration within any accuracy desired.* This implies, of course, that numerical errors will be unavoidable.

Let us classify the occurring errors based on the structure every numerical routine follows: We have input-errors, algorithmic-errors, and output-errors as indicated schematically in Fig. 1.2. This structural classification can be refined: input-errors

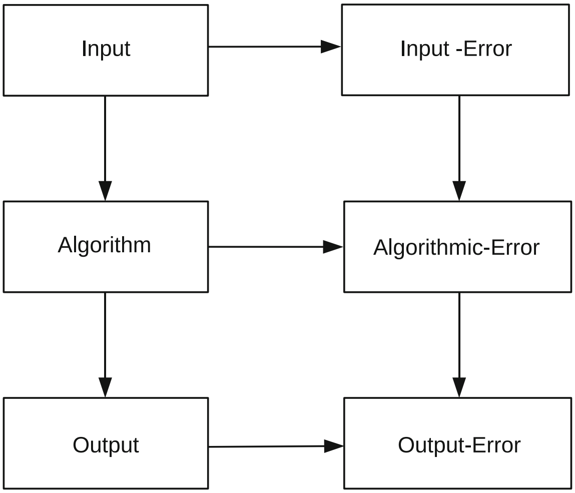

Fig. 1.2 Schematic classification of the errors occurring within a numerical procedure

are divided into rounding errors and measurement errors contained in the input data; algorithmic-errors consist of rounding errors during evaluation and of methodological errors due to mathematical approximations; finally, output errors are, in fact, rounding errors. In Sects. 1.2 and 1.3 we will concentrate on rounding errors and methodological errors. Since in most cases measurement errors cannot be influenced by the theoretical physicist concerned with numerical modeling, this particular part will not be discussed in this book. However, we will discuss the stability of numerical routines, i.e. the influence of slight modifications of the input parameters on the outcome of a particular algorithm in Sect. 1.4.

1.2 Rounding Errors

In fact, since every number is stored in a computer using a finite number of digits, we have to truncate every non-terminating number at some point. For instance, consider $\frac{2}{3} = 0.666666666666\ldots$ which will be stored as 0.6666666667 if the machine allows only ten digits. Actually, computers use binary arithmetic (for which even $0.1_{10} = 0.000110011001100\ldots_2$ is problematic) but for the moment we shall ignore this fact since the above example suffices to illustrate the crucial point. Let $\mathrm{Fl}(x)$ denote the floating-point form of a number x within the numerical range of the machine. For the above example, i.e. a ten digit storage, we have

$$\mathrm{Fl}\left(\frac{2}{3}\right) = 0.6666666667. \tag{1.20}$$

This has the consequence that, for instance, $\mathrm{Fl}(\sqrt{3}) \cdot \mathrm{Fl}(\sqrt{3}) \neq \mathrm{Fl}(\sqrt{3} \cdot \sqrt{3}) = 3$. However, $\mathrm{Fl}(\sqrt{3}) \cdot \mathrm{Fl}(\sqrt{3}) \approx 3$ within the defined range. Before we continue our discussion on rounding errors we have to introduce the concepts of the absolute and the relative error. We denote the true value of a quantity by y and its approximate value by $\overline{y}$. Then the absolute error ε_a is defined as

$$\varepsilon_a = |y - \overline{y}|, \tag{1.21}$$

while the relative error ε_r is given by

$$\varepsilon_r = \left|\frac{y - \overline{y}}{y}\right| = \frac{\varepsilon_a}{|y|}, \tag{1.22}$$

provided that $y \neq 0$. In most applications, the relative error is more significant. This is illustrated in Table 1.1, where it is intuitively obvious that in the second case the approximate value is much better although the absolute error is the same for both examples.

Table 1.1 Illustration of the significance of the relative error

	y	$\overline{y}$	ε_a	ε_r
(1)	0.1	0.09	0.01	0.1
(2)	1000.0	999.99	0.01	0.00001

Let us have a look at the relative error of an arbitrary number stored to the k-th digit: We can write an arbitrary number y in the form $y = 0.d_1d_2d_3 \dots d_kd_{k+1} \dots 10^n$ with $d_1 \neq 0$ and $n \in \mathbb{Z}$. Accordingly, we write its approximate value as $\overline{y} = 0.d_1d_2d_3 \dots d_k 10^n$, where k is the maximum number of digits stored by the machine. Hence we obtain for the relative error

$$\begin{aligned}
\varepsilon_r &= \left| \frac{0.d_1d_2d_3 \dots d_kd_{k+1} \dots 10^n - 0.d_1d_2d_3 \dots d_k 10^n}{0.d_1d_2d_3 \dots d_kd_{k+1} \dots 10^n} \right| \\
&= \left| \frac{0.d_{k+1}d_{k+2} \dots 10^{n-k}}{0.d_1d_2d_3 \dots 10^n} \right| \\
&= \left| \frac{0.d_{k+1}d_{k+2} \dots}{0.d_1d_2d_3 \dots} \right| 10^{-k} \\
&\le \frac{1}{0.1} 10^{-k} \\
&= 10^{-k+1}.
\end{aligned} \tag{1.23}$$

In the last steps we employed that, since $d_1 \neq 0$, we have $0.d_1d_2d_3 \dots \ge 0.1$ and accordingly $0.d_{k+1}d_{k+2} \dots < 1$. If the last digit would have been rounded (for $d_{k+1} \ge 5$ we set $d_k = d_k + 1$ otherwise d_k remains unchanged) instead of a simple truncation, the relative error of a variable y would be $\varepsilon_r = 0.5 \cdot 10^{-k+1}$.

Whenever an arithmetic operation is performed, the errors of the variables involved is transferred to the result. This can occur in an advantageous or disadvantageous way, where we understand disadvantageous as an increase in the relative error. Particular care is required when two nearly identical numbers are subtracted (*subtractive cancellation*) or when a large number is divided by a, in comparison, small number. In such cases the rounding error will increase dramatically. We note that it might be necessary to avoid such operations in our aim to design an algorithm which is required to produce reasonable results. An illustrative example and its remedy will be discussed in Sect. 1.3. However, before proceeding to the next section we introduce a lower bound to the accuracy which is achievable with a non-ideal computer, the *machine-number*. The machine-number is smallest positive number η which can be added to another number, such that a change in the result is observed. In particular,

$$\eta = \min_{\delta} \left\{ \delta > 0 \middle| 1 + \delta > 1 \right\}. \tag{1.24}$$

For a (nonexistent) super-computer, which is capable of saving as much digits as desired, η would be arbitrarily small. A typical value for double-precision in FORTRAN or C is $\eta \approx 10^{-16}$.

1.3 Methodological Errors

A methodological error is introduced into the routine whenever a complex mathematical expression is replaced by an approximate, simpler one. We already came across an example when we regarded the series representation of the elliptic integral (1.14) in Sect. 1.1. Although we could evaluate the series up to an arbitrary order N, we are definitely not able to sum up the coefficients to order ∞. Hence, it is not possible to get rid of methodological errors whenever we have to deal with expressions we cannot evaluate analytically. Another intriguing example is the numerical differentiation of a (analytically) given function. The standard approximation of a derivative reads

$$f'(x_0) = \frac{\mathrm{d}}{\mathrm{d}x} f(x)\bigg|_{x=x_0} \approx \frac{f(x_0+h) - f(x_0)}{h}. \tag{1.25}$$

This approximation is referred to as *finite difference* and will be discussed in more detail in Chap. 2. One would, in a first guess, expect that the obtained value gets closer to the true value of the derivative $f'(x_0)$ with decreasing values of h. From a calculus point of view, this is correct since by definition

$$\frac{\mathrm{d}}{\mathrm{d}x} f(x)\bigg|_{x=x_0} = \lim_{h\to 0} \frac{f(x_0+h) - f(x_0)}{h}. \tag{1.26}$$

However, this is not the case numerically. In particular, one can find a value $\hat{h}$ for which the relative error is minimal, while for values $h < \hat{h}$ and $h > \hat{h}$ the approximation obtained is worse in comparison. The reason is that for small values of h the rounding errors dominate the result since $f(x_0 + h)$ and $f(x_0)$ almost cancel while $1/h$ is very small. For $h > \hat{h}$, the methodological error, i.e. the replacement of a derivative by a finite difference, controls the result.

We give one further example [6] in order to illustrate the interplay between methodological errors and rounding errors. We regard the, apparently nonhazardous, numerical solution of a quadratic equation

$$ax^2 + bx + c = 0, \tag{1.27}$$

where $a, b, c \in \mathbb{R}$, $a \neq 0$. The well known solutions read

$$x_1 = \frac{-b + \sqrt{b^2 - 4ac}}{2a} \quad \text{and} \quad x_2 = \frac{-b - \sqrt{b^2 - 4ac}}{2a}. \tag{1.28}$$

Cautious because of the above examples, we immediately diagnose the danger of a subtractive cancellation in the expression of x_1 for $b > 0$ or in x_2 for $b < 0$, and rewrite the above expression for x_1:

$$x_1 = \frac{(-b + \sqrt{b^2 - 4ac})}{2a} \frac{(-b - \sqrt{b^2 - 4ac})}{(-b - \sqrt{b^2 - 4ac})} = \frac{2c}{-b - \sqrt{b^2 - 4ac}}. \tag{1.29}$$

For x_2 we obtain

$$x_2 = \frac{2c}{-b + \sqrt{b^2 - 4ac}}. \tag{1.30}$$

Consequently, if $b > 0$ x_1 should be calculated using Eq. (1.29) and if $b < 0$ Eq. (1.28) should be used to calculate x_2. Moreover, the above expressions can be cast into one expression by setting

$$x_1 = \frac{q}{a} \qquad \text{and} \qquad x_2 = \frac{c}{q}, \tag{1.31}$$

with

$$q = -\frac{1}{2}\left[b + \operatorname{sgn}(b)\sqrt{b^2 - 4ac}\right]. \tag{1.32}$$

Thus, Eqs. (1.31) and (1.32) can be used to calculate x_1 and x_2 for any sign of b.

1.4 Stability

When a new numerical method is designed *stability* is the third crucial point after rounding errors and methodological errors. We give an introductory definition:

An algorithm, equation or, even more general, a problem is referred to as unstable or ill-conditioned if small changes in the input cause a large change in the output.

It will be followed by a couple of elucidating examples [1].[1] To be more specific, let us now, for instance, consider the following system of equations

$$\begin{aligned} x + y &= 2.0, \\ x + 1.01y &= 2.01. \end{aligned} \tag{1.33}$$

The equations are easily solved and give $x = 1.0$ and $y = 1.0$. To make our point we consider now the case in which the right hand side of the second equation of (1.33) is subjected to a small perturbation, i.e. we consider in particular the following system of equations

[1] Although unstable behavior is not desirable in the first place the discovery of unstable systems was the birth of a specific branch in physics called *Chaos Theory*. We will come back to this point at the end of this section.

$$\begin{aligned} x + y &= 2.0, \\ x + 1.01y &= 2.02. \end{aligned} \tag{1.34}$$

The corresponding solution is $x = 0.0$ and $y = 2.0$. We observe that a relative change of 0.05 % on the right hand side of the second equation in (1.33) resulted in a 100 % relative change of the solution. Moreover, if the coefficient of y in the second equation of (1.33) were 1.0 instead of 1.01, which corresponds to a relative change of 1 %, the equations would be unsolvable. This is a behavior typical for ill-conditioned problems which, for obvious reasons, should be avoided whenever possible.

We give a second example: We consider the following initial value problem

$$\begin{cases} \ddot{y} - 10\dot{y} - 11y = 0, \\ y(0) = 1, \qquad \dot{y}(0) = -1. \end{cases} \tag{1.35}$$

The general solution is readily obtained to be of the form

$$y = A \exp(-x) + B \exp(11x), \tag{1.36}$$

with numerical constants A and B. The initial conditions yield the unique solution

$$y = \exp(-x). \tag{1.37}$$

The initial conditions are now changed by two small parameters $\delta, \varepsilon > 0$ to give:

$$y(0) = 1 + \delta \qquad \text{and} \qquad \dot{y}(0) = -1 + \varepsilon. \tag{1.38}$$

The unique solution which satisfies these initial conditions is:

$$\overline{y} = \left(1 + \frac{11\delta}{12} - \frac{\varepsilon}{12}\right) \exp(-x) + \left(\frac{\delta}{12} + \frac{\varepsilon}{12}\right) \exp(11x). \tag{1.39}$$

We calculate the relative error

$$\begin{aligned} \varepsilon_r &= \left|\frac{y - \overline{y}}{y}\right| \\ &= \left(\frac{11\delta}{12} - \frac{\varepsilon}{12}\right) + \left(\frac{\delta}{12} + \frac{\varepsilon}{12}\right) \exp(12x), \end{aligned} \tag{1.40}$$

which indicates that the problem is ill-conditioned since for large values of x the second term definitely overrules the first one.

Another, but not less serious kind of problem is *induced instability*:

A method is referred to as induced unstable if a small error at one point of the calculation induces a large error at some subsequent point.

Induced instability is particularly dangerous since small rounding errors are unavoidable in most calculations. Hence, if some part of the whole algorithm is ill-conditioned, the final output will be dominated by the error induced in such a way. Again, an example will help to illustrate such behavior. The definite integral

$$I_n = \int_0^1 \mathrm{d}x\, x^n \exp(x-1), \tag{1.41}$$

is considered. Integration by parts yields

$$I_n = 1 - nI_{n-1}. \tag{1.42}$$

This expression can be used to recursively calculate I_n from I_0, where

$$I_0 = 1 - \exp(-1). \tag{1.43}$$

Although the recursion formula (1.42) is exact we will run into massive problems using it. The reason is easily illustrated:

$$\begin{aligned} I_n &= 1 - nI_{n-1} \\ &= 1 - n + n(n-1)I_{n-2} \\ &= 1 - n + n(n-1) - n(n-1)(n-2)I_{n-3} \\ &\ \ \vdots \\ &= 1 + \sum_{k=1}^{n-1}(-1)^k \frac{n!}{(n-k)!} + (-1)^{n-1} n! I_0. \end{aligned} \tag{1.44}$$

Thus, the initial rounding error included in the numerical value of I_0 is multiplied with $n!$. Note that for large n we have according to STIRLING's approximation

$$n! \approx \sqrt{2\pi} n^{n+\frac{1}{2}} \exp(-n), \tag{1.45}$$

i.e. an initial error increases almost as n^n.

However, Equation (1.42) can be reformulated to give

$$I_n = \frac{1}{n+1}(1 - I_{n+1}), \tag{1.46}$$

and this opens an alternative method for a recursive calculation of I_n. We can start with some value $N \gg n$ and simply set $I_N = 0$. The error introduced in such a way may in the end not be acceptable, nevertheless, it decreases with every iteration step due to the division by n in Eq. (1.46).

Having discussed some basic features of stability in numerical algorithms we would like to add a few remarks on *Chaos Theory*. Chaos theory investigates dynamical processes which are very sensitive to initial conditions. One of the best known examples for such a behavior is the weather prediction. Although, POINCARÉ already observed chaotic behavior while working on the three body problem, one of the pioneers of chaos theory was E. N. LORENZ [7] (not to be confused with H. LORENTZ, who introduced the LORENTZ transformation). In 1961 he ran weather simulations on a small computer. However, when he tried to reproduce one particular result by restarting the calculation with new parameters calculated the days before, he observed that the outcome was completely different. The reason was that the equations he dealt with were ill-conditioned, and the rounding error he introduced by simply typing in the numbers of the graphical output, increased drastically, and, hence, produced a completely different result. Nowadays, various physical systems are known which indeed behave in such a way. Further examples are turbulences in fluids, oscillations in electrical circuits, oscillating chemical reactions, population growth in ecology, the time evolution of the magnetic field of celestial bodies, ….

It is important to note, that chaotic behavior induced in such systems is *deterministic*, yet *unpredictable*. This is due to the impossibility of an exact knowledge of the initial conditions required to predict, for instance, the weather over a reasonably long period. A feature which is referred to as the *butterfly effect*: a hurricane can form because a butterfly flapped its wings several weeks before. However, these effects have nothing to do with intrinsic in-determinism, which is solely a feature of quantum mechanics. In contrast to this, in chaos theory, the future is uniquely determined by initial conditions, however, still unpredictable. This is often referred to as *deterministic chaos*.

It has to be emphasized that chaos in physical systems is a consequence of deterministic equations describing the processes and not a consequence of the numerical method one uses for modeling. Therefore, it is important to distinguish between the stability of a numerical method and the stability of a physical system in general.

We will come across chaotic behavior again in Sect. 6.3 where we discuss chaotic behavior in the dynamics of the double pendulum.

1.5 Concluding Remarks

In this chapter we dealt with the basic features of numerical errors one is always confronted with when developing an algorithm. One point we neglected in our discussion is the *computational cost*, i.e. the time a program needs to be executed. Although this is a very important point, it is beyond the scope of this book. However, one has to find a balance between the need of achieving the most accurate result and the computing time required to achieve it. The most accurate result is useless if the programmer does not get the result within his lifetime. D. ADAMS [8] put in a nutshell: the super-computer *Deep Thought* was asked to compute the answer to *"The Ultimate Question of Life, the Universe and Everything"*, quote:

"How long?" he said.
"Seven and a half million years."

Another quite crucial point, which we neglected so far, is the error analysis of a computational method which is based on random numbers (in fact it is pseudo-random numbers, we will come back to this point in the second part of this book). In this case, the situation changes completely, because, similar to experimental results, the observed values are distributed around a mean with a certain variance. Such results have to be interpreted in a statistical context, however it turns out that for many problems the computational efficiency can be significantly increased using such methods. Typical applications are estimates of integrals or solutions to optimization problems. Such topics will be treated in the second part of this book.

References

1. Jacques, I., Judd, C.: Numerical Analysis. Chapman and Hall, London (1987)
2. Scheck, F.: Mechanics, 5th edn. Springer, Berlin (2010)
3. Abramovitz, M., Stegun, I.A. (eds.): Handbook of Mathemathical Functions. Dover, New York (1965)
4. Mathai, A.M., Haubold, H.J.: Special Functions for Applied Scientists. Springer, Berlin (2008)
5. Beals, R., Wong, R.: Special Functions. Cambridge Studies in Advanced Mathematics. Cambridge University Press, Cambridge (2010)
6. Burden, R.L., Faires, J.D.: Numerical Analysis. PWS-Kent Publishing Comp, Boston (1993)
7. Lorenz, E.N.: Deterministic nonperiodic flow. J. Atmos. Sci. **20**, 130–141 (1963)
8. Adams, D.: The Hitchhiker's Guide to the Galaxy. Pan Books, London (1979)

Part I
Deterministic Methods

Chapter 2
Numerical Differentiation

2.1 Introduction

This chapter is the first of two systematic introductions to the numerical treatment of differential equations. The importance of differential equations, and thus of derivatives and integrals, cannot be underestimated in the modern formulation of natural sciences and in particular of physics. Very often the complexity of the expressions involved does not justify an analytical approach, be it because an analytical solution simply does not exist or that the search for it is too expensive. It should be noted that modern *symbolic* software, such as MAPLE or MATHEMATICA can ease a physicists life significantly. However, in many cases a numerical treatment is unavoidable and one should be prepared.

We introduce here the notion of finite differences as a basic concept of numerical differentiation. In contrast, the next chapter will deal with the concepts of numerical quadrature. Together, these two chapters will set the stage for a comprehensive discussion of algorithms designed to solve numerically differential equations. In particular, the solution of ordinary differential equations will always be based on an integration of the equations.

This chapter is composed of four sections. The first repeats some basic concepts of calculus and introduces formally finite differences. The second formulates approximates to derivatives based on finite differences, while the third section includes a more systematic approach based on an operator technique. It allows an arbitrarily close approximation of derivatives with the advantage that the expressions discussed in this section can immediately be applied to the problems at hand. The chapter is concluded with a discussion of some additional aspects.

B. A. Stickler and E. Schachinger, *Basic Concepts in Computational Physics*,
DOI: 10.1007/978-3-319-02435-6_2, © Springer International Publishing Switzerland 2014

2.2 Finite Differences

Let us consider a smooth function $f(x)$ on the finite interval $[a, b]$ on the real axis with $x \in \mathbb{R}$. The interval $[a, b]$ is divided into $N - 1 \in \mathbb{N}$ equally spaced sub-intervals of the form $[x_i, x_{i+1}]$ where $x_1 = a$, $x_N = b$. Obviously, x_i is then given by

$$x_i = a + (i-1)\frac{b-a}{N-1}, \quad i = 1, \ldots, N. \tag{2.1}$$

We then introduce the distance h between two grid-points x_i by:

$$h = x_{i+1} - x_i = \frac{b-a}{N-1}, \quad \forall i = 1, \ldots, N-1. \tag{2.2}$$

For the sake of a more compact notation we restrict our discussion to equally spaced grid-points keeping in mind that the extension to arbitrarily spaced grid-points by replacing h by h_i is straight forward and leaves the discussion essentially unchanged.

Note that the number of grid-points and, thus, their distance h, has to be chosen in such a way that the function $f(x)$ can be sufficiently well approximated by its function values $f(x_i)$ as indicated in Fig. 2.1. We understand by *sufficiently well approximated* that some interpolation scheme in the interval $[x_i, x_{i+1}]$ will reproduce the function $f(x)$ within a given accuracy. In cases where the function is strongly varying within some sub-interval $[c, d] \subset [a, b]$ and is slowly varying within $[a, b] \setminus [c, d]$ it might be advisable to use variable grid-spacing in order to reduce the computational cost of the procedure.

We introduce the following notation: The function value of $f(x)$ at the particular grid-point x_i will be denoted by $f_i \equiv f(x_i)$ and we define its n-th derivative with respect to x at the grid-point x_i as

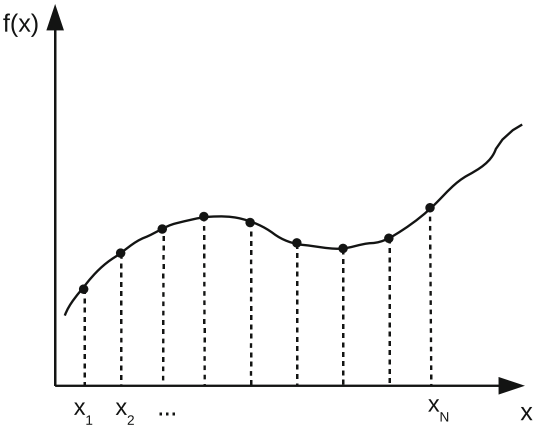

Fig. 2.1 We define equally spaced grid-points x_i on a finite interval on the real axis in such a way that the function $f(x)$ is sufficiently well approximated by its functional values $f(x_i)$ at these grid-points

$$\left.\frac{\mathrm{d}^n f(x)}{\mathrm{d}x^n}\right|_{x=x_i} = f^{(n)}(x_i) \equiv f_i^{(n)}. \tag{2.3}$$

Furthermore, we define for arbitrary $\xi \in [x_i, x_{i+1})$

$$f_{i+\varepsilon}^{(n)} = f^{(n)}(\xi), \tag{2.4}$$

where $f_{i+\varepsilon}^{(0)} \equiv f_{i+\varepsilon}$ and ε is chosen to give

$$\xi = x_i + \varepsilon h. \tag{2.5}$$

Note that $\varepsilon \in [0, 1)$.

Let us remember some basics from calculus. The first derivative, denoted $f'(x)$ of a function $f(x)$ which is continuously differentiable within the interval $[a, b]$, i.e. $f(x) \in \mathscr{C}^\infty[a, b]$, for arbitrary $x \in [a, b]$ is defined as

$$\begin{aligned} f'(x) &:= \lim_{h\to 0} \frac{f(x+h) - f(x)}{h} \\ &= \lim_{h\to 0} \frac{f(x) - f(x-h)}{h} \\ &= \lim_{h\to 0} \frac{f\left(x+\frac{h}{2}\right) - f\left(x-\frac{h}{2}\right)}{h}. \end{aligned} \tag{2.6}$$

We discussed this particular problem already in Sect. 1.3, Eq. (1.26) and learned that it is impossible to draw numerically the limit $h \to 0$. This manifests itself in a non-negligible error due to subtractive cancellation.

For the sake of a systematic treatment we remember TAYLOR's theorem, which states that if we have a function which is n-times continuously differentiable on the interval $[a, b]$ and if $f^{(n+1)}(x)$ exists we can express $f(x)$ in terms of a series expansion at point $x_0 \in [a, b]$:

$$f(x) = \sum_{k=0}^{n} \frac{f^{(k)}(x_0)}{k!}(x - x_0)^k + \frac{f^{(n+1)}[\zeta(x)]}{(n+1)!}(x - x_0)^{n+1}, \quad \forall x \in [a, b]. \tag{2.7}$$

Here, $\zeta(x)$ takes on a value between x and x_0. The last term on the right hand side of Eq. (2.7) is commonly referred to as *truncation error.* (A more general definition of this error was given in Sect. 1.1.) For $x_0 = 0$ the above series expansion is referred to as MCLAURIN series.

We introduce now the finite difference

$$\Delta f_i = f_{i+1} - f_i, \tag{2.8a}$$

as the *forward difference*,

$$\nabla f_i = f_i - f_{i-1}, \tag{2.8b}$$

as the *backward difference*, and

$$\delta f_i = f_{i+\frac{1}{2}} - f_{i-\frac{1}{2}}, \tag{2.8c}$$

as the *central difference*.[1] We can now estimate derivatives by finite differences with the help of TAYLOR's theorem (2.7). In a first step we consider (restricting to second order in h) with $f_{i+1} \equiv f(x_i + h)$:

$$\begin{aligned} f_{i+1} &= f(x_i) + hf'(x_i) + \frac{h^2}{2} f''[\zeta(x_i + h)] \\ &= f_i + hf_i' + \frac{h^2}{2} f''_{i+\varepsilon_\zeta}. \end{aligned} \tag{2.9a}$$

Here ε_ζ is the fractional part ε which has to be determined according to $\zeta(x_i + h)$. In analogue we find for f_{i-1}

$$f_{i-1} = f_i - hf_i' + \frac{h^2}{2} f''_{i+\varepsilon_\zeta}, \tag{2.9b}$$

and for $f_{i\pm\frac{1}{2}}$:

$$f_{i\pm\frac{1}{2}} = f_i \pm \frac{h}{2} f_i' + \frac{h^2}{8} f_i'' \pm \frac{h^3}{48} f'''_{i+\varepsilon_\zeta}. \tag{2.9c}$$

Here we expanded $f_{i\pm\frac{1}{2}}$ up to third order in h and the reason for this will become obvious immediately.

2.3 Finite Difference Derivatives

We define the *finite difference derivative* or difference approximations

$$D_+ f_i = \frac{\Delta f_i}{h} = \frac{f_{i+1} - f_i}{h}, \tag{2.10a}$$

as the *forward difference derivative*,

$$D_- f_i = \frac{\nabla f_i}{h} = \frac{f_i - f_{i-1}}{h}, \tag{2.10b}$$

[1] Please note that the symbols Δ, ∇, and δ in Eqs. (2.8) can also be regarded as operators acting on f_i. For a basic introduction to the theory of linear operators see for instance [1, 2].

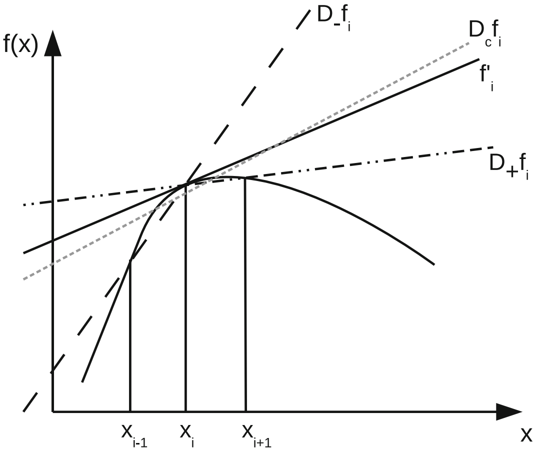

Fig. 2.2 Graphical illustration of different finite difference derivatives. The solid line labeled f_i' represents the real derivative for comparison

as the *backward difference derivative*, and

$$D_cf_i = \frac{\delta f_i}{h} = \frac{f_{i+\frac{1}{2}} - f_{i-\frac{1}{2}}}{h}, \tag{2.10c}$$

as the *central difference derivative*. A graphical interpretation of these expressions is given in Fig. 2.2.

Using the above definitions (2.10) together with the expansions (2.9) we obtain

$$\begin{aligned} f_i' &= D_+f_i - \frac{h}{2}f''_{i+\varepsilon_\zeta} \\ &= D_-f_i + \frac{h}{2}f''_{i+\varepsilon_\zeta} \\ &= D_cf_i - \frac{h^2}{24}f'''_{i+\varepsilon_\zeta}. \end{aligned} \tag{2.11}$$

We observe that in the central difference approximation of f_i' the truncation error scales like h^2 while it scales like h in the other two approximations; thus the central difference approximation should have the smallest methodological error. Note that the error cannot be dominated by the derivatives of $f(x)$ since we assumed that f is a smooth function within $[a, b]$. Furthermore we have to emphasize that the central difference approximation is essentially a *three point* approximation, including f_{i-1}, f_i and f_{i+1}, although f_i cancels. Thus, we can improve our approximation by taking even more grid-points into account. For instance, we could combine the above finite difference derivatives. Let us prepare this step by expanding Eqs. (2.9) to higher order derivatives. We then obtain for the forward difference derivative

$$D_+f_i = f_i' + \frac{h}{2}f_i'' + \frac{h^2}{6}f_i''' + \frac{h^3}{24}f_i^{IV} + \frac{h^4}{120}f_i^{V} + \cdots, \tag{2.12}$$

for the backward difference derivative

$$D_{-}f_i = f_i' - \frac{h}{2}f_i'' + \frac{h^2}{6}f_i''' - \frac{h^3}{24}f_i^{IV} + \frac{h^4}{120}f_i^{V} \mp \cdots , \tag{2.13}$$

and, finally, for the central difference derivative

$$D_c f_i = f_i' + \frac{h^2}{24}f_i''' + \frac{h^4}{1920}f_i^{V} + \cdots . \tag{2.14}$$

In order to improve the method we have to combine $D_{+}f_i$, $D_{-}f_i$ and $D_c f_i$ in such a way that at least the terms proportional to h^2 cancel. This can be achieved by observing that

$$8D_c f_i - D_{+}f_i - D_{-}f_i = 6f_i' - \frac{h^4}{60}f_{i+\varepsilon_\zeta}^{V}, \tag{2.15}$$

which gives

$$\begin{aligned} f_i' &= \frac{1}{6}\left(8D_c f_i - D_{+}f_i - D_{-}f_i\right) + \frac{h^4}{360}f_i^{V} \\ &= \frac{1}{6h}\left(f_{i-1} + 8f_{i+\frac{1}{2}} - 8f_{i-\frac{1}{2}} - f_{i+1}\right) + \frac{h^4}{360}f_{i+\varepsilon_\zeta}^{V} . \end{aligned} \tag{2.16}$$

Note that this simple combination yields an improvement of two orders in h! One can even improve the approximation in a similar fashion by simply calculating the derivative from even more points, for instance $f_{i\pm\frac{3}{2}}$.

2.4 A Systematic Approach: The Operator Technique

We would like to obtain a general expression which will allow to calculate the finite difference derivatives of arbitrary order up to arbitrary order of h in the truncation error. First of all, we redefine our grid in order to get rid of the expressions including function values between grid-points, such as $f_{i+\frac{1}{2}}$. This can easily be achieved by redefining the grid in such a way that we have in total $2N$ grid-points. However, an even more convenient method can be found by the introduction of the average operator μ

$$\mu f_i = \frac{f_{i+\frac{1}{2}} + f_{i-\frac{1}{2}}}{2} . \tag{2.17}$$

This operator ensures that there will no functional values be required between two grid-points.[2] This enables us to redefine the central difference derivative $D_c f_i$ (2.10c) as

[2] From now on, all symbols like D_c, Δ, etc. are interpreted as operators.

$$D_c f_i = \frac{\mu\delta f_i}{h} = \frac{f_{i+1} - f_{i-1}}{2h}. \tag{2.18}$$

Furthermore, we introduce the shift operator E and its inverse E^{-1}, where $EE^{-1} = \mathbb{1}$, the unity operator, by[3]

$$Ef_i = f_{i+1}, \tag{2.20}$$

and

$$E^{-1}f_i = f_{i-1}. \tag{2.21}$$

Note that we can write these operators in terms of the forward and backward difference operators Δ and ∇ of Eqs. (2.8), in particular

$$E = \Delta + \mathbb{1}, \tag{2.22}$$

and

$$E^{-1} = \mathbb{1} - \nabla. \tag{2.23}$$

Moreover, if $D \equiv \frac{\mathrm{d}}{\mathrm{d}x}$ denotes the derivative operator and if the n-th power of this operator D is understood as the n-th successive application of it, we can rewrite the TAYLOR expansions (2.9) as

$$\begin{aligned} f_{i+1} &= \left[\mathbb{1} + hD + \frac{1}{2}h^2D^2 + \frac{1}{3!}h^3D^3 + \cdots\right] f_i \\ &\equiv \exp(hD)f_i, \end{aligned} \tag{2.24}$$

and

$$\begin{aligned} f_{i-1} &= \left[\mathbb{1} - hD + \frac{1}{2}h^2D^2 - \frac{1}{3!}h^3D^3 \pm \cdots\right] f_i \\ &\equiv \exp(-hD)f_i, \end{aligned} \tag{2.25}$$

[3] We note in passing that the shift operators form the discrete translational group, a very important group in theoretical physics. Let $E(n) = E^n$ denote the shift by $n \in \mathbb{N}$ grid-points. We then have

$$E(n)E(m) = E(n+m), \tag{2.19a}$$

$$E(0) = \mathbb{1}, \tag{2.19b}$$

and

$$E(n)^{-1} = E(-n), \tag{2.19c}$$

which are the properties required to form a group. Here $\mathbb{1}$ denotes the unity element. Moreover, we have

$$E(n)E(m) = E(m)E(n), \tag{2.19d}$$

i.e. it is an Abelian group. The group of discrete translations is usually denoted by $\mathbb{T}^d$.

Hence, we find that

$$E = \mathbb{1} + \Delta \equiv \exp(hD), \tag{2.26}$$

and, accordingly, that

$$E^{-1} = \mathbb{1} - \nabla \equiv \exp(-hD). \tag{2.27}$$

In a next step we obtain from (2.9c)

$$f_{i\pm\frac{1}{2}} = E^{\pm\frac{1}{2}} f_i = \exp\left(\pm\frac{hD}{2}\right), \tag{2.28}$$

which gives

$$\delta = E^{\frac{1}{2}} - E^{-\frac{1}{2}} = \exp\left(\frac{hD}{2}\right) - \exp\left(-\frac{hD}{2}\right) \equiv 2\sinh\left(\frac{hD}{2}\right). \tag{2.29}$$

Equations (2.26), (2.27) and (2.29) can be inverted for hD because the inverse operator E^{-1} exists. This yields

$$hD = \begin{cases} \ln(\mathbb{1} + \Delta) &= \Delta - \frac{1}{2}\Delta^2 + \frac{1}{3}\Delta^3 \mp \cdots, \\ -\ln(\mathbb{1} - \nabla) &= \nabla + \frac{1}{2}\nabla^2 + \frac{1}{3}\nabla^3 + \cdots, \\ 2\sinh^{-1}\left(\frac{\delta}{2}\right) &= \delta - \frac{1}{2^2 3!}\delta^3 + \frac{3^2}{2^4 5!}\delta^5 \mp \cdots. \end{cases} \tag{2.30}$$

Again, the n-th power of the operator K (with $K = \Delta, \nabla, \delta$) $K^n f_i$ is understood as the n-th successive action of the operator K on f_i, i.e. $K^{n-1}(Kf_i)$. Expression (2.30) allows to approximate the derivatives up to arbitrary order using finite differences. Furthermore, we can take the k-th power of Eq. (2.30) in order to get an approximate k-th derivative, $(hD)^k$ [3]. A rather involved calculation results in the following relations for f_i' and f_i'':

$$f_i' = \frac{1}{h}\begin{cases} \left[\Delta - \frac{1}{2}\Delta^2 + \frac{1}{3}\Delta^3 \mp \cdots\right] f_i, \\ \left[\nabla + \frac{1}{2}\nabla^2 + \frac{1}{3}\nabla^3 + \cdots\right] f_i, \\ \left[\mu\delta - \frac{1}{3!}\mu\delta^3 + \frac{1}{30}\mu\delta^5 \mp \cdots\right] f_i, \end{cases} \tag{2.31}$$

and

$$f_i'' = \frac{1}{h^2}\begin{cases} \left[\Delta^2 - \Delta^3 + \frac{11}{12}\Delta^4 \mp \cdots\right] f_i, \\ \left[\nabla^2 + \nabla^3 + \frac{11}{12}\nabla^4 + \cdots\right] f_i, \\ \left[\delta^2 - \frac{1}{12}\delta^4 + \frac{1}{90}\delta^6 \mp \cdots\right] f_i. \end{cases} \tag{2.32}$$

In particular, for the central difference derivative we obtain

$$f_i' = \frac{f_{i+1} - f_{i-1}}{2h} + \mathcal{O}(h^2), \tag{2.33}$$

and

$$f_i'' = \frac{f_{i+1} - 2f_i + f_{i-1}}{h^2} + \mathscr{O}(h^2). \tag{2.34}$$

Here, $\mathscr{O}(h^2)$ indicates that this term is of the order of h^2, i.e., we get the important result that in this case the truncation error is of the order $\mathscr{O}(h^2)$.

2.5 Concluding Discussion

First of all, although Eq. (2.30) allows to approximate a derivative of any order k arbitrarily close, it is still an infinite series which leaves us with the decision at which order to truncate. This choice will highly depend on the choice of h, which in turn depends on the function we would like to differentiate. Let us discuss an illustrative example: Consider the function

$$f(x) = \exp(i\omega x), \tag{2.35}$$

where $\omega, x \in \mathbb{R}$ and i is the imaginary number with $i^2 = -1$. Its first derivative is

$$f'(x) = i\omega \exp(i\omega x). \tag{2.36}$$

We now introduce grid-points by

$$x_k = x_0 + kh, \tag{2.37}$$

where h is the grid-spacing and x_0 is some finite starting point on the real axis. Accordingly,

$$f_k = \exp(i\omega x_0)\exp(i\omega kh), \tag{2.38}$$

and the exact value of the first derivative is

$$f_k' = i\omega \exp(i\omega x_0)\exp(i\omega kh) = i\omega f_k. \tag{2.39}$$

We calculate the forward, backward, and central difference derivatives according to Eq. (2.10) and obtain

$$\begin{aligned} D_+ f_k &= \exp(i\omega x_0)\exp(i\omega kh)\,\frac{\exp(i\omega h) - 1}{h} \\ &= f_k \frac{\exp(i\omega h) - 1}{h}, \end{aligned} \tag{2.40a}$$

$$\begin{aligned} D_{-}f_k &= \exp(i\omega x_0)\exp(i\omega kh)\,\frac{1-\exp(-i\omega h)}{h} \\ &= f_k\,\frac{1-\exp(-i\omega h)}{h}, \end{aligned} \tag{2.40b}$$

and

$$\begin{aligned} D_{c}f_k &= \exp(i\omega x_0)\exp(i\omega kh)\,\frac{\exp(i\omega h)-\exp(-i\omega h)}{2h} \\ &= f_k\,\frac{\exp(i\omega h)-\exp(-i\omega h)}{2h}. \end{aligned} \tag{2.40c}$$

We divide the approximate derivatives by the true value (2.39) and take the modulus. We get

$$\left|\frac{D_{+}f_k}{f_k'}\right| = \left|\frac{D_{-}f_k}{f_k'}\right| = \left|\frac{2\sin\left(\frac{1}{2}h\omega\right)}{h\omega}\right|, \tag{2.41}$$

and

$$\left|\frac{D_{c}f_k}{f_k'}\right| = \left|\frac{\sin(h\omega)}{h\omega}\right|. \tag{2.42}$$

Since $|\sin(x)| \le |x|$, $\forall x \in \mathbb{R}$ we obtain that in all three cases this ratio is less than one independent of h, unless $\omega = 0$ (Please keep in mind that $\frac{\sin(x)}{x} \to 1$ as $x \to 0$). Hence, the first order finite difference approximations underestimate the true value of the derivative. The reason is easily found: $f(x)$ oscillates with frequency ω while the finite difference derivatives applied here approximate the derivative linearly. Higher order corrections will, of course, improve the approximation significantly.

We consider now the case that the function $f(x)$ is not strongly varying. Too small values of h, i.e. a very dense grid of grid-points, will definitely increase the danger of a subtractive cancellation while values of h too large, i.e. a rather coarse grid of grid-points, will decrease the rate of convergence of the series (2.30). Furthermore, it is obvious that we should prefer the method of central differences whenever possible because it converges faster.

Finally, we would like to discuss how to approximate partial derivatives of functions which depend on more than one variable. Basically this can be achieved by independently discretisizing the function of interest in each particular variable and then by defining the corresponding finite difference derivatives. We will briefly discuss the case of two variables, the extension to even more variables is straight forward. We regard a function $g(x, y)$ where $(x, y) \in [a, b] \times [c, d]$. We denote the grid-spacing in x-direction by h and in y-direction by k. The evaluation of derivatives of the form $\frac{\partial^n}{\partial x^n} g(x, y)$ or $\frac{\partial^n}{\partial y^n} g(x, y)$ for arbitrary n are approximated with the help of the schemes discussed above, only the respective grid-spacing has to be accounted for. We will now briefly discuss mixed partial derivatives, in particular the derivative $\frac{\partial^2}{\partial x \partial y} g(x, y)$. Higher orders can be easily obtained in the same fashion. Here, we will restrict to the case of the central difference derivative. Again, the extension to the other two forms of derivatives is straight forward. We would like to approximate the derivative at the point $(a+ih, c+jk)$, which will be abbreviated by (i,j). Hence, we compute

$$\begin{aligned}\frac{\partial}{\partial y}\frac{\partial}{\partial x}g(x,y)\bigg|_{(i,j)} &= \frac{1}{2h}\left[\frac{\partial}{\partial y}g(x,y)\bigg|_{(i+1,j)} - \frac{\partial}{\partial y}g(x,y)\bigg|_{(i-1,j)}\right] + \mathscr{O}(h^2)\\ &= \frac{1}{2h}\left[\frac{g_{i+1,j+1}-g_{i+1,j-1}}{2k} + \mathscr{O}(k^2)\bigg|_{(i+1,j)}\right.\\ &\qquad \left. - \frac{g_{i-1,j+1}-g_{i-1,j-1}}{2k} - \mathscr{O}(k^2)\bigg|_{(i-1,j)}\right] + \mathscr{O}(h^2), \quad (2.43)\end{aligned}$$

where we made use of the notation $g_{i,j} \equiv g(x_i, y_j)$. Neglecting higher order contributions yields

$$\frac{\partial}{\partial y}\frac{\partial}{\partial x}g(x,y)\bigg|_{(i,j)} \approx \frac{1}{2h}\frac{g_{i+1,j+1}-g_{i+1,j-1}-g_{i-1,j+1}+g_{i-1,j-1}}{2k}. \quad (2.44)$$

This simple approximation is easily improved with the help of the methods developed in the previous sections.

Finally, it should be noted that there are also other methods to approximate derivatives. One of the most powerful methods, is the method of *finite elements* [4]. The conceptual difference to the method of finite differences is that one divides the domain in finite sub-domains (elements) rather than replacing it by sets of discrete grid-points. The function of interest, say $g(x,y)$, is then replaced within each element by an interpolating polynomial. However, this method is quite complex and definitely beyond the scope of this book. Another interesting method, which is particularly useful for the solution of hyperbolic differential equations, is the method of *finite volumes*. The interested reader is referred to the book by R. J. LeVeque [5].

Summary

In a first step the notion of finite differences was introduced: even analytical functions are approximated only by their functional values at discrete grid-points and by interpolation schemes between these points. This served as a basis for the definition of finite difference derivatives. Three different kinds were discussed: the forward, the backward, and the central difference derivative. A more systematic approach to finite difference derivatives was then offered by the operator technique. It provided ready to use equations which allowed to approximate a particular derivative of arbitrary order to arbitrary order of grid-spacing. The two methodological errors introduced by this method, namely the subtractive cancellation error due to too dense a grid and the truncation error due to too coarse a grid were discussed in detail.

Problems

Consider the finite interval $I = [-5, 5]$ on the real axis. Define N equally spaced grid-points $x_i = x_1 + (i-1)h$, $i = 1, \ldots, N$. Investigate the functions

$$g(x) = \exp\left(-x^2\right) \quad \text{and} \quad h(x) = \sin(x).$$

1. Plot these functions within the interval I by defining these functions on the grid-points x_i.
2. Plot the first derivative of these functions by analytical differentiation.
3. Calculate and plot the first derivatives of these functions by employing the first order backward, forward, and central difference derivatives. For the central difference derivative use an algorithm which is based on the grid-points x_{i-1} and x_{i+1} rather than the method based on intermediate grid-points $x_{i\pm\frac{1}{2}}$.
4. Calculate and plot the first central difference derivatives of these functions by employing second order corrections. These corrections can be obtained by applying the sum representation of the derivative operator defined in Sect. 2.4, last line of Eq. (2.31), i.e. take the term proportional to δ^3 into account!
5. Calculate the absolute and the relative error of the above methods. Note that the exact values are known analytically.
6. Repeat the above steps for the second derivative of the function $h(x)$. For the second order correction of the central difference derivative take the term proportional to δ^4 in Eq. (2.32) into account.
7. Try different values of N!

References

1. Weidmann, J.: Lineare Operatoren in Hilberträumen, vol. 1: Grundlagen. Springer, Berlin (2000)
2. Davies, E.B.: Linear Operators and their Spectra. Cambridge Studies in Advanced Mathematics. Cambridge University Press, Cambridge, UK (2007)
3. Lapidus, L., Pinder, G.F.: Numerical Solution of Partial Differential Equations. Wiley, New York (1982)
4. Gockenbach, M.S.: Understanding and Implementing the Finite Element Method. Cambridge University Press, Cambridge, UK (2006)
5. LeVeque, R.J.: Finite Volume Methods for Hyperbolic Problems. Cambridge Texts in Applied Mathematics. Cambridge University Press, Cambridge, UK (2002)

Chapter 3
Numerical Integration

3.1 Introduction

Numerical integration is certainly one of the most important concepts in computational analysis since it plays a major role in the numerical treatment of differential equations. Given a function $f(x)$ which is continuous on the interval $[a, b]$, one wishes to approximate the integral by a discrete sum of the form

$$\int_a^b \mathrm{d}x f(x) \approx \sum_{i=1}^{N} \omega_i f(x_i), \tag{3.1}$$

where the ω_i are referred to as weights and x_i are the grid-points at which the function needs to be evaluated. Such methods are commonly referred to as *quadrature*.

We will mainly discuss two different approaches to the numerical integration of arbitrary functions. We start with a rather simple approach, the *rectangular* rule. The search of an improvement of this method will lead us first to the *trapezoidal* rule, then to the SIMPSON rule and, finally, to a general formulation of the method, the NEWTON-COTES quadrature. This will be followed by a more advanced technique, the GAUSS-LEGENDRE quadrature. At the end of the chapter we will discuss an elucidating example and briefly sketch extensions of all methods to more general problems, such as integration of non-differentiable functions or the evaluation of multiple integrals.

Another very important approach, which is based on random sampling methods, is the so called Monte-Carlo integration. This method will be presented in Sect. 14.2.

B. A. Stickler and E. Schachinger, *Basic Concepts in Computational Physics*,
DOI: 10.1007/978-3-319-02435-6_3, © Springer International Publishing Switzerland 2014

3.2 Rectangular Rule

The straight forward approach to numerical integration is to employ the concept of finite differences developed in Sect. 2.2. We regard a smooth function $f(x)$ within the interval $[a, b]$, i.e. $f(x) \in \mathscr{C}^{\infty}[a, b]$. The RIEMANN definition of the proper integral of $f(x)$ from a to b states that:

$$\int\limits_a^b \mathrm{d}x f(x) = \lim_{N\to\infty} \frac{b-a}{N} \sum_{i=0}^{N} f\left(a + i\frac{b-a}{N}\right). \tag{3.2}$$

We approximate the right hand side of this relation using equally spaced grid-points $x_i \in [a, b]$ according to Eq. (2.1) and find

$$\int\limits_a^b \mathrm{d}x f(x) \approx h \sum_{i=1}^{N-1} f_i. \tag{3.3}$$

However, it is clear that the quality of this approach strongly depends on the discretization chosen, i.e. on the values of x_i as illustrated schematically in Fig. 3.1. Again, a non-uniform grid may be of advantage. We can estimate the error of this approximation by expanding $f(x)$ into a TAYLOR series.

We note that

$$\int\limits_a^b \mathrm{d}x f(x) = \sum_{i=1}^{N-1} \int\limits_{x_i}^{x_{i+1}} \mathrm{d}x f(x), \tag{3.4}$$

hence, the approximation (3.3) is equivalent to the approximation

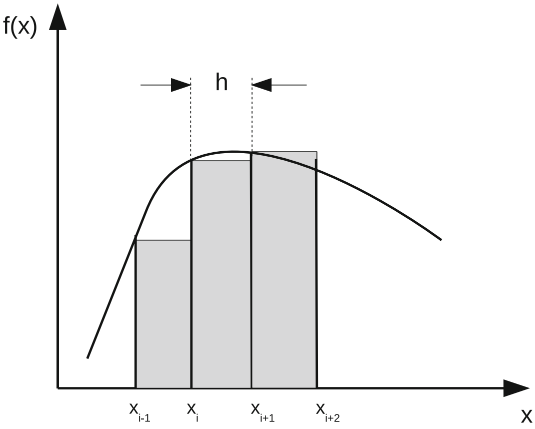

Fig. 3.1 Illustration of the numerical approximation of a proper integral according to Eq. (3.3)

$$\int_{x_i}^{x_{i+1}} \mathrm{d}x\, f(x) \approx h f_i, \tag{3.5}$$

with $\int_{x_i}^{x_{i+1}} \mathrm{d}x\, f(x)$ the elemental area. According to (2.9a) we have

$$\begin{aligned}\int_{x_i}^{x_{i+1}} \mathrm{d}x f(x) &= \int_{x_i}^{x_{i+1}} \mathrm{d}x \left[f_i + (x - x_i) f_i' + (x - x_i)^2 f_{i+\varepsilon_\zeta}'' \right] \\ &= f_i h + \frac{h^2}{2} f_i' + \mathscr{O}(h^3). \end{aligned} \tag{3.6}$$

In the last step we applied the first mean value theorem for integration which states that if $f(x)$ is continuous in $[a, b]$, then there exists a $\zeta \in [a, b]$ such that

$$\int_a^b \mathrm{d}x f(x) = (b - a) f(\zeta). \tag{3.7}$$

(We shall come back to the mean value theorem in the course of our discussion of Monte-Carlo integration in Chap. 14.) According to (3.6) the error we make with approximation (3.3) is of order $\mathscr{O}(h^2)$.

This procedure corresponds to a forward difference approach and in a similar fashion a backward difference approach can be chosen. It results in:

$$\int_a^b \mathrm{d}x f(x) = h \sum_{i=2}^{N} f_i + \mathscr{O}(h^2). \tag{3.8}$$

Let us now define the forward and backward rectangular rule by

$${}_i I_{i+1}^{+} = h f_i, \tag{3.9}$$

and

$${}_i I_{i+1}^{-} = h f_{i+1}, \tag{3.10}$$

respectively. Thus we have

$$\begin{aligned}\int\limits_{x_i}^{x_{i+1}} \mathrm{d}x f(x) &= {}_iI_{i+1}^{+} + \frac{h^2}{2} f_i' + \frac{h^3}{3!} f_i'' + \cdots \\ &= {}_iI_{i+1}^{-} - \frac{h^2}{2} f_{i+1}' + \frac{h^3}{3!} f_{i+1}'' \mp \cdots . \end{aligned} \tag{3.11}$$

However, an even more accurate way to proceed is to make use of the central difference approximation. We consider the integral

$$\int\limits_{x_i}^{x_{i+1}} \mathrm{d}x f(x), \tag{3.12}$$

expand $f(x)$ in a TAYLOR series around the midpoint $x_{i+\frac{1}{2}}$, and obtain:

$$\begin{aligned}\int\limits_{x_i}^{x_{i+1}} \mathrm{d}x f(x) &= \int\limits_{x_i}^{x_{i+1}} \mathrm{d}x \Bigg\{ f_{i+\frac{1}{2}} + \left(x - x_{i+\frac{1}{2}}\right) f_{i+\frac{1}{2}}' \\ &\qquad + \frac{\left(x - x_{i+\frac{1}{2}}\right)^2}{2} f_{i+\frac{1}{2}}'' + \mathscr{O}\left[\left(x - x_{i+\frac{1}{2}}\right)^3\right]\Bigg\} \\ &= h f_{i+\frac{1}{2}} + \frac{h^3}{24} f_{i+\varepsilon_\zeta}'' \\ &= {}_iI_{i+1} + \frac{h^3}{24} f_{i+\varepsilon_\zeta}'' . \end{aligned} \tag{3.13}$$

Thus, the error generated by this method, the central rectangular rule, scales as $\mathscr{O}(h^3)$ which is a significant improvement in comparison to Eqs. (3.3) and (3.8). We obtain

$$\int\limits_a^b \mathrm{d}x f(x) = h \sum_{i=1}^{N-1} f_{i+\frac{1}{2}} + \mathscr{O}(h^3). \tag{3.14}$$

This approximation is known as the *rectangular rule*. It is illustrated in Fig. 3.2. Note that the boundary points $x_1 = a$ and $x_N = b$ do not enter Eq. (3.14). Such a procedure is commonly referred to as an *open integration rule*. On the other hand, if the end-points are taken into account by the method it is referred to as a *closed integration rule*.

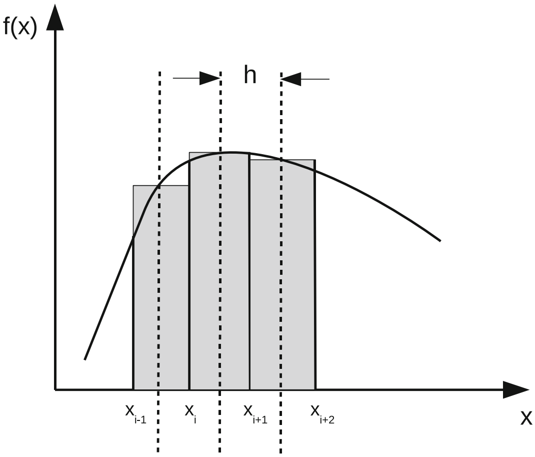

Fig. 3.2 Scheme of the rectangular integration rule according to Eq. (3.14). Note that boundary points do not enter the evaluation of the elemental areas

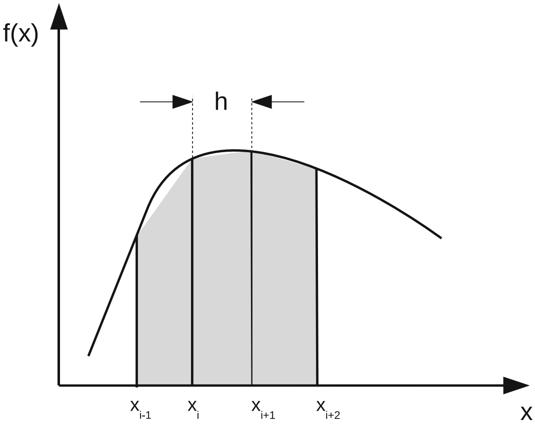

Fig. 3.3 Sketch of how the elemental areas under the curve $f(x)$ are approximated by trapezoids

3.3 Trapezoidal Rule

An elegant alternative to the rectangular rule is found when the area between two grid-points is approximated by a trapezoid as is shown schematically in Fig. 3.3. The elemental area is calculated from

$$\int_{x_i}^{x_{i+1}} \mathrm{d}x f(x) \approx \frac{h}{2}\left(f_i + f_{i+1}\right). \tag{3.15}$$

Hence, we obtain

$$\begin{aligned}\int_a^b \mathrm{d}x f(x) &\approx \frac{h}{2}\sum_{i=1}^{N-1}(f_i + f_{i+1})\\ &= h\left(\frac{f_1}{2} + f_2 + \cdots + f_{N-1} + \frac{f_N}{2}\right)\\ &= \frac{h}{2}(f_1 + f_N) + h\sum_{i=2}^{N-1} f_i\\ &= {}_1I_N^T. \end{aligned} \tag{3.16}$$

Note that this integration rule is closed, although the boundary points f_1 and f_N enter the summation (3.16) only with half the weight in comparison to all other function values f_i which is a quite reasonable result because the boundary points contribute only to one elemental area, the first and the last one. Another noticeable feature of the trapezoidal rule is that, in contrast to the rectangular rule (3.14), only function values at grid-points enter the summation, which can be desirable in some cases.

The error of this method can be estimated by inserting expansion (2.9a) into Eq. (3.16). One obtains for an elemental area:

$$\begin{aligned}{}_iI_{i+1}^T &= \frac{h}{2}(f_i + f_{i+1})\\ &= hf_i + \frac{h^2}{2}f_i' + \frac{h^3}{4}f_i'' + \cdots . \end{aligned} \tag{3.17}$$

On the other hand, we know from Eq. (3.6) that

$$hf_i = \int_{x_i}^{x_{i+1}} \mathrm{d}x f(x) - \frac{h^2}{2}f_i' - \frac{h^3}{3!}f_i'' - \cdots , \tag{3.18}$$

which, when inserted into (3.17), yields

$${}_iI_{i+1}^T = \int_{x_i}^{x_{i+1}} \mathrm{d}x f(x) + \frac{h^3}{12}f_i'' + \mathcal{O}(h^4). \tag{3.19}$$

Hence, we observe that the error induced by the trapezoidal rule is comparable to the error of the rectangular rule, namely $\mathcal{O}(h^3)$. However, since we do not have to compute function values at intermediate grid-points, this rule may be advantageous in many cases. We remember from Chap. 2 that a more accurate estimate of a derivative was achieved by increasing the number of grid-points which in the case of integration leads us to the SIMPSON rule.

3.4 The SIMPSON Rule

The basic idea of the SIMPSON rule is to include higher order derivatives into the expansion of the integrand. These higher order derivatives, which are primarily unknown, are then approximated by expressions we obtained within the context of finite difference derivatives. Let us discuss this procedure in greater detail. To this purpose we will study the integral of $f(x)$ within the interval $[x_{i-1}, x_{i+1}]$ and expand the integrand around the midpoint x_i:

$$\begin{aligned}\int_{x_{i-1}}^{x_{i+1}} \mathrm{d}x f(x) &= \int_{x_{i-1}}^{x_{i+1}} \mathrm{d}x \left[f_i + (x - x_i) f_i' + \frac{(x - x_i)^2}{2!} f_i'' \right. \\ &\quad \left. + \frac{(x - x_i)^3}{3!} f_i''' + \cdots \right] \\ &= 2h f_i + \frac{h^3}{3} f_i'' + \mathcal{O}(h^5). \end{aligned} \tag{3.20}$$

Inserting Eq. (2.34) for f_i'' yields

$$\begin{aligned}\int_{x_{i-1}}^{x_{i+1}} \mathrm{d}x f(x) &= 2h f_i + \frac{h}{3} (f_{i+1} - 2f_i + f_{i-1}) + \mathcal{O}(h^5) \\ &= h \left(\frac{1}{3} f_{i-1} + \frac{4}{3} f_i + \frac{1}{3} f_{i+1} \right) + \mathcal{O}(h^5). \end{aligned} \tag{3.21}$$

Note that in contrast to the trapezoidal rule, the procedure described here is a three point method since the function values at three different points enter the expression. We can immediately write down the resulting integral from $a \to b$. Since,

$$\int_a^b \mathrm{d}x f(x) = \int_{x_0}^{x_2} \mathrm{d}x f(x) + \int_{x_2}^{x_4} \mathrm{d}x f(x) + \cdots + \int_{x_{N-2}}^{x_N} \mathrm{d}x f(x), \tag{3.22}$$

where we assumed that N is even and employed the discretization $x_i = x_0 + ih$ with $x_0 = a$ and $x_N = b$. We obtain:

$$\int_a^b \mathrm{d}x f(x) = \frac{h}{3} (f_0 + 4f_1 + 2f_2 + 4f_3 + \cdots + 2f_{N-2} + 4f_{N-1} + f_N) + \mathcal{O}(h^5). \tag{3.23}$$

This expression is exact for polynomials of order $n \leq 3$ since the first term in the error expansion involves the fourth derivative. Hence, whenever the integrand is satisfactorily reproduceable by a polynomial of degree three or less, the SIMPSON rule might give almost exact estimates, independent of the discretization h.

The arguments applied above allow for a straightforward extension to four- or even more-point rules. We find, for instance,

$$\int\limits_{x_i}^{x_{i+3}} \mathrm{d}x f(x) = \frac{3h}{8}\left(f_i + 3f_{i+1} + 3f_{i+2} + f_{i+3}\right) + \mathcal{O}(h^5), \tag{3.24}$$

which is usually called SIMPSON's three-eight rule.

It is important to note that all the methods discussed so far are special cases of a more general formulation, the NEWTON-COTES rules which will be discussed in the next section.

3.5 General Formulation: The NEWTON-COTES Rules

We define the LAGRANGE interpolating polynomial $P(x)$ of order n [1, 2] to a function $f(x)$ as

$$P(x) = \sum_{j=1}^{n} P_j(x), \tag{3.25}$$

where

$$P_j(x) = f_j \prod_{\substack{k=1 \\ k\neq j}}^{n} \frac{x - x_k}{x_j - x_k}. \tag{3.26}$$

An arbitrary smooth function $f(x)$ can then be expressed with the help of an n-th order LAGRANGE polynomial by

$$f(x) = P(x) + \frac{f^{(n)}[\zeta(x)]}{n!}(x - x_1)(x - x_2)\ldots(x - x_n). \tag{3.27}$$

If we neglect the second term on the right hand side of this equation and integrate the LAGRANGE polynomial of order n over the n grid-points from $x_1 \to x_N$ we obtain the closed n-point NEWTON-COTES formulas. For instance, if we set $n = 2$, then

$$\begin{aligned} P(x) &= P_1(x) + P_2(x) \\ &= f_1 \frac{x - x_2}{x_1 - x_2} + f_2 \frac{x - x_1}{x_2 - x_1} \\ &= \frac{1}{h}\left[x(f_2 - f_1) - x_1 f_2 + x_2 f_1\right], \end{aligned} \tag{3.28}$$

with $f_1 \equiv f(x_1)$ and $f_2 \equiv f(x_2)$. Integration over the respective interval yields

$$\begin{aligned}\int_{x_1}^{x_2} \mathrm{d}x\, P(x) &= \frac{1}{h}\left[\frac{x^2}{2}(f_2 - f_1) + x(x_2 f_1 - x_1 f_2)\right]\Bigg|_{x_1}^{x_2} \\ &= \frac{1}{h}\left[\frac{x_2^2 - x_1^2}{2}(f_2 - f_1) + (x_2 - x_1)(x_2 f_1 - x_1 f_2)\right] \\ &= \frac{1}{2}\left[(x_2 + x_1)(f_2 - f_1) + 2x_2 f_1 - 2x_1 f_2\right] \\ &= \frac{h}{2}\left[f_2 + f_1\right] + \mathcal{O}(h^3), \end{aligned} \tag{3.29}$$

which is exactly the trapezoidal rule. By setting $n = 3$ one obtains SIMPSON's rule and setting $n = 4$ gives the SIMPSON's three-eight rule.

The *open* NEWTON-COTES rule can be obtained by integrating the polynomial $P(x)$ of order n which includes the grid-points $x_1, \ldots, x_n$ from $x_0 \rightarrow x_{n+1}$. The fact that these relations are open means that the function values at the boundary points $x_0 = x_1 - h$ and $x_{n+1} = x_n + h$ do not enter the final expressions. The simplest open NEWTON-COTES formula is the central integral approximation, which we encountered as the rectangular rule (3.14). A second order approximation is easily found with help of the two-point LAGRANGE polynomial (3.28)

$$\begin{aligned}\int_{x_0}^{x_3} \mathrm{d}x\, P(x) &= \frac{1}{h}\left[\frac{x^2}{2}(f_2 - f_1) + x(x_2 f_1 - x_1 f_2)\right]\Bigg|_{x_0}^{x_3} \\ &= \frac{1}{h}\left[\frac{x_3^2 - x_0^2}{2}(f_2 - f_1) + (x_3 - x_0)(x_2 f_1 - x_1 f_2)\right] \\ &= \frac{x_3 - x_0}{h}\left[\frac{1}{2}(x_3 + x_0)(f_2 - f_1) + (x_2 f_1 - x_1 f_2)\right] \\ &= \frac{3}{2}\left[(x_3 + x_0 - 2x_1) f_2 + (2x_2 - x_3 - x_0) f_1\right] \\ &= \frac{3h}{2}\left[f_2 + f_1\right] + \mathcal{O}(h^3). \end{aligned} \tag{3.30}$$

Higher order approximations can be obtained in a similar fashion. To conclude this section let us briefly discuss an idea which is referred to as ROMBERG's method. So far, we approximated all integrals by expressions of the form

$$I = \mathscr{I}^N + \mathcal{O}(h^m), \tag{3.31}$$

where I is the exact, unknown, value of the integral, $\mathscr{I}^N$ is the estimate obtained from an integration scheme using N grid-points and m is the leading order of the error. Let us review the error of the trapezoidal approximation: we learned that the error for the integral over the interval $[x_i, x_{i+1}]$ scales like h^3. Since we have N such intervals, we conclude that the total error behaves like $(b-a)h^2$. Similarly, the error of the three-point SIMPSON rule is for each sub-interval proportional to h^5 and this gives in total $(b-a)h^4$. We assume that this trend can be generalized and conclude that the error of an n-point method with the estimate $\mathscr{I}_n$ behaves like h^{2n-2}. Since, $h \propto N^{-1}$ we have

$$I = \mathscr{I}_n^N + \frac{C_N}{N^{2n-2}}, \tag{3.32}$$

where C_N depends on the number of grid-points N. Let us double the amount of grid-points and we obtain:

$$I = \mathscr{I}_n^{2N} + \frac{C_{2N}}{(2N)^{2n-2}}. \tag{3.33}$$

Obviously, Eqs. (3.32) and (3.33) can be regarded as a linear system of equations in I and C if $C_N \approx C_{2N} \approx C$. Solving Eqs. (3.32) and (3.33) for I yields

$$I \approx \frac{1}{4^{n-1}-1}\left(4^{n-1}\mathscr{I}_n^{2N} - \mathscr{I}_n^N\right). \tag{3.34}$$

It has to be emphasized that in the above expression I is no longer the exact value because of the approximation $C_N \approx C$. However, it is an improvement of the solution and it is possible to demonstrate that this new estimate is exactly the value one would have obtained with an integral approximation of order $n+1$ and $2N$ grid-points! Thus

$$\mathscr{I}_{n+1}^{2N} = \frac{1}{4^{n-1}-1}\left(4^{n-1}\mathscr{I}_n^{2N} - \mathscr{I}_n^N\right). \tag{3.35}$$

This suggests a very elegant and rapid procedure: We simply calculate the integrals using two point rules and add the results according to Eq. (3.35) to obtain more-point results. For instance, calculate $\mathscr{I}_2^2$ and $\mathscr{I}_2^4$, add these according to Eq. (3.35) and get $\mathscr{I}_3^4$. Now calculate $\mathscr{I}_2^8$, add $\mathscr{I}_2^4$, get $\mathscr{I}_3^8$, add $\mathscr{I}_3^4$ and get $\mathscr{I}_4^8$. This pyramid-like procedure can be continued until convergence is achieved, that is $|\mathscr{I}_m^N - \mathscr{I}_{m+1}^N| < \varepsilon$ where $\varepsilon > 0$ can be chosen arbitrarily. An illustration of this elegant method is given in Fig. 3.4.

3.6 GAUSS-LEGENDRE Quadrature

In order to prepare for the GAUSS-LEGENDRE quadrature we define the function $F(x)$ as

$$F(x) = \frac{b-a}{2} f\left(\frac{b-a}{2}x + \frac{b+a}{2}\right), \tag{3.36}$$

such that

$$\int_{a}^{b} \mathrm{d}x f(x) = \int_{-1}^{1} \mathrm{d}x F(x). \tag{3.37}$$

Furthermore, let us introduce a set of orthogonal LEGENDRE polynomials $P_\ell(x)$ [1–3] which are solutions of the LEGENDRE differential equation

$$\left(1 - x^2\right) P_\ell''(x) - 2x P_\ell'(x) + \ell(\ell + 1) P_\ell(x) = 0. \tag{3.38}$$

This equation is, for instance, the result of a transformation of the LAPLACE equation to spherical coordinates. Here, we will introduce only the most important properties of LEGENDRE polynomials which will be useful for our purpose.

LEGENDRE polynomials are defined as

$$P_\ell(x) = \sum_{k=0}^{\infty} a_{k,\ell} x^k, \tag{3.39}$$

where the coefficients $a_{k,\ell}$ can be determined recursively:

$$a_{k+2,\ell} = \frac{k(k+1) - \ell(\ell+1)}{(k+1)(k+2)} a_{k,\ell}. \tag{3.40}$$

Hence, for even values of ℓ the LEGENDRE polynomial involves only even powers of x and for odd ℓ only odd powers of x. Note also that according to Eq. (3.40) for $k \geq \ell$ the coefficients are equal to zero and, thus, the $P_\ell(x)$ are according to Eq. (3.39) polynomials of order ℓ. Furthermore, the LEGENDRE polynomials fulfill

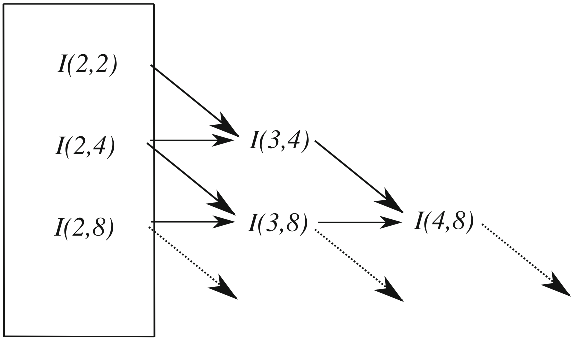

Fig. 3.4 Illustration of the ROMBERG method. Here, the $\mathscr{I}(m,n)$ are synonyms for integrals $\mathscr{I}_m^n$ where the first index m refers to the order of the quadrature while the second index n refers to the number of grid-points used. Note that we only have to use a second order integration scheme (*left row*, inside the box), all other values are determined via Eq. (3.35) as indicated by the arrows

the normalization condition

$$\int_{-1}^{1} \mathrm{d}x\, P_\ell(x) P_{\ell'}(x) = \frac{2}{2\ell' + 1}\delta_{\ell\ell'}, \tag{3.41}$$

where δ_{ij} is KRONECKER's delta. One obtains

$$P_0(x) = 1, \tag{3.42}$$

and

$$P_1(x) = x. \tag{3.43}$$

Another convenient description of the LEGENDRE polynomials is based on RODRIGUES' formula

$$P_\ell(x) = \frac{1}{2^\ell \ell!}\frac{\mathrm{d}^\ell}{\mathrm{d}x^\ell}\left(x^2 - 1\right)^\ell. \tag{3.44}$$

We now assume that the function $F(x)$ can be well approximated by some polynomial of order $2n - 1$, i.e.

$$F(x) \approx p_{2n-1}(x). \tag{3.45}$$

Please note that this means that according to Eq. (2.7) the error introduced is proportional to $F^{(2n)}(x)$.

We write the integral (3.37) as

$$\int_{-1}^{1} \mathrm{d}x\, F(x) = \sum_{i=1}^{n} \omega_i F(x_i), \tag{3.46}$$

with weights ω_i and grid-points x_i, $i = 1, \ldots, n$ which are yet undetermined! Therefore, we will determine the weights ω_i and grid-points x_i in such a way, that the integral is well approximated *even* if the polynomial p_{2n-1} in Eq. (3.45) is unknown. For this purpose we decompose $p_{2n-1}(x)$ into

$$p_{2n-1}(x) = p_{n-1}(x) P_n(x) + q_{n-1}(x), \tag{3.47}$$

where $P_n(x)$ is the LEGENDRE polynomial of order n and $p_{n-1}(x)$ and $q_{n-1}(x)$ are polynomials of order $n - 1$. Since $p_{n-1}(x)$ itself is a polynomial of order $n - 1$, it can also be expanded in LEGENDRE polynomials of orders up to $n - 1$ by

$$p_{n-1}(x) = \sum_{i=0}^{n-1} a_i P_i(x). \tag{3.48}$$

Using Eq. (3.48) in (3.47) we obtain together with normalization relation (3.41)

$$\int_{-1}^{1} \mathrm{d}x\, p_{2n-1}(x) = \sum_{i=0}^{n-1} a_i \int_{-1}^{1} \mathrm{d}x\, P_i(x) P_n(x) + \int_{-1}^{1} \mathrm{d}x\, q_{n-1}(x) = \int_{-1}^{1} \mathrm{d}x\, q_{n-1}(x). \tag{3.49}$$

Moreover, since $P_n(x)$ is a LEGENDRE polynomial of order n it has n-zeros in the interval $[-1, 1]$ and Eq. (3.47) results in

$$p_{2n-1}(x_i) = q_{n-1}(x_i), \tag{3.50}$$

where $x_1, x_2, \ldots, x_n$ denote the zeros of $P_n(x)$ and these zeros determine the grid-points of our integration routine. It is interesting to note, that these zeros are independent of the function $F(x)$ we want to integrate. We also expand $q_{n-1}(x)$ in terms of LEGENDRE polynomials

$$q_{n-1}(x) = \sum_{i=0}^{n-1} b_i P_i(x), \tag{3.51}$$

and use it in Eq. (3.50) to obtain

$$p_{2n-1}(x_i) = \sum_{k=0}^{n-1} b_k P_k(x_i), \quad i = 1, \ldots, n, \tag{3.52}$$

which can be written in a more compact form by defining $p_i \equiv p_{2n-1}(x_i)$ and $P_{ki} \equiv P_k(x_i)$:

$$p_i = \sum_{k=0}^{n-1} b_k P_{ki}, \quad i = 1, \ldots, n. \tag{3.53}$$

It has to be emphasized again that the grid-points x_i are independent of the polynomial $p_{2n-1}(x)$ and, therefore, independent of $F(x)$. Furthermore, we can replace $p_i \approx F(x_i) \equiv F_i$ according to Eq. (3.45). We recognize that Eq. (3.53) corresponds to a system of linear equations which can be solved for the weights b_k. We obtain

$$b_k = \sum_{i=1}^{n} F_i \left[\mathbf{P}^{-1}\right]_{ik}, \tag{3.54}$$

where $\mathbf{P}$ is the matrix $\mathbf{P} = \{P_{ij}\}$, which is known to be non-singular. We can now rewrite the integral (3.37) with the help of Eqs. (3.45), (3.49), and (3.51) together with the properties of the zeros of LEGENDRE polynomials [3] as

$$\int_{-1}^{1}\mathrm{d}x\ F(x) \approx \int_{-1}^{1}\mathrm{d}x p_{2n-1}(x) = \sum_{k=0}^{n-1} b_k \int_{-1}^{1}\mathrm{d}x\ P_k(x). \tag{3.55}$$

Since $P_0(x) = 1$ according to Eq. (3.42), we deduce from Eq. (3.41)

$$\int_{-1}^{1}\mathrm{d}x\, P_k(x) = \int_{-1}^{1}\mathrm{d}x\, P_k(x)P_0(x) = \frac{2}{2k+1}\delta_{k0} = 2\delta_{k0}. \tag{3.56}$$

Hence, Eq. (3.55) reads

$$\int_{-1}^{1}\mathrm{d}x\ F(x) \approx 2b_0 = 2\sum_{i=1}^{n} F_i \left[\mathbf{P}^{-1}\right]_{i0}. \tag{3.57}$$

By defining

$$\omega_i = 2\left[\mathbf{P}^{-1}\right]_{i0}, \tag{3.58}$$

we arrive at the desired expansion

$$\int_{-1}^{1}\mathrm{d}x\, F(x) \approx \sum_{i=1}^{n} \omega_i F_i. \tag{3.59}$$

Moreover, since we approximated $F(x)$ by a polynomial of order $2n-1$, the Gauss-Legendre quadrature is exact for polynomials of order $2n-1$, i.e., the error is proportional to a derivative of $F(x)$ of order $2n$. Furthermore, expression (3.58) can be put in a more convenient form. One can show that

$$\omega_i = \frac{2}{(1-x_i^2)\left[P_n'(x_i)\right]^2}, \tag{3.60}$$

where

$$P_n'(x_i) = \frac{\mathrm{d}}{\mathrm{d}x}P_n(x)\bigg|_{x=x_i}. \tag{3.61}$$

Let us make some concluding remarks. The grid-points x_i as well as the weights ω_i are independent of the actual function $F(x)$ we want to integrate. This means, that one can table these values once and for all [3] and use them for different types of problems. The grid-points x_i are symmetrically distributed around the point $x = 0$, i.e. for every x_j there is a $-x_j$. Furthermore, these two grid-points have the same weight ω_j. The density of grid-points increases approaching the boundary, however, the bound-

Table 3.1 Summary of the quadrature methods discussed in this chapter applied to the integral $\int_a^b \mathrm{d}x f(x)$

n	h	$\mathscr{I}$	Method	Comment
1	$\frac{b-a}{2}$	hf_1	Rectangular	Open
2	$b-a$	$\frac{h}{2}(f_0+f_1)$	Trapezoidal	Closed
3	$\frac{b-a}{2}$	$\frac{h}{3}(f_0+4f_1+f_2)$	SIMPSON	Closed
4	$\frac{b-a}{3}$	$\frac{3h}{8}(f_0+3f_1+3f_2+f_3)$	SIMPSON $\frac{3}{8}$	Closed
m	$\frac{b-a}{m-1}$	$\int_{x_0}^{x_{m-1}} \mathrm{d}x\, P^{(m)}(x)$	NEWTON-COTES	Closed
m	$\frac{b-a}{m+1}$	$\int_{x_0}^{x_{m+1}} \mathrm{d}x\, P^{(m)}(x)$	NEWTON-COTES	Open
m	$P_m(x_j)=0$	$\frac{b-a}{2}\sum_{j=1}^{m}\omega_j f\left(z_j\right)$	GAUSS-LEGENDRE	Open
		$z_j=\frac{a+b}{2}+\frac{a-b}{2}x_j$		
		$\omega_j=\frac{2}{(1-x_j)^2[P_m'(x_j)]^2}$		

For a detailed description consult the corresponding sections. Equal grid-spacing is assumed for all methods except for the GAUSS-LEGENDRE quadrature. The explicit values of h depend on the order of the method and are listed in the table. Furthermore, we use $x_i=a+ih$ and denote $f(x_i)=f_i$. The function $P^{(m)}(x)$ which appears in the description of the NEWTON-COTES rules denotes the m-th order LAGRANGE interpolating polynomial and $P_m(x)$ is the m-th order LEGENDRE polynomial

ary points themselves are not included, which means that the GAUSS-LEGENDRE quadrature is an *open method*. Furthermore, it has to be emphasized that low order GAUSS-LEGENDRE parameters can easily be calculated by employing relation (3.44). This makes the GAUSS-LEGENDRE quadrature the predominant integration method. In comparison to the trapezoidal rule or even the ROMBERG method, it needs in many cases a smaller number of grid-points, is simpler to implement, converges faster and yields more accurate results. One drawback of this method is that one has to compute the reduced function $F(x)$ at the zeros of the LEGENDRE polynomial x_i. This can be a problem if the integrand at hand is not known analytically.

It is important to note at this point that comparable procedures exist which use other types of orthogonal polynomials, such as HERMITE polynomials. This procedure is known as the GAUSS-HERMITE quadrature.

Table 3.1 lists the methods, discussed in the previous sections, which allow to calculate numerically an estimate of integrals of the form:

$$\int_a^b \mathrm{d}x f(x). \tag{3.62}$$

Equal grid-spacing h is assumed, with the GAUSS-LEGENDRE method as the only exception. The particular value of h depends on the order of the method employed and is given in Table 3.1.

3.7 An Example

Let us discuss as an example the following proper integral

$$I = \int_{-1}^{1} \frac{\mathrm{d}x}{x+2} = \ln(3) - \ln(1) \approx 1.09861. \tag{3.63}$$

The numerical value was obtained with a TI- 30XIIB pocket calculator. We will now apply the various methods of Table 3.1 to solve this problem. Note that these methods could give better results if a finer grid had been chosen. However, since this is only an illustrative example, we wanted to keep it as simple as possible. The rectangular rule gives

$$\mathscr{I}_R = 1 \cdot \frac{1}{2} = 0.5, \tag{3.64}$$

the trapezoidal rule

$$\mathscr{I}_T = \frac{2}{2}\left(\frac{1}{1} + \frac{1}{3}\right) = \frac{4}{3} = 1.333\ldots, \tag{3.65}$$

and an application of the SIMPSON rule yields

$$\mathscr{I}_S = \frac{1}{3}\left(\frac{1}{1} + \frac{4}{2} + \frac{1}{3}\right) = \frac{10}{9} = 1.111\ldots. \tag{3.66}$$

Finally, we apply the GAUSS-LEGENDRE quadrature in a second order approximation. We could look up the parameters in Ref. [3], however, for illustrative reasons we will calculate those in this simple case. For a second order approximation we need the LEGENDRE polynomial of second order. It can be obtained from RODRIGUES' formula (3.44):

$$\begin{aligned} P_2(x) &= \frac{1}{2^2 2!} \frac{\mathrm{d}^2}{\mathrm{d}x^2} \left(x^2 - 1\right)^2 \\ &= \frac{1}{8} \frac{\mathrm{d}}{\mathrm{d}x} 4x(x^2 - 1) \\ &= \frac{1}{2}\left[(x^2 - 1) + 2x^2\right] \\ &= \frac{1}{2}\left(3x^2 - 1\right). \end{aligned} \tag{3.67}$$

In a next step the zeros x_1 and x_2 of $P_2(x)$ are determined from Eq. (3.67) which results immediately in:

$$x_{1,2} = \pm \frac{1}{\sqrt{3}} \approx \pm 0.57735. \tag{3.68}$$

The weights ω_1 and ω_2 can now be evaluated according to Eq. (3.60):

$$\omega_i = \frac{2}{(1 - x_i^2)\left[P_2'(x_i)\right]^2}. \tag{3.69}$$

It follows from Eq. (3.67) that

$$P_2'(x) = 3x, \tag{3.70}$$

and, thus,

$$P_2'(x_1) = -\sqrt{3} \qquad \text{and} \qquad P_2'(x_2) = \sqrt{3}. \tag{3.71}$$

This is used to calculate the weights from Eq. (3.69):

$$\omega_1 = \omega_2 = \frac{2}{\left(1 - \frac{1}{3}\right) \cdot 3} = 1. \tag{3.72}$$

We combine the results (3.68) and (3.72) to arrive at the GAUSS-LEGENDRE estimate of the integral (3.63):

$$\mathscr{I}_{GL} = \frac{1}{-\frac{1}{\sqrt{3}} + 2} + \frac{1}{\frac{1}{\sqrt{3}} + 2} = 1.090909\ldots. \tag{3.73}$$

Obviously, a second order GAUSS-LEGENDRE approximation results already in a much better estimate of the integral (3.63) than the trapezoidal rule which is also of second order. It is also better than the estimate by the SIMPSON rule which is of third order. Another point which makes the GAUSS-LEGENDRE quadrature so attractive from the numerical point of view is the fact that all coefficients in the GAUSS-LEGENDRE quadrature are *independent* of the function one wishes to integrate.

There is a drawback though: it is not easy to apply the GAUSS-LEGENDRE algorithm to calculate numerically estimates of integrals over functions $f(x)$ not defined analytically. All other methods listed in Table 3.1 are not restricted at all to an analytic representation of the integrand.

3.8 Concluding Discussion

Let us briefly discuss some further aspects of numerical integration. In many cases one is confronted with improper integrals of the form

$$\int_a^\infty \mathrm{d}x f(x), \qquad \int_{-\infty}^a \mathrm{d}x f(x), \qquad \text{or} \qquad \int_{-\infty}^\infty \mathrm{d}x f(x). \tag{3.74}$$

The question arises whether or not we can treat such an integral with the methods discussed so far. The answer is yes, it is possible as we will demonstrate using the integral

$$I = \int_a^\infty \mathrm{d}x f(x). \tag{3.75}$$

as an example; other integrals can be treated in a similar fashion. We rewrite Eq. (3.75) as

$$I = \lim_{b\to\infty} \int_a^b \mathrm{d}x f(x) = \lim_{b\to\infty} I(b). \tag{3.76}$$

One now calculates $I(b_1)$ for some $b_1 > a$ and $I(b_2)$ for some $b_2 > b_1$. If $|I(b_2) - I(b_1)| < \varepsilon$, where $\varepsilon > 0$ is the required accuracy, the resulting value $I(b_2)$ can be regarded as the appropriate estimate to I.[1] However, in many cases it is easier to perform an integral transform in order to map the infinite interval onto a finite interval. For instance, consider [4]

$$I = \int_0^\infty \mathrm{d}x \frac{1}{\left(1+x^2\right)^{\frac{4}{3}}}. \tag{3.77}$$

The transformation

$$t = \frac{1}{1+x} \tag{3.78}$$

gives

$$I = \int_0^1 \mathrm{d}t \frac{t^{\frac{2}{3}}}{\left[t^2 + (1-t)^2\right]^{\frac{4}{3}}}. \tag{3.79}$$

Thus, we mapped the interval $[0, \infty) \to [0, 1]$. Integral (3.79) can now be approximated with help of the methods discussed in the previous sections. These can also be applied to approximate convergent integrals whose integrand shows singular behavior within $[a, b]$.

An interesting situation arises when the integrand $f(x)$ is not smooth within the interval $I : x \in [a, b]$. Nevertheless, it will be safe to assume that $f(x)$ will at least be piecewise smooth within this interval. In this case the total integral is split into a

[1] Particular care is required when dealing with periodic functions!

sum over sub-intervals within which $f(x)$ is smooth. Let us, for instance, regard the function

$$f(x) = \begin{cases} x\ \cos(x), & x < 0, \\ x\ \sin(x), & x \geq 0, \end{cases}$$

and calculate the integral over the interval $I : x \in [-10, 10]$ as

$$\int_{-10}^{10} \mathrm{d}x\ f(x) = \int_{-10}^{0} \mathrm{d}x\, x \cos(x) + \int_{0}^{10} \mathrm{d}x\, x \sin(x).$$

We generalize this result and write

$$\int_{I} \mathrm{d}x\ f(x) = \sum_{k} \int_{I_k} \mathrm{d}x\ f(x), \tag{3.80}$$

with sub-intervals $I_k \in I, \forall k$ and the integrand $f(x)$ is assumed to be smooth within each sub-interval I_k but not necessarily within the interval I. We can then apply one of the methods discussed in this chapter to calculate an estimate of the integral over any of the sub-intervals I_k.

Another interesting question is whether or not we can also evaluate multiple integrals with the help of the above formalisms. Again, the answer is yes. Similar to the discussion in Sect. 2.5 about the approximation of partial derivatives on the basis of finite differences, one can apply the rules of quadrature developed here for different dimensions to obtain an estimate of the desired integral. However, the complexity of the problem is significantly increased if the integration boundaries are functions of the variables rather than constants. For instance,

$$\int_{a}^{b} \mathrm{d}x \int_{\phi_1(x)}^{\phi_2(x)} \mathrm{d}y f(x, y). \tag{3.81}$$

Such cases are rather difficult to handle and the method to choose depends highly on the form of the functions $\phi_1(x)$, $\phi_2(x)$ and $f(x, y)$. We will not deal with integrals of this kind because this is beyond the scope of this book. The interested reader is referred to books by Dahlquist and Björk [5] and by Press et al. [6].

Summary

The starting point was the concept of finite differences (Sect. 2.2). Based on this concept proper integrals over smooth functions $f(x)$ have been approximated by a sum over elemental areas with the elemental area defined as the area under

$f(x)$ between two consecutive grid-points. The simplest method, the *rectangular rule*, was based on forward/backward differences. It is a *closed* method, i.e. the functional values at the boundaries are included. On the other hand, a rectangular rule based on central differences is an *open* method, i.e. the functional values at the boundaries are not included. Using the TAYLOR expansion (2.7) revealed that the methodological error of the rectangular rule was of order $\mathscr{O}(h^2)$. With the elemental area approximated by a trapezoid we arrived at the *trapezoidal rule*. It is a closed method and the methodological error is of order $\mathscr{O}(h^3)$. If higher order derivatives of $f(x)$ are included the SIMPSON rules of quadrature are derived. They allowed a remarkable reduction of the methodological error. A more general formulation of all these methods was based on the interpolation of the function $f(x)$ using LAGRANGE interpolating polynomials of order n and resulted in the class of NEWTON-COTES rules. For various orders of n of the interpolating polynomial all the above rules have been derived. Within this context a particularly useful method, the ROMBERG method, was discussed. By adding diligently only two-point rules the error of the numerical estimate of the integral has been made arbitrarily small. An even more general approach was offered by the GAUSS-LEGENDRE quadrature which used LEGENDRE polynomials of order ℓ to approximate the function $f(x)$. The grid-points were defined by the zeros of the ℓ-th order polynomial and the weights ω_i in Eq. (3.1) were proportional to the square of the inverse first derivative of the polynomial. This method had the enormous advantage that the grid-points and weights were independent of the function $f(x)$ and, thus, can be determined once and for all for any polynomial order ℓ. Error analysis proved that this method had the smallest methodological error.

Problems

We consider the interval $I = [-5, 5]$ together with the functions $g(x)$ and $h(x)$:

$$g(x) = \exp\left(-x^2\right) \quad \text{and} \quad h(x) = \sin(x).$$

We discretize the interval I by introducing N equally spaced grid-points. The corresponding $N-1$ sub-intervals are denoted by I_j, $j = 1, \dots N-1$. In the following we wish to calculate estimates of the integrals

$$\mathscr{I}_1 = \int_I \mathrm{d}x\, g(x) \qquad \text{and} \qquad \mathscr{I}_2 = \int_I \mathrm{d}x\, h(x).$$

Furthermore, we add a third integral of the form

$$\mathscr{I}_3 = \int_I \mathrm{d}x\, h^2(x) = \int_I \mathrm{d}x\ \sin^2(x),$$

to our discussion.

1. Evaluate $\mathscr{I}_1$ with the help of the *error function* $\mathrm{erf}(x)$, which should be supplied by the environment you use as an intrinsic function. Note that the error function is defined as
$$\mathrm{erf}(x) = \frac{2}{\sqrt{\pi}} \int_0^x \mathrm{d}z \exp(-z^2). \tag{3.82}$$
Hence you should be able to express $\mathscr{I}_1$ in terms of $\mathrm{erf}(x)$.
2. Calculate $\mathscr{I}_2$ and $\mathscr{I}_3$ analytically.
3. In order to approximate $\mathscr{I}_1$, $\mathscr{I}_2$ and $\mathscr{I}_3$ with the help of the two second order methods we discussed in this chapter, employ the following strategy: First the integrals are rewritten as
$$\int_I \mathrm{d}x \cdot = \sum_i \int_{I_i} \mathrm{d}x \cdot ,$$
where $\cdot$ is a placeholder for $g(x)$, $h(x)$ and $h^2(x)$. In a second step the integrals are approximated by
$$\int_{I_i} \mathrm{d}x \cdot, \qquad i = 1, \ldots, N-1 ,$$
with (i) the central rectangular rule and (ii) the trapezoidal rule.
4. In addition, we approximate the integrals $\mathscr{I}_1$, $\mathscr{I}_2$ and $\mathscr{I}_3$ by employing SIMPSON's rule for odd N. Here
$$\int_I \mathrm{d}x \cdot = \int_{I_1 \cup I_2} \mathrm{d}x \ \cdot + \int_{I_3 \cup I_4} \mathrm{d}x \ \cdot + \cdots + \int_{I_{N-2} \cup I_{N-1}} \mathrm{d}x \cdot ,$$
is used as it was discussed in Sect. 3.4.
5. Compare the results obtained with different algorithms and different numbers of grid-points, N. Plot the absolute- and the relative error as a function of N.

References

1. Mathai, A.M., Haubold, H.J.: Special Functions for Applied Scientists. Springer, Berlin (2008)
2. Beals, R., Wong, R.: Special Functions. Cambridge Studies in Advanced Mathematics. Cambridge University Press, Cambridge (2010)

3. Abramovitz, M., Stegun, I.A. (eds.): Handbook of Mathemathical Functions. Dover, New York (1965)
4. Sormann, H.: Numerische Methoden in der Physik. Lecture Notes. Institute of Theoretical and Computational Physics, Graz University of Technology, Austria (2011)
5. Dahlquist, G., Björk, A.: Numerical Methods in Scientific Computing. Cambridge University Press, Cambridge (2008)
6. Press, W.H., Teukolsky, S.A., Vetterling, W.T., Flannery, B.P.: Numerical Recipes in C++, 2nd edn. Cambridge University Press, Cambridge (2002)

Chapter 4
The Kepler Problem

4.1 Introduction

The Kepler problem is certainly one of the most important problems in the history of physics and natural sciences in general. We will study this problem for several reasons: (i) it is a nice demonstration of the applicability of the methods introduced in the previous chapters, (ii) important concepts of the numerical treatment of ordinary differential equations can be introduced quite naturally, and (iii) it allows to revisit some of the most important aspects of classical mechanics.

The Kepler problem is a special case of the two-body problem, which is discussed in Appendix A. Let us summarize the main results. The symmetries of the two body problem allow several simplifications: (i) one can reduce the problem to a two dimensional one body problem in a central potential, (ii) they guarantee conservation of the energy E, and (iii) the angular momentum ℓ is conserved. Due to the reduction to a two dimensional problem in a central potential, one usually regards the problem in polar coordinates (ρ, φ).

The final differential equations, which have to be solved are of the form

$$\dot{\varphi} = \frac{|\ell|}{\mu\rho^2}, \tag{4.1}$$

and

$$\dot{\rho} = \pm\sqrt{\frac{2}{\mu}\left(E - U(\rho) - \frac{|\ell|^2}{2\mu\rho^2}\right)}, \tag{4.2}$$

which gives an implicit equation for ρ

$$t = t_0 + \int_{\rho_0}^{\rho} \mathrm{d}\rho' \frac{\mu\rho'}{\sqrt{\mu\rho'^2\left[E - U(\rho')\right] - |\ell|^2}}, \tag{4.3}$$

B. A. Stickler and E. Schachinger, *Basic Concepts in Computational Physics*,
DOI: 10.1007/978-3-319-02435-6_4, © Springer International Publishing Switzerland 2014

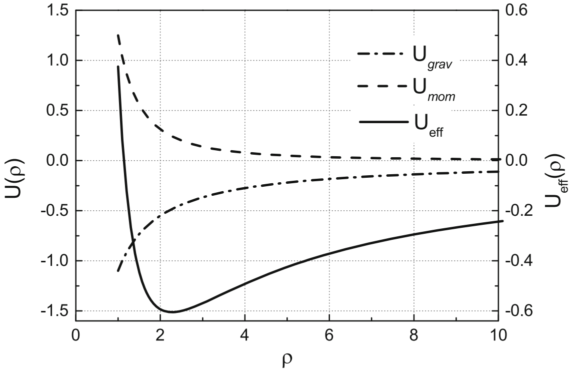

Fig. 4.1 Schematic illustration of the effective potential $U_{eff}(\rho)$ versus ρ (*solid line, right hand scale*). The axis annotations are in arbitrary units, $U_{grav}(\rho)$ (*dashed-dotted line*) denotes the gravitational contribution while $U_{mom}(\rho)$ (*dashed line*) denotes the contribution due to the conservation of angular momentum (*Left hand scale* applies)

Furthermore, one can show that the angle φ is related to the radius ρ by

$$\varphi = \varphi_0 \pm |\ell| \int_{\rho_0}^{\rho} \frac{\mathrm{d}\rho'}{\rho'\sqrt{2\mu\rho'^2\left[E - U(\rho')\right] - |\ell|^2}}, \tag{4.4}$$

where $\varphi_0 = \varphi(t_0)$ and t_0 is some starting point on the time scale. Here, one commonly defines the *effective* potential $U_{eff}(\rho)$ as

$$U_{eff}(\rho) = U(\rho) + \frac{|\ell|^2}{2\mu\rho^2}, \tag{4.5}$$

which is shown schematically in Fig. 4.1 (solid black line) together with the gravitational contribution $U_{grav}(\rho) = U(\rho)$ (dashed-dotted line) and the contribution $U_{mom} = |\ell|^2/(2\mu\rho^2)$ (dashed line), the potential due to conservation of angular momentum.

In case of the KEPLER problem a gravitational potential of the form

$$U(\rho) = -\frac{\alpha}{\rho}, \qquad \alpha > 0 \tag{4.6}$$

is applied.

4.2 The Problem

Let us investigate the particular case of a gravitational potential of the form (4.6). Hence, we rewrite Eq. (4.4) as

$$\varphi = \varphi_0 \pm \int_{\rho_0}^{\rho} \mathrm{d}\rho' \frac{|\ell|}{\mu\rho'^2} \left[\frac{2}{\mu}\left(E + \frac{\alpha}{\rho'} - \frac{|\ell|^2}{2\mu\rho'^2}\right)\right]^{-\frac{1}{2}} . \tag{4.7}$$

The substitution

$$u = \frac{1}{\rho}, \quad \mathrm{d}u = -\frac{\mathrm{d}\rho}{\rho^2}, \tag{4.8}$$

simplifies (4.7) to

$$\begin{aligned} \varphi &= \varphi_0 \mp \int_{u_1}^{u_2} \mathrm{d}u \frac{|\ell|}{\mu} \left[\frac{2}{\mu}\left(E + \alpha u - \frac{|\ell|^2 u^2}{2\mu}\right)\right]^{-\frac{1}{2}} \\ &= \varphi_0 \mp \int_{u_1}^{u_2} \mathrm{d}u \left[\frac{2\mu E}{|\ell|^2} + \frac{2\mu\alpha}{|\ell|^2} u - u^2\right]^{-\frac{1}{2}} , \end{aligned} \tag{4.9}$$

where the integration boundaries u_1 and u_2 are given by $1/\rho_0$ and $1/\rho$, respectively. Let us evaluate this integral. We recognize that

$$\frac{2\mu E}{|\ell|^2} + \frac{2\mu\alpha}{|\ell|^2} u - u^2 = \frac{2\mu E}{|\ell|^2} + \frac{\mu^2\alpha^2}{|\ell|^4} - \left(u - \frac{\mu\alpha}{|\ell|^2}\right)^2 . \tag{4.10}$$

Therefore, the substitution

$$v = u - \frac{\mu\alpha}{|\ell|^2}, \tag{4.11}$$

gives

$$\begin{aligned} \int \mathrm{d}u \left[\frac{2\mu E}{|\ell|^2} + \frac{2\mu\alpha}{|\ell|^2} u - u^2\right]^{-\frac{1}{2}} &= \int \mathrm{d}v \left[\frac{2\mu E}{|\ell|^2} + \frac{\mu^2\alpha^2}{|\ell|^4} - v^2\right]^{-\frac{1}{2}} \\ &= \int \frac{\mathrm{d}w}{\sqrt{1 - w^2}}, \end{aligned} \tag{4.12}$$

where we employed one more substitution, namely:

$$w = \left(\frac{2\mu E}{|\ell|^2} + \frac{\mu^2\alpha^2}{|\ell|^4}\right)^{-\frac{1}{2}} v. \tag{4.13}$$

Equation (4.12) is easily integrated with the help of the substitution $w = \cos(z)$:

$$\begin{aligned}\int \frac{\mathrm{d}w}{\sqrt{1-w^2}} &= -\cos^{-1}(w)\\ &= -\cos^{-1}\left(\frac{\frac{|\ell|}{\rho}-\frac{\mu\alpha}{|\ell|}}{\sqrt{2\mu E+\frac{\mu^2\alpha^2}{|\ell|^2}}}\right).\end{aligned} \tag{4.14}$$

Hence, Eq. (4.7) yields for a gravitational potential of the form (4.6) the equation:

$$\varphi = \varphi_0 \pm \cos^{-1}\left(\frac{\frac{|\ell|}{\rho}-\frac{\mu\alpha}{|\ell|}}{\sqrt{2\mu E+\frac{\mu^2\alpha^2}{|\ell|^2}}}\right) + \text{const.} \tag{4.15}$$

In order to characterize the solution (4.15), we introduce the parameters

$$a = \frac{|\ell|^2}{\mu\alpha} \tag{4.16}$$

and the *eccentricity* ε

$$\varepsilon = \sqrt{1+\frac{2E|\ell|^2}{\mu\alpha^2}}. \tag{4.17}$$

Hence, neglecting the integration constant and setting $\varphi_0 = 0$, Eq. (4.15) reads

$$\frac{a}{\rho} = 1 + \varepsilon\cos(\varphi). \tag{4.18}$$

This equation describes for $\varepsilon > 1$ a hyperbola, for $\varepsilon = 1$ a parabola and for $\varepsilon < 1$ an ellipse. The case $\varepsilon = 0$ is a special case of the ellipse and describes a circle with radius $\rho = a$. A more detailed discussion of this result, in particular the derivation of KEPLER's laws can be found in any textbook on classical mechanics [1]. We discuss now some numerical aspects.

4.3 Numerical Treatment

In the previous section we solved the KEPLER problem by evaluating the integrand Eq. (4.7) expressing the angle φ as a function of the radius ρ. However, in this section we aim at solving the integral equation Eq. (4.3) numerically with the help of the methods discussed in the previous chapter. Remember that Eq. (4.3) expresses the time t as a function of the radius ρ. This implicit equation has to be inverted, in order to obtain $\rho(t)$, which, in turn, is then inserted into Eq. (4.1) which allows to obtain the angle $\varphi(t)$ as a function of time. This discussion will lead us in a natural way to the most common techniques applied to solve ordinary differential equations, which is of no surprise since we remember that Eq. (4.3) is nothing but the integral representation of Eq. (4.2).

We give a short outline of what we plan to do. We discretize the time axis in equally spaced time steps Δt, i.e. $t_n = t_0 + n\Delta t$. Accordingly, we define the radius ρ at time $t = t_n$ as $\rho(t_n) = \rho_n$. We can use the methods introduced in Chap. 3 to approximate the integral Eq. (4.3) from some ρ_n to ρ_{n+1}. According to Chap. 3, the absolute error introduced will behave like $\delta = |\rho_n - \rho_{n+1}|^\beta$, where the explicit value of β depends on the method used. However, since the radius ρ changes continuously with time t we know that for sufficiently small values of Δt the error δ will also become arbitrarily small. If we start from some initial values t_0 and ρ_0, we can successively calculate the values ρ_1, ρ_2, ..., by applying a small time step Δt.

Let us start by rewriting Eq. (4.3) as:

$$t - t_0 = \int\limits_{\rho_0}^{\rho} \mathrm{d}\rho' f(\rho'). \tag{4.19}$$

As we discretized the time axis in equally spaced increments $t_n = t_0 + n\Delta t$ and defined $\rho_n = \rho(t_n)$, we can rewrite Eq. (4.19) as

$$\Delta t = t_n - t_{n-1} = \int_{\rho_n}^{\rho_{n+1}} \mathrm{d}\rho' f(\rho'). \tag{4.20}$$

The forward rectangular rule, (3.9) results in the approximation

$$\Delta t = (\rho_{n+1} - \rho_n) f(\rho_n). \tag{4.21}$$

We solve this equation for ρ_{n+1} and and obtain the expression

$$\rho_{n+1} = h(\rho_n)\Delta t + \rho_n, \tag{4.22}$$

where we defined

$$h(\rho) = \frac{1}{f(\rho)} = \sqrt{\frac{2}{\mu}\left[E - U_{eff}(\rho)\right]}, \tag{4.23}$$

following Eqs. (4.2) and (4.5). As (4.3) is the integral representation of the ordinary differential equation (4.2), approximation (4.22) corresponds to the approximation

$$D_+\rho_n = h(\rho_n), \tag{4.24}$$

where $D_+\rho_n$ is the forward difference derivative (2.10a), given by

$$D_+\rho_n = \frac{\rho_{n+1} - \rho_n}{\Delta t}. \tag{4.25}$$

The left hand side of the discretized differential equation (4.24) is independent of ρ_{n+1}, this method is referred to as an *explicit* method. In particular, consider an ordinary differential equation of the form

$$\dot{y} = F(y). \tag{4.26}$$

Then the approximation method is referred to as an *explicit* EULER *method* if it is of the form

$$y_{n+1} = y_n + F(y_n)\Delta t. \tag{4.27}$$

Note that y might be a vector.

Let us use the backward rectangular rule (3.10) to solve Eq. (4.20). We obtain

$$t_{n+1} - t_n = (\rho_{n+1} - \rho_n) f(\rho_{n+1}), \tag{4.28}$$

or equivalently

$$\rho_{n+1} = \rho_n + h(\rho_{n+1})\Delta t. \tag{4.29}$$

Again, this corresponds to an approximation of the differential equation (4.2) by

$$D_- \rho_{n+1} = h(\rho_{n+1}), \tag{4.30}$$

where $D_-(\rho_{n+1})$ is the backward difference derivative (2.10b) given by

$$D_- \rho_{n+1} = \frac{\rho_{n+1} - \rho_n}{\Delta t}. \tag{4.31}$$

Note, that on the left hand side of Eq. (4.29) the quantity of interest ρ_{n+1} still appears in the argument of the function h (4.23). Therefore, (4.29) is an *implicit* equation for ρ_{n+1} which has to be solved. In general, if the problem (4.26) is approximated by an algorithm of the form

$$y_{n+1} = y_n + F(y_{n+1})\Delta t, \tag{4.32}$$

it is referred to as an *implicit* EULER *method*. Note that the implicit equation (4.32) might be be analytically unsolvable. Hence, one has to employ a numerical method to solve (4.32) which will also imply a numerical error. However, in case of Eq. (4.29) we can solve the equation analytically since it is a fourth order polynomial in ρ_{n+1} of the form

$$\rho_{n+1}^4 - 2\rho_n \rho_{n+1}^3 + \rho_n^2 \rho_{n+1}^2 - \frac{2\alpha \Delta t^2}{\mu} \rho_{n+1} + \left(|\ell|^2 + \frac{2E}{\mu} \right) \Delta t^2 = 0. \tag{4.33}$$

The solution of the above Eq. (4.33) is quite tedious and will not be discussed here, however, the method one employs is referred to as FERRARI's method [2].

A natural way to proceed is to regard the central rectangular rule (3.13) in a next step. Within this approximation we obtain for Eq. (4.19)

$$\Delta t = (\rho_{n+1} - \rho_n) f\left(\frac{\rho_{n+1} + \rho_n}{2}\right), \tag{4.34}$$

which is equivalent to the implicit equation

$$\rho_{n+1} = \rho_n + h\left(\frac{\rho_{n+1} + \rho_n}{2}\right)\Delta t. \tag{4.35}$$

It can be written as an approximation to Eq. (4.2) with help of the central difference derivative $D_c \rho_{n+\frac{1}{2}}$:

$$D_c \rho_{n+\frac{1}{2}} = h\left(\frac{\rho_{n+1} + \rho_n}{2}\right). \tag{4.36}$$

In general, for a problem of the form (4.26) a method of the form

$$y_{n+1} = y_n + F\left(\frac{y_{n+1} + y_n}{2}\right)\Delta t, \tag{4.37}$$

is referred to as the *implicit midpoint rule*. We note that this method might be more accurate since the error of the rectangular rule scales like $\mathcal{O}(h^2)$ while the error of the forward and backward rectangular rules scale like $\mathcal{O}(h)$. Nevertheless, in case of the Kepler problem, one can solve the implicit equation (4.35) analytically for ρ_{n+1} which is certainly of advantage.

In summary we discussed three methods which we can employ to solve an ordinary differential equation of the form (4.26). These methods were introduced with the help of the particular case of the Kepler problem. More general and advanced methods to solve ordinary differential equations and a more systematic description of these methods will be offered in the next chapter.

However, let us discuss another point before proceeding to the chapter on the numerics of ordinary differential equations. As demonstrated in Sect. 1.3 the approximation of the integral (4.3) involves a numerical error. What will be the consequence of this error? Since we demonstrated that the approximations we discussed result in a differential equation in finite difference form, i.e. Eqs. (4.24), (4.30), and (4.35), we know that the derivative $\dot{\rho}$ will exhibit an error. Consequently, energy conservation, as discussed in Appendix A, Eq. (A.27) will be violated.

This is definitely not desirable. There is a special class of methods, known as *symplectic integrators* which were specifically designed for such cases. They are based on a formulation of the problem using Hamilton's equations of motion. Let us regard the particular case of the Kepler problem. In this case the Hamilton function reads (in some scaled units)

$$H(p,q) = \frac{1}{2}\left(p_1^2 + p_2^2\right) - \frac{1}{\sqrt{q_1^2 + q_2^2}}. \tag{4.38}$$

Here $p = (p_1, p_2)$ are the generalized momentum coordinates of the mass point in the two-dimensional plane and (q_1, q_2) are the generalized position coordinates. From this HAMILTON's equations of motion

$$\begin{pmatrix} \dot{q} \\ \dot{p} \end{pmatrix} = \begin{pmatrix} \nabla_p H(p,q) \\ -\nabla_q H(p,q) \end{pmatrix} = \begin{pmatrix} a(q,p) \\ b(q,p) \end{pmatrix}, \tag{4.39}$$

follow. Here the functions $a(q, p)$ and $b(q, p)$ have been introduced for a more convenient notation. Note that these functions are two dimensional objects in the case of KEPLER's problem. In this case the so called *symplectic* EULER *method* is given by

$$\begin{aligned} q_{n+1} &= q_n + a(q_n, p_{n+1})\Delta t, \\ p_{n+1} &= p_n + b(q_n, p_{n+1})\Delta t. \end{aligned} \tag{4.40}$$

Obviously, the first equation is explicit while the second is implicit. An alternative formulation reads

$$\begin{aligned} q_{n+1} &= q_n + a(q_{n+1}, p_n)\Delta t, \\ p_{n+1} &= p_n + b(q_{n+1}, p_n)\Delta t, \end{aligned} \tag{4.41}$$

where the first equation is implicit and the second equation is explicit. Of course, (4.39) may be solved with the help of the explicit EULER method (4.27), the implicit EULER method (4.32) or the implicit midpoint rule (4.37). The solution should be equivalent to solving Eq. (4.3) with the respective method and then calculating (4.1) successively. Again, a more systematic discussion of symplectic integrators can be found in the following chapters.

Let us conclude this chapter with a final remark. We decided to solve Eqs. (4.3) and (4.1) because we wanted to reproduce the dynamics of the system, i.e. we wanted to obtain $\rho(t)$ and $\varphi(t)$. This directed us to the numerical solution of two integrals. If we wanted to employ symplectic methods, which provide several advantages, we would have to solve four differential equations Eq. (4.39) instead of two integrals. Moreover, if we are not interested in the time evolution of the system but in the form of the trajectory in general, we could simply evaluate the integral (4.4) analytically or, if an analytical solution is not feasible for the potential $U(\rho)$ one is interested in, numerically. Methods to approximate such an integral were extensively discussed in Chap. 3.

Summary

KEPLER's two-body problem was used as an incentive to introduce intuitively numerical methods to solve ordinary first order differential equations. To serve this purpose the basic differential equations were transformed into integral form. These integrals were then solved with the help of the rules discussed in Sect. 3.2. Three basic methods have been identified, namely the *explicit* EULER method (based on the forward difference derivative), the *implicit* EULER method (based on the backward difference derivative), and the *explicit midpoint rule* (based on the central rectangular rule). Shortcomings of these methods have been discussed briefly as were remedies to overcome those shortcomings.

References

1. Scheck, F.: Mechanics, 5th edn. Springer, Berlin (2010)
2. Clark, A.: Elements of Abstract Algebra. Dover, New York (1971)

Chapter 5
Ordinary Differential Equations: Initial Value Problems

5.1 Introduction

In this chapter we will introduce common numeric methods designed to solve *initial value problems*. Within our discussion of the KEPLER problem in the previous chapter we introduced four concepts, namely the implicit EULER method, the explicit EULER method, the implicit midpoint rule, and we mentioned the symplectic EULER method. In this chapter we plan to put these methods into a more general context and to discuss more advanced techniques.

Let us define the problem: We consider initial value problems of the form

$$\begin{cases} \dot{y}(t) &= f(y, t), \\ y(0) &= y_0, \end{cases} \tag{5.1}$$

where $y(t) \equiv y$ is an n-dimensional vector and y_0 is referred to as the *initial value* of y. Let us make some remarks about the form of Eq. (5.1).

(i) We note that by posing Eq. (5.1), we assume that the differential equation is *explicit* in $\dot{y}$; i.e. initial value problems of the form

$$\begin{cases} G(\dot{y}) &= f(y, t), \\ y(0) &= y_0, \end{cases} \tag{5.2}$$

are only considered if $G(\dot{y})$ is analytically invertible. For instance, we will not deal with differential equations of the form

$$\dot{y} + \log(\dot{y}) = 1. \tag{5.3}$$

(ii) We note that Eq. (5.1) is a *first order* differential equation in y. However, this is in fact not a restriction since we can transform every explicit differential equation of order n into a coupled set of explicit first order differential equations. Let us demonstrate this. We regard an explicit differential equation of the form

B. A. Stickler and E. Schachinger, *Basic Concepts in Computational Physics*,
DOI: 10.1007/978-3-319-02435-6_5, © Springer International Publishing Switzerland 2014

$$y^{(n)} = f(t; y, \dot{y}, \ddot{y}, \ldots, y^{(n-1)}), \tag{5.4}$$

where we defined $y^{(k)} \equiv \frac{\mathrm{d}^k}{\mathrm{d}t^k} y$. This equation is equivalent to the set

$$\begin{aligned} \dot{y}_1 &= y_2, \\ \dot{y}_2 &= y_3, \\ \vdots \;\; & \;\; \vdots \\ \dot{y}_{n-1} &= y_n, \\ \dot{y}_n &= f(t, y_1, y_2, \ldots, y_n), \end{aligned} \tag{5.5}$$

which can be written as Eq. (5.1). Hence, we can attenuate the criterion discussed in point (i), i.e. that the differential equation has to be explicit in $\dot{y}$, to the criterion that the differential equation of order n has to be explicit in the n-th derivative of y, namely $y^{(n)}$.

There is another point required to be discussed before moving on. The numerical treatment of initial value problems is of inestimable value in physics because many differential equations, which appear unspectacular at first glance, cannot be solved analytically. For instance, consider a first order differential equation:

$$\dot{y} = t^2 + y^2. \tag{5.6}$$

Although this equation appears to be simple, one has to rely on numerical methods in order to obtain a solution. However, Eq. (5.6) is not *well posed* since the solution is ambiguous as long as no initial values are given. A numerical solution is only possible if the problem is completely defined. In many cases, one uses numerical methods although the problem is solvable with the help of analytic methods, simply because the solution would be too complicated. A numerical approach might be justified, however, one should always remember that [1], quote:

"Numerical methods are no excuse for poor analysis."

This chapter is augmented by a chapter on the double pendulum, which will serve as a demonstration of the applicability of Runge-Kutta methods and by a chapter on molecular dynamics which will demonstrate the applicability of the leap-frog algorithm.

5.2 Simple Integrators

We start by reintroducing the methods already discussed in the previous chapter. Again, we discretize the time coordinate t via the relation $t_n = t_0 + n\Delta t$ and define $f_n \equiv f(t_n)$ accordingly. In the following we will refrain from noting the initial condition explicitly for a more compact notation. We investigate Eq. (5.1) at some particular time t_n:

$$\dot{y}_n = f(y_n, t_n). \tag{5.7}$$

Integrating both sides of (5.7) over the interval $[t_n, t_{n+1}]$ gives

$$y_{n+1} = y_n + \int_{t_n}^{t_{n+1}} \mathrm{d}t' f[y(t'), t']. \tag{5.8}$$

Note that Eq. (5.8) is exact and it will be our starting point in the discussion of several paths to a numeric solution of initial value problems. These solutions will be based on an approximation of the integral on the right hand side of Eq. (5.8) with the help of the methods already discussed in Chap. 3.

In the following we list four of the best known simple integration methods for initial value problems:

(1)

Applying the forward rectangular rule (3.9) to Eq. (5.8) yields

$$y_{n+1} = y_n + f(y_n, t_n)\Delta t + \mathscr{O}(\Delta t^2), \tag{5.9}$$

which is the explicit EULER method we encountered already in Sect. 4.3. This method is also referred to as the *forward* EULER *method* . In accordance to the forward rectangular rule, the leading term of the error of this method is proportional to Δt^2 as was pointed out in Sect. 3.2.

(2)

We use the backward rectangular rule (3.10) in Eq. (5.8) and obtain

$$y_{n+1} = y_n + f(y_{n+1}, t_{n+1})\Delta t + \mathscr{O}(\Delta t^2), \tag{5.10}$$

which is the implicit EULER method, also referred to as *backward* EULER *method*. As already highlighted in Sect. 4.3, it may be necessary to solve Eq. (5.10) numerically for y_{n+1} (Some notes on the numeric solution of non-linear equations can be found in Appendix B).

(3)

The central rectangular rule (3.13) approximates Eq. (5.8) by

$$y_{n+1} = y_n + f(y_{n+\frac{1}{2}}, t_{n+\frac{1}{2}})\Delta t + \mathscr{O}(\Delta t^3), \tag{5.11}$$

and we rewrite this equation in the form:

$$y_{n+1} = y_{n-1} + 2f(y_n, t_n)\Delta t + \mathcal{O}(\Delta t^3). \tag{5.12}$$

This method is sometimes referred to as the *leap-frog* routine or STÖRMER-VERLET method. We will come back to this point in Chap. 7. Note that the approximation

$$y_{n+\frac{1}{2}} \approx \frac{y_n + y_{n+1}}{2}, \tag{5.13}$$

gives the implicit midpoint rule as it was introduced in Sect. 4.3.

(4)

Employing the trapezoidal rule (3.15) in an approximation to Eq. (5.8) yields

$$y_{n+1} = y_n + \frac{\Delta t}{2}\left[f(y_n, t_n) + f(y_{n+1}, t_{n+1})\right] + \mathcal{O}(\Delta t^3). \tag{5.14}$$

This is an implicit method which has to be solved for y_{n+1}. It is generally known as the CRANK-NICOLSON method or simply as *trapezoidal method*.

Methods (1), (2), and (4) are also known as one-step methods, since only function values at times t_n and t_{n+1} are used to propagate in time. In contrast, the leap-frog method is already a *multi-step* method since three different times appear in the expression. Basically, there are three different strategies to improve these rather simple methods:

- TAYLOR series methods: Use more terms in the TAYLOR expansion of y_{n+1}.
- Linear Multi-Step methods: Use data from previous time steps y_k, $k < n$ in order to cancel terms in the truncation error.
- RUNGE-KUTTA method: Use intermediate points within one time step.

We will briefly discuss the first two alternatives and then turn our attention to the RUNGE- KUTTA methods in the next section.

Taylor Series Methods

From Chap. 2 we are already familiar with the TAYLOR expansion (2.7) of the function y_{n+1} around the point y_n,

$$y_{n+1} = y_n + \Delta t\dot{y}_n + \frac{\Delta t^2}{2}\ddot{y}_n + \mathcal{O}(\Delta t^3). \tag{5.15}$$

We insert Eq. (5.7) into Eq. (5.15) and obtain

$$y_{n+1} = y_n + \Delta t f(y_n, t_n) + \frac{\Delta t^2}{2}\ddot{y}_n + \mathscr{O}(\Delta t^3). \tag{5.16}$$

So far nothing has been gained since the truncation error is still proportional to Δt^2. However, calculating $\ddot{y}_n$ with the help of Eq. (5.7) gives

$$\ddot{y}_n = \frac{\mathrm{d}}{\mathrm{d}t} f(y_n, t_n) = \dot{f}(y_n, t_n) + f'(y_n, t_n)\dot{y}_n = \dot{f}(y_n, t_n) + f'(y_n, t_n) f(y_n, t_n), \tag{5.17}$$

and this results together with Eq. (5.16) in:

$$y_{n+1} = y_n + \Delta t f(y_n, t_n) + \frac{\Delta t^2}{2}\left[\dot{f}(y_n, t_n) + f'(y_n, t_n) f(y_n, t_n)\right] + \mathscr{O}(\Delta t^3). \tag{5.18}$$

This manipulation reduced the local truncation error to orders of Δt^3. The derivatives of $f(y_n, t_n)$, $f'(y_n, t_n)$ and $\dot{f}(y_n, t_n)$ can be approximated with the help of the methods discussed in Chap. 2, if an analytic differentiation is not feasible.

The above procedure can be repeated up to arbitrary order in the TAYLOR expansion (5.15).

Linear Multi-Step Methods

A k-th order linear multi-step method is defined by the approximation

$$y_{n+1} = \sum_{j=0}^{k} a_j y_{n-j} + \Delta t \sum_{j=0}^{k+1} b_i f(y_{n+1-j}, t_{n+1-j}), \tag{5.19}$$

of Eq. (5.8). The coefficients a_j and b_j have to be determined in such a way that the truncation error is reduced. Two of the best known techniques are the so called second order ADAMS–BASHFORD methods

$$y_{n+1} = y_n + \frac{\Delta t}{2}\left[3f(y_n, t_n) - f(y_{n-1}, t_{n-1})\right] \tag{5.20}$$

and the second order rule (*backward differentiation formula*)

$$y_{n+1} = \frac{1}{3}\left[4y_n - y_{n-1} + \frac{\Delta t}{2} f(y_{n+1}, t_{n+1})\right]. \tag{5.21}$$

We note in passing that the backward differentiation formula of arbitrary order can easily be obtained with the help of the operator technique introduced in Sect. 2.4, Eq. (2.30). One simply replaces the first derivative on the left hand side by the function $f(y_n, t_n)$ according to Eq. (5.7) and calculates the backward difference series on the right hand side to arbitrary order.

In many cases, multi-step methods are based on the interpolation of previously computed values y_k by LAGRANGE polynomials. This interpolation is then inserted into Eq. (5.8) and integrated. However, a detailed discussion of such procedures is beyond the scope of this book. The interested reader is referred to Refs. [2, 3].

Nevertheless, let us make one last point. We note that Eq. (5.19) is explicit for $b_0 = 0$ and implicit for $b_0 \neq 0$. In many numerical realizations one combines implicit and explicit multi-step methods in such a way that the explicit result (solve Eq. (5.19) with $b_0 = 0$) is used as a guess to solve the implicit equation (solve Eq. (5.19) with $b_0 \neq 0$). Hence, the explicit method *predicts* the value y_{n+1} and the implicit method *corrects* it. Such methods yield very good results and are commonly referred to as *predictor–corrector* methods [4].

5.3 RUNGE-KUTTA Methods

In contrast to linear multi-step methods, the idea in RUNGE-KUTTA methods is to improve the accuracy by calculating intermediate grid-points within the interval $[t_n, t_{n+1}]$. We note that the approximation (5.11) resulting from the central rectangular rule is already such a method since the function value $y_{n+\frac{1}{2}}$ at the grid-point $t_{n+\frac{1}{2}} = t_n + \frac{\Delta t}{2}$ is taken into account. We investigate this in more detail and rewrite Eq. (5.11):

$$y_{n+1} = y_n + f(y_{n+\frac{1}{2}}, t_{n+\frac{1}{2}})\Delta t + \mathcal{O}(\Delta t^3). \tag{5.22}$$

We now have to find appropriate approximations to $y_{n+\frac{1}{2}}$ which will increase the accuracy of Eq. (5.11). Our first choice is to replace $y_{n+\frac{1}{2}}$ with the help of the explicit EULER method, Eq. (5.9),

$$y_{n+\frac{1}{2}} = y_n + \frac{\Delta t}{2}\dot{y}_n = y_n + \frac{\Delta t}{2} f(y_n, t_n), \tag{5.23}$$

which, inserted into Eq. (5.22) yields

$$y_{n+1} = y_n + f\left[y_n + \frac{\Delta t}{2} f(y_n, t_n), t_n + \frac{\Delta t}{2}\right]\Delta t + \mathcal{O}(\Delta t^2). \tag{5.24}$$

We note that Eq. (5.24) is referred to as the *explicit midpoint rule*. In analogy we could have approximated $y_{n+\frac{1}{2}}$ with the help of the implicit EULER method (5.10) which yields

$$y_{n+1} = y_n + f\left[y_n + \frac{\Delta t}{2} f(y_{n+1}, t_{n+1}), t_n + \frac{\Delta t}{2}\right]\Delta t + \mathcal{O}(\Delta t^2). \tag{5.25}$$

This equation is referred to as the *implicit midpoint rule.* Let us explain how we obtain an estimate for the error in Eqs. (5.24) and (5.25). In case of Eq. (5.24) we investigate the term

$$y_{n+1} - y_n - f\left[y_n + \frac{\Delta t}{2} f(y_n, t_n), t_n + \frac{\Delta t}{2}\right]\Delta t.$$

The TAYLOR expansion of y_{n+1} and $f(\cdot)$ around the point $\Delta t = 0$ yields

$$\Delta t\left[\dot{y}_n - f(y_n, t_n)\right] + \frac{\Delta t^2}{2}\left[\ddot{y} - \dot{f}(y_n, t_n) - f'(y_n, t_n)\dot{y}_n\right] + \cdots . \tag{5.26}$$

We observe that the first term cancels because of Eq. (5.7). Consequently, the error is of order Δt^2. A similar argument holds for Eq. (5.25).

Let us introduce a more convenient notation for the above examples before we concentrate on a more general topic. It is presented in algorithmic form, i.e. it defines the sequence in which one should calculate the various terms. This is convenient for two reasons, first of all it increases the readability of complex methods such as Eq. (5.25) and, secondly, it can be easily identified which part of the method involves an implicit step which has to be solved separately for the corresponding variable. For this purpose let us introduce variables Y_i of some index $i \geq 1$ and we use a simple example to illustrate this notation. Consider the explicit EULER method (5.9). It can be written as

$$\begin{aligned} Y_1 &= y_n, \\ y_{n+1} &= y_n + f(Y_1, t_n)\Delta t. \end{aligned} \tag{5.27}$$

In a similar fashion we write the implicit EULER method (5.10) as

$$\begin{aligned} Y_1 &= y_n + f(Y_1, t_{n+1})\Delta t, \\ y_{n+1} &= y_n + f(Y_1, t_{n+1})\Delta t. \end{aligned} \tag{5.28}$$

It is understood that the first equation of (5.28) has to be solved for Y_1 first and this result is then plugged into the second equation in order to obtain y_{n+1}. One further example: the CRANK–NICOLSON (5.14) method can be rewritten as

$$\begin{aligned} Y_1 &= y_n, \\ Y_2 &= y_n + \frac{\Delta t}{2}\left[f(Y_1, t_n) + f(Y_2, t_{n+1})\right], \\ y_{n+1} &= y_n + \frac{\Delta t}{2}\left[f(Y_1, t_n) + f(Y_2, t_{n+1})\right], \end{aligned} \tag{5.29}$$

where the second equation is to be solved for Y_2 in the second step.

In analogy, the algorithmic form of the explicit midpoint rule (5.24) is defined as

$$\begin{aligned} Y_1 &= y_n, \\ Y_2 &= y_n + \frac{\Delta t}{2} f\left(Y_1, t_n + \frac{\Delta t}{2}\right), \\ y_{n+1} &= y_n + \frac{\Delta t}{2} f\left(Y_2, t_n + \frac{\Delta t}{2}\right), \end{aligned} \tag{5.30}$$

and we find for the implicit midpoint rule (5.25):

$$\begin{aligned} Y_1 &= y_n + \frac{\Delta t}{2} f\left(Y_1, t_n + \frac{\Delta t}{2}\right), \\ y_{n+1} &= y_n + \Delta t f\left(Y_1, t_n + \frac{\Delta t}{2}\right). \end{aligned} \tag{5.31}$$

The above algorithms are all examples of the so called Runge-Kutta methods. We introduce the general representation of a d-stage Runge-Kutta method:

$$\begin{aligned} Y_i &= y_n + \Delta t \sum_{j=1}^{d} a_{ij} f\left(Y_j, t_n + c_j \Delta t\right), \qquad i = 1, \ldots, d, \\ y_{n+1} &= y_n + \Delta t \sum_{j=1}^{d} b_i f\left(Y_j, t_n + c_j \Delta t\right). \end{aligned} \tag{5.32}$$

We note that Eq. (5.32) it is completely determined by the coefficients a_{ij}, b_j and c_j. In particular $a = \{a_{ij}\}$ is a $d \times d$ matrix, while $b = \{b_j\}$ and $c = \{c_j\}$ are d dimensional vectors.

Butcher tableaus are a very useful tool to characterize such methods. They provide a structured representation of the coefficient matrix a and the coefficient vectors b and c:

$$\begin{array}{c|cccc} c_1 & a_{11} & a_{12} & \ldots & a_{1d} \\ c_2 & a_{21} & a_{22} & \ldots & a_{2d} \\ \vdots & \vdots & \vdots & \ddots & \vdots \\ c_d & a_{d1} & a_{d2} & \ldots & a_{dd} \\ \hline & b_1 & b_2 & \ldots & b_d \end{array} \tag{5.33}$$

We note that the Runge-Kutta method (5.32) or (5.33) is explicit if the matrix a is zero on and above the diagonal, i.e. $a_{ij} = 0$ for $j \geq i$. Let us rewrite all the methods described here in the form of Butcher tableaus:

Explicit EULER:

$$\begin{array}{c|c} 0 & 0 \\ \hline & 1 \end{array} \tag{5.34}$$

Implicit EULER:

$$\begin{array}{c|c} 1 & 1 \\ \hline & 1 \end{array} \tag{5.35}$$

CRANK- NICOLSON:

$$\begin{array}{c|cc} 0 & 0 & 0 \\ 1 & \frac{1}{2} & \frac{1}{2} \\ \hline & \frac{1}{2} & \frac{1}{2} \end{array} \tag{5.36}$$

Explicit Midpoint:

$$\begin{array}{c|cc} 0 & 0 & 0 \\ \frac{1}{2} & \frac{1}{2} & 0 \\ \hline & \frac{1}{2} & \frac{1}{2} \end{array} \tag{5.37}$$

Implicit Midpoint:

$$\begin{array}{c|c} \frac{1}{2} & \frac{1}{2} \\ \hline & 1 \end{array} \tag{5.38}$$

With the help of RUNGE–KUTTA methods of the general form (5.32) one can develop methods of arbitrary accuracy. One of the most popular methods is the explicit four stage method (we will call it *e-RK-4*) which is defined by the algorithm:

$$\begin{aligned}
Y_1 &= y_n, \\
Y_2 &= y_n + \frac{\Delta t}{2} f(Y_1, t_n), \\
Y_3 &= y_n + \frac{\Delta t}{2} f\left(Y_2, t_n + \frac{\Delta t}{2}\right), \\
Y_4 &= y_n + \Delta t f\left(Y_3, t_n + \frac{\Delta t}{2}\right), \\
y_{n+1} &= y_n + \frac{\Delta t}{6}\left[f(Y_1, t_n) + 2f\left(Y_2, t_n + \frac{\Delta t}{2}\right)\right.
\end{aligned}$$

$$+2f\left(Y_3, t_n+\frac{\Delta t}{2}\right)+f(Y_4, t_n)\Bigg]. \tag{5.39}$$

This method is an analogue to the Simpson rule of numerical integration as discussed in Sect. 3.4. However, a detailed compilation of the coefficient array a and coefficient vectors b, and c is quite complicated. A closer inspection reveals that the methodological error of this method behaves as Δt^5. The algorithm *e-RK-4*, Eq. (5.39), is represented by a Butcher tableau of the form

$$\begin{array}{c|cccc} 0 & 0 & 0 & 0 & 0 \\ \frac{1}{2} & \frac{1}{2} & 0 & 0 & 0 \\ \frac{1}{2} & 0 & \frac{1}{2} & 0 & 0 \\ 1 & 0 & 0 & 1 & 0 \\ \hline & \frac{1}{6} & \frac{1}{3} & \frac{1}{3} & \frac{1}{6} \end{array} \tag{5.40}$$

Another quite popular method is given by the Butcher tableau

$$\begin{array}{c|cc} \frac{1}{2}-\frac{\sqrt{3}}{6} & \frac{1}{4} & \frac{1}{4}-\frac{\sqrt{3}}{6} \\ \frac{1}{2}+\frac{\sqrt{3}}{6} & \frac{1}{4}+\frac{\sqrt{3}}{6} & \frac{1}{4} \\ \hline & \frac{1}{2} & \frac{1}{2} \end{array} \tag{5.41}$$

We note that this method is implicit and mention that it corresponds to the two point Gauss-Legendre quadrature of Sect. 3.6.

A further improvement of implicit Runge-Kutta methods can be achieved by *choosing* the Y_i in such a way that they correspond to solutions of the differential equation (5.7) at intermediate time steps. The intermediate time steps at which one wants to reproduce the function are referred to as *collocation points*. At these points the functions are approximated by interpolation on the basis of Lagrange polynomials, which can easily be integrated analytically. However, the discussion of such collocation methods [4] is far beyond the scope of this book.

In general Runge-Kutta methods are very useful. However one always has to keep in mind that there could be better methods for the problem at hand. Let us close this section with a quote from the book by Press et al. [5]:

> "*For many scientific users, fourth-order Runge-Kutta is not just the first word on ODE integrators, but the last word as well. In fact, you can get pretty far on this old workhorse, especially if you combine it with an adaptive step-size algorithm. Keep in mind, however, that the old workhorse's last trip may well take you to the poorhouse: Bulirsch-Stoer or predictor-corrector methods can be very much more efficient for problems where high accuracy is a requirement. Those methods are the high-strung racehorses. Runge-Kutta is for ploughing the fields.*"

5.4 Hamiltonian Systems: Symplectic Integrators

Let us define a symplectic integrator as a numerical integration in which the mapping

$$\Phi_{\Delta t} : y_n \mapsto y_{n+1}, \tag{5.42}$$

is symplectic. Here $\Phi_{\Delta t}$ is referred to as the *numerical flow* of the method. If we regard the initial value problem (5.1) we can define in an analogous way the *flow of the system* φ_t as

$$\varphi_t(y_0) = y(t). \tag{5.43}$$

For instance, if we consider the initial value problem

$$\begin{cases} \dot{y} = Ay, \\ y(0) = y_0, \end{cases} \tag{5.44}$$

where $y \in \mathbb{R}^n$ and $A \in \mathbb{R}^{n \times n}$, then the flow of the system φ_t is given by:

$$\varphi_t(y_0) = \exp(At)y_0. \tag{5.45}$$

On the other hand, if we regard two vectors $v, w \in \mathbb{R}^2$, we can express the area ω of the parallelogram spanned by these vectors as

$$\omega(v, w) = \det(vw) = v \begin{pmatrix} 0 & 1 \\ -1 & 0 \end{pmatrix} w = ad - bc, \tag{5.46}$$

where we put $v = (a, b)^T$ and $w = (c, d)^T$. More generally, if $v, w \in \mathbb{R}^{2d}$, we have

$$\omega(v, w) = v \begin{pmatrix} 0 & I \\ -I & 0 \end{pmatrix} w \equiv vJw, \tag{5.47}$$

where I is the $d \times d$ dimensional unity matrix. Hence (5.47) represents the sum of the projected areas of the form

$$\det \begin{pmatrix} v_i & w_i \\ v_{i+d} & w_{i+d} \end{pmatrix}. \tag{5.48}$$

If we regard a mapping $M : \mathbb{R}^{2d} \mapsto \mathbb{R}^{2d}$ and require that

$$\omega(Mv, Mw) = \omega(v, w), \tag{5.49}$$

i.e. the area is preserved, we obtain the condition that

$$M^T JM = J, \tag{5.50}$$

which is equivalent to $\det(M) = 1$. Finally, a differentiable mapping $f : \mathbb{R}^{2d} \mapsto \mathbb{R}^{2d}$ is referred to as *symplectic* if the linear mapping $f'(x)$ (JACOBI matrix) conserves ω for all $x \in \mathbb{R}^{2d}$. One can easily prove that the flow of Hamiltonian systems (energy conserving) is symplectic, i.e. area preserving in phase space. Every Hamiltonian system is characterized by its HAMILTON function $H(p, q)$ and the corresponding HAMILTON equations of motion:

$$\dot{p} = -\nabla_q H(p, q) \qquad \text{and } \dot{q} = \nabla_p H(p, q). \tag{5.51}$$

We define the flow of the system via

$$\varphi_t(x_0) = x(t), \tag{5.52}$$

where

$$x_0 = \begin{pmatrix} p_0 \\ q_0 \end{pmatrix} \quad \text{and} \quad x(t) = \begin{pmatrix} p(t) \\ q(t) \end{pmatrix}. \tag{5.53}$$

Hence we rewrite (5.51) as

$$\dot{x} = J^{-1} \nabla_x H(x), \tag{5.54}$$

and note that $x \equiv x(t, x_0)$ is a function of time and initial conditions. In a next step we define the Jacobian of the flow via

$$P_t(x_0) = \nabla_{x_0} \phi_t(x_0), \tag{5.55}$$

and calculate

$$\begin{aligned} \dot{P}_t(x_0) &= \nabla_{x_0} \dot{x} \\ &= J^{-1} \nabla_{x_0} \nabla_x H(x) \\ &= J^{-1} \Delta_x H(x) \nabla_{x_0} x \\ &= J^{-1} \Delta_x H(x) P_t(x_0) \\ &= \begin{pmatrix} -\nabla_{qp} H(p, q) & -\nabla_{qq} H(p, q) \\ \nabla_{pp} H(p, q) & \nabla_{pq} H(p, q) \end{pmatrix} P_t(x_0). \end{aligned} \tag{5.56}$$

Hence, P_t is given by the solution of the equation

$$\dot{P}_t = J^{-1} \Delta_x H(x) P_t. \tag{5.57}$$

Symplecticity ensures that the area

$$P_t^T J P_t = \text{const}, \tag{5.58}$$

which can be verified by calculating $\frac{\mathrm{d}}{\mathrm{d}t} \left(P_t^T J P_t \right)$ where we keep in mind that $J^T = -J$. Hence,

$$\begin{aligned}\frac{\mathrm{d}}{\mathrm{d}t}P_t^T J P_t &= \dot{P}_t^T J P_t + P_t^T J \dot{P}_t \\ &= P_t^T \Delta_x H(x)(J^{-1})^T J P_t + P_t^T J J^{-1} \Delta_x H(x) P_t \\ &= 0, \end{aligned} \tag{5.59}$$

if the HAMILTON function is conserved, i.e.

$$\frac{\partial}{\partial t} H(p, q) \overset{!}{=} 0. \tag{5.60}$$

This means that the flow of a Hamiltonian system is symplectic, i.e. area preserving in phase space.

Since this conservation law is violated by methods like *e-RK-4* or explicit EULER, one introduces so called *symplectic integrators*, which have been particularly designed as a remedy to this shortcoming. A detailed investigation of these techniques is far too engaged for this book. The interested reader is referred to Refs. [6–9].

However, we provide a list of the most important integrators.

Symplectic EULER

$$q_{n+1} = q_n + a(q_n, p_{n+1})\Delta t, \tag{5.61a}$$

$$p_{n+1} = p_n + b(q_n, p_{n+1})\Delta t. \tag{5.61b}$$

Here $a(p, q) = \nabla_p H(p, q)$ and $b(p, q) = -\nabla_q H(p, q)$ have already been defined in Sect. 4.3.

Symplectic RUNGE–KUTTA

It can be demonstrated that a RUNGE-KUTTA method is symplectic if the coefficients fulfill

$$b_i a_{ij} + b_j a_{ji} = b_i b_j, \tag{5.62}$$

for all i, j [7]. This is a property of the collocation methods based on GAUSS points c_i.

5.5 An Example: The KEPLER Problem, Revisited

It has already been discussed in Sect. 4.3 that the HAMILTON function of this system takes on the form

$$H(p, q) = \frac{1}{2}\left(p_1^2 + p_2^2\right) - \frac{1}{\sqrt{q_1^2 + q_2^2}}, \tag{5.63}$$

and HAMILTON's equations of motion read

$$\dot{p}_1 = -\nabla_{q_1} H(p,q) = -\frac{q_1}{(q_1^2 + q_2^2)^{\frac{3}{2}}}, \tag{5.64a}$$

$$\dot{p}_2 = -\nabla_{q_2} H(p,q) = -\frac{q_2}{(q_1^2 + q_2^2)^{\frac{3}{2}}}, \tag{5.64b}$$

$$\dot{q}_1 = \nabla_{p_1} H(p,q) = p_1, \tag{5.64c}$$

$$\dot{q}_2 = \nabla_{p_2} H(p,q) = p_2. \tag{5.64d}$$

We now introduce the time instances $t_n = t_0 + n\Delta t$ and define $q_i^n \equiv q_i(t_n)$ and $p_i^n \equiv p_i(t_n)$ for $i = 1, 2$. In the following we give the discretized recursion relation for three different methods, namely explicit EULER, implicit EULER, and symplectic EULER.

Explicit EULER

In case of the explicit EULER method we have simple recursion relations

$$p_1^{n+1} = p_1^n - \frac{q_1^n \Delta t}{[(q_1^n)^2 + (q_2^n)^2]^{\frac{3}{2}}}, \tag{5.65a}$$

$$p_2^{n+1} = p_2^n - \frac{q_2^n \Delta t}{[(q_1^n)^2 + (q_2^n)^2]^{\frac{3}{2}}}, \tag{5.65b}$$

$$q_1^{n+1} = q_1^n + p_1^n \Delta t, \tag{5.65c}$$

$$q_2^{n+1} = q_2^n + p_2^n \Delta t. \tag{5.65d}$$

Implicit EULER

We obtain the implicit equations

$$p_1^{n+1} = p_1^n - \frac{q_1^{n+1} \Delta t}{[(q_1^{n+1})^2 + (q_2^{n+1})^2]^{\frac{3}{2}}}, \tag{5.66a}$$

$$p_2^{n+1} = p_2^n - \frac{q_2^{n+1} \Delta t}{[(q_1^{n+1})^2 + (q_2^{n+1})^2]^{\frac{3}{2}}}, \tag{5.66b}$$

$$q_1^{n+1} = q_1^n + p_1^{n+1} \Delta t, \tag{5.66c}$$

$$q_2^{n+1} = q_2^n + p_2^{n+1} \Delta t. \tag{5.66d}$$

These implicit equations can be solved, for instance, by the use of the NEWTON method discussed in Appendix B.

Symplectic EULER

Employing Eqs. (5.61) gives

$$p_1^{n+1} = p_1^n - \frac{q_1^n \Delta t}{[(q_1^n)^2 + (q_2^n)^2]^{\frac{3}{2}}}, \tag{5.67a}$$

$$p_2^{n+1} = p_2^n - \frac{q_2^n \Delta t}{[(q_1^n)^2 + (q_2^n)^2]^{\frac{3}{2}}}, \tag{5.67b}$$

$$q_1^{n+1} = q_1^n + p_1^{n+1} \Delta t, \tag{5.67c}$$

$$q_2^{n+1} = q_2^n + p_2^{n+1} \Delta t. \tag{5.67d}$$

These implicit equations can be solved analytically and we obtain

$$p_1^{n+1} = p_1^n - \frac{q_1^n \Delta t}{[(q_1^n)^2 + (q_2^n)^2]^{\frac{3}{2}}}, \tag{5.68a}$$

$$p_2^{n+1} = p_2^n - \frac{q_2^n \Delta t}{[(q_1^n)^2 + (q_2^n)^2]^{\frac{3}{2}}}, \tag{5.68b}$$

$$q_1^{n+1} = q_1^n + p_1^n \Delta t - \frac{q_1^n \Delta t^2}{[(q_1^n)^2 + (q_2^n)^2]^{\frac{3}{2}}}, \tag{5.68c}$$

$$q_2^{n+1} = q_2^n + p_2^n \Delta t - \frac{q_2^n \Delta t^2}{[(q_1^n)^2 + (q_2^n)^2]^{\frac{3}{2}}}. \tag{5.68d}$$

A second possibility of the symplectic EULER is given by Eq. (4.41). It reads

$$p_1^{n+1} = p_1^n - \frac{q_1^{n+1} \Delta t}{[(q_1^{n+1})^2 + (q_2^{n+1})^2]^{\frac{3}{2}}}, \tag{5.69a}$$

$$p_2^{n+1} = p_2^n - \frac{q_2^{n+1} \Delta t}{[(q_1^{n+1})^2 + (q_2^{n+1})^2]^{\frac{3}{2}}}, \tag{5.69b}$$

$$q_1^{n+1} = q_1^n + p_1^n \Delta t, \tag{5.69c}$$

$$q_2^{n+1} = q_2^n + p_2^n \Delta t. \tag{5.69d}$$

The trajectories calculated using these four methods are presented in Figs. 5.1 and 5.2, the time evolution of the total energy of the system is plotted in Fig. 5.3. The initial conditions were [7]

$$p_1(0) = 0, \qquad q_1(0) = 1 - e, \tag{5.70}$$

and

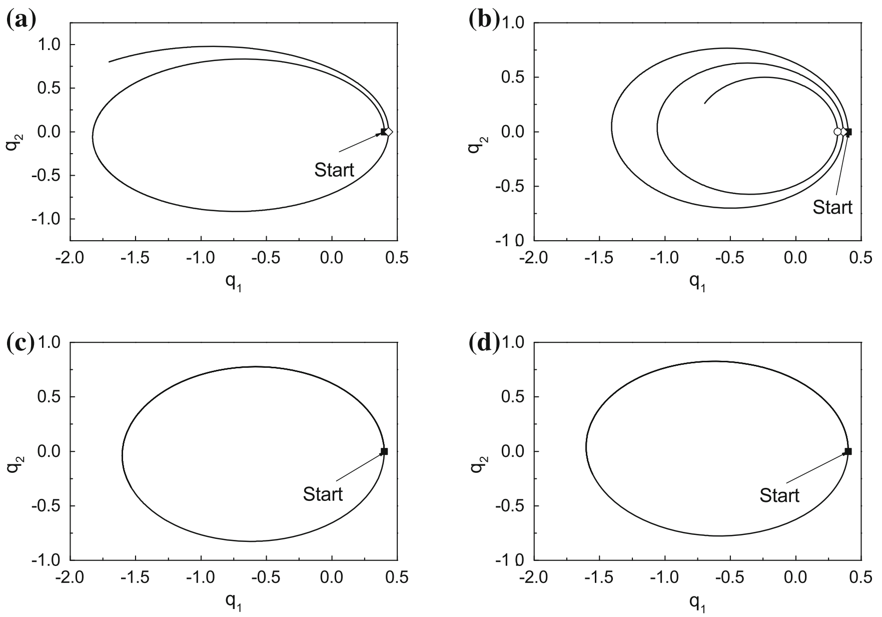

Fig. 5.1 Kepler trajectories in position space for the initial values defined in Eqs. (5.70) and (5.71). They are indicated by a *solid square*. Solutions have been generated **(a)** by the explicit Euler method (5.65), **(b)** by the implicit Euler method (5.66), **(c)** by the symplectic Euler method (5.68), and **(d)** by the symplectic Euler method (5.69)

$$p_2(0) = \sqrt{\frac{1+e}{1-e}}, \qquad q_2(0) = 0, \tag{5.71}$$

with $e = 0.6$ which gives $H = -1/2$. Furthermore, we set $\Delta t = 0.01$ for the symplectic Euler methods and $\Delta t = 0.005$ for the forward and backward Euler methods in order to reduce the methodological error. The implicit equations were solved with help of the Newton method as discussed in Appendix B. The Jacobi matrix was calculated analytically, hence no methodological error enters because approximations of derivatives were unnecessary.

According to theory the q-space and p-space projections of the phase space trajectory are ellipses. Furthermore, energy and angular momentum are conserved. Thus, the numerical solutions of Hamilton's equations of motion (5.64) should reflect these properties. Figures 5.1a, b and 5.2a, b present the results of the explicit Euler method, Eq. (5.65), and the implicit Euler method, Eq. (5.66), respectively. Obviously, the result does not agree with the theoretical expectation and the trajectories are open instead of closed. The reason for this behavior is the methodological error of the method which is accumulative and, thus, causes a violation of energy conservation. This violation becomes apparent in Fig. 5.3 where the total energy $H(t)$ is plotted versus time t. Neither the explicit Euler method (dashed line) nor the

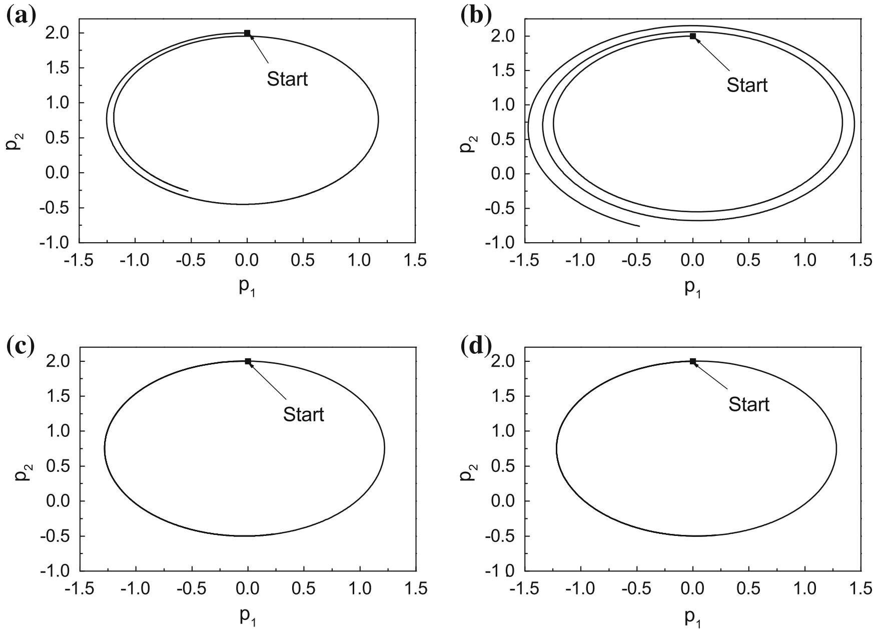

Fig. 5.2 Kepler trajectories in momentum space for the initial values defined in Eqs. (5.70) and (5.71). They are indicated by a *solid square*. Solutions have been generated **(a)** by the explicit Euler method (5.65), **(b)** by the implicit Euler method (5.66), **(c)** by the symplectic Euler method (5.68), and **(d)** by the symplectic Euler method (5.69)

implicit Euler method (short dashed line) conform to the requirement of energy conservation. We also see step-like structures of $H(t)$. At the center of these steps an open diamond symbol and in the case of the implicit Euler method an additional open circle indicate the position in time of the perihelion of the point-mass (point of closest approach to the center of attraction). It is indicated by the same symbols in Fig. 5.1a, b. At this point the point-mass reaches its maximum velocity, the pericenter velocity, and it covers the biggest distances along its trajectory per time interval Δt. Consequently, the methodological error is biggest in this part of the trajectory which manifests itself in those steps in $H(t)$. As the point-mass moves 'faster' when the implicit Euler method is applied, again, the distances covered per time interval are greater than those covered by the point-mass in the explicit Euler method. Thus, it is not surprising that the error of the implicit Euler method is bigger as well when $H(t)$ is determined.

These results are in strong contrast to the numerical solutions of Eqs. (5.64) obtained with the help of symplectic Euler methods which are presented in Figs. 5.1c, d and 5.2c, d. The trajectories are almost perfect ellipses for both symplectic methods Eqs. (5.68) and (5.69). Moreover, the total energy $H(t)$ (solid and dashed-dotted lines in Fig. 5.3) varies very little as a function of t. Deviations from the mean value can only be observed around the perihelion which is indicated by

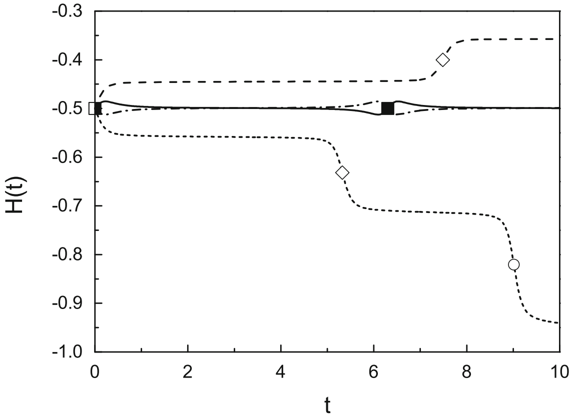

Fig. 5.3 Time evolution of the total energy H calculated with the help of the four methods discussed in the text. The initial values are given by Eqs. (5.70) and (5.71). Solutions have been generated **(a)** by the explicit EULER method (5.65) (*dashed line*), **(b)** by the implicit EULER method (5.66) (*dotted line*), **(c)** by the symplectic EULER method (5.68) (*solid line*), and **(d)** by the symplectic EULER method (5.69) (*dashed-dotted line*)

a solid square. Moreover, these deviations compensate because of the symplectic nature of the method. This proves that symplectic integrators are the appropriate technique to solve the equations of motion of Hamiltonian systems.

Summary

We concentrated on numerical methods to solve the initial value problem. The methods discussed here rely heavily on the various methods developed for numerical integration because we can always find an integral representation of this kind of ordinary differential equations. The simple integrators known from Chap. 4 were augmented by the more general CRANK-NICHOLSON method which was based on the trapezoidal rule introduced in Sect. 3.3. The simple single-step methods were improved in their methodological error by TAYLOR series methods, linear multi-step methods, and by the RUNGE-KUTTA method. The latter took intermediate points within the time interval $[t_n, t_{n+1}]$ into account. In principle, it is possible to achieve almost arbitrary accuracy with such a method. Nevertheless, all those methods had the disadvantage that because of their methodological error energy conservation was violated when applied to Hamiltonian systems. As this problem can be remedied by symplectic integrators a short introduction into this topic was provided and the most important symplectic integrators have been presented. The final discussion of KEPLER'S two-body problem elucidated the various points discussed throughout this chapter.

Problems

1. Write a program to solve numerically the KEPLER problem. The HAMILTON function of the problem is defined as

$$H(p,q)=\frac{1}{2}\left(p_1^2+p_2^2\right)-\frac{1}{\sqrt{q_1^2+q_2^2}},$$

and the initial conditions are given by

$$p_1(0)=0,\quad q_1(0)=1-e,\quad p_2(0)=\sqrt{\frac{1+e}{1-e}},\quad q_2(0)=0,$$

where $e=0.6$. Derive HAMILTON'S equations of motion and implement an algorithm which solves these equations based on the following methods

(a) Explicit EULER,
(b) Symplectic EULER.

2. Plot the trajectories and the total energy as a function of time. You can use the results presented in Figs. 5.1 and 5.2 to check your code. Modify the initial conditions and discuss the results! Try to confirm KEPLER'S laws of planetary motion with the help of your algorithm.

References

1. Dorn, W.S., McCracken, D.D.: Numerical Methods with Fortran IV Case Studies. Wiley, New York (1972)
2. Colliatz, L.: The Numerical Treatment of Differential Equations. Springer, Berlin (1960)
3. van Winckel, G.: Numerical methods for differential equations. Lecture Notes. Karl-Franzens Universität Graz, Austria (2012).
4. Ascher, U.M., Petzold, L.R.: Computer Methods for Ordinary Differential Equations and Differential-Algebraic Equations. Society for Industrial and Applied Mathematics, Philadelphia (1998)
5. Press, W.H., Teukolsky, S.A., Vetterling, W.T., Flannery, B.P.: Numerical Recipes in C++, 2nd edn. Cambridge University Press, Cambridge, UK (2002)
6. Guillemin, V., Sternberg, S.: Symplectic Techniques in Physics. Cambridge University Press, Cambridge, UK (1990)
7. Hairer, E.: Geometrical integration - symplectic integrators. Lecture Notes, TU München, Germany (2010)
8. Scheck, F.: Mechanics, 5th edn. Springer, Berlin (2010)
9. Levi, D., Oliver, P., Thomova, Z., Winteritz, P. (eds.): Symmetries and integrability of Difference Equations. London Mathematical Society Lecture Note Series. Cambridge University Press, Cambridge, UK (2011)

Chapter 6
The Double Pendulum

6.1 HAMILTON's Equations

We investigate the dynamics of a double pendulum illustrated schematically in Fig. 6.1 in two spatial dimensions. It is the aim of this section to derive HAMILTON's equations of motion for this system. In a first step we introduce generalized coordinates and determine the LAGRANGE function of the system [1].

We determine the kinetic and potential energy, introduce generalized momenta and derive the HAMILTON function from which HAMILTON's equations of motion follow. These equations will serve as a starting point for the formulation of a numerical method.

From Fig. 6.1 we find the coordinates of the two masses:

$$x_1 = \ell \sin(\varphi_1), \qquad z_1 = 2\ell - \ell \cos(\varphi_1), \tag{6.1}$$

and

$$x_2 = \ell \left[\sin(\varphi_1) + \sin(\varphi_2)\right], \qquad z_2 = 2\ell - \ell \left[\cos(\varphi_1) + \cos(\varphi_2)\right]. \tag{6.2}$$

Here, 2ℓ is the pendulum's total length. The angles $\varphi_i, i = 1, 2$ are defined in Fig. 6.1.

We note that $\ell = \text{const}$ and obtain the time derivatives of the coordinates (6.1) and (6.2):

$$\dot{x}_1 = \ell\dot{\varphi}_1 \cos(\varphi_1), \tag{6.3}$$
$$\dot{z}_1 = \ell\dot{\varphi}_1 \sin(\varphi_1), \tag{6.4}$$
$$\dot{x}_2 = \ell\left[\dot{\varphi}_1 \cos(\varphi_1) + \dot{\varphi}_2 \cos(\varphi_2)\right], \tag{6.5}$$
$$\dot{z}_2 = \ell\left[\dot{\varphi}_1 \sin(\varphi_1) + \dot{\varphi}_2 \sin(\varphi_2)\right]. \tag{6.6}$$

The LAGRANGE function of the system is defined by

B. A. Stickler and E. Schachinger, *Basic Concepts in Computational Physics*,
DOI: 10.1007/978-3-319-02435-6_6, © Springer International Publishing Switzerland 2014

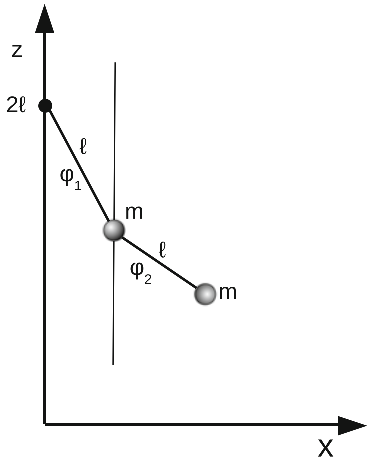

Fig. 6.1 Schematic illustration of the double pendulum. m are the point-masses, 2ℓ is the total length of the pendulum and φ_1, φ_2 are the corresponding angles

$$L = T - U, \tag{6.7}$$

with the kinetic energy T and the potential U. The kinetic energy T is given by[1]

$$\begin{aligned} T &= \frac{m}{2}\left(\dot{x}_1^2 + \dot{z}_1^2 + \dot{x}_2^2 + \dot{z}_2^2\right) \\ &= \frac{m\ell^2}{2}\left\{2\dot{\varphi}_1^2 + \dot{\varphi}_2^2 + 2\left[\sin(\varphi_1)\sin(\varphi_2) + \cos(\varphi_1)\cos(\varphi_2)\right]\dot{\varphi}_1\dot{\varphi}_2\right\} \\ &= \frac{m\ell^2}{2}\left[2\dot{\varphi}_1^2 + \dot{\varphi}_2^2 + 2\dot{\varphi}_1\dot{\varphi}_2\cos(\varphi_1 - \varphi_2)\right]. \end{aligned} \tag{6.8}$$

The potential energy U is determined by the gravitational force

$$\begin{aligned} U &= mgz_1 + mgz_2 \\ &= mg\ell\left[4 - 2\cos(\varphi_1) - \cos(\varphi_2)\right], \end{aligned} \tag{6.9}$$

where g is the acceleration due to gravity. Hence, the LAGRANGE function L is determined by:

$$L = \frac{m\ell^2}{2}\left[2\dot{\varphi}_1^2 + \dot{\varphi}_2^2 + 2\dot{\varphi}_1\dot{\varphi}_2\cos(\varphi_1 - \varphi_2)\right] - mg\ell\left[4 - 2\cos(\varphi_1) - \cos(\varphi_2)\right]. \tag{6.10}$$

Let us introduce generalized momenta p_i, $i = 1, 2$ as

[1] We make use of the relation:

$$\sin(x)\sin(y) + \cos(x)\cos(y) = \cos(x - y).$$

$$p_1 = \frac{\partial}{\partial \dot{\varphi}_1} L = m\ell^2 \left[2\dot{\varphi}_1 + \dot{\varphi}_2 \cos(\varphi_1 - \varphi_2)\right], \tag{6.11}$$

and

$$p_2 = \frac{\partial}{\partial \dot{\varphi}_2} L = m\ell^2 \left[\dot{\varphi}_2 + \dot{\varphi}_1 \cos(\varphi_1 - \varphi_2)\right]. \tag{6.12}$$

In the following we solve Eqs. (6.11) and (6.12) for $\dot{\varphi}_1$ and $\dot{\varphi}_2$. This will allow to express the kinetic energy (6.8) in terms of generalized momenta p_1 and p_2.

In a first step we solve Eq. (6.12) for $\dot{\varphi}_2$ and obtain

$$\dot{\varphi}_2 = \frac{p_2}{m\ell^2} - \dot{\varphi}_1 \cos(\varphi_1 - \varphi_2). \tag{6.13}$$

This result is used to rewrite Eq. (6.11) and we find

$$\frac{p_1}{m\ell^2} = 2\dot{\varphi}_1 + \left[\frac{p_2}{m\ell^2} - \dot{\varphi}_1 \cos(\varphi_1 - \varphi_2)\right] \cos(\varphi_1 - \varphi_2). \tag{6.14}$$

Solving for $\dot{\varphi}_1$ gives

$$\dot{\varphi}_1 = \left[2 - \cos^2(\varphi_1 - \varphi_2)\right]^{-1} \left[\frac{p_1}{m\ell^2} - \frac{p_2}{m\ell^2} \cos(\varphi_1 - \varphi_2)\right]. \tag{6.15}$$

The trigonometric identity

$$\cos^2(x) + \sin^2(x) = 1, \tag{6.16}$$

changes Eq. (6.15) into

$$\dot{\varphi}_1 = \frac{1}{m\ell^2} \frac{p_1 - p_2 \cos(\varphi_1 - \varphi_2)}{1 + \sin^2(\varphi_1 - \varphi_2)}. \tag{6.17}$$

This is then used to transform Eq. (6.13) into

$$\begin{aligned}
\dot{\varphi}_2 &= \frac{1}{m\ell^2} \left[p_2 - \frac{p_1 \cos(\varphi_1 - \varphi_2) - p_2 \cos^2(\varphi_1 - \varphi_2)}{1 + \sin^2(\varphi_1 - \varphi_2)}\right] \\
&= \frac{1}{m\ell^2} \frac{p_2 + p_2 \sin^2(\varphi_1 - \varphi_2) - p_1 \cos(\varphi_1 - \varphi_2) + p_2 \cos^2(\varphi_1 - \varphi_2)}{1 + \sin^2(\varphi_1 - \varphi_2)} \\
&= \frac{1}{m\ell^2} \frac{2p_2 - p_1 \cos(\varphi_1 - \varphi_2)}{1 + \sin^2(\varphi_1 - \varphi_2)}.
\end{aligned} \tag{6.18}$$

Hence, with help of Eqs. (6.17) and (6.18) we can reevaluate the kinetic energy (6.8) to give

$$\begin{aligned}
T &= \frac{m\ell^2}{2}\left[2\dot{\varphi}_1^2 + \dot{\varphi}_2^2 + 2\dot{\varphi}_1\dot{\varphi}_2\cos(\varphi_1-\varphi_2)\right] \\
&= \frac{m\ell^2}{2}\left(\frac{1}{m\ell^2}\frac{1}{1+\sin^2(\varphi_1-\varphi_2)}\right)^2 \Big\{2\left[p_1 - p_2\cos(\varphi_1-\varphi_2)\right]^2 \\
&\quad + \left[2p_2 - p_1\cos(\varphi_1-\varphi_2)\right]^2 \\
&\quad + 2\left[p_1 - p_2\cos(\varphi_1-\varphi_2)\right]\left[2p_2 - p_1\cos(\varphi_1-\varphi_2)\right]\cos(\varphi_1-\varphi_2)\Big\} \\
&= \frac{1}{2m\ell^2}\frac{1}{\left[1+\sin^2(\varphi_1-\varphi_2)\right]^2}\Big\{p_1^2\left[2-\cos^2(\varphi_1-\varphi_2)\right] \\
&\quad + 2p_2^2\left[2-\cos^2(\varphi_1-\varphi_2)\right] - 2p_1p_2\cos(\varphi_1-\varphi_2)\left[2-\cos^2(\varphi_1-\varphi_2)\right]\Big\} \\
&= \frac{1}{2m\ell^2}\frac{2-\cos^2(\varphi_1-\varphi_2)}{\left[1+\sin^2(\varphi_1-\varphi_2)\right]^2}\Big\{p_1^2 + 2p_2^2 - 2p_1p_2\cos(\varphi_1-\varphi_2)\Big\} \\
&= \frac{1}{2m\ell^2}\frac{p_1^2 + 2p_2^2 - 2p_1p_2\cos(\varphi_1-\varphi_2)}{1+\sin^2(\varphi_1-\varphi_2)}.
\end{aligned} \tag{6.19}$$

In the very last step we made, again, use of the trigonometric property (6.16).

With the help of the kinetic energy (6.19) and the potential energy (6.9) we can write the Hamilton function $H(p_1, p_2, \varphi_1, \varphi_2)$ as

$$\begin{aligned}
H &= T + U \\
&= \frac{1}{2m\ell^2}\frac{p_1^2 + 2p_2^2 - 2p_1p_2\cos(\varphi_1-\varphi_2)}{1+\sin^2(\varphi_1-\varphi_2)} \\
&\quad + mg\ell\left[4 - 2\cos(\varphi_1) - \cos(\varphi_2)\right],
\end{aligned} \tag{6.20}$$

and this allows to formulate, finally, Hamilton's equations of motion:

$$\dot{\varphi}_i = \frac{\partial}{\partial p_i}H, \quad \dot{p}_i = -\frac{\partial}{\partial \varphi_i}H, \quad i = 1, 2. \tag{6.21}$$

Hence, we have to solve the following set of equations

$$\dot{\varphi}_1 = \frac{1}{m\ell^2}\frac{p_1 - p_2\cos(\varphi_1-\varphi_2)}{1+\sin^2(\varphi_1-\varphi_2)}, \tag{6.22a}$$

$$\dot{\varphi}_2 = \frac{1}{m\ell^2}\frac{2p_2 - p_1\cos(\varphi_1-\varphi_2)}{1+\sin^2(\varphi_1-\varphi_2)}, \tag{6.22b}$$

$$\dot{p}_1 = \frac{1}{m\ell^2}\frac{1}{1+\sin^2(\varphi_1-\varphi_2)}\Bigg[-p_1p_2\sin(\varphi_1-\varphi_2) \\ + \frac{p_1^2+2p_2^2-2p_1p_2\cos(\varphi_1-\varphi_2)}{1+\sin^2(\varphi_1-\varphi_2)}\cos(\varphi_1-\varphi_2)\sin(\varphi_1-\varphi_2)\Bigg] \\ - 2mg\ell\sin(\varphi_1), \tag{6.22c}$$

and

$$\dot{p}_2 = \frac{1}{m\ell^2}\frac{1}{1+\sin^2(\varphi_1-\varphi_2)}\Bigg[p_1p_2\sin(\varphi_1-\varphi_2) \\ - \frac{p_1^2+2p_2^2-2p_1p_2\cos(\varphi_1-\varphi_2)}{1+\sin^2(\varphi_1-\varphi_2)}\sin(\varphi_1-\varphi_2)\cos(\varphi_1-\varphi_2)\Bigg] \\ - mg\ell\sin(\varphi_2). \tag{6.22d}$$

In the following section we will discuss the numerical solution of Eqs. (6.22) with the help of the explicit RUNGE-KUTTA algorithm *e-RK-4* introduced in Sect. 5.3.

6.2 Numerical Solution

In a first step we recognize that Eqs. (6.22) are of the form

$$\dot{y} = F(y), \tag{6.23}$$

where $y \in \mathbb{R}^4$. Let us define

$$y = \begin{pmatrix} y_1 \\ y_2 \\ y_3 \\ y_4 \end{pmatrix} = \begin{pmatrix} \varphi_1 \\ \varphi_2 \\ p_1 \\ p_2 \end{pmatrix}, \tag{6.24}$$

and consequently

$$F(y) = \begin{pmatrix} f_1(y) \\ f_2(y) \\ f_3(y) \\ f_4(y) \end{pmatrix} = \begin{pmatrix} \dot{\varphi}_1 \\ \dot{\varphi}_2 \\ \dot{p}_1 \\ \dot{p}_2 \end{pmatrix}, \tag{6.25}$$

as defined in Eq. (6.22). We will, furthermore, introduce the time instances $t_n = n\Delta t$, $n \in \mathbb{N}$ and denote by $y_n = y(t_n) = (y_1^n, y_2^n, y_3^n, y_4^n)^T$. Since the function $F(y)$ of Eq. (6.25) does not depend explicitly on time t we reformulate the *e-RK-4* algorithm of Eq. (5.39) as

$$\begin{aligned}
Y_1 &= y_n, \\
Y_2 &= y_n + \frac{\Delta t}{2} F(Y_1), \\
Y_3 &= y_n + \frac{\Delta t}{2} F(Y_2), \\
Y_4 &= y_n + \Delta t F(Y_3), \\
y_{n+1} &= y_n + \frac{\Delta t}{6} \left[F(Y_1) + 2F(Y_2) + 2F(Y_3) + F(Y_4) \right].
\end{aligned} \tag{6.26}$$

Hence, the remaining challenge is to correctly implement the function $F(y) = [f_1(y), f_2(y), f_3(y), f_4(y)]^T$ according to Eqs. (6.22).

The following graphs discuss the dynamics (trajectories in φ- and p-space, as well as in configuration space) of the pendulum and for this purpose we defined the parameters $m = \ell = 1$ and $g = 9.8067$. The time step was chosen to be $\Delta t = 0.001$ and we calculated $N = 60000$ time steps.

We start with Fig. 6.2. The two masses numbered 1 and 2 are initially in the equilibrium position (solid circles). Both masses are pushed to the right but the push on mass 1 $[p_1(0) = 4.0]$ is much stronger than the one mass 2 experiences $[p_2(0) = 2.0]$. Thus, mass 2 is 'dragged' along in the process. This is made transparent by two 'snapshots' indicated by solid light gray circles and solid gray circles. The motion of the whole system is quite regular.

We proceed with Fig. 6.3. In this case mass 1 is displaced from its position by the initial angular displacement $\varphi_1 = 1.0$. This initial configuration is indicated by the solid circles numbered 1 and 2 representing the two point-masses. Mass 2 is then pushed to the right with $p_2(0) = 3.0$. In contrast to the previous situation mass 1 is now following mass 2 and the requirement that mass 1 remains on a circular trajectory centered around the point (0,2) in configuration space, Fig. 6.3c, results in a very lively trajectory of mass 2. Again two snapshots indicated by solid light gray circles and solid gray circles illustrate configurations of particular interest.

The situation illustrated by Fig. 6.4 is quite similar to the one already discussed in Fig. 6.2. Initially both masses are in the equilibrium position and then mass 2 is pushed to the right $[p_2(0) = 4.0]$. Thus, mass 1 is trailing behind. In contrast to the previous figure the trajectory of mass 2 will now be symmetric around the z-axis given enough time. Again, snapshots indicated by solid light gray circles and solid gray circles indicate interesting configurations.

The situation which resulted in Fig. 6.5 was quite similar to the one discussed in Fig. 6.4. The only difference is that mass 2 is now pushed more strongly to the right $[p_2(0) = 5.0]$. Of course, mass 1 is again dragging behind mass 2. In contrast to Fig. 6.4 the initial momentum of mass 2 is now sufficient to allow mass 2 to pass through the center of the inner mass' circular trajectory. Snapshots indicated by light gray solid circles and solid gray circles emphasize interesting configurations.

The situation shown in Fig. 6.6 differs from the one of Fig. 6.5 only by the initial condition for mass 2. It is now pushed even more strongly to the right $[p_2(0) = 6.5]$ and this initial momentum is sufficient to cause mass 1 to rotate around the point

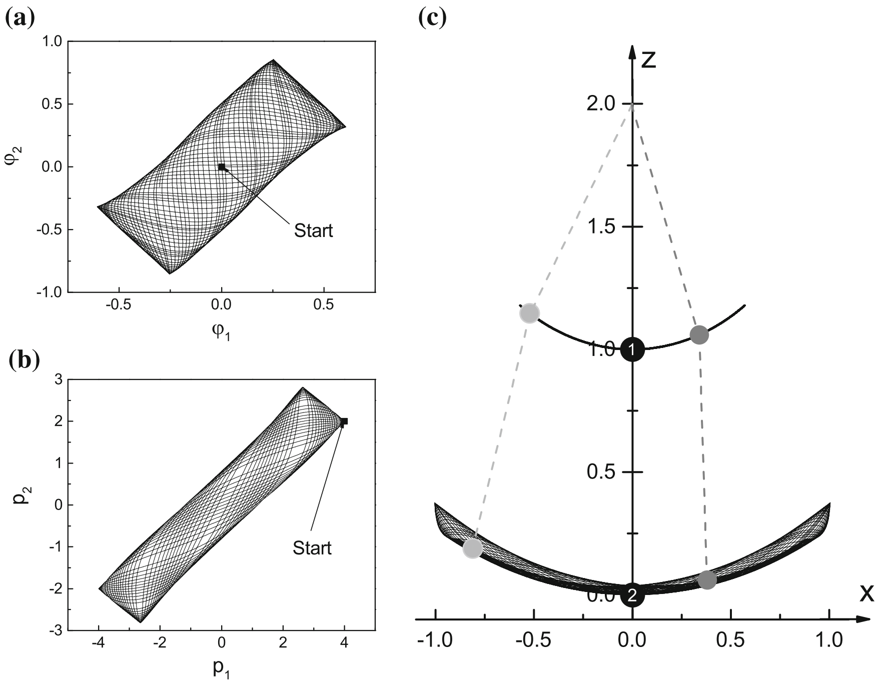

Fig. 6.2 Numerical solution of the double pendulum with initial conditions $\varphi_1(0) = \varphi_2(0) = 0.0$, $p_1(0) = 4.0$ and $p_2(0) = 2.0$. (**a**) Trajectory in φ-space, (**b**) trajectory in p-space, and (**c**) trajectory in local (x, z)-space. The *solid circles* numbered 1 and 2 represent the two masses in their initial configuration

(0,2). Nevertheless, mass 1 is permanently dragging behind mass 2. Two interesting configurations are depicted by snapshots (solid light gray circles and solid gray circles).

A comparison between trajectories as a result of different initial conditions reveals that the physical system is highly sensitive to the choice of the initial conditions $y_0 = [\varphi_1(0), \varphi_2(0), p_1(0), p_2(0)]^T$. For instance, consider Figs. 6.4, 6.5 and 6.6. In all three cases we chose y_0 in such a way that the initial angles $\varphi_1(0) = \varphi_2(0) = 0$ and the generalized momentum coordinate $p_1(0) = 0$. The only difference is that we used different values for the initial value of the second momentum coordinate p_2. However, the resulting dynamics of φ_1 versus φ_2 as well as p_1 versus p_2 are entirely different and so are the local (x, z)-space trajectories. Hence, the system is *chaotic*. In the following section we will briefly discuss a method designed to characterize chaotic behavior of physical systems [2, 3].

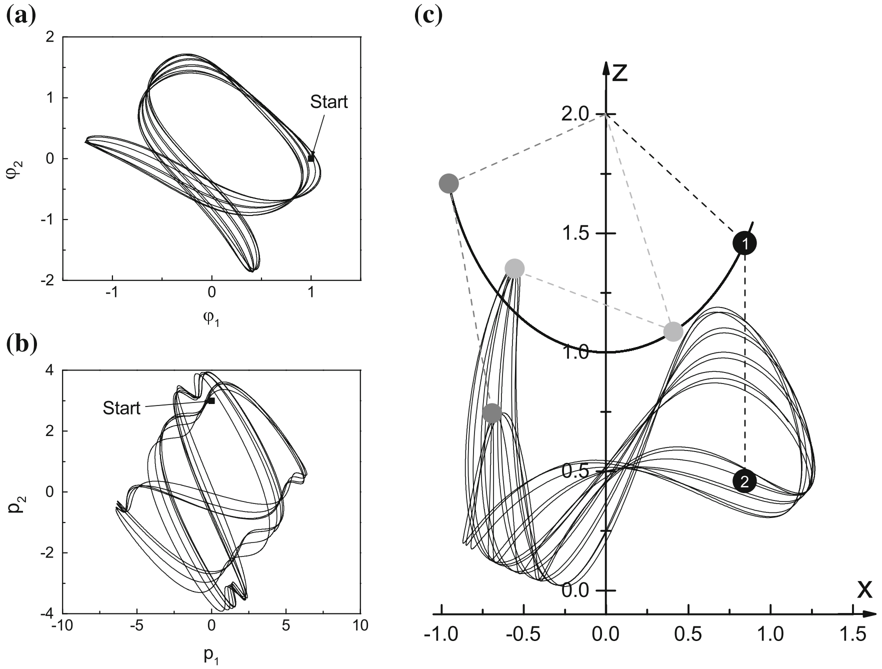

Fig. 6.3 Numerical solution of the double pendulum with initial conditions $\varphi_1(0) = 1.0$, $\varphi_2(0) = 0.0$, $p_1(0) = 0.0$ and $p_2(0) = 3.0$. (**a**) Trajectory in φ-space, (**b**) trajectory in p-space, and (**c**) trajectory in local (x, z)-space. The *solid circles* numbered 1 and 2 represent the two masses in their initial configuration

6.3 Numerical Analysis of Chaos

Let us introduce some basic notations. We consider a physical system with f degrees of freedom. Furthermore, let $q_1(t), \ldots, q_f(t)$ denote the generalized coordinates and $p_1(t), \ldots, p_f(t)$ denote the corresponding generalized momenta which allow a full characterization of the system. Consequently, the f-dimensional vector $q(t) = [q_1(t), q_2(t), \ldots, q_f(t)]^T$ describes a point in *configuration space* of the physical system. In case of a pendulum consisting of f point-masses connected in a similar fashion as the double pendulum discussed above, which corresponds to the particular case $f = 2$, the configuration space is constrained to values $\varphi_i \in (-\pi, \pi]$, $i = 1, \ldots, f$. This resembles an f-dimensional torus.

The $2f$-dimensional vector $x(t) = [q_1(t), \ldots, q_f(t), p_1(t), \ldots, p_f(t)]^T$ describes a point within the *phase space* of the physical system at some particular time t. The time evolution of a physical system is represented by its *phase space trajectory*. Note that the phase space trajectories $x(t)$ are differentiable with respect to t.

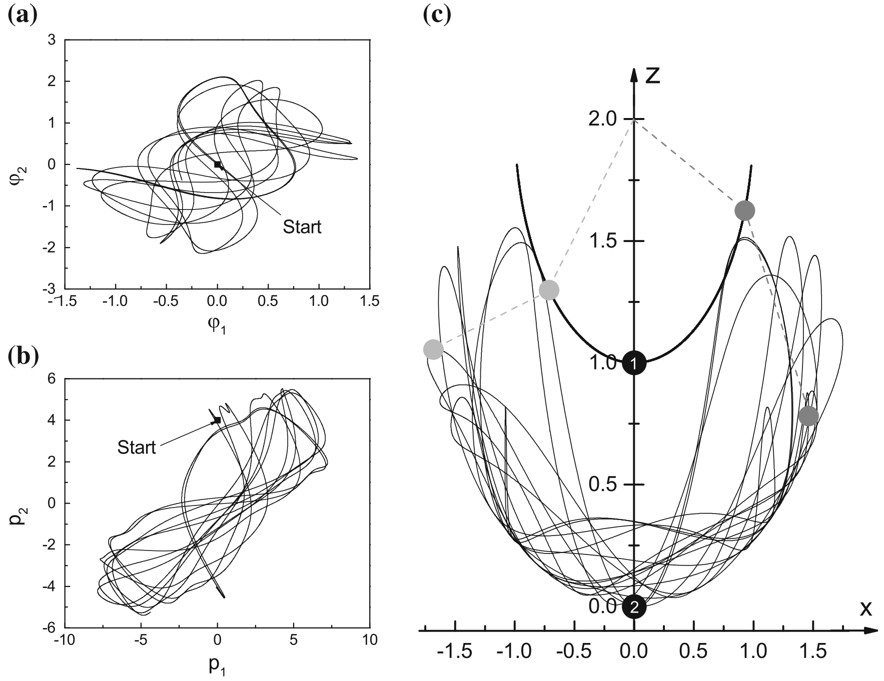

Fig. 6.4 Numerical solution of the double pendulum with initial conditions $\varphi_1(0) = \varphi_2(0) = 0.0$, $p_1(0) = 0.0$ and $p_2(0) = 4.0$. (**a**) Trajectory in φ-space, (**b**) trajectory in p-space, and (**c**) trajectory in local (x, z)-space. The *solid circles* numbered 1 and 2 represent the two masses in their initial configuration

We define an *autonomous system* as a system which is *time-invariant*, i.e. the HAMILTON function $H(x, t)$ does not depend explicitly on time t, $H(x, t) \equiv H(x)$. Hence, a physical system is referred to as autonomous if the HAMILTON function $H(x, t)$ of the system obeys the relation

$$\frac{\partial}{\partial t} H(x, t) = \frac{\partial}{\partial t} H(x) = 0 \; . \tag{6.27}$$

In other words, energy is conserved.

An autonomous system is referred to as *integrable* if it has f independent invariants $I_1, \ldots, I_f$

$$I_j(x) = I_j = \text{const}, \quad j = 1, \ldots, f \; . \tag{6.28}$$

One of these is the energy. Each particular invariant I_j reduces the dimension of the manifold on which the phase space trajectories can propagate. Hence, an integrable system propagates on an f-dimensional subspace of the $2f$-dimensional phase space.

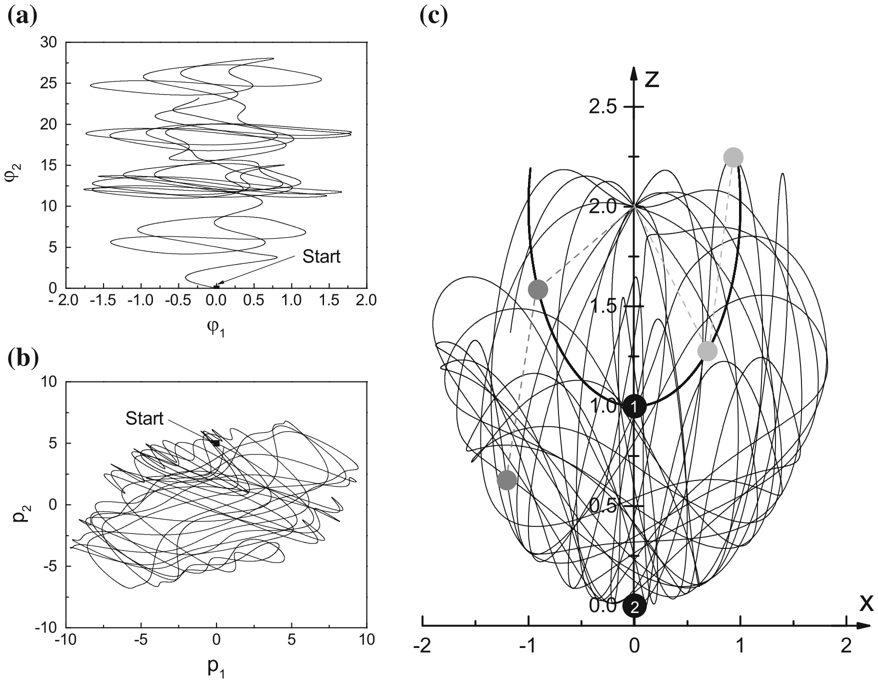

Fig. 6.5 Numerical solution of the double pendulum with initial conditions $\varphi_1(0) = \varphi_2(0) = 0.0$, $p_1(0) = 0.0$ and $p_2(0) = 5.0$. (**a**) Trajectory in φ-space, (**b**) trajectory in p-space, and (**c**) trajectory in local (x, z)-space. The *solid circles* numbered 1 and 2 represent the two masses in their initial configuration

We note that a one-dimensional autonomous system is integrable since the conservation of energy delivers the required invariant.

Non-integrable systems can show chaotic behavior. In such a case one can only obtain special solutions of the system by means of analytical methods. On the other hand, the formulation of a general solution is only possible with the aid of numerical methods. From all this the question arises whether or not these solutions are stable. In order to study this stability problem let us introduce the concept of LYAPUNOV stability [4].

Given the initial conditions x_0 and x_0' we obtain at time t the phase space coordinates $x(t) = \varphi_t(x_0)$ and $x'(t) = \varphi_t(x_0')$ as a solution of Hamilton's equations of motion. Here $\varphi_t(x_0)$ denotes the flow of the Hamiltonian system as defined in Sect. 5.4. A solution is referred to as LYAPUNOV stable if

$$\forall \varepsilon > 0 \, \exists \delta(\varepsilon) > 0 : \forall x_0' : |x_0 - x_0'| < \delta \Rightarrow |\varphi_t(x_0) - \varphi_t(x_0')| < \varepsilon, \quad \forall t > 0 \, . \tag{6.29}$$

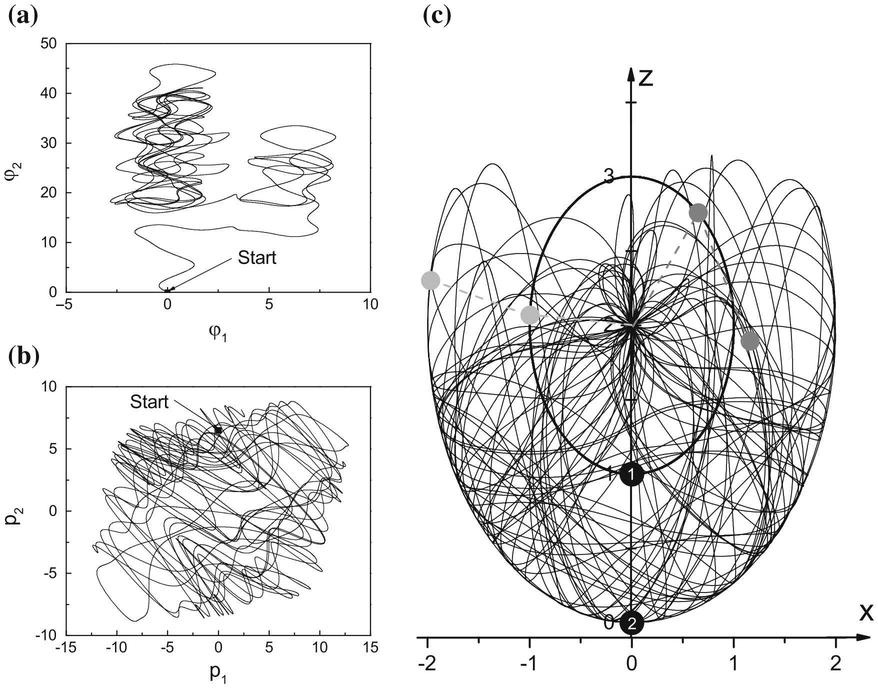

Fig. 6.6 Numerical solution of the double pendulum with initial conditions $\varphi_1(0) = \varphi_2(0) = 0.0$, $p_1(0) = 0.0$ and $p_2(0) = 6.5$. (**a**) Trajectory in φ-space, (**b**) trajectory in p-space, and (**c**) trajectory in configuration space. The *solid circles* numbered 1 and 2 represent the two masses in their initial configuration

In words: The trajectory which corresponds to the perturbed initial condition x_0' stays within a tube of radius ε around the unperturbed trajectory $\varphi_t(x_0)$ *for all* $t > 0$ if the solution is LYAPUNOV stable.

This definition suggests the introduction of the so called LYAPUNOV length $d(t)$. It is defined as the distance given by the Euclidean norm $\|\varphi_t(x_0) - \varphi_t(x_0')\|$ in phase space between two trajectories $\varphi_t(x_0)$ and $\varphi_t(x_0')$ corresponding to different initial conditions x_0 and x_0'.

Asymptotically stable solutions tend to *attract* trajectories from their neighborhood. Hence they are referred to as *attractors*.

Furthermore, let us define a *periodic orbit* as a trajectory for which one can find a time t such that

$$\varphi_t(x) = x, \tag{6.30}$$

for all x.

In order to find an answer to the question whether or not the solutions of non-integrable systems are stable we introduce the method of POINCARÉ maps. The idea is to reduce the investigation of the complete $2f$-dimensional phase space trajectory $x(t) = \varphi_t(x_0)$ to the investigation of its *intersection* points through a plane Σ which is transverse to the flow of the system. This plane is a subspace of dimension $2f-1$ and is commonly referred to as Poincaré section [1]. The transversality of the Poincaré section Σ means that periodic flows intersect this section and do not flow parallel to or within it.

Consider a trajectory which is bound to a finite domain, i.e. it does not tend to infinity in some phase space coordinate. In this case it is possible to define the Poincaré section in such a way that the trajectory will intersect this section not only once but several times. A Poincaré map is the mapping of one intersection point P onto the next intersection point P'.

Let us substantiate this idea: we consider the initial condition x_0 for which the trajectory is periodic. We choose the initial time $t = 0$ in such a way that $x_0 \in \Sigma$, where Σ is the Poincaré section. We suppose that after a time $\tau(x_0)$ the trajectory intersects the Poincaré section again. Note that we denoted $\tau \equiv \tau(x_0)$ in order to emphasize that the recurrence time will depend on the initial condition x_0. Since we demanded that the trajectory which starts in x_0 is periodic, we deduce that it intersects the Poincaré section at some point $\varphi_{\tau(x_0)}(x_0) = x_0$. We consider now a slightly perturbed initial condition $x' \in U(x_0)$, where $U(x_0)$ is referred to as the *neighborhood* of x_0. In this case the trajectory will in general not be periodic, and the next intersection point $\varphi_{\tau(x')}(x') \neq x'$. The mapping from one intersection point x' onto the next intersection point $\varphi_{\tau(x')}(x')$ is called the Poincaré map $P(x') = \varphi_{\tau(x')}(x')$. We note that the particular point x_0 is a fixed point of this mapping, $P(x_0) = x_0$. Furthermore, we note that if $x' \in U(x_0)$ we will have $P(x') \in U_1(x_0)$, where $U_1(x_0)$ is the neighborhood of first return, see Fig. 6.7.

Let us give an example: in case of the double pendulum we have four generalized coordinates which, with the help of conservation of energy, are constrained to

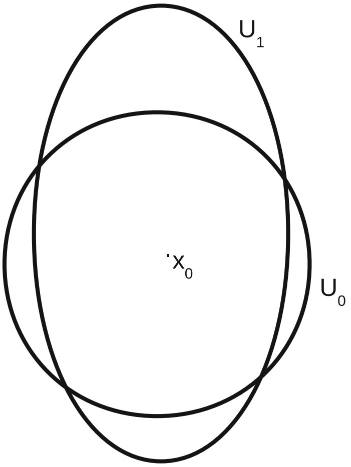

Fig. 6.7 Schematic illustration of the neighborhood $U_0(x_0)$ and the neighborhood of first return $U_1(x_0)$

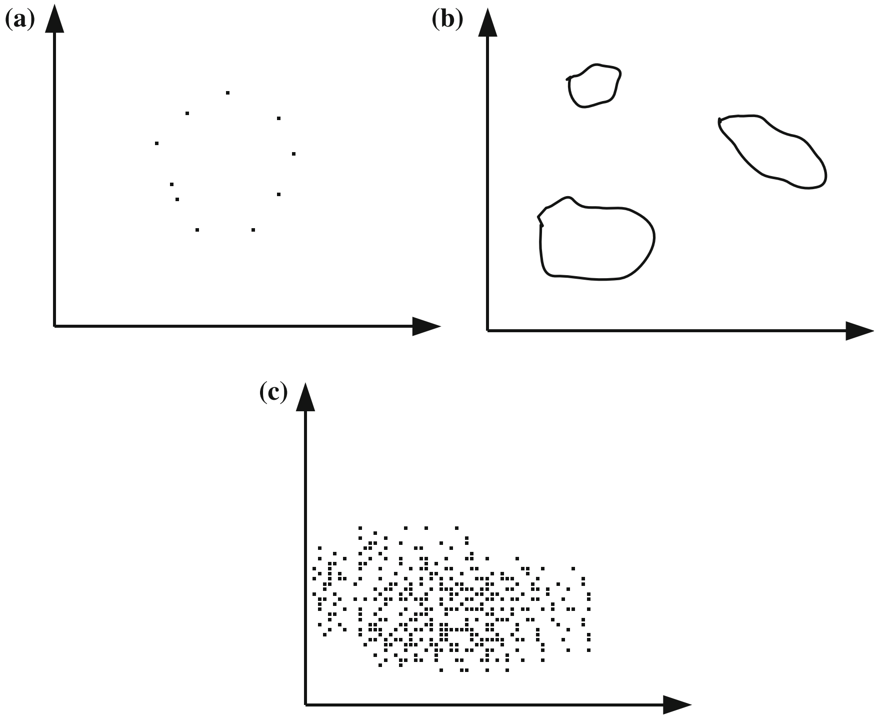

Fig. 6.8 Schematic illustration of the three types of Poincaré plots as discussed in the text. (**a**) Finite number of intersection points, (**b**) infinite number of intersection points which, however, form closed lines, (**c**) space-filling and, consequently, chaotic behavior

a three-dimensional manifold within the four-dimensional phase space. Since the investigation of these three dimensional trajectories is very complex we consider a two-dimensional section. For instance, the coordinates $[\varphi_1(t), p_1(t)]^T$ can be 'measured' whenever $\varphi_2(t) = 0$ and $p_2 > 0$. Thus, the system's state is registered whenever the second pendulum crosses the vertical plane from the left hand side. In the particular case that the acceleration $g = 0$ we note that the system is integrable: We deduce from Eq. (6.9) that the potential energy $U = 0$ and the Lagrange function is independent of the actual positions x_1, z_1, x_2, z_2 and depends only on the respective velocities. This means that the angular momentum is conserved which gives us, together with the conservation of energy, a second invariant. Hence the system moves on a two-dimensional manifold in the four dimensional phase space.

We discuss now some of the most typical scenarios for Poincaré plots. Note that this discussion is not restricted to the case of the double pendulum. In case of integrable systems one distinguishes between two different scenarios: first, the set of intersection points $(\eta_1, \eta_2, \ldots, \eta_N)$ is finite. In the second, more general case, the dimension N of the set of intersection points is infinite. In both cases the intersection points form one-dimensional lines which do not have to be connected.

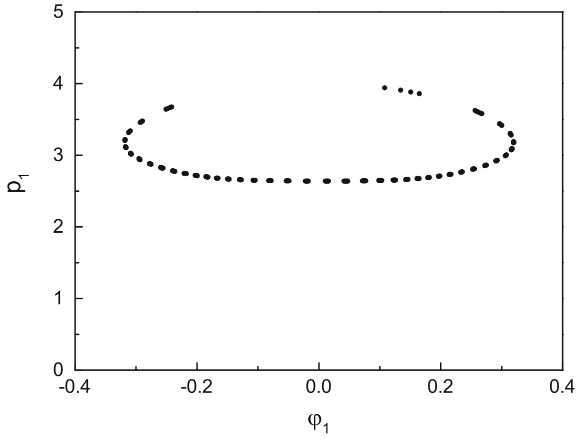

Fig. 6.9 POINCARÉ plot of the double pendulum with initial conditions $\varphi_1(0) = \varphi_2(0) = 0.0$, $p_1(0) = 4.0$ and $p_2(0) = 2.0$. It corresponds to the situation discussed in Fig. 6.2

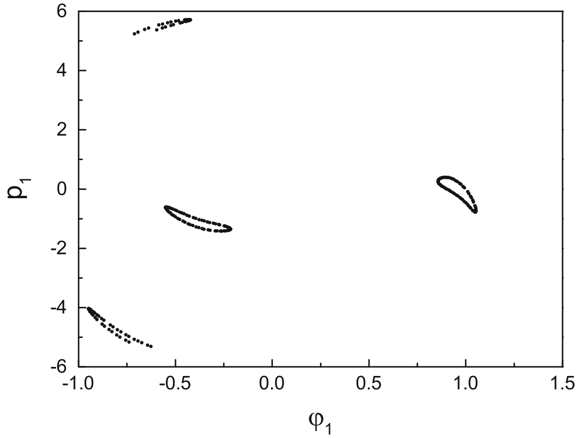

Fig. 6.10 POINCARÉ plot of the double pendulum with initial conditions $\varphi_1(0) = 1.0, \varphi_2(0) = 0.0$, $p_1(0) = 0.0$ and $p_2(0) = 3.0$. It corresponds to the situation discussed in Fig. 6.3

Figure 6.8 discusses this schematically. However, if the system is non-integrable, a third scenario is possible: chaotic behavior. In this case the intersection points seem to be randomly distributed on the two dimensional plane and one observes space-filling behavior. This is illustrated schematically in Fig. 6.8c. Whether one observes chaotic behavior or not depends on the choice of the initial conditions.

In Figs. 6.9, 6.10 and 6.11 we present POINCARÉ plots of the double pendulum. The plots were obtained with help of the method discussed above, i.e. $\varphi_2 = 0$ and $p_2 > 0$. Again, we set $m = \ell = 1$ and $g = 9.8067$. The time step was chosen to be $\Delta t = 0.001$ and we calculated $N = 36 \times 10^4$ time steps. In Figs. 6.9 and 6.11 we observe regular behavior as it was illustrated in Fig. 6.8b. In Fig. 6.10 the points are space filling and, consequently, chaotic behavior is observed in this particular case. Keeping in mind that this particular POINCARÉ plot refers to the initial value problem of Fig. 6.4 we conclude that all problems of this series, i.e. Figs. 6.4, 6.5 and 6.6, are non-integrable and chaotic.

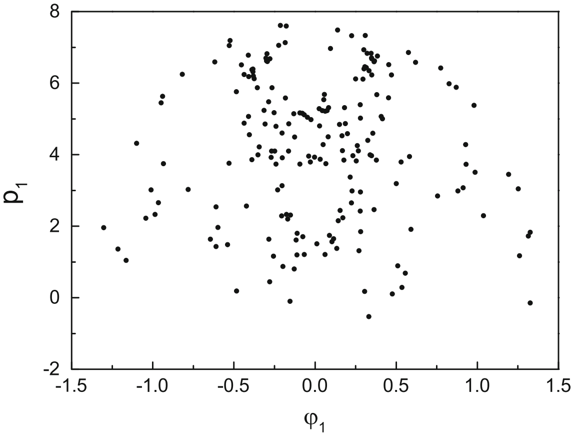

Fig. 6.11 POINCARÉ plot of the double pendulum with initial conditions $\varphi_1(0) = \varphi_2(0) = 0.0$, $p_1(0) = 0.0$ and $p_2(0) = 4.0$. It corresponds to the situation discussed in Fig. 6.4

Summary

The dynamics of the double pendulum is described by a system of four ordinary first order differential equations. It is a typical initial value problem and, thus, the methods introduced in Chap. 5 are all candidates to find a numerical solution. Here we concentrated on the explicit RUNGE-KUTTA algorithm *e-RK-4* of Sect. 5.3. Solutions were studied in detail for several classes of initial conditions. One of the results was that rather small changes of the initial conditions could result in rather strong, chaotic reactions of the outer mass. This triggered the obvious question about the stability of a numerical analysis and of physical dynamics in general. While the stability of numerical methods has already been discussed in Chap. 1 we focused here on the chaotic behavior of Hamiltonian systems. Consequently, a short section on the numerical analysis of chaos was added. It contained the most important concepts and in particular the concept of the LYAPUNOV stability which allowed to classify the stability of a phase space trajectory. Finally, the importance of POINCARÉ plots in recognizing whether a system is integrable or non-integrable was explained. Non-integrable systems can develop chaotic behavior. Thus, POINCARÉ plots are an important tool to study chaos in mechanics.

Problems

1. Verify HAMILTON's equations of motion derived in Sect. 6.1. Implement the *e-RK-4* algorithm discussed in Sects. 5.3 and 6.2 to integrate the equations of motion. Plot the trajectories for various initial conditions. Use the examples illustrated in Sect. 6.2 to check the code.

2. Produce POINCARÉ plots by plotting (φ_1, p_1) whenever $\varphi_2 = 0$ and $p_2 > 0$. The condition $\varphi_2 = 0$ is substituted by $|\varphi_2| < \varepsilon$ in the numerically realization. Note that if the points are space filling the dynamics are chaotic, as discussed in Sect. 6.3. Try to find different initial conditions which result in regular behavior and different initial conditions which produce chaotic dynamics.
3. Let $x(t) = [\varphi_1(t), \varphi_2(t), p_1(t), p_2(t)]^T$ and $x'(t) = [\varphi_1'(t), \varphi_2'(t), p_1'(t), p_2'(t)]^T$ be two trajectories which correspond to different initial conditions x_0 and x_0'. In this case the LYAPUNOV distance is defined as

$$d(t) = \sqrt{[\varphi_1(t) - \varphi_1'(t)]^2 + [\varphi_2(t) - \varphi_2'(t)]^2 + [p_1(t) - p_1'(t)]^2 + [p_2(t) - p_2'(t)]^2}.$$

Plot the LYAPUNOV distance $d(t)$ as a function of time t for two different initial conditions.

References

1. Scheck, F.: Mechanics, 5th edn. Springer, Berlin (2010)
2. McCauley, J.L.: Chaos. Dynamics and Fractals. Cambridge University Press, Cambridge, UK (1994)
3. Schuster, H.G., Just, W.: Deterministic Chaos, 4th edn. Wiley, New York (2006)
4. Lyapunov, A.M.: The General Problem of Stability of Motion. Taylor and Francis, London (1992)

Chapter 7
Molecular Dynamics

7.1 Introduction

It is the aim of many branches of research in physics to describe macroscopic observable properties of matter on the basis of microscopic dynamics. However, a description of the simultaneous motion of a large number of interacting particles is in most cases not feasible by analytic methods. Moreover, if the interaction between the particles is strong a description is particularly difficult. Within the framework of statistical mechanics one tries to remedy these difficulties by employing some simplifying assumptions and by treating the system from a statistical point of view. However, most of these simplifying assumptions are only justified within certain limits, such as the *weak coupling limit* or the *low density limit*. Nevertheless, it is not easy to establish how the solutions acquired are influenced by these limits and how the physics beyond these limits can be perceived. This makes the necessity of numerical solutions quite apparent. There are essentially two methods to determine physical quantities over a restricted set of states, namely *molecular dynamics* [1–3] and *Monte Carlo* methods. The technique of molecular dynamics will be discussed within this chapter while an introduction into some basic features of Monte Carlo algorithms is postponed to the second part of this book.

We strictly focus on a particular sub-field of molecular dynamics, namely on *classical molecular dynamics*, i.e. the treatment of classical physical systems. Extensions to quantum mechanical systems, which are commonly referred to as quantum molecular dynamics, will not be discussed here.

7.2 Classical Molecular Dynamics

We consider N particles with positions $r_i \equiv r_i(t)$, velocities $v_i \equiv v_i(t) = \dot{r}_i(t)$ and masses m_i, where $i = 1, 2, \ldots, N$. We note that r_i and v_i are vectors of the same dimension. We can write NEWTON's equations of motion as

B. A. Stickler and E. Schachinger, *Basic Concepts in Computational Physics*,
DOI: 10.1007/978-3-319-02435-6_7, © Springer International Publishing Switzerland 2014

$$m_i \ddot{r}_i = f_i(r_1, r_2, \dots, r_N), \tag{7.1}$$

where we introduced the forces $f_i \equiv f_i(r_1, r_2, \dots, r_N)$. Again, we note that the forces f_i are vectors of the same dimension as r_i and v_i. We specify the forces f_i by demanding them to be *conservative*. Thus, we write

$$f_i(r_1, r_2, \dots, r_N) = -\nabla_i U(r_1, r_2, \dots, r_N), \tag{7.2}$$

where we note that ∇_i is the gradient pertaining to the spatial components of the i-th particle and $U(r_1, r_2, \dots, r_N)$ is some potential which we will abbreviate with $U \equiv U(r_1, r_2, \dots r_N)$. We then specify this potential U as the sum of two-particle interactions U_{ij} and some external potential U_{ext} as, for instance, the gravitational field or a constant electric potential applied to the system:

$$U = \frac{1}{2} \sum_i \sum_{j \neq i} U_{ij} + U_{ext}. \tag{7.3}$$

In our discussion of the two-body problem (Appendix A) and, in particular, of the KEPLER problem in Chap. 4 we considered a central force, which was proportional to $-1/r$. Due to the conservation of angular momentum, it was convenient to introduce an effective potential U_{eff} as the sum of an attractive and repulsive part as it was defined in Eq. (4.5) and illustrated in Fig. 4.1. In contrast, in molecular dynamics the most prominent two-body interaction potential is known as the LENNARD-JONES potential. It is of the form

$$U(|r|) = 4\sigma \left[\left(\frac{\varepsilon}{|r|} \right)^{12} - \left(\frac{\varepsilon}{|r|} \right)^{6} \right], \tag{7.4}$$

where ε and σ are real parameters and $|r|$ is the distance between two particles. The significance of the parameters ε and σ as well as the form of $U(|r|)$ defined by Eq. (7.4) is illustrated in Fig. 7.1. The LENNARD-JONES potential was particularly developed to model the interaction between neutral atoms or molecules. The repulsive term, which is proportional to $|r|^{-12}$, describes the PAULI repulsion while the attractive $|r|^{-6}$ term accounts for attractive VAN DER WAALS forces.

We introduce the distance between particles i and j via

$$r_{ij} = |r_i - r_j| = |r_j - r_i| = r_{ji}, \tag{7.5}$$

and define the two-body potential

$$U_{ij} = U(r_{ij}), \tag{7.6}$$

where U is approximated by the LENNARD-JONES potential (7.4). Furthermore, we deduce from Eq. (7.4) that

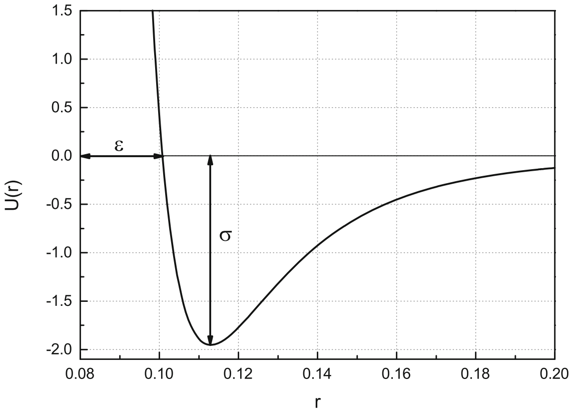

Fig. 7.1 Illustration of the LENNARD-JONES potential, Eq. (7.4). σ describes the depth of the potential well and ε is the position of the root of the LENNARD-JONES potential

$$f(|r|) = -\nabla_r U(|r|) = \frac{24\sigma}{|r|^2}\left[2\left(\frac{\varepsilon}{|r|}\right)^{12} - \left(\frac{\varepsilon}{|r|}\right)^{6}\right] r, \tag{7.7}$$

where we keep in mind that r is a vector. Hence, we write the forces f_i which appear in NEWTON's equations of motion (7.1) with the help of (7.3) in the form

$$\begin{aligned} f_i &= -\nabla_i U \\ &= -\nabla_i \left(\frac{1}{2}\sum_k \sum_{l\neq k} U_{kl} + U_{ext}\right) \\ &= -\sum_{j\neq i} \nabla_i U_{ij} - \nabla_i U_{ext} \\ &= \sum_{j\neq i} f(r_{ij}) + f_{ext}^i \\ &= \sum_{j\neq i} f_{ij} + f_{ext}^i, \end{aligned} \tag{7.8}$$

where we implicitly defined the external force f_{ext}^i acting on particle i and the two particle forces f_{ij} acting between particle i and j. Let us introduce the vectors $R = (r_1, r_2, \dots, r_N)^T$, $V = (v_1, v_2, \dots, v_N)^T = \dot{R}$ and $F = (f_1/m_1, f_2/m_2, \dots, f_N/m_N)^T$ in order to rewrite (7.1) as

$$\ddot{R} = F, \tag{7.9}$$

which is equivalent to two first order ordinary differential equations

$$\begin{pmatrix} \dot{R} \\ \dot{V} \end{pmatrix} = \begin{pmatrix} V \\ F \end{pmatrix}. \tag{7.10}$$

Note that (7.10) is of the form (5.1). Let us introduce now a more convenient notation which will help in the discussion of some numerical methods which have been developed to solve this initial value problem. We regard discrete time instances $t_k = k\Delta t$, where $k \in \mathbb{N}_0$ and function values at these discrete time instances t_k are denoted by a subscript k, as for instance $R_k \equiv R(t_k)$.

(i) In a first approximation we apply the symplectic EULER method [see Eq. (4.41)] to Eq. (7.10) and obtain

$$\begin{pmatrix} R_{k+1} \\ V_{k+1} \end{pmatrix} = \begin{pmatrix} R_k \\ V_k \end{pmatrix} + \begin{pmatrix} V_{k+1} \\ F_k \end{pmatrix} \Delta t. \tag{7.11}$$

Inserting the second into the first equation results in

$$R_{k+1} = R_k + V_k \Delta t + F_k \Delta t^2. \tag{7.12}$$

The velocity V_k at time t_k is then approximated by the backward difference derivative (2.10b) and we find the recursion relation:

$$R_{k+1} = 2R_k - R_{k-1} + F_k \Delta t^2. \tag{7.13}$$

We note that it is only valid for $k \geq 1$. The initialization step necessary to complete the analysis is found by expanding R_1 in a TAYLOR series up to second order:

$$R_1 = R_0 + \Delta t V_0 + \frac{1}{2} F_0 \Delta t^2. \tag{7.14}$$

This method is referred to as the STRÖMER-VERLET algorithm. Note that Eq. (7.14) serves as the initialization of the sequence of time steps. Furthermore, we remark that Eq. (7.13) could have also been obtained using the central difference derivative to approximate the second time derivative in Eq. (7.1):

$$\ddot{R}_k \approx \frac{R_{k+1} - 2R_k + R_{k-1}}{\Delta t^2} = F_k. \tag{7.15}$$

In summary, the VERLET or STÖRMER–VERLET algorithm is defined by the following set of equations:

$$\begin{aligned} R_{k+1} &= 2R_k - R_{k-1} + F_k \Delta t^2, \qquad k \geq 1, \\ R_1 &= R_0 + \Delta t V_0 + \frac{1}{2} F_0 \Delta t^2. \end{aligned} \tag{7.16}$$

(ii) We employ the central rectangular rule of integration (Sect. 3.2) in order to obtain approximations which are formally equivalent to Eq. (5.11). In particular, we obtain from Eq. (7.10):

$$R_{k+1} = R_k + V_{k+\frac{1}{2}} \Delta t. \tag{7.17}$$

We note that the value of $V_{k+\frac{1}{2}}$ is yet undetermined. However, it can be determined in a similar fashion via

$$V_{k+\frac{1}{2}} = V_{k-\frac{1}{2}} + F_k \Delta t. \tag{7.18}$$

This method which is referred to as the *leap-frog* algorithm is initialized by the relation

$$V_{\frac{1}{2}} = V_0 + \frac{\Delta t}{2} F_0. \tag{7.19}$$

Equation (7.19) can also be obtained by expanding $V_{\frac{1}{2}}$ in a TAYLOR series up to first order around the point $t_0 = 0$ and by noting that $\dot{V}_k = F_k$. In summary we write the leap-frog algorithm as

$$\begin{aligned} R_{k+1} &= R_k + V_{k+\frac{1}{2}} \Delta t, \\ V_{k+\frac{1}{2}} &= V_{k-\frac{1}{2}} + F_k \Delta t, \\ V_{\frac{1}{2}} &= V_0 + \frac{1}{2} F_0 \Delta t. \end{aligned} \tag{7.20}$$

(iii) A third, very elegant alternative is the so-called *velocity* VERLET algorithm. We expand R_{k+1}:

$$R_{k+1} = R_k + V_k \Delta t + \frac{1}{2} F_k \Delta t^2. \tag{7.21}$$

This equation allows to calculate the spatial coordinates at time t_{k+1} if R_k and V_k are given. Note that $F_k = F(R_k)$ is completely determined by the positions R_k. Nevertheless, we need one more relation in order to determine the velocities at times t_{k+1}. Again, we expand V_{k+1} in a TAYLOR series, however, we approximate the remainder by the arithmetic mean between t_k and t_{k+1}:

$$V_{k+1} = V_k + \frac{1}{2} \left(F_k + F_{k+1} \right) \Delta t. \tag{7.22}$$

The strategy is clear: we calculate the positions R_{k+1} from Eq. (7.21) for given values of R_k and V_k. With the help of R_{k+1} we compute F_{k+1}, which is then inserted into Eq. (7.22) which determines V_{k+1}. In summary, the complete algorithm of the velocity VERLET method is defined by the steps:

$$
\begin{aligned}
R_{k+1} &= R_k + V_k \Delta t + \frac{1}{2} F_k \Delta t^2, \\
V_{k+1} &= V_k + \frac{1}{2} \left(F_k + F_{k+1} \right) \Delta t. \qquad (7.23)
\end{aligned}
$$

We note some properties of these methods. The Verlet algorithm of Eq. (7.16) is time invariant (symmetry under the transformation $\Delta t \to -\Delta t$), hence reversible. This is a direct consequence of its relation to the symplectic Euler method. Moreover, the positions R_k obtained with this method are highly accurate, however, the procedure suffers under an inaccurate approximation of the velocities V_k. This shortcoming is clearly remedied by the leap-frog algorithm (7.20) or the velocity Verlet algorithm (7.23). However, these methods are not time invariant. Hence, one has to decide whether or not very accurate values for the velocities are required for the problem at hand. In many cases the velocity Verlet algorithm is the most popular choice.

In the following section we discuss some numerical details to be considered when implementing the routine.

7.3 Numerical Implementation

The rough structure of a molecular dynamics code consists of three crucial steps, namely

- Initialization,
- start simulation and equilibrate,
- continue simulation and store results.

In the following we discuss some of the most important subtleties associated with these three parts. In particular we will focus on the choice of appropriate boundary conditions and on the choice of the scales of characteristic quantities.

Boundary Conditions

Basically, there are two possibilities: (i) The system is of finite size and the implementation of boundary conditions might be straightforward. For instance, let us assume that we regard N particles within a finite box of reflecting boundaries, we simply propagate the particle-coordinates in time and if a particle tries to leave the box, we correct its trajectory according to a reflection law. The velocity is adjusted accordingly. This is illustrated in Fig. 7.2 for a two-dimensional case and the particular situation that the particle is reflected from the right hand boundary of the box. The corresponding equations read

Fig. 7.2 Illustration of the reflection principle for a box of finite dimension with reflecting boundaries

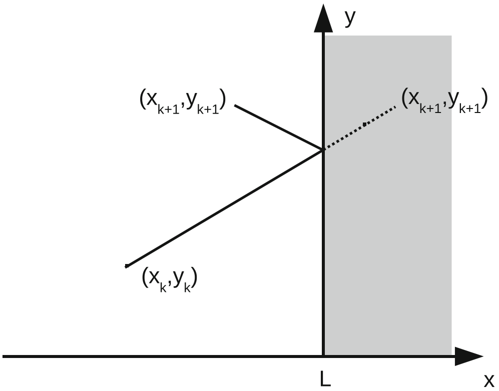

$$r_{k+1} = \begin{pmatrix} x_{k+1} \\ y_{k+1} \end{pmatrix} = \begin{pmatrix} L - (\tilde{x}_{k+1} - L) \\ \tilde{y}_{k+1} \end{pmatrix}, \tag{7.24}$$

and

$$v_{k+1} = \begin{pmatrix} v_{k+1,x} \\ v_{k+1,y} \end{pmatrix} = \begin{pmatrix} -\tilde{v}_{k+1,x} \\ \tilde{v}_{k+1,y} \end{pmatrix}. \tag{7.25}$$

Here L denotes the length of the box and $\tilde{x}_{k+1}$, $\tilde{y}_{k+1}$, $\tilde{v}_{k+1,x}$ and $\tilde{v}_{k+1,y}$ are the positions and velocities one would have obtained in the absence of the boundary, see Fig. 7.2.

(ii) The system is not confined. Then the situation is entirely different. Of course, one could approximate the infinite volume by a large but finite volume. In such a case the influence of a constraint to finite size is usually not negligible. The induced errors are referred to as *finite volume effects*. A very popular choice are so called *periodic boundary conditions* which means that a finite system is surrounded by an infinite number of completely identical replicas of the system, where the forces are allowed to act across the boundaries. Because of this, calculating the force on one particle requires the evaluation of an infinite sum. This is numerically not manageable and we have to find ways to truncate the sum. For instance, it might be a good approximation to restrict the sum to nearest-neighbor cells. However, the applicability of such an approach highly depends on the properties of the system under investigation and, in particular, on the range of the interaction potential. In case of a LENNARD-JONES potential the quantity defining the range of the interaction potential is ε, see Fig. 7.1.

If a particle leaves the box, it enters the box at the same time on the opposite side. More generally, due to the requirement of identical replicas, we have for all observables $O(r)$ that $O(r + nK) = O(r)$, where r lies within the central box, K is a lattice vector pointing to one of the neighboring cells and $n \in \mathbb{N}_0$.

There is another crucial point concerning periodic boundary conditions. In case of a closed system, the system is definitely at rest. However, if periodic boundary conditions are imposed it is possible that the particles move with constant velocity from one cell to another, which, in our case, resembles circling trajectories. This is definitely not desirable since the total velocity is a measure of the kinetic energy and therefore of the temperature of the system. However, one can *shift* the total velocity in order to remedy this problem. In particular, if

$$v_{tot} = \sum_{i=1}^{N} v_i \neq 0, \tag{7.26}$$

the shift

$$v_i' = v_i - \frac{1}{N} v_{tot}, \tag{7.27}$$

yields the desired result. We note that in case that all masses are identical, i.e. $m_1 = m_2 = \cdots = m_N \equiv m$, this is equivalent to $p_{tot} = m v_{tot} = 0$.

In conclusion, we remark that the choice of boundary conditions is not the only item to be considered in the definition of the system. Another quite crucial point might be the size of the box. If an infinite system is modeled using finite systems, the dimension of the box *must* fairly exceed the mean free path of the particles. Otherwise, the influence of the boundaries is going to perturb significantly the outcome of our numerical experiment.

Initialization and Equilibration

We remember from statistical physics [4] that every degree of freedom in a classical system contributes $k_B T/2$ to the total kinetic energy. Here k_B is BOLTZMANN's constant and T is the temperature. If we regard N particles, which move in a d-dimensional space, we have $d(N-1)$ degrees of freedom, if we demand that $v_{tot} = 0$. Hence, we have

$$E_{kin} = \frac{1}{2} \sum_{i=1}^{N} m_i v_i^2 = \frac{d(N-1)}{2} k_B T, \tag{7.28}$$

which gives a relation from which we can determine the temperature of the system:

$$k_B T = \frac{1}{d(N-1)} \sum_{i=1}^{N} m_i v_i^2. \tag{7.29}$$

However, in many applications the system is supposed to be simulated at a *given* temperature, i.e. the temperature T is an input rather than an output parameter and is supposed to stay constant during the simulation. We can control the temperature by rescaling the velocities and this might be necessary at several times during the simulation in order to guarantee a constant temperature. We define

$$v_i' = \lambda v_i, \tag{7.30}$$

where λ is a rescaling parameter. The temperature associated with the velocities v_i' is given by

$$k_B T' = \frac{\lambda^2}{d(N-1)} \sum_{i=1}^{N} m_i v_i^2. \tag{7.31}$$

This allows to determine how to choose λ in order to obtain a certain temperature T':

$$\lambda = \sqrt{\frac{d(N-1)k_B T'}{2E_{kin}}}. \tag{7.32}$$

We note that if the total velocity, which is the sum of all velocities v_i, is zero, the total velocity corresponding to the rescaled velocities v_i' is also equal to zero since

$$\sum_{i=1}^{N} v_i' = \lambda \sum_{i=1}^{N} v_i = 0. \tag{7.33}$$

This ensures that rescaling of the velocities does not induce a bias.

The choice of the initial conditions highly influences the time the system needs to reach thermal equilibrium. For instance, if a gas is to be simulated at a given temperature T it might be advantageous to choose the initial velocities according to a MAXWELL-BOLTZMANN distribution. The MAXWELL-BOLTZMANN distribution states that the probability [more precisely: the pdf (*probability density function* describing the probability, see Appendix D)] that a particle with mass m has velocity v is proportional to

$$p(|v|) \propto |v|^2 \exp\left(-\frac{m|v|^2}{2k_B T}\right). \tag{7.34}$$

Another intriguing question is how to check whether or not thermal equilibrium has been reached. In statistical mechanics one is usually confronted with expectation values of observables $O(t)$ as a function of time. The expectation value $\langle O \rangle$ is defined as

$$\langle O \rangle = \lim_{\tau \to \infty} \frac{1}{\tau} \int_0^{\tau} \mathrm{d}t\, O(t). \tag{7.35}$$

Since $O(t)$ is not known analytically one replaces the mean value by its arithmetic mean

$$\langle O \rangle \approx \overline{O} = \frac{1}{n} \sum_{j=k}^{k+n} O(t_j). \tag{7.36}$$

If n and k are sufficiently large, the average value can be regarded as converged. In particular, one has to choose n reasonably large and then find k in such a way, that for all values $k' \geq k$ the same result for $\overline{O}$ is obtained. Hence, equilibrium has been reached after k time-steps and it is now possible to 'measure' the observables by calculating their mean values. A more detailed discussion of such a procedure, as, for instance, the influence of time correlations or a discussion of more advanced techniques is postponed to Chap. 19.

There is one last point: In many cases the *natural units* of the physical system might be disadvantageous because they are likely to induce numerical instabilities. In such cases a common technique is to switch to *rescaled variables* by introducing new units, which are characteristic quantities for the system and all physical quantities are expressed in these new units. For instance one might introduce the length L of the box as the unit of space. The new spatial coordinates would then be given by

$$r' = \frac{r}{L}. \tag{7.37}$$

Hence all coordinates take on values within the interval $r' \in [0, 1]$. However, one cannot introduce an arbitrary set of characteristic quantities due to the physical relations they have to obey. For instance, one might introduce a characteristic energy ε_0, a characteristic length λ, and a characteristic mass m. In this case the characteristic temperature $\tilde{T}$ is determined via

$$\tilde{T} = \frac{\varepsilon_0}{k_B}. \tag{7.38}$$

Moreover the characteristic time τ is fixed to the value

$$\tau = \sqrt{\frac{m\lambda^2}{\varepsilon_0}}, \tag{7.39}$$

which results from the relation between the kinetic energy and the velocity.

To illustrate a molecular dynamics simulation we study a set of $N = 100$ particles of mass $m = 1$ which are subject to a LENNARD-JONES potential (7.4) characterized by $\varepsilon = \sigma = 1$ and to a gravitational force mg, $g = 9.81$. At initialization the particles are placed in a 10×10 lattice starting with the lower left hand edge at $x = 10.5$ and $y = 10$. The particles are equally spaced with $\Delta x = \Delta y = \varepsilon$. This initial configuration is shown in Fig. 7.3a. Furthermore, the left hand side, the right hand side, and the bottom of the confinement ($L = 30$) are described by reflecting boundary conditions, Eqs. (7.24) and (7.25). The confinement is open at the top, i.e. it extends to infinity. The time step is given by $\Delta t = 10^{-3}$. Figure 7.3b–d demonstrate how the system developed after 1200, 1800, and 3000 time steps, respectively.

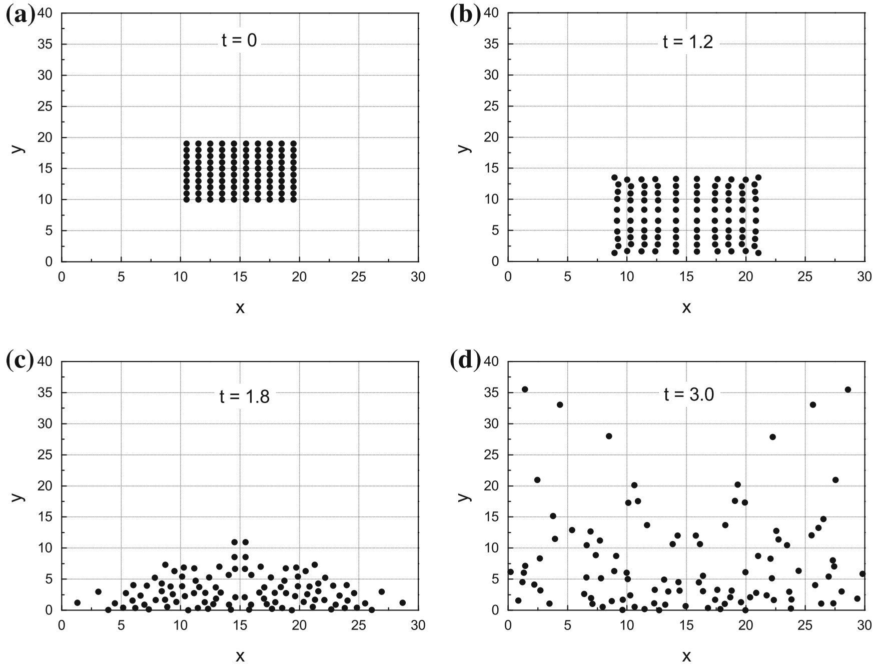

Fig. 7.3 (**a**) Initial configuration: the particles are placed in a 10 × 10 equally spaced lattice starting with $x = 10.5$ and $y = 10.0$; $g = 9.81$. The initial velocities are equal to zero. (**b**) Configuration after 1200 time steps. (**c**) Configuration after 1800 time steps. (**d**) Configuration after 3000 time steps

This chapter closes our discussion of the numerics of initial value problems. In the following chapters we will introduce some of the basic concepts developed to solve boundary value problems with numerical methods.

Summary

This chapter dealt with the classical dynamics of many particles (not necessarily identical particles) which are confined in a box of finite dimension or which are allowed to roam freely in infinite space. The particles are subject to a particle-particle interaction and to an external force. The discussion was restricted to classical molecular dynamics. From HAMILTON's equations of motion for N interacting particles numerical methods were developed which allowed the simulation of the particles' dynamics. Based on the symplectic EULER method the STRÖMER-VERLET algorithm was derived. Another approach was based on the central rectangular rule and resulted in the *leap-frog* algorithm. Finally, the *velocity* VERLET algorithm was introduced. All three methods do have their merits. The first gives very accurate results for the particles' positions but calculates inaccurate velocities. It has the advantage that it is time reversible. The other two methods lack this property but give very accurate estimates of the particles' velocities. The final part of this chapter was dedicated to the discussion of various subtleties of the numerical implementation of these algorithms as there are: (i) definition of boundary conditions, (ii) initialization of the algorithm, (iii) equilibration to a given temperature, (iv) ensuring constant temperature throughout the simulation, and (v) transformation to rescaled variables.

Problems

1. We investigate the pendulum of Chap. 1 and write its equation of motion as

$$\ddot{x} + \omega^2 x = 0,$$

with ω defined in Eq. (1.7). The STRÖMER–VERLET algorithm is applied to simulate the pendulum's motion and to compare the numerical results with the exact solution. Demonstrate that the result is very sensitive to the choice of the time step Δt and, in particular, of the product $\omega\Delta t$. Note that in this particular case the STRÖMER–VERLET algorithm can also be studied analytically! What happens for the choice $\omega\Delta t = 1$ or $\omega\Delta t \geq 2$? Which conclusions can be drawn from this example for a proper choice of the time discretization?
Try the other two methods to simulate the pendulums dynamics.

2. Write a molecular dynamics code with the help of the following instructions. You can use either the leap-frog or the velocity VERLET algorithm. We consider the following system:

- There are $N = 100$ particles in a two-dimensional box with side length $L = 30$. The boundaries at the bottom, at the left- and at right-hand side are considered as reflecting, as in Fig. 7.2. The top of the box is regarded as open (no periodic boundary condition or reflecting boundary is imposed).
- The particles interact through a LENNARD-JONES potential of the form (7.4) where ε and σ define the interaction.
- Furthermore, a gravitational force $F_{ext} = -mge_y$ acts on each particle, where m is the particle's mass, g is the acceleration due to gravity, and e_y denotes the unit vector in y-direction.
- As an initial condition, the particles can be placed within the box on a regular lattice, where the distance between the particles is the characteristic distance according to the LENNARD-JONES potential, i.e. ε. The form and position of this lattice is arbitrary. This is illustrated in Fig. 7.3.

We measure the velocities and the positions of all particles. Since the particle's velocities and positions are to be analyzed with the help of an extra program, the data are written to external files (it is not necessary to save *all* time steps!).

Perform the following analysis:

- Determine the temperature T from the kinetic energy as discussed in in this chapter. Note that in this particular case we do not demand that $v_{tot} = 0$!
- Try different initial conditions. For instance, set the initial velocity equal to zero and stack the particles in different geometric configurations (rectangle, triangle, ..., one can also use more than one configurations at the same time!). The nearest neighbor distance between the particles can be set equal to ε. Choose one configuration and place it at different positions in the box. What happens?
- Set $\varepsilon = \sigma = m = 1$ (we change the units) and set in the initial condition to the inter-atomic distance of $2^{\frac{1}{6}}\varepsilon$. (Why?) Vary the gravitational acceleration g (different systems of units) in order to simulate different states of matter. The reference program developed solid behavior for $g \approx 0$, liquid behavior for $g \approx 0.1$ and gaseous behavior for $g > 1$. Explain this behavior!
- Measure the particle density $\rho(h)$ as a function of the height h. You should be able to reproduce the barometric formula:

$$\rho \propto \rho_0 \exp\{-\gamma h/T\}, \quad \gamma > 0.$$

- Determine the momentum distribution ($p_i = mv_i$) of the particles and demonstrate that it follows a Maxwell-Boltzmann distribution

$$p(|v|) \propto |v|^2 \exp\{-\gamma |v|^2/T\}, \quad \gamma > 0,$$

  with $|v| = \sqrt{v_x^2 + v_y^2}$, the Euclidean norm.
- Illustrate the results of the simulation graphically.

References

1. Hoover, W.G.: Molecular Dynamics. Springer, Berlin (1986)
2. Griebel, M., Knapek, S., Zumbesch, G.: Numerical Simulation in Molecular Dynamics. Texts in Computational Science and Engeneering, vol. 5. Springer, Berlin (2007)
3. Marx, D., Hutter, J.: Ab Initio Molecular Dynamics. Cambridge University Press, Cambridge (2012)
4. Mandl, F.: Statistical Physics, 2nd edn. Wiley, New York (1988)

Chapter 8
Numerics of Ordinary Differential Equations: Boundary Value Problems

8.1 Introduction

It is the aim of this chapter to introduce some of the basics methods developed to solve boundary value problems. Since a treatment of all available concepts is far too extensive, we will concentrate on two approaches, namely the finite difference approach and the shooting methods [1–3]. Furthermore, we will strictly focus on *linear boundary value problems* defined on a finite interval $[a, b] \subset \mathbb{R}$. A boundary value problem is referred to as linear if both the differential equation and the boundary conditions are linear. Such a problem of order n is of the form

$$\begin{cases} L[y] = f(x) & x \in [a, b], \\ U_\nu[y] = \lambda_\nu & \nu = 1, \dots, n. \end{cases} \tag{8.1}$$

Here, $L[y]$ is a linear operator

$$L[y] = \sum_{k=0}^{n} a_k(x) y^{(k)}(x), \tag{8.2}$$

where $y^{(k)}(x)$ denotes the k-th spatial derivative of $y(x)$, i.e. $y^{(k)} = \frac{\mathrm{d}^k y(x)}{\mathrm{d}x^k}$ and $f(x)$ as well as the $a_k(x)$ are given functions which we assume to be continuous. Accordingly, linear boundary conditions $U_\nu[y]$ can be formulated as

$$U_\nu[y] = \sum_{k=0}^{n-1} \left[\alpha_{\nu k} y^{(k)}(a) + \beta_{\nu k} y^{(k)}(b) \right] = \lambda_\nu, \tag{8.3}$$

where the $\alpha_{\nu k}$, $\beta_{\nu k}$ and λ_ν are given constants. The question in which cases a solution to the boundary value problem (8.1) exists and whether or not this solution will be unique, will not be discussed here.

B. A. Stickler and E. Schachinger, *Basic Concepts in Computational Physics*,
DOI: 10.1007/978-3-319-02435-6_8, © Springer International Publishing Switzerland 2014

Let us introduce some further notations. If the function $f(x) = 0$ for all $x \in [a, b]$ the differential equation in the first line of Eq. (8.1) is referred to as *homogeneous*. In analogy, if the constants $\lambda_\nu = 0$ for all $\nu = 1, \dots, n$, the boundary conditions are referred to as *homogeneous*. If the differential equation is homogeneous and the boundary conditions are homogeneous as well, the boundary value problem (8.1) is referred to as homogeneous. In all other cases it is referred to as *inhomogeneous*.

The boundary conditions are said to be *decoupled* if the function values at the two different boundaries do not mix.

One of the most important types of boundary value problems in physics are linear second order boundary value problems with decoupled boundary conditions. It is of the form:

$$a_2(x)y''(x) + a_1(x)y'(x) + a_0(x)y(x) = f(x), \quad x \in [a, b], \tag{8.4a}$$

$$\alpha_0 y(a) + \alpha_1 y'(a) = \lambda_1, \quad |\alpha_0| + |\alpha_1| \neq 0, \tag{8.4b}$$

$$\beta_0 y(b) + \beta_1 y'(b) = \lambda_2, \quad |\beta_0| + |\beta_1| \neq 0. \tag{8.4c}$$

This chapter focuses mainly on problems of this kind.

In particular, for second order differential equations, boundary conditions of the form

$$y(a) = \alpha, \qquad y(b) = \beta, \tag{8.5}$$

are referred to as *boundary conditions of the first kind* or DIRICHLET boundary conditions, on the other hand boundary conditions of the form

$$y'(a) = \alpha, \qquad y'(b) = \beta, \tag{8.6}$$

are referred to as *boundary conditions of the second kind* or NEUMANN *boundary conditions* and boundary conditions of the form (8.4) are referred to as *boundary conditions of the third kind* or STURM *boundary conditions*.

We note, that the particular case of decoupled boundary conditions does not include problems like

$$y(a) = y(b) \neq 0. \tag{8.7}$$

We encountered such a condition in Sect. 7.3 where we introduced boundary conditions of this form as periodic boundary conditions.

In the following section the method of finite differences will be applied to solve boundary value problems of the form (8.4). On the other hand, shooting methods, in particular the method developed by NUMEROV, will be the topic of the third section.

8.2 Finite Difference Approach

For illustrative purposes, we regard a boundary value problem of the form (8.4). The extension to more complex problems might be tedious but follows the same procedure. We discretize the interval $[a, b]$ according to the recipe introduced in Chap. 2: the positions x_k are given by $x_k = a + (k-1)h$, where the grid-spacing h is determined via the maximum number of grid-points N as $h = (b-a)/(N-1)$. Hence, we have $x_1 = a$ and $x_N = b$. Furthermore, we use the notation $y_k \equiv y(x_k)$ for all $k = 1, \ldots, N$. It will be used for all functions which appear in Eqs. (8.4). Let us employ the central difference derivative (2.10c) in order to approximate

$$y''(x_k) = y_k'' \approx \frac{y_{k+1} - 2y_k + y_{k-1}}{h^2}, \tag{8.8}$$

for $k = 2, \ldots, N-1$ and

$$y'(x_k) = y_k' \approx \frac{y_{k+1} - y_{k-1}}{2h} \;. \tag{8.9}$$

The boundary points x_1 and x_N will be treated in a separate step. In order to abbreviate the notation we will rewrite the differential equation (8.4) as

$$a(x)y''(x) + b(x)y'(x) + c(x)y(x) = f(x). \tag{8.10}$$

Equations (8.8) and (8.9) are then applied and we arrive at the difference equation

$$a_k \frac{y_{k+1} - 2y_k + y_{k-1}}{h^2} + b_k \frac{y_{k+1} - y_{k-1}}{2h} + c_k y_k = f_k, \tag{8.11}$$

where $k = 2, \ldots, N-1$. Sorting the y_k yields furthermore:

$$\left(\frac{a_k}{h^2} - \frac{b_k}{2h}\right) y_{k-1} + \left(c_k - \frac{2a_k}{h^2}\right) y_k + \left(\frac{a_k}{h^2} + \frac{b_k}{2h}\right) y_{k+1} = f_k. \tag{8.12}$$

This equation is only valid for $k = 2, \ldots, N-1$ because we defined N grid-points within the interval $[a, b]$.

In a final step it is necessary to incorporate the boundary conditions and this will enable us to reduce the whole problem to a system of linear equations. Decoupled boundary conditions of a second order differential equation for the left hand boundary (8.4b) are of the form:

$$\alpha_0 y(a) + \alpha_1 y'(a) = \lambda_1, \quad |\alpha_0| + |\alpha_1| \neq 0, \tag{8.13}$$

and we find for the right hand boundary (8.4c):

$$\beta_0 y(b) + \beta_1 y'(b) = \lambda_2, \quad |\beta_0| + |\beta_1| \neq 0. \tag{8.14}$$

We discretize $y'(a)$ as

$$y'(a) = y_1' \approx \frac{y_2 - y_0}{2h}, \tag{8.15}$$

and set $y_1 \equiv y(a)$. Note that the function value y_0 in Eq. (8.15) is unknown since $x_0 = a - h$ is not a point within our interval $[a, b]$. Nevertheless, we use Eq. (8.15) in Eq. (8.13) and obtain:

$$\alpha_0 y_1 + \alpha_1 \frac{y_2 - y_0}{2h} = \lambda_1. \tag{8.16}$$

In a next step we solve Eq. (8.16) for y_0 under the premise that $\alpha_1 \neq 0$,

$$y_0 = y_2 - \frac{2h}{\alpha_1} \left(\lambda_1 - \alpha_0 y_1\right), \tag{8.17}$$

rewrite (8.12) for $k = 1$,

$$\left(\frac{a_1}{h^2} - \frac{b_1}{2h}\right) y_0 + \left(c_1 - \frac{2a_1}{h^2}\right) y_1 + \left(\frac{a_1}{h^2} + \frac{b_1}{2h}\right) y_2 = f_1, \tag{8.18}$$

and insert (8.17) into (8.18):

$$\left[c_1 - \frac{2a_1}{h^2} + \frac{\alpha_0}{\alpha_1}\left(\frac{2a_1}{h} - b_1\right)\right] y_1 + \frac{2a_1}{h^2} y_2 = f_1 - \frac{\lambda_1}{\alpha_1}\left(b_1 - \frac{2a_1}{h}\right). \tag{8.19}$$

In the specific case that $\alpha_1 = 0$ we obtain immediately from Eq. (8.16) that

$$y_1 = \frac{\lambda_1}{\alpha_0}. \tag{8.20}$$

We follow the same strategy and incorporate the boundary condition at the right hand boundary, Eq. (8.14), i.e. we discretize (8.14) by introducing a grid-point y_{N+1} via

$$\beta_0 y_N + \beta_1 \frac{y_{N+1} - y_{N-1}}{2h} = \lambda_2, \tag{8.21}$$

solve this equation for y_{N+1} under the premise that $\beta_1 \neq 0$

$$y_{N+1} = y_{N-1} + \frac{2h}{\beta_1} \left(\lambda_2 - \beta_0 y_N\right), \tag{8.22}$$

and insert this into Eq. (8.12) for $k = N$. This results in:

$$\frac{2a_N}{h^2} y_{N-1} + \left[c_N - \frac{2a_N}{h^2} - \frac{\beta_0}{\beta_1} \left(b_N + \frac{2a_N}{h} \right) \right] y_N = f_N - \frac{\lambda_2}{\beta_1} \left(b_N + \frac{2a_N}{h} \right). \tag{8.23}$$

In the specific case $\beta_1 = 0$, the value y_N is fixed at the boundary and one obtains from (8.14) that

$$y_N = \frac{\lambda_2}{\beta_0}. \tag{8.24}$$

We note that as a result of this procedure the boundary value problem was reduced to a system of inhomogeneous linear equations, namely Eqs. (8.12), (8.19) and (8.23). It can be written as

$$Ay = F, \tag{8.25}$$

where we introduced the vectors $y = (y_1, y_2, \dots, y_N)^T$, F as

$$F = \begin{pmatrix} f_1 - \frac{\lambda_1}{\alpha_1}\left(b_1 - \frac{2a_1}{h} \right) \\ f_2 \\ f_3 \\ \vdots \\ f_{N-1} \\ f_N - \frac{\lambda_2}{\beta_1}\left(b_N + \frac{2a_N}{h} \right) \end{pmatrix}, \tag{8.26}$$

and the tridiagonal matrix A as

$$A = \begin{pmatrix} B_1 & C_1 & 0 & & \cdots & 0 \\ A_2 & B_2 & C_2 & & \cdots & \vdots \\ 0 & \ddots & \ddots & \ddots & & \\ \vdots & & \ddots & \ddots & \ddots & 0 \\ & & & A_{N-1} & B_{N-1} & C_{N-1} \\ 0 & \cdots & & 0 & A_N & B_N \end{pmatrix}. \tag{8.27}$$

Here we defined,

$$A_k = \begin{cases} \left(\frac{a_k}{h^2} - \frac{b_k}{2h} \right) & k = 2, \dots, N-1, \\ \frac{2a_N}{h^2} & k = N, \end{cases} \tag{8.28}$$

$$B_k = \begin{cases} \left[c_1 - \frac{2a_1}{h^2} + \frac{\alpha_0}{\alpha_1}\left(\frac{2a_1}{h} - b_1\right)\right] & k = 1, \\ \left(c_k - \frac{2a_k}{h^2}\right) & k = 2, \dots N-1, \\ \left[c_N - \frac{2a_N}{h^2} - \frac{\beta_0}{\beta_1}\left(b_N + \frac{2a_N}{h}\right)\right] & k = N, \end{cases} \tag{8.29}$$

and, finally,

$$C_k = \begin{cases} \frac{2a_1}{h^2} & k = 1, \\ \left(\frac{a_k}{h^2} + \frac{b_k}{2h}\right) & k = 2, \dots, N-1. \end{cases} \tag{8.30}$$

We remark in conclusion that the remaining task is to solve this linear system of equations (8.25) (A brief introduction to the numerical treatment of linear systems of equations can be found in Appendix C). Very effective methods exist for cases where the matrix A is tridiagonal [4] as it is the case here. Although we discussed the method of finite differences for the particular case of a second order differential equation with decoupled boundary conditions, the same strategy can be employed to derive similar methods for higher order boundary value problems. However, these methods will in general be more complex. Furthermore, we note that in cases where $\alpha_1 = \beta_1 = 0$ the function values at the boundaries y_1 and y_N are fixed and the corresponding system of linear equations reduces to $(N-2)$-dimensions.

Let us briefly investigate the differential equation which corresponds to the problem (8.4) together with periodic boundary conditions of the form (8.7). In this case we have to consider that

$$y_1 = y_N, \tag{8.31}$$

and, in order to a solution to exist, we have necessarily

$$a_1 = a_N, \quad b_1 = b_N, \quad \text{and} \quad c_1 = c_N. \tag{8.32}$$

The approximation (8.12) is again employed to transform the differential equation (8.4) for $k = 2, \dots, N-1$. For instance, for $k = 2$ it changes into

$$\left(\frac{a_2}{h^2} - \frac{b_2}{2h}\right) y_1 + \left(c_2 - \frac{2a_2}{h^2}\right) y_2 + \left(\frac{a_2}{h^2} + \frac{b_2}{2h}\right) y_3 = f_2, \tag{8.33}$$

and we obtain for $k = N-1$

$$\begin{aligned} \left(\frac{a_{N-1}}{h^2} - \frac{b_{N-1}}{2h}\right) y_{N-2} + \left(c_{N-1} - \frac{2a_{N-1}}{h^2}\right) y_{N-1} & \\ + \left(\frac{a_{N-1}}{h^2} + \frac{b_{N-1}}{2h}\right) y_N = f_{N-1}. & \end{aligned} \tag{8.34}$$

Since $y_1 = y_N$ Eq. (8.34) can be rewritten as

$$\left(\frac{a_{N-1}}{h^2} - \frac{b_{N-1}}{2h}\right) y_{N-2} + \left(c_{N-1} - \frac{2a_{N-1}}{h^2}\right) y_{N-1} \\ + \left(\frac{a_{N-1}}{h^2} + \frac{b_{N-1}}{2h}\right) y_1 = f_{N-1}. \tag{8.35}$$

Finally, Eq. (8.12) results for $k = 1$ in

$$\left(\frac{a_1}{h^2} - \frac{b_1}{2h}\right) y_{N-1} + \left(c_1 - \frac{2a_1}{h^2}\right) y_1 + \left(\frac{a_1}{h^2} + \frac{b_1}{2h}\right) y_2 = f_1, \tag{8.36}$$

where we identified $y_0 = y(x_1 - h) \equiv y(x_N - h) = y_{N-1}$. All this results in a closed system of $N - 1$ equations, which is of the form (8.25)

$$Ay = F, \tag{8.37}$$

where $y = (y_1, y_2, \dots, y_{N-1})^T$,

$$F = \begin{pmatrix} f_1 \\ f_2 \\ \vdots \\ f_{N-1} \end{pmatrix}, \tag{8.38}$$

and the $(N-1) \times (N-1)$ matrix A is given by

$$A = \begin{pmatrix} B_1 & C_1 & 0 & \cdots & 0 & A_1 \\ A_2 & B_2 & C_2 & & \cdots & 0 \\ 0 & \ddots & \ddots & \ddots & & \vdots \\ \vdots & & \ddots & \ddots & \ddots & 0 \\ 0 & & & A_{N-2} & B_{N-2} & C_{N-2} \\ C_{N-1} & 0 & \cdots & 0 & A_{N-1} & B_{N-1} \end{pmatrix}. \tag{8.39}$$

Here, we defined

$$A_k = \left(\frac{a_k}{h^2} - \frac{b_k}{2h}\right), \qquad k = 1, \dots, N-1, \tag{8.40}$$

$$B_k = \left(c_k - \frac{2a_k}{h^2}\right), \qquad k = 1, \dots, N-1, \tag{8.41}$$

and

$$C_k = \left(\frac{a_k}{h^2} + \frac{b_k}{2h}\right), \qquad k = 1, \dots, N-1. \tag{8.42}$$

In contrast to the matrix (8.27) matrix (8.39) is not tridiagonal since the matrix elements $(A)_{1,N-1}$ and $(A)_{N-1,1}$ are non-zero. Nevertheless, it was possible to reduce the boundary value problem to a system of linear equations which can be solved iteratively.

8.3 Shooting Methods

Again, for illustrative purposes, we restrict the discussion to a second order boundary value problem with decoupled boundary conditions of the form (8.4). The essential idea of shooting methods is to treat the boundary value problem as an initial value problem. The resulting equations can then be solved with the help of methods discussed in Chap. 5. Of course, such an approach can, in general, not be exact. The trick is, that one modifies the initial conditions iteratively in such a way that the boundary conditions are fulfilled. Let us put this train of thoughts into a mathematical form: We rewrite the second order differential equation (8.4a) as

$$y'' = f(y, y', x), \tag{8.43}$$

which can be reduced to a set of first order differential equations as was demonstrated in Chap. 5. We note that Eq. (8.43) is not yet well posed since the initial conditions have not been defined. The boundary condition on the left hand side reads:

$$\alpha_0 y(a) + \alpha_1 y'(a) = \lambda_1. \tag{8.44}$$

We now *assume* that $y'(a) = z$, where z is some number. This gives the well posed initial value problem

$$\begin{cases} y'' = f(y, y', x), \\ y(a) = \frac{\lambda_1}{\alpha_0} - \frac{\alpha_1}{\alpha_0} z, \\ y'(a) = z, \end{cases} \tag{8.45}$$

under the assumption that $\alpha_0 \neq 0$. The solution of this problem will be written as $y(x; z)$ in order to indicate its dependence on the particular choice $y'(a) = z$. We remember, that the boundary condition at the right hand boundary reads:

$$\beta_0 y(b) + \beta_1 y'(b) = \lambda_2. \tag{8.46}$$

Let us define the function

$$F(z) = \beta_0 y(b; z) + \beta_1 y'(b; z) - \lambda_2, \tag{8.47}$$

and we observe that the solution of the equation

$$F(z) = 0, \tag{8.48}$$

gives the desired solution to the boundary value problem (8.4), because in this case the second boundary condition (8.46) is fulfilled. In practice, one tries several values of z until relation (8.48) is fulfilled. However, from a numerical point of view this method is very inefficient since usually several initial value problems have to be solved until the correct value of z is found. Nevertheless, in some cases shooting methods proved to be very useful.

For instance, shooting methods are particularly effective if a solution to an eigenvalue problem of the form

$$a(x)y''(x) + b(x)y'(x) + c(x)y(x) = \lambda y(x), \tag{8.49a}$$

in combination with homogeneous boundary conditions,

$$\alpha_0 y(a) + \alpha_1 y'(a) = 0, \tag{8.49b}$$

and

$$\beta_0 y(b) + \beta_1 y'(b) = 0. \tag{8.49c}$$

is to be found. We note that Eq. (8.49a) has the trivial solution $y(x) \equiv 0$ for all values of λ. However a non-trivial solution will only exist for particular values of λ. These particular values will be indexed by λ_n and are referred to as *eigenvalues* of Eq. (8.49a). The corresponding functions $y_n(x)$ are referred to as *eigenfunctions*. We note that the differential equation (8.49a) in combination with the boundary conditions (8.49b) and (8.49c) define a homogeneous boundary value problem. Such a problem is commonly referred to as an *eigenvalue problem*. Furthermore, we note the following property of homogeneous boundary value problems: Suppose that $y(x)$ is a solution of the boundary value problem (8.49). Then $\tilde{y}(x) = \gamma y(x)$, with $\gamma =$ const will also be a solution of (8.49). Hence, the solution of a homogeneous boundary value problem is not unique but invariant under multiplication by a constant γ. Typically, the multiplicative factor γ is fixed by some additional condition, such as a normalization condition of the form

$$\int_a^b \mathrm{d}x |y(x)|^2 = 1. \tag{8.50}$$

We now employ this property and *choose* $y(a) = 1$. Inserting this choice into (8.49b) yields

$$y'(a) = -\frac{\alpha_0}{\alpha_1}. \tag{8.51}$$

Note that for $\alpha_0 = 0$ or $\alpha_1 = 0$, we are restricted to the choices $y'(a) = 0$ and $y(a)$ is arbitrary or $y(a) = 0$ and $y'(a)$ is arbitrary, respectively. If we assume that $a(x) \neq 0$

for all $x \in [a, b]$, we can solve the initial value problem

$$\begin{cases} y''(x) &= -\frac{b(x)}{a(x)} y'(x) - \frac{c(x)-\lambda}{a(x)} y(x), \\ y(a) &= 1, \\ y'(a) &= -\frac{\alpha_0}{\alpha_1}. \end{cases} \tag{8.52}$$

The solutions are denoted by $y(x; \lambda)$ in order to emphasize that they will highly depend on the choice of the parameter λ. The strategy is to solve the initial value problem (8.52) for several values of λ and whenever one finds that

$$F(\lambda) = \beta_0 y(b; \lambda) + \beta_1 y'(b; \lambda) = 0, \tag{8.53}$$

an eigenvalue λ_n and the corresponding eigenfunction $y_n(x) = y(x; \lambda_n)$ to the eigenvalue problem (8.49) have been found.

However, this strategy is also very time consuming. The most common application of the shooting method is its combination with a very fast and accurate solution of initial value problems. This method is known as the NUMEROV method. It is applicable whenever one is confronted with a differential equation of the form

$$y''(x) + k(x) y(x) = 0, \tag{8.54}$$

in combination with homogeneous boundary conditions. Here $k(x)$ is some function. If we are particularly interested in eigenvalue problems then $k(x)$ has the form $k(x) = q(x) - \lambda$, where $q(x)$ is some function and λ is the eigenvalue [see the discussion after equation (8.49)]. For instance, consider the one-dimensional stationary SCHRÖDINGER equation,

$$\psi''(x) + \frac{2m}{\hbar^2} \left[E - V(x)\right] \psi(x) = 0, \tag{8.55}$$

where $\psi(x)$ is the wave-function, m is the mass, $\hbar$ denotes the reduced PLANCK constant, E is the energy, and $V(x)$ is some potential. In this case we identify

$$k(x) = \frac{2m}{\hbar^2} \left[E - V(x)\right]. \tag{8.56}$$

We note that Eq. (8.55) together with its boundary conditions defines an eigenvalue problem with eigenvalues E_n, the possible energies of the system. We remember from Chap. 2, Eq. (2.34), that

$$y_j'' = \frac{y_{j+1} - 2y_j + y_{j-1}}{h^2} - \frac{h^2}{12} y_j^{(4)} - \cdots = -k_j y_j. \tag{8.57}$$

In the last step we made use of Eq. (8.54) and introduced $k_j \equiv k(x_j)$. Furthermore, we write the fourth derivative of $y(x)$ at point $x = x_j$ as

$$y_j^{(4)} \approx \frac{y''_{j+1} - 2y''_j + y''_{j-1}}{h^2} = \frac{-k_{j+1}y_{j+1} + 2k_j y_j - k_{j-1}y_{j-1}}{h^2}, \tag{8.58}$$

where we employed Eq. (8.54). Truncating (8.57) after the fourth order derivative $y_j^{(4)}$, inserting relation (8.58), and solving for y_{j+1} yields

$$y_{j+1} = \frac{2\left(1 - \frac{5h^2}{12}k_j\right) y_j - \left(1 + \frac{h^2}{12}k_{j-1}\right) y_{j-1}}{1 + \frac{h^2}{12}k_{j+1}}. \tag{8.59}$$

This gives a very fast algorithm to solve the differential equation (8.54) with some initial values of the form (8.52). The remaining strategy is the same as discussed above, i.e. one *screens* the parameter λ in order to find the eigenvalues λ_n and eigenfunctions $y_n(x)$. In case of the SCHRÖDINGER equation, one can screen the energy E in order to obtain the energy eigenvalues E_n which satisfy a condition of the form (8.53).

Let us conclude this section with two important remarks on the NUMEROV method before we present two illustrating examples in the next chapters. We note from Eq. (8.59) that in order to compute y_3 one already needs the function values y_1 and y_2. Usually, one obtains these values from the boundary conditions in combination with some additional condition for the problem at hand. Such an additional condition might be, for instance, the normalization of the function $y(x)$, like Eq. (8.50). Let us make a second comment. As already emphasized, one has to run the NUMEROV algorithm several times for different *trial values* of the parameter λ. In order to reduce the computational cost of the method it is in many cases advantageous to store the function values q_i, where $k_i = q_i - \lambda$, in an array, which is then regarded as an input argument of the NUMEROV algorithm.

Summary

We focused on linear boundary value problems defined on a finite interval $[a, b] \subset \mathbb{R}$. Most important for physics are second order boundary value problems with decoupled boundary conditions, i.e. the boundary conditions at the two different boundaries do not mix. The numerical treatment of the second order differential equation together with its boundary conditions concentrated either on the application of finite differences or on shooting methods. In the finite difference approach the methods developed in Chap. 2 were applied and the boundary conditions were incorporated directly. This resulted in a set of linear algebraic equations which is to be solved for each grid-point of the discretisized interval $[a, b]$. The case of periodic boundary conditions was also discussed in detail.

The shooting methods, on the other hand, try to link the decoupled boundary value problem to an initial value problem. This allowed the application of the methods discussed in Chap. 5. The idea was to start with some initial value at one of the two boundaries, solve the differential equation numerically and to modify the initial value iteratively until it agreed with the original boundary condition within some predefined error. Such a procedure is rather time consuming. Nevertheless, shooting methods, in particular its NUMEROV variation, are very useful in the numerical solution of eigenvalue problems, as was demonstrated by the homogeneous boundary value problem of the one-dimensional stationary SCHRÖDINGER equation.

References

1. Colliatz, L.: The Numerical Treatment of Differential Equations. Springer, Berlin (1960)
2. Lapidus, L., Pinder, G.F.: Numerical Solution of Partial Differential Equations. Wiley, New York (1982)
3. Asher, U.M., Mattheij, R.M.M., Russell, R.D.: Numerical solution of boundary value problems for ordinary differential equations. Classics in Applied Mathematics, vol. 13. Cambridge University Press, Cambridge, UK (1995)
4. Press, W.H., Teukolsky, S.A., Vetterling, W.T., Flannery, B.P.: Numerical Recipes in C++, 2nd edn. Cambridge University Press, Cambridge (2002)

Chapter 9
The One-Dimensional Stationary Heat Equation

9.1 Introduction

This is the first of two chapters which illustrate the applicability of the methods introduced in Chap. 8. Within this chapter the finite difference approach is employed to solve the stationary heat equation. Let us motivate briefly this particular problem. We consider a rod of length L which is supposed to be kept at constant temperatures T_0 and T_N at its ends as illustrated in Fig. 9.1. The homogeneous heat equation is a linear partial differential equation of the form

$$\frac{\partial}{\partial t} T = \kappa \Delta T. \tag{9.1}$$

Here $T = T(x, t)$ is the temperature as a function of space $x \in \mathbb{R}^3$ and time $t \in \mathbb{R}$, $\Delta = \nabla^2 = \partial_x^2 + \partial_y^2 + \partial_z^2$ is the LAPLACE operator, and $\kappa =$ const is the thermal diffusivity.

We remark, that Eq. (9.1) is a partial differential equation together with initial and boundary conditions. Moreover, we note in passing that the heat equation is equivalent to the diffusion equation

$$\frac{\partial}{\partial t} \rho(x, t) = D \Delta \rho(x, t), \tag{9.2}$$

with particle density $\rho(x, t)$ and the diffusion coefficient $D =$ const. Here we restrict ourselves to a simplified situation in order to test the validity of the finite difference approach discussed in Sect. 8.2. The general solution of the heat or diffusion equation will be discussed in Sect. 11.3.

If we assume that the cylindrical surface of the rod is perfectly isolated, we can restrict the problem to a one-dimensional problem. Furthermore, we assume that the steady-state has been reached, i.e. $\frac{\partial}{\partial t} T(x, t) = 0$. Hence, the remaining boundary value problem is of the form

B. A. Stickler and E. Schachinger, *Basic Concepts in Computational Physics*,
DOI: 10.1007/978-3-319-02435-6_9, © Springer International Publishing Switzerland 2014

Fig. 9.1 We consider a rod of length L. Its ends are kept at constant temperatures T_0 and T_N, respectively

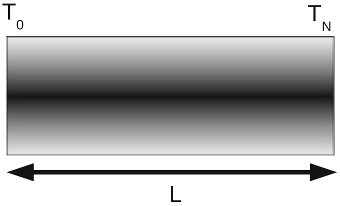

$$\begin{cases} \frac{\mathrm{d}^2}{\mathrm{d}x^2}T = 0, & x \in [0, L], \\ T(0) = T_0, & \\ T(L) = T_N. & \end{cases} \tag{9.3}$$

The solution can easily be found analytically and one obtains

$$T(x) = T_0 + (T_N - T_0)\,\frac{x}{L}. \tag{9.4}$$

In the following section we will apply the approach of finite differences to the boundary value problem (9.3) as discussed in Sect. 8.2.

9.2 Finite Differences

We discretize the interval $[0, L]$ according Chap. 2 by the introduction of N grid-points $x_n = nh$, with $h = L/N$, $x_0 = 0$, and $x_N = L$. Furthermore, $T_n \equiv T(x_n)$ and, in particular, we refer to the boundary conditions (9.3) as T_0 and T_N, respectively.

On the basis of this discretization, we approximate Eq. (9.3) by

$$\frac{T_{n+1} - 2T_n + T_{n-1}}{h^2} = 0, \tag{9.5}$$

or equivalently

$$T_{n+1} - 2T_n + T_{n-1} = 0. \tag{9.6}$$

We can rewrite this as a matrix equation,

$$AT = F, \tag{9.7}$$

where the boundary conditions have already been included. In Eq. (9.7) the vector $T = (T_1, T_2, \dots, T_{N-1})^T$, the tridiagonal matrix A is given by

$$A = \begin{pmatrix} -2 & 1 & 0 & & \dots & 0 \\ 1 & -2 & 1 & 0 & \dots & 0 \\ 0 & 1 & -2 & 1 & & \\ \vdots & & \ddots & \ddots & \ddots & \\ 0 & \dots & & & 1 & -2 \end{pmatrix}, \tag{9.8}$$

and the vector F is given by

$$F = \begin{pmatrix} -T_0 \\ 0 \\ \vdots \\ 0 \\ -T_N \end{pmatrix}. \tag{9.9}$$

It is an easy task to solve Eq. (9.7) analytically. It follows from Eq. (9.6) that

$$T_{n+1} = 2T_n - T_{n-1}, \qquad n = 1, \dots, N-1. \tag{9.10}$$

We insert $n = 1, 2, 3$ in order to obtain

$$T_2 = 2T_1 - T_0, \tag{9.11}$$

$$\begin{aligned} T_3 &= 2T_2 - T_1, \\ &= 3T_1 - 2T_0, \end{aligned} \tag{9.12}$$

$$\begin{aligned} T_4 &= 2T_3 - T_2, \\ &= 4T_1 - 3T_0. \end{aligned} \tag{9.13}$$

We recognize the pattern and conclude that T_n has the general form

$$T_n = nT_1 - (n-1)T_0, \tag{9.14}$$

which we prove by complete induction:

$$\begin{aligned} T_{n+1} &= 2T_n - T_{n-1} \\ &= 2(nT_1 - (n-1)T_0) - [(n-1)T_1 - (n-2)T_0] \\ &= (n+1)T_1 - nT_0. \end{aligned} \tag{9.15}$$

Hence, expression (9.14) is valid for all $n = 1, \dots, N$. However, since T_N is kept constant according to the boundary condition, we can determine T_1 from

$$T_N = NT_1 - NT_0 + T_0, \tag{9.16}$$

which yields

$$T_1 = \frac{T_N - T_0}{N} + T_0. \tag{9.17}$$

Inserting (9.17) into (9.14) gives

$$\begin{aligned} T_n &= T_0 + (T_N - T_0)\frac{n}{N} \\ &= T_0 + (T_N - T_0)\frac{nh}{L}, \end{aligned} \tag{9.18}$$

which is exactly the discretized version of Eq. (9.4). Hence the finite difference approach to the boundary value problem (9.3) is exact and independent of the grid-spacing h. This is not surprising since we proved already in Chap. 2 that finite difference derivatives are exact for linear functions.

9.3 A Second Scenario

We consider the inhomogeneous heat equation

$$\frac{\partial}{\partial t}T = \kappa \Delta T - \Gamma(x,t). \tag{9.19}$$

Here $\Gamma(x,t) \equiv \Gamma(x)$ is some heat source or heat drain, which is assumed to be independent of time t. Again, we consider the one dimensional, stationary case, i.e.

$$\frac{\mathrm{d}^2}{\mathrm{d}x^2}T = \frac{1}{\kappa}\Gamma(x), \tag{9.20}$$

with the same boundary conditions as in Eq. (9.4). Furthermore, we assume $\Gamma(x)$ to be of the form

$$\Gamma(x) = \frac{\Theta}{\ell}\exp\left[-\frac{\left(x - \frac{L}{2}\right)^2}{\ell^2}\right], \tag{9.21}$$

i.e. $\Gamma(x)$ has the form of a Gauss peak which is centered at $x = L/2$ and has a width determined by the parameter ℓ and a maximum height given by the constant Θ. Such a situation might occur, for instance, when the rod is heated with some kind of a heat gun or cooled by a cold spot. (In the case of the diffusion equation one could imagine, that the density of electrons ρ is constant at the contacts at $x = 0$ and $x = L$. The source/drain term $\Gamma(x)$ then accounts for a constant generation or recombination rate of electrons, for instance, through incoming light or intrinsic traps, respectively.)

Furthermore, we note that in the limiting case $\ell \to 0$ we have

$$\lim_{\ell \to 0} \Gamma(x) = \Theta\delta\left(x - \frac{L}{2}\right), \tag{9.22}$$

where $\delta(\cdot)$ is the DIRAC δ-distribution; in this case the spatial extension of the source/drain term $\Gamma(x)$ is infinitesimal.

We now employ the results of Sect. 8.2 and rewrite the system of equations in the familiar form

$$AT = F, \tag{9.23}$$

where A has already been given in Eq. (9.8), $T = (T_1, T_2, \ldots, T_{N-1})^T$ and F is given by

$$F = \frac{h^2}{\kappa} \begin{pmatrix} \Gamma_1 - \frac{\kappa}{h^2} T_0 \\ \Gamma_2 \\ \vdots \\ \Gamma_{N-2} \\ \Gamma_{N-1} - \frac{\kappa}{h^2} T_N \end{pmatrix}. \tag{9.24}$$

Here we used the notation $\Gamma_n \equiv \Gamma(x_n)$.

The system is solved numerically quite easily using methods discussed by PRESS et al. [1] for the solution of sets of algebraic equations of the kind (9.24) with tridiagonal matrix A. We chose $L = 10$, $\kappa = 1$, $\Theta = -0.4$, $\ell = 1$, $T_0 = 0$ and $T_N = 2$. The resulting temperature profiles $T(x)$ (solid line) for different values of N can be found in Figs. 9.2, 9.3 and 9.4 as well as the respective form of the function $\Gamma(x)$ (dashed line). With increasing number of steps we see, as it was to be expected, a refinement of the temperature profile. Its maximum does not quite agree with the minimum of $\Gamma(x)$, it is shifted slightly towards the end of the rod because of the boundary conditions, i.e. $T_0 < T_N$.

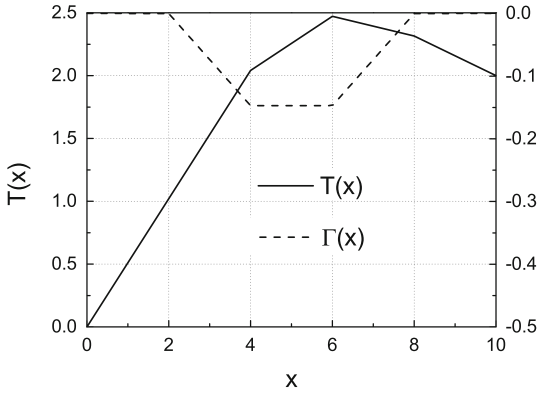

Fig. 9.2 Temperature profile $T(x)$ (*solid line*, *left hand scale*) and the source function $\Gamma(x)$ (*dashed line*, *right hand scale*) for $N = 5$

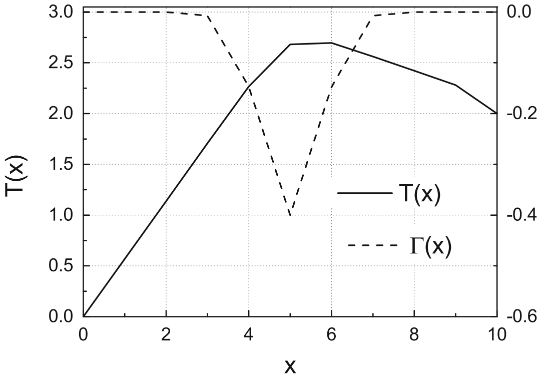

Fig. 9.3 Temperature profile $T(x)$ (*solid line*, *left hand scale*) and the source function $\Gamma(x)$ (*dashed line*, *right hand scale*) for $N = 10$

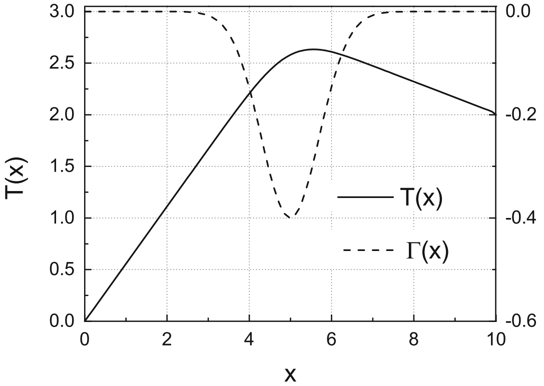

Fig. 9.4 Temperature profile $T(x)$ (*solid line*, *left hand scale*) and the source function $\Gamma(x)$ (*dashed line*, *right hand scale*) for $N = 100$

Summary

The methods of Sect. 8.2 were applied to find the numerical solution of the stationary heat equation with DIRICHLET boundary conditions. We studied the particular case of an isolated rod of length L. This reduced the dimensionality of the differential equation to one. The length of the rod was then divided into N discrete grid-points. Using finite differences the one-dimensional ordinary second order differential equation which described this particular problem was transformed into a set of linear algebraic equations which determined the temperatures at each grid-point. This set of algebraic equations was characterized by a tridiagonal coefficient matrix. Solutions have been studied with and without a heat source which was described as a 'point' source characterized by a Gaussian of given width and amplitude. In the first case analytic solutions were easily derived. They described a linear temperature profile increasing (decreasing) from T_0 to T_N. In the latter case solutions were generated numerically using specific algorithms designed for sets of algebraic equations with a tridiagonal coefficient matrix A.

Problems

1. Calculate the stationary temperature profile across the cylindrical rod of Fig. 9.1 which is exposed to a heat sink centered around $x = L/2$. This heat sink is described by a function $\Gamma(x)$ which is of rectangular shape of width a and depth θ. Both ends of the rod are kept at constant temperatures T_0 and T_N, respectively.
2. Investigate the three cases $T_0 > T_N$, $T_0 < T_N$, $T_0 = T_N > 0$, and study the influence of the width a of the heat sink on the temperature profile.

Reference

1. Press, W.H., Teukolsky, S.A., Vetterling, W.T., Flannery, B.P.: Numerical recipes in C++, 2nd edn. Cambridge University Press, Cambridge (2002)

Chapter 10
The One-Dimensional Stationary SCHRÖDINGER Equation

10.1 Introduction

The numerical solution of the stationary SCHRÖDINGER equation is discussed to illustrate the application of NUMEROV's shooting method as it was described in Sect. 8.3.

We start the discussion with a brief survey of basic quantum mechanics (see for instance the books by G. BAYM [1], by C. COHEN-TANNOUDJI et al. [2], or by J.J. SAKURAI [3]). Of course, this chapter is not supposed to give a self-contained introduction to quantum mechanics and the reader not familiar with quantum mechanics should, therefore, regard the following discussion from a purely mathematical point of view.

A quantum-mechanical wave-function $\Psi \equiv \Psi(x,t) \in \mathbb{C}$ as a function of time $t \in \mathbb{R}^+$ and space $x \in \mathbb{R}^3$, obeys the SCHRÖDINGER equation

$$i\hbar \frac{\mathrm{d}}{\mathrm{d}t}\Psi = H\Psi, \tag{10.1}$$

where $\hbar = h/(2\pi)$ is the reduced PLANCK constant, i is the imaginary unit, and H is the HAMILTON operator or Hamiltonian. If $H \neq H(t)$, i.e. the Hamiltonian is independent of time t, we can employ a product ansatz

$$\Psi(x,t) = \exp\left(-\frac{i}{\hbar}Et\right)\psi(x), \tag{10.2}$$

where E is the energy and $\psi(x)$ is the time-independent part of the wave-function. This ansatz transforms Eq. (10.1) into

$$\begin{aligned} i\hbar\frac{\mathrm{d}}{\mathrm{d}t}\left[\exp\left(-\frac{i}{\hbar}Et\right)\psi(x)\right] &= i\hbar\left(-\frac{i}{\hbar}E\right)\exp\left(-\frac{i}{\hbar}Et\right)\psi(x) \\ &= \exp\left(-\frac{i}{\hbar}Et\right)H\psi(x), \end{aligned} \tag{10.3}$$

B. A. Stickler and E. Schachinger, *Basic Concepts in Computational Physics*,
DOI: 10.1007/978-3-319-02435-6_10, © Springer International Publishing Switzerland 2014

and $\psi(x)$ is determined by the eigenvalue problem

$$H\psi = E\psi, \tag{10.4}$$

augmented by appropriate boundary conditions. We already came across Eq. (10.4) when we discussed shooting methods in Sect. 8.3. The one-particle Hamiltonian is of the general form

$$H = T + V = \frac{P^2}{2m} + V, \tag{10.5}$$

where T is the kinetic energy operator, V is the potential operator, P is the momentum operator and m is the particle's mass. If the system is not exposed to an external magnetic field, P can be expressed in position space by

$$P = -i\hbar\nabla_x, \tag{10.6}$$

and the potential operator V by $V(x)$. Thus we get for Eq. (10.5):

$$H = -\frac{\hbar^2}{2m}\Delta + V(x). \tag{10.7}$$

Hence, we have to solve the linear, second order partial differential equation:

$$-\frac{\hbar^2}{2m}\Delta\psi(x) + V(x)\psi(x) = E\psi(x). \tag{10.8}$$

Equation (10.8) will certainly not have solutions for arbitrary values of the energy E. The particular values $E = E_n$ for which (10.7) has a solution are referred to as *eigenenergies* and the corresponding solution $\psi_n(x)$ is referred to as *eigenfunction* to the eigenenergy E_n. We rewrite Eq. (10.8) in order to emphasize this point as

$$-\frac{\hbar^2}{2m}\Delta\psi_n(x) + V(x)\psi_n(x) = E_n\psi_n(x)\ , \qquad n = 1, 2, 3, \ldots. \tag{10.9}$$

We define the scalar product between two functions $\chi(x)$ and $\varphi(x)$

$$\langle\chi|\varphi\rangle = \int \mathrm{d}x\,\chi^*(x)\varphi(x), \tag{10.10}$$

where $\chi^*(x)$ denotes the complex conjugate of $\chi(x)$. The corresponding L^2-norm reads

$$|\chi| = \sqrt{\langle\chi|\chi\rangle} = \sqrt{\int \mathrm{d}x|\chi(x)|^2}. \tag{10.11}$$

The expectation value of an operator O in the quantum mechanical state Ψ is given by

$$\langle O \rangle = \frac{\langle \Psi | O \Psi \rangle}{\langle \Psi | \Psi \rangle} = \frac{\int \mathrm{d}x \Psi^*(x) O \Psi(x)}{\int \mathrm{d}x |\Psi(x)|^2}. \tag{10.12}$$

We note from Eq. (10.4) that the energy is the expectation value of the HAMILTON operator H

$$\langle H \rangle = \frac{\int \mathrm{d}x \Psi^*(x) H \Psi(x)}{\int \mathrm{d}x |\Psi(x)|^2} = E. \tag{10.13}$$

In the following we quote some important properties. A detailed discussion can be found in any textbook on quantum mechanics.

- The expectation value $\langle O \rangle$ of a Hermitian operator O, $O^\dagger = O$, is real, i.e. $\langle O \rangle = \langle O \rangle^*$. Here $O^\dagger$ denotes the adjoint of O, i.e. $O^\dagger = (O^*)^T$.
- Every real expectation value can be described by a Hermitian operator.
- All observables can be described by Hermitian operators, in particular, the Hamiltonian *has* to be a *Hermitian* operator to ensure that the eigenenergies E_n are real, $E_n \in \mathbb{R}$.
- It follows from the hermiticity of H that the eigenfunctions $\psi_n(x)$ form a complete, orthogonal basis in HILBERT space. Furthermore, the functions can be normalized and the relation

$$\langle \psi_n | \psi_m \rangle = \delta_{nm}, \tag{10.14}$$

holds, with δ_{nm} the KRONECKER-δ.

The expectation value of a Hermitian operator O (10.12) can be rewritten with the help of (10.14) as

$$\langle O \rangle = \int \mathrm{d}x \Psi^*(x) O \Psi(x). \tag{10.15}$$

Furthermore, the total wave-function $\Psi(x,t)$ (10.2) consists of contributions from different eigenenergies. We define

$$\Psi_n(x,t) = \exp\left(-\frac{i}{\hbar} E_n t\right) \psi_n(x), \tag{10.16}$$

and write the total wave-function $\Psi(x,t)$ as a superposition of wave-functions $\Psi_n(x,t)$

$$\Psi(x,t) = \sum_n c_n \Psi_n(x,t), \tag{10.17}$$

because the $\Psi_n(x,t)$ constitute a complete, orthogonal basis. We note that this is only possible because the SCHRÖDINGER equation is linear. Again, we demand $\Psi(x,t)$ to be normalized for all t. Employing Eq. (10.14) in Eq. (10.17) yields

$$\int \mathrm{d}x |\Psi(x,t)|^2 = \sum_n |c_n|^2 = 1. \tag{10.18}$$

We give the following interpretation of the squared modulus of the wave-function without going into detail:

$$|\Psi(x,t)|^2 \mathrm{d}x = \text{The probability that the particle described by the wave-function } \Psi(x,t) \text{ can be found at time } t \text{ within a volume } dx \text{ around the point } x. \tag{10.19}$$

This interpretation justifies the requirement of a normalization of the wave-function $\Psi(x,t)$

$$\int \mathrm{d}x |\Psi(x,t)|^2 \overset{!}{=} 1, \tag{10.20}$$

because, by definition the particle has to be found somewhere anytime.

Suppose we start with an initial state $\chi(x) = \Psi(x, t = 0)$. Since the functions $\psi_n(x)$ form a complete basis in HILBERT space, $\chi(x)$ may be written with the help of (10.17) as

$$\chi(x) = \sum_n c_n \psi_n(x). \tag{10.21}$$

We deduce from (10.14) that

$$\langle \psi_m | \chi \rangle = \sum_n c_n \int \mathrm{d}x \psi_m^*(x) \psi_n(x) = c_m. \tag{10.22}$$

We note that $|c_m|^2$ is the probability that the particle was initially in state m. This allows us to interpret Eq. (10.17) in the following way: The coefficients c_m determine the composition of the initial state. The exponential factor describes an oscillation and we note that different eigenfunctions, which correspond to different eigenenergies, oscillate with different frequencies. This can, for instance, induce the diffluence of a wave packet.

In what follows, we will concentrate on the one-dimensional SCHRÖDINGER equation, that is $x \in \mathbb{R}$. We give a simple example, which will then be solved numerically in Sect. 10.3

10.2 A Simple Example: The Particle in a Box

Since $x \in \mathbb{R}$ we rewrite (10.7) as

$$-\frac{\hbar^2}{2m}\frac{\mathrm{d}^2}{\mathrm{d}x^2}\psi_n(x) + V(x)\psi_n(x) = E_n\psi_n(x), \tag{10.23}$$

and specify

$$V(x) = \begin{cases} 0 & 0 \le x \le L, \\ \infty & \text{elsewhere,} \end{cases} \tag{10.24}$$

together with the boundary conditions

$$\psi_n(0) = \psi_n(L) = 0, \qquad n = 1, 2, 3, \ldots\ , \tag{10.25}$$

and the normalization condition

$$\int \mathrm{d}x |\psi_n(x)|^2 = \int_0^L \mathrm{d}x |\psi_n(x)|^2 = 1, \qquad n = 1, 2, 3, \ldots . \tag{10.26}$$

We note that the boundary conditions are dictated by the particular form of the potential (10.24) which requires that $\psi_n(x) = 0$ for $x \notin [0, L]$. This problem is commonly referred to as the *particle in a one-dimensional box*.

Let us introduce dimensionless variables in order to simplify the numerics of Eq. (10.23). We define new variables

$$s = \frac{x}{L}, \qquad \varepsilon_n = \frac{E_n}{\overline{E}}, \tag{10.27}$$

where L is the length scale and $\overline{E}$ is the energy scale. The energy scale $\overline{E}$ is fully determined by the relation

$$\overline{E} = \frac{\hbar^2}{mL^2}. \tag{10.28}$$

We note that $s \in [0, 1]$, hence the rescaled wave-function is given by

$$\varphi_n(s) = \sqrt{L}\psi_n(x), \tag{10.29}$$

which satisfies the normalization condition

$$\int_0^L \mathrm{d}x |\psi_n(x)|^2 = \int_0^1 \mathrm{d}s |\varphi_n(s)|^2 = 1. \tag{10.30}$$

The rescaled SCHRÖDINGER equation can be obtained by multiplying Eq. (10.23) with $1/\overline{E}$:

$$
\begin{aligned}
-\frac{\hbar^2}{2m\overline{E}}\frac{\mathrm{d}^2}{\mathrm{d}x^2}\psi_n(x) + \frac{V(x)}{\overline{E}}\psi_n(x) &= -\frac{L^2}{2}\frac{\mathrm{d}^2}{\mathrm{d}x^2}\psi_n(x) + v(s)\psi_n(x) \\
&= -\frac{1}{2}\frac{\mathrm{d}^2}{\mathrm{d}s^2}\psi_n(x) + v(s)\psi_n(x) \\
&= \frac{E_n}{\overline{E}}\psi_n(x) \\
&= \varepsilon_n\psi_n(x) \ . \qquad (10.31)
\end{aligned}
$$

Here we introduced the rescaled potential $v(s)$

$$
v(s) = \begin{cases} 0 & 0 \le s \le 1, \\ \infty & \text{elsewhere.} \end{cases} \qquad (10.32)
$$

Hence, the rescaled wave-function (10.29) is a solution of the differential equation:

$$
-\frac{1}{2}\frac{\mathrm{d}^2}{\mathrm{d}s^2}\varphi_n(s) + v(s)\varphi_n(s) = \varepsilon_n\varphi_n(s). \qquad (10.33)
$$

We already stated that the form of the potential implies that $\varphi_n(s) = 0$ for all $s \notin [0, 1]$. Therefore, the complete boundary value problem can be written for $n = 1, 2, 3, \dots$ as

$$
\begin{cases} -\frac{1}{2}\frac{\mathrm{d}^2}{\mathrm{d}s^2}\varphi_n(s) = \varepsilon_n\varphi_n(s), & s \in [0, 1], \\ \varphi_n(0) = 0, \\ \varphi_n(1) = 0. \end{cases} \qquad (10.34)
$$

It is an easy task to solve this boundary value problem analytically. For $s \in [0, 1]$ we choose the ansatz

$$
\varphi_n(s) = A_n \sin(k_n s) + B_n \cos(k_n s), \qquad (10.35)
$$

where A_n and B_n are some constants and k_n is given by

$$
k_n = \sqrt{2\varepsilon_n} \ . \qquad (10.36)
$$

From the boundary conditions we obtain

$$
\varphi_n(0) = B_n = 0, \qquad (10.37)
$$

and

$$
\varphi_n(1) = A_n \sin(k_n) = 0. \qquad (10.38)
$$

It follows from Eq. (10.38) that

$$k_n = n\pi, \qquad n = 1, 2, 3, \dots, \tag{10.39}$$

and, therefore, that the eigenenergies ε_n are quantized

$$\varepsilon_n = \frac{n^2\pi^2}{2}, \tag{10.40}$$

and the corresponding eigenfunctions $\varphi_n(s)$ are of the form

$$\varphi_n(s) = \begin{cases} A_n \sin(n\pi s) & s \in [0, 1], \\ 0 & \text{elsewhere.} \end{cases} \tag{10.41}$$

The constants A_n are determined from the normalization condition (10.30)[1]

$$\begin{aligned} \int_0^1 \mathrm{d}s |\varphi_n(s)|^2 &= A_n^2 \int_0^1 \mathrm{d}s \sin^2(n\pi s) \\ &= \frac{A_n^2}{n\pi} \int_0^{n\pi} \mathrm{d}u \sin^2(u) \\ &= \frac{A_n^2}{\pi} \int_0^{\pi} \mathrm{d}u \sin^2(u) \\ &= \frac{A_n^2}{\pi} \frac{\pi}{2} \\ &= \frac{A_n^2}{2} \\ &\overset{!}{=} 1, \end{aligned} \tag{10.44}$$

and:

$$A_n = \sqrt{2}\,. \tag{10.45}$$

[1] Here we make use of

$$\begin{aligned} \int \mathrm{d}u \sin^2(u) &= -\cos(u)\sin(u) + \int \mathrm{d}u \cos^2(u) \\ &= -\cos(u)\sin(u) + \int \mathrm{d}u \left[1 - \sin^2(u)\right], \end{aligned} \tag{10.42}$$

and, therefore

$$\int \mathrm{d}u \sin^2(u) = \frac{1}{2}\left[u - \cos(u)\sin(u)\right]. \tag{10.43}$$

Finally, we employ relations (10.27), (10.28) and (10.29) to obtain

$$\psi_n(x) = \frac{1}{\sqrt{L}}\varphi_n\left(\frac{x}{L}\right) = \begin{cases} \sqrt{\frac{2}{L}}\sin\left(\frac{n\pi x}{L}\right) & x \in [0, L], \\ 0 & \text{elsewhere,} \end{cases} \tag{10.46}$$

and

$$E_n = \varepsilon_n \overline{E} = \frac{\hbar^2\pi^2 n^2}{2mL^2}\ . \tag{10.47}$$

In most cases it is required to calculate expectation values of some observables. We might, for instance, be interested in the expectation value $\langle x\rangle$ of the position operator x or its variance $\text{var}\,(x) = \left\langle (x - \langle x\rangle)^2\right\rangle$. It follows from Eq. (10.27) that

$$\langle x\rangle = L\,\langle s\rangle\,, \quad \text{and} \quad \left\langle (x - \langle x\rangle)^2\right\rangle = L^2\left\langle (s - \langle s\rangle)^2\right\rangle = L^2 \text{var}\,(s)\,. \tag{10.48}$$

Employing definition (10.15) together with the solution (10.41) gives $\langle s\rangle$:

$$\begin{aligned}
\langle s\rangle &= 2\int_0^1 \mathrm{d}s\,\sin^2(n\pi s)s \\
&= \frac{2}{n^2\pi^2}\int_0^{n\pi} \mathrm{d}u\,\sin^2(u)u \\
&= \frac{2}{n\pi^2}\left\{\frac{1}{2}\left[u^2 - u\cos(u)\sin(u)\right]_0^{n\pi} - \frac{1}{2}\int_0^{n\pi}\mathrm{d}u\,[u - \cos(u)\sin(u)]\right\} \\
&= \frac{2}{n\pi^2}\left(\frac{n^2\pi^2}{2} - \frac{n^2\pi^2}{4} + \frac{\sin^2(u)}{4}\bigg|_0^{n\pi}\right) \\
&= \frac{1}{2}\,.
\end{aligned} \tag{10.49}$$

Here we made again use of relation (10.43). Furthermore, we obtain for $\left\langle s^2\right\rangle$:

$$\begin{aligned}
\left\langle s^2\right\rangle &= 2\int_0^1 \mathrm{d}s\,\sin^2(n\pi s)s^2 \\
&= \frac{2}{n^3\pi^3}\int_0^{n\pi}\mathrm{d}u\,\sin^2(u)u^2
\end{aligned}$$

$$
\begin{aligned}
&= \frac{2}{n^3\pi^3}\left\{\frac{1}{2}\Big[u^3 - u^2\cos(u)\sin(u)\Big]_0^{n\pi} - \int\limits_0^{n\pi} \mathrm{d}u\Big[u^2 - u\cos(u)\sin(u)\Big]\right\} \\
&= \frac{2}{n^3\pi^3}\left[\frac{n^3\pi^3}{2} - \frac{n^3\pi^3}{3} + \int\limits_0^{n\pi} \mathrm{d}u u\cos(u)\sin(u)\right] \\
&= \frac{2}{n^3\pi^3}\left\{\frac{n^3\pi^3}{6} + \left[u\frac{\sin^2(u)}{2}\right]_0^{n\pi} - \frac{1}{2}\int\limits_0^{n\pi} \mathrm{d}u\sin^2(u)\right\} \\
&= \frac{2}{n^3\pi^3}\left(\frac{n^3\pi^3}{6} - \frac{n\pi}{4}\right) \\
&= \frac{1}{3} - \frac{1}{2n^2\pi^2}\,. \qquad (10.50)
\end{aligned}
$$

Hence, the variance var (s) is determined by

$$
\left\langle (s - \langle s\rangle)^2 \right\rangle = \left\langle s^2 \right\rangle - \langle s\rangle^2 = \frac{1}{3} - \frac{1}{2n^2\pi^2} - \frac{1}{4} = \frac{1}{12}\left(1 - \frac{6}{n^2\pi^2}\right). \qquad (10.51)
$$

We note that the variance increases with increasing n. In the following we shall reproduce the above results with help of the shooting NUMEROV method. Furthermore, the numerical formulation will allow us to find solutions for more complex potentials.

10.3 Numerical Solution

The following discussion is based on the scaled SCHRÖDINGER equation (10.33). However, we consider a more general potential of the form

$$
v(s) = \begin{cases} \tilde{v}(s) & 0 \le s \le 1, \\ \infty & \text{elsewhere.} \end{cases} \qquad (10.52)
$$

Hence, the boundary value problem (10.34) takes on the form

$$
\begin{cases} -\frac{1}{2}\frac{\mathrm{d}^2}{\mathrm{d}s^2}\varphi_n(s) + \tilde{v}(s)\varphi_n(s) = \varepsilon_n\varphi_n(s) & s \in [0, 1], \\ \varphi_n(0) = 0, \\ \varphi_n(1) = 0. \end{cases} \qquad (10.53)
$$

Moreover, our numerical treatment will be based on shooting methods, discussed in Sect. 8.3. Therefore, we rewrite the second order differential equation in Eq. (10.53) in a form which corresponds to Eq. (8.54), namely:

$$\varphi_n''(s) + 2\left[\varepsilon_n - \tilde{v}(s)\right]\varphi_n(s) = 0. \tag{10.54}$$

The interval [0, 1] is discretized using $N + 1$ grid-points $s_\ell = \ell/N$, $\ell = 0, 1, 2, \ldots, N$ $(h = 1/N)$ and we denote with $\varphi_n(s_\ell)$ and $\tilde{v}(s_\ell) \equiv v_\ell$ the values of $\varphi_n(s)$ and $\tilde{v}(s)$ at those grid-points. This allows to rewrite Eq. (8.59) as

$$\varphi_n(s_{\ell+1}) = \frac{2\left[1 - \frac{5}{6N^2}\left(\varepsilon_n - \tilde{v}_\ell\right)\right]\varphi_n(s_\ell) - \left[1 + \frac{1}{6N^2}\left(\varepsilon_n - \tilde{v}_{\ell-1}\right)\right]\varphi_n(s_{\ell-1})}{1 + \frac{1}{6N^2}\left(\varepsilon_n - \tilde{v}_{\ell+1}\right)}. \tag{10.55}$$

Again, we will denote solutions of this equation by $\varphi_n(s_\ell;\varepsilon)$ to emphasize their dependence on the eigenvalue ε.

We use the initial conditions $\varphi_n(s_0) = 0$ and $\varphi_n'(s_0) = 1$, which is always possible, since (10.53) is a homogeneous boundary value problem. This gives

$$\varphi_n'(s_0) \approx \frac{\varphi_n(s_1) - \varphi_n(s_{-1})}{2h} = 1 \quad \Rightarrow \quad \varphi_n(s_1) = \frac{2}{N}\,. \tag{10.56}$$

The normalization of the wave-function (10.30) is then approximated with the help of the forward rectangular rule (3.9):

$$\int_0^1 \mathrm{d}s|\varphi_n(s)|^2 \approx h\sum_{\ell=0}^{N}\left[\varphi_n(s_\ell)\right]^2 \overset{!}{=} 1. \tag{10.57}$$

Consistently, we approximate the expectation value $\langle s\rangle$ via

Table 10.1 Comparison between analytic and numerical eigenenergies for the particle in a box for $N = 100$

n	ε_n-analytic	ε_n-numeric
1	4.934802	4.934802
2	19.739209	19.739208
3	44.413219	44.413205
4	78.956835	78.956753
5	123.370055	123.369742
6	177.652879	177.651943
7	241.805308	241.802947
8	315.827341	315.822077
9	399.718978	399.708300
10	493.480220	493.460113

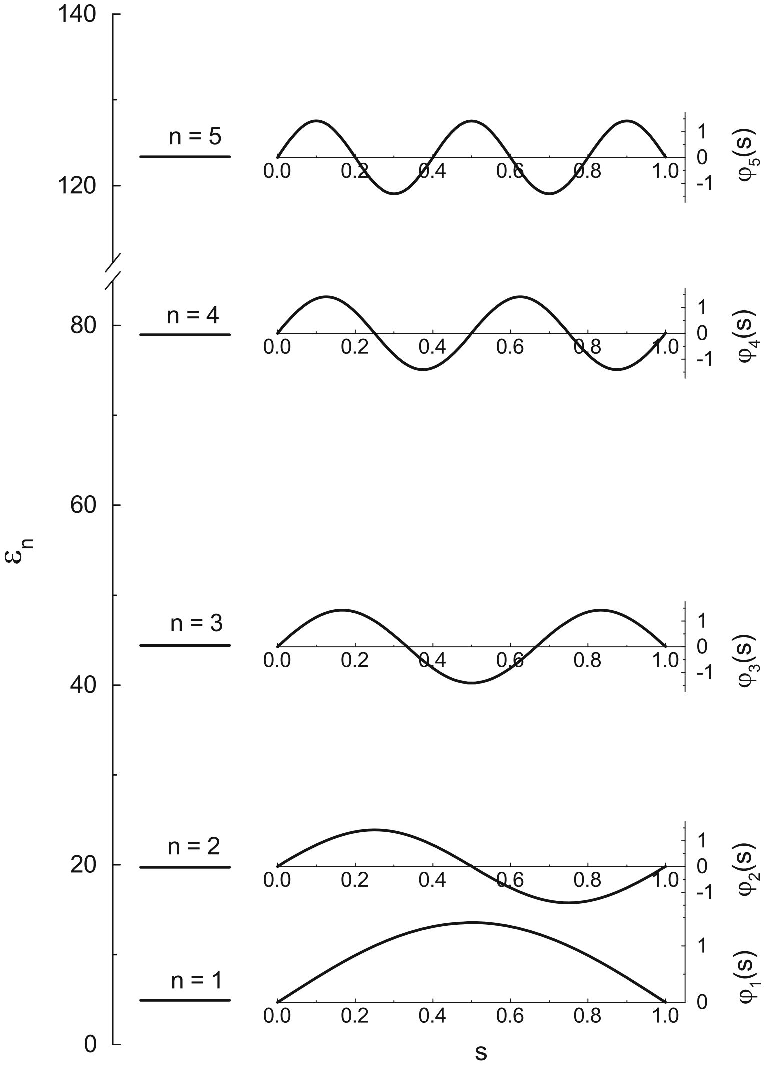

Fig. 10.1 The first five numerically determined eigenvalues ε_n of Table 10.1 are presented has horizontal lines (*left hand scale*). Aligned with these eigenvalues are the corresponding eigenfunctions $\varphi_n(s)$ versus s for $N = 100$ (*right hand scales*)

$$\int_0^1 \mathrm{d}s\, s|\varphi_n(s)|^2 \approx h \sum_{\ell=0}^{N} [\varphi_n(s_\ell)]^2\, s_\ell \ . \tag{10.58}$$

The NUMEROV shooting algorithm is then defined by the following steps:

1. Choose two trial energies ε_a and ε_b and define the required accuracy η.
2. Calculate $\varphi(s_N; \varepsilon_a) \equiv \varphi_a$ and $\varphi(s_N; \varepsilon_b) \equiv \varphi_b$ using Eq. (10.55).

3. If $\varphi_a \varphi_b > 0$, choose new values for ε_a or ε_b and go to step 1.
4. If $\varphi_a \varphi_b < 0$, calculate $\varepsilon_c = (\varepsilon_a + \varepsilon_b)/2$ and determine $\varphi(s_N; \varepsilon_c) \equiv \varphi_c$ using Eq. (10.55).
5. If $\varphi_a \varphi_c < 0$, set $\varepsilon_b = \varepsilon_c$ and go to step 4.
6. If $\varphi_c \varphi_b < 0$, set $\varepsilon_a = \varepsilon_c$ and go to step 4.
7. Terminate the loop when $|\varepsilon_a - \varepsilon_b| < \eta$.

These steps have been carried out for 100 grid-points, a potential $\tilde{v} = 0$, and a required accuracy of $\eta = 10^{-10}$. The first ten eigenenergies are given in Table 10.1 and are compared with the analytic results (10.40).

In addition, Fig. 10.1 presents the first five eigenvalues ε_n (right hand scale) as horizontal straight lines. Aligned with these eigenvalues we find on the right hand side of this figure the corresponding normalized eigenfunctions calculated using $N = 100$ grid-points. The agreement with the analytic result of Eq. (10.41) is excellent.

10.4 Another Case

Here we discuss briefly some results achieved with the help of NUMEROV's shooting algorithm. In particular, we discuss the particle in the box for three different potentials $\tilde{v}(s)$ [see Eq. (10.52)],

$$\tilde{v}_1(s) = 50\cos(\pi s), \quad \tilde{v}_2(s) = 50\exp\left[-\frac{\left(s - \frac{1}{2}\right)^2}{0.08}\right], \quad \tilde{v}_3(s) = 50s. \qquad (10.59)$$

The potentials are illustrated in Fig. 10.2. All calculations were carried out with $N = 100$ grid-points and an accuracy $\eta = 10^{-10}$. The first five eigenenergies ε_n are shown in Figs. 10.3, 10.4 and 10.5, respectively, as horizontal lines (left hand scale).

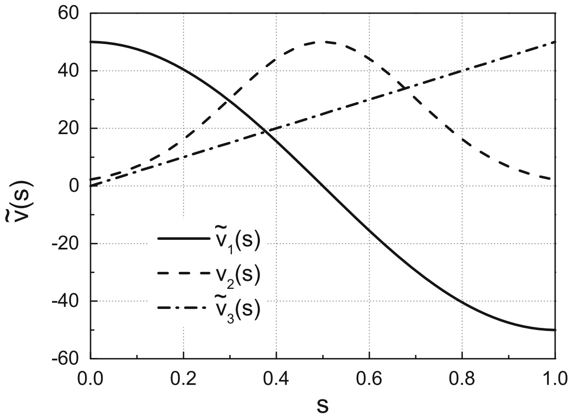

Fig. 10.2 The three different potentials $\tilde{v}(s)$ introduced by Eq. (10.59)

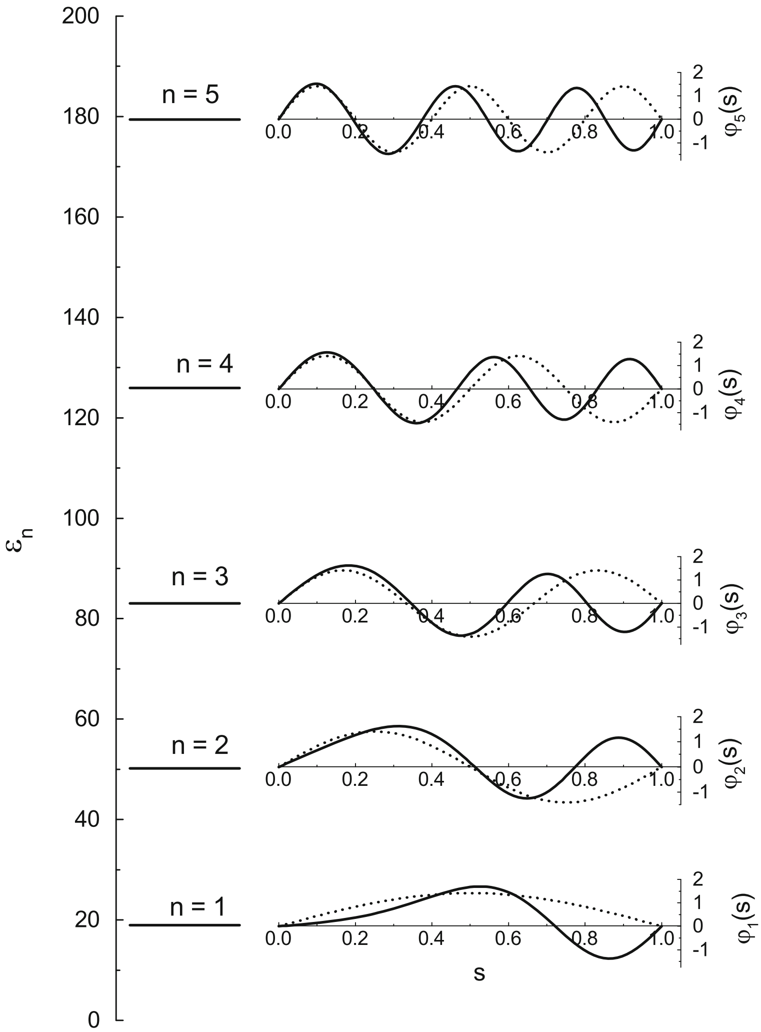

Fig. 10.3 Numerically determined eigenvalues ε_n (*left hand scale*) and eigenfunctions $\varphi_n(s)$ versus s (*right hand scales*) for the potential $\tilde{v}_1(s)$. The first five eigenvalues are presented as straight *horizontal lines*. Aligned with these lines the eigenfunctions are shown on the *right hand side* of this figure. The *dotted lines* indicate the eigenfunctions of the particle in the box with $\tilde{v}(s) = 0$ (see Fig. 10.1)

The numerically determined normalized eigenfunctions $\varphi_n(s)$ versus s (solid lines) are presented on the right hand side of these figures and are aligned with their respective eigenvalues. They are also compared with the eigenfunctions (dotted lines) of the particle in a box, i.e. $\tilde{v}(s) = 0$. In all cases the eigenfunctions reflect the symmetry of the various potentials $\tilde{v}(s)$ which becomes particularly transparent in Fig. 10.3 for the potential $\tilde{v}_1(s)$. The eigenfunctions develop an additional node in

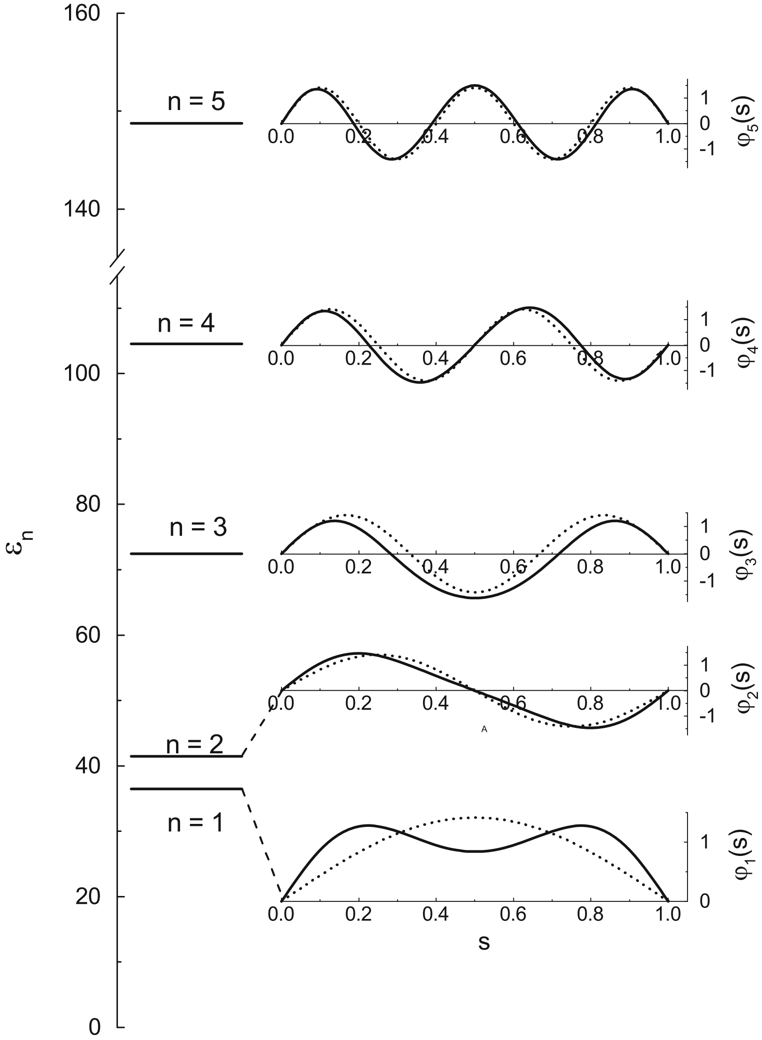

Fig. 10.4 Numerically determined eigenvalues ε_n (*left hand scale*) and eigenfunctions $\varphi_n(s)$ versus s (*right hand scales*) for the potential $\tilde{v}_2(s)$. The first five eigenvalues are presented as straight *horizontal lines*. Aligned with these lines the eigenfunctions are shown on the *right hand side* of this figure. The *dotted lines* indicate the eigenfunctions of the particle in the box with $\tilde{v}(s) = 0$ (see Fig. 10.1)

comparison to the eigenfunctions calculated for $\tilde{v}(s) = 0$. In the other two cases only the very first eigenfunctions $n \geq 3$ appear to be affected by the potential. Moreover, in all three cases, the respective eigenvalues are shifted towards higher values which is consistent with a general result of quantum mechanical perturbation theory.

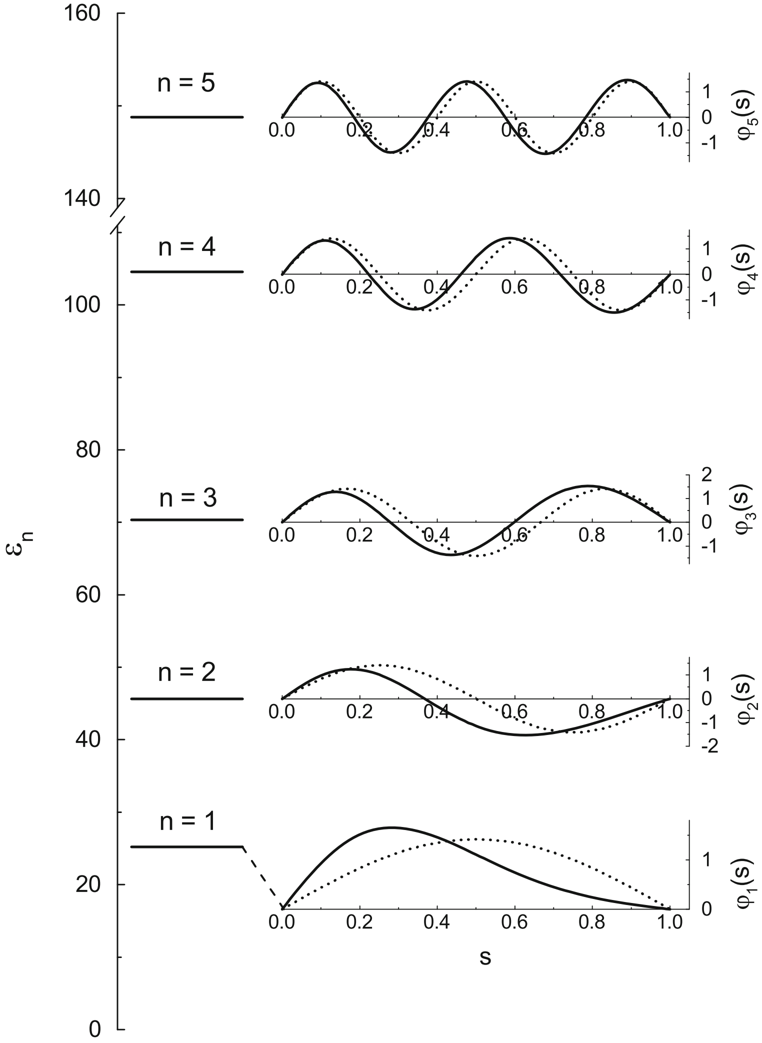

Fig. 10.5 Numerically determined eigenvalues ε_n (*left hand scale*) and eigenfunctions $\varphi_n(s)$ versus s (*right hand scales*) for the potential $\tilde{v}_3(s)$. The first five eigenvalues are presented as straight *horizontal lines*. Aligned with these lines the eigenfunctions are shown on the *right hand side* of this figure. The *dotted lines* indicate the eigenfunctions of the particle in the box with $\tilde{v}(s) = 0$ (see Fig. 10.1)

Summary

The quantum-mechanical problem of a particle in a box was described by a homogeneous boundary value problem which could be solved analytically if the box' potential $\tilde{v}(s) = 0$. On the other hand, NUMEROV's shooting algorithm was particularly designed to treat effectively homogeneous boundary value problems.

Consequently, the problem of the particle in the box was used to design a NUMEROV shooting algorithm which was then tested against the analytic results. The agreement between numerics and analytical results turned out to be excellent and proved the quality of the method. For illustrative purposes the problem of the particle in the box was then solved numerically for three different, more complex, box-potentials $\tilde{v}(s)$.

Problems

1. Solve the one-dimensional stationary SCHRÖDINGER equation in an infinitely deep potential well by employing the shooting method according to NUMEROV of Sect. 8.3. The total potential $v(s)$ is assumed to be of the form (10.52). Choose different potentials $\tilde{v}(s)$ within the well.
   You can check your code by reproducing the results presented in Sects. 10.3 and 10.4. In addition, determine numerically the expectation value $\langle x \rangle$ and the variance var (x) of the position operator x for the first five eigenfunctions. This can be achieved by employing the rectangular rule of Chap. 3, as illustrated in Eq. (10.58).
2. Solve the SCHRÖDINGER equation for some potential $\tilde{v}(s)$ of your choice and plot the first five eigenfunctions. This potential should not be equal to one of the potentials discussed in this chapter. Again, calculate $\langle x \rangle$ and var (x) for the first five eigenfunctions.

References

1. Baym, G.: Lectures on Quantum Mechanics. Lecture Notes and Supplements in Physics. The Benjamin/Cummings Publ. Comp., Inc., London (1969)
2. Cohen-Tannoudji, C., Diu, B.: Laloë: Quantum Mechanics, vol. I. John Wiley, New York (1977)
3. Sakurai, J.J.: Modern Quantum Mechanics. Addison-Wesley Publishing Comp, Menlo Park (1985)

Chapter 11
Partial Differential Equations

11.1 Introduction

This section discusses some fundamental aspects of the numerics of partial differential equations and this discussion will be based on methods already encountered in previous chapters, i.e. on finite difference methods. More advanced techniques, such as finite element methods or finite volume methods for conservation laws, are beyond the scope of this book. A detailed discussion of these methods can be found in any textbook on numerics of partial differential equations [1].

Since we already introduced the concepts of finite difference derivatives in Chap. 2 and their application to boundary value problems of ordinary differential equations in Sect. 8.2, we concentrate mainly on the application of these methods to specific types of partial differential equations. In detail, we investigate the POISSON equation as an example for *elliptic partial differential equations*, the time dependent heat equation as an example for *parabolic partial differential equations*, and the wave equation as an example for *hyperbolic partial differential equations*. The concepts presented here are, of course, also applicable to other problems. However, in contrast to the numerics of ordinary differential equations, there exists no general recipe for the solution of partial differential equations.

We remark that the method of finite differences for partial differential equations is particularly useful to find solutions of linear partial differential equations. In case of nonlinear equations, such as the NAVIER-STOKES equations, more advanced techniques have to be employed. However, as in our discussion of ordinary differential equations we strictly restrict to linear partial differential equations. The interested reader is referred to textbooks on advanced computational methods [2, 3].

Another important point to note is that, as in the theory of ordinary differential equations, the problem is only fully determined when initial and/or boundary conditions have been defined. For instance, in the case of the POISSON equation only boundary conditions are required, while for the time-dependent heat equation initial conditions are required as well. In general, pure boundary value problems are easier from a numerical point of view because the question whether or not the algorithm

B. A. Stickler and E. Schachinger, *Basic Concepts in Computational Physics*,
DOI: 10.1007/978-3-319-02435-6_11, © Springer International Publishing Switzerland 2014

is stable does not play such an important role. For combined boundary and initial value problems it is essential to check carefully that the discretization of the time axis is not in conflict with the discretization of the space domain. This is of particular importance in the numerical treatment of hyperbolic partial differential equations, where the so called COURANT-FRIEDRICHS-LEWY (CFL) condition determines the stability of the algorithm. We shall come back to this point in Sects. 11.3 and 11.4.

This chapter will be concluded by a discussion of the numerical solution of the time-dependent SCHRÖDINGER equation in Sect. 11.5.

11.2 The POISSON Equation

We consider the POISSON equation as a model for an elliptic partial differential equation. Nevertheless, we review briefly some basics of electrodynamics. The force $F(r, t)$ as a function of position r and time t acting on a particle with charge q, which moves with velocity ν within an electromagnetic field described by the electric field $E(r, t)$ and the magnetic field $B(r, t)$, is determined from[1]:

$$F(r,t) = q\left[E(r,t) + \frac{\nu}{c} \wedge B(r,t)\right]. \tag{11.1}$$

In the following we shall consider the static, i.e. time-independent case, and, moreover, $B(r, t) = 0$. The electric field E itself is described by the equation

$$\nabla \cdot E(r) = \frac{1}{\varepsilon}\rho(r), \tag{11.2}$$

where the charge density $\rho(r, t)$ acts as the source of the electric field $E(r, t)$. Here ε is the dielectric function and is assumed to be constant in what follows. Furthermore, the electric field E is connected to the electrostatic potential $\varphi(r)$ via

$$E(r) = -\nabla\varphi(r). \tag{11.3}$$

Thus, Eq. (11.2) is reformulated as:

$$\Delta\varphi(r) = -\frac{\rho(r)}{\varepsilon}. \tag{11.4}$$

This equation is referred to as the POISSON equation and in the particular case of $\rho(r) = 0$ it is referred to as the LAPLACE equation.

In what follows we focus on the numerical solution of the two dimensional POISSON equation (11.4) on a square domain $\Omega = [0, L_x] \times [0, L_y]$ together with boundary conditions $\varphi(x, y) = g(x, y)$ on $\partial\Omega$. In detail, we want to solve the two-dimensional boundary value problem

[1] $a \wedge b$ denotes the vector product of the two vectors a and b.

$$\begin{cases} \frac{\partial^2}{\partial x^2}\varphi(x,y) + \frac{\partial^2}{\partial y^2}\varphi(x,y) = -\rho(x,y), & (x,y) \in \Omega, \\ \varphi(x,y) = \ g(x,y), & (x,y) \in \partial\Omega, \end{cases} \tag{11.5}$$

where we absorbed ε into the charge density $\rho(x, y)$. Note that a treatment of the three dimensional case can be carried out in analogue.

We employ a finite difference approximation to the derivatives which appear in Eq. (11.5) (see Chap. 2). Thus, we define grid-points in x and y direction via

$$x_i = x_0 + ih, \quad i = 0, 1, 2, \ldots, n, \tag{11.6a}$$

$$y_j = y_0 + jk, \quad j = 0, 1, 2, \ldots, m, \tag{11.6b}$$

where h and k denote the grid-spacing in x- and y-direction, respectively. As in our discussion in Chap. 2 we will consider only equally spaced grid-points. An extension to non-uniform grids is straightforward.

We define the function values on the grid-points as

$$\varphi_{i,j} \equiv \varphi(x_i, y_j), \tag{11.7}$$

and similarly $\rho_{i,j} \equiv \rho(x_i, y_j)$. Consequently, we find the finite difference approximation of Eq. (11.5):

$$\frac{\varphi_{i-1,j} - 2\varphi_{i,j} + \varphi_{i+1,j}}{h^2} + \frac{\varphi_{i,j-1} - 2\varphi_{i,j} + \varphi_{i,j+1}}{k^2} = -\rho_{i,j}. \tag{11.8}$$

The boundary conditions (11.5) can be written as

$$\varphi_{0,j} = g_{0,j}, \qquad j = 0, 1, \ldots, m, \tag{11.9a}$$
$$\varphi_{n,j} = g_{n,j}, \qquad j = 0, 1, \ldots, m, \tag{11.9b}$$
$$\varphi_{i,0} = g_{i,0}, \qquad i = 1, 2, \ldots, n-1, \tag{11.9c}$$
$$\varphi_{i,m} = g_{i,m}, \qquad i = 1, 2, \ldots, n-1. \tag{11.9d}$$

Equation (11.8) is multiplied by $-k^2h^2/2$ and after rearranging terms we obtain

$$\left(h^2 + k^2\right)\varphi_{i,j} - \frac{1}{2}\left[k^2\left(\varphi_{i-1,j} + \varphi_{i+1,j}\right) + h^2\left(\varphi_{i,j-1} + \varphi_{i,j+1}\right)\right] = \frac{(hk)^2}{2}\rho_{i,j}, \tag{11.10}$$

for $i = 1, \ldots, n$ and $j = 1, \ldots, m$. There are different strategies how the set of equations (11.10) might be solved. The common strategy is to employ the assignments

$$\begin{aligned}\varphi_{1,1} &\to \varphi_1,\\ \varphi_{1,2} &\to \varphi_2,\\ \vdots\ & \quad \vdots\\ \varphi_{n,m} &\to \varphi_\ell,\end{aligned} \tag{11.11}$$

where $\ell = nm$. Equation (11.10) is then rewritten as a matrix equation with a vector of unknowns $\varphi = (\varphi_1, \varphi_2, \dots, \varphi_\ell)^T$ according to Eq. (11.11), where the boundary conditions have to be included in the matrix. This matrix equation is then solved either by direct or iterative methods discussed in Appendix C.

We solve Eq. (11.10) iteratively. For this purpose we introduce the iteration index t, where $\varphi^t_{i,j}$ is the function value at the grid-point (x_i, y_j) after t-iteration steps. There are two different implementations of an iterative solution of Eq. (11.10), namely the GAUSS-SEIDEL or the JACOBI method (Appendix C) which differ only in the update procedure of the function values $\varphi^t_{i,j}$ at the grid-points. The basic idea is to develop an update algorithm which expresses the function values $\varphi^t_{i,j}$ with the help of function values at already updated grid-points and of function values $\varphi^{t-1}_{i,j}$ determined in the preceding iteration step [Eq. (C.27)].

We formulate this iteration rule as

$$\begin{aligned}\varphi^{t+1}_{i,j} = &\ \frac{(hk)^2}{2(h^2+k^2)}\rho_{i,j}\\ &+ \frac{1}{2(h^2+k^2)}\left[k^2\left(\varphi^{t+1}_{i-1,j} + \varphi^t_{i+1,j}\right) + h^2\left(\varphi^{t+1}_{i,j-1} + \varphi^t_{i,j+1}\right)\right],\end{aligned} \tag{11.12}$$

where we abstained from incorporating a relaxation parameter (see Appendix C). Note that by using the iteration rule (11.12) the boundary conditions have to be accounted for in an additional step.

Let us specify the boundary conditions in order to define a concrete example: We impose DIRICHLET boundary conditions in x-direction, i.e. $\varphi(0, y) = \varphi(L_x, y) = 0$. In this case the boundary conditions are included into Eq. (11.12) by restricting the loop over the x-grid from $i = 2, \dots, N - 1$, which leaves the boundary points $\varphi(0, y)$ and $\varphi(L_x, y)$ unchanged. In y-direction we impose DIRICHLET boundary conditions as well. They are given by $\varphi(x, 0) = \varphi(x, L_y) = 0$. Furthermore we set, to be distinct, $L_x = L_y = 10$ and set the number of grid-points on both axes to $n = m = 100$. Furthermore we define the domains:

$$\Omega_1 = \left(x_{\frac{n}{2}-10}, x_{\frac{n}{2}}\right] \times \left(y_{\frac{m}{2}-10}, y_{\frac{m}{2}}\right], \tag{11.13a}$$

$$\Omega_2 = \left(x_{\frac{n}{2}}, x_{\frac{n}{2}+10}\right] \times \left(y_{\frac{m}{2}-10}, y_{\frac{m}{2}}\right], \tag{11.13b}$$

$$\Omega_3 = \left(x_{\frac{n}{2}-10}, x_{\frac{n}{2}}\right] \times \left(y_{\frac{m}{2}}, y_{\frac{m}{2}+10}\right], \tag{11.13c}$$

$$\Omega_4 = \left(x_{\frac{n}{2}}, x_{\frac{n}{2}+10}\right] \times \left(y_{\frac{m}{2}}, y_{\frac{m}{2}+10}\right]. \tag{11.13d}$$

The charge density $\rho(x, y)$ is described by three different scenarios, i.e.

$$\rho_1(x, y) = \begin{cases} 50 & (x, y) \in \Omega_1 \cup \Omega_2 \cup \Omega_3 \cup \Omega_4, \\ 0 & \text{elsewhere}, \end{cases} \tag{11.14a}$$

$$\rho_2(x, y) = \begin{cases} 50 & (x, y) \in \Omega_1 \cup \Omega_2, \\ -50 & (x, y) \in \Omega_3 \cup \Omega_4, \\ 0 & \text{elsewhere}, \end{cases} \tag{11.14b}$$

$$\rho_3(x, y) = \begin{cases} 50 & (x, y) \in \Omega_1 \cup \Omega_4, \\ -50 & (x, y) \in \Omega_2 \cup \Omega_3, \\ 0 & \text{elsewhere}. \end{cases} \tag{11.14c}$$

Here $\rho_1(x, y)$, $\rho_2(x, y)$, and $\rho_3(x, y)$ describe an electric monopole, dipole, and quadrupole, respectively. The charge densities are shown in Fig. 11.1.

The solution of Eq. (11.12) is regarded to be converged if the potential $\varphi(x, y)$ does not change significantly between two consecutive iteration steps, i.e.

$$\max_{i,j} \left(|\varphi^t_{i,j} - \varphi^{t-1}_{i,j}| \right) < \eta, \tag{11.15}$$

where $\eta = 10^{-4}$ is the required accuracy. A criterion to check the relative change can be formulated in a similar fashion.

The resulting potential profiles are illustrated in Fig. 11.2a–c. They reflect perfectly the symmetries of the charge densities $\rho_1(x, y)$, $\rho_2(x, y)$, and $\rho_3(x, y)$, respectively. Finally, the electric field $E(x, y)$ can be calculated from $\varphi(x, y)$ with the help of Eq. (11.3) using standard finite difference methods.

11.3 The Time-Dependent Heat Equation

Here we discuss the numerical solution of the time-dependent heat equation which is a representative of parabolic partial differential equations. This equation has already been introduced in Sect. 9.1, Eq. (9.1), and is, reduced to the one-dimensional case, of the form

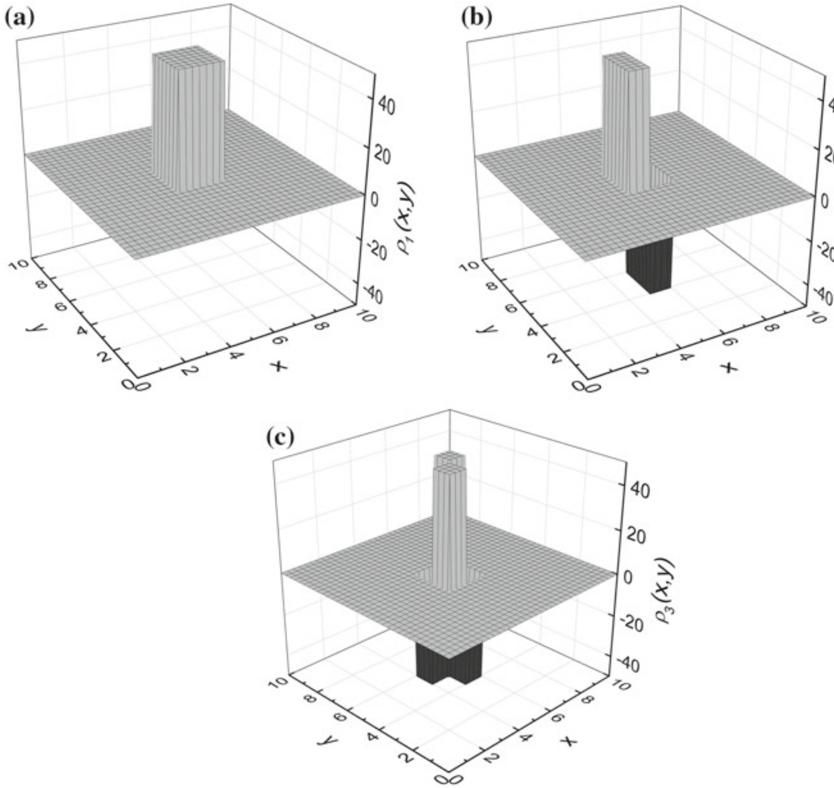

Fig. 11.1 Charge densities. **(a)** $\rho_1(x, y)$, **(b)** $\rho_2(x, y)$, and **(c)** $\rho_3(x, y)$ as defined in Eqs. (11.14)

$$\frac{\partial}{\partial t} T(x, t) = \kappa \frac{\partial^2}{\partial x^2} T(x, t). \tag{11.16}$$

It is augmented by appropriate boundary and initial conditions. Again, we will not discuss the extension to higher dimensions since it is straightforward, however, maybe tedious. We approximate the right hand side of Eq. (11.16) with the help of the central finite difference approximation (Sect. 2.2) and obtain

$$\frac{\partial}{\partial t} T_k(t) = \kappa \frac{T_{k-1}(t) - 2T_k(t) + T_{k+1}(t)}{h^2}. \tag{11.17}$$

Here we imposed the usual discretization, i.e. $x_k = x_0 + kh$, $k = 1, \ldots, N$, in combination with the notation $T_k(t) \equiv T(x_k, t)$.

The time derivative in Eq. (11.17) can be approximated with the help of methods already discussed in Chap. 5. In particular, one has to decide whether Eq. (11.17) should be approximated by an explicit or implicit integrator. In what follows we shall apply both, the explicit EULER and the implicit EULER method to solve Eq. (11.17).

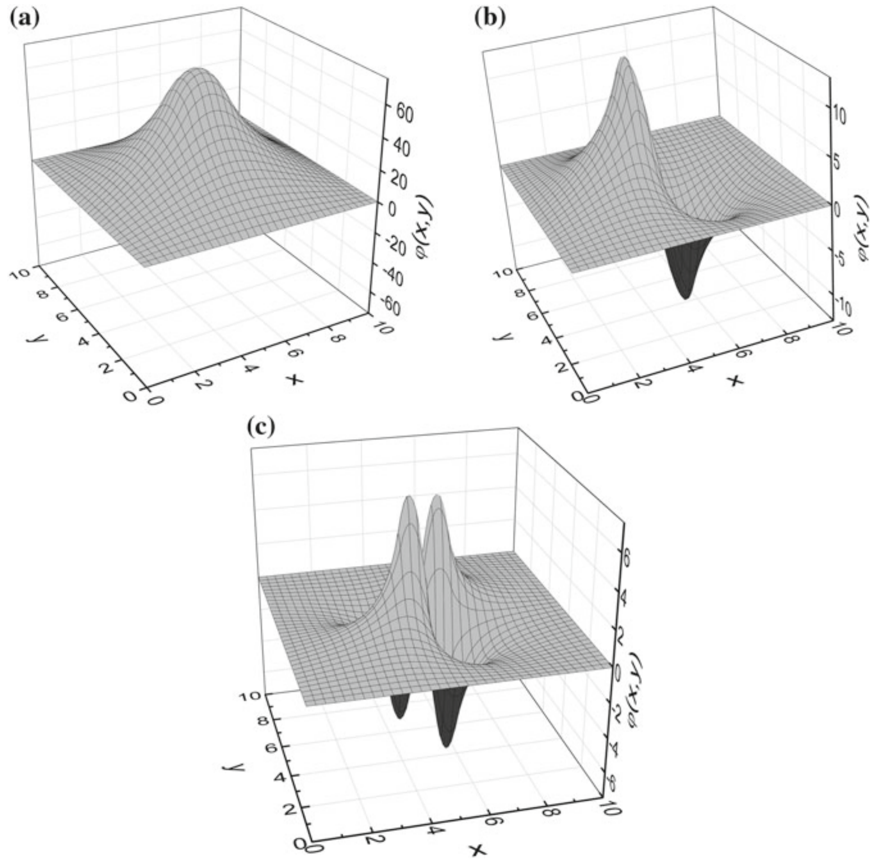

Fig. 11.2 Potential profile obtained for charge density. **(a)** $\rho_1(x, y)$, **(b)** $\rho_2(x, y)$, and **(c)** $\rho_3(x, y)$

However, more complex integrators may be applied as well. In particular, the method according to CRANK-NICOLSON proved to be very useful in the theory of parabolic differential equations. The extensions are straightforward and will therefore not be discussed here.

We define $t_n = t_0 + n\Delta t$ and $T_k^n \equiv T_k(t_n)$ and employ, furthermore, the explicit EULER scheme (5.9) in Eq. (11.17) to get

$$\frac{T_k^{n+1} - T_k^n}{\Delta t} = \kappa \frac{T_{k-1}^n - 2T_k^n + T_{k+1}^n}{h^2}, \tag{11.18}$$

with the solution:

$$T_k^{n+1} = T_k^n + \kappa \Delta t \frac{T_{k-1}^n - 2T_k^n + T_{k+1}^n}{h^2}. \tag{11.19}$$

We note that the right hand side of this equation depends only on temperatures of the previous time step, since we used an explicit method. Although this might seem advantageous on a first glance, it turns out that the above scheme is not stable for arbitrary choices of Δt and h. In particular, it is possible prove that the above discretization is stable only for

$$\frac{\kappa \Delta t}{h^2} \leq \frac{1}{2}. \tag{11.20}$$

A detailed discussion and proof of this property can be found in any advanced textbook on numerics of partial differential equations [1].

On the other hand, if we apply the implicit EULER method (5.10) to solve Eq. (11.17) we obtain

$$\frac{T_k^{n+1} - T_k^n}{\Delta t} = \kappa \frac{T_{k-1}^{n+1} - 2T_k^{n+1} + T_{k+1}^{n+1}}{h^2}, \tag{11.21}$$

which is unconditionally stable. However, Eq. (11.21) is an implicit equation, i.e. the function values T_{k+1}^{n+1} and T_{k-1}^{n+1} are required in order to evaluate T_k^{n+1}. Hence, Eq. (11.21) has to be solved as a system of linear equations. This system may be written as

$$AT^{n+1} = T^n + F, \tag{11.22}$$

where the vector $T^\ell = (T_0^\ell, T_1^\ell, \dots, T_N^\ell)^T$, the tridiagonal matrix A is given by

$$A = \begin{pmatrix} \ddots & \ddots & \ddots & & \\ & -\frac{\kappa \Delta t}{h^2} & 1 + \frac{2\kappa \Delta t}{h^2} & -\frac{\kappa \Delta t}{h^2} & \\ & & \ddots & \ddots & \ddots \end{pmatrix}, \tag{11.23}$$

and the boundary conditions are incorporated in the matrix A and in the vector F, see Sects. 9.2 and 9.3. The linear system (11.22) can be solved numerically using a direct or an iterative method. Employing an iterative method, imposes a third index t on the function values of the temperature T, which accounts for the iteration step.

In a similar fashion, other integrators can be applied to solve Eq. (11.17). Such integrators have been discussed in Chap. 5.

Let us give a brief numerical example. We consider the time-dependent homogeneous heat equation (11.16) on a finite interval $\Omega = [0, L]$ together with the boundary conditions of Sect. 9.1, i.e.

$$T(0) = T_0, \qquad T(L) = T_N. \tag{11.24}$$

In addition we regard the initial condition

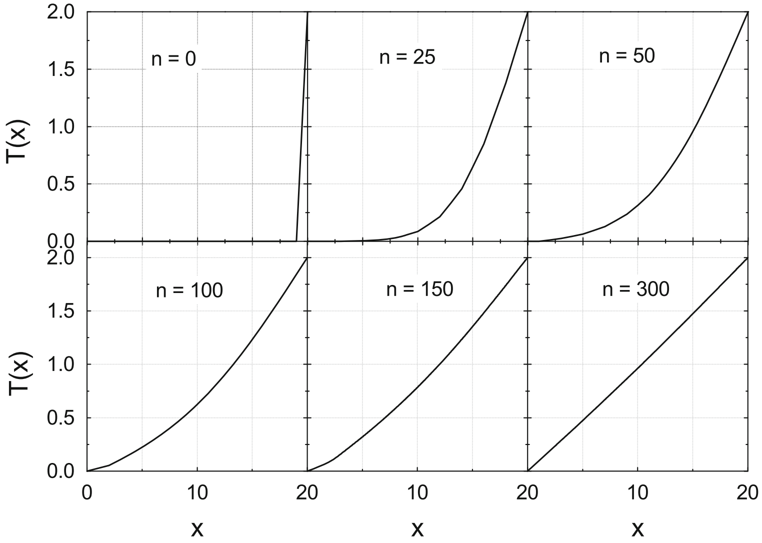

Fig. 11.3 Solutions of the time-dependent heat equation achieved with the explicit EULER method. The stability criterion (11.20) is fulfilled. Results after $n = 25$, 50, 100, 150, and 300 time steps are presented. $n = 0$ represents the initial conditions

$$T(x, 0) = 0, \qquad x \in [0, L]. \tag{11.25}$$

In Fig. 11.3 we show the time evolution of $T(x, t)$ at six different times as obtained with the explicit EULER method (11.19). Here we chose $T_0 = 0$, $T_N = 2$, $N = 20$, $L = 10$, $\kappa = 1$ as well as $\Delta t \approx 0.5$. Note that for this choice of parameters, the condition (11.20) is fulfilled since $h \approx 1.05$ and therefore

$$\frac{\kappa \Delta t}{h^2} \approx 0.45 \leq \frac{1}{2}. \tag{11.26}$$

In Fig. 11.4 we show the results obtained with the same procedure, however Δt was chosen to be approximately 0.7, such that

$$\frac{\kappa \Delta t}{h^2} \approx 0.63 > \frac{1}{2}. \tag{11.27}$$

Moreover, in Fig. 11.5 we show the results obtained with the same parameters as for Fig. 11.4 but with the help of the implicit EULER method (11.21).

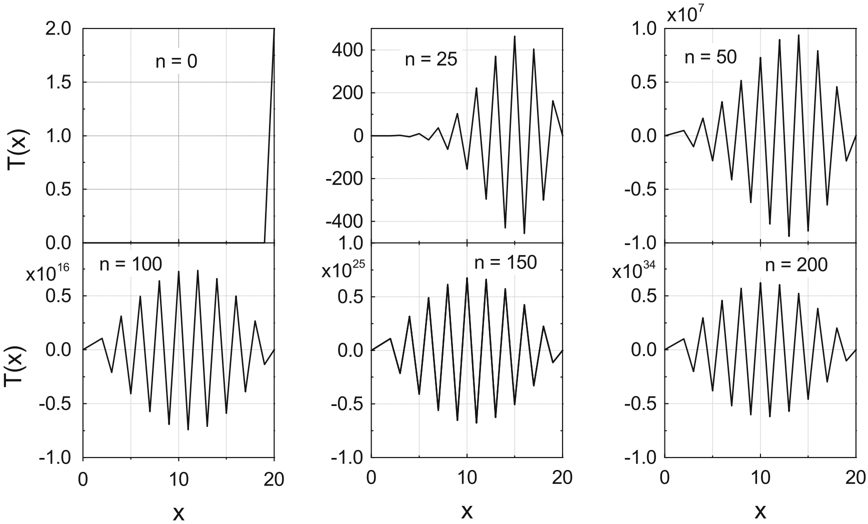

Fig. 11.4 Solutions of the time-dependent heat equation achieved with the explicit EULER method. The stability criterion (11.20) is not fulfilled and, therefore, the solution is apparently unstable. Results after $n = 25, 50, 100, 150$, and 200 time steps are presented. $n = 0$ represents the initial conditions

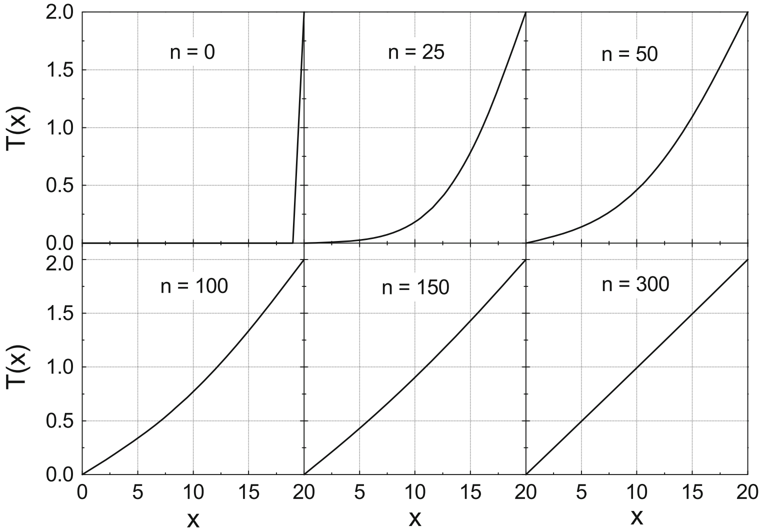

Fig. 11.5 Solutions of the time-dependent heat equation achieved with the implicit EULER method. Results after $n = 25, 50, 100, 150$, and 300 time steps are presented. $n = 0$ represents the initial conditions

11.4 The Wave Equation

As a model hyperbolic partial differential equation we consider briefly the wave equation. Again, we regard only the one-dimensional case, i.e.

$$\frac{\partial^2}{\partial t^2} u(x,t) = c^2 \frac{\partial^2}{\partial x^2} u(x,t), \tag{11.28}$$

where c is the speed at which the wave propagates. Again, Eq. (11.28) is to be augmented by appropriate boundary and initial conditions. We shall employ a finite difference approach similar to the one discussed in Sect. 11.3. Furthermore, we will restrict the discussion to the explicit EULER approximation. Consequently, Eq. (11.28) is replaced by

$$\frac{u_k^{n-1} - 2u_k^n + u_k^{n+1}}{\Delta t^2} = c^2 \frac{u_{k-1}^n - 2u_k^n + u_{k+1}^n}{h^2}. \tag{11.29}$$

We define the parameter $\lambda = \frac{c\Delta t}{h}$ and solve Eq. (11.29) for u_k^{n+1}:

$$u_k^{n+1} = 2(1-\lambda^2)u_k^n - u_k^{n-1} + \lambda^2 (u_{k-1}^n + u_{k+1}^n). \tag{11.30}$$

We note two important points. (i) To calculate the solution for time step $n+1$ we need to know the solutions for the time steps n and $n-1$. In particular, we need $n=0$ and $n=1$ in order to obtain $n=2$. The function values for $n=1$ can be obtained from the initial conditions, which must include a first order time derivative of $u(x,t)$ since (11.28) is a second order differential equation with respect to time t. (ii) As in the case of parabolic problems, the explicit EULER approximation (11.30) will not be stable for arbitrary values of λ. It is only stable for

$$\lambda = \frac{c\Delta t}{h} \leq 1. \tag{11.31}$$

This condition is referred to as the COURANT-FRIEDRICHS-LEWY or CFL condition. Its importance stems from the fact, that this condition is not limited to the wave equation but holds for hyperbolic problems in general. In particular, since the wave equation can always be viewed as a combination of a right- and a left-going advection equation, i.e.

$$\frac{\partial}{\partial t} u(x,t) = \pm c \frac{\partial}{\partial x} u(x,t), \tag{11.32}$$

we have the very important property that explicit time integrators applied to solve (11.32) are only stable if relation (11.31) is obeyed.

Let us return to the discretization (11.30). Suppose we have initial conditions of the form

$$u(x,0) = f(x), \qquad \frac{\partial}{\partial t} u(x,0) = g(x). \tag{11.33}$$

They can be approximated by

$$u_k^0 = f_k, \qquad \frac{u_k^1 - u_k^0}{\Delta t} = g_k, \tag{11.34}$$

and the solution of the second relation in (11.34) yields the desired function values for $n = 1$, i.e.

$$u_k^1 = u_k^0 + \Delta t g_k. \tag{11.35}$$

However, in many cases it is beneficial to take higher order terms into account. This can be achieved by employing a TAYLOR expansion of the form (Chap. 2):

$$\frac{u_k^1 - u_k^0}{\Delta t} = \frac{\partial}{\partial t} u(x, 0) + \frac{\Delta t}{2} \frac{\partial^2}{\partial t^2} u(x, 0) + \mathcal{O}(\Delta t^2). \tag{11.36}$$

We make now use of the initial conditions (11.33), employ the wave equation (11.28), and solve for u_k^1. This gives

$$u_k^1 = u_k^0 + \Delta t g_k + \frac{\Delta t^2 c^2}{2} f_k'' + \mathcal{O}(\Delta t^3). \tag{11.37}$$

Here we assumed that the second spatial derivative $f_k'' = \frac{\partial^2}{\partial x^2} f(x_k)$ of the initial condition $f(x)$ exists. It may then be approximated by a finite difference approach.

To be specific we consider a vibrating string of length L, which is fixed at its ends, i.e. $u(0, t) = u(L, t) = 0$. Furthermore, we assume that the string was initially at rest, i.e.

$$\frac{\partial}{\partial t} u(x, 0) = 0, \tag{11.38}$$

and impose initial conditions

$$u(x, 0) = \begin{cases} \sin\left(\frac{2\pi x}{L}\right) & x \in \left(\frac{L}{2}, L\right], \\ 0 & \text{elsewhere}. \end{cases} \tag{11.39}$$

In Fig. 11.6 we show the results obtained with $L = 1$, $c = 2$, $N = 100$. Δt was chosen in such a way that $\lambda = 0.5$. In Fig. 11.7 we show the results obtained using the same parameter set, however $\lambda = 1.01$.

Let us conclude this section with a final remark. In general, the numerical solution of hyperbolic partial differential equations might be very difficult since in many cases these equations represent conservation laws. A very popular class of methods in this context is referred to as *finite volume methods*. A detailed discussion of these methods can be found in the book by R. J. LEVEQUE [2].

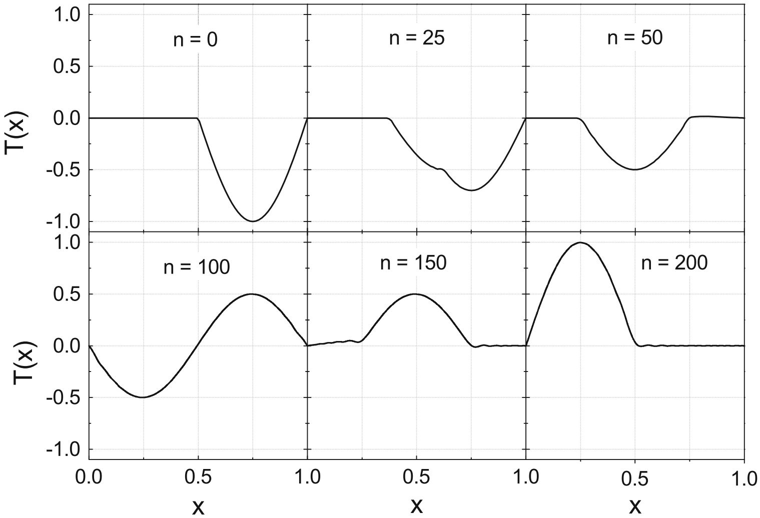

Fig. 11.6 Solutions of the wave equation generated by the explicit EULER method with $\lambda = 0.5$. Results after $n = 25, 50, 100, 150$, and 200 time steps are presented. $n = 0$ represents the initial conditions

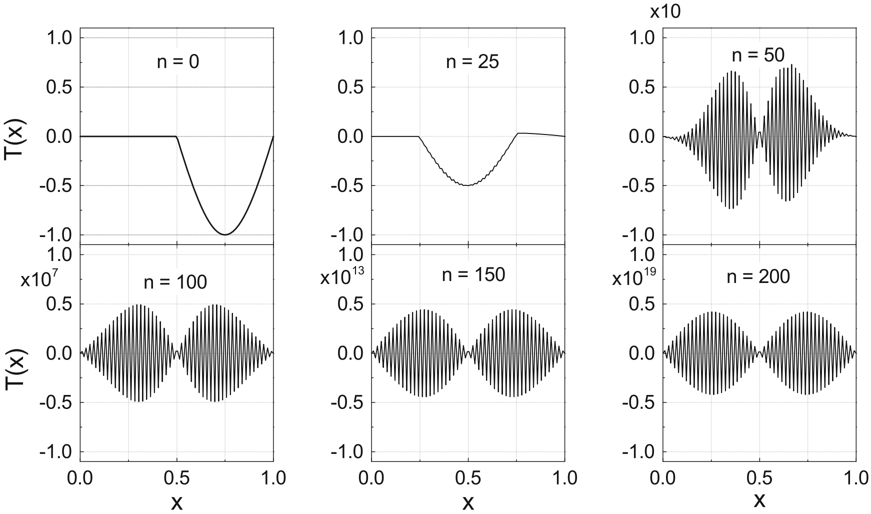

Fig. 11.7 Solutions of the wave equation generated by the explicit EULER method with $\lambda = 1.01$. Results after $n = 25, 50, 100, 150$, and 200 time steps are presented. $n = 0$ represents the initial conditions

11.5 The Time-Dependent SCHRÖDINGER Equation

We already came across the time-dependent SCHRÖDINGER equation in Chap. 10. It reads

$$i\hbar\frac{\partial}{\partial t}\Psi(x,t) = H\Psi(x,t), \tag{11.40}$$

where $\hbar$ is the reduced PLANCK constant, $\Psi(x,t)$ is the wave-function and H is the HAMILTON operator. Since the SCHRÖDINGER equation contains a complex coefficient, it cannot be categorized as a differential equation of one of the familiar types, i.e. elliptic, parabolic or hyperbolic. In fact, the SCHRÖDINGER equation shows parabolic as well as hyperbolic behavior (it is of the form of the diffusion equation but allows for wave solutions). In what follows we discuss briefly a very elegant method developed to numerically approximate solutions of the time-dependent SCHRÖDINGER equation.

We note that Eq. (11.40) has the formal solution

$$\Psi(x,t) = \exp\left(-\frac{it}{\hbar}H\right)\Psi(x,0) = U(t)\Psi(x,0), \tag{11.41}$$

where we assumed that H is independent of t and introduced the initial wave-function $\Psi(x,0) = \Psi(x,t=0)$. We note that the prefactor $U(t)$ on the right hand side of Eq. (11.41) *propagates* the solution in time. Furthermore, it is a unitary operator and therefore preserves the norm of the wave-function $\Psi(x,t)$. $U(t)$ is usually referred to as the *unitary time-evolution operator*. We remember that unitary means that $UU^\dagger = U^\dagger U = \mathbb{1}$.

We employ relation (11.41) in order to obtain

$$\Psi(x,t+\Delta t) = \exp\left(-\frac{i(t+\Delta t)}{\hbar}H\right)\Psi(x,0) = \exp\left(-\frac{i\Delta t}{\hbar}H\right)\Psi(x,t). \tag{11.42}$$

Expanding the exponential in this equation in its series representation and truncating the series after the second term results in the approximation

$$\Psi(x,t+\Delta t) \approx \left(1-\frac{i\Delta t}{\hbar}H\right)\Psi(x,t). \tag{11.43}$$

Again, we introduce grid-spacing and the correspondingly indexed functions in order to obtain

$$\Psi_k^{n+1} = \left(1-\frac{i\Delta t}{\hbar}H\right)\Psi_k^n. \tag{11.44}$$

In the following we will denote the position grid-spacing by Δx instead of h in order to avoid confusion with the reduced PLANCK constant $\hbar$. Using Eq. (10.23) for the Hamiltonian in its local space representation in the one-dimensional case and by approximating the second derivative with the help of the central difference approximation we arrive at

$$\Psi_k^{n+1} = \Psi_k^n - \frac{i\Delta t}{\hbar}\left(-\frac{\hbar^2}{2m}\frac{\Psi_{k-1}^n - 2\Psi_k^n + \Psi_{k+1}^n}{\Delta x^2} + V_k\Psi_k^n\right), \tag{11.45}$$

where we defined $V_k \equiv V(x_k)$.

We note that this equation is equivalent to the explicit EULER approximation (11.18) of the heat equation, with the exception that an imaginary coefficient appears in Eq. (11.45). An implicit procedure for the time-dependent SCHRÖDINGER equation (11.40) can be obtained by inversion of Eq. (11.42):

$$\Psi(x,t) = U^\dagger(\Delta t)\Psi(x,t+\Delta t) = \exp\left(\frac{i\Delta t}{\hbar}H\right)\Psi(x,t+\Delta t). \tag{11.46}$$

A series expansion of the exponential results in the desired relation:

$$\Psi_k^n = \left(1 + \frac{i\Delta t}{\hbar}H\right)\Psi_k^{n+1}. \tag{11.47}$$

We emphasize that the unitarity of the time-evolution operator is of fundamental importance, since it preserves the norm of the wave-function. However, in truncating the series representation of the unitary time evolution operator $U(\Delta t)$ we certainly violate the unitarity of $U(\Delta t)$. This problem can be remedied by imposing unitarity of the time evolution as an additional requirement. This requirement can be incorporated by normalizing the wave-function after each time step.

In what follows we shall employ a CRANK-NICOLSON scheme in order to solve Eq. (11.40) numerically for a particular potential. The CRANK-NICOLSON scheme can be obtained by realizing that

$$\begin{aligned}
U(\Delta t) &= \exp\left(-\frac{i\Delta t}{\hbar}H\right) \\
&= \exp\left(-\frac{i\Delta t}{2\hbar}H\right)\exp\left(-\frac{i\Delta t}{2\hbar}H\right) \\
&= \exp\left(\frac{i\Delta t}{2\hbar}H\right)^{-1}\exp\left(-\frac{i\Delta t}{2\hbar}H\right) \\
&= \left[U^\dagger\left(\frac{\Delta t}{2}\right)\right]^{-1} U\left(\frac{\Delta t}{2}\right).
\end{aligned} \tag{11.48}$$

Hence, we obtain from Eq. (11.45)

$$U^\dagger\left(\frac{\Delta t}{2}\right)\Psi_k^{n+1} = U\left(\frac{\Delta t}{2}\right)\Psi_k^n, \tag{11.49}$$

or by expanding U in a series and truncating after the second term

$$\left(1+\frac{i\Delta t}{2\hbar}H\right)\Psi_k^{n+1}=\left(1-\frac{i\Delta t}{2\hbar}H\right)\Psi_k^n. \tag{11.50}$$

Again, inserting the finite difference approximation of the Hamiltonian H and rearranging terms yields

$$\left[1+\frac{i\Delta t}{2\hbar}\left(\frac{\hbar^2}{m\Delta x^2}+V_k\right)\right]\Psi_k^{n+1}-\frac{i\Delta t\hbar}{4m\Delta x^2}\left(\Psi_{k-1}^{n+1}+\Psi_{k+1}^{n+1}\right)=\hat{\Omega}_k^n, \tag{11.51}$$

where we defined $\hat{\Omega}_k^n$ as

$$\hat{\Omega}_k^n=\left[1-\frac{i\Delta t}{2\hbar}\left(\frac{\hbar^2}{m\Delta x^2}+V_k\right)\right]\Psi_k^n+\frac{i\Delta t\hbar}{4m\Delta x^2}\left(\Psi_{k-1}^n+\Psi_{k+1}^n\right). \tag{11.52}$$

Both sides of Eq. (11.51) are now multiplied by $i4m\Delta x^2/(\hbar\Delta t)$ and this gives

$$\Psi_{k-1}^{n+1}+2\left(\frac{i2m\Delta x^2}{\Delta t\hbar}-1-\frac{m\Delta x^2}{\hbar^2}V_k\right)\Psi_k^{n+1}+\Psi_{k+1}^{n+1}=\Omega_k^n, \tag{11.53}$$

where

$$\Omega_k^n=-\Psi_{k-1}^n+2\left(\frac{i2m\Delta x^2}{\Delta t\hbar}+1+\frac{m\Delta x^2}{\hbar^2}V_k\right)\Psi_k^n-\Psi_{k+1}^n. \tag{11.54}$$

We recognize that Eq. (11.53) establishes a system of linear equations and rewrite it in matrix form as

$$A\Psi^{n+1}=\Omega^n, \tag{11.55}$$

where we defined the vectors $\Psi^{n+1}=\left(\Psi_0^n,\Psi_1^n,\dots,\Psi_N^n\right)^T$, $\Omega^n=\left(\Omega_0^n,\Omega_1^n,\dots,\Omega_N^n\right)^T$ and the tridiagonal matrix

$$A=\begin{pmatrix} \ddots & \ddots & \ddots & & \\ & 1 & \Gamma_k & 1 & \\ & & \ddots & \ddots & \ddots \end{pmatrix}, \tag{11.56}$$

with Γ_k for $k=1,2,\dots,N$ given by

$$\Gamma_k=2\left(\frac{i2m\Delta x^2}{\Delta t\hbar}-1-\frac{m\Delta x^2}{\hbar^2}V_k\right), \tag{11.57}$$

according to Eq. (11.53).

Again, we solve the system (11.56) iteratively. However, in this case we employ a more elegant ansatz which is allowed for tridiagonal matrices. We set in particular

$$\Psi_{k+1}^{n+1} = a_k \Psi_k^{n+1} + b_k^n, \tag{11.58}$$

and apply it to Eq. (11.53). After rearranging terms we arrive at:

$$2\left(1 + \frac{m\Delta x^2}{\hbar^2} V_k - \frac{i2m\Delta x^2}{\Delta t\hbar} - \frac{a_k}{2}\right)\Psi_k^{n+1} = \Psi_{k-1}^{n+1} + b_k^n - \Omega_k^n. \tag{11.59}$$

We define furthermore

$$\alpha_k = 2\left(1 + \frac{m\Delta x^2}{\hbar^2} V_k - \frac{i2m\Delta x^2}{\Delta t\hbar} - \frac{a_k}{2}\right), \tag{11.60}$$

and obtain from Eq. (11.59)

$$\Psi_k^{n+1} = \frac{1}{\alpha_k}\Psi_{k-1}^{n+1} + \frac{b_k^n - \Omega_k^n}{\alpha_k}. \tag{11.61}$$

However, due to the ansatz (11.58) we also have

$$\Psi_k^{n+1} = a_{k-1}\Psi_{k-1}^{n+1} + b_{k-1}^n, \tag{11.62}$$

which results in the relations

$$a_{k-1} = \frac{1}{\alpha_k}, \tag{11.63}$$

and

$$b_{k-1}^n = \frac{b_k^n - \Omega_k^n}{\alpha_k} = \left(b_k^n - \Omega_k^n\right) a_{k-1}. \tag{11.64}$$

Equation (11.63) results in the recursion relation

$$a_k = 2\left(1 + \frac{m\Delta x^2}{\hbar^2} V_k - \frac{i2m\Delta x^2}{\Delta t\hbar}\right) - \frac{1}{a_{k-1}}, \tag{11.65}$$

and from Eq. (11.64) we find

$$b_k^n = \frac{b_{k-1}^n}{a_{k-1}} + \Omega_k^n. \tag{11.66}$$

The remaining question is how to choose a_0 and b_0^n. We impose the boundary conditions $\Psi_0^n = 0$ and $\Psi_N^n = 0$ and from Eq. (11.53) we find

$$\Omega_1^n = 2\left(\frac{i2m\Delta x^2}{\Delta t\hbar} - 1 - \frac{m\Delta x^2}{\hbar^2}V_1\right)\Psi_1^{n+1} + \Psi_2^{n+1}. \tag{11.67}$$

A comparison of this equation with the ansatz (11.58), i.e. $\Psi_2^{n+1} = a_1\Psi_1^{n+1} + b_1^n$, reveals that

$$a_1 = 2\left(1 + \frac{m\Delta x^2}{\hbar^2}V_k - \frac{i2m\Delta x^2}{\Delta t\hbar}\right), \tag{11.68}$$

and

$$b_1^n = \Omega_1^n. \tag{11.69}$$

These expressions are equivalent to $a_0 = \infty$ and it is, thus, impossible to calculate Ψ_1^{n+1} from Ψ_0^{n+1}. However, this is not really a problem because we can determine the function values Ψ_k^{n+1} via a backward recursion

$$\Psi_k^{n+1} = \frac{1}{a_k}\left(\Psi_{k+1}^{n+1} - b_k^n\right), \tag{11.70}$$

which is initialized with the boundary condition $\Psi_N^{n+1} = 0$. We can summarize the algorithm:

1. Choose the initial conditions Ψ_k^0, $k = 0, 1, \ldots, N$ which satisfy the boundary conditions $\Psi_0^0 = 0$ and $\Psi_N^0 = 0$.
2. Set

$$a_1 = 2\left(1 + \frac{m\Delta x^2}{\hbar^2}V_k - \frac{i2m\Delta x^2}{\Delta t\hbar}\right), \tag{11.71}$$

   and calculate for $k = 2, \ldots, N-1$

$$a_k = 2\left(1 + \frac{m\Delta x^2}{\hbar^2}V_k - \frac{i2m\Delta x^2}{\Delta t\hbar}\right) - \frac{1}{a_{k-1}}. \tag{11.72}$$

3. Start the time loop: $n = 1, 2, \ldots, M$.
4. Calculate for $k = 1, 2, \ldots, N-1$

$$\Omega_k^n = -\Psi_{k-1}^n + 2\left(\frac{i2m\Delta x^2}{\Delta t\hbar} + 1 + \frac{m\Delta x^2}{\hbar^2}V_k\right)\Psi_k^n - \Psi_{k+1}^n. \tag{11.73}$$

5. Set

$$b_1^n = \Omega_1^n, \tag{11.74}$$

   and calculate for $k = 2, \ldots, N-1$

$$b_k^n = \frac{b_{k-1}^n}{a_{k-1}} + \Omega_k^n. \tag{11.75}$$

6. Calculate for $k = N-1, N-2, \dots, 1$
$$\Psi_k^{n+1} = \frac{1}{a_k}\left(\Psi_{k+1}^{n+1} - b_k^n\right), \tag{11.76}$$
where the boundary conditions $\Psi_0^n = \Psi_N^n = 0$ are to be considered.
7. Set $n = n + 1$ and go to step 4.

In the following we discuss a specific example to illustrate the application of this algorithm. We choose the initial condition

$$\Psi(x, 0) = \exp(iqx)\exp\left[-\frac{(x-x_0)^2}{2\sigma^2}\right], \tag{11.77}$$

a GAUSS wave packet centered at $x = x_0$ which propagates in positive x-direction with momentum q. Note that this wave-function is not yet normalized. Furthermore, we regard a potential barrier

$$V_1(x) = \begin{cases} V_0 & x \in [a, b], \\ 0 & \text{elsewhere}, \end{cases} \tag{11.78}$$

or a double barrier

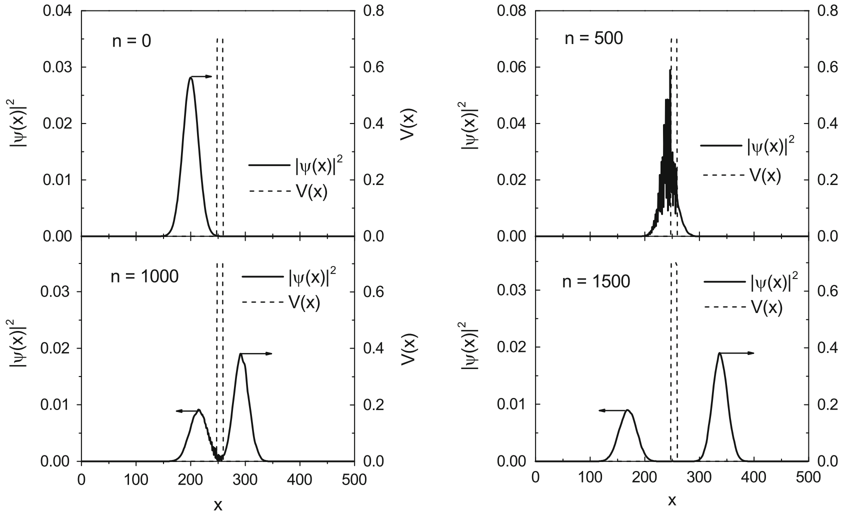

Fig. 11.8 Time evolution of the square modulus of the wave-function $|\psi(x)|^2$ versus x (*solid line, left hand scale*). The potential $V(x) = V_1(x)$ is also plotted versus x (*dashed line, right hand scale*). We present the results for $n = 500$, 1,000, and 1,500 time steps. The graph labeled by $n = 0$ represents the initial configuration

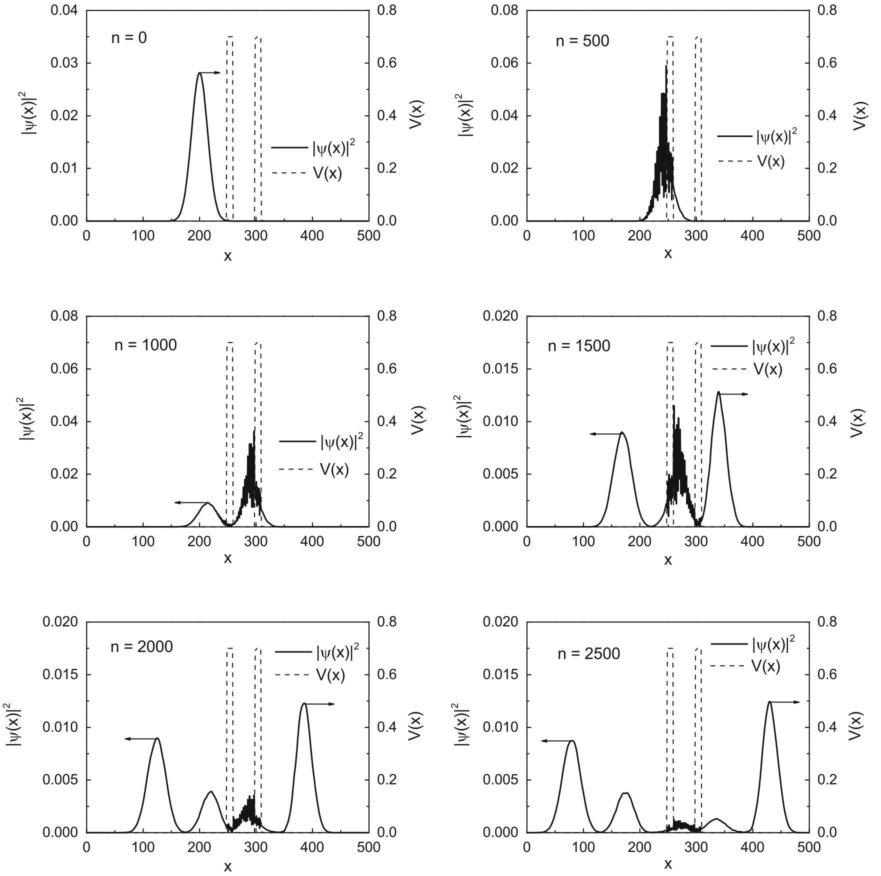

Fig. 11.9 Time evolution of the square modulus of the wave-function $|\psi(x)|^2$ versus x (*solid line*, *left hand scale*). The potential $V(x) = V_2(x)$ is also plotted versus x (*dashed line*, *right hand scale*). We present the results for $n = 500$, 1,000, 1,500, 2,000, and 2,500 time steps. The graph labeled by $n = 0$ represents the initial configuration

$$V_2(x) = \begin{cases} V_0 & x \in [a, b] \cup [c, d], \\ 0 & \text{elsewhere.} \end{cases} \tag{11.79}$$

The scales and parameters are chosen in the following way: $L = 500$, $\Delta x = 1$, $\Delta t = 0.1$, $m = \hbar = 1$, $x_0 = 200$, $q = 2$, $\sigma = 20$, $V_0 = 0.7$, $a = 250$, $b = 260$, $c = 300$, and $d = 310$. Figures 11.8 and 11.9 display the squared modulus of the resulting wave-function, $|\Psi(x,t)|^2$, versus x (solid line, left hand scale) at different times steps $n = 500$, 1000, and 1500, and for the two potentials $V_1(x)$ and $V_2(x)$ (dashed lines, right hand scale) for additional time steps $n = 2000$, and 2500, respectively. $n = 0$ corresponds to the initial configuration.

In both figures a typical quantum mechanical effect which is referred to as *tunneling* can be observed. In particular, there exists a finite probability that the potential barrier can be crossed, although, from a classical point of view, the particle's energy is not sufficient to overcome the barrier. A detailed discussion of this effect and its technological importance can be found in any standard textbook on quantum mechanics [4–6].

Summary

This chapter was about linear partial differential equations and how to find solutions numerically. The dominating theme was the application of the various finite difference methods. The two-dimensional POISSON equation served as an example of an elliptic partial differential equation. The algorithm to solve this equation developed here was based on the central difference derivative. Parabolic partial differential equations were represented by the time-dependent one-dimensional heat equation. The numerical solution proved to be possible by either using an explicit or an implicit EULER scheme. For the explicit EULER scheme the appropriate choice of time and space discretization proved to be essential for the stability of the algorithm. The one-dimensional wave equation was introduced as an example of a hyperbolic partial differential equation. The solution was found by employing an explicit EULER approximation. Again time and space discretization had to follow a specific stability criterion, the COURANT-FRIEDRICHS-LEWY condition. Finally, the one-dimensional time-dependent SCHRÖDINGER equation was studied. It does not fit into any of the above categories. The algorithm to find a numerical solution was developed here on the basis of a CRANK-NICOLSON scheme and it was tested with the quantum mechanical tunneling effect.

Problems

1. Write a program which solves the two-dimensional POISSON equation for an arbitrary charge density distribution $\rho(x, y)$. Use the numerical method discussed in Sect. 11.2.
   (a) Impose DIRICHLET boundary conditions $\varphi(x, 0) = \varphi(x, L_y) = \varphi(0, y) = \varphi(L_x, y) = 0$ as described in Sect. 11.2. Test the program by first reproducing Fig. 11.2.
   (b) Solve the POISSON equation for different charge densities of your choice.
   (c) Calculate the electric field $E(x, y)$ with the help of Eq. (11.3).

2. Calculate the time evolution of the temperature distribution $T(x, t)$ along a cylindrical rod described in Sect. 9.3. The rod is kept at constant temperatures T_0 and T_N at its ends. The parameters used in Sect. 9.3 stay unchanged. Study also the case of a heat sink as suggested in the Problems section of Chap. 9.

3. Calculate the time evolution of the square modulus of the wave-function $|\psi(x)|^2$ versus x for a potential $V_1(x)$ according to Eq. (11.78) with $V_0 < 0$ (quantum well). Modify the potential according to

$$V(x) = \begin{cases} V_1 & x \in [a, b] \cup [c, d] \\ V_2 & x \in [b, c] \\ 0 & \text{elsewhere,} \end{cases}$$

with $V_1 > 0$, $V_2 < 0$, and $|V_1| < |V_2|$.

References

1. Lapidus, L., Pinder, G.F.: Numerical Solution of Partial Differential Equations. John Wiley and Sons, New York (1982)
2. LeVeque, R.J.: Finite Volume Methods for Hyperbolic Problems. Cambridge Texts in Applied Mathematics. Cambridge University Press, Cambridge (2002)
3. Gockenbach, M.S.: Understanding and Implementing the Finite Element Method. Cambridge University Press, Cambridge (2006)
4. Baym, G.: Lectures on Quantum Mechanics. Lecture Notes ans Supplements in Physics. The Benjamin Cummings Publlishing Company, London (1969)
5. Cohen-Tannoudji, C., Diu, B.: Laloë: Quantum Mechanics, vol. I. John Wiley, New York (1977)
6. Sakurai, J.J.: Modern Quantum Mechanics. Addison-Wesley Publishing Company, Menlo Park (1985)

Part II
Stochastic Methods

Chapter 12
Pseudo Random Number Generators

12.1 Introduction

We shall discuss here briefly the most important methods available to generate random numbers or, more precisely, pseudo random numbers. The reader not familiar with the basic concepts of probability theory is highly encouraged to read Appendix D before proceeding. Let us now motivate the problem and discuss some preliminary points.

A first example of randomness in physical systems is certainly the outcome of a dice-throw or the drawing of lotto numbers. Even though the outcome of a dice-throw is completely determined by the initial conditions, it is effectively unpredictable because the initial conditions cannot be determined accurately enough. A probabilistic description, which assigns the *random variables* $1, 2, 3, 4, 5,$ and 6 a probability of $1/6$, respectively, is much more convenient and promising. It has to be kept in mind, ofcourse, that results obtained on the basis of such an approach are also clearly probabilistic in their nature.

We note that quantum mechanics is the only physical theory known which includes randomness intrinsically. However, even in the case of classical systems, a *stochastic* description, that is a description based on random numbers, can be very advantageous. For instance, consider the typical example of a classical interacting gas consisting of N particles. The motion is fully determined by N NEWTON's equations of motion or, equivalently, by the LIOUVILLE equation. However, if N is large (for instance in the range of one mol, that is $N = 6.022 \times 10^{23}$ particles) a full treatment or complete solution of the system is not feasible and in most cases not desired. One possibility is to employ the BOLTZMANN transport equation, which is an evolution equation of the *distribution function* $f(x, p, t)$. The distribution function gives the probability of finding a particle at a particular time t within a particular phase space volume $\mathrm{d}x\ \mathrm{d}p$.

Another interesting example is Brownian motion or diffusion, i.e. the random motion of dust particles on a fluid surface. The description with the help of a *stochastic*

B. A. Stickler and E. Schachinger, *Basic Concepts in Computational Physics*,
DOI: 10.1007/978-3-319-02435-6_12, © Springer International Publishing Switzerland 2014

differential equation, such as the LANGEVIN equation, is completely sufficient and much easier than a description of N interacting particles.

Further examples of stochastic descriptions can be found in various fields of expertise, such as biology (e.g. the foraging behavior of animals), economics (e.g. the prediction of market prize behaviors), medicine (e.g. genome mutation), and many others. Another quite interesting and purely mathematical application can be found in the evaluation of integrals as an alternative to the methods discussed in Chap. 3. This method is referred to as Monte-Carlo integration and will be discussed in Chap. 14 together with a basic introduction to stochastics and its applications in physics.

All these methods have in common that the numerical treatment requires random numbers and, therefore, generators of random numbers are a necessary item. This justifies a closer inspection of randomness in general and the generation of random numbers or sequences in particular. However, the clarification of some points is in order before we introduce the basics of random number generators. In particular, we have to explain, what we understand by randomness and how it can be measured. Moreover, based on this discussion we have to formulate requirements to be imposed on the random number generators required to deliver useful random numbers.

Let us begin with the question of how to define randomness in general. Although, we might have an intuitive picture of randomness it is hard to put it into words without mathematical tools. For instance, consider the sequence s_1, which consists of N elements:

$$s_1 = 0, 0, 0, 0, 0, \ \dots, \qquad N \text{ elements}. \tag{12.1}$$

Is it random? The question cannot be answered without further information. Suppose, the numbers in the sequence s_1 were drawn from a set $\mathscr{S}$. Now, if the set is of the form

$$\mathscr{S}_1 = \{0\}, \tag{12.2}$$

the above sequence s_1 *is* random. But even this additional information is insufficient. Suppose the numbers of the sequence s_1 were drawn from the set $\mathscr{S}_2$

$$\mathscr{S}_2 = \{0, 1\}, \tag{12.3}$$

with the *events* 0 and 1 together with assigned probabilities $P(0)$ and $P(1)$. These probabilities describe the probability that the outcome of a measurement on the set $\mathscr{S}_2$ yields either the event 0 or 1, respectively. For instance, in the case of tossing a coin the event 0 may correspond to *heads* while 1 stands for *tails*. (To register this result is within this context a *measurement*.) In this case the probabilities are given by $P(0) = P(1) = 1/2$, under the premise that the coin is perfectly ideal and has not been manipulated.

Even, if we know that the coin has not been manipulated, sequence (12.1) is still a possible outcome, although it is rather improbable for a large number N of measurements (repeated tosses of the coin).

We quote the literal definition of randomness within the context of a random sequence. It goes back to Chaitin [1]:

> *[...] a series of numbers is random if the smallest algorithm capable of specifying it to a computer has about the same number of bits of information as the series itself.*

This definition seems to include the most important features of randomness, which we are used to from our experience. Since, no universal trend is observable, reproducing the sequence requires the knowledge of every single constituent. Hence, one may employ the sloppy definition that randomness is the lack of an universal trend.

So far, we defined randomness of a sequence of numbers. However, what is a random number? Although the simplest answer is that it is a number drawn at random, a more useful answer is found if we regard a random sequence drawn from the set

$$\mathscr{S}_3 = \{0, 1, 2, 3, 4, 5, 6, 7, 8, 9\}. \tag{12.4}$$

If the random number is to be uniformly distributed, we assign probabilities $P(k) = 1/10$, $k = 0, 1, \ldots, 9$ and if we would like to obtain a random number from the interval

$$\Omega_1 = [0, 1), \tag{12.5}$$

we may simply draw the sequence $s_2 = a_1, a_2, a_3, \ldots$ from $\mathscr{S}_3$ and compose the random number r as

$$r = 0.a_1a_2a_3 \ldots . \tag{12.6}$$

In what follows we shall restrict our discussion to random numbers, which are uniformly distributed over a finite set, i.e. we assign to all possible outcomes the same probability. Generation of non-uniformly distributed random numbers from uniformly distributed random numbers is not a difficult task and will be discussed in more detail in Chap. 13.

We shall now focus briefly on the question of how one can test whether or not a sequence together with a given set is truly a random sequence (again, under the premise of a uniform distribution). From an intuitive point of view, one would simply exploit the statistical definition of probability (D.4), i.e. one would *measure* the probability of a certain outcome by counting the particular results. This procedure can be quite promising, however, it has to be kept in mind that the statistical definition of probability is only valid in the limit $m \to \infty$, where m is the number of measurements. Hence, it is fundamentally impossible to determine whether or not a sequence is random because an infinite number of elements would have to be evaluated and analyzed. More promising appears to be the calculation of moments or correlations from the sequence and to compare such a result with known values for real random numbers. These statistical tests will be discussed in Sect. 12.3. If we consider the sequence (12.1) drawn from the set $\mathscr{S}_3$, (12.3) (uniform distribution), we can deduce that it is a very improbable result for large N, although it is certainly a possible outcome. Methods based on this train of thoughts are known as *hypothesis testings* and we discuss the χ^2 test as a simple representative of such tests in Sect. 12.3.

Section 12.2 is dedicated to the discussion of different methods of how to generate so called *pseudo random numbers*. A pseudo random number is a number generated with the help of a deterministic algorithm, however, it shows a behavior as if it were random, i.e. its statistical properties are close to that of true random numbers. In contrast to pseudo random numbers, *real random numbers* are truly random. A real random number can be obtained from experiments. One could, for instance, simply toss a coin and register the resulting sequence of zeros and ones. A more sophisticated method is to exploit the radioactive decay of a nucleus, which is believed to be purely stochastic. There are also more exotic ideas, such as using higher digits of π, which are assumed to behave as if they were random. However, all these methods have in common that they are far too slow for computational purposes. Moreover, an *experimental* approach is obviously not *reproducible* in the sense, that a random sequence cannot be reproduced on demand, but the reproducibility of a random number sequence is essential for many applications.

Let us formulate several criteria, which we require from a random number generator: The algorithm should

- produce pseudo random numbers whose statistical properties are as close as possible to that of real random numbers.
- have a long period, i.e. it should generate a non-repeating sequence of random numbers which is sufficiently long for computational purposes.
- be reproducible in the sense defined above, as well as restartable from an arbitrary break-point.
- be fast and parallelizable, i.e. it should not be the limiting component in simulations.

There is one last point: the division of this book into one part which discusses deterministic methods and one which discusses stochastic methods may seem weird in the light of the above discussion, since the numerically important random number generators are deterministic in nature. However, we will maintain this somehow arbitrary separation since the concepts discussed within this second part are fundamentally different from the concepts discussed in the first part.

12.2 Different Approaches

In what follows, we discuss pseudo random number generators which generate a pseudo random number r uniformly distributed within the interval $[0, 1)$. Hence, its *probability density function* (pdf) is given by

$$p(r) = \begin{cases} 1 & r \in [0, 1), \\ 0 & \text{elsewhere}, \end{cases} \tag{12.7}$$

and from this follows the *cumulative distribution function* (cdf; see Appendix D):

$$P(r) = \int_0^r \mathrm{d}r' \; p(r') = \begin{cases} 0 & r < 0, \\ r & 0 \le r < 1, \\ 1 & r \ge 1. \end{cases} \tag{12.8}$$

We shall now introduce briefly some of the most basic concepts for pseudo random number generators. However, in huge simulations based on random numbers standard pseudo random number generators provided by the various compilers may not be sufficient due to their rather short period and bad statistical properties. In this case it is, therefore, recommended to consult the literature [2] and use more advanced techniques in order to obtain reliable results.

Linear Congruential Generators

Linear congruential generators are the simplest and most prominent random number generators. They produce a sequence of integers $\{x_n\}$, $n \in \mathbb{N}$ following the rule

$$x_{n+1} = (ax_n + c) \mod m, \tag{12.9}$$

where a, c and m are positive integers which obey $0 \le a, c < m$. Furthermore, the generator is initialized by its *seed* x_0, which is also a positive (in most cases odd) integer in the range $0 \le x_0 < m$. The seed is commonly taken from, for instance, the system time in order to avoid repetition at a restart of the sequence. In many environments it is therefore necessary to fix the seed artificially whenever one wants to perform reproducible tests.

We note that the sequence resulting from Eq. (12.9) is bounded to the interval $x_n = [0, m-1]$ and, hence, its maximum period is m. However, the actual period of the sequence highly depends on the choices of the parameters a, c and m as well as on the seed x_0. In general, linear congruential generators are very fast and simple, however, they have rather short periods. Moreover, they are very susceptible to correlations since the value x_{n+1} is calculated from x_n only. (This is obviously a property which does not apply to real random numbers and it should therefore be eliminated!) In Sect. 12.3 we will discuss some simple methods which allow to identify such correlations.

One of the most prominent choices for the parameters in Eq. (12.9) are the PARK-MILLER parameters:

$$a = 7^5, \quad c = 0, \quad m = 2^{31} - 1. \tag{12.10}$$

Note that one has to be particularly careful when choosing $c = 0$. It follows from Eq. (12.9) that if $c = 0$ and if for any n, $x_n = 0$ one obtains $x_k = 0$ for all $k > n$.

The random numbers r_n described by the pdf (12.7) are obtained via

$$r_n = \frac{x_n}{m} \in [0, 1). \tag{12.11}$$

Let us briefly discuss two famous improvements which concentrate on the reduction of correlations and an elongation of the period: The first idea, which is referred to as *shuffling*, includes a second *pseudo random* step. One calculates N numbers r_n from Eqs. (12.9) and (12.11) and stores these numbers in an array. If a random number is needed by the executing program, a second random integer $k \in [1, N]$ is drawn and the kth element is taken from this array. In order to avoid that the same random number is used again, the kth element of the array is now replaced by a new random number which, again, is calculated from (12.9) and (12.11).

The second idea to improve the linear congruential generator is simply to include more previous elements of the sequence:

$$x_{n+1} = \left(\sum_{k=0}^{\ell} a_k x_{n-k} \right) \mod m, \tag{12.12}$$

where $\ell > 0$ and $a_\ell \neq 0$. Again, the periodicity depends highly on the choice of the parameters, as well as on the seed. In the following we will discuss a special type of generators of the form (12.12), the FIBONACCI generators.

FIBONACCI *Generators*

The FIBONACCI sequence is given by

$$x_{n+1} = x_n + x_{n-1}, \qquad x_0 = 0, \quad x_1 = 1, \tag{12.13}$$

which results for $n \geq 1$ in

$$1, 1, 2, 3, 5, 8, 13, 21, 34, 55, 89, \ldots. \tag{12.14}$$

Choosing in Eq. (12.12) $m = 10$, $\ell = 1$ and $a_0 = a_1 = 1$ simply leaves the last digits of the sequence (12.14):

$$1, 1, 2, 3, 5, 8, 3, 1, 4, 5, 9, \ldots. \tag{12.15}$$

This suggests the definition of a pseudo random number generator based on the Fibonacci sequence. It is of the form

$$x_{n+1} = (x_n + x_{n-1}) \mod m, \tag{12.16}$$

which, according to our previous discussion, allows a periodicity exceeding m. A straightforward generalization results in the so called *lagged Fibonacci generators:*

$$x_{n+1} = (x_{n-p} \otimes x_{n-q}) \mod m, \tag{12.17}$$

where $p, q \in \mathbb{N}$ and the operator $\otimes$ stands for any binary operation, such as addition, subtraction, multiplication or some logical operation. Two of the most popular lagged FIBONACCI generators are the *shift register generator* and the MARSAGLIA-ZAMAN *generator*.

The shift register generator is based on the *exclusive or* (XOR; $\oplus$) operation, which acts on each bit of the numbers x_{n-p} and x_{n-q}. In particular, the recurrence relation reads

$$x_n = x_{n-p} \oplus x_{n-q}. \tag{12.18}$$

The XOR operation $\oplus$ is shown in the following multiplication table:

a	b	$a \oplus b$
0	0	0
1	0	1
0	1	1
1	1	0

Hence, suppose that the binary representation of x_{n-p} is of the form 01001110... while for x_{n-q} we have 11110011 .... This results in

x_{n-p}	0	1	0	0	1	1	1	0	...
x_{n-q}	1	1	1	1	0	0	1	1	...
x_{n+1}	1	0	1	1	1	1	0	1	...

A very prominent choice is given by $p = 250$ and $q = 103$ which yields a superior periodicity which is of order $\mathcal{O}(10^{75})$. The algorithm is initialized with the help of, for instance, a linear congruential generator.

In contrast, the MARSAGLIA-ZAMAN generator, uses the subtraction operation and may be written by introducing the so called *carry bit* Δ as

$$\Delta = x_{n-p} - x_{n-q} - c_{n-1}, \tag{12.19}$$

where $x_i \in [0, m]$ for all i. Then,

$$x_n = \begin{cases} \Delta & \Delta \geq 0, \\ \Delta + m & \Delta < 0. \end{cases} \tag{12.20}$$

and c_n is obtained via

$$c_n = \begin{cases} 0 & \Delta \geq 0, \\ 1 & \Delta < 0. \end{cases} \tag{12.21}$$

For the particular choice $p = 10$, $q = 24$ and $m = 2^{24}$ one finds an amazingly large periodicity which is of order $\mathscr{O}(10^{171})$. The random numbers x_n are integers in the interval $x_n \in [0, m]$, hence dividing the random numbers by m gives $r_n \in [0, 1]$.

12.3 Quality Tests

Here, we discuss some tests to check whether or not a given, finite sequence of numbers x_n consists of uniformly distributed random numbers out of the interval $x_n \in [0, 1]$.[1]

Statistical Tests

These statistical tests are generally the most simple methods to achieve a first idea of the quality of a pseudo random number generator. Statistical tests are typically based on the calculation of moments or correlations. Since we regard the simplified case of uniformly distributed, uncorrelated random numbers within the interval [0, 1], the moments can be calculated immediately via (see Appendix D)

$$\left\langle X^k \right\rangle = \int \mathrm{d}x\ x^k p(x) = \int_0^1 \mathrm{d}x\ x^k = \frac{1}{k+1}, \tag{12.22}$$

for $k \in \mathbb{N}$. These moments are only approximated by the generated finite sequence of numbers $\{x_n\}_{n=1,\ldots,N}$ via

$$\left\langle X^k \right\rangle \approx \overline{x^k} = \frac{1}{N} \sum_{n=1}^{N} x_n^k. \tag{12.23}$$

As illustrated in Appendix D, the error of this approximation is of order $\mathscr{O}\left(\frac{1}{\sqrt{N}}\right)$, i.e.

$$\left\langle X^k \right\rangle = \overline{x^k} + \mathscr{O}\left(\frac{1}{\sqrt{N}}\right). \tag{12.24}$$

In a similar fashion, we can calculate correlations from the values of the sequence and compare it with the analytical result. We remember that if we regard uncorrelated random numbers we obtain

[1] From now on we define quite generally the interval out of which random numbers x_n are drawn by $x_n \in [0, 1]$ keeping in mind that this interval depends on the actual method applied. This method determines whether zero or one is contained in the interval.

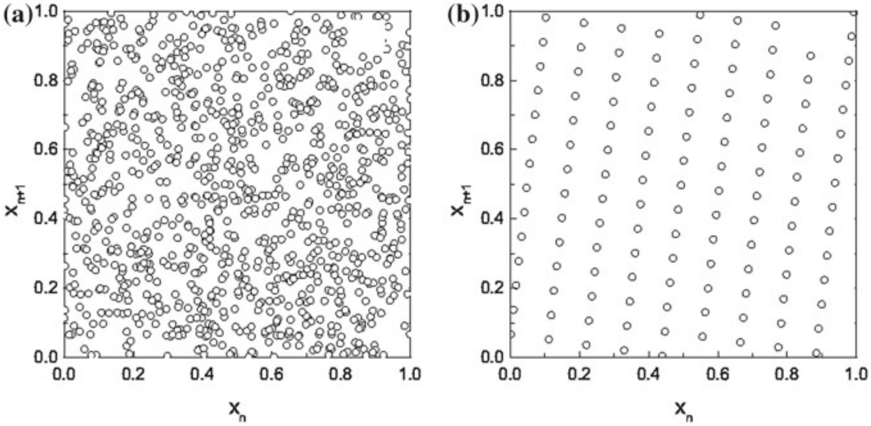

Fig. 12.1 Spectral test for a linear congruential generator. We used the PARK-MILLER parameters, **(a)** $a = 7^5$, $c = 0$, and $m = 2^{31} - 1$, **(b)** $a = 137$, $c = 0$, and $m = 2^{11}$, and plotted $N = 10^3$ subsequent pairs (x_n, x_{n+1}) of random numbers. In frame (**a**) the random numbers evolve nicely distributed within the unit square, showing no obvious correlations. On the other hand, in frame (**b**) subsequent random numbers lie on hyperplanes and, thus, develop correlations, i.e. they do not fill the unit square uniformly

$$\langle X_n X_{n+k} \rangle = \langle X_n \rangle^2 = \frac{1}{4}. \tag{12.25}$$

Another, quite evident test, is the analysis of the symmetry of the distribution. If $X_n \in [0, 1]$ is uniformly distributed then it follows that $(1 - X_n) \in [0, 1]$ should also be uniformly distributed.

Finally, we discuss a graphical test, known as the *spectral test*. The spectral test consists of plotting subsequent random numbers, i.e. x_n versus x_{n+1} and of inspecting the resulting plot by eye. One expects that the random numbers uniformly fill the unit-square, however, if correlations exist, particular patterns might evolve. We illustrate this method in Fig. 12.1 where it is applied to a linear congruential generator with two different sets of parameters, see Eq. (12.9).

Hypothesis Testing

Basically, one could employ different hypothesis tests, such as the KOLMOGOROV-SMIRNOV test, to test random numbers. These tests are rather basic and are discussed in numerous books on statistics. In what follows we shall briefly discuss the χ^2-test; for more advanced techniques we refer the reader to the literature [3, 4].

The χ^2-test tests the pdf directly. One starts by sorting the N elements of the sequence into a histogram. Suppose we would like to have M bins and, hence, the width of every bin is given by $\frac{1}{M}$. We now count the number of elements which

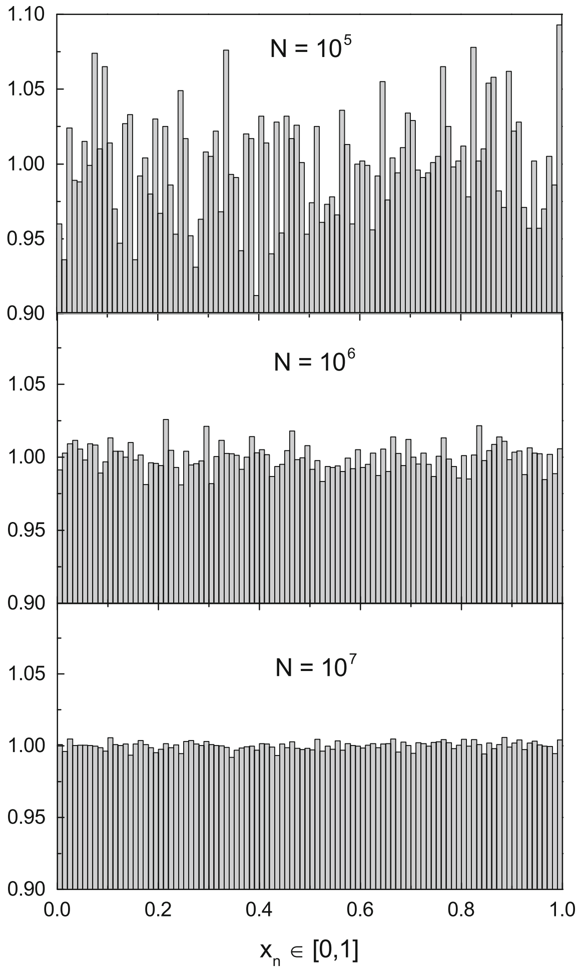

Fig. 12.2 Histograms for $N = 10^5$, $N = 10^6$ and $N = 10^7$, $M = 100$ bins as obtained with the PARK-MILLER linear congruential generator, $a = 7^5$, $c = 0$ and $m = 2^{31} - 1$

lie within bin k, i.e. within the interval $\left[\frac{k-1}{M}, \frac{k}{M}\right]$ and denote this number by n_k. The histogram array h is given by $h = c(n_1, n_2, \ldots, n_M)^T$ where the constant $c = \frac{M}{N}$ normalizes the histogram. In Fig. 12.2 we show three different histograms for $N = 10^5$, $N = 10^6$ and $N = 10^7$ uniformly distributed random numbers as obtained with the PARK-MILLER linear congruential generator. In Fig. 12.3 we show a histogram for $N = 10^7$ obtained with the bad linear congruential generator defined in Fig. 12.1b.

Let us briefly remember some points from probability theory [5, 6]. One can show, that if numbers Q_n are normally distributed random variables, their sum

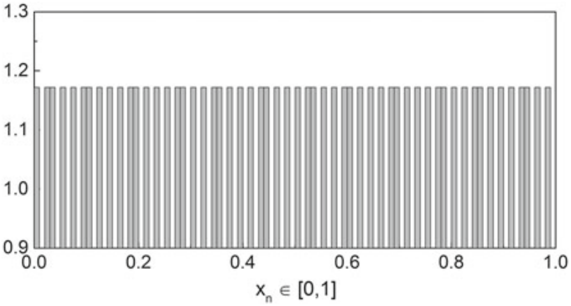

Fig. 12.3 Histogram for $N = 10^7$ and $M = 100$ bins as obtained with a linear congruential generator with parameters $a = 137$, $c = 0$ and $m = 2^{11}$

$$x = \sum_{n=1}^{\nu} Q_n^2, \tag{12.26}$$

follows a χ^2-distribution where ν is the number of degrees of freedom. The pdf of the χ^2-distribution is given by

$$p(x;\nu) = \frac{x^{\frac{\nu}{2}-1} e^{-\frac{x}{2}}}{2^{\frac{\nu}{2}} \Gamma\left(\frac{\nu}{2}\right)}, \quad x \geq 0, \tag{12.27}$$

where $\Gamma(\cdot)$ denotes the Γ-function. The probability of finding the variable x within the interval $[a, b] \subset \mathbb{R}^+$ can be calculated as

$$P(x \in [a,b];\nu) = \int_a^b \mathrm{d}x \; p(x;\nu), \tag{12.28}$$

and in particular for $a = 0$ we obtain

$$P(x < b;\nu) = \int_0^b \mathrm{d}x \; p(x;\nu) = F(b;\nu). \tag{12.29}$$

Here we introduced the cdf $F(b;\nu)$. Let us consider the inverse problem: the probability that $x \leq b$ is equal to α, i.e. $F(b;\nu) = \alpha$, then we calculate the upper bound b by inverting Eq. (12.29) in order to obtain

$$b = F^{-1}(\alpha;\nu). \tag{12.30}$$

These values are tabulated [7].

We return to our particular example: the hypothesis is that the sequence $\{x_n\}$ generated by some pseudo random number generator follows a uniform distribution. It then follows from the central limit theorem that the deviations from the theoretically expected values follow a normal distribution. We define the variable

$$x = \chi^2 = \sum_{k=1}^{M} \frac{(n_k - n_k^{th})^2}{n_k^{th}}. \tag{12.31}$$

If our hypothesis is true, χ^2 follows a χ^2-distribution with $\nu = M - 1$, since the degrees of freedom are reduced by one because of the requirement that the sum of all numbers n_k is equal to N. We employ relation (12.30) for $\alpha = 0.85$ and $\nu = 99$ in order to obtain $b = 113$. Hence, values $\chi^2 < b$ are very likely if χ^2 really follows a χ^2 distribution, while values $\chi^2 > b$ are unlikely and therefore the hypothesis may require a review. However, it has to be emphasized that it is fundamentally impossible to *verify* a hypothesis. It can only be falsified or strengthened. We note that the resulting value of χ^2 will highly depend on the seed number of the generator as long as the maximum period has not been reached.

Summary

We first concentrated on a possible definition of randomness and on a mathematical definition of random numbers and sequences. As the generation of random numbers is the main topic of this section we moved on to describe the requirements an 'ideal' random number generator will have to obey. On the other hand, the numerics of computational physics demand reproducible sequences of random numbers and this resulted in the notion of 'pseudo' random numbers which will be generated by deterministic methods and, thus, cannot possibly be 'ideal'. A number of rather simple but quite effective pseudo random number generators was discussed before the question of how to test the quality (randomness) of these numbers was raised. We discussed statistical tests and demonstrated the simple spectral test using a linear congruential generator. More sophisticated is the method of quality testing. The histogram technique as a direct test for the probability density function from which the random numbers are drawn is discussed in detail. Finally, some basics of the χ^2-test have been presented.

Problems

1. Write the computer code for a linear congruential generator. This generator is described by

$$x_{j+1} = (ax_j + c) \mod m.$$

The random numbers $r_j \in [0, 1]$ can be obtained by normalizing x_j as was discussed in Sect. 12.2. Use the following parameters

(a) $a = 16807, \quad c = 0, \quad m = 2^{31} - 1, \quad x_0 = 3141549,$
(b) $a = 5, \quad c = 0, \quad m = 2^7, \quad x_0 = 1.$

2. Perform the following analysis:

   (a) Compute the mean $\langle r \rangle$ and the variance var (r) for random numbers generated in N steps. Plot the result.
   (b) Plot two successive random numbers r_k versus r_{k+1} for $k = 1, 2, \ldots, N - 1$ in a two dimensional plot.
   (c) Repeat the above steps for random numbers generated by your system's software.
   (d) Discuss the results!

References

1. Chaitin, G.J.: Randomness and mathematical proof. Sci. Am. **232**, 47 (1975)
2. Press, W.H., Teukolsky, S.A., Vetterling, W.T., Flannery, B.P.: Numerical Recipes in C++, 2nd edn. Cambridge University Press, Cambridge (2002)
3. Iversen, G.P., Gergen, I.: Statistics. Springer Undergraduate Textbooks in Statistics. Springer, Berlin (1997)
4. Keener, R.W.: Theoretical Statistics. Springer, New York (2010)
5. Chow, Y.S., Teicher, H.: Probability Theory, 3rd edn. Springer Texts in Statistics. Springer, Berlin (1997)
6. Kienke, A.: Probability Theory. Universitext. Springer, Heidelberg (2008)
7. Abramovitz, M., Stegun, I.A. (eds.): Handbook of Mathemathical Functions. Dover, New York (1965)

Chapter 13
Random Sampling Methods

13.1 Introduction

In most applications random numbers are required which follow a certain probability density function (pdf) which is not a uniform distribution on the interval [0, 1]. Of course, one could employ natural sources if available. However, we would like to formulate methods which will allow us to obtain random numbers which follow some arbitrary pdf from uniformly distributed random numbers which in turn can be generated with the help of the methods we discussed in Chap. 12.

Within this chapter we shall introduce two methods to obtain random numbers from some arbitrary pdf, i.e. the *inverse transformation method* and the *rejection method*. Furthermore, in Sect. 13.4 we shall discuss the generalization of these methods to piecewise defined pdfs and combined pdfs. It has to be emphasized that these methods are in many cases not sufficient and a more powerful approach is required. One of these approaches which is based on the idea of *importance sampling* and is referred to as the Metropolis method. It will be discussed briefly in Chap. 14.

Apart from these methods we are going to discuss in the following sections, it is possible to obtain quite easily random numbers for special pdfs by an almost trivial approach, namely the *direct sampling*. For instance, suppose x_1, x_2 are two uniformly distributed random numbers. Hence, their pdf is given by

$$p_u(x) = \begin{cases} 1 & x \in [0, 1], \\ 0 & \text{elsewhere.} \end{cases} \tag{13.1}$$

and the corresponding *cumulative distribution function* (cdf) follows:

$$P_u(x) = \int_0^x \mathrm{d}x' \; p_u(x') = \begin{cases} 0 & x < 0, \\ x & x \in [0, 1], \\ 1 & x > 1. \end{cases} \tag{13.2}$$

B. A. Stickler and E. Schachinger, *Basic Concepts in Computational Physics*,
DOI: 10.1007/978-3-319-02435-6_13, © Springer International Publishing Switzerland 2014

One can show, that the new random number y

$$y = \max(x_1, x_2), \tag{13.3}$$

possesses the cdf

$$F(y) = y^2, \tag{13.4}$$

and, thus, the pdf

$$f(y) = 2y, \tag{13.5}$$

follows. This results in a very elegant method of constructing random numbers z which follow the pdf

$$g(z) = kz^{k-1}, \tag{13.6}$$

by defining

$$z = \max(x_1, x_2, \dots, x_k). \tag{13.7}$$

Here, the random numbers x_i are uniformly distributed and can be obtained with the help of the methods introduced in Chap. 12.

Another quite elegant method can be employed to calculate random numbers z_i according to a normal distribution. In this case, the pdf is of the form

$$p(z) = \frac{1}{\sqrt{2\pi}} \exp\left(-\frac{z^2}{2}\right). \tag{13.8}$$

Again, we act on the assumption that the x_i are uniformly distributed random numbers taken from the unit interval [0, 1]. We take two random numbers (x_1, x_2) in order to construct two random numbers (z_1, z_2), which follow the pdf (13.8). It is an easy task to prove that the transformation

$$z_1 = \sqrt{-2\ln x_1}\cos(2\pi x_2), \qquad z_2 = \sqrt{-2\ln x_1}\sin(2\pi x_2), \tag{13.9}$$

gives the desired result. We introduce the joint distribution $p_u(x_1, x_2) = p_u(x_1)$ $p_u(x_2)$ (i.e. no correlations). The transformation of probabilities gives

$$p(z_1, z_2)\mathrm{d}z_1\,\mathrm{d}z_2 = p_u(x_1, x_2)\mathrm{d}x_1\,\mathrm{d}x_2, \tag{13.10}$$

or, equivalently, the JACOBIAN determinant

$$p(z_1, z_2) = \frac{\partial(x_1, x_2)}{\partial(z_1, z_2)}, \tag{13.11}$$

where we employed Eq. (13.1). We recognize that Eq. (13.9) is equivalent to

$$x_1 = \exp\left(-\frac{z_1^2+z_2^2}{2}\right), \qquad x_2 = \frac{1}{2\pi}\cos^{-1}\left(\frac{z_1}{\sqrt{z_1^2+z_2^2}}\right)$$
$$= \frac{1}{2\pi}\sin^{-1}\left(\frac{z_2}{\sqrt{z_1^2+z_2^2}}\right). \qquad (13.12)$$

The JACOBIAN determinant is readily evaluated to give

$$\begin{aligned}\frac{\partial(x_1,x_2)}{\partial(z_1,z_2)} &= \begin{vmatrix} \frac{\partial x_1}{\partial z_1} & \frac{\partial x_1}{\partial z_2} \\ \frac{\partial x_2}{\partial z_1} & \frac{\partial x_2}{\partial z_2} \end{vmatrix} \\ &= \begin{vmatrix} z_1 x_1 & z_2 x_1 \\ -\frac{z_2}{2\pi\sqrt{z_1^2+z_2^2}} & \frac{z_1}{2\pi\sqrt{z_1^2+z_2^2}} \end{vmatrix} \\ &= \frac{x_1}{2\pi} \\ &= \frac{1}{2\pi}\exp\left(-\frac{z_1^2+z_2^2}{2}\right) \\ &= p(z_1)p(z_2), \end{aligned} \qquad (13.13)$$

i.e. it is the product of two normal distributions. Here we employed, that

$$\frac{\mathrm{d}}{\mathrm{d}x}\sin^{-1}(x) = -\frac{\mathrm{d}}{\mathrm{d}x}\cos^{-1}(x) = \frac{1}{\sqrt{1-x^2}}. \qquad (13.14)$$

Hence, z_1 and z_2 indeed follow a normal distribution. We shall now turn our attention to methods which allow sampling from arbitrary pdfs.

13.2 Inverse Transformation Method

The inverse transformation method is one of the simplest and most useful methods to sample random variables from an arbitrary pdf. Let $p(x)$, $x \in [x_{\min}, x_{\max}]$, denote the pdf from which we want to obtain our random numbers. The corresponding cdf will be denoted by

$$P(x) = \int_{x_{\min}}^{x} \mathrm{d}x'\, p(x'). \qquad (13.15)$$

It follows immediately from the positivity and the normalization condition of pdfs (Appendix D) that $P(x)$ is monotonically increasing and, furthermore, that

$P(x_{\min}) = 0$ and $P(x_{\max}) = 1$. Let ξ denote some random number uniformly distributed within the interval [0, 1], i.e. pertaining to the pdf $p_u(\xi)$. In the following we shall demonstrate, that the number

$$x = P^{-1}(\xi), \tag{13.16}$$

indeed follows the pdf $p(x)$, i.e. x is indeed the random number we are interested in. We employ the conservation of probability and obtain

$$p_u(\xi)\mathrm{d}\xi = p(x)\mathrm{d}x \implies 1 = p_u(\xi) = p(x)\left(\frac{\mathrm{d}\xi}{\mathrm{d}x}\right)^{-1}. \tag{13.17}$$

The choice $\xi = P(x)$, finally, gives the desired result, since

$$\frac{\mathrm{d}}{\mathrm{d}x}P(x) = p(x), \tag{13.18}$$

and, hence, we have

$$x = P^{-1}(\xi), \tag{13.19}$$

where P^{-1} denotes the inverse of P. This is an obvious caveat of this method, as it requires the $P^{-1}(\xi)$ to exist and that $P(x)$ can be calculated and inverted analytically. This is, for instance, not possible in the case of the normal distribution (13.8).

Let us give an illustrating example. Suppose we want to draw random numbers which are uniformly distributed within the interval $[a, b]$. The corresponding pdf reads

$$p(x) = \frac{1}{b-a}, \tag{13.20}$$

and the cdf takes on the form

$$P(x) = \frac{x-a}{b-a}, \tag{13.21}$$

where we employed that in this particular example $x_{\min} = a$. Hence, we have

$$\xi = \frac{x-a}{b-a}, \tag{13.22}$$

which is uniformly distributed within [0, 1]. Consequently, we determine random numbers $x \in [a, b]$ uniformly distributed via

$$x = a + (b-a)\xi. \tag{13.23}$$

We give a second example. The pdf we are interested in is the exponential distribution

$$p(x) = \frac{1}{\lambda}\exp\left(-\frac{x}{\lambda}\right), \tag{13.24}$$

where $\lambda > 0$ and $x \in [0, \infty)$. This could, for instance, describe the free path x of a particle between interactions, where the mean free path $\langle x \rangle = \lambda$. From Eq. (13.16) we obtain

$$\xi = \frac{1}{\lambda} \int_0^x \mathrm{d}x' \, \exp\left(-\frac{x'}{\lambda}\right) = 1 - \exp\left(-\frac{x}{\lambda}\right), \tag{13.25}$$

and consequently

$$x = -\lambda \ln(1 - \xi), \tag{13.26}$$

gives random variables according to the exponential distribution (13.24) if ξ follows the pdf $p_u(\xi)$ defined in Eq. (13.1). We note that it follows from the symmetry of the uniform distribution that

$$x = -\lambda \ln(\xi), \tag{13.27}$$

without affecting the resulting random numbers. In Fig. 13.1 we show a histogram with random numbers drawn according to (13.27).

We pointed out already that it is certainly a caveat of this method that the cdf $P(x)$ has to be calculated and inverted analytically. However, even if $P(x)$ is not analytically invertible, it is possible to employ the inverse transformation method by calculating $P(x)$ for certain grid-points x_i and then interpolating $P(x)$ piecewise between these points with the help of an invertible function. However, in many cases it is advantageous to employ the rejection method, which will be discussed next.

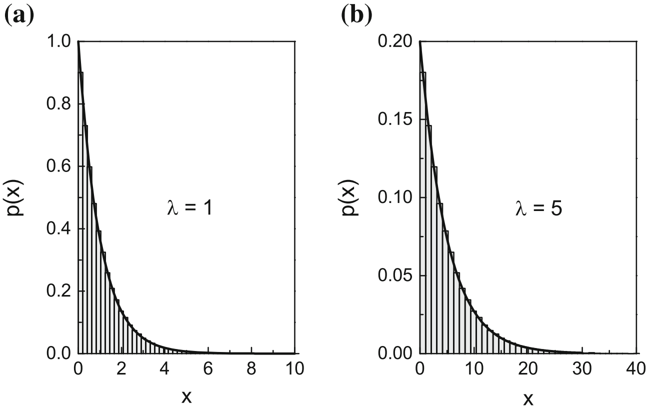

Fig. 13.1 The histogram representation of the pdf $p(x)$ versus x generated by random numbers drawn from an exponential distribution Eq. (13.24) with the help of the inverse transformation sampling method. *Two* different values for λ have been considered, namely **(a)** $\lambda = 1$ and **(b)** $\lambda = 5$. $N = 10^5$ random numbers have been sampled. The *solid line* corresponds to the pdf $p(x)$ according to Eq. (13.24)

13.3 Rejection Method

The rejection method is particularly suitable if the inverse transformation method fails. One of the most prominent versions of the rejection method is the Metropolis algorithm, as it will be introduced in Sect. 14.3.

The basic idea of the rejection method is quickly formulated: we draw random numbers x from another, preferably analytically invertible pdf $h(x)$ and check whether or not they lie within the desired pdf $p(x)$. If this is the case the random number x is accepted, otherwise it will be rejected. This is also the basic idea of the *hit and miss* version of Monte-Carlo integration which will be discussed in Sect. 14.2.

We specify the rejection method: Let $p(x)$ denote the pdf from which we want to draw random numbers. Furthermore, let $h(x)$ be another pdf, which can easily be sampled (for instance with the help of the inverse transformation method) and which is chosen in a such a way that the inequality

$$p(x) \leq c\,h(x), \tag{13.28}$$

holds for all $x \in [x_{\min}, x_{\max}]$, where c is some constant. The function $ch(x)$ is referred to as the *envelope* of $p(x)$ within the interval $[x_{\min}, x_{\max}]$. The strategy is clear: we sample a random variable x^t (trial state) from $h(x)$ and accept it with probability $p(x)/[c\,h(x)]$. This procedure is sketched in Fig. 13.2. Let $p(A|x)$ denote the probability that a given value x is accepted and $g(x)$ denotes the probability that we produce a variable x with this algorithm. Furthermore, $P(x = x^t)$ stands for the probability that a trial state x^t is generated. We have

$$\begin{aligned} g(x) &\propto P(x = x^t)p(A|x^t) \\ &= h(x^t)\frac{p(x^t)}{c\,h(x^t)} \\ &\propto p(x^t). \end{aligned} \tag{13.29}$$

Hence, we indeed generate random numbers according to $p(x)$. We may also calculate the probability $P(A)$ that an arbitrary trial state x^t is accepted. This is done with the help of the marginalization rule (see Appendix D):

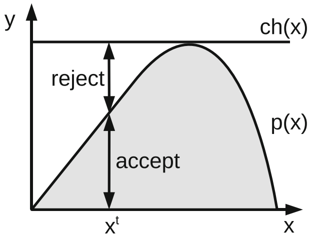

Fig. 13.2 Schematic illustration of the rejection method. The trial state x^t is accepted with probability $p(x)/[ch(x)]$

$$\begin{aligned} P(A) &= \int \mathrm{d}x^t \; p(A \wedge x^t) \\ &= \int \mathrm{d}x^t \; p(A|x^t) P(x = x^t) \\ &= \int \mathrm{d}x^t \; \frac{p(x^t)}{c\, h(x^t)} h(x^t) \\ &= \frac{1}{c} \int \mathrm{d}x^t \; p(x^t) \\ &= \frac{1}{c}. \end{aligned} \tag{13.30}$$

In a similar fashion, we obtain for a d-dimensional random variable that

$$P(A) = \frac{1}{c^d}. \tag{13.31}$$

We deduce that the bigger c the worse is the acceptance probability of the rejection method. It is therefore advisable to choose the envelope $h(x)$ very carefully.

We give an illustrating example: We aim at sampling the normal distribution for $x \in \mathbb{R}$

$$p(x) = \frac{1}{\sqrt{2\pi\sigma^2}} \exp\left(-\frac{x^2}{2\sigma^2}\right), \tag{13.32}$$

with expectation value $\langle x \rangle = 0$ and variance σ^2. In a first step we restrict our investigation to $x \in [0, \infty)$ due to the symmetry of the pdf. The slightly modified pdf for the right-half axis reads

$$q(x) = \sqrt{\frac{2}{\pi\sigma^2}} \exp\left(-\frac{x^2}{2\sigma^2}\right), \qquad x \in [0, \infty), \tag{13.33}$$

where we adjusted the normalization. The complete normal distribution (13.32) is re-obtained by sampling the sign of x in an additional step. We choose as the envelope $h(x)$ the exponential distribution Eq. (13.24). We choose λ and c in such a way, that the acceptance probability (13.30) has a maximum under the constraint (13.28). Since this is equivalent to $c \to \min$ we have to solve the optimization problem

$$c \geq \frac{q(x)}{h(x)} \to \max\,. \tag{13.34}$$

The resulting $c_{\min}$ is then given by

$$c_{\min} = \frac{q(x_{\mathrm{opt}})}{h(x_{\mathrm{opt}})}. \tag{13.35}$$

Here x_{opt} is the yet unknown optimal value for x. We obtain

$$\begin{aligned}\frac{\mathrm{d}}{\mathrm{d}x}\frac{q(x)}{p(x)} &= \sqrt{\frac{2\lambda^2}{\pi\sigma^2}}\frac{\mathrm{d}}{\mathrm{d}x}\exp\left(\frac{x}{\lambda}-\frac{x^2}{2\sigma^2}\right)\\ &= \sqrt{\frac{2\lambda^2}{\pi\sigma^2}}\exp\left(\frac{x}{\lambda}-\frac{x^2}{2\sigma^2}\right)\left[\frac{1}{\lambda}-\frac{x}{\sigma^2}\right]\\ &\overset{!}{=} 0,\end{aligned} \tag{13.36}$$

and, therefore,

$$x_{\text{opt}} = \frac{\sigma^2}{\lambda}. \tag{13.37}$$

Consequently, we have

$$c_{\min} = \sqrt{\frac{2\lambda^2}{\pi\sigma^2}}\exp\left(\frac{\sigma^2}{2\lambda^2}\right). \tag{13.38}$$

The above relation gives the minimum c for arbitrary λ. However, since $h(x)$ is our envelope, we can choose λ in such a way, that $c_{\min} \to$ min. This is achieved in a second step:

$$\begin{aligned}\frac{\mathrm{d}}{\mathrm{d}\lambda}c_{\min} &= \sqrt{\frac{2}{\pi\sigma^2}}\exp\left(\frac{\sigma^2}{2\lambda^2}\right)\left(1-\frac{\sigma^2}{\lambda^2}\right)\\ &\overset{!}{=} 0.\end{aligned} \tag{13.39}$$

This gives the optimum value λ_{opt} as

$$\lambda_{\text{opt}} = \sigma. \tag{13.40}$$

Finally, we obtain that with the help of the above choice $c_{\min}$ takes on the final form

$$c_{\min} = \sqrt{\frac{2e}{\pi}}. \tag{13.41}$$

The algorithm is executed in the following steps:

1. Draw a uniformly distributed random number $\xi \in [0, 1]$.
2. Calculate $x^t = -\lambda_{\text{opt}} \ln(\xi)$, where $\lambda_{\text{opt}} = \sigma$.
3. Draw a uniformly distributed random number $r \in [0, 1]$. If $r \le \frac{q(x^t)}{c_{\min}h(x^t)}$, then $x = x^t$ is accepted and if $r > \frac{q(x^t)}{c_{\min}h(x^t)}$, x^t is rejected and we return to step 1.
4. If x^t was accepted, we draw a uniformly distributed random number $r \in [0, 1]$ and only if $r < 0.5$ we set $x = -x$ otherwise x stays as is.

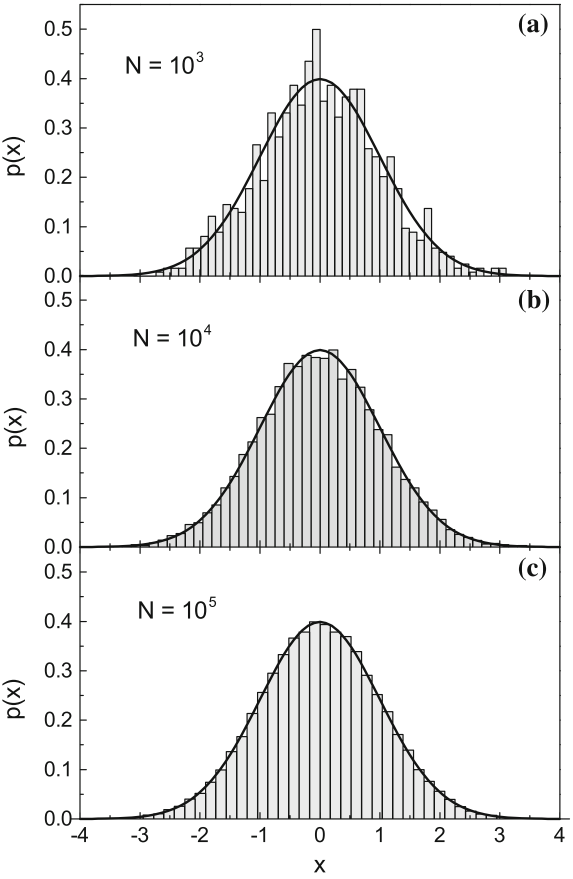

Fig. 13.3 The histogram representation of the pdf $p(x)$ versus x generated by random numbers drawn from the normal distribution Eq. (13.32) ($\sigma = 1$) with the help of the rejection method. We sampled **(a)** $N = 10^3$, **(b)** $N = 10^4$, and **(c)** $N = 10^5$ random numbers. The *solid line* represents the pdf $p(x)$ (13.32)

5. We repeat steps 1–4 until the number N of desired random numbers has been reached.

Figure 13.3 shows random numbers obtained with the help of this method in a histogram representation . We calculated (a) $N = 10^3$, (b) $N = 10^4$, and (c) $N = 10^5$ random numbers for $\sigma = 1$. It is quite obvious that the original pdf (13.32) is the better approximated the bigger the number N of sampled random number becomes.

13.4 Probability Mixing

Probability mixing is a method developed to generate random numbers by sampling from piecewise defined or composite pdfs. Such a pdf is of the general form

$$p(x) = \sum_{i=1}^{N} \alpha_i f_i(x), \quad \alpha_i \neq 0, \tag{13.42}$$

where the sub-pdfs $f_i(x)$ fulfill the normalization requirement

$$\int \mathrm{d}x' \, f_i(x') = 1, \tag{13.43}$$

and are non-negative, i.e.

$$f_i(x) \geq 0, \tag{13.44}$$

for all $i = 1, \ldots, N$. It follows that

$$\sum_{i=1}^{N} \alpha_i = 1, \tag{13.45}$$

so that

$$\int \mathrm{d}x' \, p(x') = 1, \tag{13.46}$$

is fulfilled. The question is how to sample random numbers from such a pdf, since in most cases it might be hard to invert the sum (inverse transformation method) or find a suitable envelope (rejection method). However, the question can easily be answered: We define

$$q_i = \sum_{\ell=1}^{i} \alpha_\ell. \tag{13.47}$$

Thus, $q_N = 1$ and the interval [0, 1] has been divided according to:

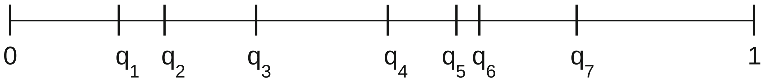

A uniformly distributed random number $r \in [0, 1]$ can now be employed to determine the index i for which the condition

$$q_{i-1} < r < q_i, \tag{13.48}$$

is fulfilled and we draw the random number x according to the sub-pdf $f_i(x)$ with any of the methods discussed above.

This procedure is quite plausible, since the coefficients α_i give the relative weight of the sub-pdfs $f_i(x)$, i.e. α_i determines the importance of the particular sub-pdf $f_i(x)$. It is therefore a natural approach to use it as a measure of the probability that a random variable is to be sampled from the particular sub-pdf $f_i(x)$.

Summary

To generate high quality random numbers from some non-uniform pdf $p(x) \neq p_u(x)$ is one of the most important tasks in computational physics, but from the outside it appears to play only a supportive role. This chapter concentrated on basic methods to generate the desired random numbers: (a) the *direct sampling method* uses transformations of the uniform distribution to generate the required random numbers; (b) the *inverse transformation method* is based on the availability of an inverse cdf in most cases required to be calculated analytically; finally, (c) the *rejection method* which is basically a hit or miss method. It uses an easily invertible pdf $h(x)$ which envelops the desired pdf $p(x)$ completely within some interval $x \in [x_{min}, x_{max}]$. The effectiveness of this method depends on how 'well' the envelope $h(x)$ encloses the original pdf $p(x)$. In a last step the method of *probability mixing* was discussed. It is an easily verifiable method which allows to sample random numbers from composite pdfs.

Problems

Draw random numbers from the following pdfs:

1. *Direct Sampling*:
   Sample the normal distribution with $\langle x \rangle = 0$ with the help of the method discussed in Sect. 13.1. Check the result by plotting the random numbers against the pdf $p(x)$ in a histogram.
2. *Inverse Transformation Method*:
   Write a function which samples random numbers from the exponential distribution with the help of the inverse transformation method as discussed in Sect. 13.2. Compare the generated random numbers to the pdf in a histogram.
3. *Rejection Method*:
   Sample the normal distribution with $\langle x \rangle = 0$ with the help of the exponential distribution as discussed in Sect. 13.3. Compare the generated random numbers with the pdf in a histogram. Determine the acceptance probability numerically.
4. *Probability Mixing*:
   We choose an alternative envelope for the normal distribution. This envelope is chosen to be constant for all $|x| < x_0$ and decays exponentially for $|x| \geq x_0$. The parameters do not need to optimize the acceptance probability. Again, plot the generated random numbers in a histogram and compare the acceptance probability with the acceptance probability of point (3).

Chapter 14
A Brief Introduction to Monte-Carlo Methods

14.1 Introduction

It is the aim of this chapter to give a brief introduction to Monte-Carlo methods in general, and to Monte-Carlo integration as well as to the METROPOLIS-HASTINGS algorithm in particular. A detailed discussion of the fundamental concepts involved is postponed to Chap. 16. The introduction given here is not supposed to be self-contained. Actually, we shall introduce concepts without referring to the origin of the relations employed.

The notion of Monte-Carlo methods, Monte-Carlo algorithms or Monte-Carlo techniques is not well defined. In particular, the term *Monte-Carlo* summarizes a wide field of methods, which are based on the sampling of random numbers. In general, the advantage of Monte-Carlo algorithms can be found in their computational strength. In many cases it is simply not feasible to employ deterministic methods due to their very high computational cost. However, in many cases the use of methods based on random sampling is also motivated by the nature of the processes to be described. We mentioned in the previous chapter as a typical example the radioactive decay of some nucleus. This process is believed to be purely stochastic in nature.

The development of Monte-Carlo techniques was initialized in the 1940s by VON NEUMANN, ULAM and METROPOLIS, who actually also coined the term *Monte-Carlo methods*. In particular, ULAM's uncle used to gamble (and loose his money) in a casino named *Monte-Carlo casino*, which they apparently regarded as their inspiration.

One of the earliest and most impressive illustration of the principle of Monte-Carlo techniques in general, and of Monte-Carlo integration in particular is the Monte-Carlo approximation of π. The discussion which follows now includes the essential ideas of Monte-Carlo integration.

We regard the unit square characterized by the corner points $(0, 0)$, $(0, 1)$, $(1, 0)$, and $(1, 1)$. The area A_s of this square is one. We insert a quarter-circle of radius $r = 1$ which, consequently, possesses the area $A_c = \pi/4$. Suppose, we are throwing darts on this unit square in such a way that the impact points are uniformly distributed; then the probability P that a certain dart becomes stuck within the interior of the

B. A. Stickler and E. Schachinger, *Basic Concepts in Computational Physics*,

DOI: 10.1007/978-3-319-02435-6_14,

Table 14.1 Approximate values $\pi_a^{(i)}$ obtained with the method discussed in the text

N	$\pi_a^{(1)}$	$\lvert\pi_a^{(1)} - \pi\rvert$	$\pi_a^{(2)}$	$\lvert\pi_a^{(2)} - \pi\rvert$
10	2.8000	0.34159	2.8000	0.34159
10^2	2.9200	0.22159	3.1600	0.01841
10^3	3.1600	0.01841	3.1840	0.04241
10^4	3.1304	0.01119	3.1868	0.04521
10^5	3.1358	0.00579	3.1875	0.04589
10^6	3.1393	0.00229	3.1875	0.04599
10^7	3.1413	0.00028	3.1875	0.04599

The linear congruential generators are initialized by the following parameters: generator (1): $a = 7^5$, $c = 0$, $m = 2^{31} - 1$, and $x_0 = 281$ (PARK-MILLER) and generator (2): $a = 7^5$, $c = 0$, $m = 2^{10}$, and $x_0 = 281$. We also give the absolute errors $|\pi_a^{(i)} - \pi|$

quarter-circle is given by

$$P = \frac{A_c}{A_s} = A_c = \frac{\pi}{4} = 0.785398\ldots. \tag{14.1}$$

From a probabilistic point of view, we have after N throws of which n hit the interior of the quarter-circle the probability:

$$P = \lim_{N\to\infty} \frac{n}{N}. \tag{14.2}$$

The strategy is clear: we draw random numbers x_i, y_i from the interval $[0, 1]$. These are the intersection points of the darts. Repeating this *experiment* several times and counting the number of hits n within the quarter-circle allows us to approximate π via

$$P = \frac{\pi}{4} \approx \frac{n}{N}. \tag{14.3}$$

The resulting approximation of π will be strongly influenced by the number of experiments N as well as by the performance of the random number generator used. Table 14.1 lists computed approximations of π for different numbers of experiments N as they were obtained with the help of a linear congruential generator. Linear congruential generators have been introduced and discussed in Sect. 12.2. The parameters used to initialize the generators are given in the caption of the table. Furthermore, Fig. 14.1 illustrates the result after $N = 10^3$ experiments for both generators.

14.2 Monte-Carlo Integration

We generalize the ideas formulated above: we consider a function $f(x) \geq 0$ for $x \in [a, b] \subset \mathbb{R}$ where the area of interest is

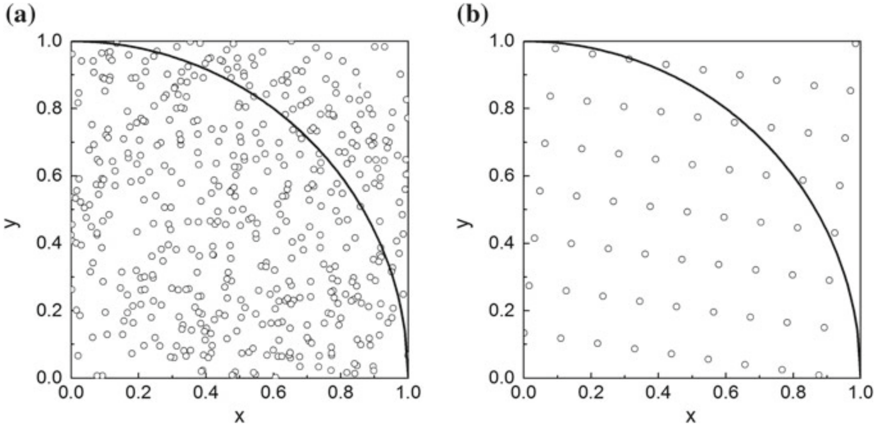

Fig. 14.1 $N = 10^3$ uniformly distributed random numbers within the unit-square. Frame (**a**) gives the results for generator (1) while frame (**b**) is for generator (2). The number of elements within the quarter-circle indicated by the solid line determines the value of $\pi_a^{(i)}$. The inferior result of the approximation obtained with generator (2) [frame (**b**)] originates in correlations between the x and y coordinates

$$A = \int_a^b \mathrm{d}x\ f(x). \tag{14.4}$$

We denote

$$\xi = \max_{x \in [a,b]} f(x), \tag{14.5}$$

and obtain using the above example

$$A = A_s \lim_{N \to \infty} \frac{n}{N}, \tag{14.6}$$

where n is the number of random points under the curve indicated schematically in Fig. 14.2. The area A_s is given by

$$A_s = (b - a)\xi, \tag{14.7}$$

and the random numbers $r_i = (x_i, y_i)$ are uniformly distributed within the intervals $x_i \in [a, b]$ and $y_i \in [0, \xi]$. This method is referred to as *hit and miss integration*.

Another way to perform a Monte-Carlo integration is the so called *mean-value integration* . It is essentially based on the mean value theorem of calculus which we already employed in our discussion of quadrature in Chap. 3. We will restate the theorem here for the sake of a more transparent illustration. The mean-value theorem states that if $f(x)$ is a continuous function for $x \in [a, b]$ then there exists a $z \in (a, b)$ such that

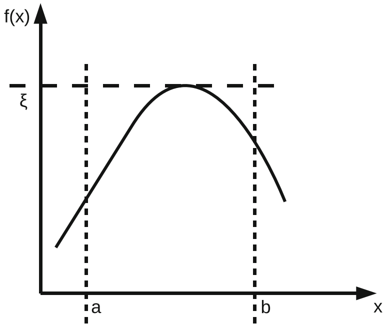

Fig. 14.2 Schematic illustration of the Monte-Carlo integration technique

$$\int_a^b \mathrm{d}x\ f(x) = f(z)(b-a). \tag{14.8}$$

The function value $f(z) = \langle f \rangle$ is referred to as the *expectation value* or *mean value* of $f(x)$. Now we know from probability theory [1, 2], that the expectation value can be approximated by the arithmetic mean $\overline{f}$, with the error given by the standard error, i.e.

$$\frac{1}{b-a}\int_a^b \mathrm{d}x'\ f(x') = \overline{f} \pm \sqrt{\frac{\overline{f^2} - \overline{f}^2}{N}}. \tag{14.9}$$

The arithmetic mean $\overline{f}$, on the other hand, is given by

$$\overline{f} = \frac{1}{N}\sum_{i=1}^{N} f(x_i), \tag{14.10}$$

and consequently

$$\overline{f^2} = \frac{1}{N}\sum_{i=1}^{N} f^2(x_i). \tag{14.11}$$

Note that here the variables x_i are assumed to be uniformly distributed random numbers within the interval $[a, b]$. We will immediately discuss this result in more detail. However, first of all we note from the law of large numbers, Appendix D, that this approach is exact in the limit $N \to \infty$, i.e.

$$\frac{1}{b-a}\int_a^b \mathrm{d}x'\ f(x') = \lim_{N\to\infty}\frac{1}{N}\sum_{i=1}^{N} f(x_i). \tag{14.12}$$

Let us consider the more general case: We want to evaluate the expectation value

$$\langle f \rangle = \int \mathrm{d}x \; f(x) p(x), \tag{14.13}$$

where $x \in \mathbb{R}^d$ and $p(x)$ is a pdf. A typical example is the calculation of the thermal expectation value in statistical physics where the pdf $p(x)$ is given by the normalized BOLTZMANN distribution

$$p(x) = \frac{1}{Z} \exp\left[-\frac{E(x)}{k_B T}\right]. \tag{14.14}$$

Here $E(x)$ denotes the energy as a function of the parameter $x \in \mathbb{R}^d$, k_B stands for BOLTZMANN's constant, T is the temperature, and the normalization factor Z is referred to as the canonical partition function.

Equation (14.13) may be rewritten as

$$\langle f \rangle = \int \mathrm{d}x \; f(x) p(x) = \int \mathrm{d}f \; f q(f), \tag{14.15}$$

where we introduced the probability density $q(f)$ of f via

$$q(f) = \int \mathrm{d}x \; \delta\left[f - f(x)\right] p(x). \tag{14.16}$$

with $\delta(\cdot)$ DIRAC's δ-distribution. Let us briefly explain how we arrived at this definition. Let the cdf $P(x)$ be defined by[1]

$$P(x) = \Pr(X \le x) = \int\limits_{-\infty}^{x} \mathrm{d}x \; p(x). \tag{14.17}$$

We define in a similar fashion the cdf $Q(f)$ via

$$Q(f) = \Pr(F \le f) = \Pr[f(X) \le f]. \tag{14.18}$$

Note that we distinguish between the function $f(X)$ of the random variable X—which in turn follows the pdf $p(X)$—and the particular function value $f \in \mathbb{R}$. Furthermore, the probability $\Pr[f(X) \le f]$ can be rewritten as

$$\Pr[f(X) \le f] = \sum_n \Pr(a_n \le X \le b_n), \tag{14.19}$$

where the values $a_n < b_n$ are the ordered intersection points $a_1 < b_1 < a_2 < b_2 < \cdots < a_N < b_N$ chosen in such a way that

[1] Please note that according to the conventions established in Appendix D capital letters denote random variables.

$$f(a_n) = f(b_n) = f, \quad \text{and} \quad f[x \in (a_n, b_n)] < f. \tag{14.20}$$

It is a matter of the particular form of $f(x)$ whether or not the boundary points have to be included. Equation (14.19) can be rewritten:

$$\Pr(a_n \le X \le b_n) = P(b_n) - P(a_n) = \int\limits_{a_n}^{b_n} \mathrm{d}x \; p(x). \tag{14.21}$$

The pdf $q(f)$ is related to the cdf $Q(f)$ via

$$q(f) = \frac{\mathrm{d}}{\mathrm{d}f} Q(f), \tag{14.22}$$

and we obtain

$$\begin{aligned} q(f) &= \sum_n \frac{\mathrm{d}}{\mathrm{d}f} \Pr(a_n \le X \le b_n) \\ &= \sum_n \frac{\mathrm{d}}{\mathrm{d}f} \int\limits_{a_n}^{b_n} \mathrm{d}x \; p(x) \\ &= \sum_n \left[\frac{\mathrm{d}b_n}{\mathrm{d}f} p(b_n) - \frac{\mathrm{d}a_n}{\mathrm{d}f} p(a_n) \right] \\ &= \sum_n \left[\left(\frac{\mathrm{d}f(x)}{\mathrm{d}x} \right)^{-1} p(x) \Bigg|_{x=b_n} - \left(\frac{\mathrm{d}f(x)}{\mathrm{d}x} \right)^{-1} p(x) \Bigg|_{x=a_n} \right]. \end{aligned} \tag{14.23}$$

However, from Eq. (14.20) we know that

$$\frac{\mathrm{d}f(x)}{\mathrm{d}x}\Bigg|_{x=b_n} \overset{!}{>} 0 \quad \text{and} \quad \frac{\mathrm{d}f(x)}{\mathrm{d}x}\Bigg|_{x=a_n} \overset{!}{<} 0. \tag{14.24}$$

We introduce the intersection points x_k where $x_1 < x_2 < \cdots < x_K$ and $K = 2N$—if the boundary points are not included—for which $f(x_1) = f(x_2) = \cdots = f(x_K) = f$. Hence, Eq. (14.23) may be rewritten as

$$\begin{aligned} q(f) &= \sum_k \left| \frac{\mathrm{d}f\;(x)}{\mathrm{d}x} \right|^{-1} \Bigg|_{x=x_k} p(x_k) \\ &= \sum_k \frac{p(x_k)}{|f'(x_k)|}. \end{aligned} \tag{14.25}$$

The DIRAC δ-distribution of an arbitrary function $g(y)$ can be expressed as

$$\delta[g(y)] = \sum_i \frac{\delta(y - y_i)}{|g'(y_i)|}, \tag{14.26}$$

where the y_i are the zeros of $g(y)$, i.e. $g(y_i) = 0$. Hence, we arrive at the final result and find for Eq. (14.23):[2]

$$q(f) = \int \mathrm{d}x \; \delta\left[f - f(x)\right] p(x). \tag{14.27}$$

Furthermore, we note that

$$\int \mathrm{d}f \; q(f) = \int \mathrm{d}f \; \int \mathrm{d}x \; \delta\left[f - f(x)\right] p(x) = \int \mathrm{d}x \; p(x) = 1. \tag{14.28}$$

As a result, the variance of f, $\operatorname{var}(f)$ can be expressed as

$$\operatorname{var}(f) = \int \mathrm{d}x \; \left[f(x) - \langle f\rangle\right]^2 p(x) = \int \mathrm{d}f \; \left[f - \langle f\rangle\right]^2 q(f). \tag{14.29}$$

Let us define in a next step the arithmetic mean

$$\mathscr{F} = \frac{1}{N}\sum_{i=1}^{N} f(x_i) = \frac{1}{N}\sum_{i=1}^{N} f_i, \tag{14.30}$$

calculated with the help of N random numbers. Hence, we have

$$\langle \mathscr{F}\rangle = \langle f\rangle, \tag{14.31}$$

and

$$\operatorname{var}(\mathscr{F}) = \frac{\operatorname{var}(f)}{N}, \tag{14.32}$$

according to Appendix D. It follows from the central limit theorem, that for large values of N, the pdf of $\mathscr{F}$, $p(\mathscr{F})$ converges to a normal distribution $\mathscr{N}$ with $\langle \mathscr{F}\rangle$ and $\operatorname{var}(\mathscr{F})$, i.e.

[2] We give an example. Suppose $f(x) = \exp(x)$. Then we deduce that

$$\delta\left[f - \exp(x)\right] = \frac{\delta(x - \ln f)}{f},$$

and, consequently,

$$q(f) = \frac{p(\ln f)}{f}.$$

$$p(\mathscr{F}) \approx \mathscr{N}\left(\mathscr{F}\,\middle|\,\langle f\rangle\,,\,\frac{\mathrm{var}\,(f)}{N}\right). \tag{14.33}$$

This property can now be employed to estimate $\langle f\rangle$ according to

$$\langle f\rangle = \mathscr{F} \pm \sqrt{\frac{\mathrm{var}\,(f)}{N}} = \frac{1}{N}\sum_{i=1}^{N} f(x_i) \pm \sqrt{\frac{\mathrm{var}\,(f)}{N}}, \tag{14.34}$$

with random numbers x_i sampled from the pdf $p(x)$. This method is the most prominent formulation of Monte-Carlo integration.

We shall briefly discuss some properties of this method. We deduce from Eq. (14.34) that the error scales like $N^{-\frac{1}{2}}$. In contrast to the integration methods we discussed in Chap. 3, N is no longer the number of grid-points but the number of random numbers sampled.[3] In principle, the error scaling is worse than in the case of classical integrators. For instance, in the case of the central rectangular rule (Sect. 3.2) we had an error scaling of N^{-2} when summed over the whole interval. However, we obtained this result for the one-dimensional case, in higher dimensions we will certainly need much more grid-points. On the other hand, in Eq. (14.34) N corresponds the number of d-dimensional random numbers x. Hence, Monte-Carlo integration can be of advantage whenever one has to deal with complicated, high dimensional integrals. In contrast, restricted to one dimension it is in most cases not an improvement of the methods discussed already.

Monte-Carlo integration can also be of advantage whenever the integrand $f(x)$ is not well behaved, i.e. if one would need a very fine grid in order to compute a reasonable estimate of the true value of the integral. In such cases Monte-Carlo integration offers a very convenient approach due to its conceptual simplicity.

It is certainly a drawback of Monte-Carlo integration in its formulation (14.34), that the error is also proportional to $\sqrt{\mathrm{var}\,(f)}$, which is a yet unknown quantity. One has to approximate it with an adequate estimator, for instance with the help of the sampling variance. Moreover, if the variance $\mathrm{var}\,(f)$ diverges, the central limit theorem does not hold and the procedure (14.34) is no longer justified and will fail for sure.

Closely related to the problem of how to determine $\mathrm{var}\,(f)$, is the question of how many random numbers should be drawn. In most cases an iterative approach is the most promising strategy. In a first step N random numbers are drawn and the integral is computed using Eq. (14.34). Then another set of N random numbers is sampled and Eq. (14.34) is reevaluated now using all $2N$ random numbers. If the change in the resulting estimate of the integral is less than some given tolerance ε, the loop is terminated otherwise another set of N random numbers is added.

We mention that this form of Monte-Carlo integration can be improved particularly by sampling only from points which dominantly contribute to the integral. This

[3] Nevertheless, there is certainly some conceptual similarity between grid-points and random numbers within this context.

method is referred to as *importance sampling* and will be discussed in more detail later on.

14.3 The METROPOLIS Algorithm: An Introduction

Within this section we shall briefly discuss the METROPOLIS algorithm as a more sophisticated method to produce random numbers from given distributions. In fact, the METROPOLIS algorithm is a special form of the rejection method (Sect. 13.3). The aim of this particular section is to introduce the algorithm on a very basic level in order to allow a first view at an interesting model out of statistical physics, namely the ISING model which will be discussed in Chap. 15. A more detailed discussion of the METROPOLIS algorithm is postponed to Sect. 16.4.

The METROPOLIS algorithm is particularly useful to treat problems in statistical physics where thermodynamic expectation values of some observable O are the interesting objects. They are defined as

$$\langle O \rangle = \int \mathrm{d}x \; O(x) q(x), \tag{14.35}$$

where x is a set of parameters and $q(x)$ is the BOLTZMANN distribution (14.14). The set of parameters x could be, for instance, the position- and momentum-space coordinates of N different particles. In most cases x is a high dimensional object, which makes classical numerical integration (Chap. 3) cumbersome. Instead Monte-Carlo integration is employed and the integral (14.35) is approximated with the help of Eq. (14.34)

$$\langle O \rangle \approx \frac{1}{N} \sum_{i=1}^{N} O(x_i) \pm \sqrt{\frac{\mathrm{var}\,(O)}{N}}, \tag{14.36}$$

where the uncorrelated random numbers x_i, $i = 1, 2, \ldots, N$ are drawn according to the pdf $q(x)$ Eq. (14.14). We recognize immediately the problem: we need to know the exact functional form of $q(x)$ if we want to apply either the inverse transformation method or the rejection method discussed in Chap. 13. However, the partition function Z itself is determined by an integral which can be approximated using Eq. (14.36). We set

$$q(x) = \frac{p(x)}{Z}, \tag{14.37}$$

and

$$Z = \int \mathrm{d}x \; p(x) \tag{14.38}$$

follows from the normalization of $q(x)$. The METROPOLIS algorithm was designed to avoid precisely this problem. We concentrate on a pdf which is of the form (14.37), but $q(x)$ must not necessarily be of the form (14.14), i.e. $p(x)$ is arbitrary but it ensures that

$$\int \mathrm{d}x\ q(x) = 1 \Longleftrightarrow \int \mathrm{d}x\ p(x) = Z, \tag{14.39}$$

and $q(x) \geq 0$ for all x. In other words, $q(x)$ is a pdf. Suppose we already have a sequence $x_0, x_1, \ldots, x_n = \{x_n\}$ of parameters which indeed follows the pdf $q(x)$.[4] We now add to the last element of this sequence x_n a small perturbation δ and set

$$x_t = x_n + \delta. \tag{14.40}$$

Note that the perturbation δ is of the same dimension as the vector x. In similarity to the rejection method we seek for a criterion which helps us to decide whether or not the value x_t can be accepted as the next element of the sequence $\{x_n\}$.

The METROPOLIS method proposes an acceptance probability of the form

$$\Pr(A|x_t, x_n) = \begin{cases} 1 & \text{if } \frac{q(x_t)}{q(x_n)} \geq 1\ , \\ \frac{q(x_t)}{q(x_n)} & \text{otherwise.} \end{cases} \tag{14.41}$$

Hence, if $\Pr(A|x_t, x_n) = 1$, we set $x_{n+1} = x_t$, and if $\Pr(A|x_t, x_n) < 1$, we draw a random number $r \in [0, 1]$ and accept x_t if $r \leq \Pr(A|x_t, x_n)$ and reject x_t otherwise. We note that in this formulation the knowledge of the normalization factor Z is no longer required since it follows from Eq. (14.37) that

$$\frac{q(x_t)}{q(x_n)} = \frac{p(x_t)}{p(x_n)}. \tag{14.42}$$

Consequently we rewrite Eq. (14.41) as

$$\Pr(A|x_t, x_n) = \min\left(\frac{p(x_t)}{p(x_n)}, 1\right) = p(x_t|x_n), \tag{14.43}$$

where we introduced in the last step a more compact notation.

A discussion of the underlying concepts and why the choice (14.41) indeed samples random numbers according to the pdf $q(x)$ requires some basic knowledge of stochastics in general and of MARKOV-chains in particular. Hence, we postpone this discussion to Chap. 16. We will solely emphasize here a particular property which is referred to as *detailed balance* and which we shall acknowledge to be crucial for the METROPOLIS algorithm: let $p(x_t|x_n)$ denote the pdf for the probability that a random number x_t is generated from the random number x_n as defined in Eq. (14.43). Then the condition of detailed balance is given by

$$p(x_t|x_n)q(x_n) = p(x_n|x_t)q(x_t). \tag{14.44}$$

[4] The question of how one can obtain such a sequence will be discussed in Sect. 16.3.

In words: The probability $p(x_t|x_n)$ that a random number x_t is generated from a random number x_n times the probability $q(x_n)$ that the random number x_n occurred at all is equal to the probability $p(x_n|x_t)$ that the random number x_n is generated from x_t times the probability $q(x_t)$ that x_t occurred. Detailed balance is motivated by physics and is a condition of thermodynamic equilibrium.

Let us briefly demonstrate that the METROPOLIS algorithm (14.43) satisfies detailed balance (14.44). We distinguish three different cases: (i) Suppose that $p(x_t|x_n) = p(x_n|x_t) = 1$. From Eq. (14.43) we note that this is only possible if $p(x_t) = p(x_n)$ and therefore $q(x_t) = q(x_n)$ which is already Eq. (14.44) for this particular case. (ii) We assume that $p(x_t|x_n) = 1$ but $p(x_n|x_t) \neq 1$. It then follows from Eq. (14.43)

$$\begin{aligned} p(x_n|x_t)q(x_t) &= \frac{p(x_n)}{p(x_t)}q(x_t) \\ &= q(x_n), \end{aligned} \tag{14.45}$$

which corresponds to Eq. (14.44) for $p(x_t|x_n) = 1$. Note that we made use of definition (14.37) in order to achieve this result. (iii) In a similar fashion we have for $p(x_n|x_t) = 1$ and $p(x_t|x_n) \neq 1$ that

$$\begin{aligned} p(x_t|x_n)q(x_n) &= \frac{p(x_t)}{p(x_n)}q(x_n) \\ &= q(x_t), \end{aligned} \tag{14.46}$$

which, again, is Eq. (14.44). Hence, the METROPOLIS algorithm (14.43) indeed obeys detailed balance.

A question we did not answer so far is how to choose the initialization point x_0 of the sequence. This is clearly not trivial and is strongly related to one of the major disadvantages of the METROPOLIS algorithm, namely that subsequent random numbers (x_n, x_{n+1}) are strongly correlated. One of the most pragmatic approaches is to choose a starting point x_0 at random from the parameter space and then discard it together with the first few members of the sequence. This approach is strongly motivated by a clear physical picture: the sequence of random numbers resembles the evolution of the physical system from an arbitrary initial point x_0 toward equilibrium which manifests itself in the condition of detailed balance. Hence, the approach of discarding the first few members of the sequence is referred to as *thermalization*.

The integral of interest, Eq. (14.35) is then approximated with the help of Eq. (14.36), where the random numbers $x_k, x_{k+1}, \ldots, x_{k+N}$ are used, if the thermalization required k steps. There is a remedy which helps to reduce correlations between subsequent random numbers within the sequence which is based on a similar strategy. In particular, the modified sequence

$$x_k, x_{k+\ell}, x_{k+2\ell}, \ldots, \tag{14.47}$$

generated by discarding ℓ intermediate random numbers will reduce correlations between the members of this final sequence of random numbers.

Summary

This chapter set the stage for an important numerical tool in computational physics: the Monte-Carlo techniques. It started with the conceptual transparent task of how to calculate π using a sequence of uniformly distributed random numbers of the range [0, 1]. This established the so-called hit and miss technique. It moved on to a discussion of Monte-Carlo integration in a more formal way and discussed in detail the error involved by this type of integration as opposed to the error experienced by deterministic methods. The conclusion was, that Monte-Carlo integration is certainly preferable whenever estimates of highly dimensional integrals are required. It also has advantages when the integrand is heavily structured. The second part of this chapter dealt with the METROPOLIS algorithm which allowed to generate a sequence of random numbers from some pdf $p(x)$. It is conceptually similar to the rejection method discussed earlier. The mathematical background which is more involved was not discussed within this first contact with the METROPOLIS algorithm. Instead, the emphasis was to demonstrate that this algorithm obeyed detailed balance a property purely based on physics as a condition of thermodynamic equilibrium. It was, furthermore, pointed out that the random numbers generated by this algorithm are highly correlated and some strategies to remedy this problem have been discussed.

References

1. Chow, Y.S., Teicher, H.: Probability Theory, 3rd edn. Springer Texts in Statistics. Springer, Berlin (1997)
2. Kienke, A.: Probability Theory. Universitext. Springer, Heidelberg (2008)

Chapter 15
The Ising Model

15.1 The Model

Ferromagnetic materials are materials which develop a non-vanishing magnetization M even in the absence of an external magnetic field B. It is an experimental observation, that this magnetization decreases smoothly with increasing temperature, and vanishes above the critical temperature T_C, referred to as Curie temperature. This typical situation is illustrated in Fig. 15.1. In a theoretical description of this phase transition the magnetization M serves as an order parameter.[1] At $T = T_C$ the system exhibits a second order phase transition, i.e. the magnetization is not differentiable with respect to T; it is, however, continuous.

The microscopic origin of this macroscopic phenomenon is based on the exchange interaction between identical particles, i.e. between the atoms or molecules forming the material. The exchange interaction is a purely quantum mechanical effect which is a consequence of the Coulomb interaction in combination with the Pauli exclusion principle. For a more detailed discussion, the reader may consult any textbook on quantum mechanics [1–3].

Given two atoms or molecules with spins S_1 and S_2, where $S_1, S_2 \in \mathbb{R}^3$, the exchange interaction energy is of the form[2]

$$E = JS_1 \cdot S_2, \tag{15.1}$$

with the exchange constant J. The magnitude of J as well as its sign are determined by overlap integrals which include the Coulomb interaction. If $J < 0$ a parallel orientation of the spins is favorable and ferromagnetic behavior arises if $T < T_C$. On the other hand, if $J > 0$, antiparallel orientation is established as long as the temperature does not exceed the Néel temperature T_N. However, in both cases the system undergoes a phase transition to a paramagnetic state if the temperature T

[1] For a short introduction to phase transitions in general please consult Appendix E.

[2] In this discussion we regard the spin as a classical quantity. In the quantum mechanic case one has to replace the vectors by vector operators S_i.

DOI: 10.1007/978-3-319-02435-6_15, © Springer International Publishing Switzerland 2014

Fig. 15.1 Schematic illustration of the magnetization M as a function of temperature T in a ferromagnetic material

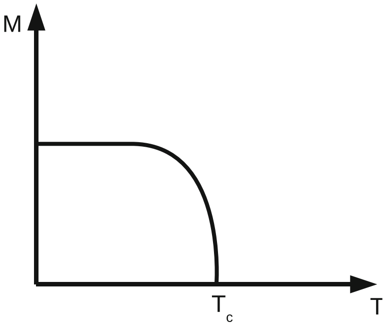

Fig. 15.2 Schematic illustration of the spin-orientation in (**a**) ferromagnetic ($J < 0$) or (**b**) antiferromagnetic ($J > 0$) two-dimensional crystal

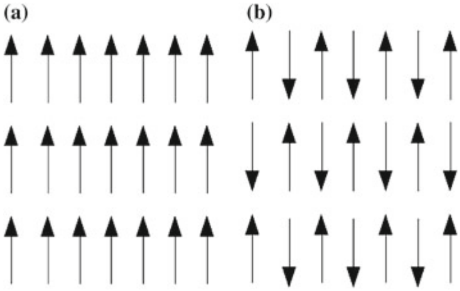

exceeds the Curie temperature (ferromagnetic case) or the Néel temperature (antiferromagnetic case). A schematic illustration of ferro- and antiferromagnetism for a two-dimensional crystal is illustrated in Fig. 15.2. We summarize the different scenarios:

$$\begin{cases} J < 0 & \text{ferromagnetic,} \\ J > 0 & \text{antiferromagnetic,} \\ J = 0 & \text{non-interacting.} \end{cases} \tag{15.2}$$

We concentrate now on a cubic crystal lattice in which the atoms are localized at positions x_ℓ. The spin of atom ℓ will be denoted by $S_\ell \in \mathbb{R}^3$ and the exchange parameter between atom ℓ and atom ℓ' by $J_{\ell\ell'}$. Furthermore, we consider the ferromagnetic case, i.e. $J_{\ell\ell'} < 0$. The Hamilton function is of the form

$$H = \frac{1}{2} \sum_{\ell\ell'} J_{\ell\ell'} S_\ell \cdot S_{\ell'} = \frac{1}{2} \sum_{\ell\ell'} J_{\ell-\ell'} S_\ell \cdot S_{\ell'}. \tag{15.3}$$

Here $J_{\ell\ell'}$ was replaced by $J_{\ell-\ell'} = J_{\ell'-\ell}$ to account for translational invariance. Moreover, we define that $J_{\ell\ell} = 0$, otherwise we would have to exclude the contributions $\ell = \ell'$ from the above sum. The Hamilton function (15.3) is genuine to the Heisenberg model [4]. We note that in this model there is no distinguished direction of spin orientation, i.e. the HAMILTON function is invariant under a rotation of all spin vectors S_ℓ. The actual orientation may be determined by an external magnetic field or by an anisotropy of the crystal lattice. Furthermore, the restriction of the spin orientation to the positive or negative z-direction is the characteristic of the ISING model. In a quantum mechanical description the HAMILTON operator (Hamiltonian) of this model is defined by

$$H = \frac{1}{2} \sum_{\ell\ell'} J_{\ell-\ell'} S_\ell^z S_{\ell'}^z, \tag{15.4}$$

where S_ℓ^z are the spin operators in z-direction. In the specific case of spin $1/2$ particles the spin operators S_ℓ^z in this Hamiltonian are replaced by $(\hbar/2)\sigma_\ell^z$ with σ_ℓ^z the PAULI matrix and $\hbar$ the reduced PLANCK's constant. Furthermore, we redefine $J'_{\ell-\ell'} = -(\hbar^2/4)J_{\ell-\ell'}$, $J'_{\ell-\ell'} > 0$, and represent the Hamiltonian in the basis of eigenstates of the operators σ_ℓ^z. These eigenstates have eigenvalues $\sigma_\ell = \pm 1$, which correspond to *spin up* and *spin down* states, respectively. Hence we obtain

$$H = -\frac{1}{2} \sum_{\ell\ell'} J_{\ell-\ell'} \sigma_\ell \sigma_{\ell'} - h \sum_\ell \sigma_\ell, \tag{15.5}$$

where we dropped the prime of the exchange parameter $J_{\ell-\ell'}$ for the sake of a more compact notation. We added, furthermore, a term which accounts for the possible coupling of the spins to an external magnetic field,[3] where h stands for the reduced field $h = -\mu_B g B/2$.[4]

There are some special cases in which the ISING model can be solved analytically [5, 6]. For instance, one can solve the general case described by Eq. (15.5) with the help of the *mean field* approximation. In this case, the contribution h_ℓ acting on site ℓ, namely

$$h_\ell = h + \sum_{\ell'} J_{\ell-\ell'} \sigma_{\ell'}, \tag{15.6}$$

is replaced by its mean value

$$\langle h_\ell \rangle = h + \tilde{J} m, \tag{15.7}$$

where $m = \langle \sigma_\ell \rangle$ and $\tilde{J} = \sum_\ell J_\ell$. (The term $\tilde{J}m$ is commonly referred to as the *molecular field*.) With the help of this ansatz it is, for instance, possible to reproduce the experimentally observed CURIE-WEISS-law of ferromagnetic materials, i.e. the temperature dependence of the magnetic susceptibility χ for $T > T_C$ can be described by:

[3] We note in passing that the Hamiltonian (15.5) is invariant under a spin flip of all spins if $h = 0$ ($\mathbb{Z}_2$ symmetry). This symmetry is broken if $h \neq 0$, i.e. the spins align with the external field h.

[4] We note that $H \propto \mu \cdot B$ where B is the magnetic field and μ is the magnetic moment. Furthermore, μ can be expressed as $\mu = -\mu_B g S/\hbar = -\mu_B g \sigma/2$, where μ_B is the BOHR magneton, g is the LANDÉ g-factor and σ is the vector of PAULI matrices. The sign is convention.

$$\chi \propto \frac{1}{T - T_C}. \tag{15.8}$$

Another very interesting special case of the general model (15.5) is the restriction to nearest neighbor (n. n.) interaction with the assumption that the interaction between non-nearest neighbor spins is negligible. One step further goes the approximation that $J_{\ell-\ell'} \equiv J$ for nearest neighbors. Hence, we have

$$J_{\ell-\ell'} = \begin{cases} J & \text{if} \quad \ell, \ell' \quad \text{n. n.}, \\ 0 & \text{otherwise}. \end{cases} \tag{15.9}$$

In this case Eq. (15.5) is rewritten as

$$H = -\frac{J}{2} \sum_{\langle \ell\ell' \rangle} \sigma_\ell \sigma_{\ell'} - h \sum_{\ell} \sigma_\ell, \tag{15.10}$$

where $\sum_{\langle \ell\ell' \rangle}$ denotes the sum over all nearest neighbors. This model can be solved analytically in one and two dimensions if one assumes that the system is spatially unlimited. The solution in one dimension was published by E. ISING [7], the solution in two dimensions, which is much more involved, was reported by L. ONSAGER [8]. We shall briefly discuss ISING's solution in one dimension:

We rewrite the Hamiltonian (15.10) for N-particles aligned in a one-dimensional chain as

$$H = -J \sum_{\ell=1}^{N} \sigma_\ell \sigma_{\ell+1} - h \sum_{\ell=1}^{N} \sigma_\ell, \tag{15.11}$$

under the assumption of periodic boundary conditions, i.e. $\sigma_{N+1} = \sigma_1$ and the factor $1/2$ was absorbed into J. Let us briefly elaborate on the kind of observables we would like to describe within this model. (We note in passing that the following discussion is not restricted to the one-dimensional case.) Given a particular spin configuration $\mathscr{C} = \{\sigma_i\}$, we assume that the probability of finding the system in this configuration is given by the BOLTZMANN distribution $p(\mathscr{C})$[5]:

$$p(\mathscr{C}) = \frac{1}{Z_N} \exp\left[-\frac{E(\mathscr{C})}{k_B T}\right]. \tag{15.12}$$

Here, T is the temperature and k_B is BOLTZMANN's constant. The energy $E(\mathscr{C})$ associated with configuration $\mathscr{C}$ is given by Eq. (15.11). Please note that this is now, obviously, a classical model although we consider spin degrees of freedom. The partition function Z_N is given by the sum over all possible configurations $\mathscr{C}$:

[5] In particular we assume ergodicity of the system as will be explained in Chap. 16.

$$Z_N = \sum_{\mathscr{C}} \exp\left[-\frac{E(\mathscr{C})}{k_B T}\right]. \tag{15.13}$$

In the general case the problem of solving the ISING problem is a problem of evaluating the sum (15.13). This is certainly not an easy task since, for instance, in the one dimensional case with $N = 100$ grid-points one has $2^N = 2^{100} \approx 1.3 \times 10^{30}$ different configurations $\mathscr{C}$. However, if Z_N is known a lot more follows [5, 6, 9]. For instance, the expectation value of the energy[6] is given by

$$\langle E \rangle = \sum_{\mathscr{C}} p(\mathscr{C}) E(\mathscr{C}) = (k_B T)^2 \frac{\partial}{\partial T} \ln Z_N, \tag{15.14}$$

and the expectation value of the magnetization is given by

$$\langle M \rangle = \sum_{\mathscr{C}} p(\mathscr{C}) \mathscr{M}(\mathscr{C}) = k_B T \frac{\partial}{\partial h} \ln Z_N, \tag{15.15}$$

where we defined the magnetization $\mathscr{M}(\mathscr{C})$ of the configuration $\mathscr{C}$ via

$$\mathscr{M}(\mathscr{C}) = \left(\sum_{\ell} \sigma_\ell\right)_{\mathscr{C}} . \tag{15.16}$$

Here we put the term $\sum_\ell \sigma_\ell$ within parenthesis indexed by $\mathscr{C}$ in order to emphasize its dependence on the particular configuration $\mathscr{C}$. From the observables (15.14) and (15.15) the *fluctuation quantities* the magnetic susceptibility, χ, and the heat capacity, c_h, can be derived. The following relations hold:

$$\chi = \frac{\partial}{\partial h} \langle M \rangle \quad \text{and} \quad c_h = \frac{\partial}{\partial T} \langle E \rangle . \tag{15.17}$$

Equation (15.14) allows to rewrite the expression for the heat capacity as:

$$c_h = \sum_{\mathscr{C}} E(\mathscr{C}) \frac{\partial}{\partial T} p(\mathscr{C}). \tag{15.18}$$

Here we made use of the fact that $E(\mathscr{C})$ is independent of temperature T. We evaluate, furthermore, the derivative of $p(\mathscr{C})$ with respect to temperature T:

$$\begin{aligned} \frac{\partial}{\partial T} p(\mathscr{C}) &= \frac{\partial}{\partial T}\left[\frac{\exp\left(-\frac{E(\mathscr{C})}{k_B T}\right)}{Z_N}\right] \\ &= \frac{p(\mathscr{C})}{(k_B T)^2}\left[E(\mathscr{C}) - \langle E \rangle\right]. \end{aligned} \tag{15.19}$$

[6] $\langle E \rangle$ is also referred to as internal energy U.

This is inserted into Eq. (15.18) and results in a final expression for the heat capacity:

$$\begin{aligned} c_h &= \frac{1}{(k_B T)^2} \sum_{\mathscr{C}} p(\mathscr{C}) \left[E^2(\mathscr{C}) - E(\mathscr{C}) \langle E \rangle \right] \\ &= \frac{1}{(k_B T)^2} \left(\langle E^2 \rangle - \langle E \rangle^2 \right) \\ &= \frac{1}{(k_B T)^2} \mathrm{var}\,(E)\,. \end{aligned} \tag{15.20}$$

This expression for the heat capacity c_h justifies why it is referred to as a fluctuation quantity.

In a similar fashion we calculate the magnetic susceptibility using relation (15.15):

$$\chi = \sum_{\mathscr{C}} \mathscr{M}(\mathscr{C}) \frac{\partial}{\partial h} p(\mathscr{C}). \tag{15.21}$$

We note that

$$\frac{\partial}{\partial h} E(\mathscr{C}) = -\mathscr{M}(\mathscr{C}), \tag{15.22}$$

and obtain:

$$\begin{aligned} \frac{\partial}{\partial h} p(\mathscr{C}) &= \frac{\partial}{\partial h} \left[\frac{\exp\left(-\frac{E(\mathscr{C})}{k_B T} \right)}{Z_N} \right] \\ &= \frac{p(\mathscr{C})}{k_B T} \left[\mathscr{M}(\mathscr{C}) - \langle M \rangle \right]. \end{aligned} \tag{15.23}$$

This results in a final expression for the magnetic susceptibility χ which relates it to the variance of the magnetization M:

$$\begin{aligned} \chi &= \frac{1}{k_B T} \sum_{\mathscr{C}} p(\mathscr{C}) \left[\mathscr{M}^2(\mathscr{C}) - \mathscr{M}(\mathscr{C}) \langle M \rangle \right] \\ &= \frac{1}{k_B T} \left(\langle M^2 \rangle - \langle M \rangle^2 \right) \\ &= \frac{1}{k_B T} \mathrm{var}\,(M)\,. \end{aligned} \tag{15.24}$$

We return after this excursion to the analytic treatment of the infinite one-dimensional ISING model with nearest neighbor interaction, Eq. (15.11). If it were possible to evaluate the partition function Z_N, the required observables would be directly accessible via the above relations. In most cases this task is not analytically feasible. Nevertheless, in our particular case it appears to be possible because we recognize that:

$$\begin{aligned} Z_N &= \sum_{\mathscr{C}} p(\mathscr{C}) \\ &= \sum_{\mathscr{C}} \exp\left[\frac{1}{k_B T}\left(J\sum_{\ell=1}^{N}\sigma_\ell\sigma_{\ell+1} + h\sum_{\ell=1}^{N}\sigma_\ell\right)\right] \\ &= \sum_{\mathscr{C}}\prod_{\ell=1}^{N}\exp\left[\frac{J}{k_B T}\sigma_\ell\sigma_{\ell+1} + \frac{h}{2k_B T}\left(\sigma_\ell + \sigma_{\ell+1}\right)\right]. \end{aligned} \tag{15.25}$$

In the last step the sum over σ_ℓ was replaced by an alternative sum

$$\sum_{\ell=1}^{N}\sigma_\ell = \frac{1}{2}\sum_{\ell=1}^{N}\left(\sigma_\ell + \sigma_{\ell+1}\right), \tag{15.26}$$

as a consequence of the periodic boundary conditions $\sigma_{N+1} = \sigma_1$. Obviously, Eq. (15.25) can be rewritten as

$$Z_N = \mathrm{tr}\left(\mathscr{T}^N\right), \tag{15.27}$$

where tr $(\cdot)$ denotes the *trace* operation and we introduced the *transfer* matrix:

$$\mathscr{T}_{\sigma,\sigma'} = \exp\left[\frac{J}{k_B T}\sigma\sigma' + \frac{h}{2k_B T}\left(\sigma + \sigma'\right)\right]. \tag{15.28}$$

Let us briefly clarify this point: The trace operation in the basis of the spin eigenvalues $\sigma = \pm 1$ results in

$$\mathrm{tr}\left(\mathscr{T}\right) = \sum_{\sigma}\mathscr{T}_{\sigma,\sigma} = T_{-1,-1} + T_{1,1}. \tag{15.29}$$

Hence, we have

$$\begin{aligned} \mathrm{tr}\left(\mathscr{T}^N\right) &= \sum_{\sigma}\left(\mathscr{T}^N\right)_{\sigma\sigma} \\ &= \sum_{\sigma}\sum_{\substack{\{\sigma_i\} \\ i=1,\dots,N-1}}\mathscr{T}_{\sigma,\sigma_1}\mathscr{T}_{\sigma_1,\sigma_2}\cdots\mathscr{T}_{\sigma_{N-1},\sigma} \\ &= \sum_{\substack{\{\sigma_i\} \\ i=1,\dots,N}}\mathscr{T}_{\sigma_1,\sigma_2}\mathscr{T}_{\sigma_2,\sigma_3}\cdots\mathscr{T}_{\sigma_N,\sigma_1}. \end{aligned} \tag{15.30}$$

In the last step we redefined the sum indices and we used the notation $\{\sigma_i\}$ to indicate that the sum runs over all possible values of $\sigma_1, \sigma_2, \dots, \sigma_N$ in order to abbreviate the notation. However, the sum over all possible values of $\sigma_1, \sigma_2, \dots, \sigma_N$ can be replaced by a sum over all configurations $\mathscr{C}$ where one configuration is a specific combination of definite values $\sigma_1, \sigma_2, \ldots, \sigma_N$. For these definite values the product of transfer matrices in Eq. (15.30) is equivalent to the product of exponentials in Eq. (15.25) due to our definition of the transfer matrix $\mathscr{T}_{\sigma,\sigma'}$, Eq. (15.28). Hence we demonstrated that expression (15.27) is indeed equivalent to Eq. (15.25).

It follows from definition (15.28) that

$$\mathscr{T} = \begin{pmatrix} \exp\left(\frac{J+h}{k_BT}\right) & \exp\left(-\frac{J}{k_BT}\right) \\ \exp\left(-\frac{J}{k_BT}\right) & \exp\left(\frac{J-h}{k_BT}\right) \end{pmatrix}. \tag{15.31}$$

It is an easy task to determine the eigenvalues of this matrix. The characteristic polynomial

$$\det \begin{pmatrix} \exp\left(\frac{J+h}{k_BT}\right) - \lambda & \exp\left(-\frac{J}{k_BT}\right) \\ \exp\left(-\frac{J}{k_BT}\right) & \exp\left(\frac{J-h}{k_BT}\right) - \lambda \end{pmatrix} \tag{15.32}$$

is of the form

$$\begin{aligned} &\left[\exp\left(\frac{J+h}{k_BT}\right) - \lambda\right]\left[\exp\left(\frac{J-h}{k_BT}\right) - \lambda\right] - \exp\left(-\frac{2J}{k_BT}\right) \\ &= \lambda^2 - 2\lambda \exp\left(\frac{J}{k_BT}\right)\cosh\left(\frac{h}{k_BT}\right) + 2\sinh\left(\frac{2J}{k_BT}\right) \\ &\overset{!}{=} 0, \end{aligned} \tag{15.33}$$

which is easily solved. Thus, we get for the eigenvalues $\lambda_{1,\,2}$:

$$\begin{aligned} \lambda_{1,2} = {} & \exp\left(\frac{J}{k_BT}\right)\cosh\left(\frac{h}{k_BT}\right) \\ & \pm \sqrt{\exp\left(\frac{2J}{k_BT}\right)\sinh^2\left(\frac{h}{k_BT}\right) + \exp\left(-\frac{2J}{k_BT}\right)}. \end{aligned} \tag{15.34}$$

We note that $\lambda_1 \geq \lambda_2$ for all temperatures $T \geq 0$.

We now make use of the fact that the trace is invariant under a basis transformation Γ. Hence we can express the transfer matrix in a basis in which it is diagonal and set

$$\mathscr{T}' = \Gamma \mathscr{T} \Gamma^{-1} = \begin{pmatrix} \lambda_1 & 0 \\ 0 & \lambda_2 \end{pmatrix}, \tag{15.35}$$

which immediately results in:

$$Z_N = \lambda_1^N + \lambda_2^N. \tag{15.36}$$

Everything required to calculate the expectation value of energy *per particle* $\langle \varepsilon \rangle$

$$\langle \varepsilon \rangle = \frac{(k_B T)^2}{N} \frac{\partial}{\partial T} \ln Z_N, \tag{15.37}$$

in the *thermodynamic* limit $N \to \infty$ is now in place and so we can investigate the possibility of a phase transition. Thus, we first consider the limit

$$\lim_{N\to\infty} \frac{1}{N} Z_N = \lim_{N\to\infty} \frac{1}{N} \ln\left(\lambda_1^N + \lambda_2^N\right) = \ln \lambda_1, \tag{15.38}$$

since $\lambda_1 \geq \lambda_2$ for all $T \geq 0$.[7]

If there is no external field, i.e. $h = 0$, we have

$$\lim_{N\to\infty} \frac{1}{N} Z_N = \ln\left[2\cosh\left(\frac{J}{k_B T}\right)\right], \tag{15.39}$$

which is a smooth function of T for $T \geq 0$. Consequently, we do not observe a phase transition in the one dimensional Ising model. More information about the system can be provided by the spin correlation function $\langle \sigma_\ell \sigma_{\ell'} \rangle$

$$\langle \sigma_\ell \sigma_{\ell'} \rangle = \sum_{\mathscr{C}} p(\mathscr{C}) \sigma_\ell \sigma_{\ell'}. \tag{15.40}$$

A basic, however, tedious calculation shows that in the thermodynamic limit it is described by

$$\langle \sigma_\ell \sigma_{\ell'} \rangle = \left(\frac{\lambda_2}{\lambda_1}\right)^{\ell-\ell'}, \tag{15.41}$$

with the result that the spin correlation decreases with increasing distance $\ell - \ell'$ since $\lambda_2 < \lambda_1$ for $T > 0$.

We move on and briefly sketch the solution of the infinite two-dimensional Ising model according to L. Onsager [8]. The Hamiltonian (15.11) reads

$$H = -J \sum_{\ell\ell'} \sigma_{\ell,\ell'} \left(\sigma_{\ell+1,\ell'} + \sigma_{\ell-1,\ell'} + \sigma_{\ell,\ell'-1} + \sigma_{\ell,\ell'+1}\right) - h \sum_{\ell,\ell'} \sigma_{\ell,\ell'}. \tag{15.42}$$

The strategy follows the one which has already been discussed in the one-dimensional case: The Hamiltonian is inserted in the expression for the partition function Z_N and with the help of the correct basis one can rewrite Z_N as the trace over a product

[7] We transform

$$\lambda_1^N + \lambda_2^N = \lambda_1^N \left[1 + \left(\frac{\lambda_2}{\lambda_1}\right)^N\right],$$

and use that

$$\left(\frac{\lambda_2}{\lambda_1}\right)^N \to 0, \qquad \text{as} \qquad N \to \infty.$$

of transfer matrices. However, in this case the transfer matrix $\mathscr{T}$ is of dimension $2N \times 2N$ rather than 2×2. It is obvious that the search for the largest eigenvalue for arbitrary N is not a trivial task. We will therefore limit our discussion to a summary of the most important results for the particular case $h = 0$.

In the two-dimensional case one indeed observes a phase transition, i.e. the magnetic susceptibility becomes singular at a particular temperature T_C. This temperature is given as the solution of equation

$$2\tanh^2\left(\frac{2J}{k_B T_C}\right) = 1. \tag{15.43}$$

The expectation value of the energy per particle takes on the form

$$\langle\varepsilon\rangle = -J\coth\left(\frac{2J}{k_B T}\right)\left\{1 + \frac{2}{\pi}K_1(\xi)\left[2\tanh^2\left(\frac{2J}{k_B T}\right) - 1\right]\right\}, \tag{15.44}$$

where $K_1(\xi)$ is the complete elliptic integral of the first kind [see also Eq. (1.16)]

$$K_1(x) = \int\limits_0^{\frac{\pi}{2}} \mathrm{d}y \, \frac{1}{\sqrt{1 - x^2\sin^2 y}}, \tag{15.45}$$

with argument

$$\xi = \frac{2\sinh\left(\frac{2J}{k_B T}\right)}{\cosh^2\left(\frac{2J}{k_B T}\right)}. \tag{15.46}$$

The magnetization per particle $\langle m\rangle$ is proved to be determined from

$$\langle m\rangle = \begin{cases} \frac{(1+z^2)^{\frac{1}{4}}(1-6z^2+z^4)^{\frac{1}{8}}}{\sqrt{1-z^2}} & \text{for } T < T_C, \\ 0 & \text{for } T > T_C, \end{cases} \tag{15.47}$$

with

$$z = \exp\left(-\frac{2J}{k_B T}\right).$$

Equation (15.47) clearly describes a phase transition at $T = T_C$.

15.2 Numerics

We study a finite two-dimensional Ising model on a square lattice Ω with grid-points (x_i, y_j), $i, j = 1, 2, \ldots, N$, which will be denoted by (i, j). We write the Hamiltonian in the form

$$H = -J \sum_{\left\langle \substack{ij \\ i'j'} \right\rangle} \sigma_{i,j}\sigma_{i',j'} - h \sum_{ij} \sigma_{i,j}, \tag{15.48}$$

where $\sigma_{i,j} \in \{-1, 1\}$. Hence, we consider nearest neighbor interaction and regard the exchange parameter as independent of the actual positions i, j. The problem is easily motivated: we would like to calculate numerically observables like the expectation value of the energy or of the magnetization which will then be compared with the analytic results. This allows a rather simple check of the quality of our numerical approach which can then be extended to similar models which cannot any longer be treated analytically. We need numerical methods because summing over all possible configurations in a calculation of the partition function Z_N is simply no longer feasible since, for instance, for $N = 100$ we have $2^{N^2} = 2^{10000} \approx 10^{3000}$ possible configurations which will have to be considered as follows from Eqs. (15.13), (15.14) and (15.15). A more convenient approach would be to approximate the sums with the help of methods we encountered within the context of Monte-Carlo integration, Sect. 14.2. For instance, the estimate of the energy expectation value is given by

$$\langle E \rangle = \frac{1}{M} \sum_{i=1}^{M} E(\mathscr{C}_i) \pm \sqrt{\frac{\text{var}\,(E)}{M}}. \tag{15.49}$$

Here, $\mathscr{C}_i$, $i = 1, 2, \ldots, M$ are M configurations drawn from the pdf (15.12), the Boltzmann distribution. Equation (15.49) is referred to as the *estimator* of the internal energy. We note that we also have to calculate an estimate of the variance of E using a similar approach in order to determine the error induced by this approximation.[8]

Hence, the remaining task is to find configurations $\mathscr{C}_i$ which indeed follow the Boltzmann distribution (15.12). The inverse transformation method of Sect. 13.2 cannot be employed since $E(\mathscr{C}_i)$ is not invertible. Furthermore, the rejection method is useless since we would need the partition function Z_N in order to apply it. However, calculating the partition function is a task as difficult as calculating the internal energy (15.14) without any approximations. Therefore, the method of choice will be the Metropolis algorithm discussed in Sect. 14.3.

Let $\mathscr{C}$ be a given spin configuration on the two-dimensional square lattice Ω. We modify the spin on one particular grid-point (i, j) and obtain a *trial* spin configuration $\mathscr{C}^t$. According to our discussion in Sect. 14.3, the probability of accepting the new configuration $\mathscr{C}^t$ is then given by

[8] In particular var $(E) = \langle E^2 \rangle - \langle E \rangle^2$ is to be determined and only the second term is already known. The first term, $\langle E^2 \rangle$, is then estimated with the help of

$$\left\langle E^2 \right\rangle = \frac{1}{M} \sum_{i=1}^{M} E_i^2.$$

$$\Pr(A|\mathscr{C}^t,\mathscr{C}) = \min\left(\frac{p(\mathscr{C}^t)}{p(\mathscr{C})},1\right) = \min\left\{\exp\left[-\frac{E(\mathscr{C}^t)-E(\mathscr{C})}{k_BT}\right],1\right\}$$
$$= \min\left[\exp\left(-\frac{\Delta E_{ij}}{k_BT}\right),1\right]. \tag{15.50}$$

The spin orientation was changed only on one grid-point (i,j), with $\sigma_{i,j} \to \hat{\sigma}_{i,j} = -\sigma_{i,j}$; thus, the energy difference ΔE_{ij} is easily evaluated using

$$\Delta E_{ij} = 2J\sigma_{i,j}\left(\sigma_{i+1,j}+\sigma_{i-1,j}+\sigma_{i,j-1}+\sigma_{i,j+1}\right)+2h\sigma_{i,j}. \tag{15.51}$$

with $\sigma_{i,j}$ the original spin orientation.

We will now discuss numerical details, some particular to the numerical treatment of the ISING model, and some of rather general nature which should be considered whenever a Monte-Carlo simulation is planned.

(1) Lattice Geometry

We regard a two-dimensional $N \times N$ square lattice with periodic boundary conditions[9] in order to reduce finite volume effects. It is advisable to write a program which helps to identify the nearest neighbors of some grid-point, since we will need this information in the METROPOLIS run whenever we calculate the energy difference due to a spin flip according to Eq. (15.51). In particular, we would like to generate a matrix *neighbor*(*site*, *i*), where $i = 1, 2, 3, 4$ are the directions to the neighboring grid-points. Such a matrix will have to be generated only once for each choice of a system of size N. First we relabel the sites of the system following the scheme[10]

$$\begin{array}{ccc} N(N-1)+1 & \cdots & N^2 \\ \vdots & \vdots & \vdots \\ N+1 & \cdots & 2N \\ 1 & 2\cdots & N. \end{array} \tag{15.52}$$

Then we initialize the matrix *neighbor* as an array of size $N^2 \times 4$. Every *site* has four nearest neighbors: *up*, *right*, *down* and *left*. The following method can be applied to evaluate the corresponding entries for periodic boundary conditions:

- for *up* we have:

[9] Periodic boundary conditions in two dimensions imply that

$$\sigma_{N+1,j} = \sigma_{1,j} \qquad \text{and} \qquad \sigma_{i,N+1} = \sigma_{i,1},$$

for all i, j.

[10] In the following we will refer to the notation (i), $i = 1, 2, \ldots, N^2$ as the *single-index* notation while the notation (i,j), $i,j = 1, 2, \ldots, N$ will be referred to as the *double-index* notation.

(a) If $site + N \leq N^2$: $up = site + N$,
(b) else if $site + N > N^2$: $up = site - N(N-1)$.

- For *right* we have:

(a) If $\mathrm{mod}(site, N) \neq 0$: $right = site + 1$,
(b) else if $\mathrm{mod}(site, N) = 0$: $right = site - N + 1$.

- For *down* we have:

(a) If $site - N \geq 1$: $down = site - N$,
(b) else if $site - N < 1$: $down = site + N(N-1)$

- For *left* we have:

(a) If $\mathrm{mod}(site - 1, N) \neq 0$: $left = site - 1$,
(b) else if $\mathrm{mod}(site - 1, N) = 0$: $left = site + N - 1$.

Finally, we arrange the array according to

$$neighbor(site, :) = [up, right, down, left], \tag{15.53}$$

where $site = 1, 2, \ldots, N^2$.

(2) Initialization

As already discussed in Sect. 14.3, the quality of the random numbers obtained with the help of the METROPOLIS algorithm is highly dependent on the choice of initial conditions, i.e. the initial configuration $\mathscr{C}_0$. Of course, it would be favorable to start with a configuration which was already drawn from the BOLTZMANN distribution $p(\mathscr{C})$. However, in practice this is not feasible *ab initio*. But, as will be elucidated in Chap. 16, the METROPOLIS algorithm produces configurations, which become independent of the initial state and follow the BOLTZMANN distribution. Hence we can simply start with some arbitrary configuration and discard it together with the first n constituents of the sequence $\mathscr{C}_0, \mathscr{C}_1, \ldots, \mathscr{C}_n$. This method is referred to as *thermalization*.[11] The question arises: can n be determined to ensure that the following sequence, starting with $\mathscr{C}_{n+1}$ will be in accordance with the pdf $p(\mathscr{C})$?

There are two different possibilities to approach this problem: (i) The first is to measure auto-correlations between configurations $\mathscr{C}_i$ where it has to be ensured that the set of states is sufficiently large to allow for a significant conclusion. We will discuss auto-correlations in more detail in Chap. 19. (ii) The second approach is to empirically check whether equilibrium has been reached or not. For instance, one could simply plot some selected observables and check when the initial bias vanishes, i.e. the observable reaches some saturation value as a function of the number

[11] The number of configurations discarded is referred to as the thermalization length.

of measurements. A particularly useful method is to start the algorithm using at least two different configurations. As soon as equilibrium has been reached, the observables should approach the same saturation values after a certain (finite) number of measurements. A typical choice is the *cold start* and the *hot start*. Cold start means that the temperature is initially below the critical temperature, i.e. in the ISING model all spins are aligned (ferromagnetic state), whereas hot start means that the temperature is well above the critical temperature and for the ISING model the spin orientation is chosen at random for any site (paramagnetic state).

(3) Execution of the Code

The METROPOLIS algorithm for the ISING model is executed in the following steps:

1. Choose an initial configuration $\mathscr{C}_0$.
2. We migrate through the lattice sites systematically.[12] Suppose we just reached site (i, j) (we use the double-index notation $i, j = 1, 2, \dots, N$, to improve the readability) and our current configuration was $\mathscr{C}_k$, i.e. k configurations have been accepted so far.
3. Generate a new configuration $\mathscr{C}^t$ from $\mathscr{C}_k$ by replacing in $\mathscr{C}_k$ the entry $\sigma_{i,j}$ by $-\sigma_{i,j}$.
4. The new configuration is accepted with probability

$$\Pr(A|\mathscr{C}^t, \mathscr{C}_k) = \min\left[\exp\left(-\frac{\Delta E_{ij}}{k_B T}\right), 1\right], \tag{15.54}$$

   where ΔE_{ij} is determined from Eq. (15.51). $\mathscr{C}^t$ is accepted if $\Pr(A|\mathscr{C}^t, \mathscr{C}_k)$ is equal to one or if $\Pr(A|\mathscr{C}^t, \mathscr{C}_k) \geq r \in [0, 1]$ otherwise $\mathscr{C}^t$ is rejected. If $\mathscr{C}^t$ was accepted we set $\mathscr{C}_{k+1} = \mathscr{C}^t$.
5. Go to the next lattice site [step 2].

We note that instead of sampling the lattice sites sequentially as suggested in step 2 the lattice sites can also be sampled randomly with the help of

$$i = \text{int}(rN^2) + 1, \tag{15.55}$$

where $r \in [0, 1]$ is a uniformly distributed random number and $\text{int}(\cdot)$ denotes the integer part of a given quantity. Obviously, Eq. (15.55) is only useful in the single-index notation $i = 1, 2, \dots, N^2$.

[12] A run through all lattice sites is referred to as a *sweep*.

(4) Measurement

As soon as thermalization was achieved the procedure to measure interesting observables can be started. Such a procedure consists of collecting the data required and in calculating expectation values as was illustrated in Eq. (15.49) for the case of the expectation value of the energy. A more detailed study of estimator techniques is postponed to Chap. 19. However, there is one crucial point one should be aware of: We already mentioned in our discussion of the METROPOLIS algorithm in Sect. 14.3 that subsequent configurations $\mathscr{C}_k$ may be strongly correlated. This problem can be circumvented by simply neglecting intermediate configurations. For instance, one may allow a couple of 'empty' sweeps between two measurements.

In the following we discuss some selected results obtained with the numerical approach described above.

15.3 Selected Results

We investigate the two-dimensional ISING model with periodic boundary conditions. Moreover, we chose $h = 0$ and $J = 0.5$ for all following illustrations.

In a first experiment we plan to check the thermalization process and, thus, measure after every single sampling step and skip thermalization. The observables of interest, the expectation value of the energy per particle, $\langle \varepsilon \rangle$, and the expectation value of the magnetization per particle, $\langle m \rangle$, are illustrated in Fig 15.3 for 30 sweeps in a system of the size $N = 50$ which corresponds to $m \sim 8 \times 10^4$ measurements. Moreover, we set $k_B T = 3$ which should be well above T_C according to Eq. (15.43). Hence, we expect paramagnetic behavior, i.e. $\langle m \rangle = 0$ in the equilibrium since the acceptance probability is rather large because the spins are randomly orientated. In addition, Fig. 15.4 shows a typical spin configuration for a temperature well above T_C.

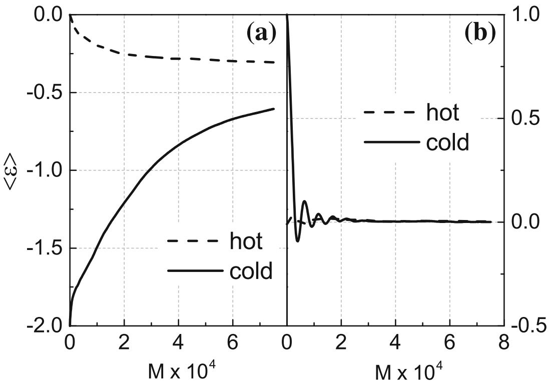

Fig. 15.3 Time evolution of **(a)** the expectation value of the energy per particle $\langle \varepsilon \rangle$ and **(b)** of the expectation value of the magnetization per particle $\langle m \rangle$ versus the number of measurements M. We used a cold start (*solid line*) and a hot start (*dashed line*) to achieve these results

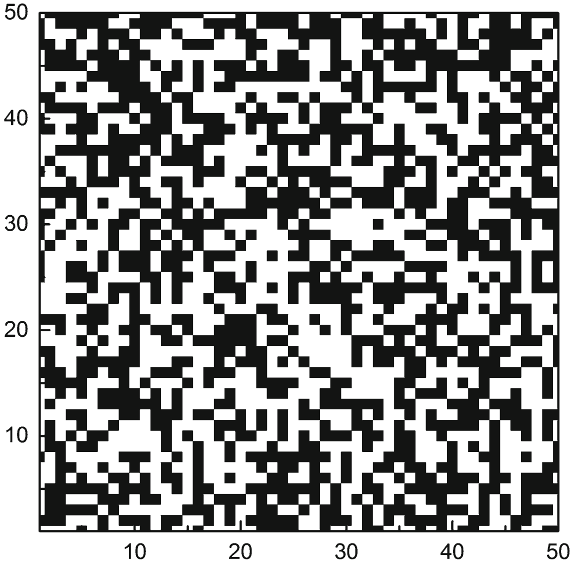

Fig. 15.4 Typical spin configuration for a temperature well above the critical temperature T_C. *Black shaded areas* correspond to spin up sites while the *white areas* are spin down sites

According to Fig. 15.3b the expectation value of the magnetization per particle $\langle m \rangle$ approaches indeed zero after a rather short thermalization period independently of the starting procedure. This is certainly not the case for the energy expectation value per particle $\langle \varepsilon \rangle$, Fig. 15.3a, which does not approach saturation even after $M \sim 8 \times 10^4$ measurements for both starting procedures. The consequence is that the thermalization period certainly needs to be longer than only 30 sweeps.

Keeping this result in mind we move on to perform the next check of our numerics, namely to study the influence of the system size N on the numerical results we get for the observables $\langle \varepsilon \rangle$, $\langle m \rangle$ as well as c_h and χ as functions of temperature T. Let us outline the strategy: a thermalization period of 500 sweeps will be used and 10 sweeps between each measurement will be discarded. Moreover, we start with the *hot start* configuration and at a temperature $k_B T_0 = 3$ well above T_C. After the measurements at T_0 have been finished, the temperature is slightly decreased, $T_1 < T_0$.

One more point should be addressed: suppose we perform a simulation using the strategy outlined above and obtain as a result some observable O as a function of temperatures $\{T_n\}$, with T_0 the initial temperature well above T_C and $T_{n+1} < T_n$. The temperature dependence of the observable will, of course, be most interesting for temperatures $T \approx T_C$. Thus, what we will need is an adaptive cooling strategy designed in such a way that the temperature is decreased rapidly for temperatures $T \gg T_C$ or $T \ll T_C$, but for $T \approx T_C$ the temperature is modified only minimally. (This question will also be a very important point in the discussion of *simulated annealing*, a stochastic optimization strategy.) At the moment we are satisfied with equally spaced temperatures, i.e. $T_{k+1} = T_k - \delta$, where $\delta = \text{const}$ because we are mainly interested to study the influence of the system size N on our calculations.

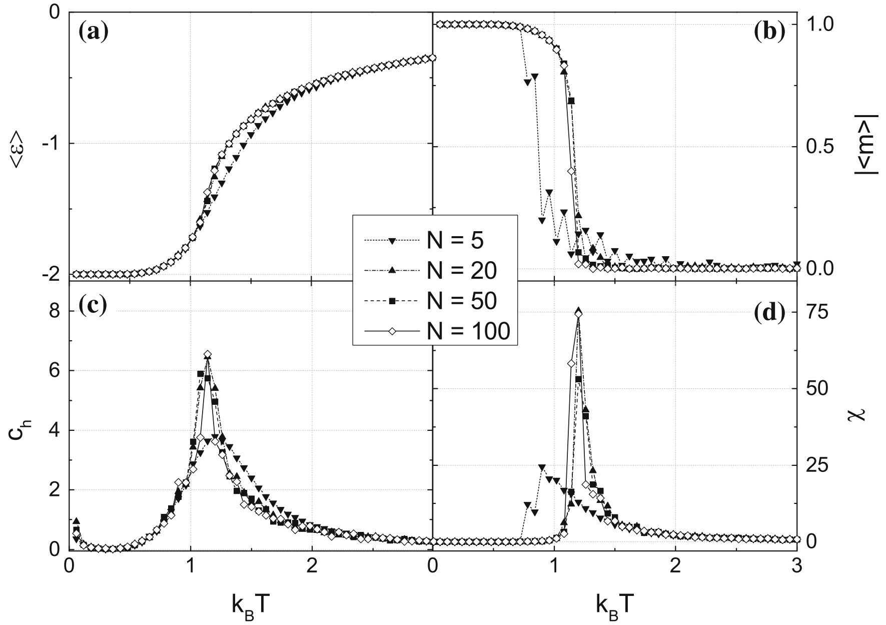

Fig. 15.5 **(a)** The expectation value of the energy per particle $\langle \varepsilon \rangle$, **(b)** the absolute value of the expectation value of the magnetization per particle $|\langle m \rangle|$, **(c)** the heat capacity c_h, and **(d)** the magnetic susceptibility χ vs temperature $k_B T$ for the two-dimensional ISING model. The system sizes are $N = 5, 20, 50, 100$

The error bars of the calculated expectation values have been obtained with the help of Eq. (15.49). The error estimates for the heat capacity c_h as well as for the magnetic susceptibility χ are more complex to evaluate. The method employed is referred to as *statistical bootstrap*, where $M = 100$ samples have been generated. This method will be explained in some detail in Chap. 19.

In Fig. 15.5 we compare the expectation value of the energy per particle, $\langle \varepsilon \rangle$, the absolute value of the magnetization per particle $|\langle m \rangle|$, the overall heat capacity c_h and the overall magnetic susceptibility χ for four system sizes N = 5, 20, 50, 100. Furthermore, in Fig. 15.6 we show the curves for the system size of N = 50 together with corresponding error bars.

We observe that the phase transition gets sharper with increasing system size, i.e. increasing values of N. In fact we know, that the phase transition is infinitely sharp as $N \to \infty$ from the analytic solution given by ONSAGER. It is a quite obvious result of this study that the system size N should be greater than 20 to achieve acceptable results.

Furthermore, we presented the absolute value of the magnetization rather than the magnetization itself. The reason is that for $T < T_C$ the ground state is degenerate. In particular, the state with all spins up or all spins down is equally probable since

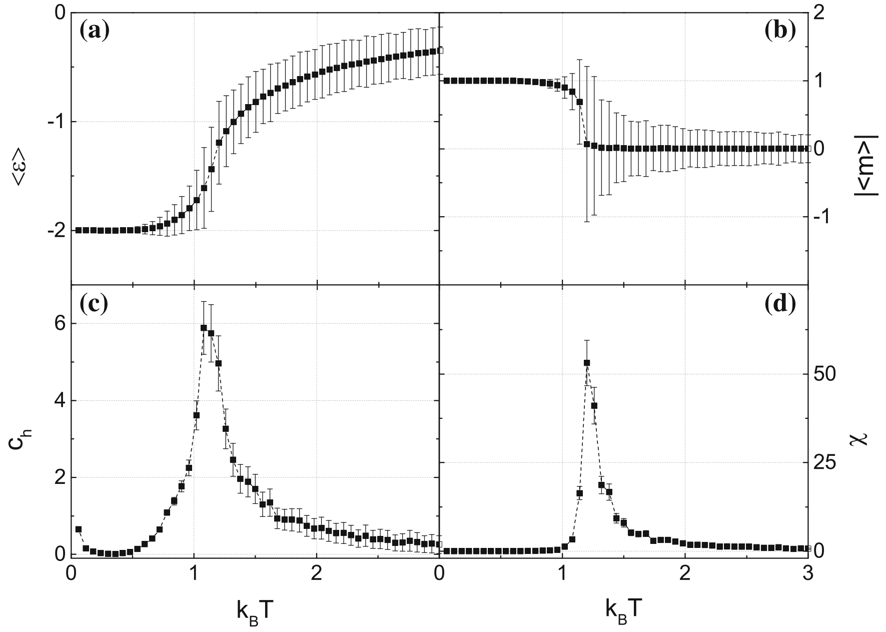

Fig. 15.6 **(a)** The expectation value of the energy per particle $\langle \varepsilon \rangle$, **(b)** the expectation value of the magnetization per particle $|\langle m \rangle|$, **(c)** the heat capacity c_h, and **(d)** the magnetic susceptibility χ with error bars vs temperature $k_B T$ obtained for the two-dimensional ISING model of size $N = 50$

we set the external magnetic field $h = 0$. This is a manifestation of $\mathbb{Z}_2$ symmetry of the Hamiltonian discussed in Sect. 15.1.

Of particular interest is the region around the critical temperature, referred to as the *critical region*. In this region, the spins are not perfectly aligned and not randomly orientated either. In this region the spins align in so called *magnetic domains*, which are also referred to as WEISS domains. A typical spin configuration for such a domain is shown in Fig. 15.7.

We conclude this chapter with an interesting note: Fig. 15.6 makes it quite clear that the error of the expectation value of the magnetization and of the energy is biggest for values around the transition temperature. In fact, if we increase the system size the error will get even larger. The reason is quite obvious: the error of our Monte-Carlo integration is proportional to the square root of the variance of the investigated observable. However, since we deal with a second order phase transition, this variance tends to infinity as $N \to \infty$. There is one cure to the problem: We are dealing here with finite-sized systems, thus, the variance will never actually be infinitely large. Furthermore, according to Eq. (15.49) we can decrease the error by increasing the

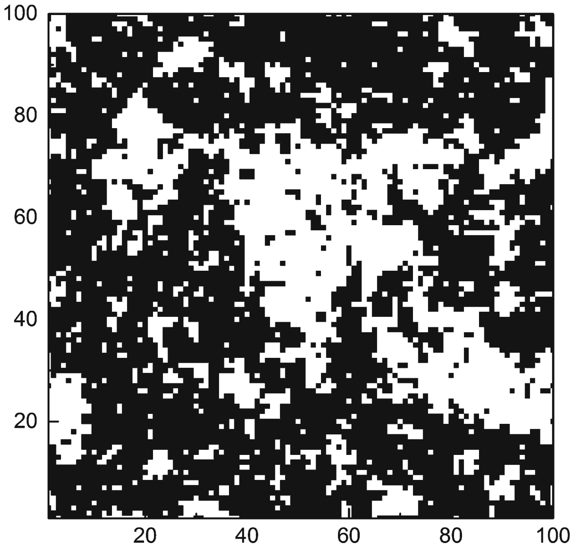

Fig. 15.7 For $T \approx T_C$ the spins organize in WEISS domains. Here we show a typical spin configuration for $N = 100$ and $k_B T = 1.15$. The *black shaded areas* correspond to spin up sites while the *white areas* indicate spin down sites

number of measurements. Hence, if one is confronted with large systems, one has also to perform many measurements in order to reduce the error.[13]

Summary

The ISING model is a rather simple model which describes effectively a second order phase transition. Such phase transitions are the topic of extensive numerical studies and, therefore, this model served here as a tool to demonstrate how to proceed from the problem analysis to a numerical algorithm which will allow to simulate the physics. The advantage of the ISING model was that under certain simplifications solutions could be derived analytically. In the course of this analysis the important concept of observables was introduced. Observables are certain physical properties of a system which characterize the specific phenomenon of interest. Numerically, observables are certain variables which are to be 'measured' within the course of a simulation. After the extensive analysis of the ISING model the transition to the numerical analysis of the two-dimensional ISING model was a rather easy part. The required modification of spin configurations turned out to be the key element of the simulation and this suggested the application of the METROPOLIS algorithm for sampling. Finally, important problems like initialization of the simulation, thermalization, finite size effects, measurement of observables, and the prevention of correlations between subsequent spin configurations caused by the METROPOLIS algorithm have been discussed

[13] We note from Eq. (15.49) that we have to perform four times as many measurements in order to reduce the error by a factor 2.

on the basis of concrete calculations. This chapter was motivated by the remark, quote [10]:

"Numerical methods are no excuse for poor analysis."

Problems

1. Write a program to simulate the two-dimensional ISING model with periodic boundary conditions with the help of the METROPOLIS algorithm. Follow the strategy outlined in Sect. 15.2 and try to reproduce the results illustrated in Sect. 15.3 for $N = 5, 20, 50$.

   In particular, as a first step write a routine which stores the nearest neighbors of the square lattice in an array. As a second step, write a program which performs a sweep through the lattice geometry. You can either choose the lattice sites systematically or at random. As a third step, set up the main program which calls the sweep routine. Choose some initial configuration and thermalize the system. Measure the expectation value of the energy per particle as well as the absolute value of the expectation value of the magnetization for different temperatures $k_B T$ and determine the respective errors, see Eq. (15.49). Calculate also the overall magnetic susceptibility and the overall heat capacity. The determination of the error is more complicated in this case and can therefore be neglected for the moment.

   Good parameters to start with are $J = 0.5$, $N_{therm} = 500$, $N_{skip} = 10$ and $h = 0.0$.
2. Try also different values of J and $h \neq 0$.

References

1. Baym, G.: Lectures on quantum mechanics. Lecture Notes and Supplements in Physics. The Benjamin/Cummings Publ. Comp., Inc., London, Amsterdam (1969)
2. Cohen-Tannoudji, C., Diu, B.: Laloë: Quantum Mechanics, vol. I. John Wiley, New York (1977)
3. Sakurai, J.J.: Modern Quantum Mechanics. Addison-Wesley Publishing Comp, Menlo Park (1985)
4. White, R.M.: Quantum theory of magnetism, 3rd edn. Springer Series in Solid-State Sciences. Springer, Berlin, Heidelberg (2007)
5. Mandl, F.: Statistical Physics, 2nd edn. John Wiley, New York (1988)
6. Schwabl, F.: Statistische Physik, 3rd edn. Springer Lehrbuch. Springer, Berlin, Heidelberg (2006)
7. Ising, E.: Zeitschrift für Physik **31**, 253 (1925)
8. Onsager, L.: Crystal statistics. i. a two-dimensional model with an order-disorder transition. Phys. Rev. **65**, 117–149 (1944). doi:10.1103/PhysRev.65.117
9. Landau, L.D., Lifshitz, E.M.: Course of Theoretical Physics, vol. 5: Statistical Physics. Pergamon Press, London (1963)
10. Dorn, W.S., McCracken, D.D.: Numerical Methods with Fortran IV Case Studies. Wiley, New York (1972)

Chapter 16
Some Basics of Stochastic Processes

16.1 Introduction

This chapter is devoted to an introduction to some basic concepts of the huge field of stochastic processes. This introduction serves two purposes: First of all, it will allow for a more systematic treatment of non-deterministic methods in computational physics, which is certainly necessary if we really aim at an understanding of these methods. The second reason can be found in the elementary importance of stochastics in modern theoretical physics and chemistry in general. Hence, many of the concepts elaborated within this chapter will be of profound importance in subsequent chapters. For instance, we present a discussion of diffusion theory in Chap. 17 as a motivating example.

In the following we use the notation introduced in Appendix D. The reader non familiar with the basics of probability theory [1] is highly encouraged to at least consult Appendix D before proceeding.

This chapter consists of five sections including this introduction. In Sect. 16.2 we introduce the basic definitions associated with stochastic processes in general. Here we discuss concepts which will serve as a basis for understanding the concepts elaborated within the subsequent sections. Section 16.3 deals with a special class of stochastic processes, the so called MARKOV processes. As we shall see, these processes are of fundamental importance for statistical physics and for computational methods. Moreover, in Sect. 16.4 we consider so called MARKOV-chains, which are discrete MARKOV processes defined on a discrete time span. This will serve as the basis of a very important method in computational physics, the so called MARKOV-Chain Monte Carlo technique. We already encountered a simple example of this method in Sect. 14.3 and in Chap. 15, the METROPOLIS algorithm. Finally, in Sect. 16.5 continuous-time MARKOV-chains will be discussed, in particular discrete MARKOV processes on a continuous time span. These processes are very important, for instance, in diffusion theory as will be demonstrated in Chap. 17.

We note that a discussion of detailed balance will be included in the section MARKOV processes, Sect. 16.3, although detailed balance follows from physical

B. A. Stickler and E. Schachinger, *Basic Concepts in Computational Physics*,
DOI: 10.1007/978-3-319-02435-6_16, © Springer International Publishing Switzerland 2014

arguments. Please note that we already mentioned detailed balance in our discussion of the METROPOLIS algorithm in Sect. 14.3.

16.2 Stochastic Processes

The following discussion is primarily restricted to one-dimensional processes.

A stochastic process is a time dependent process depending on randomness. From a mathematical point of view, a stochastic process $Y_X(t)$ is a random variable Y, which is a function of another random variable X and time $t \geq 0$, i.e.

$$Y_X(t) = f(X, t). \tag{16.1}$$

Here we apply the notation of Appendix D and denote random variables by capital letters, such as X, and their realization by lower case characters, such as x. Consequently, the realization of a stochastic process is described by

$$Y_x(t) = f(x, t). \tag{16.2}$$

The set of all possible realizations of $Y_X(t)$ span the *state space* of the stochastic process. We note that it is in principle not necessary to define t as the time in a classical sense. It suffices to denote $t \in T$, where T is a totally ordered set such as, for instance, $T = \mathbb{N}$ the natural numbers. The set T is referred to as the *time span*. We distinguish four different scenarios:

- discrete state space, discrete time span,
- continuous state space, discrete time span,
- discrete state space, continuous time span,
- continuous state space, continuous time span.

Stochastic processes on a continuous time span are referred to as continuous-time stochastic processes.

Suppose the random variable X follows the pdf $p_X(x)$. It is then an easy task to calculate averages $\langle Y(t) \rangle$ of the stochastic process $Y_X(t)$ via

$$\langle Y(t) \rangle = \int \mathrm{d}x Y_x(t) p_X(x). \tag{16.3}$$

This concept is easily extended to multiple times $t_1, t_2, \ldots, t_n$ by

$$\langle Y(t_1)Y(t_2)\cdots Y(t_n) \rangle = \int \mathrm{d}x Y_x(t_1)Y_x(t_2)\cdots Y_x(t_n) p_X(x), \tag{16.4}$$

which defines the *moments* of the stochastic process [1–3]. Similar to the concept of the correlation coefficient, see Appendix D, we define the so called *auto-correlation* *function* $\kappa(t_1, t_2)$ by

$$\begin{aligned}\kappa(t_1, t_2) &= \frac{\langle [Y(t_1) - \langle Y(t_1)\rangle]\,[Y(t_2) - \langle Y(t_2)\rangle]\rangle}{\sqrt{\langle [Y(t_1) - \langle Y(t_1)\rangle]^2\rangle \langle [Y(t_2) - \langle Y(t_2)\rangle]^2\rangle}} \\ &= \frac{\langle Y(t_1)Y(t_2)\rangle - \langle Y(t_1)\rangle\langle Y(t_2)\rangle}{\sqrt{\mathrm{var}[Y(t_1)]\mathrm{var}[Y(t_2)]}} \\ &= \frac{\gamma[Y(t_1), Y(t_2)]}{\sqrt{\mathrm{var}[Y(t_1)]\mathrm{var}[Y(t_2)]}}. \end{aligned} \tag{16.5}$$

The function $\gamma[Y(t_1), Y(t_2)]$ is referred to as the *auto-covariance function* and is defined as

$$\gamma[Y(t_1), Y(t_2)] = \mathrm{cov}[Y(t_1), Y(t_2)]. \tag{16.6}$$

We proceed by defining the pdf of a stochastic process $Y_X(t)$. The pdf $p_1(y, t)$, which describes the probability that the stochastic process $Y_X(t)$ takes on its representation y at time t, is given by (see Sect. 14.2)

$$p_1(y, t) = \int \mathrm{d}x \delta[y - Y_x(t)] p_X(x). \tag{16.7}$$

In a similar fashion we define the pdf $p_n(y_1, t_1, y_2, t_2, \dots, y_n, t_n)$ which describes the probability that the stochastic process takes on the realization y_1 at time t_1, y_2 at time t_2, ..., and y_n at time t_n as

$$\begin{aligned} p_n(y_1, t_1, y_2, t_2, \dots, y_n, t_n) = \int \mathrm{d}x \delta[y_1 - Y_x(t_1)]\delta[y_2 - Y_x(t_2)] \cdots \\ \times \delta[y_n - Y_x(t_n)] p_X(x), \end{aligned} \tag{16.8}$$

for arbitrary n. This is referred to as the *hierarchy of pdfs*. We note the following important properties of the pdf $p_n(y_1, t_1, y_2, t_2, \dots, y_n, t_n)$ [3]:

- $p_n(y_1, t_1, y_2, t_2, \dots, y_n, t_n) \geq 0,$ (16.9)
- $p_n(\dots, y_k, t_k \dots, y_l, t_l, \dots) = p_n(\dots, y_l, t_l \dots, y_k, t_k, \dots),$ (16.10)
- $\int dy_n p_n(y_1, t_1, \dots, y_n, t_n) = p_{n-1}(y_1, t_1, \dots, y_{n-1}, t_{n-1}),$ (16.11)
- $\int dy p_1(y, t) = 1.$ (16.12)

The moments defined in Eq. (16.4) can also be expressed with the help of the pdfs p_n by

$$\langle Y(t_1)Y(t_2) \cdots Y(t_n)\rangle = \int \mathrm{d}y_1 \dots \mathrm{d}y_n y_1 \cdots y_n p_n(y_1, t_1, \dots, y_n, t_n). \tag{16.13}$$

Conditional pdfs $p_{l|k}$ can also be introduced. They describe the probability that we have y_{k+1} at t_{k+1}, ..., y_{k+l} at t_{k+l} if there existed y_1 at t_1, ..., y_k at t_k via

$$p_{l|k}(y_{k+1}, t_{k+1}, \ldots, y_{k+l}, t_{k+l}|y_1, t_1, \ldots, y_k, t_k) = \frac{p_{k+l}(y_1, t_1, \ldots, y_{k+l}, t_{k+l})}{p_k(y_1 t_1, \ldots, y_k, t_k)}. \tag{16.14}$$

It follows that

$$\int \mathrm{d}y_2 p_{1|1}(y_2, t_2|y_1, t_1) = 1. \tag{16.15}$$

Let us give some further definitions:

- A stochastic process is referred to as a *stationary process* if the moments defined in Eq. (16.4) are invariant under a time-shift $\varDelta t$, i.e.

$$\langle Y(t_1)Y(t_2)\cdots Y(t_n)\rangle = \langle Y(t_1 + \varDelta t)Y(t_2 + \varDelta t)\cdots Y(t_n + \varDelta t)\rangle. \tag{16.16}$$

  In particular, one has $\langle Y(t)\rangle = \text{const}$ and the auto-covariance depends only on the time difference $|t_1 - t_2|$, i.e.

$$\gamma(t_1, t_2) = \text{cov}[Y(t_1), Y(t_2)] = \text{cov}[Y(0), Y(|t_1 - t_2|)] \equiv \gamma(t_1 - t_2). \tag{16.17}$$

  It is understood that $\gamma(t) = \gamma(-t)$. Moreover, we have

$$p_n(y_1, t_1 + \varDelta t, \ldots, y_n, t_n + \varDelta t) = p_n(y_1, t_1, \ldots, y_n, t_n), \tag{16.18}$$

  and in particular, $p_1(y, t) = p_1(y)$.
- A *time-homogeneous* process is a stochastic process whose conditional pdfs are stationary

$$p_{1|1}(y_2, t_2|y_1, t_2 - \tau) = p_{1|1}(y_2, s_2|y_1, s_2 - \tau), \tag{16.19}$$

  for all t_2, τ, s_2. The pdf $p_{1|1}$ is referred to as *transition probability*.
- A *process of stationary increments* is a stochastic process $Y_X(t)$ for which the difference $Y_X(t_2) - Y_X(t_1)$ is stationary for all $t_2 - t_1$, with $t_2 > t_1 \geq 0$. This means, in particular, that the pdf of this process depends only on the time difference $t_2 - t_1$. The quantities $Y_X(t_2) - Y_X(t_1)$ are referred to as increments.
- A *process of independent increments* is a stochastic process $Y_X(t)$ for which the differences

$$Y_X(t_2) - Y_X(t_1), Y_X(t_3) - Y_X(t_2), \ldots, Y_X(t_n) - Y_X(t_{n-1}),$$

  are independent for all $t_n > t_{n-1} > \cdots > t_2 > t_1$.
- A LÉVY *process* is a continuous-time stochastic process with stationary independent increments which starts with $Y_X(0) = 0$.

- A *Gaussian process* is a stochastic process $Y_X(t)$ for which all finite linear combinations of $Y_X(t)$, $t \in T$ follow a normal distribution. We shall come back to this kind of process in Chap. 17.
- A WIENER *process* is a continuous-time stochastic process with independent increments which starts with $Y_X(0) = 0$ and for which the increments $Y_X(t_2) - Y_X(t_1)$ follow a normal distribution with mean 0 and variance $t_2 - t_1$. The WIENER process is a special case of a LÉVY process. One of the main applications of the WIENER process is to study *Brownian motion* or diffusion. This process will be discussed in more detail in Sect. 16.3 and in Chap. 17.
- The *random walk* is the discrete analogy to the WIENER process. This means in particular that if the step size of the random walk goes to zero, the WIENER process is reestablished. This point will be elucidated in Chap. 17.

After stating the most important definitions, we proceed to the next section in which the attention is on a special class of stochastic processes, the so called MARKOV processes.

16.3 MARKOV Processes

A MARKOV process is a stochastic process $Y_X(t)$ for which the conditional pdf $p_{1|n-1}$ satisfies for arbitrary n and $t_1 < t_2 < \cdots < t_n$ the relation

$$p_{1|n-1}(y_n, t_n | y_1, t_1, \ldots, y_{n-1}, t_{n-1}) = p_{1|1}(y_n, t_n | y_{n-1}, t_{n-1}). \tag{16.20}$$

Hence, a MARKOV process is a process in which any state y_n, t_n is uniquely defined by its precursor state y_{n-1}, t_{n-1} and is independent of the entire rest of the past. MARKOV processes are of particular importance in natural sciences because of their rather simple structure. This outstanding importance will become clear throughout the rest of this book.

We note in passing that a process with independent increments is *always* a MARKOV process because

$$Y_X(t_{n+1}) = Y_X(t_n) + \left[Y_X(t_{n+1}) - Y_X(t_n)\right], \tag{16.21}$$

is satisfied. Since the increment $Y_X(t_{n+1}) - Y_X(t_n)$ is independent of all previous increments which gave rise to $Y_X(t_n)$ *by definition*, $Y_X(t_{n+1})$ depends only on $Y_X(t_n)$, which is exactly the MARKOV property (16.20).

The quantity $p_{1|1}(y_n, t_n | y_{n-1}, t_{n-1})$ which appears in Eq. (16.20) is referred to as *transition probability*. Given the transition probability $p_{1|1}$ together with the pdf p_1, one can construct the whole hierarchy of pdfs (16.8) of the MARKOV process by calculating successively [3]

$$\begin{aligned}
p_2(y_1,t_1,y_2,t_2) &= p_{1|1}(y_2,t_2|y_1,t_1)p_1(y_1,t_1),\\
p_3(y_1,t_1,y_2,t_2,y_3,t_3) &= p_{1|2}(y_3,t_3|y_1,t_1,y_2,t_2)p_2(y_1,t_1,y_2,t_2),\\
&= p_{1|1}(y_3,t_3|y_2,t_2)p_{1|1}(y_2,t_2|y_1,t_1)p_1(y_1,t_1),\\
\vdots \quad &\quad \vdots
\end{aligned} \tag{16.22}$$

Here we employed definition (16.14) and in the second step of the second equation we employed for $p_{1|2}$ the MARKOV property (16.20).

The fact that the whole hierarchy of pdfs can be constructed by repeating the steps illustrated in Eq. (16.22) reveals the rather simple structure of MARKOV processes. However, Eq. (16.22) contains another useful information. We regard the pdf p_3 of (16.22) for three successive times $t_1 < t_2 < t_3$. First we integrate the left-hand side with respect to y_2 which yields with the help of property (16.9)

$$\int \mathrm{d}y_2 p_3(y_1,t_1,y_2,t_2,y_3,t_3) = p_2(y_1,t_1,y_3,t_3). \tag{16.23}$$

Hence, we have

$$p_2(y_1,t_1,y_3,t_3) = p_1(y_1,t_1)\int \mathrm{d}y_2 p_{1|1}(y_3,t_3|y_2,t_2)p_{1|1}(y_2,t_2|y_1,t_1), \tag{16.24}$$

or after dividing both sides by $p_1(y_1,t_1)$ and by keeping in mind Eq. (16.14) we arrive at:

$$p_{1|1}(y_3,t_3|y_1,t_1) = \int \mathrm{d}y_2 p_{1|1}(y_3,t_3|y_2,t_2)p_{1|1}(y_2,t_2|y_1,t_1). \tag{16.25}$$

This equation is known as the CHAPMAN–KOLMOGOROV equation. The interpretation of this equation is straight-forward: the transition probability from (y_1,t_1) to (y_3,t_3) is equivalent to the transition probability from (y_1,t_1) to (y_2,t_2) multiplied by the transition probability from (y_2,t_2) to (y_3,t_3) when summed over all intermediate positions y_2. This is illustrated in Fig. 16.1.

We state a very important theorem: Any two non-negative functions $p_{1|1}$ and p_1 uniquely define a MARKOV process if

$$p_{1|1}(y_3,t_3|y_1,t_1) = \int \mathrm{d}y_2 p_{1|1}(y_3,t_3|y_2,t_2)p_{1|1}(y_2,t_2|y_1,t_1), \tag{16.26}$$

is obeyed, i.e. the CHAPMAN-KOLMOGOROV equation (16.25), and if

$$p_1(y_2,t_2) = \int \mathrm{d}y_1 p_{1|1}(y_2,t_2|y_1,t_1)p_1(y_1,t_1), \tag{16.27}$$

which follows immediately from the first equation in Eq. (16.22) in combination with property (16.9).

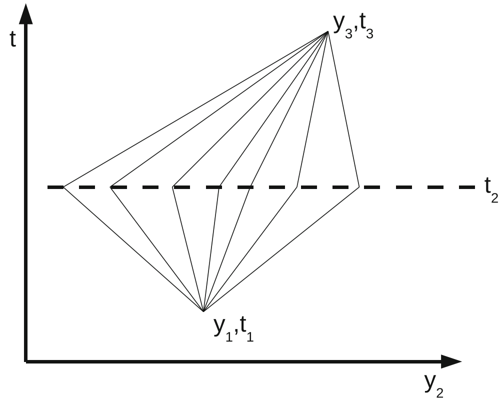

Fig. 16.1 Illustration of the CHAPMANN-KOLMOGOROV equation.

As a first example we consider one of the most important MARKOV processes in physics, the WIENER process. Its importance stems from its application to the description of Brownian motion, i.e. the random motion of dust particles on a fluid surface. (In Chap. 17 we shall have a closer look on diffusion phenomena.) The transition probability of the WIENER process is of the form[1]

$$p_{1|1}(y_2, t_2|y_1, t_1) = \frac{1}{\sqrt{2\pi(t_2 - t_1)}} \exp\left[-\frac{(y_2 - y_1)^2}{2(t_2 - t_1)}\right]. \tag{16.28}$$

The initial condition is given by

$$p_1(y_1, t_1 = 0) = \delta(y_1). \tag{16.29}$$

A simple, however, tedious calculation proves that (16.28) indeed obeys the CHAPMAN-KOLMOGOROV equation (16.25). Moreover, we deduce from Eq. (16.29) together with (16.27) that

$$p_1(y, t) = \frac{1}{\sqrt{2\pi t}} \exp\left(-\frac{y^2}{2t}\right). \tag{16.30}$$

The WIENER process is easily realized on the computer. We regard the one-dimensional case and start at the origin $Y_X(0) = 0$. From the property of normally distributed increments, i.e.

$$Y_X(t + \mathrm{d}t) - Y_X(t) \propto \mathcal{N}(\mathrm{d}y|0, \mathrm{d}t), \tag{16.31}$$

[1] This form is equivalent to the above definition of the WIENER process, in particular to the requirement of normally distributed increments with variance $t_2 - t_1$.

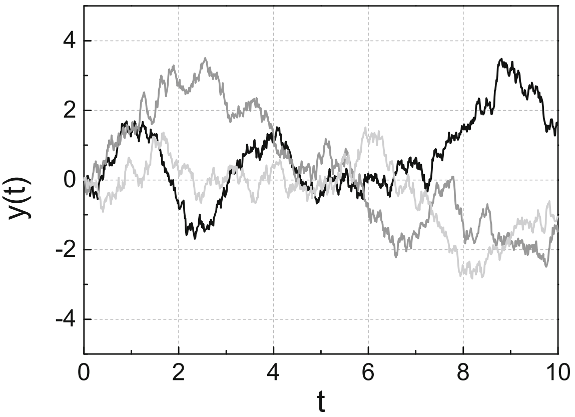

Fig. 16.2 Three possible realizations of the WIENER process.

where $\mathcal{N}$ denotes the normal distribution, we draw the step size dy. Hence, we start with $y_0 = 0$, draw the displacement dy within a time-step dt from the normal distribution with mean zero and variance dt and calculate the next position according to $y_{n+1} = y_n + \mathrm{d}y$.[2] The result is depicted in Fig. 16.2.

Let us mention a second very important MARKOV process, the POISSON process. The POISSON process is particularly interesting for problems involving *waiting times*, such as the decay of some radioactive nucleus. However, we shall also come across the POISSON process within the context of diffusion in Chap. 17. The transition probability of the POISSON process is defined as

$$p_{1|1}(n_2, t_2|n_1, t_1) = \frac{(t_2 - t_1)^{n_2 - n_1}}{(n_2 - n_1)!} \exp\left[-(t_2 - t_1)\right]. \tag{16.32}$$

Here it is understood that $n_1, n_2 \in \mathbb{N}$ and $n_2 > n_1$. Hence, the POISSON process counts the number of occurrences n_2 of a certain event until the time t_2 is reached, under the premise that n_1 events have already occurred at time t_1. The POISSON process is initialized by the pdf

$$p_1(n_1, t_1 = 0) = \delta_{n_1 0}, \tag{16.33}$$

here δ_{ij} is the KRONECKER-δ. Hence we have according to Eq. (16.27)

$$p_1(n, t) = \sum_{n_1} p_{1|1}(n, t|n_1, t_1 = 0) p_1(n_1, t_1 = 0) = \frac{t^n}{n!} \exp\left(-t\right), \tag{16.34}$$

i.e. a POISSON distribution. Let us briefly consider the time between two events. Suppose we had n_1 events at time t_1. Then, we search the probability that at time $t_2 = t_1 + \tau$ we still counted $n_2 = n_1$ events, i.e. nothing happened. We have

[2] Alternatively, we may draw dy from a normal distribution with variance 1 and multiply it by $\sqrt{\mathrm{d}t}$. This follows from a simple transformation of variables.

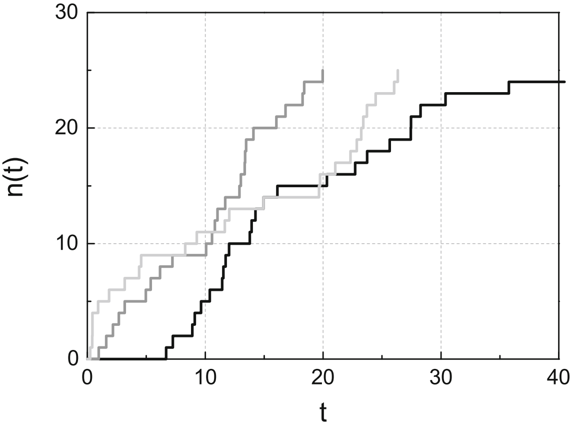

Fig. 16.3 Three possible realizations of a POISSON process.

$$p_{1|1}(n_1, t_1 + \tau | n_1, t_1) = \exp(-\tau) , \tag{16.35}$$

i.e. the waiting times are independent and follow an exponential distribution. We may simulate the POISSON process by starting at $t_1 = 0$ with $n_1 = 0$ and by increasing $n_2, n_3, \ldots$ by one, i.e. $n_{i+1} = n_i + 1$ after successive waiting times $\tau_1, \tau_2, \ldots$ which we draw from the exponential distribution, see Sect. 13.2. The result is illustrated in Fig. 16.3.

Finally we remark that for a time-homogeneous MARKOV process the transition probability $p_{1|1}(y_2, t_2 | y_1, t_1)$ depends by definition on the time difference $t_2 - t_1 \equiv \tau$ rather than explicitly on the two times t_1 and t_2 and is usually denoted by $T_\tau(y_2, y_1)$.

We shall now turn our attention to another very important general concept of MARKOV processes, the *master equation*. This equation is in fact the differential form of the CHAPMAN-KOLMOGOROV equation. We regard the CHAPMAN-KOLMOGOROV equation (16.25) for three successive times $t_1 < t_2 < t_3 = t_2 + \tau$ where τ is assumed to be small, i.e. $\tau \ll 1$. We expand the conditional pdf $p_{1|1}$ in a TAYLOR series with respect to τ:

$$p_{1|1}(y_3, t_2 + \tau | y_2, t_2) = p_{1|1}(y_3, t_2 | y_2, t_2) + \tau \frac{\partial}{\partial \tau} p_{1|1}(y_3, t_2 + \tau | y_2, t_2)\tau \Big|_{\tau=0} + \mathscr{O}(\tau^2). \tag{16.36}$$

Let us define the transition rate $w(y_3 | y_2, t_2)$ from y_2 to y_3, where $y_2 \neq y_3$, at time t_2 by

$$w(y_3 | y_2, t_2) = \frac{\partial}{\partial \tau} p_{1|1}(y_3, t_2 + \tau | y_2, t_2)\tau \Big|_{\tau=0}. \tag{16.37}$$

We now regard the first term on the right-hand side of Eq. (16.36) and note that it has to be of the form

$$p_{1|1}(y_3, t_2 | y_2, t_2) = \delta(y_3 - y_2). \tag{16.38}$$

We note that we defined the transition rate (16.37) only for elements $y_2 \neq y_3$. The remaining part with $y_2 = y_3$ will be denoted by $a(y_2, t_2)$ and we rewrite (16.36) as

$$p_{1|1}(y_3, t_2 + \tau | y_2, t_2) = [1 + a(y_2, t_2)]\delta(y_3 - y_2) + \tau w(y_3|y_2, t_2), \tag{16.39}$$

where we neglected terms of order $\mathscr{O}(\tau^2)$. We require Eq. (16.39) to be normalized according to Eq. (16.15) and obtain

$$a(y_2, t_2) = -\tau \int \mathrm{d}y_3 w(y_3|y_2, t_2). \tag{16.40}$$

Hence, the term $1 + a(y_2, t_2)$ describes indeed the probability that no event occurs within the time interval $[t_2, t_2 + \tau]$. We insert expansion (16.39) into the CHAPMAN-KOLMOGOROV equation (16.25) with the result:

$$\begin{aligned} \frac{p_{1|1}(y_3, t_2 + \tau | y_1, t_1) - p_{1|1}(y_3, t_2 | y_1, t_1)}{\tau} = \int \mathrm{d}y_2 \big[& w(y_3|y_2, t_2) p_{1|1}(y_2, t_2|y_1, t_1) \\ & - w(y_2|y_3, t_2) p_{1|1}(y_3, t_2|y_1, t_1) \big]. \end{aligned} \tag{16.41}$$

In the limit $\tau \to 0$ we arrive, finally, at the master equation:

$$\begin{aligned} \frac{\partial}{\partial t} p_{1|1}(y, t|y', t') = \int \mathrm{d}y'' \big[& w(y|y'', t) p_{1|1}(y'', t|y', t') \\ & - w(y''|y, t) p_{1|1}(y, t|y', t') \big]. \end{aligned} \tag{16.42}$$

If we now multiply both sides of this equation with $p_1(y', t')$ and integrate over y', see property (16.27), a master equation for the pdf $p_1(y, t)$ is obtained:

$$\frac{\partial}{\partial t} p_1(y, t) = \int \mathrm{d}y' \left[w(y|y', t) p_1(y', t) - w(y'|y, t) p_1(y, t) \right]. \tag{16.43}$$

Let us briefly discuss this equation. In its derivation we assumed the state space to be continuous. However, the master equation for a discrete state space is obtained by replacing the integral by a sum over discrete states. The physical interpretation of an equation of this kind is straight-forward: The time evolution of the quantity $p_1(y, t)$ is governed by the sum over all transitions into state y (first term) minus all transitions out of state y. We remark that master equations occur commonly in physical applications; for instance, the collision integral of the BOLTZMANN equation is of a similar form. The transitions rates $w(y|y', t)$ can be determined in many physical applications.[3]

[3] As an example we quote FERMI's golden rule, where the transition rate $w_{nn'}$ from unperturbed states n to n' is of the form

$$w_{nn'} = \frac{2\pi}{\hbar} |H'_{nn'}| \rho(E_n),$$

Furthermore, if we have a stationary distribution $p_1(y,t) = p_1(y)$, i.e. if the system is in a stationary state, we obtain from (16.43)

$$\int \mathrm{d}y' w(y|y',t)p_1(y') = \int \mathrm{d}y' w(y'|y,t)p_1(y), \tag{16.44}$$

which is referred to as *global balance*. The much stronger condition

$$w(y|y',t)p_1(y') = w(y'|y,t)p_1(y), \tag{16.45}$$

is referred to as *detailed balance* and will be discussed next.

We demonstrate now that the equilibrium distribution function $p_e(X)$ of a classical physical system will, under certain restrictions, indeed fulfill detailed balance [2]. In what follows the following notation will be applied: the vector $x = (q_k, p_k)^T \in \mathbb{R}^{6N}$ represents the phase space trajectory of the N particles constituting the system under investigation. The equations of motion are of the form

$$\dot{q_k} = \frac{\partial}{\partial p_k} H(x), \qquad \dot{p_k} = -\frac{\partial}{\partial q_k} H(x). \tag{16.46}$$

Furthermore, let $Y_X(t)$ denote a stochastic process which describes some observable of the physical system. We require that $Y_X(t)$ is invariant under time reversal. Furthermore, we assume the equilibrium distribution function $p_e(x)$ to be invariant under time reversal, which in most cases is equivalent to the requirement that the Hamilton function $H(x)$ is invariant under time reversal. We will denote the operation of time reversal with the help of an over-line, i.e.

$$\bar{t} = -t, \quad \overline{x} = (q_k, -p_k)^T. \tag{16.47}$$

Hence, the above assumptions read

$$\overline{Y_x(t)} = Y_{\overline{x}}(\bar{t}) = Y_{\overline{x}}(-t) = Y_x(t), \tag{16.48}$$

and

$$\overline{p_e(x)} = p_e(\overline{x}) = p_e(x). \tag{16.49}$$

In particular, we deduce from (16.48) that

$$Y_{\overline{x}}(0) = Y_x(0), \tag{16.50}$$

and

$$Y_{\overline{x}}(t) = Y_x(-t). \tag{16.51}$$

(Footnote 3 continued)
where $H'_{nn'}$ are the matrix element of the perturbation Hamiltonian H' and $\rho(E_n)$ denotes the density of states of the unperturbed system.

We calculate the pdf p_2 from

$$p_2(y_1, 0, y_2, t) = \int \mathrm{d}x \delta[y_1 - Y_x(0)]\delta[y_2 - Y_x(t)]p_e(x). \tag{16.52}$$

However, since we integrate over the whole phase space we recognize that the volume is invariant under a change d$x \to d\overline{x}$. Thus, we can change the variable of integration from x to $\overline{x}$ which results in

$$\begin{aligned} p_2(y_1, 0, y_2, t) &= \int \mathrm{d}\overline{x} \delta[y_1 - Y_{\overline{x}}(0)]\delta[y_2 - Y_{\overline{x}}(t)]p_e(\overline{x}) \\ &= \int \mathrm{d}x \delta[y_1 - Y_x(0)]\delta[y_2 - Y_x(-t)]p_e(x) \\ &= p_2(y_2, -t, y_1, 0) \\ &= p_2(y_2, 0, y_1, t). \end{aligned} \tag{16.53}$$

Hence we have

$$p_2(y_1, 0, y_2, t) = p_2(y_2, 0, y_1, t), \tag{16.54}$$

and obtain immediately

$$p_{1|1}(y_2, t|y_1, 0)p_e(y_1) = p_{1|1}(y_1, t|y_2, 0)p_e(y_2). \tag{16.55}$$

Differentiating both sides with respect to t and employing definition (16.37) for small t yields

$$w(y_2|y_1)p_e(y_1) = w(y_1|y_2)p_e(y_2), \tag{16.56}$$

which is the condition of detailed balance, Eq. (16.45), for stationary distributions.

It should be noted at this point that detailed balance in physical systems is strongly connected to the entropy growth (the H-theorem by BOLTZMANN). Detailed balance was based on the condition that the stochastic process $Y_X(t)$ was invariant under time reversal and that the equilibrium distribution $p_e(x)$ had the same property. This has in most cases the consequence that the HAMILTON function is also invariant under time reversal transformations. However, a detailed discussion of these properties is far beyond the scope of this book.

We shall continue our discussion with so called MARKOV-chains, which are a special class of MARKOV processes. MARKOV-chains will prove to be very important for the understanding of MARKOV-chain Monte Carlo techniques, such as the METROPOLIS algorithm.

16.4 MARKOV-Chains

A MARKOV-chain is a time-homogeneous MARKOV process defined on a discrete time span and in a discrete state space. Hence, we may express the time instances by integers, i.e. $T = \mathbb{N}_0$, $t_n = n$ where $n \in \mathbb{N}_0$. Furthermore, possible outcomes can be indexed by integers, i.e. $Y_X(t_n) \in \{m\}$ where $m \in \mathbb{N}$. As a first consequence of the discreteness of the state space we may replace all pdfs p by probabilities Pr. Hence the MARKOV property reads

$$\Pr(Y_{n+1} = y|Y_n = y_n, \ldots, Y_1 = y_1) = \Pr(Y_{n+1} = y|Y_n = y_n), \tag{16.57}$$

where we used the notation $Y_n \equiv Y_X(t_n)$. Furthermore, $y_n \in \{m\}$ is one particular realization out of the discrete state space. Since we assume that the transition probabilities are independent of the actual time, we can define a *transition matrix* $P = \{p_{ij}\}$ via

$$p_{ij} = \Pr(Y_{n+1} = j|Y_n = i). \tag{16.58}$$

Consequently, we write

$$\Pr(Y_n = i_n, Y_{n-1} = i_{n-1}, \ldots, Y_0 = i_0) = \Pr(Y_0 = i_0) p_{i_0 i_1} p_{i_1 i_2} \cdots p_{i_{n-1} i_n}. \tag{16.59}$$

We note that the transition matrix is a *stochastic matrix*. This is a matrix with only non-negative elements such that the sum of each row is equal to one. Furthermore, one can show that the product of two stochastic matrices results, again, in a stochastic matrix.

We define the *state vector at time n*, $\pi^{(n)} = \{\pi_i^{(n)}\}$ as

$$\pi_i^{(n)} = \Pr(Y_n = i). \tag{16.60}$$

From the marginalization rule (Sect. D.6) we have for the particular case $n = 1$

$$\Pr(Y_1 = i) = \sum_k \Pr(Y_0 = k) \Pr(Y_1 = i|Y_0 = k), \tag{16.61}$$

or with the help of the above definitions (16.58) and (16.60)

$$\pi_i^{(1)} = \sum_k p_{ki} \pi_k^{(0)}, \tag{16.62}$$

for all i. Hence, we have for $n = 1$

$$\pi^{(1)} = \pi^{(0)} P, \tag{16.63}$$

and for $n = 2$

$$\pi^{(2)} = \pi^{(1)}P = \pi^{(0)}P^2. \tag{16.64}$$

Obviously, for arbitrary n follows

$$\pi^{(n)} = \pi^{(0)}P^n. \tag{16.65}$$

Hence the probability matrix for an n step transition $P^{(n)}$ reads $P^{(n)} = P^n$. We immediately deduce that the CHAPMAN–KOLMOGOROV equation for MARKOV-chains is indeed fulfilled since

$$P^{(n)}P^{(m)} = P^nP^m = P^{n+m} = P^{(n+m)}, \tag{16.66}$$

for two integers n and m.

Let us give some further definitions in order to classify MARKOV-chains [2, 3].

- The notation $i \to j$ means *state i leads to state j* and is true whenever there is a path of length n, $i_0 = i, i_1, \ldots, i_n = j$ such that for all $p_{i_k i_{k+1}} > 0$ for $k = 0, 1, \ldots, n-1$. This is equivalent to $(P^n)_{ij} > 0$.
- The notation $i \leftrightarrow j$ means *state i communicates with state j*. This relation is true whenever $i \to j$ and $j \to i$.
- A class of states is given if (i) all states within one class communicate with each other and (ii) two states of different classes never communicate with each other. These classes are referred to as the *irreducible* classes of the MARKOV-chain.
- An *irreducible* MARKOV-*chain* is a MARKOV-chain in which the whole state space forms an irreducible class, i.e. *all* states communicate with each other.
- A *closed set of states* is a set of states which never leads to states which are outside of this set.
- An *absorbing state* is a state which does not lead to any other states, i.e. it forms itself a closed set. We note that an absorbing state can be reached from the outside but there is no escape from it.
- A state is referred to as *transient* if the probability of returning to the state is less than one.
- A state is referred to as *recurrent* if the probability of returning to the state is equal to one.
- Furthermore, we call a state *positive recurrent* if the expectation value of the first return time is less than infinity and *null recurrent* if it is infinity. We may formulate this in a more mathematical language: The time of first return to state i is defined via

$$T_i = \inf\left(n \geq 1 : X_n = i | X_0 = i\right). \tag{16.67}$$

The probability that we return to state i for the first time after n steps is defined as

$$f_{ii}^n = \Pr(T_i = n). \tag{16.68}$$

Hence, a state is referred to as recurrent if

$$F_i = \sum_n f_{ii}^n = 1, \tag{16.69}$$

positive recurrent if

$$\langle T_i \rangle = \sum_n n f_{ii}^n < \infty, \tag{16.70}$$

and null recurrent if

$$\langle T_i \rangle = \sum_n n f_{ii}^n = \infty. \tag{16.71}$$

We note that we also have $\langle T_i \rangle = \infty$ if state i is transient. Furthermore, one can show that a state is only recurrent if

$$\sum_n p_{ii}^n = \infty. \tag{16.72}$$

- A state is referred to as *periodic* if the return time of the state can only be a multiple of some integer $d > 1$.
- A state is referred to as *aperiodic* if $d = 1$.
- We call a state *ergodic* if it is positive recurrent and aperiodic.
- A MARKOV-chain is called *ergodic* if all its states are *ergodic*.

We give some useful theorems in the context of the above definitions: First of all, it can be proved that if a MARKOV-chain is irreducible it follows that either *all* states are transient, or *all* states are null recurrent, or *all* states are positive recurrent.

Furthermore, a theorem by KOLMOGOROV states that if a MARKOV-chain is irreducible and aperiodic then the limit

$$\pi_j = \lim_{n \to \infty} \pi_j^{(n)} = \frac{1}{\langle T_j \rangle}, \tag{16.73}$$

exists. It follows from the above discussion that if all states j are transient or null recurrent we have

$$\pi_j = 0, \tag{16.74}$$

and if all states j are positive recurrent, we have

$$\pi_j \neq 0, \tag{16.75}$$

for all j. In this case the state vector $\pi = \{\pi_j\}$ is referred to as the *stationary distribution* or *equilibrium distribution*. We note that in this context the term equilibrium does not mean that nothing changes, but that the system *forgets* its own past. In particular, as soon as the system reaches the stationary distribution, it is independent of the initial state $\pi^{(0)}$.

We concentrate now on equilibrium distributions. It follows from Eq. (16.65) that π satisfies

$$\pi = \pi P, \tag{16.76}$$

i.e. π is the *left-eigenvector* to the transition probability matrix P with eigenvalue 1. We note that Eq. (16.76) states a homogeneous eigenvalue problem, i.e. the solution is only determined up to a constant multiplicator (see Sect. 8.3). However, it is clear that the vector π satisfies

$$\sum_j \pi_j = 1. \tag{16.77}$$

One can show that the unique solution of the eigenvalue problem (16.76) together with the normalization condition (16.77) for n states can be written as

$$\pi = e \cdot (P - E - I)^{-1}, \tag{16.78}$$

where e is an n-element row vector containing only ones, E is a $n \times n$ matrix containing only ones and I is the $n \times n$ identity.

Let us briefly elaborate on this point: if it is possible to construct a MARKOV-chain which possesses a unique stationary distribution, we know that it will definitely reach this distribution independent of the choice of initial conditions. The existence as well as the form of the stationary distribution is clearly determined by the transition probabilities p_{ij}. A sufficient condition for a unique stationary distribution to exist is the requirement of reversibility. A MARKOV-chain is referred to as *reversible* if

$$p_{ij}\pi_i = p_{ji}\pi_j, \tag{16.79}$$

for all i, j, i.e. if the transition probabilities ensure *detailed balance* for the stationary distribution π.

Now we are in a position to understand better why detailed balance is such an important concept of the METROPOLIS algorithm discussed in Sect. 14.3: Invoking the detailed balance condition ensures that for all possible initial states the MARKOV-chain converges towards the equilibrium distribution for which detailed balance is fulfilled. Of course, the convergence time will highly depend on the choice of the initial state as well as on the choice of the transition matrix. Hence, we may produce random numbers with the help of such a MARKOV-chain and after a *thermalization* period these numbers follow the required pdf. Methods based on this concept are commonly referred as MARKOV-*chain Monte Carlo sampling methods*.

We give a brief example, the *spread of a rumor*. Let Z_1 and Z_2 be two distinct versions of a report. If a person receives the report Z_1 it will pass this report on as Z_1 with probability $(1 - p)$ and as Z_2 with probability p. In a similar fashion, if the person receives Z_2 it will pass it on as Z_2 with probability $(1 - q)$ and modify it to Z_1 with probability q. We summarize

- $\Pr(Z_1 \to Z_1) = (1 - p) = p_{11}$,

- $\Pr(Z_1 \to Z_2) = p = p_{12}$,
- $\Pr(Z_2 \to Z_1) = q = p_{21}$,
- $\Pr(Z_2 \to Z_2) = (1-q) = p_{22}$.

The transition matrix is of the form

$$P = \begin{pmatrix} 1-p & p \\ q & 1-q \end{pmatrix}. \tag{16.80}$$

We note that the two states communicate with each other $Z_1 \leftrightarrow Z_2$, hence the MARKOV-chain is irreducible. Furthermore, since the process can reach either state Z_1 or Z_2 within a single time step, it is clearly aperiodic. Let us briefly investigate the probabilities of first recurrence f_{ii}^n after n steps. Due to the theorem by KOLMOGOROV it is sufficient to investigate the state Z_1 since the MARKOV-chain is irreducible and it follows that also Z_2 has the same recurrence properties. We note the following possible paths for a first return to state Z_1:

- $1: \quad \Pr(Z_1 \to Z_1) = (1-p) = f_{11}^1$,
- $2: \quad \Pr(Z_1 \to Z_2 \to Z_1) = pq = f_{11}^2$,
- $3: \quad \Pr(Z_1 \to Z_2 \to Z_2 \to Z_1) = p(1-q)q = f_{11}^3$,
- $n: \quad \Pr(Z_1 \to Z_2 \to \cdots \to Z_2 \to Z_1) = p(1-q)^{n-2}q = f_{11}^n$.

The probability of returning to Z_1 is, see Eq. (16.69),

$$\begin{aligned} F_1 &= \sum_{n=1}^{\infty} f_{11}^n \\ &= (1-p) + pq \sum_{n=0}^{\infty} (1-q)^n \\ &= (1-p) + pq \frac{1}{1-(1-q)} \\ &= 1, \end{aligned} \tag{16.81}$$

where we employed that $0 < (1-q) < 1$ as well as the convergence of the geometric series. Hence state Z_1 is recurrent and, therefore, also state Z_2 is recurrent. We calculate the expectation value of the first return time $\langle T_1 \rangle$:

$$\begin{aligned} \langle T_1 \rangle &= \sum_{n=1}^{\infty} n f_{11}^n \\ &= (1-p) + pq \sum_{n=0}^{\infty} (n+2)(1-q)^n \end{aligned}$$

$$
\begin{aligned}
&= (1-p) + 2pq \underbrace{\sum_{n=0}^{\infty}(1-q)^n}_{=\frac{1}{q}} + pq \sum_{n=0}^{\infty} n(1-q)^n \\
&= 1 + p - pq(1-q)\frac{d}{dq}\underbrace{\sum_{n=0}^{\infty}(1-q)^n}_{=\frac{1}{q}} \\
&= 1 + p + \frac{p}{q}(1-q) \\
&= \frac{p+q}{q}. \qquad (16.82)
\end{aligned}
$$

Hence, the states Z_1 and Z_2 are positive recurrent as long as $p \neq 0$ and $q \neq 0$. This means that an equilibrium distribution exists and it can be obtained from Eq. (16.73). We have

$$\pi_1 = \frac{1}{\langle T_1 \rangle} = \frac{q}{p+q}. \qquad (16.83)$$

Due to the normalization condition (16.77) we obtain

$$\pi_2 = 1 - \pi_1 = \frac{p}{p+q}, \qquad (16.84)$$

and, therefore,

$$\langle T_2 \rangle = \frac{p+q}{p}. \qquad (16.85)$$

Since all states are positive recurrent and aperiodic, the above MARKOV-chain is ergodic. Finally, we remark that this example also fulfills detailed balance since

$$\pi_1 p_{12} = \frac{qp}{p+q} = \pi_2 p_{21}. \qquad (16.86)$$

Let us briefly interpret this example: Suppose the original, i.e. true version Z_1 of a report is *'Mr. X is going to resign'* while Z_2 is just the opposite, i.e. *'Mr. X is not going to resign'*. The property of irreducibility of the MARKOV-chain reflects the fact that there is no version of the report which cannot be reached or modified. Moreover, we just demonstrated that the process is positive recurrent, i.e. even if the probability p that Z_1 was modified to Z_2 is very small and the probability q that Z_2 was modified to Z_1 is very high, the report will infinitely often return to version Z_2 with probability one. This means that the public will be told infinitely often that Mr. X is *not* going to resign with probability one. The equilibrium probabilities π_1 and π_2 display the asymptotic probability of versions one and two of the report, respectively. However, as has already been emphasized, this does not mean that the report cannot be modified in equilibrium, it simply displays the fact that the probabilities reached a steady state. Finally, we note an interesting effect in passing: Suppose that the probabilities that any of the two versions is modified is very small but equal, i.e. $p = q \ll 1$. Then the equilibrium distribution is

$$\pi_1 = \pi_2 = \frac{1}{2}, \tag{16.87}$$

i.e. the public will believe Z_1 and Z_2 with the same probability after some time independent of the initial version and also independent of the actual decision of Mr. X. Detailed balance expresses the property that the probability of receiving Z_2 and passing it on as Z_1 is the same as the probability of receiving Z_2 and passing it on as Z_1.

We close this section with a final remark: It is an easy task to generalize the ideas of Markov-chains to continuous state spaces since we already introduced the required tools in Sect. 16.3. Let $\pi(x)$ denote the stationary distribution density and $p(x|y)$ the accompanying transition rate pdf. Then relation (16.76) reads

$$\pi(x) = \int \mathrm{d}y \pi(y) p(x|y), \tag{16.88}$$

together with

$$\int \mathrm{d}x \pi(x) = 1, \tag{16.89}$$

the usual normalization of pdfs. In this case, the detailed balance condition reads

$$\pi(x) p(y|x) = \pi(y) p(x|y), \tag{16.90}$$

which is equivalent to Eq. (16.55).

The extension of this discussion to a continuous time span is not as straightforward as the extension to a continuous state span. We will discuss this generalization, i.e. continuous-time Markov-chains, in the following section.

16.5 Continuous-Time Markov-Chains

A continuous-time Markov-chain is a time-homogeneous Markov process on a discrete state space but with a continuous time span, $t \geq 0$. Thus

$$\Pr[X(t+s) = n | X(s) = m] = p_{nm}(t), \tag{16.91}$$

is *independent* of $s \geq 0$. In this case the transition matrix $P(t) = \{p_{ij}(t)\}$ is an explicit function of time t. For its elements $p_{nm}(t)$ we note the following four properties:

(a) All matrix elements $p_{nm}(t)$ of the transition matrix P are positive, i.e.

$$p_{nm}(t) \geq 0, \qquad \forall t > 0. \tag{16.92}$$

(b) Moreover, we have the usual normalization of the rows of the transition matrix P,

$$\sum_m p_{nm}(t) = 1, \qquad \forall n \text{ and } t > 0. \tag{16.93}$$

(c) As for every MARKOV process, the transition matrix of the continuous time MARKOV-chain obeys the CHAPMAN-KOLMOGOROV equation:

$$\sum_k p_{nk}(t)p_{km}(t') = p_{nm}(t+t'), \tag{16.94}$$

which can alternatively be expressed as

$$P(t+t') = P(t)P(t'). \tag{16.95}$$

(d) Furthermore, we assume that $p_{nm}(t)$ is a continuous function of t and that

$$\lim_{t\to 0} p_{nm}(t) = \begin{cases} 1 \text{ for } n = m, \\ 0 \text{ for } n \neq m. \end{cases} \tag{16.96}$$

It follows from Eq. (16.96) that the matrix elements $p_{nm}(t)$ can be written as

$$p_{nm}(t) = \begin{cases} 1 + q_{nn}t + \mathcal{O}(t^2) & \text{for } n = m, \\ q_{nm}t + \mathcal{O}(t^2) & \text{for } n \neq m, \end{cases} \tag{16.97}$$

where we introduced with $\{q_{nm}\} = Q$ the *transition rate matrix*. The transition rate matrix Q obeys:

(a) All off-diagonal elements q_{nm}, $n \neq m$, are non-negative since

$$q_{nm} = \lim_{t\to 0} \frac{p_{nm}(t)}{t} \geq 0 \qquad \text{for } n \neq m. \tag{16.98}$$

(b) All diagonal elements q_{nn} are non-positive since

$$q_{nn} = -\lim_{t\to 0} \frac{1 - p_{nn}(t)}{t} \leq 0. \tag{16.99}$$

(c) Differentiating Eq. (16.93) with respect to t yields that the sum over all elements in a row is equal to zero. Therefore, we conclude

$$q_{nn} = -\sum_{\substack{m \\ n\neq m}} q_{nm}. \tag{16.100}$$

Moreover, differentiating the Chapman-Kolmogorov equation with respect to t or t' gives the Kolmogorov forward—or Kolmogorov backward equations

$$\dot{P}(t) = P(t)Q \qquad \text{and} \qquad \dot{P}(t) = QP(t), \tag{16.101}$$

respectively. We obtain $P(t) = \exp(Qt)$ where the exponential function of a matrix has to be understood in the following way

$$\exp(Qt) = \sum_{k=0}^{\infty} \frac{t^k}{k!} Q^k, \tag{16.102}$$

where $Q^0 = I$ is the identity matrix.

We define s as the time of the first jump of our process for the particular case $X(0) = n$

$$s = \min\left[t | X(t) \neq X(0)\right]. \tag{16.103}$$

It can be shown that $P_n(s > t)$, the probability that the jump occurs at *some* time $s > t$, is given by

$$P_n(s > t) = \exp(q_{nn} t), \tag{16.104}$$

where we note that $q_{nn} \leq 0$. Moreover,

$$P_n[X(s) = m] = -\frac{q_{nm}}{q_{nn}}, \tag{16.105}$$

and the process starts again at time s and in state m. This means that in a continuous-time Markov-chain the waiting times between two consecutive jumps are *exponentially distributed*. One of the simplest examples of a continuous time Markov-chain is the Poisson process as discussed in Sect. 16.3.

Summary

This chapter introduced the concept of stochastic processes $Y_X(t)$ as 'time' dependent processes depending on randomness. Y is a random variable which depends on another random variable X and t the time. All realizations of $Y_X(t)$ span the state space. Each stochastic process is coupled to a pdf which describes the probability that the process takes on the realization y at time t. In the course of this introduction a series of general properties which classify such processes have been defined. This was followed by the discussion of a particular class of stochastic processes, the Markov processes. They have the remarkable property that a future realization of the process solely depends on its current realization and not on the history how this current realization had been reached (Markov property). A huge class of processes in physics and related sciences are Markovian in nature. The next refinement in our discussion was the introduction of MARKOV-chains. These are processes defined on a discrete time span and in a discrete state space. This allowed to replace the pdfs by probabilities. Again, various specific properties of MARKOV-chains opened the possibility of a distinctive classification. A very important observation was that under certain conditions a MARKOV-chain reaches a stationary or equilibrium distribution and it will definitely arrive at this distribution independent of the choice of initial conditions. Moreover, detailed balance is obeyed by this equilibrium condition. This observation is the backbone of MARKOV-chain Monte Carlo sampling methods, in particular of the METROPOLIS algorithm. Finally, continuous-time MARKOV-chains have been discussed with the emphasis on the fact that they are not merely a generalization of discrete-time MARKOV processes.

Problems

1. Write a program to simulate the WIENER process in one dimension. Follow the method explained in Sect. 16.2 and perform the following analysis:
   (a) Illustrate graphically some typical sample paths.
   (b) Calculate the mean $\langle x(t)\rangle$ and the variance $\mathrm{var}[x(t)]$ by restarting the process several times with different seeds and plot the result.
   (c) Measure the position x of the particle at a particular time t for several runs (with different seeds) and illustrate the result $p(x, t)$ graphically.

2. Realize numerically a POISSON process according to the instructions given in Sect. 16.2. Again, plot some typical sample paths. Moreover, calculate the mean waiting time $\langle\tau\rangle$ as well as the variance var (τ) numerically as well as analytically.

References

1. Chow Y.S., Teicher, H.: Probability theory, 3rd edn. Springer Texts in Statistics. Springer, Berlin (1997)
2. van Kampen, N.G.: Stochastic Processes in Physics and Chemistry. Elsevier, Amsterdam (2008)
3. Breuer, H.P., Petruccione, F.: Open Quantum Systems. Clarendon Press, Oxford, UK (2010)

Chapter 17
The Random Walk and Diffusion Theory

17.1 Introduction

Diffusion is one of the most fascinating and widely spread processes in science. Its occurrence ranges from random motion of dust particles on fluid surfaces—which is historically known as Brownian motion—over gradient induced motion of particles in numerous physical systems to the spreading of malaria by migration of mosquitoes or even to the description of fluctuations in stock markets.

For instance, let us regard N neutral, identical, classical particles which solely interact through collisions, e.g. an H_2-gas in a box, where $N = N_A \approx 6.022 \times 10^{23}$. We are interested in the dynamics of one particle under the influence of all others in the particular case of no influence by an external force; we expect that diffusion will be the dominating process. From the microscopic point of view such a situation can be described with the help of N coupled Newtonian equations. Anyhow, such a procedure will not be feasible due to the size of the system, i.e. the magnitude of N. However, a statistical description can be obtained from BOLTZMANN's equation

$$\frac{\mathrm{d}}{\mathrm{d}t} f(r, \eta, t) = \frac{\partial}{\partial t} f(r, \eta, t)\Big|_{\text{coll.}}, \tag{17.1}$$

where $f(r, \eta, t)$ is the phase space distribution function. Hence, $f(r, \eta, t)\mathrm{d}r\mathrm{d}\eta$ is the number of particles within the phase-space volume $\mathrm{d}r\mathrm{d}\eta$ centered around position r at time t and which have a momentum η. In particular, we have

$$\frac{\partial}{\partial t} f(r, \eta, t) + \frac{\eta}{m} \cdot \frac{\partial}{\partial r} f(r, \eta, t) + F \cdot \frac{\partial}{\partial \eta} f(r, \eta, t) = C[f](r, \eta, t), \tag{17.2}$$

where $C[f](r, \eta, t)$ is the collision integral and F describes an external force. In cases where collisions result solely from two-body interactions between particles

B. A. Stickler and E. Schachinger, *Basic Concepts in Computational Physics*,
DOI: 10.1007/978-3-319-02435-6_17, © Springer International Publishing Switzerland 2014

that are assumed to be uncorrelated prior to the collision,[1] the collision integral can be written as

$$C[f](r,\eta,t) = \int d\xi_1 \int d\xi_2 \int d\xi_3 g(\xi_1,\xi_2,\xi_3,\eta)\,[f(r,\xi_1,t)f(r,\xi_2,t) \\ -f(r,\eta,t)f(r,\xi_3,t)]\,. \tag{17.3}$$

Here, $g(\xi_1,\xi_2,\xi_3,\eta)$ accounts for the probability that a collision between two particles with initial momenta ξ_1 and ξ_2 and final momenta ξ_3 and η occurs. This function depends on the particular type of particles under investigation and has, in general, to be determined from a microscopic theory.[2] We now define the particle density $\rho(r,t)$ as a function of space r and time t via

$$\rho(r,t) = \int d\eta f(r,\eta,t). \tag{17.4}$$

A detailed, very complicated and time-consuming mathematical analysis results in a diffusion equation of the well-known form

$$\frac{\partial}{\partial t}\rho(r,t) = D\frac{\partial^2}{\partial r^2}\rho(r,t)\;, \tag{17.5}$$

if collisions dominate the dynamics (*diffusion limit*). Here $D = \text{const}$ is the diffusion coefficient of dimension length$^2\times$ time^{-1}. Note that

$$\int dr\rho(r,t) = N, \tag{17.6}$$

is the number of particles within our system.[3] Thus, in our example we can interpret diffusion as the average evolution of the integrated phase space distribution function governed by collisions between particles. Such an interpretation will certainly not hold in the case of fluctuations in stock markets or in the case of the spreading of malaria because typically mosquitoes do not *collide* with humans.

It is the aim of the first part of this chapter to present a purely stochastic approach to diffusion, the so called *random walk* model. This stochastic description will prove to have several precious advantages: (i) We will be able to identify criteria for the validity of the diffusion model even for systems lacking a straight-forward physical

[1] This assumption is known as the approximation of *molecular chaos*. In fact it represents the MARKOV approximation to the dynamics of a many particle system.

[2] For instance, one can employ FERMI's golden rule to obtain this function on a quantum mechanical level. We already came across an expression of the form (17.3) on the right hand side of the master equation, see Sect. 16.3, Eq. (16.44).

[3] The function $\rho(r,t)$ is referred to as a *physical distribution function* due to the normalization condition (17.6). This is in contrast to distribution functions we encountered so far within this book, which are normalized to unity.

interpretation. (ii) The stochastic formulation will give us the opportunity to perform diffusion 'experiments' on the computer without much computational effort. The methods employed are based on algorithms discussed in previous chapters. (iii) Within this framework it will be an easy task to generalize the approach to stochastic models of anomalous diffusion, i.e. the *fractal time random walk* and the LÉVY *flight* models. These models play an increasingly important role in modern statistical physics.

We conclude this introduction with a quote from a review article by E. W. MONTROLL and M. F. SCHLESINGER [1]:

Since traveling was onerous (and expensive), and eating, hunting and wenching generally did not fill the seventeenth century gentleman's day, two possibilities remained to occupy the empty hours, praying and gambling; many preferred the latter.

17.2 The Random Walk

The random walk is one of the classical examples of MARKOV-chains. Its application ranges from economics,[4] genetics, foraging behavior of animals, polymer dynamics to Brownian motion, i.e. the random motion of dust particles on a fluid surface, brain research (neuron dynamics), and many more. In this section we will discuss some of the basic properties of random walks in one dimension. For convenience, we will use the familiar picture of one diffusing particle.

Basics

We define the random walk process:We regard a single particle which moves at time instances

$$0, \Delta t, 2\Delta t, \dots, n\Delta t, \dots, \tag{17.7}$$

between grid-points

$$\dots, -n\Delta x, \dots, -\Delta x, 0, \Delta x, \dots, n\Delta x, \dots\ . \tag{17.8}$$

In what follows the lattice point $n\Delta x$ will be denoted by x_n, where $n \in \mathbb{Z}$ and the instance $k\Delta t$ will be denoted by t_k where $k \in \mathbb{N}_0$, following the conventions of Chap. 2. The initial position is given by

$$\Pr[X(t_0 = 0) = x_i] = \delta_{i0}, \tag{17.9}$$

[4] The assumption that stock fluctuations can be described by a random walk is known as the *random walk hypothesis.*

and the transition rates p_{ij} from position i to position j within a single time step Δt are defined as

$$\Pr[X(t_{n+1}) = x_i | X(t_n) = x_j] = p\delta_{ji-1} + q\delta_{ji+1} + r\delta_{ij} \; . \tag{17.10}$$

Here p denotes the probability that the particle jumps to the neighboring grid-point on the right-hand side, q stands for the probability that the particle jumps to the neighboring grid-point on the left-hand side, and r denotes the probability of staying at the same-grid point within this time step. Naturally, we have

$$p + q + r = 1 \; . \tag{17.11}$$

Consequently, we have a MARKOV-chain with time instances t_n and a state space spanned by the positions x_k. Moreover, we note that the stochastic process is clearly irreducible since all states communicate with each other. Hence, it follows that either all states are recurrent or all states are transient. Furthermore, in the case that $r \neq 0$ the MARKOV-chain is aperiodic, otherwise, if $r = 0$ the chain is periodic with periodicity $d = 2$ because it takes at least two steps to return to the starting position.

We concentrate first on the *classical random walk*, that is a one-dimensional random walk with $\Delta t = \Delta x = 1$, $r = 0$ and $p + q = 1$, i.e. the probability of remaining in the actual position within one time step is equal to zero. If, furthermore, $p = q = 1/2$ the random walk is referred to as *unbiased* for $p \neq q$ we call it *biased*. We write the position $X(t_n) = x_n$ at time $t_n = n$ as

$$x_n = \sum_{i=1}^{n} \xi_i , \tag{17.12}$$

where $\xi_i \in \{-1, 1\}$ and $\Pr(\xi_i = +1) = p$, $\Pr(\xi_i = -1) = q$. Let us assume that within these n steps the particle moved m times to the right and, consequently, $n - m$ times to the left. The actual position x_n after n steps can then be described by

$$x_n = m - (n - m) = 2m - n \equiv k , \tag{17.13}$$

where we used that $x_0 = 0$. It is interesting to calculate the probability $\Pr(x_n = k)$ to find the particle after n time steps at some particular position k. This is simply the sum over all paths along which the particle moved $m = (n + k)/2$ times to the right and $n - m = (n - k)/2$ times to the left multiplied by the probability for m steps to the right and $n - m$ steps to the left. In total, this yields $\binom{n}{m} = \binom{n}{(n+k)/2}$ different contributions and we have

$$\begin{aligned} \Pr(x_n = k) &= \binom{n}{m} p^m q^{n-m} \\ &= \binom{n}{(n + k)/2} p^{\frac{n+k}{2}} q^{\frac{n-k}{2}} \; . \end{aligned} \tag{17.14}$$

In particular, we have for the unbiased random walk:

$$\Pr(x_n = k) = \binom{n}{(n+k)/2}\left(\frac{1}{2}\right)^n . \tag{17.15}$$

First of all, we note that due to the aperiodicity of the classical random walk, k can only take on the values $k = -n, -n+2, \ldots, n-2, n$, i.e. $n \pm k$ has to be even. For all other k we have $\Pr(x_n = k) = 0$. Furthermore,

$$\begin{aligned}\sum_{\substack{k=-n\\ n\pm k \text{ even}}}^{n} \Pr(x_n = k) &= \sum_{m=0}^{n}\binom{n}{m}p^m q^{n-m}\\ &= (p+q)^n\\ &= 1,\end{aligned} \tag{17.16}$$

and the probability of finding the particle at time n within $[-n, n]$ is equal to one. A simple algorithm to simulate the one-dimensional biased random walk consists of the following steps:

1. Define values x_0, p and $q = 1 - p$.
2. Draw a random number $r \in [0, 1]$.
3. If $r < p$ we set $x_{n+1} = x_n + 1$,
4. otherwise we set $x_{n+1} = x_n - 1$.
5. Return to step 2.

In Fig. 17.1 we present three different realizations of an unbiased one-dimensional random walk for (a) $N = 50$, (b) $N = 100$, and (c) $N = 1000$ consecutive steps.

Comparison between Figs. 17.1 and 16.2 already suggests a connection between the random walk and the WIENER process, however, we shall come back to this point in the course of this chapter.

Moments

Let us briefly elaborate on the moments of the random walk. The first moment or expectation value $\langle x_n\rangle$ is given by

$$\begin{aligned}\langle x(t_n)\rangle &= \sum_{\substack{k=-n\\ n\pm k \text{ even}}}^{n} k\binom{n}{(n+k)/2}p^{(n+k)/2}q^{(n-k)/2}\\ &= \sum_{m=0}^{n}(2m-n)\binom{n}{m}p^m q^{n-m}\\ &= (2\langle m\rangle - n)\\ &= n(2p-1).\end{aligned} \tag{17.17}$$

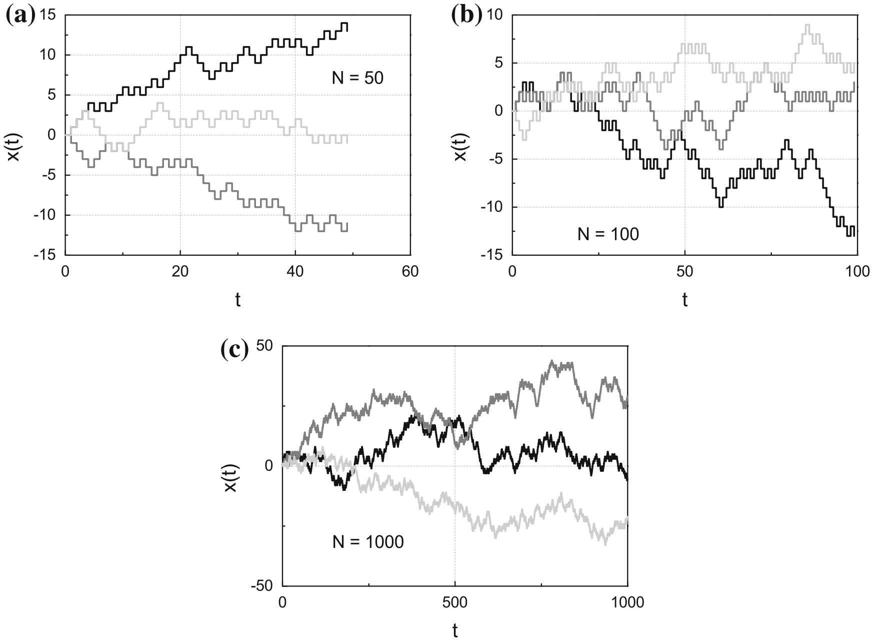

Fig. 17.1 Three different realizations of an unbiased one-dimensional random walk for (**a**) $N = 50$, (**b**) $N = 100$, and (**c**) $N = 1000$ time steps and different seeds

We now introduce the *bias* v such that

$$p = \frac{1}{2}(1 + v) \quad \text{and} \quad q = \frac{1}{2}(1 - v), \tag{17.18}$$

and obtain

$$\langle x_n \rangle = nv. \tag{17.19}$$

We calculate the second moment $\left\langle x_n^2 \right\rangle$ using the same method and get:

$$\left\langle x_n^2 \right\rangle = n(1 - v^2) + n^2 v^2. \tag{17.20}$$

From this, the variance var (x_n) follows immediately:

$$\text{var}\,(x_n) = \left\langle x_n^2 \right\rangle - \langle x_n \rangle^2 = n(1 - v^2). \tag{17.21}$$

We note the following: The expectation value $\langle x_n \rangle$ moves according to Eq. (17.19) with a uniform velocity defined by the bias $v = p - q$. In particular, for the unbiased random walk $v = 0$ and, thus, $\langle x_n \rangle = 0$ for all n. Furthermore, we observe that var (x_n) increases linearly with time n—a property we already noted for the WIENER process in Sect. 16.3—and it is maximal for $v = 0$. For $v = \pm 1$, which describes a pure drift motion in the positive or negative x direction, the variance is equal to zero.

Recurrence

Let us briefly investigate the recurrence behavior of the random walk. We are interested in the probability $f_{00}^{(2\ell)}$ of a first return to the origin $x_0 = 0$ after 2ℓ steps. We already know that $f_{00}^{(2\ell)} \propto p^\ell q^\ell$ from our previous analysis. In the very first time step the particle moves either to $x_1 = 1$ or to $x_1 = -1$ and, consequently, within the following $2\ell - 2$ steps it must not cross or touch the line $x_k = 0$ and the particle has to terminate at position $x_{2\ell-1} = x_1$. Therefore, the walker performs $\ell - 1$ steps to the left and $\ell - 1$ steps to the right within these $2\ell - 2$ steps. The total number of possible paths N from x_1 to $x_{2\ell-1} = x_1$ is given by

$$N = \binom{2\ell - 2}{\ell - 1} . \tag{17.22}$$

Moreover, N may also be written as the sum of the number N_c of paths which cross or touch the line $x_k = 0$ and the number N_{nc} of paths which do not cross or touch the line $x_k = 0$, i.e.

$$N = N_c + N_{nc}. \tag{17.23}$$

Obviously, we are only interested in the paths which do not cross or touch the line $x_k = 0$. We employ the reflection principle to solve this problem. In general, the number of paths which go from $x_1 = i > 0$ to $x_{k+1} = j > 0$ within k-steps and cross the line $x_\ell = 0$ is equal to the total number of paths which go from $x_1 = -i$ to $x_{k+1} = j$, as is schematically illustrated in Fig. 17.2.

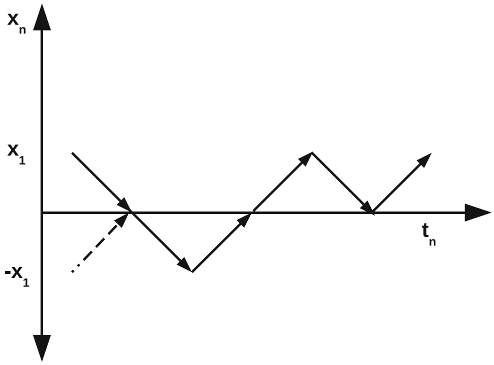

Fig. 17.2 Illustration of the reflection principle

Let us regard the case $x_1 = 1$, i.e. the walker moved in the first step to the right. Hence, from the reflection principle we obtain that the number of paths from x_1 to $x_{2\ell-2} = x_1$ in $2\ell - 2$ steps which cross or touch the line $x_k = 0$ is given by the total number of paths from $-x_1$ to $x_{2\ell-2} = x_1$, i.e.

$$N_c = \binom{2\ell - 2}{\ell}. \tag{17.24}$$

We note that in this picture, the walker moves ℓ steps to the right and $\ell - 2$ steps to the left. Hence, we obtain that the number of paths which do not cross or touch the line $x_k = 0$ is given by

$$2N_{nc} = 2(N - N_c) = \frac{1}{2\ell - 1}\binom{2\ell}{\ell}. \tag{17.25}$$

The prefactor 2 accounts for the fact that the walker can move in its first step either to $x_1 = -1$ or to $x_1 = 1$. Thus, the probability for the first return of the particle after 2ℓ steps is described by:

$$f_{00}^{(2\ell)} = \frac{1}{2\ell - 1}\binom{2\ell}{\ell} p^\ell q^\ell. \tag{17.26}$$

We calculate the recurrence probability according to Eq. (16.69) and this results in

$$\sum_{\ell=0}^{\infty} f_{00}^{(2\ell)} = \begin{cases} 1 & \text{for } p = q = \frac{1}{2}, \\ 2p & \text{for } p < q, \\ 2q & \text{for } p > q, \end{cases} \tag{17.27}$$

with the consequence that the one-dimensional random walk is only recurrent in the unbiased case $v = 0$.

Another possibility to demonstrate the recurrence of the unbiased one-dimensional random walk is provided by Eq. (16.72). The probability that a walker returns to $x_0 = 0$ after $2n$ steps is given by

$$P^{(2n)}(x_0) = \binom{2n}{n} p^n q^n = \frac{(2n)!}{n!n!}(pq)^n. \tag{17.28}$$

In this case we are not interested in the question whether or not it is the particle's first return. By STIRLING's approximation, see Appendix D, we approximate

$$n! \propto n^{n+\frac{1}{2}} e^{-n}\sqrt{2\pi}, \tag{17.29}$$

and obtain for $P^{(2n)}(x_0)$

$$P^{(2n)}(x_0) \propto \frac{(4pq)^n}{\sqrt{n\pi}}. \tag{17.30}$$

We assume $p \leq \frac{1}{2}$ and since $pq = p(1-p) = p - p^2 \leq \frac{1}{2} - \frac{1}{4} = \frac{1}{4}$ where the equality holds for $p = q = \frac{1}{2}$, and obtain

$$\sum_{n=0}^{\infty} P^{(2n)}(x_0) \to \infty \quad \text{only for} \quad p = q = \frac{1}{2}. \tag{17.31}$$

The same argument holds for $p > \frac{1}{2}$ since we can write $pq = q - q^2 \leq \ldots$. According to (16.72) this means that the process is recurrent only for $p = q$, in accordance with our previous result (17.27), and transient otherwise. We note that this result agrees with the physical picture of an external force inducing a bias or *drift* velocity $v \neq 0$.

It should be noted that the unbiased random walk in two dimensions is also recurrent while it can be proved to be transient in higher dimensions. In 3D, for instance, the recurrence probability is approximately 0.34.

17.3 The Wiener Process and Brownian Motion

It is the purpose of this section to demonstrate that the Wiener process is the scaling limit of the random walk. Moreover, we shall briefly discuss the Langevin equation and derive the diffusion equation.

As a starting point we consider the one-dimensional unbiased random walk on an equally spaced grid according to Eq. (17.8) and time instances given by Eq. (17.7). We denote the stochastic process by $X_n = X(t_n)$ and have

$$X_n = \sum_{i=1}^{n} \xi_i \Delta x, \tag{17.32}$$

where $\xi \in \{-1, 1\}$ together with $X_0 = 0$. Since we regard the unbiased case we have $\Pr(\xi_i = \pm 1) = 1/2$, $\langle \xi_i \rangle = 0$, and $\mathrm{var}\,(\xi_i) = 1$. This is equivalent to

$$\langle X_n \rangle = 0 \quad \text{and} \quad \mathrm{var}\,(X_n) = n \Delta x^2, \tag{17.33}$$

as we already demonstrated in the previous section, Eq. (17.21). The variance $\mathrm{var}\,(X_n)$ can be rewritten using the definition $t_n \equiv n\Delta t$ as:

$$\mathrm{var}\,(X_n) = t_n \frac{\Delta x^2}{\Delta t}. \tag{17.34}$$

We would now like to perform the simultaneous limit $\Delta t, \Delta x \to 0$ in such a way, that

$$\lim_{\substack{\Delta t\to 0\\ \Delta x\to 0}} \frac{\Delta x^2}{\Delta t} = D = \text{const}, \tag{17.35}$$

is the diffusion coefficient D. This limit is known as the *continuous limit* and will in the following be denoted by the operator $\mathscr{L}$. Hence, in the continuous limit we have

$$\mathscr{L}\left[\text{var}\left(X_n\right)\right] = Dt, \tag{17.36}$$

where we renamed $t_n = t$. We note that the limit $\Delta t \to 0$ for constant t is equivalent to $n \to \infty$. Therefore, we obtain in accordance with the central limit theorem

$$\mathscr{L}\left(X_n\right) \to W_t \sim \mathscr{N}(0, Dt), \tag{17.37}$$

where $\mathscr{N}(0, Dt)$ denotes the normal distribution of mean zero and variance Dt, see Appendix D. We introduced, furthermore, the symbol W_t to represent the WIENER process and, finally, the symbol $\sim$ which stands, within this context, for the notion *follows the distribution*. In order to demonstrate that W_t is indeed the WIENER process, we have to prove that W_t has independent increments $W_{t_2} - W_{t_1}$ which follow, according to Chap. 16, a normal distribution with mean zero and a variance proportional to $t_2 - t_1$. This is easily demonstrated: From the random walk we know that

$$X_n - X_m = \sum_{i=1}^{n} \xi_i - \sum_{i=1}^{m} \xi_i = \sum_{i=m+1}^{n} \xi_i, \tag{17.38}$$

and, therefore, $X_n - X_m$ and $X_m - X_k$ are clearly independent for $n > m > k$ and it follows that also $W_t - W_s$ and $W_s - W_u$ are independent. Furthermore, we have

$$X_n - X_m \overset{d}{=} X_{n-m}, \tag{17.39}$$

where the symbol $\overset{d}{=}$ stands for the notion *to follow the same distribution* or *to be distributionally equivalent*. Therefore, in the limit $\mathscr{L}$ for $t > s$

$$W_t - W_s \overset{d}{=} W_{t-s} \sim \mathscr{N}\left[0, D(t-s)\right] \ , \tag{17.40}$$

which completes the proof. We note that the particular case $D = 1$ is commonly referred to as the *standard* WIENER *process*. We remark that in many cases the terms WIENER process and Brownian motion are used as synonyms for a stochastic process satisfying the above properties. However, strictly speaking, the stochastic process is the WIENER process while Brownian motion is the physical phenomenon which can be described by the WIENER process.

If we suppose that $p \neq q$, i.e.

$$\mathscr{L}\left(\langle X_n \rangle\right) = \mu t, \tag{17.41}$$

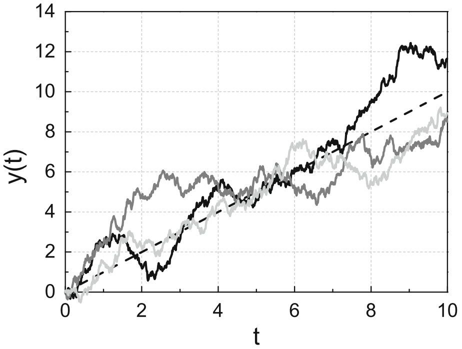

Fig. 17.3 Three different realizations of the standard WIENER process with drift $\mu = 1$ according to Eq. (17.42). The expectation value $\langle x \rangle = \mu t$ of the process is presented as a *dashed line*

with the drift constant μ, a WIENER process with a drift term

$$\mathscr{L}(X_n) \to \tilde{W}_t = \mu t + W_t, \tag{17.42}$$

is described. This process behaves like W_t with the only difference that it fluctuates around mean μt instead of mean zero. Note that for $\mu > 0$ the mean $\left\langle \tilde{W}_t \right\rangle$ increases, while for $\mu < 0$ it decreases with time t.

Another interesting property of the WIENER process is its *self-similarity*. In particular, we have the property that for $\alpha > 0$

$$W_t \stackrel{d}{=} \alpha^{-\frac{1}{2}} W_{\alpha t}, \tag{17.43}$$

with the consequence that it is completely sufficient to study the properties of the WIENER process for $t \in [0, 1]$ to know its properties for arbitrary time intervals. Relation (17.43) follows from the fact that $W_t \sim \mathscr{N}(0, Dt)$.

Furthermore, *white noise*, $\eta(t)$, is defined as the formal derivative of the WIENER process W_t with respect to time. We give its most important properties without going into details[5]:

$$\langle \eta(t) \rangle = 0, \quad \text{and} \quad \langle \eta(t)\eta(s) \rangle = \delta(t - s). \tag{17.44}$$

White noise is referred to as *Gaussian white noise* if $\eta(t)$ follows a normal distribution.

Figure 17.3 presents three different realizations of the standard WIENER process with drift according to Eq. (17.42).

[5] In fact, it can be shown that W_t is non-differentiable with probability one. This is the reason why it is defined as the *formal* derivative of W_t. Let $\varphi(t)$ be a test function and $f(t)$ an arbitrary function which does not need to be differentiable with respect to t. Then the formal derivative $\dot{f}(t)$ is defined by

$$\int_0^\infty \mathrm{d}t\; \dot{f}(t)\varphi(t) = -\int_0^\infty \mathrm{d}t\; f(t)\dot{\varphi}(t).$$

Let us briefly derive the diffusion equation from the random walk model. The probability $\Pr(x,t)$ of finding the particle at time t at position x can be expressed by

$$\begin{aligned}\Pr(x,t) &= \Pr(x,t-\Delta t)r + \Pr(x-\Delta x,t-\Delta t)p \\ &\quad + \Pr(x+\Delta x,t-\Delta t)q \qquad (17.45)\\ &= \Pr(x,t-\Delta t)(1-p-q) + \Pr(x-\Delta x,t-\Delta t)p \\ &\quad + \Pr(x+\Delta x,t-\Delta t)q, \qquad (17.46)\end{aligned}$$

i.e. the probability of being at point x at time t is the same as the probability of being at time $t-\Delta t$ either at point x and remaining there, or at point $x-\Delta x$ and moving one step to the right, or at point $x+\Delta x$ and moving one step to the left. Expanding each term in a Taylor series up to order $\mathscr{O}(\Delta x^2)$ and $\mathscr{O}(\Delta t)$, respectively, yields

$$\begin{aligned}p(x,t) &= (1-p-q)\Big[p(x,t) - \Delta t\frac{\partial p(x,t)}{\partial t}\Big] \\ &\quad + p\Big[p(x,t) - \Delta t\frac{\partial p(x,t)}{\partial t} - \Delta x\frac{\partial p(x,t)}{\partial x} \\ &\quad + \frac{1}{2}\Delta x^2\frac{\partial^2 p(x,t)}{\partial x^2}\Big] \\ &\quad + q\Big[p(x,t) - \Delta t\frac{\partial p(x,t)}{\partial t} + \Delta x\frac{\partial p(x,t)}{\partial x} \\ &\quad + \frac{1}{2}\Delta x^2\frac{\partial^2 p(x,t)}{\partial x^2}\Big]. \qquad (17.47)\end{aligned}$$

Note that we replaced the probabilities $\Pr(\cdot)$ by the pdfs $p(\cdot)$ because we switched from a discrete to a continuous state space. From Eq. (17.47) we obtain

$$\frac{\partial p(x,t)}{\partial t} = -\frac{(p-q)\Delta x}{\Delta t}\frac{\partial p(x,t)}{\partial x} + \frac{(p+q)\Delta x^2}{2\Delta t}\frac{\partial^2 p(x,t)}{\partial x^2}. \qquad (17.48)$$

We draw the continuous limit and define the drift constant

$$\mu = \mathscr{L}\left[(p-q)\frac{\Delta x}{\Delta t}\right] = \lim_{\substack{\Delta t\to 0\\ \Delta x\to 0}}\frac{(q-p)}{\Delta t}\Delta x, \qquad (17.49)$$

the diffusion constant

$$D = \mathscr{L}\left[(p+q)\frac{\Delta x^2}{2\Delta t}\right] = \lim_{\substack{\Delta t\to 0\\ \Delta x\to 0}}\frac{(p+q)}{2\Delta t}\Delta x^2, \qquad (17.50)$$

and arrive at the one-dimensional diffusion equation with drift term:

$$\frac{\partial p(x,t)}{\partial t} = \mu\frac{\partial p(x,t)}{\partial x} + D\frac{\partial^2 p(x,t)}{\partial x^2}. \qquad (17.51)$$

This equation is referred to as a Fokker-Planck equation. In the specific case $p = q$ the drift term disappears and we obtain, as expected, the classical diffusion equation

$$\frac{\partial}{\partial t} p(x, t) = D \frac{\partial^2}{\partial x^2} p(x, t), \tag{17.52}$$

which we solved already numerically in Chaps. 9 and 11. It follows from this discussion that the position of a diffusing particle can be described as a stochastic process where, in the continuous limit, the jump-lengths follow a normal distribution. Moreover, we know from our discussion of continuous-time Markov-chains in Sect. 16.5, that the waiting times between two successive jumps will certainly follow an exponential distribution. These insights will serve as a starting point in the discussion of general diffusion models in Sect. 17.4. Moreover, we note that the anisotropy of the jump-length distribution is a model for the presence of an external field which manifests itself in a drift term.

A completely different approach to the formal description of Brownian motion goes back to Langevin. He considered the classical equation of motion of a particle in a fluid which reads

$$\dot{v} = -\beta v, \tag{17.53}$$

where β denotes the friction coefficient and we set the particle's mass m equal to one. Langevin argued that this equation may only be valid for the average motion of the particle, i.e. the long time behavior or the motion of massive particles. However, if the particle is not heavy at all its trajectory may be highly affected by collisions with solvent's molecules. He supposed that a reasonable generalization of Eq. (17.53) should be of the form

$$\dot{v} = -\beta v + F(t), \tag{17.54}$$

where $F(t)$ is a *randomforce*. In particular, $F(t)$ is a stochastic process which satisfies

$$\langle F(t) \rangle = 0 \quad \text{and} \quad \langle F(t) F(s) \rangle = A\delta(t - t'), \tag{17.55}$$

where A is a constant and we obtain

$$F(t) \overset{d}{=} \sqrt{A}\eta(t). \tag{17.56}$$

Equation (17.54) is referred to as the Langevin equation and it is *the* prototype *stochastic differential equation*. From the definition of white noise $\eta(t)$ we note that we can rewrite the Langevin equation as

$$\mathrm{d}v \ = -\beta v \mathrm{d}t \ + \sqrt{A} \mathrm{d}W_t \,. \tag{17.57}$$

The solution of the Langevin equation describes a stochastic process referred to as the Ornstein–Uhlenbeck *process*. This process is essentially the only stochastic process which is stationary, Gaussian and Markovian. Its master equation is a

FOKKER-PLANCK equation of the form

$$\frac{\partial}{\partial t} p(v,t) = \beta \frac{\partial}{\partial v} v p(v,t) + \frac{A}{2} \frac{\partial^2}{\partial v^2} p(v,t), \tag{17.58}$$

where $p(v,t)$ is the pdf of the ORNSTEIN–UHLENBECK process. If the initial velocity v_0 is given then the pdf $p(v,t)$ can proved to be defined by:

$$p(v,t) = \frac{\sqrt{\beta}}{\sqrt{\pi A \left(1 - e^{-2\beta t}\right)}} \exp\left[-\frac{\beta \left(v - v_0 e^{-\beta t}\right)^2}{A \left(1 - e^{-2\beta t}\right)} \right]. \tag{17.59}$$

The LANGEVIN Eq. (17.54) can be solved analytically and one obtains

$$v(t) = v_0 \exp\left(-\beta t\right) + \sqrt{A} \int_0^t \mathrm{d}t' \, \eta(t') \exp\left[-\beta(t - t')\right]. \tag{17.60}$$

In particular, we can write

$$v(t_{n+1}) = v(t_n) \exp\left(-\beta \Delta t\right) + Z_n, \tag{17.61}$$

where we defined Z_n as

$$Z_n = \sqrt{A} \int_0^{\Delta t} \mathrm{d}t' \, \eta(t_n + t') \exp\left[-\beta(\Delta t - t')\right]. \tag{17.62}$$

Since $\eta(t)$ was assumed to be Gaussian white noise, Z_n can be proved to be described by

$$Z_n \sim \mathcal{N}\left\{0, \frac{A}{2\beta}\left[1 - \exp\left(-2\beta \Delta t\right)\right]\right\}, \tag{17.63}$$

which offers a very convenient way to simulate the ORNSTEIN–UHLENBECK process. This particular formulation of Brownian motion allows to model this process by sampling changes in the velocity Z_n from the normal distribution with mean zero and the variance given in Eq. (17.63). The walker's position $x(t)$ can then be obtained by approximating the velocity $v = \dot{x}$ with the help of finite difference derivatives, as described in Chap. 2. In conclusion we remark that although the LANGEVIN equation was introduced in a heuristic manner, it represents a very useful tool due to its rather simple interpretation.

In Fig. 17.4 we show three different realizations of the ORNSTEIN–UHLENBECK process corresponding to three different initial velocities v_0. The corresponding random trajectories of the Brownian particle are illustrated in Fig. 17.5.

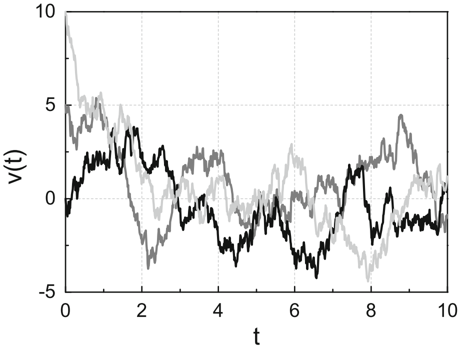

Fig. 17.4 Three different realizations of the ORNSTEIN-- UHLENBECK process. For this simulation we chose $\beta = 1$, $A = 5$, $\mathrm{d}t = 10^{-2}$ and $N = 10^3$ time steps. Furthermore, we chose three different initial velocities, i.e. $v_0 = 0$ (*black*), $v_0 = 5$ (*gray*) and $v_0 = 10$ (*light gray*)

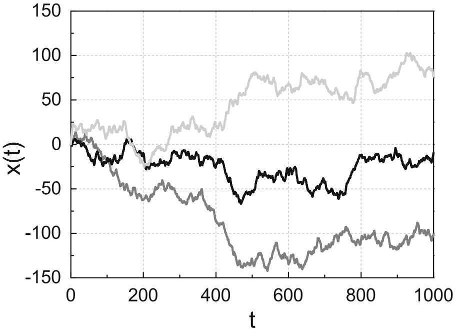

Fig. 17.5 Random trajectories of the Brownian particle corresponding to the velocities illustrated in Fig. 17.4 with initial position $x_0 = 0$. Note that we used for this figure $N = 10^5$ time steps

17.4 Generalized Diffusion Models

We formulate now a very general approach to diffusive behavior which is based on continuous random variables. We start with the introduction of the pdf $\Lambda(x, t)$. Its purpose is to describe the event that a particle arrives at time t at position x. It can be expressed as [2]

$$\Lambda(x, t) = \int \mathrm{d}x \int_0^t \mathrm{d}t' \Psi(x, t; x', t') \Lambda(x', t'), \tag{17.64}$$

where $\Psi(x, t; x', t')$ is the *jump pdf*. It can be understood in the following way: $\Psi(x, t; x', t')$ describes the probability for an event that a particle which arrived at time t' at position x'—with pdf $\Lambda(x', t')$—waited at position x' until the time t was reached and then jumped within an infinitesimal time interval from position x' to x. If we regard a space and time homogeneous process, we can replace $\Psi(x, t; x', t')$ by $\Psi(x - x', t - t')$. This allows us to introduce a jump length pdf $p(x)$ and a waiting time pdf $q(t)$. They are related to the jump pdf by

$$p(x) = \int_0^\infty \mathrm{d}t' \Psi(x, t') \quad \text{and} \quad q(t) = \int_{-\infty}^\infty \mathrm{d}x' \Psi(x', t). \tag{17.65}$$

If the jump length pdf and the waiting time pdf are conditionally independent one can simply write $\Psi(x, t) = p(x)q(t)$. The probability $\varphi(x, t)$ of finding a particle at position x at time t is, furthermore, given by

$$\varphi(x, t) = \int_0^t \mathrm{d}t' \Lambda(x, t') \Psi(t - t'), \tag{17.66}$$

where $\Psi(t)$ is the probability, that a particle stayed at least for a time interval t at the same position, i.e.

$$\Psi(t) = 1 - \int_0^t \mathrm{d}t' q(t - t'). \tag{17.67}$$

Finally, the jump length variance Σ^2 and the characteristic waiting time T are given by

$$\Sigma^2 = \int_{-\infty}^\infty \mathrm{d}x' x'^2 p(x') \quad \text{and} \quad T = \int_0^\infty \mathrm{d}t' t' q(t'). \tag{17.68}$$

Our discussion of the WIENER process in the previous section allowed us to conclude that for Brownian motion the jump length pdf is a Gaussian and the waiting time pdf is an exponential distribution, i.e.

$$p(x) = \frac{1}{\sqrt{2\pi\Sigma^2}} \exp\left(-\frac{x^2}{2\Sigma^2}\right) \quad \text{and} \quad q(t) = \frac{1}{T} \exp\left(-\frac{t}{T}\right). \tag{17.69}$$

The characteristic function, see Appendix D, of the waiting time pdf $q(t)$ is given by

$$\hat{q}(s) = \int_0^\infty \mathrm{d}t q(t) e^{-st} = \frac{1}{T} \frac{1}{s - \frac{1}{T}} = \frac{1}{1 + sT}, \tag{17.70}$$

and we find for the jump length pdf $p(x)$:

$$\hat{p}(k) = \int \mathrm{d}x e^{-ikx} p(x) = \exp\left(-\sigma^2 k^2\right). \tag{17.71}$$

Here we defined $\Sigma^2 \equiv 2\sigma^2$. For $x, t \to \infty$, i.e. $k,\ s \to 0$, the characteristic functions $\hat{q}(s)$ and $\hat{p}(k)$ develop the asymptotic behavior

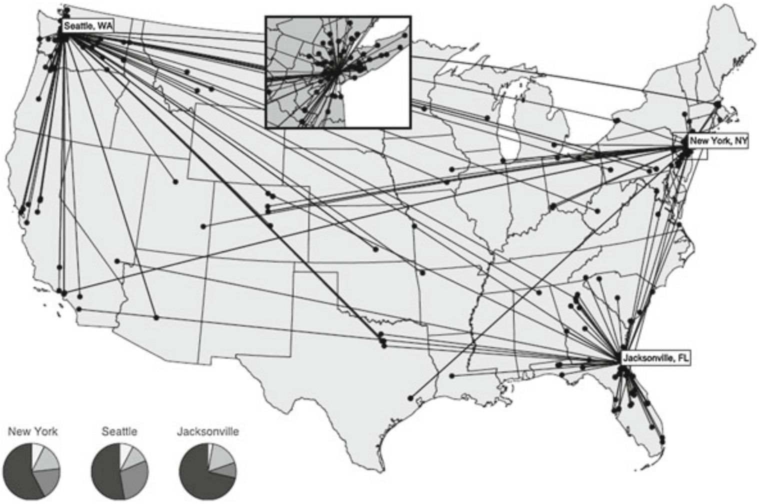

Fig. 17.6 Travelling behavior of humans. Adapted from [3]. Copyright © 2006, Rights Managed by Nature Publishing Group

$$\lim_{s\to 0} \frac{1}{1+sT} \approx 1 - sT + \mathscr{O}(s^2), \tag{17.72}$$

and

$$\lim_{k\to 0} \exp\left(-\sigma^2 k^2\right) \approx 1 - \sigma^2 k^2 + \mathscr{O}(k^4). \tag{17.73}$$

In fact, it can be shown that any pair of jump length and waiting time pdfs lead to the same asymptotic behavior in first order, i.e. $\mathscr{O}(T)$ and $\mathscr{O}(\sigma^2)$, as long as the moments T and Σ^2 exist.

However, there is a variety of processes which cannot be accounted for within the basic framework of Brownian motion. Such processes are described within the concept of anomalous diffusion. Examples for such a behavior are, for instance, the foraging behavior of spider monkeys, particle trajectories in a rotating flow, diffusion of proteins across cell membranes, diffusion of tracers in polymer-like breakable micelles, the traveling behavior of humans, see Fig. 17.6 which was adapted from [3], charge carrier transport in disordered organic molecules, etc.

In what follows, we plan to concentrate on two different models of anomalous diffusion. The first model can, from a qualitative point of view, be characterized as a diffusion process which consists of small clustering jumps which are intersected by very long *flights*. Such behavior is, for instance, encountered in the context of human travel behavior, see Fig. 17.6, charge carrier transport in disordered solids, etc. The incorporation of these long jumps on a stochastic level is referred to as Lévy *flight*.

The second model, which is referred to as the *fractal time random walk*[6] incorporates anomalously long waiting times between two successive jumps. In particular, these long waiting times account for non-Markovian effects which could be due to, for instance, trapping processes of charge carriers in disordered solids. It has to be emphasized at this point that the resulting diffusion models are still linear in the pdf $\varphi(x,t)$. The inclusion of non-linear effects will not be discussed here, however, can be achieved within the framework of *non-extensive thermodynamics* formulated by C. TSALLIS [4], an immediate application was reported by [5].

Let us start our discussion with LÉVY flights. In this case one modifies the asymptotic behavior of the characteristic function of the jump length pdf according to

$$\hat{p}(k) \propto 1 - (\sigma |k|)^{\alpha}, \tag{17.74}$$

where $\alpha \in (0,2]$. We recognize that this is the asymptotic behavior $|k| \to 0$ of the characteristic function of a symmetric LÉVY α-stable distribution following Eq. (D.75) of Appendix D. In the limit $\alpha \to 2$ normal, i.e. Gaussian behavior is recovered. Such a characteristic function corresponds to a jump length pdf of the form

$$p(x) \propto |x|^{-\alpha-1} \qquad \text{for} \qquad |x| \to \infty, \tag{17.75}$$

according to Eq. (D.76). A jump-length pdf of this form is commonly referred to as a *fat-tailed jump length pdf* due its asymptotic behavior.

A LÉVY flight is, in principle, a random walk where the length of the jumps at discrete time instances t_n follow the pdf (17.75). In the continuous time limit, the waiting times are distributed exponentially as was illustrated in Sect. 16.5. It has to be noted that in such a case the jump length variance diverges, i.e. $\Sigma^2 \to \infty$, consequently, LÉVY stable distributions are *not* subject to the central limit theorem. In particular, the distance from the origin after some finite time t follows a LÉVY stable distribution. Moreover, we note that if $0 < \alpha < 1$ even the mean jump length $\langle x \rangle$ diverges. A detailed mathematical analysis proves, that Lévy flights result in a diffusion equation of the form

$$\frac{\partial}{\partial t} p(x,t) = D_{\alpha} \mathcal{D}^{\alpha}_{|x|} p(x,t), \tag{17.76}$$

where D_{α} is the fractional diffusion coefficient of dimension length$^{\alpha}$ × time^{-1} and $\mathscr{D}^{\alpha}_{|x|}$ is the symmetric RIESZ fractional derivative operator of order $\alpha \in (1,2)$[7]:

$$\mathscr{D}^{\alpha}_{|x|} f(x) = \frac{1}{2\Gamma(2-\alpha)\cos\left(\frac{\alpha\pi}{2}\right)} \int \mathrm{d}x' \frac{f''(x')}{|x-x'|^{\alpha-1}}, \tag{17.77}$$

[6] This model is also sometimes referred to as the *continuous-time random walk*, which is somehow misleading since also classical diffusion is defined on a continuous time span.

[7] A short introduction to fractional derivatives and integrals can be found in Appendix F.

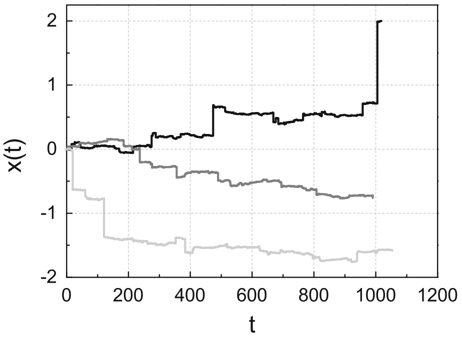

Fig. 17.7 Three different realizations of the one dimensional Lévy flight. The parameters are $\ell = 0.001, \alpha = 1.3$ and we performed $N = 1000$ time steps

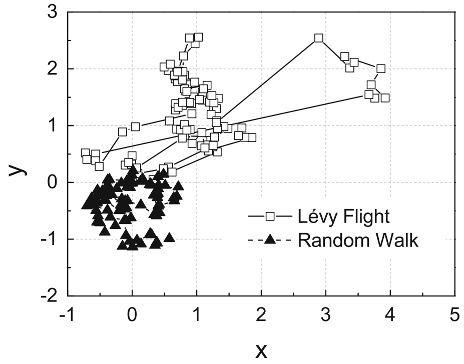

Fig. 17.8 Comparison between the two-dimensional Wiener process (*solid up-triangles*) and the two-dimensional Lévy flight (*open squares*) for $\alpha = 1.3$. The minimal flight length of the Lévy flight as well as the jump length variance of the Wiener process were set $\ell = \Sigma^2 = 0.1$ and we performed $N = 100$ time steps

where $f''(x)$ is the second spatial derivative of f.

In Fig. 17.7 a one-dimensional Lévy flight is illustrated. Furthermore, we give in Fig. 17.8 a comparison between a two-dimensional Lévy flight and a two-dimensional Wiener process. In order to obtain these figures, we sampled the waiting times from an exponential distribution with mean $\langle t \rangle = 1$. The jump length of the Lévy flight were sampled by writing the jump length pdf (17.75) in the form

$$p(x) = \alpha \ell^{\alpha} \frac{\Theta(x - \ell)}{x^{\alpha+1}}, \quad x > 0. \tag{17.78}$$

Here α is referred to as the Lévy index, $\Theta(\cdot)$ denotes the Heaviside Θ function and $\ell > 0$ is the *minimal flight length*. We introduced this particular form of the pdf because it is rather easy to sample with the help of the inverse transformation method—Sect. 13.2—and it features the asymptotic behavior, Eq. (17.75). Moreover, it can be demonstrated that it gives the correct behavior in the limit $\ell \to 0$. We note that the direction of the jump has to be sampled in an additional step. Figure 17.8 is particularly instructive because the different physics described by these two models becomes immediately apparent.

Let us turn our attention to the second scenario, the fractal time random walk. In this case the asymptotic behavior of the waiting time pdf is modified according to

$$\hat{q}(s) \propto 1 - (Ts)^{\beta}, \tag{17.79}$$

where $\beta \in (0, 1]$ and for $\beta \to 1$ regular behavior, i.e. an exponentially distributed waiting time, is recovered. A pdf of such a form is commonly referred to as a *fat-tailed waiting time pdf*. After an inverse LAPLACE transform we obtain

$$q(t) \propto t^{-\beta-1} \quad \text{for} \quad t \to \infty. \tag{17.80}$$

We note that in this case the mean waiting time $T = \langle t \rangle$ diverges for $\beta < 1$. This clearly indicates a non-Markovian time evolution since we demonstrated in Sect. 16.5 that every Markovian discrete time process converges in the continuous time limit to a process with exponentially distributed waiting times. Again, the ansatz

$$q(t) = \beta \tau^{\beta} \frac{\Theta(t - \tau)}{t^{\beta+1}}, \tag{17.81}$$

is employed, where $\tau > 0$ is the *minimal waiting time*. The process is essentially a random walk with waiting times distributed according to Eq. (17.81), i.e. the jump length Δx is constant. In the continuous space limit $\Delta x \to 0$ one obtains that the jump lengths follow a Gaussian, as in the case of a regular random walk. A detailed analysis shows that in the limit $\tau \to 0$ the corresponding diffusion equation is of the form

$${}^{C}D_t^{\beta} p(x, t) = D_{\beta} \frac{\partial^2}{\partial x^2} p(x, t), \tag{17.82}$$

where the diffusion constant D_{β} is of dimension length^2× time$^{-\beta}$. Here, ${}^{C}D_t^{\beta}$ is the CAPUTO fractional time derivative of order $\beta \in (0, 1)$, see Appendix F. It is of the form

$${}^{C}D_t^{\beta} f(t) = \frac{1}{\Gamma(1 - \beta)} \int_0^t \mathrm{d}t' \frac{\dot{f}(t')}{(t - t')^{\beta}}. \tag{17.83}$$

It follows from the properties of fractional derivatives that an alternative form of Eq. (17.82) can be found, namely

$$\frac{\partial}{\partial t} p(x, t) = D_{\beta} \frac{\partial^2}{\partial x^2} D_t^{\beta} p(x, t), \tag{17.84}$$

where D_t^{β} is the RIEMANN-LIOUVILLE fractional derivative of order β, see Appendix F.

In Fig. 17.9 we show three different realizations of the fractal time random walk. The waiting times are drawn from the pdf (17.81) with the help of the inverse trans-

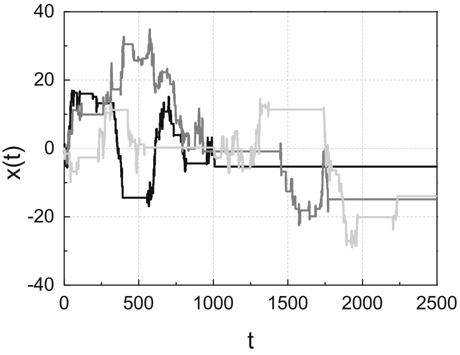

Fig. 17.9 Three different realizations of the fractal time random walk in one dimension for $\beta = 0.8$ and $\tau = 0.1$

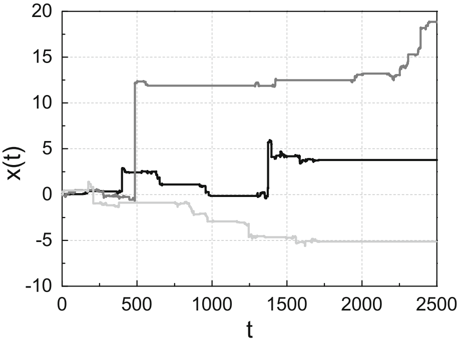

Fig. 17.10 Three possible realizations of the fractal time Lévy flight in one dimension. The parameters are $\tau = 0.1$, $\beta = 0.8$, $\ell = 0.01$ and $\alpha = 1.3$

formation method—Sect. 13.2—and the jump lengths are drawn from a normal distribution with jump length variance $\Sigma^2 = 1$.

It is a straight-forward task to combine fractal time random walks and Lévy flights to so called *fractal time* Lévy *flights*. The resulting diffusion equation can be written as

$$^C D_t^\beta p(x,t) = D_{\alpha\beta} \mathscr{D}_{|x|}^\alpha p(x,t), \tag{17.85}$$

where the diffusion constant $D_{\alpha\beta}$ has units length$^\alpha$ × time$^{-\beta}$ and $^C D_t^\beta$ and $\mathcal{D}_{|x|}^\alpha$ are the fractional Caputo and Riesz derivatives, respectively.

In Fig. 17.10 we show three different realizations of such a diffusion process. The waiting times were drawn from Eq. (17.81) where we set $\tau = 0.1$ and $\beta = 0.8$. The jump lengths were drawn from (17.78) with $\alpha = 1.3$ and $\ell = 0.01$. The direction of the jump was sampled in an additional step.

We close this chapter with a short discussion: The description of diffusion processes with the help of stochastics proofed to be one of the most powerful approaches in modern theoretical physics. Within this chapter we discussed several different approaches toward a description of Brownian motion, namely the random walk, the Wiener process, and the Langevin equation, as well as models which describe phenomena beyond Brownian motion. It has to be emphasized that the field of anomalous diffusion in general is still developing rapidly, however, its importance for the description of various phenomena in science is already impressive. We refer the interested reader to the excellent review articles by R. METZLER and J. KLAFTER on anomalous diffusion [6, 7].

Summary

The random walk, a classical example of MARKOV-chains, was used to open the door to the realm of diffusion theory. Random walks have been used for a long time to simulate Brownian motion and related problems, and from a theoretical point of view it is the scaling limit of the WIENER process. The biased WIENER process was then used to demonstrate that the Fokker-Planck equation follows in the limit of a continuous state space, as the classical diffusion equation follows from the unbiased WIENER process in the same limit. Brownian motion was also the basis for the rather heuristic introduction of the stochastic differential equation by LANGEVIN. A direct consequence of this equation was the ORNSTEIN-UHLENBECK process with its master equation, the Fokker-Planck equation. It is the only stationary, Gaussian, and Markovian process in this class of stochastic diffusion processes. An extension of these processes was then possible by the introduction of a jump pdf which in turn allowed to define a jump length pdf and a waiting time pdf. These two pdfs resulted in a more general description of diffusion processes in a space and time homogeneous environment. Furthermore, the observation that many diffusive processes (not only in physics) cannot be understood within the framework of 'classical' Brownian motion resulted in the introduction of LÉVY flights. This was particularly motivated by the need for a process whose jump-length variance diverges, which enabled, for instance the simulation of human travel behavior. In the very last step the fractal time random walk was introduced. It was characterized by a specific form of the waiting time pdf which made it possible to describe on a stochastic level anomalously long waiting times between two consecutive jumps. Such behavior can, for instance, be observed by trapping phenomena in solids. The combination of both extensions resulted in the fractal time LÉVY flight.

Problems

1. Write a program which simulates different realizations of the following stochastic processes in one spatial dimension:

   (a) A random walk,
   (b) a standard WIENER process and a WIENER process with drift,
   (c) an OHRNSTEIN- UHLENBECK process,
   (d) a LÉVY flight,

(e) a fractal time random walk,
(f) and a fractal time LÉVY flight.

Illustrate three different sample paths graphically for each process. Furthermore, perform the following tests:

(a) Calculate the expectation value $\langle x_n \rangle$ and the variance $\text{var}\,(x_n)$ of the random walk numerically by restarting the process several times with different seeds.
(b) In a similar fashion, calculate numerically $\langle W_t \rangle$ and $\text{var}\,(W_t)$.
(c) Try different parameters $\alpha,\ \beta$ for LÉVY flights and fractal time random walks.

2. Write a program which simulates the WIENER process in two dimensions. This can be achieved by drawing the jump length from a normal distribution and sampling the *jump angle*, i.e. the direction, in an additional step. Augment this program with LÉVY flight jump lengths pdfs.

References

1. Montroll, E.W., Schlesinger, M.F.: The wonderful world of random walks. In: Lebowitz, J.L., Montroll, E.W. (eds.) Non-Equilibrium Phenomena II, Studies in Statistical Mechanics, vol. 11. North-Holland, Amsterdam (1984)
2. Stickler, B.A., Schachinger, E.: Continuous time anomalous diffusion in a composite medium. Phys. Rev. E **84**, 021116 (2011). doi:10.1103/PhysRevE.84.021116
3. Brockmann, D., Hufnagl, L., Geisl, T.: The scaling laws of human travel. Nature (London) **439**, 462–465 (2006). doi:10.1038/nature04292
4. Tsallis, C.: Introduction to Nonextensive Statistical Mechanics. Springer, Berlin (2009)
5. Plastino, A.R., Plastino, A.: Non-extensive statistical mechanics and generalized fokker-planck equation. Physica A. **222**, 347–354 (1995)
6. Metzler, R., Klafter, J.: The random walk's guide to anomalous diffusion: a fractional dynamics approach. Phys. Rep. **339**, 1–77 (2000)
7. Metzler, R., Klafter, J.: The restaurant at the end of random walk: recent developments in the description of anomalous transport by fractional dynamics. J. Phys. A **37**, R161 (2004)

Chapter 18
MARKOV-Chain Monte Carlo and the POTTS Model

18.1 Introduction

This chapter will discuss in more detail the concept of MARKOV-chain Monte Carlo techniques. We already came across the METROPOLIS algorithm in Sect. 14.3, where the condition of *detailed balance* proved to be the crucial point of the method. The reason for imposing such a condition was explained in general later on in our discussion of MARKOV-chains within Sect. 16.4. The ISING model, analyzed in Chap. 15, served as a first illustration of the applicability of MARKOV-chain Monte Carlo methods in physics.

Let us briefly summarize what we learned so far: We discussed several methods to draw pseudo random numbers from a given distribution in Chap. 13. The two most important methods, i.e. the inverse transformation method and the rejection method, are based on an exact knowledge of the analytic form of the distribution function which the random numbers are supposed to follow. However, when simulating the physics of the ISING model it is required to draw random configurations from the equilibrium distribution of the system and, unfortunately, the exact form of this distribution is primarily unknown. On the other hand, in the discussion of MARKOV-chains we came across the condition of detailed balance. Invoking this condition ensures that the constructed MARKOV-chain converges toward a stationary distribution, independently of the initial conditions. Hence we can also draw random numbers by constructing a MARKOV-chain with a stationary distribution which is equal to the distribution from which we would like to obtain our random numbers. In this case the distribution function has to be known, at least in principle. However, the formulation of the METROPOLIS algorithm allows for an unknown normalization constant of the distribution function which, in turn, makes this method such a powerful tool in computational physics.

Here we want to discuss MARKOV-chain Monte Carlo techniques in some more detail and start by introducing the concept of *importance sampling*, review the METROPOLIS algorithm, and discuss the straight-forward generalization to the

B. A. Stickler and E. Schachinger, *Basic Concepts in Computational Physics*,
DOI: 10.1007/978-3-319-02435-6_18, © Springer International Publishing Switzerland 2014

Metropolis-Hastings algorithm. Finally, the applicability of the Metropolis- -Hastings algorithm will be demonstrated by simulating the physics of the q-states Potts model [1] which is closely related to the Ising model. This chapter is closed with a brief presentation of some of the more advanced techniques within this context.

18.2 Markov-Chain Monte Carlo Methods

Before turning our focus toward the Markov-chain Monte Carlo methods we shall briefly discuss *importance sampling*. Let $p(x)$ be a certain pdf from which we would like to draw a sequence of random numbers $\{x_i\}$, $i \geq 1$. Furthermore, let $f(x)$ be some arbitrary function and we would like to estimate its expectation value $\langle f \rangle_p$, i.e. the integral

$$\langle f \rangle_p = \int dx f(x) p(x). \tag{18.1}$$

In equivalence, $\langle f \rangle_p$ can also be regarded as the expectation value $\langle a \rangle \equiv \langle a \rangle_u$ of the function $a(x) := f(x)p(x)$, with $u(x)$ (in the standard notation) the pdf of the uniform distribution. Hence, we may evaluate $\langle a \rangle$ by drawing uniformly distributed random numbers on a given interval $[a, b] \subset \mathbb{R}$ and by estimating the expectation value by its arithmetic mean as discussed in Sect. 14.2. This approach is the easiest version of a method referred to as *simple sampling*. On the other hand, we might approximate $\langle f \rangle_p$ by sampling x_i according to $p(x)$ and by employing the central limit theorem as was demonstrated in Sect. 14.2. The basic idea of *importance sampling*, however, is to improve this approach by sampling from a different distribution $q(x)$ which is in most cases chosen in such a way that the expectation value $\langle f \rangle_p$ is easier to calculate.

Let $g(x)$ be some function with $g(x) > 0$ for all x. Then

$$\langle f \rangle_p = \int dx f(x) p(x) = \int dx \frac{f(x)}{g(x)} p(x) g(x) = c \left\langle \frac{f}{g} \right\rangle_q , \tag{18.2}$$

where we defined the function $q(x) = \frac{1}{c} p(x) g(x)$ and c is chosen in such a way that $\int dx q(x) = 1$. We note that $g(x)$ can be *any* positive function. Hence, such an approach might be interesting in two different scenarios: (i) if it is easier to sample from the distribution $q(x)$ rather than from $p(x)$ and, (ii) if such a sampling results in a variance reduction which is equivalent to a decrease in error, and less random numbers are to be sampled to obtain comparable results.

Let us briefly elaborate on this point: we have

$$\text{var}\left(\frac{f}{g}\right)_q = \left\langle \left(\frac{f}{g} - \left\langle \frac{f}{g} \right\rangle_q \right)^2 \right\rangle_q , \tag{18.3}$$

and for the particular choice $g(x) \equiv f(x)$ we obtain that

$$\mathrm{var}\left(\frac{f}{g}\right)_q = 0, \tag{18.4}$$

i.e. the error of our Monte Carlo integration vanishes. However, the ideal case of $g(x) \equiv f(x)$ is unrealistic because we obtain for the normalization constant c

$$c = \int dx\, p(x)g(x) = \langle g \rangle_p \equiv \langle f \rangle_p\,, \tag{18.5}$$

which is exactly the integral we want to evaluate. However, the function $g(x)$ can be adapted to improve the result and $g(x)$ can be chosen in such a way that the integral $\langle g \rangle_p$ is easy to evaluate and that $g(x)$ follows $f(x)$ as closely as possible; in other words, the quotient $f(x)/g(x)$ becomes as constant as possible. This means that we do not sample from $p(x)$ on a given interval but only from points which matter for the particular function $f(x)$. Such an approach is referred to as *importance sampling*.

The attentive reader might have observed that, on a first glance, importance sampling has nothing to do with MARKOV-chain Monte Carlo methods in general. Nevertheless, it can be demonstrated that MARKOV-chain Monte Carlo methods corresponds indeed to importance sampling.

To prove this, we remember that MARKOV-chain Monte Carlo techniques are based on the generation of a sequence of configurations $S^{(n)}$:

$$S^{(1)} \to S^{(2)} \to \cdots \to S^{(n)} \to \cdots\ . \tag{18.6}$$

Each individual configuration $S^{(n)}$ is generated from the previous configuration $S^{(n-1)}$ at random with a certain transition probability $P(S^{(n-1)} \to S^{(n)})$. These transition probabilities obey

$$P(S \to S') \geq 0 \qquad \text{and} \qquad \sum_{S'} P(S \to S') = 1, \tag{18.7}$$

and this property ensures that the sequence (18.6) is a MARKOV-chain. In Sect. 16.4 we observed that the detailed balance condition for a stationary distribution $P(S)$

$$P(S)P(S \to S') = P(S')P(S' \to S) \tag{18.8}$$

guarantees convergence of the MARKOV-chain toward the stationary distribution. Hence, the remaining task is to find transition probabilities which fulfill detailed balance. In a typical situation, the transition probabilities can be written as

$$P(S \to S') = P_p(S \to S')P_a(S \to S'), \tag{18.9}$$

where $P(S \to S')$ is the probability that a configuration S' is proposed and $P_a(S \to S')$ is the probability that the proposed configuration is accepted. In many cases one simplifies the situation by assuming that

$$P_p(S \to S') = P_p(S' \to S), \tag{18.10}$$

and, thus, the detailed balance condition changes into

$$P(S)P_a(S \to S') = P(S')P_a(S' \to S). \tag{18.11}$$

The METROPOLIS algorithm uses *one* possible choice for the acceptance probability, namely

$$P_a(S \to S') = \min\left[1, \frac{P(S')}{P(S)}\right]. \tag{18.12}$$

It was demonstrated in Sect. 14.3 that (18.12) indeed fulfills Eq. (18.11). The execution of the algorithm was already illustrated in Chap. 15 in the course of our discussion of the numerics of the ISING model.

A rather straight-forward generalization of the METROPOLIS algorithm (18.12) is obtained by considering an asymmetric proposal probability $P_p(S \to S')$. It is easily demonstrated that the choice

$$P_a(S \to S') = \min\left[1, \frac{P(S')}{P(S)} \frac{P_p(S' \to S)}{P_p(S \to S')}\right], \tag{18.13}$$

also fulfills detailed balance (18.8). The choice (18.13) is referred to as the METROPOLIS-HASTINGS algorithm.[1]

By exploiting the MARKOV property in order to sample configurations according to the BOLTZMANN distribution we perform *importance sampling* as illustrated above. An alternative approach would be to select different configurations according to a uniform distribution which obviously increases the numerical cost of the method by magnitudes. Hence, sampling with the help of a MARKOV-chain yields a variance reduction in comparison to the crude approach of simple sampling. Furthermore, the algorithm can be optimized by a clever choice of $P_p(S \to S')$ which does not need to be symmetric. Clearly, this choice will have to depend on the particular problem at hand.

We shall briefly discuss two alternative approaches to MARKOV-chain Monte Carlo sampling, namely GIBBS *sampling* and *slice sampling*.

Suppose we want to sample a sequence of m-dimensional variables $x^{(n)} = (x_1^{(n)}, x_2^{(n)}, \dots, x_m^{(n)})^T$ from a multivariate distribution function $p(x) = p(x_1, x_2, \dots, x_m)$. Gibbs sampling is particularly interesting if the joint distribution functions are well-known and simple to sample. One sets for a particular component

[1] Please note that it is common in the literature to refer even to Eq. (18.12) as a METROPOLIS–HASTINGS algorithm, despite the fact that here $P_p(S' \to S) = P_p(S \to S')$.

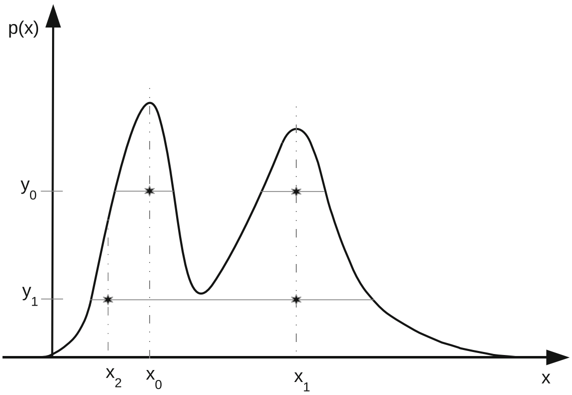

Fig. 18.1 Schematic illustration of *slice sampling*. The following steps are required: (**a**) Choose x_0, (**b**) draw $y_0 \in [0, p(x_0)]$, (**c**) draw $x_1 \in \mathscr{S}[p^{-1}(y_0)]$, (**d**) draw $y_1 \in [0, p(x_1)]$, (**e**) draw $x_2 \in \mathscr{S}[p^{-1}(y_1)]$, (**f**) ....

of the vector $x^{(n)}$

$$P_a(x_j^{(n+1)}|x^{(n)}) = p(x_j^{(n+1)}|x_1^{(n+1)}, \dots, x_{j-1}^{(n+1)}, x_{j+1}^{(n)}, \dots, x_m^{(n)}). \tag{18.14}$$

We note that this is possible since we have

$$\begin{aligned} p(x_j|x_1, \dots, x_{j-1}, x_{j+1}, \dots, x_m) &= \frac{p(x_1, \dots, x_m)}{p(x_1, \dots, x_{j-1}, x_{j+1}, \dots, x_m)} \\ &\propto p(x_1, \dots, x_m), \end{aligned} \tag{18.15}$$

because the denominator of the left hand side of Eq. (18.15) is independent of x_j. It can therefore be treated as a normalization constant when sampling x_j.

Let us briefly discuss *slice sampling*: For reasons of simplicity we shall regard the uni-variate case, where $p(x)$ denotes the pdf from which we would like to sample. In a first step we draw a random variable y_0 uniformly from the interval $[0, p(x_0)]$, where x_0 is some initial value. The next random variable x_1 is then obtained by uniformly sampling it from the slice $\mathscr{S}[p^{-1}(y_0)]$. The sequence $\{x_j\}$ is constructed by ignoring the y_0 values. This procedure is illustrated in Fig. 18.1.

18.3 The Potts Model

As an illustrative example of the Metropolis algorithm we already discussed the two-dimensional Ising model in Chap. 15. Within this section, we shall discuss another example, the q-states Potts model, which can be regarded as a generalization of the Ising model. The model is characterized by the Hamiltonian

$$H = -\sum_{ij} J_{ij} \delta_{\sigma_i \sigma_j}, \tag{18.16}$$

where the notation used for the ISING model applies. In particular, we shall regard the case $J_{ij} = J$ for i, j nearest neighbors and $J_{ij} = 0$ otherwise. In contrast to the ISING model, the spin realizations σ_i on grid-point i can take integer values $\sigma_i = 1, 2, \ldots, q$. For $q = 2$, the POTTS model is equivalent to the ISING model, which can be easily proved by rewriting the Hamiltonian as

$$H = \frac{J}{2} \sum_{\langle ij \rangle} 2 \left(\frac{1}{2} - \delta_{\sigma_i \sigma_j} \right) - J \sum_i \frac{1}{2}. \tag{18.17}$$

Here $\langle ij \rangle$ denotes sum over nearest neighbors. We observe that $2\left[\frac{1}{2} - \delta_{\sigma_i \sigma_j}\right]$ is equal to $+1$ for $\sigma_i = \sigma_j$ and -1 for $\sigma_i \neq \sigma_j$. Moreover, the constant energy shift in Eq. (18.17) can be neglected and we recover the ISING model of Chap. 15.

The calculation of the observables of interest, i.e. $\langle E \rangle$, $\langle M \rangle$, c_h and χ, as well as the basic algorithm can be adopted from Chap. 15 as it is.[2] The only main difference occurs at step 3 of the algorithm discussed in Sect. 15.2: Instead of setting $\sigma_{ij} = -\sigma_{ij}$ we draw the new value of σ_{ij} uniformly distributed from $1, 2, \ldots, q$ excluding the old value of σ_{ij}.

In Figs. 18.2, 18.3, 18.4 and 18.5 we show the mean energy per particle $\langle \varepsilon \rangle$, the mean magnetization per particle $\langle m_1 \rangle$ (with $Q = 1$ in Eq. (18.18)), the heat capacity c_h as well as the magnetic susceptibility χ for $q = 1, 2, \ldots, 8$ and $J = 0.5$ (Eq. (18.16)) versus temperature $k_B T$. The size of the system was $N \times N$ with $N = 40$. We performed 10^4 measurements per temperature and 10 sweeps where discarded between two successive measurements in order to reduce correlations. The equilibration time was set to 10^3 sweeps. A typical spin configuration for $q = 4$ and $k_B T = 0.47$ can be found in Fig. 18.6.

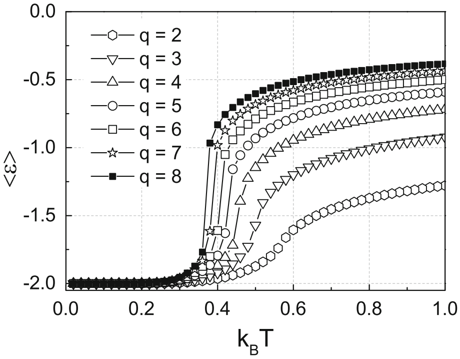

Fig. 18.2 The mean free energy per particle $\langle \varepsilon \rangle$ versus temperature $k_B T$ for a q-states POTTS model on a 40×40 square lattice, with $q = 1, 2, \ldots, 8$ and $J = 0.5$. 10^4 measurements have been performed

[2] We calculate the magnetization in a particular spin configuration Q via

$$\mathscr{M}_Q(\mathscr{C}) = \left(\sum_i \delta_{\sigma_i, Q} \right)_{\mathscr{C}}. \tag{18.18}$$

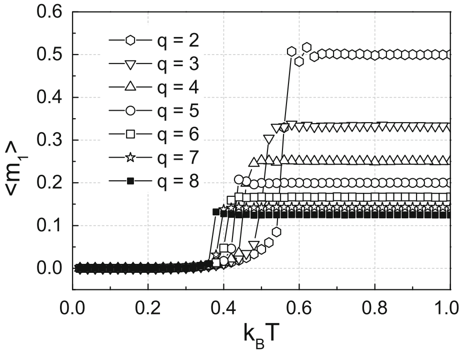

Fig. 18.3 The mean magnetization per particle $\langle m_1 \rangle$ versus temperature $k_B T$ for a q-states POTTS model on a 40×40 square lattice, for $q = 1, 2, \ldots, 8$ and $J = 0.5$. 10^4 measurements have been performed

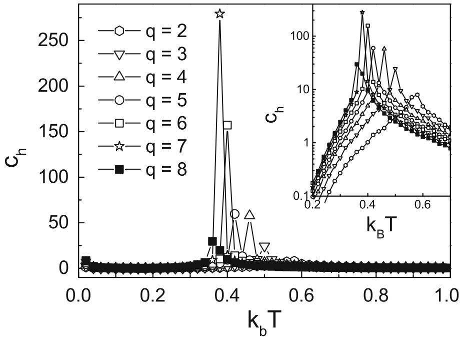

Fig. 18.4 The heat capacity c_h versus temperature $k_B T$ for a q-states POTTS model on a 40×40 square lattice, with $q = 1, 2, \ldots, 8$ and $J = 0.5$. 10^4 measurements have been performed. The inset shows the specific heat c_h on a logarithmic scale in the region around the transition temperature

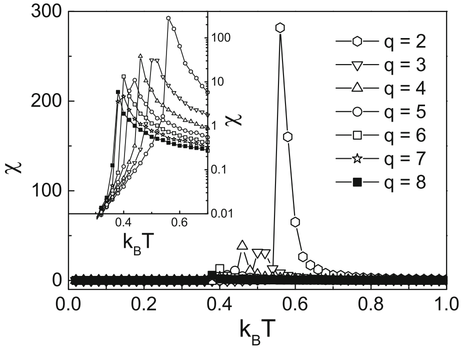

Fig. 18.5 The magnetic susceptibility χ versus temperature $k_B T$ for a q-states POTTS model on a 40×40 square grid, with $q = 1, 2, \ldots, 8$ and $J = 0.5$. 10^4 measurements have been performed. The inset shows the magnetic susceptibility χ on a logarithmic scale in the region around the transition temperature

A number of interesting details can be observed in Figs. 18.2 and 18.3. First of all, we observe that the mean magnetization above the critical temperature decreases with increasing values of q. The reason for this is obvious: the mean magnetization for $T \gg T_c$ represents the probability of finding a particular spin in state $\sigma_i = 1$, which is equivalent to $1/q$ for a uniform distribution and therefore decreases with increasing q. Please note that the expectation value of the magnetization $\langle m_Q \rangle$ is restricted to take the values from $\{0, 1\}$ for $T \ll T_C$ due to the modified definition

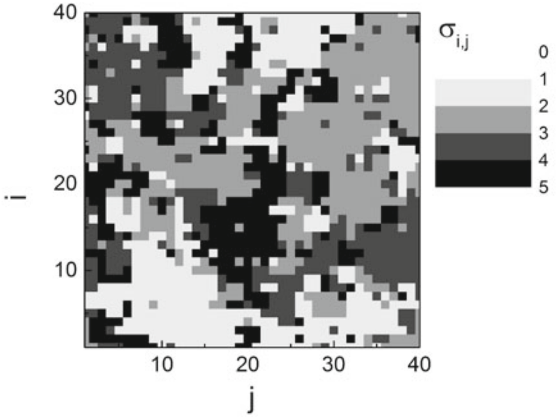

Fig. 18.6 A typical spin configuration $\sigma_{i,j}$ for a q-states POTTS model on a 40×40 square lattice with $q = 4$, $J = 0.5$, and $k_B T = 0.47$

Table 18.1 List of the critical $\alpha_c = \frac{J}{k_B T_c}$ of the q-states POTTS model for $q = 2, 3, \ldots, 8$

q	α_c
2	0.89
3	1.00
4	1.09
5	1.16
6	1.22
7	1.28
8	1.35

of $\mathscr{M}_Q(\mathscr{C})$. This is in contrast to the ISING model where $\langle m \rangle \in \{-1, 1\}$ for $T < T_c$. Hence, we obtain for $T \ll T_C$ $\langle m_1 \rangle = 0$ with probability $(q-1)/q$ and $\langle m_1 \rangle = 1$ with probability $1/q$. However, the particular definition (18.18) of $\mathscr{M}_Q(\mathscr{C})$ is not important since the physically relevant property of the POTTS model Hamiltonian (18.16) is the $\mathbb{Z}_q$ symmetry with a degenerate ground state.

A second interesting feature is the observation that the critical temperature also decreases with increasing q which becomes particularly transparent from Figs. 18.4 and 18.5. The critical temperatures are quoted in Table 18.1. Finally, we deduce from Fig. 18.2 that the phase transition is smoother for $q = 2$ and becomes discontinuous for large values of q. In particular, the q-states POTTS model exhibits a second order phase transition for $q = 2, 3, 4$ and a first order phase transition for $q > 4$, which is hard to see from Figs. 18.2 and 18.3. However, there is another method to unambiguously identify a first order phase transition. It is referred to as the histogram technique. The mean energies of consecutive measurements near the critical temperature are simply collected in a histogram. If one peak is observed, the system fluctuates around a single phase, i.e. a second order phase transition was observed. However, the existence of two or more peaks means that the system fluctuates between two or more different phases and, therefore, exhibits a first order phase

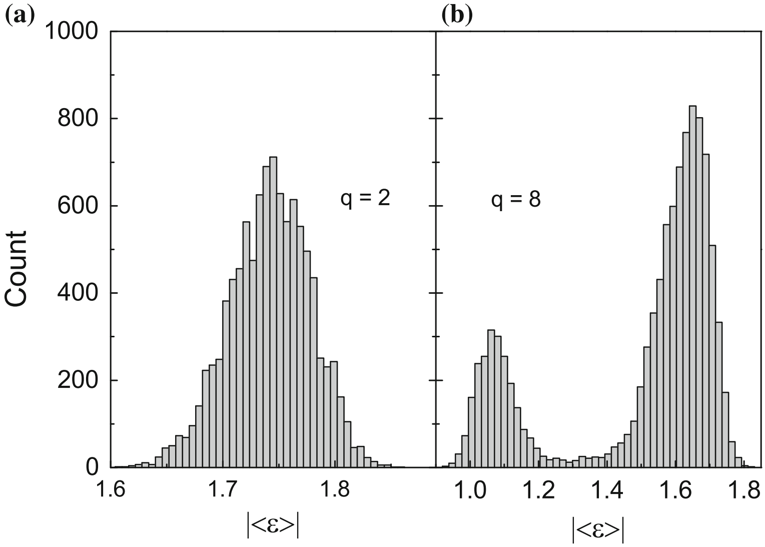

Fig. 18.7 (**a**) Histogram of 10^4 measurements of the absolute value of the mean free energy per particle $|\langle \varepsilon \rangle|$ for a q-states POTTS model on a 40×40 square lattice at temperature $k_B T = 0.56$ with $q = 2$. We observe *one single peak* which indicates that the system exhibits a second order phase transition. (**b**) The same as (**a**) but for $q = 8$ and temperature $k_B T = 0.37$. We observe two well separated peaks, thus the system exhibits a first order phase transition

transition. In Fig. 18.7 we show two histograms for $q = 2$ ($k_B T = 0.56$) and $q = 8$ ($k_B T = 0.37$) from 10^4 measurements to prove our case.

One possible realization of the $q = 3$ states POTTS model was discussed by M. KARDAR and A. N. BERKER [2]. They studied the oversaturated adsorption of Krypton atoms on a graphite surface. A detailed analysis of this system revealed that three energetically degenerate sublattices are formed. It was further demonstrated that the thermodynamic properties can be explained by a $q = 3$ states POTTS model. For a more detailed discussion we refer to the original paper by M. KARDAR and A. N. BERKER. Further applications of the POTTS model are found in the review by Wu [3].

The attentive reader may have noticed that our results do not carry error-bars. We neglected error-bars for a clearer illustration. A short discussion of methods used to calculate numerical errors was presented in Sect. 15.2 for the ISING model and they can easily be adapted for the POTTS model. More advanced techniques will be introduced in the next chapter.

18.4 Advanced Algorithms for the POTTS Model

Within this section we shall briefly discuss some advanced techniques for the POTTS model. Although these algorithms are applicable for arbitrary q we shall restrict our discussion to the case $q = 2$, i.e. the ISING model, for reasons of simplicity. Let us briefly motivate the problem. For large N we observe the formation of spin domains (regions in which all spins point in the same direction; WEISS regions) for temperatures $T \approx T_c$. In such a case this particular METROPOLIS algorithm is disadvantageous because single spin flips will only affect the boundaries of these domains (*critical slowing down*). It is therefore necessary to perform many sweeps in order to produce configurations which are entirely different. It might therefore be a better approach to flip the whole spin *cluster* at once. Such algorithms are referred to as *cluster* algorithms. The main problem is the identification of clusters as well as the assignment of a probability to the flip of a particular cluster.

As a first example we shall discuss the SWENDSEN-WANG algorithm [4]. The algorithm is executed in the following steps:

1. Identify all *links* between two neighboring identical spins.
2. Define a *bond* between two linked spins with probability

$$P = 1 - \exp(-2\beta J), \tag{18.19}$$

with $\beta = 1/(k_B T)$.
3. Identify all *clusters*, i.e. spins which are connected by bonds.
4. Flip every cluster with probability $1/2$.
5. Delete the bonds and restart the iteration for the next spin configuration.

Figure 18.8 shows a schematic illustration of a cluster.

We note the following properties of the SWENDSEN-WANG algorithm:

- The algorithm is ergodic because every spin forms a cluster on its own with a non-vanishing probability according to Eq. (18.19).
- The algorithm fulfills detailed balance for the BOLTZMANN distribution and thus reproduces the correct stationary distribution.

Since the algorithm breaks domain walls or flips whole clusters, this algorithm can be regarded to be very efficient from a numerical point of view. However, it

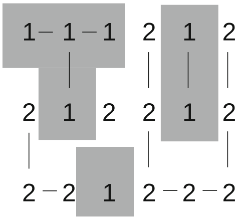

Fig. 18.8 Schematic illustration of the identification of clusters according to the SWENDSEN-WANG algorithm. 1 and 2 denote two different spin orientations, bonds are denoted by *solid lines* and all bonded spins form clusters

outperforms the single spin Metropolis algorithm only for temperatures near the critical temperature because only then spin domains dominate the observables.

A simpler version of this algorithm consists of the following four steps:

1. Randomly pick a lattice site.
2. Find all neighbors with the same spin and form bonds with probability (18.19).
3. Move to the boundary of the cluster and repeat step 2, i.e. the cluster *grows*.
4. If no new bond is formed, flip the cluster with probability 1.

In this simplified version the identification of clusters is not necessary because each cluster is built dynamically during the simulation. Such a formulation of a cluster algorithm is the Wolff algorithm [5] which is essentially a generalization of the work of Swendsen and Wang [4]. The question arises why it is possible to accept every step, i.e. flip every formed cluster, without contradicting the condition of detailed balance. The reason can be found in the definition of the probability of bond-formation. An even more effective extension to quantum systems of the Wolff algorithm is the *loop* algorithm [6]. For a more detailed discussion of all these methods we refer the interested reader to the literature [7] and to the particular papers cited here.

Before proceeding to the next chapter, let us briefly mention that there is also an entirely different approach to improve the Metropolis algorithm for quantum systems, the so called *worm* algorithms [6]. However, a detailed discussion of such algorithms is beyond the scope of this book.

Summary

The dominant topic of this chapter was importance sampling, a method to improve Monte Carlo methods by reducing the variance. In this method some hard to sample pdf is approximated as closely as possible by another, easy to sample pdf and one concentrates on intervals which particularly matter for an as accurate as possible estimate of, for instance, an expectation value of some property $f(x)$. In this sense Markov-chain Monte Carlo techniques correspond to importance sampling as long as detailed balance is obeyed. In this particular case the Markov-chain is known to approach the equilibrium distribution which must not necessarily be known in detail. The Metropolis algorithm with its symmetric acceptance probability is one possible realization of Markov-chains which obey detailed balance. Another method is the Metropolis-Hastings algorithm with its asymmetric acceptance probability. It also obeys detailed balance and improves the variance over the 'classical' Metropolis algorithm. The second part of this chapter was dedicated to the simulation of the q-state Potts model, an extension of the Ising model. The Potts model has the fascinating feature that it develops a second order phase transition for $q \leq 4$ and a first order phase transition for $q > 4$. Moreover, the transition temperature is q-dependent. The numerical simulation of the physics of this model proved to be able to pick up on all these particular features. Finally, some advanced algorithms developed for a more precise handling of various properties of spin-models, particularly around the phase transition, have been presented without going into great detail.

Problems

1. Modify the program designed to solve the Ising model (see Problems in Chap. 15) in such a way that the physics of the q-states Potts model can be simulated for arbitrary values of q. Try to reproduce the figures presented within this chapter. In order to investigate the order of the phase transition, plot the internal energy per particle $\langle \varepsilon \rangle$ for $T \approx T_c$ in a histogram for different measurements.

   The critical temperatures listed in Table 18.1 for $q = 2, 3, \dots, 8$ can be used to validate your code.
2. Include a non-zero external field h and study its influence on the physics of the q-states Potts model for different values of q.

References

1. Potts, R.B.: Some generalized order-disorder transformations. Math. Proc. Cambridge Philos. Soc. **48**, 106–109 (1952). doi:10.1017/S0305004100027419
2. Kardar, M., Berker, A.N.: Commensurate-incommensurate phase diagrams for overlayers from a helical potts model. Phys. Rev. Lett. **48**, 1552–1555 (1982). doi:10.1103/PhysRevLett.48.1552
3. Wu, F.Y.: The potts model. Rev. Mod. Phys. **54**, 235–268 (1982). doi:10.1103/RevModPhys.54.235
4. Swendsen, R.H., Wang, J.S.: Nonuniversal critical dynamics in monte carlo simulations. Phys. Rev. Lett. **58**, 86–88 (1987). doi:10.1103/PhysRevLett.58.86
5. Wolff, U.: Collective monte carlo updating for spin systems. Phys. Rev. Lett. **62**, 361–364 (1989). doi:10.1103/PhysRevLett.62.361
6. Evertz, H.G.: The loop algorithm. Ad. Phy. **52**, 1–66 (2003). doi:10.1080/0001873021000049195
7. Newman, M.E.J., Barkema, G.T.: Monte Carlo Methods in Statistical Physics. Oxford University Press, Oxford (1999)

Chapter 19
Data Analysis

19.1 Introduction

This chapter will discuss some of the most important techniques to analyze data sets of general origin and Monte-Carlo generated data in particular.

This program is easily motivated: the enormous importance of data analysis in theoretical as well as experimental physics is hard to overestimate and it is a common superstition, that data generated by numerical methods do not require to be analyzed by means of statistical methods. This is quite generally not true and statistical analysis of the data becomes even more important if the data themselves have been generated by stochastic algorithms. For instance, simple tests for the quality of data generated by random number generators have already been discussed within Chap. 12 and some simple estimators to approximate observables and to calculate respective errors have been discussed in Chap. 15. This chapter aims to summarize these techniques and to introduce some of the more advanced techniques.

19.2 Calculation of Errors

We shall briefly reintroduce the simple estimators which have already been in use. We approximate the expectation value $\langle x \rangle$ of some variable x

$$\langle x \rangle = \int \mathrm{d}x \, x p(x), \tag{19.1}$$

where $p(x)$ is a pdf, by its arithmetic mean

$$\langle x \rangle \approx \overline{x} = \frac{1}{N} \sum_{i=1}^{N} x_i, \tag{19.2}$$

DOI: 10.1007/978-3-319-02435-6_19, © Springer International Publishing Switzerland 2014

where the numbers x_i follow the distribution $p(x)$. It is of conceptual importance to distinguish between the expectation value $\langle x \rangle$, which is a c-number while the estimator $\overline{x}$ is a random number fluctuating around $\langle x \rangle$. The error of approximating $\langle x \rangle$ by $\overline{x}$ can be estimated by calculating the variance

$$\mathrm{var}\,(\overline{x}) = \frac{\mathrm{var}\,(x)}{N} = \frac{\left\langle x^2 \right\rangle - \langle x \rangle^2}{N}, \tag{19.3}$$

for uncorrelated random numbers x_i (see Appendix D). In case of correlated measurements, the treatment becomes more involved and will be discussed in Sect. 19.3. In Eq. (19.3), the expectation values $\left\langle x^2 \right\rangle$ and $\langle x \rangle$ may again be replaced by the corresponding estimators $\overline{x^2}$ and $\overline{x}$ in order to obtain a reasonable estimate of the variance $\mathrm{var}\,(\overline{x})$. In particular, we approximate

$$\left\langle x^2 \right\rangle \approx \overline{x^2} = \frac{1}{N} \sum_{i=1}^{N} x_i^2. \tag{19.4}$$

This approximation has already been applied during the discussion of the ISING model in Chap. 15. In the case of MARKOV-chain Monte Carlo simulations, the result (19.3) can be interpreted in a rather obvious way. If the simulation is repeated under identical conditions roughly 68 % of all simulations would yield a mean value $\overline{x}$ within the range $[\overline{x} - \sigma_{\overline{x}}, \overline{x} + \sigma_{\overline{x}}]$, where $\sigma_{\overline{x}} = \sqrt{\mathrm{var}\,(\overline{x})}$ is the standard error.

Let us briefly consider the quite familiar case where the underlying distribution $p(x)$ of a sequence of random numbers $\{x_i\}$ is unknown. In such a case one cannot simply use a particular estimator without caring about the particular form of $p(x)$. A common way to proceed is the *poor person's assumption*: The underlying distribution is symmetric. This assumption has its origin in the central limit theorem (see Appendix D). However, in order to avoid fatal misconceptions some intuitive checks may be necessary. If the data sample is reasonably large one may obtain essential information from presenting the data points in form of a histogram or, if the index i refers to time instances, by plotting the time sequence. We shall briefly elaborate on these intuitive checks.

From a histogram of the data set a first idea about the form of the underlying distribution can be obtained. For instance, if there is only one peak, like in Fig. 19.1, quantities like the mean or the variance might be useful. Anyhow, if there are two (or more) separate peaks, like in Fig. 19.2, it may make no sense to calculate the mean or variance by summing over the data points of both peaks. Such a situation may for instance occur in statistical spin models, with two phases, for instance in the q-state POTTS model as illustrated in Fig. 18.7a, b.

In a similar fashion, plotting the time series, i.e. the data points x_i as a function of t_i where the t_i are discrete time instances, could reveal important information on the properties of the data set. For instance systematic trends, outliers, or hints for correlations may be observed.

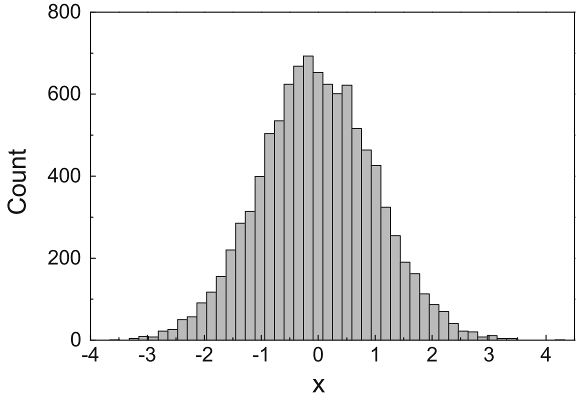

Fig. 19.1 Histogram generated by random sampling of a Gaussian of mean zero and variance one

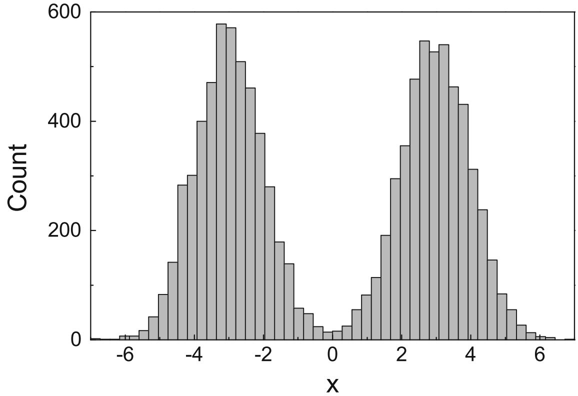

Fig. 19.2 Histogram generated by random sampling of two Gaussians of mean zero and variance one, displaced by +3 and −3, respectively

Let us turn our attention to some more advanced estimator techniques. So far we discussed the sample mean and sample variance as candidates for unbiased estimators.[1] In a more general context the calculation of observables from data sets might be more complex. In the following we assume a data set of N data points $(x_1, x_2, \dots, x_N)$. Basically, we would like to estimate a quantity of the form $f(\langle x \rangle)$ where$f$ is some particular function (for instance $\langle x \rangle^2$). A bad (*biased*) estimate would be to calculate

$$\overline{f} = \frac{1}{N} \sum f(x_i), \tag{19.5}$$

which is definitely not the quantity we are interested in because for $N \to \infty$ we have $\overline{f} \to \langle f \rangle$. A better estimate would be to calculate

[1] Since mean and variance are calculated from the same data points, they are usually not unbiased. Therefore a common choice is the so called *bias corrected variance* $\text{var}\,(\overline{x})_B$ which is given by $\text{var}\,(\overline{x})_B = \frac{N}{N-1} \text{var}\,(\overline{x})$ where N is the number of data points. A more detailed discussion can be found in any textbook on statistics [1].

$$f(\overline{x}) = f\left(\frac{1}{N}\sum x_i\right), \tag{19.6}$$

which converges to $f(\langle x \rangle)$ for $N \to \infty$. The error of $\overline{x}$ is given by $\sigma_{\overline{x}}$ as was outlined above. The question immediately arises: how can we estimate the error attached to $f(\overline{x})$? This will be answered exemplary on the basis of two different methods which proved to be very successful in this context, the *Jackknife* method and the *statistical bootstrap* method.

We define Jackknife averages

$$x_i^J = \frac{1}{N-1}\sum_{j \neq i} x_j, \tag{19.7}$$

and x_i^J is the average of all values $x_j \neq x_i$. Moreover, we define

$$f_i^J \equiv f(x_i^J), \tag{19.8}$$

and this opens the possibility to estimate $f(\langle x \rangle)$ following

$$f(\langle x \rangle) \approx \overline{f}^J = \frac{1}{N}\sum_i f_i^J, \tag{19.9}$$

with the statistical error

$$\sigma_{\overline{f}^J}^2 = (N-1)\left[\overline{(f^J)^2} - (\overline{f}^J)^2\right], \tag{19.10}$$

which can be written as

$$\sigma_{\overline{f}^J}^2 = \frac{N-1}{N}\sum_i (f_i^J - \overline{f}^J)^2, \tag{19.11}$$

for uncorrelated f_i^J (see Appendix D).

In the case of the statistical bootstrap we consider again a set of N data-points $\{x_i\}$. We randomly choose N elements from this data set *without removal* and calculate for these N points the observable $f_i = f(1/N \sum_j x_j^i)$. This is repeated M-times and we get

$$f(\langle x \rangle) \approx \overline{f}_{BS} = \frac{1}{M}\sum_i f_i, \tag{19.12}$$

and

$$\sigma_{\overline{f}_{BS}}^2 = \frac{1}{M}\sum_i \left(f_i - \overline{f}_{BS}\right)^2. \tag{19.13}$$

We note that this method has been employed in Chap. 15 in order to calculate the error-bars of the observables as a function of temperature in Fig. 15.6. In the same fashion the methods discussed here can be employed to estimate the errors attached to the observables calculated for the POTTS model in Chap. 18.

Let us close this section with a short comment on systematic errors. As already highlighted within Chap. 1 one also has to take care of possible systematic errors. Like in experimental data, these errors are more likely to be overlooked since they are rather hard to identify. In general, there is no method available to investigate systematic errors. For instance, in the simulation of the ISING model, the main source of errors is that we do not allow our MARKOV-chain to equilibrate completely, which would be equivalent to running the simulation forever. Within the following section, however, we will introduce the notion of an auto-correlation time which, at least, allows for a systematic investigation of this fundamental problem.

However, in general it is not possible to give a standard procedure which allows to determine an estimate of systematic errors.

19.3 Auto-Correlations

The situation becomes more involved whenever the random numbers of the sequence $\{x_i\}$ are correlated, i.e. $\operatorname{cov}\left(x_i, x_j\right) \neq 0$ for $i \neq j$. We interpret now the elements of the series $\{x_i\}$ as successive members of a time series. Hence, the covariances between elements x_i and x_j account for auto-correlations of a certain observable between different time steps. We rewrite Eq. (19.3):

$$\begin{aligned}
\operatorname{var}(\overline{x}) &= \left\langle \overline{x^2} \right\rangle - \langle \overline{x} \rangle^2 \\
&= \frac{1}{N^2} \sum_{i,j=1}^{N} \left\langle x_i x_j \right\rangle - \frac{1}{N^2} \sum_{i,j=1}^{N} \langle x_i \rangle \left\langle x_j \right\rangle \\
&= \frac{1}{N^2} \sum_{i=1}^{N} \left(\left\langle x_i^2 \right\rangle - \langle x_i \rangle^2 \right) \\
&\quad + \frac{1}{N^2} \sum_{i \neq j} \left(\left\langle x_i x_j \right\rangle - \langle x_i \rangle \left\langle x_j \right\rangle \right) .
\end{aligned} \tag{19.14}$$

The first term on the right hand side of Eq. (19.14) is identified as $\operatorname{var}(x_i)/N$ which is assumed to be identical for all i, i.e. $\operatorname{var}(x_i) \equiv \operatorname{var}(x)$. Furthermore, we rewrite the sum

$$\sum_{i \neq j} \cdot = 2 \sum_{i=1}^{N} \sum_{j=i+1}^{N} \cdot ,$$

in order to obtain

$$\operatorname{var}(\overline{x}) = \frac{1}{N}\left[\operatorname{var}(x) + \frac{2}{N}\sum_{i=1}^{N}\sum_{j=i+1}^{N}\operatorname{cov}\left(x_i, x_j\right)\right]. \qquad (19.15)$$

Let us assume time translational invariance, i.e.

$$\operatorname{cov}\left(x_i, x_j\right) \equiv C(j-i), \qquad (19.16)$$

for $j > i$. Plugging expression (19.16) into Eq. (19.15) yields

$$\begin{aligned}\operatorname{var}(\overline{x}) &= \frac{1}{N}\left[\operatorname{var}(x) + \frac{2}{N}\sum_{i=1}^{N}\sum_{j=i+1}^{N} C(j-i)\right]\\ &= \frac{1}{N}\left[\operatorname{var}(x) + \frac{2}{N}\sum_{k=1}^{N} C(k)\,(N-k)\right]\\ &= \frac{1}{N}\left[\operatorname{var}(x) + 2\sum_{k=1}^{N} C(k)\left(1-\frac{k}{N}\right)\right]. \qquad (19.17)\end{aligned}$$

Hence, we have

$$\operatorname{var}(\overline{x}) = \frac{\operatorname{var}(x)}{N} 2\hat{\tau}_x^i, \qquad (19.18)$$

where we introduced the (proper) *integrated auto-correlation time* $\hat{\tau}_x^i$ via

$$\hat{\tau}_x^i = \frac{1}{2} + \sum_{k=1}^{N} A(k)\left(1-\frac{k}{N}\right), \qquad (19.19)$$

with the normalized auto-correlation function

$$A(k) = \frac{C(k)}{C(0)} = \frac{\operatorname{cov}(x_i, x_{i+k})}{\operatorname{var}(x_i)}. \qquad (19.20)$$

In most cases we are interested in the limit $N \to \infty$ of Eq. (19.19):

$$\tau_x^i = \lim_{N\to\infty}\hat{\tau}_x^i = \frac{1}{2} + \sum_{k=1}^{\infty} A(k). \qquad (19.21)$$

Let us briefly investigate the particular form of the auto-correlation function $A(k)$ in order to further simplify relation (19.21). During our discussion of Markov-chains in Sect. 16.4 we observed that the stationary distribution π is the left-eigenvector of the transition matrix P with eigenvalue 1, as expressed in Eq. 16.76. Let $\{\varphi_\ell\}$ denote the set of all left-eigenvectors of the matrix P with eigenvalues λ_ℓ, i.e. $\varphi_\ell P = \lambda_\ell \varphi_\ell$.[2] We may then express an arbitrary state $q(0)$ in this basis as

$$q(0) = \sum_i \alpha_i \varphi_i. \tag{19.22}$$

It follows from Eq. (16.4) that after n consecutive time steps we have

$$q(n) = q(0)P^n = \sum_i \alpha_i \varphi_i P^n = \sum_i \alpha_i \lambda_i^n \varphi_i. \tag{19.23}$$

Let us assume that we are interested in some observable $O(n)$ at some time n. The observable can be expressed as

$$O(n) = \sum_i [q(n)]_i o_i = \sum_i \alpha_i \lambda_i^n o_i, \tag{19.24}$$

where we defined with o_i the expectation value of O in the i-th eigenstate φ_i. For large n the value of $O(n)$ will be dominated by the largest eigenvalue of P, say λ_0, and we denote this value by $O(\infty) = \alpha_0 o_0$. This allows to rewrite Eq. (19.24) as

$$O(n) = O(\infty) + \sum_{i \neq 0} \alpha_i o_i \lambda_i^n. \tag{19.25}$$

Let $\lambda_1 \in \mathbb{R}$ be the second largest eigenvalue and let us define the exponential auto-correlation time τ_x^e via

$$\tau_x^e = -\frac{1}{\log(\lambda_1)}. \tag{19.26}$$

This allows to approximate $O(n)$ for large n by

$$O(n) \approx O(\infty) + \beta \exp\left(-\frac{n}{\tau_x^e}\right), \tag{19.27}$$

where β is some constant. Hence, the auto-correlation obeys

$$C(n) \propto [O(0) - O(\infty)]\,[O(n) - O(\infty)] \propto \beta \exp\left(-\frac{n}{\tau_x^e}\right), \tag{19.28}$$

and we can simply set for the auto-correlation function $A(k)$

$$A(k) = \gamma \exp\left(-\frac{k}{\tau_x^e}\right), \tag{19.29}$$

[2] Note that since P is a stochastic matrix, it follows that $|\lambda_\ell| \leq 1$ for all ℓ. Furthermore, it can be shown that the largest eigenvalue of a stochastic matrix is equal to 1.

where γ is some constant.

This result is now used in the expression for the integrated auto-correlation time (19.21) and the result is:

$$\begin{aligned}\tau_x^i &= \frac{1}{2} + \gamma \sum_{k=1}^{\infty} \left[\exp\left(-\frac{1}{\tau_x^e}\right)\right]^k \\ &= \frac{1}{2} + \gamma \left[\frac{1}{1 - \exp\left(-\frac{1}{\tau_x^e}\right)} - 1\right] \\ &= \frac{1}{2} + \gamma \frac{\exp\left(-\frac{1}{\tau_x^e}\right)}{1 - \exp\left(-\frac{1}{\tau_x^e}\right)}. \end{aligned} \tag{19.30}$$

For large $\tau_x^e \gg 1$ the exponential function can be expanded into a TAYLOR series up to first order and we obtain

$$\tau_x^i = \frac{1}{2} + \gamma \frac{1 - \frac{1}{\tau_x^e}}{\frac{1}{\tau_x^e}} = \frac{1}{2} + \gamma \left(\tau_x^e - 1\right) \propto \gamma \tau_x^e. \tag{19.31}$$

However, we note that in general relation (19.31) is a poor approximation because usually the exponential auto-correlation time is very different from the integrated auto-correlation time.

Let us briefly discuss our results. A comparison between Eqs. (19.3) and (19.18) reveals that due to correlations in the time series, the number of effective data points is reduced by a factor $2\hat{\tau}_x^i$, i.e.

$$N_{eff} = \frac{N}{2\hat{\tau}_x^i}. \tag{19.32}$$

In the limit $\tau_x^e \to 0$ we obtain $\tau_x^i = 1/2$ and therefore recover Eq. (19.3). We note that the effective number of measurements is the relevant quantity whenever the error of a Monte Carlo integration is calculated.

Moreover, one can measure the exponential auto-correlation time τ_x^e for an estimate of the number of steps that should be neglected between two successive measurements. This is achieved by fitting the auto-correlation $A(k)$ with an exponential function. A brief introduction to least squares fits can be found in Appendix G.

In a final remark we note that the auto-correlation times may be very different for different observables.

19.4 The Histogram Technique

The histogram technique is a method which allows to approximate the expectation value of some observable for temperatures near a given temperature T_0 without performing further MARKOV-chain Monte Carlo simulations. The basic idea is easily sketched. Suppose the observable O is solely a function of energy E. We perform a MARKOV-chain Monte Carlo simulation for a given temperature T_0 and measure the energy E several times. The resulting measurements are sorted in a histogram with bin width ΔE as was demonstrated in Sect. 18.3. In what follows $n(E)$ shall denote the number of configurations measured within the interval $(E, E + \Delta E)$. Hence, the probability of measuring an energy within the interval $(E, E + \Delta E)$ is given by

$$P_H(E, T_0) = \frac{n(E)}{M}, \tag{19.33}$$

where the index H refers to histogram and $M = \sum_E n(E)$ is the number of measurements. However, we note that this probability can also be expressed by the BOLTZMANN distribution

$$P(E, T) = \frac{N(E) \exp\left(-\frac{E}{k_B T}\right)}{\sum_E N(E) \exp\left(-\frac{E}{k_B T}\right)}, \tag{19.34}$$

where $N(E)$ denotes the number of micro-states within the interval $(E, E + \Delta E)$. We note that $N(E)$ is independent of the temperature T and that relation (19.34) is valid for all temperatures T. In particular for $T = T_0$ we have

$$P_H(E, T_0) = P(E, T_0), \tag{19.35}$$

which immediately yields

$$N(E) = \alpha n(E) \exp\left(\frac{E}{k_B T_0}\right), \tag{19.36}$$

where α is some constant. We remember that $n(E)$ is the distribution of configurations measured at T_0. Inserting Eq. (19.36) into (19.34) yields

$$P(E, T) = \frac{n(E) \exp\left[-\left(\frac{1}{k_B T} - \frac{1}{k_B T_0}\right) E\right]}{\sum_E n(E) \exp\left[-\left(\frac{1}{k_B T} - \frac{1}{k_B T_0}\right) E\right]}, \tag{19.37}$$

for arbitrary T. The expectation value of the observable O at some temperature T, i.e. $\langle O \rangle_T$, can now be calculated from

$$
\begin{aligned}
\langle O\rangle_T &= \sum_E O(E)P(E,T) \\
&= \frac{\sum_E O(E)n(E)\exp\left[-\left(\frac{1}{k_BT}-\frac{1}{k_BT_0}\right)E\right]}{\sum_E n(E)\exp\left[-\left(\frac{1}{k_BT}-\frac{1}{k_BT_0}\right)E\right]}.
\end{aligned}
\tag{19.38}
$$

It is, therefore, not necessary to run an additional MARKOV-chain Monte Carlo simulation in an attempt to compute the expectation value for T in the vicinity of T_0. However, if T_0 deviates strongly from T, the above procedure (19.38) is not a good approximation because the relevant configurations for T may have been very improbable at T_0 and may therefore not have been reproduced sufficiently often in the original MARKOV-chain Monte Carlo simulation.

Summary

Data analysis is an important but often neglected part of natural sciences and in particular of numerical simulations. It consists mainly of consistency checks and error analysis. This chapter concentrated in a first step on error analysis. It discussed the most common methods to arrive at an estimate of the error involved whenever expectation values of some property are analyzed. These went beyond all those methods which have already been discussed in some detail throughout this book. In a second step auto-correlations have been discussed. They should be part of consistency checks and give valuable information about possible systematic errors. The auto-correlation analysis is of particular importance whenever the quality of the sequence of random numbers is crucial to a particular simulation. (Experiments in which the events are expected to be random, like radioactive decay, fall also into this category.) Nevertheless, this method can also be very useful in MARKOV-chain Monte Carlo simulations as it allows to define and determine an auto-correlation time which can be used as a measure of the number of sweeps which have to be neglected between two consecutive measurements. Finally, the histogram technique was introduced as a method of data interpolation. It allows in addition to the applications which have already been presented within this book to estimate the expectation value of some property at some 'temperature' T if the expectation value of this same property is known at some other temperature T_0 if $T \sim T_0$ and if the equilibrium distribution is known. Thus, in most cases there is no need to run an additional simulation at temperature T.

Problems

1. Calculate the auto-correlation function for random numbers generated by the two linear congruential generators discussed in Sect. 12.2. Check also the random number generator provided by your system. Discuss the results.
2. POTTS model: Calculate the error attached to the specific heat c_h and the susceptibility χ using the Jackknife method for all values of $q = 1, \ldots, 8$. Plot the corresponding diagrams and discuss the results. Determine the exponential and integrated correlation time.

Reference

1. Iversen, G.P., Gergen, I.: Statistics. Springer Undergraduate Textbooks in Statistics. Springer, Berlin (1997)

Chapter 20
Stochastic Optimization

20.1 Introduction

Let us define the problem: Suppose $x \in \mathbb{S}$ is some vector in an n-dimensional search space $\mathbb{S}$ and let $\mathbb{H} : \mathbb{S} \to \mathbb{R}$ be a mapping from the search space $\mathbb{S}$ onto the real axis $\mathbb{R}$. The function $\mathbb{H}$ plays a particular role and is usually referred to as the *cost function*. A minimization problem can be defined in a very compact form:

Find $x_0 \in \mathbb{S}$, *such that* $\mathbb{H}(x_0)$ *is the* global *minimum of the cost function* $\mathbb{H}$.

In analogue, a maximization problem with cost function $\mathbb{H}$ defines a minimization problem with cost function $\mathbb{G} = -\mathbb{H}$. The class of both problems is referred to as the class of optimization problems. In what follows only minimization problems are considered.

The reader might be aware that there is an uncountable number of examples of applications in physics and related sciences which actually are optimization problems. We list a few in order to remind ourselves of their fundamental importance:

- The set of linear equations $Ax = b$ is in many cases regarded as a minimization problem: $\mathbb{H}(x) = \|Ax - b\|^2$ for high dimensional problems.
- The quantum mechanical ground state energy E_0 is given by

$$E_0 = \min_{\Psi} \frac{\langle \Psi \mid H \mid \Psi \rangle}{\langle \Psi \mid \Psi \rangle} , \tag{20.1}$$

  where $|\Psi\rangle$ denotes the wave function and H is the Hamiltonian of the system.
- High dimensional and highly non-linear least squares fits. (More details can be found in Appendix G).
- The equilibrium crystal structure of solids is obtained by minimization of the free energy.
- Protein folding is described by minimization of the forces in a *molecular dynamics* problem.
- etc.

B. A. Stickler and E. Schachinger, *Basic Concepts in Computational Physics*,
DOI: 10.1007/978-3-319-02435-6_20, © Springer International Publishing Switzerland 2014

Whenever the cost function is at least once differentiable, methods of deterministic optimization can be applied. (Two simple deterministic optimization methods are presented in Appendix H.) On the other hand, if $\mathbb{H}$ is not differentiable or too complex, due to a huge search space $\mathbb{S}$ or many local minima, methods of stochastic optimization can be employed. The term stochastic optimization is used for methods which contain at least one step which is based on random number generation. Let us briefly give some examples of problems for which deterministic methods fail:

- The *Traveling Salesperson Problem*: A traveling salesperson has to visit L cities in a tour as short as possible under the constraint that he/she has to return to the starting point in the end. Each city has to be visited only once, hence the cities have to be ordered in such a way that the travel length becomes a global minimum. In particular, the cost function

$$\mathbb{H}(\{i\}) = \sum_{\ell=1}^{L} |x_{i_{\ell+1}} - x_{i_\ell}| \, , \tag{20.2}$$

  has to be minimized. Here $\{i\}$ denotes a certain configuration of cities and we set $i_{L+1} = i_1$. Obviously, we cannot calculate the first derivative of $\mathbb{H}$ with respect to $\{i\}$, set it zero, and solve the problem in the classical way. On the other hand, a brute force approach of calculating $\mathbb{H}(\{i\})$ for all possible arrangements $\{i\}$ is not possible since we have $L!$ different possible routes. Since for one particular choice all L starting points and both travel directions yield the same result, we have to calculate $\frac{L!}{2L} = \frac{(L-1)!}{2}$ different configurations $\{i\}$. We would have about 10^{155} different choices for $L = 100$ cities! This clearly makes such an approach intractable.
- The arrangement of timetables under certain constraints. In particular, the design of timetables in schools, universities or at airports. This problem is also referred to as the *Nurse Scheduling Problem* for obvious reasons.
- The Ising *spin glass*: In contrast to the classical Ising model, the Ising spin glass is characterized by nearest neighbor interactions J_{ij} which are, in the most simple case, chosen to be $J_{ij} = +1$ and $J_{ij} = -1$ with the same probability. In this case the ground state below the critical temperature is not simply given by a configuration in which all spins point in the same direction. Of course, the ground state configuration in such a case can be highly degenerate. The fact that such a model can be simulated using Markov-chain Monte Carlo methods as they have been discussed within Chaps. 15 and 18 gives us some idea of how one may employ stochastic methods to solve optimization problems.
- The *N-Queens Problem*: Place N queens on a $N \times N$ chessboard in such a way that no two queens attack each other. In particular, this means that two queens are not allowed to share the same row, the same column, and the same diagonal. It can be shown that the problem possesses solutions for $N \geq 4$. One defines a function $\mathbb{H}(\{n\})$ which counts the number of attacks in a certain configuration $\{n\}$. For instance, for $N = 4$, the configuration

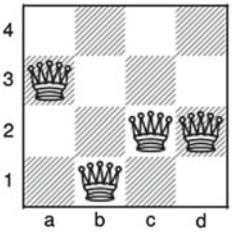

has $\mathbb{H}(\{n\}) = 2$. On the contrary, the configuration

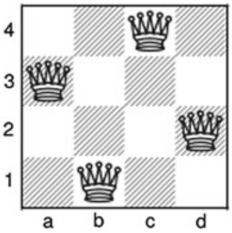

solves the 4-queens problem, i.e. $\mathbb{H}(\{n\}) = 0$.

We will discuss here some of the most basic methods of stochastic optimization: the method of *hill climbing*, the method of *simulated annealing*, and *genetic algorithms*. The ideas on which several more advanced techniques are based will be sketched in Sect. 20.5.

20.2 Hill Climbing

The method of *hill climbing* is probably one of the most simple methods of stochastic optimization. Given a cost function $\mathbb{H}(x)$, we proceed with the following steps:

1. Choose an initial position x_0.
2. Randomly pick a new x_n from the *neighborhood* of x_{n-1}.
3. Keep x_n if $\mathbb{H}(x_n) \leq \mathbb{H}(x_{n-1})$.
4. Terminate the search if no new x_n can be found in the neighborhood of x_{n-1}.

We note that in order to execute the algorithm a *neighborhood* relation is required. In particular, for instance in the case of the traveling salesperson problem it is by no means clear what a configuration in the *neighborhood* of a certain route $\{i\}$ should mean. This neighborhood relation has to be defined for each problem and we discuss here two possibilities.

In the case of the traveling salesperson or the Ising spin glass model the neighborhood of a route $\{i\}$ or of a configuration $\mathscr{C}$ can be defined as the set of all routes

$\{i\}$ in which two cities have been interchanged or as the set of all configurations $\mathscr{C}$ in which one spin has been flipped.

On the other hand, if the search space $\mathbb{S} = \mathbb{R}^n$ we may define the neighborhood as the number of points within an n-sphere of radius r centered at $z \equiv x_{n-1}$. It is rather simple to sample points from an n-sphere centered at the origin by applying the method of G. Marsaglia [1]: For an n-dimensional vector we sample all components $x_1, \ldots, x_n$ from the normal distribution $\mathscr{N}(0, 1)$ with mean zero and variance one. The points are then transformed according to

$$x_j \to x'_j = \frac{r}{\|x\|} x_j + z_j \ , \tag{20.3}$$

where $\|x\|$ denotes the Euclidean norm of the vector x. The points given by Eq. (20.3) lie on the surface of the n-sphere with radius r. In order to obtain uniformly distributed random points *within* a sphere with radius r we draw a random number $u \in [0, 1]$ and calculate

$$x_j \to x'_j = u^{\frac{1}{n}} x_j \ , \tag{20.4}$$

where the factor $1/n$ in the exponent of u ensures that the points are uniformly distributed.

Let us briefly summarize the most important properties of the method of hill climbing:

- The way the algorithm is defined it will terminate in a *local* minimum, not in the global minimum. A possible remedy to this caveat is achieved by restarting the algorithm several times from different initial positions. Information gathered from previous runs can help to make a good choice for the initial positions of restarts.
- How the global minimum is obtained depends highly on the choice of the initial conditions and this is very similar to the situation when deterministic methods of optimization (Appendix H) are employed. Sometimes it may even be of advantage to accept points which result in a slight increase of the cost function's value just to escape a local minimum.
- For most problems this method is very expensive from a computational point of view.

We apply the method of hill climbing to the N-queens problem for $N = 8$. The algorithm is executed in the following way: In the initial configuration the queens are set randomly on the chessboard and we place only one queen in each row and column. It is then checked whether or not two queens attack each other. If they do, a new configuration is generated by picking two queens at random and by changing their respective positions. This is repeated until a configuration arises in which none of the queens attacks another. Hence, the algorithm resembles a random walk in parameter space (i.e. possible configurations under the constraint that only one queen is placed in each row and column), which is terminated as soon as no queen is attacked by any other queen. It is rather obvious that this strategy is not very fast, however, one possible solution to the problem for $N = 8$ can easily be found within a couple of iterations:

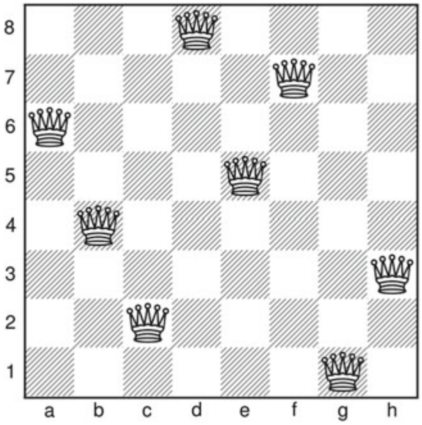

However, for large N the method of hill climbing is definitely not a good method for the N-queens problem.

20.3 Simulated Annealing

Let us turn our attention to another method, i.e. *simulated annealing*. Simulated annealing is a method which is highly motivated by physics. In order to reconstruct its train of thoughts let us consider the ISING spin glass introduced in Sect. 20.1. As in the case of the ISING model, Chap. 15, we know from thermodynamics that the equilibrium distribution of configurations $P(\mathscr{C}, T)$ at a certain temperature T is a BOLTZMANN distribution

$$P(\mathscr{C}, T) = \frac{1}{Z} \exp\left[-\frac{H(\mathscr{C})}{k_B T}\right] , \tag{20.5}$$

where $H(\mathscr{C})$ is the HAMILTON function of the system. In particular, we expect that the system is in its ground state (let us assume a non-degenerate ground-state for the time being) with probability one in the limit $T \to 0$, provided that we cooled sufficiently slow, i.e. let the system enough time to equilibrate. This provides a rather interesting method to solve an optimization problem: We take the cost function $\mathbb{H}(x)$ and define the probability for the realization of a particular point in the search space $x_0 \in \mathbb{S}$ by

$$P(x_0, T) = \frac{1}{Z} \exp\left[-\frac{\mathbb{H}(x_0)}{T}\right] , \tag{20.6}$$

where T is some external parameter which we refer to as *temperature* for reasons of convenience. Moreover, in Eq. (20.6) Z denotes the normalization constant, i.e.

$$Z = \sum\!\!\!\!\!\!\!\int_{x\in\mathbb{S}} \mathrm{d}x \ \exp\left[-\frac{\mathbb{H}(x)}{T}\right] . \tag{20.7}$$

We then take some finite initial temperature $T_0 \neq 0$ and construct a Markov-chain of realizations $\{x_n\}$ which converges towards the distribution (20.6), as we did in the case of a Markov-chain Monte Carlo methods in Chap. 18. Of course, we choose a sampling technique which does not require the explicit knowledge of the normalization Z, such as the Metropolis-Hastings algorithm of Sect. 18.2. As soon as the Markov-chain reaches its stationary distribution for a given temperature T, we slightly decrease the temperature and restart the Markov-chain with the last configuration of the previous temperature.

It is of advantage to choose an initial temperature at which a large part of the search space $\mathbb{S}$ can be covered, i.e. the acceptance probability for a new realization in the Markov-chain is almost equal for all $x \in \mathbb{S}$. Otherwise, some regions of the search space might be excluded from our search routine by an unlucky choice of the initial configuration. In particular the result might be a configuration in the neighborhood of the initial configuration of the Markov-chain and it is, therefore, most likely a local minimum rather than the global minimum.

The method outlined in the above paragraphs is commonly referred to as the classical version of *simulated annealing*. The name for the algorithm stems from the annealing process in metallurgy, where a metal is first heated and then slowly cooled in order to reduce the amount of defects in the material. The same principles hold for this algorithm: by slowly *cooling* the search Markov-chain, we slowly exclude unimportant parts of the search space by decreasing their acceptance probability. Nevertheless, the chain is given enough time to explore the whole remaining search space at each temperature.

We note that the algorithm consists of the following essential ingredients: (i) a proposal probability for new states x within search space $\mathbb{S}$, (ii) an acceptance probability $P_A(x' \to x)$ for a proposed x from a previous state x', and (iii) a cooling strategy $T = T(t)$, where t is time. Let us briefly elaborate on these points.

(i) Proposal Probability

The question of how to generate new states x from a previous state x' within the search space $\mathbb{S}$ is closely related or even identical to the definition of a neighborhood in the case of hill climbing in Sect. 20.2. It is therefore not necessary to repeat the above discussion, we simply refer to it. The proposal probability will be denoted by $P_p(x \to x')$ in what follows.

(ii) Acceptance of Probability

The acceptance probability has to be chosen in such a way that the sequence of generated states constitutes a MARKOV-chain which converges towards the distribution (20.6). Hence, detailed balance has to be imposed and the implications of this requirement have been discussed extensively in Chap. 18. Note that the proposal probability has to be included into the definition of the acceptance probability, see Sect. 18.2.

We note that the particular choice of a METROPOLIS-HASTINGS acceptance probability

$$P_a(x \to x', T) = \min\left(1, \frac{P(x', T)}{P(x, T)} \frac{P_p(x' \to x)}{P_p(x \to x')}\right) , \tag{20.8}$$

appears to be quite natural for several reasons:

- It is very general and can, thus, also handle asymmetric proposal probabilities.
- In the symmetric case, i.e. for $P_p(x \to x') = P_p(x' \to x)$, we have for $\mathbb{H}(x') \leq \mathbb{H}(x)$ according to our choice (20.6)

  $$\frac{P(x', T)}{P(x, T)} = \exp\left\{\frac{1}{T}\left[\mathbb{H}(x) - \mathbb{H}(x')\right]\right\} \geq 1 , \tag{20.9}$$

  and the state x' is accepted with probability 1. Moreover, for $\mathbb{H}(x') > \mathbb{H}(x)$, x' may still be accepted with some finite probability $P_a(x \to x', T)$ which offers an opportunity to escape a local minimum.

Let us now turn our attention to the choice of a proper cooling strategy.

(iii) Cooling Strategy

The design of a proper cooling strategy includes both, the choice of an appropriate initial temperature T_0 as well as the formulation of a mathematical rule which defines $T_{n+1} = f(T_n)$ where $T_{n+1} < T_n$.

We discuss the choice of the initial temperature in a first step. A common choice for the initial temperature is to choose it in such a way that at least 80 % of all generated states can be accepted. One determines this temperature by taking some arbitrary $T_0 > 0$ and generating N states. If the number of rejected states N_r is greater than $0.2N$, then the temperature T_0 is doubled and the number of rejected states is measured again.

Another more sophisticated choice is based on the following idea: In the best case the initial temperature reaches infinity, i.e. $T_0 \to \infty$, because in this case the acceptance probability is one for all states independent of $\mathbb{H}(x)$, and we perform a random walk in search space $\mathbb{S}$. We calculate the mean value $\langle\mathbb{H}\rangle_\infty$ and the variance $\mathrm{var}\,(\mathbb{H})_\infty$. Thus, the function values $\mathbb{H}$ fluctuate between $[\langle\mathbb{H}\rangle_\infty - \sqrt{\mathrm{var}\,(\mathbb{H})_\infty}, \langle\mathbb{H}\rangle_\infty + \sqrt{\mathrm{var}\,(\mathbb{H})_\infty}]$. We consider now the expectation value $\langle\mathbb{H}\rangle_{T_0}$ for large T_0, when $\varepsilon = 1/T_0$ is small, and find with $p(x,\varepsilon) = P(x,T) = q(x,\varepsilon)/Z(\varepsilon)$

$$\begin{aligned}
\langle\mathbb{H}\rangle_\varepsilon &= \int \mathrm{d}x\; p(x,\varepsilon)\mathbb{H}(x) \\
&\equiv \frac{1}{Z(\varepsilon)} \int \mathrm{d}x\; q(x,\varepsilon)\mathbb{H}(x) \\
&\approx \frac{1}{Z(\varepsilon)} \int \mathrm{d}x\; q(x,\varepsilon)\mathbb{H}(x)\bigg|_{\varepsilon=0} + \varepsilon \int \mathrm{d}x\; \frac{\mathrm{d}}{\mathrm{d}\varepsilon}\left(\frac{1}{Z(\varepsilon)} q(x,\varepsilon)\right)\mathbb{H}(x)\bigg|_{\varepsilon=0} \\
&= \langle\mathbb{H}\rangle_0 + \varepsilon \int \mathrm{d}x\; \big[p(x,\varepsilon)\,\langle\mathbb{H}\rangle_\varepsilon - \mathbb{H}(x)p(x,\varepsilon)\big]\,\mathbb{H}(x)\bigg|_{\varepsilon=0} \\
&= \langle\mathbb{H}\rangle_0 - \varepsilon\left[\left\langle\mathbb{H}^2\right\rangle_0 - \langle\mathbb{H}\rangle_0^2\right] . \qquad (20.10)
\end{aligned}$$

Re-substituting $T_0 = 1/\varepsilon$ results, finally, in:

$$\langle\mathbb{H}\rangle_{T_0} \approx \langle\mathbb{H}\rangle_\infty - \frac{\mathrm{var}\,(\mathbb{H})_\infty}{T_0} . \qquad (20.11)$$

T_0 is now chosen in such a way that the expectation value $\langle\mathbb{H}\rangle_{T_0}$ borders infinite temperature fluctuations and we set consequently

$$\langle\mathbb{H}\rangle_{T_0} = \langle\mathbb{H}\rangle_\infty - \sqrt{\mathrm{var}\,(\mathbb{H})_\infty} , \qquad (20.12)$$

with the implication that

$$T_0 = \sqrt{\mathrm{var}\,(\mathbb{H})_\infty} . \qquad (20.13)$$

Having discussed in quite some detail the choice of an initial temperature it is now time to investigate possibilities of an appropriate cooling strategy. An often used cooling strategy is the *geometric cooling schedule*

$$T_n = T_0 q^n , \qquad (20.14)$$

with $0 \ll q < 1$. However, for a particular cost function $\mathbb{H}(x)$ one might observe several *phase transitions* during the cooling process. Naturally, the expectation value $\langle\mathbb{H}\rangle$ changes rapidly in the region $T \approx T_c$ and it is therefore advantageous to take such a possibility into account and to design the cooling strategy accordingly.

Hence, a more appropriate strategy is to use temperature changes which cause only slightly modified acceptance probabilities. In particular, we demand that

$$\frac{1}{1+\delta} < \frac{P(x,T_n)}{P(x,T_{n+1})} < 1+\delta , \qquad (20.15)$$

with $0 < \delta \ll 1$. Assuming a BOLTZMANN type distribution for $P(x, T_n)$, we obtain

$$\exp\left[-\mathbb{H}(x)\left(\frac{1}{T_n} - \frac{1}{T_{n+1}}\right)\right] < 1 + \delta \ , \tag{20.16}$$

or

$$T_{n+1} > \frac{T_n}{1 + \frac{T_n}{\mathbb{H}(x)} \ln(1+\delta)} \ . \tag{20.17}$$

Hence, we can choose

$$T_{n+1} \approx \frac{T_n}{1 + \frac{T_n}{3\sqrt{\operatorname{var}(\mathbb{H})_{T_n}}} \ln(1+\delta)} \ , \tag{20.18}$$

where we replaced $\mathbb{H}(x) \approx 3\sqrt{\operatorname{var}(\mathbb{H})_{T_n}}$. This choice is plausible if one recognizes that we can replace $\mathbb{H}(x) \to \mathbb{H}(x) - \mathbb{H}_{\min}$ in the above calculations, where $\mathbb{H}_{\min}$ represents the (unknown) minimum of $\mathbb{H}(x)$. This cooling schedule is known as the AARTS schedule.

The final question concerns the termination of the algorithm. Typically, there are several choices. We shall briefly note the most popular procedures. Obviously, the first choice is to terminate the algorithm as soon as the acceptance ratio is below a predefined threshold value. A more sophisticated choice is to terminate the algorithm whenever the mean value $\langle \mathbb{H} \rangle \approx \text{const}$ reaches some constant value. A totally different approach would be to initially choose a maximum number of iterations or to set the final temperature T_f to some reasonable value. Of course, the termination condition has to be defined for each particular problem individually.

Before discussing a specific example, let us briefly present some further points which can be found in the literature. It has been demonstrated [2] that the optimal cooling strategy for a BOLTZMANN type distribution is of the form

$$T_n \propto \frac{1}{\ln(n)} \ . \tag{20.19}$$

In this case one finds the global minimum with probability one. However, the convergence toward this minimum is rather slow. Moreover, several extensions of classical simulated annealing have been suggested in the literature. For instance, *fast simulated annealing* uses a CAUCHY distribution instead of a BOLTZMANN distribution:

$$P(x, T) = \frac{T}{\left(x^2 + T^2\right)^{\frac{d+1}{2}}} \ . \tag{20.20}$$

Here d is the dimension of the search space $\mathbb{S}$. The optimal cooling strategy for such a distribution function is of the form

$$T_n \propto \frac{1}{n} \, , \tag{20.21}$$

which signifies a considerable increase in convergence speed in comparison to Eq. (20.19). A further generalization is referred to as *generalized simulated annealing* and is based on the TSALLIS distribution which depends on an external parameter ε:

$$P_\varepsilon(x, T) = \frac{1}{Z}\left[1 + \frac{\varepsilon \mathbb{H}(x)}{k_B T}\right]^{-\frac{1}{\varepsilon}} \, . \tag{20.22}$$

It can be demonstrated that P_ε converges towards the BOLTZMANN distribution for $\varepsilon \to 0$. Furthermore, we mention that the concept of the TSALLIS distribution is closely intertwined with the definition of the TSALLIS entropy and the formulation of non-extensive thermodynamics [3].

As a first illustrative example we discuss the *traveling salesperson problem* for cities on a regular grid because in this case the optimal route is easily identified. We calculate the initial temperature from Eq. (20.13) and employ the geometric cooling schedule (20.14) with $q = 0.99$ together with a termination criterion of the form

$$\langle \mathbb{H} \rangle_{T_n} - \langle \mathbb{H} \rangle_{T_{n-1}} < \eta \, , \tag{20.23}$$

where η is the required accuracy. In Fig. 20.1 we show the path for two different temperatures T and $N = 36$ cities. This case will in what follows be called the *first scenario*. In a *second scenario* we place 36 cities in four equally spaced clusters. Results for the optimal route are presented in Fig. 20.2.

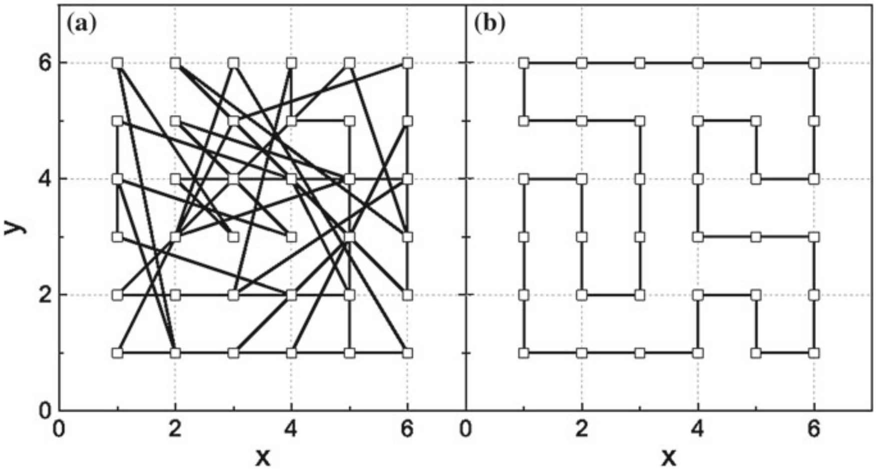

Fig. 20.1 (**a**) Initial route of the traveling salesperson for 36 cities on a regular grid. (**b**) One of many optimal routes of the traveling salesperson for 36 cities on a regular grid

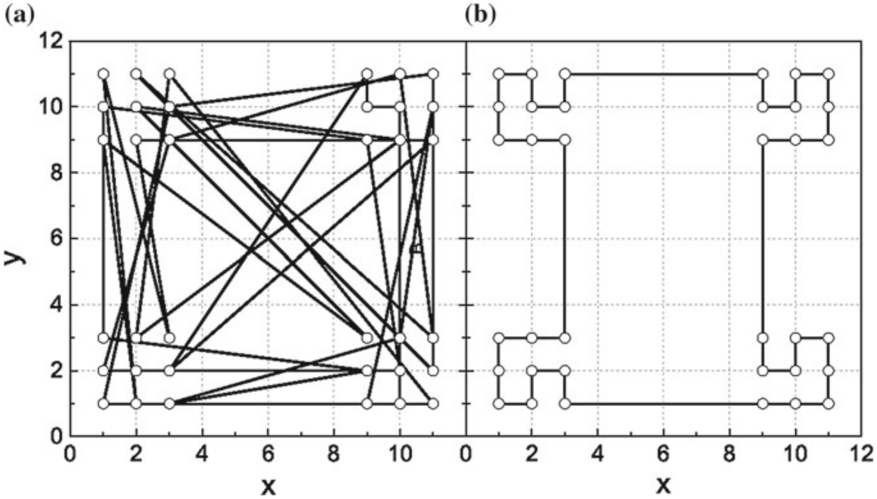

Fig. 20.2 (**a**) Initial route of the traveling salesperson for 36 cities placed in four equally spaced clusters. (**b**) One of many optimal routes of the traveling salesperson for 36 cities placed in four equally spaced clusters

Fig. 20.3 (**a**) The expectation value $\langle \mathbb{H} \rangle_T$ and (**b**) the 'specific heat' c_h versus temperature T for scenario one

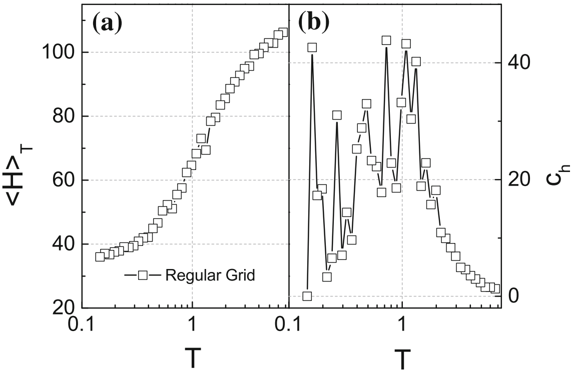

In a genuine physical system the question whether a possible phase transition is of first or second order is solely determined by the HAMILTON function $H(x)$ of the system. As an intriguing example we refer to the q-states POTTS model of Sect. 18.3 where a second order phase transition was observed for $q \leq 4$ and a first order phase transition for $q > 4$. In analogue, the order of a 'phase transition' during the iteration process toward the global minimum in simulated annealing is completely determined by the particular form of the cost function $\mathbb{H}(x)$. To follow up on this comment, the expectation values of $\langle \mathbb{H} \rangle_T$ and of the 'specific heat' c_h are compared for the two scenarios as functions of temperature T. Figures 20.3a, b presents the results for scenario one and Figs. 20.4a, b those for scenario two. The second scenario develops two second order phase transitions while in the first scenario only one second order

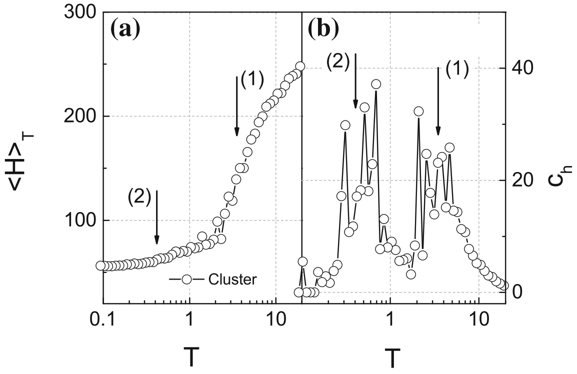

Fig. 20.4 The same as Fig. 20.3 but for scenario two. Two first order phase transitions are observed. They are indicated by *down arrows* labeled (*1*) and (*2*)

phase transition can be observed. The first phase transition of the second scenario (at $T \approx 3.5$) can be related to the optimization of the clusters' sequence while in the second phase transition (at $T \approx 0.42$) the sequence of cities within the clusters becomes finalized. These two transitions are indicated by down arrows labeled (1) and (2).

20.4 Genetic Algorithms

The sparkling idea of *genetic algorithms* has originally been lent from natures *survival* of the fittest. The basic intentions are quickly summarized by remembering the natural evolution of a particular species within a hostile environment: The individuals of the species *reproduce* from one *generation* to another. During this process the *genes* of the individuals are modified by local *mutations*. Individuals best accustomed to the environment then survive with higher probability. This very last process is referred to as *selection*. By iterating this process for large *populations* the individuals of the whole species will adjust their properties to the environment *on average*,[1] and, thus, the individuals will be better equipped for survival within the hostile environment. A large population is compulsory in order to obtain a huge variety in the *phenotype* of the individuals. Algorithms based on such a scheme are referred to as *genetic algorithms*.

We are not going into the details of the implementation of genetic algorithms because this is beyond the scope of this book. However, the ideas sketched above will be applied to the problem of the traveling salesperson passing through m-cities just to illustrate the method. Let $s = (s_1, \dots, s_m) \in \mathbb{N}^m$ denote a list of m integers, which obey $s_i \leq i$. For instance, for $m = 10$, s might be given by

[1] Note that in the real world the environment (in particular the natural enemies of a species) develop as well. Moreover, we do not consider any communication within a species, like the formation of *societies*, *learning*, and related processes.

Table 20.1 Sample tour to illustrate the recovery of the order of cities within a genetic algorithm

$\hat{s}$	1	2	3	4	5	6	7	8	9	10		Tour
9	1	2	3	4	5	6	7	8	[9]	10	→	9
4	1	2	3	[4]	5	6	7	8	10		→	4
3	1	2	[3]	5	6	7	8	10			→	3
3	1	2	[5]	6	7	8	10				→	5
5	1	2	6	7	[8]	10					→	8
1	[1]	2	6	7	10						→	1
4	2	6	7	[10]							→	10
2	2	[6]	7								→	6
2	2	[7]									→	7
1	[2]										→	2

Elements indicated by [x] are ‘selected’ elements which are added to the column Tour

$$s = (1, 2, 2, 4, 1, 5, 3, 3, 4, 9). \tag{20.24}$$

The order of cities is then recovered by setting $\hat{s} = (s_m, \dots, s_1)$ and performing the steps illustrated in Table 20.1.

In words: The vector $\hat{s}$ labels the elements taken from the list $(1, 2, \dots, m)$ *with* removal. The resulting list Tour specifies the optimum sequence of the cities. The genetic algorithm is executed in the following steps:

- Define M initial individuals.
- *Mutation*: for each individual we introduce a single random local modification with probability p_{mut}.
- *Reproduction*: We produce M additional individuals by pairwise combining the *parents*. This is performed by

  (a) Pick two individuals at random.
  (b) Draw a random integer $r \in [1, m-1]$ and replace the first r genes of the first individual by the first r genes of the second individual and vice versa.

  In this way, we obtain $2M$ individuals.
- *Selection*: The M individuals with the highest *fitness*, i.e. the lowest value of the cost function survive.

The above steps are repeated until the desired number of generations has been achieved.

In Fig. 20.5 we show the optimal path for the traveling salesperson problem discussed in the previous section, but now for $N = 30$ cities. It was obtained with the genetic algorithm described here. The number of individuals was chosen to be $M = 5000$ and the number of generations to be $G = 5000$.

Some remarks are appropriate: First of all we note that there are many different permutations of how a genetic algorithm can be realized. In particular, it is the problem which determines the most convenient form to implement the essential ingredients: mutation, reproduction, and selection. However, particular care is required in

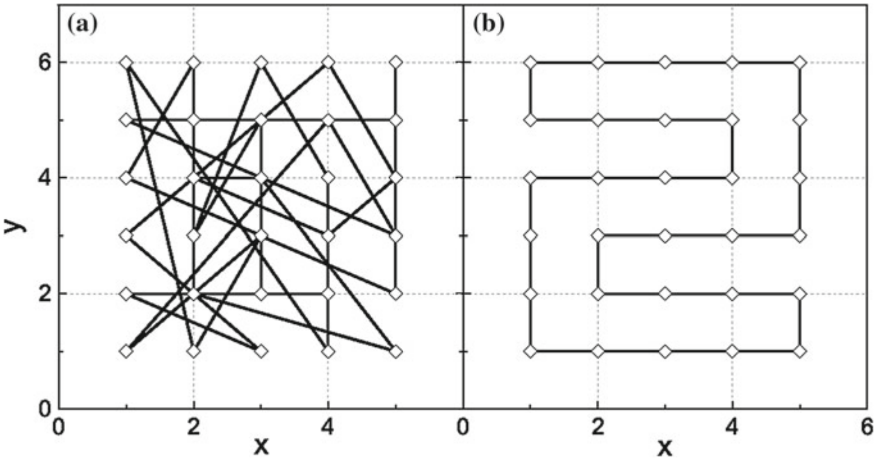

Fig. 20.5 (**a**) The random route of one individual out of the population of 5000. (**b**) One of many optimal routes of the traveling salesperson for $N = 30$ cities as obtained by a genetic algorithm

formulating the algorithm so that it does not produce individuals which are *too* similar. In such a case the algorithm very likely terminates in a local minimum.

A second remark concerns the treatment of optimization problems with continuous variables x. Here it might be advantageous to represent the variable x in its binary form because it makes the reproduction step particularly simple.

20.5 Some Further Methods

We briefly list some alternative stochastic optimization techniques without going into detail. Two famous alternatives which are closely related to simulated annealing are:

- *Threshold Accepting Algorithms*: The new configuration x' is accepted with probability one if $\mathbb{H}(x') \leq \mathbb{H}(x) + T$. During the simulation the *temperature* or *threshold level* T is continuously decreased. The above choice of an acceptance is a very effective choice to allow for escaping local minima.
- *Deluge Algorithms*: These algorithms are very similar to threshold accepting algorithms. We present it in the original formulation which is suited to find the global maximum of a function $\mathbb{G}(x)$. The global minimum of $\mathbb{H}(x)$ can be found by searching the maximum of $\mathbb{G}(x) = -\mathbb{H}(x)$. One accepts a new state x' with probability one if $\mathbb{G}(x') > T$, where T is continuously increased during the simulation. Hence, the whole *landscape* of $\mathbb{G}(x)$ is *flooded* with increasing T until only the summits of $\mathbb{G}(x)$ are left. Finally, only the biggest *mountain* will reach out of the *water* and the global maximum has been found.

Two famous ideas which are closely related to genetic algorithms are:

- *Grouping Genetic Algorithms*: The idea is to put the individuals of the population in distinct *groups*. These groups may for instance be formed by comparing the genes or grouping individuals with similar cost function values. All members of a group have one part of the genes in common, and all operators acting on genes act on the whole group. Such an approach can significantly improve the convergence rate of a classical genetic algorithm.
- *Ant Colony Optimization*: The idea is, again, borrowed from nature, in particular from an ant colony searching the optimum path between two or more fixed or variable points. In real world an ant travels from one point to another randomly, leaving a trail of pheromone on its traveled path. Following ants are very likely to follow the pheromone trail, however, some random nature remains. The key point is that with time the pheromone trail starts to evaporate, hence its impact on the path of following ants is reduced if the path is not traveled frequently or often enough so that the pheromones already evaporated. In this way one prevents the algorithm to get stuck in a local minimum and the global minimum may be found by sending out artificial ants.

There are many further methods available in the literature [see, for instance, [4]] to which we refer the interested reader.

Summary

The local maximum/minimum of some cost function $\mathbb{H}(x)$ within a search space $\mathbb{S}$ can be determined using stochastic methods, thus establishing a particular class of algorithms known as *Stochastic Optimization*. The most straightforward method was the algorithm of *hill climbing* which resembled a controlled random walk within a restricted search space $\mathbb{S}$ called neighborhood. Because of this feature hill climbing will find in general local minima within this neighborhood and the global minimum has to be found under variation of initial conditions. This made this method too expensive for complex problems from a computational point of view. To move from a random walk formulation to a formulation on the basis of MARKOV-chain Monte Carlo was the logical next step. The method of choice was named *simulated annealing*. It uses the METROPOLIS-HASTINGS algorithm to generate new configurations within search space $\mathbb{S}$ from a temperature dependent equilibrium distribution using a cooling strategy to slowly restrict the search space to the neighborhood of the global minimum. It can be proved that this method always converges to the global minimum if the cooling strategy obeys some specific conditions, albeit rather slowly. There are many flavors of this basic algorithm which either differ in the definition of the acceptance probability or in the cooling strategy. A completely different class of algorithms was established with the so-called *genetic algorithms*. They are borrowed from nature's concept of the survival of the fittest. They are based on the notions of: (i) Mutation, a single random local modification of certain probability.

(ii) Reproduction, additional 'individuals' are generated by pairwise combining parents. (iii) Selection: Individuals with the lowest value of the cost function survive and mutation starts again. Genetic algorithms are very versatile and a huge body of optimization problems can actually be covered by this kind of methods.

Problems

Solve the traveling salesperson problem for $N = 20$ cities on a regular grid with the help of simulated annealing. As a cooling schedule, use the geometric cooling as explained in Sect. 20.3. Determine the initial temperature by demanding an acceptance rate of 90 % and terminate the algorithm if the mean value of the cost function $\langle \mathbb{H} \rangle$ remains unchanged for at least 10 successive temperatures. Calculate the expectation value $\langle \mathbb{H} \rangle_T$ for different temperatures and identify the transition temperature. In a second step produce a list of 20 cities which are randomly distributed on a two-dimensional plane. Optimize this problem as well. Note that you should produce the list of cities only *once* in order to obtain comparable and reproducible results.

References

1. Marsaglia, G.: Choosing a point from the surface of a sphere. Ann. Math. Stat. **43**, 645–646 (1972). doi:10.1214/aoms/1177692644
2. Kirkpatrik, S., Gellat Jr., C.D.: Simulated annealing. Science **220**, 671 (1983)
3. Tsallis, C.: Introduction to Nonextensive Statistical Mechanics. Springer, Berlin (2009)
4. Hartmann, A.H., Rieger, H.: Optimization Algorithms in Physics. Wiley, Berlin (2002)

Appendix A
The Two-Body Problem

Consider two mass points with position $r_i(t) \in \mathbb{R}^3$, $i = 1, 2$ and masses m_i, $i = 1, 2$. It is assumed that the point masses interact through a central potential $U = U(|r_1(t) - r_2(t)|)$ and external forces are neglected, i.e. the system is closed. In the following we will omit the explicit notation of time t for the sake of a more compact notation. Furthermore, let $p_i \in \mathbb{R}^3$, $i = 1, 2$ denote the point mass' momentum. Then the LAGRANGE function takes on the form

$$L(r_1, r_2, p_1, p_2) = \frac{p_1^2}{2m_1} + \frac{p_2^2}{2m_2} - U(|r_1 - r_2|) \quad \Rightarrow \text{CS} : \mathbb{R}^{12}. \tag{A.1}$$

and defines a twelve-dimensional configuration space (CS). Replacing the mass momenta p_i by

$$p_i = m_i \dot{r}_i, \quad i = 1, 2, \tag{A.2}$$

yields for the LAGRANGE function (A.1)

$$L(r_1, r_2, \dot{r}_1, \dot{r}_2) = \frac{m_1}{2}\dot{r}_1^2 + \frac{m_2}{2}\dot{r}_2^2 - U(|r_1 - r_2|), \tag{A.3}$$

where $\dot{r}_i$ denotes the time derivative of r_i. We note the following symmetries: the LAGRANGE function (A.3) is (i) translational invariant, (ii) rotational invariant, and, (iii) time invariant. We know from mechanics [1] that each symmetry of the LAGRANGE function corresponds to a constant of motion (a quantity that is conserved throughout the motion) and, thus, results in a reduction of the dimensionality of the twelve-dimensional configuration space.

Let us demonstrate these symmetries: In order to prove translational invariance, we transform to center of mass coordinates, which are given by

$$R = \frac{m_1 r_1 + m_2 r_2}{m_1 + m_2} \qquad \text{and} \qquad r = r_2 - r_1. \tag{A.4}$$

B. A. Stickler and E. Schachinger, *Basic Concepts in Computational Physics*,
DOI: 10.1007/978-3-319-02435-6, © Springer International Publishing Switzerland 2014

It is easily verified that we can express the original coordinates r_1 and r_2 with the help of (A.4) as

$$r_1 = R + \frac{m_2}{m_1 + m_2} r \qquad \text{and} \qquad r_2 = R - \frac{m_1}{m_1 + m_2} r. \tag{A.5}$$

Rewriting the LAGRANGE function (A.3) in the new coordinates (A.4) yields

$$\begin{aligned} L(r, R, \dot{r}, \dot{R}) &= \frac{M}{2}\dot{R}^2 + \frac{\mu}{2}\dot{r}^2 - U(|r|) \\ &\equiv L(r, \dot{r}, \dot{R}), \end{aligned} \tag{A.6}$$

where we introduced the total mass M and the *reduced* mass μ:

$$M = m_1 + m_2 \qquad \text{and} \qquad \mu = \frac{m_1 m_2}{m_1 + m_2}. \tag{A.7}$$

Note that in Eq. (A.6) the center of mass coordinate R is a *cyclic* coordinate, i.e. it does not appear explicitly in the LAGRANGE function. Hence, the system is translational invariant and we can deduce from LAGRANGE's equations that

$$\frac{\mathrm{d}}{\mathrm{d}t}\frac{\partial}{\partial \dot{R}} L = \frac{\partial}{\partial R} L = 0, \tag{A.8}$$

i.e. the center of mass momentum is conserved. Hence, we obtain that

$$\frac{\partial}{\partial \dot{R}} L = M\dot{R} = \text{const}, \tag{A.9}$$

or equivalently,

$$R(t) = At + B, \tag{A.10}$$

where $A, B \in \mathbb{R}^3$ are constants determined by the initial conditions of the problem. Note that this means that the center of mass moves along a straight line with constant velocity. It is now possible to reformulate the LAGRANGE function (A.6) as

$$\begin{aligned} L(r, \dot{r}) &= \frac{M}{2}A^2 + \frac{\mu}{2}\dot{r}^2 - U(|r|) \\ &\equiv \tilde{L}(r, \dot{r}) + \text{const} \quad \Rightarrow \text{CS} : \mathbb{R}^6. \end{aligned} \tag{A.11}$$

Hence, the problem was reduced to a one-body problem with the LAGRANGE function $\tilde{L}(r, \dot{r})$. We shall omit the tilde in the following for the sake of a more compact notation and regard the LAGRANGE function

$$L(r, \dot{r}) = \frac{\mu}{2}\dot{r}^2 - U(|r|), \tag{A.12}$$

instead of (A.11). We note that the translational invariance allowed us to reduce the two-body problem to an effective one body problem.

We proceed by investigating rotational invariance. Equation (A.12) resembles the LAGRANGE function of a particle located at position r in the field of a central force $F \in \mathbb{R}^3$ pointing to the center of the coordinate system (or pointing from the center of the coordinate system to the particle). This situation is clearly invariant under a rotation of the coordinate system since U depends only on the modulus of r, i.e. $U = U(|r|)$. We note that, therefore, $r \| F$, i.e. r is parallel to F for all $t \geq 0$. In such a case the angular momentum $\ell \in \mathbb{R}^3$ is conserved, since

$$\frac{\mathrm{d}}{\mathrm{d}t}\ell = M = r \wedge F = 0, \quad \rightarrow \ell = \text{const}, \tag{A.13}$$

where M is the *torque*. This allows us to arbitrarily rotate our coordinate system. We take advantage if this result to rotate it in such a way that

$$\ell = |\ell| e_z, \tag{A.14}$$

where e_z is the unit vector in z-direction. Moreover, since the angular momentum ℓ is given by

$$\ell = \mu r \wedge \dot{r} = \text{const}, \tag{A.15}$$

and because $\ell \| e_z$ we conclude that $r \perp e_z$. This allows us to put $z = 0$, which means that the whole motion of the point mass can be described in the $x - y$ plane $\Rightarrow$ CS : $\mathbb{R}^4$. We note that the rotational invariance led us to the conservation of angular momentum which allowed a reduction from a three-dimensional problem to a two dimensional problem. In a next step, we rewrite the LAGRANGE function (A.6) as (A.12) in polar coordinates (ρ, φ):

$$L(\rho, \dot{\rho}, \dot{\varphi}) = \frac{\mu}{2}\left(\dot{\rho}^2 + \rho^2\dot{\varphi}^2\right) - U(\rho) \quad \Rightarrow \text{CS} : \mathbb{R}^3. \tag{A.16}$$

Let us calculate LAGRANGE's equations (A.6) as from (A.16): First we regard the differential equation for the radius ρ

$$\frac{\mathrm{d}}{\mathrm{d}t}\frac{\partial}{\partial \dot{\rho}}L = \mu\ddot{\rho} = \frac{\partial}{\partial \rho}L = \rho\dot{\varphi}^2 - \frac{\partial}{\partial \rho}U(\rho), \tag{A.17}$$

thus

$$\mu\ddot{\rho} - \mu\rho\dot{\varphi}^2 + \frac{\mathrm{d}}{\mathrm{d}\rho}U(\rho) = 0. \tag{A.18}$$

For φ we obtain

$$\frac{\mathrm{d}}{\mathrm{d}t}\frac{\partial}{\partial \dot{\varphi}}L = \frac{\mathrm{d}}{\mathrm{d}t}\mu\rho^2\dot{\varphi} = \frac{\partial}{\partial \varphi}L = 0, \tag{A.19}$$

which is

$$\frac{\mathrm{d}}{\mathrm{d}t}\left(\mu\rho^2\dot{\varphi}\right)=0. \tag{A.20}$$

Equation (A.20) is trivially fulfilled since according to Eq. (A.15)

$$\mu\rho^2\dot{\varphi}=|\ell|=\text{const.} \tag{A.21}$$

However, we solve Eq. (A.21) for $\dot{\varphi}$

$$\dot{\varphi}=\frac{|\ell|}{\mu\rho^2}, \tag{A.22}$$

and plug (A.22) into (A.18) and obtain

$$\mu\ddot{\rho}-\frac{|\ell|^2}{\mu\rho^3}+\frac{\mathrm{d}}{\mathrm{d}\rho}U(\rho)=0. \tag{A.23}$$

We can now make use of the time invariance of the LAGRANGE function (A.16). Since this equation does not explicitly depend on time t we have

$$\frac{\partial}{\partial t}L=0. \tag{A.24}$$

This implies conservation of energy, Eq. (A.6), as can easily be demonstrated. We regard the total time derivative of the LAGRANGE function L

$$\frac{\mathrm{d}}{\mathrm{d}t}L=\dot{\rho}\frac{\partial}{\partial\rho}L+\ddot{\rho}\frac{\partial}{\partial\dot{\rho}}L+\ddot{\varphi}\frac{\partial}{\partial\dot{\varphi}}L+\frac{\partial}{\partial t}L, \tag{A.25}$$

and solve for $\frac{\partial}{\partial t}L$

$$\frac{\mathrm{d}}{\mathrm{d}t}\left(\dot{\rho}\frac{\partial}{\partial\dot{\rho}}L+\dot{\varphi}\frac{\partial}{\partial\dot{\varphi}}L-L\right)=-\frac{\partial}{\partial t}L=0. \tag{A.26}$$

Consequently

$$\dot{\rho}\frac{\partial}{\partial\dot{\rho}}L+\dot{\varphi}\frac{\partial}{\partial\dot{\varphi}}L-L=\text{const}, \tag{A.27}$$

which states the conservation of energy. Let us evaluate this expression with the help of Eq. (A.16). We obtain

$$\begin{aligned}\dot{\rho}\frac{\partial}{\partial\dot{\rho}}L+\dot{\varphi}\frac{\partial}{\partial\dot{\varphi}}L-L&=\frac{\mu}{2}\left(\dot{\rho}^2+\rho^2\dot{\varphi}^2\right)+U(\rho)\\&=\frac{\mu}{2}\dot{\rho}^2+\frac{|\ell|^2}{2\mu\rho^2}+U(\rho)\\&=E.\end{aligned} \tag{A.28}$$

Here we employed, in a second step, relation (A.22). In summary, time invariance led us to the result

$$\frac{\mu}{2}\dot{\rho}^2 + \frac{|\ell|^2}{2\mu\rho^2} + U(\rho) = E \quad \Rightarrow \text{CS} : \mathbb{R}^2. \tag{A.29}$$

We note that time reversal allowed us to reduce the problem to a first order differential equation in ρ, Eq. (A.29). Hence the way to solve the two-body problem can be outlined as follows: (i) calculate $R(t)$ according to Eq. (A.10), (ii) solve Eq. (A.29) in order to obtain $\rho(t)$, (iii) plug $\rho(t)$ into Eq. (A.22) and solve for $\varphi(t)$, (iv) since $z(t) = 0$, the original vectors $r_1(t)$, $r_2(t)$ can be constructed from $\rho(t)$ and $\varphi(t)$. All integration constants are uniquely determined by the initial conditions of the problem at hand.

From Eq. (A.29) we obtain

$$\dot{\rho} = \pm\sqrt{\frac{2}{\mu}\left(E - U(\rho) - \frac{|\ell|^2}{2\mu\rho^2}\right)}, \tag{A.30}$$

which results in an implicit equation for ρ

$$t = t_0 + \int\limits_{\rho_0}^{\rho} \mathrm{d}\rho' \frac{\mu\rho'}{\sqrt{\mu\rho'^2\left[E - U(\rho')\right] - |\ell|^2}}, \tag{A.31}$$

where we defined $\rho_0 \equiv \rho(t_0)$, and t_0 is some initial time and we neglected the negative root. The integral in Eq. (A.31) yields t as a function of ρ, $t = t(\rho)$, which then has to be inverted to, finally, obtain $\rho = \rho(t)$. Whether Eq. (A.31) can be solved analytically depends on the particular form of the potential $U(\rho)$. If Eq. (A.31) cannot be solved analytically one has to employ numerical approximations.

Furthermore, let us express the angle φ as a function of the radius ρ, $\varphi = \varphi(\rho)$. We get from Eqs. (A.22) and (A.30):

$$\frac{\mathrm{d}\varphi}{\mathrm{d}\rho} = \frac{\mathrm{d}\varphi}{\mathrm{dt}}\frac{\mathrm{d}t}{\mathrm{d}\rho} = \pm\frac{|\ell|}{\mu\rho^2}\left[\frac{2}{\mu}\left(E - U(\rho) - \frac{|\ell|^2}{2\mu\rho^2}\right)\right]^{-\frac{1}{2}}. \tag{A.32}$$

We integrate this equation over ρ and find the desired relation

$$\varphi = \varphi_0 \pm |\ell| \int\limits_{\rho_0}^{\rho} \frac{\mathrm{d}\rho'}{\rho'\sqrt{2\mu\rho'^2\left[E - U(\rho')\right] - |\ell|^2}}, \tag{A.33}$$

where $\varphi_0 \equiv \varphi(t_0)$.

Appendix B
Solving Non-Linear Equations: The NEWTON Method

We give a brief introduction into the solution of non-linear equations with the help of NEWTON's method. We regard a differentiable function $F(x)$ and we would like to find the solution of the equation

$$F(x) = 0. \tag{B.1}$$

The simplest approach is to transform the equation into an equation of the form

$$x = f(x), \tag{B.2}$$

which is always possible. This equation could be solved iteratively by simply repeating

$$x_{t+1} = f(x_t), \tag{B.3}$$

where we start with some initial value x_0. If this method converges, one can approximate the solution arbitrarily close, however, convergence is not guaranteed and will in fact depend on the transformation from Eqs. (B.1) to (B.2). A more advanced technique is the so called NEWTON method. It is based on the definition of $f(x)$ as

$$f(x) = x - \frac{F(x)}{F'(x)}, \tag{B.4}$$

which allows the iteration

$$x_{t+1} = x_t - \frac{F(x_t)}{F'(x_t)}. \tag{B.5}$$

Here $F'(x)$ denotes the derivative of $F(x)$ with respect to x. The convergence behavior of the iteration (B.5) highly depends on the form of the function $F(x)$ and on the choice of the starting point x_0. The routine can be regarded as converged if $|x_{t+1} - x_t| < \varepsilon$, where ε is the accuracy required.

B. A. Stickler and E. Schachinger, *Basic Concepts in Computational Physics*,
DOI: 10.1007/978-3-319-02435-6, © Springer International Publishing Switzerland 2014

If $F(x)$ is not differentiable one can use the *regula falsi* or employ *stochastic methods* which will be discussed in the second part of this book. The iteration of the method known as *regula falsi* is

$$x_{t+1} = x_t - F(x_t)\frac{x_t - x_{t-1}}{F(x_t) - F(x_{t-1})}. \tag{B.6}$$

A more detailed discussion on methods to solve transcendental equations numerically can be found in any textbook on numerical methods, see for instance [2, 3]. We shall also briefly introduce the case of a non-linear system of equations of the form (B.1) where $F(x) \in \mathbb{R}^N$ and $x \in \mathbb{R}^N$. In this case the iteration scheme is given by

$$x_{t+1} = x_t - J^{-1}(x_t)F(x_t), \tag{B.7}$$

where

$$J(x) = \nabla_x F(x) = \begin{pmatrix} \frac{\partial F_1(x)}{\partial x_1} & \frac{\partial F_1(x)}{\partial x_2} & \cdots & \frac{\partial F_1(x)}{\partial x_N} \\ \frac{\partial F_2(x)}{\partial x_1} & \frac{\partial F_2(x)}{\partial x_2} & \cdots & \frac{\partial F_2(x)}{\partial x_N} \\ \vdots & \vdots & \ddots & \vdots \\ \frac{\partial F_N(x)}{\partial x_1} & \frac{\partial F_N(x)}{\partial x_2} & \cdots & \frac{\partial F_N(x)}{\partial x_N} \end{pmatrix}. \tag{B.8}$$

is the JACOBI matrix of $F(x)$. We can also make use of the methods discussed in Chap. 2 to calculate numerically the derivatives in Eqs. (B.5) or (B.8).

Appendix C
Numerical Solution of Linear Systems of Equations

Here we would like to discuss briefly two of the most important methods to solve non-homogeneous systems of linear equations applying numerical methods. We consider n equations of the form

$$\begin{aligned} a_{11}x_1 + a_{12}x_2 + \cdots + a_{1n}x_n &= b_1, \\ a_{21}x_1 + a_{22}x_2 + \cdots + a_{2n}x_n &= b_2, \\ \vdots \quad &\quad \vdots \\ a_{n1}x_1 + a_{n2}x_2 + \cdots + a_{nn}x_n &= b_n, \end{aligned} \tag{C.1}$$

which is usually expressed in a matrix equation,

$$Ax = b. \tag{C.2}$$

The coefficients of the matrix $A = \{a_{ij}\}$ as well as the vector $b = \{b_i\}$ are assumed to be real valued and, furthermore, if

$$\sum_{i=1}^{n} |b_i| \neq 0, \tag{C.3}$$

the problem (C.2) is referred to as non-homogeneous (inhomogeneous). The solution of non-homogeneous linear systems of equations is one of the central problems in numerical analysis, since numerous numerical methods, such as the finite difference approach to a boundary value problem, see Chap. 8, can be reduced to such a problem.

From a purely theoretical point of view we note that the solution to (C.2) is well defined as long as the matrix A is non-singular, i.e. as long as

$$\det(A) \neq 0. \tag{C.4}$$

B. A. Stickler and E. Schachinger, *Basic Concepts in Computational Physics*,
DOI: 10.1007/978-3-319-02435-6, © Springer International Publishing Switzerland 2014

Then the unique solution of (C.2) can be written as

$$x = A^{-1}b. \tag{C.5}$$

However, the inversion of matrix A is very complex for $n \geq 4$ and one would prefer methods which are computationally more effective. Basically, one distinguishes between *direct* and *iterative* methods. Since a complete discussion of this huge topic would be too extensive, we will mainly focus on two methods.

In contrast to iterative procedures, direct procedures do not contain any methodological errors and can, therefore, be regarded as *exact*. However, these methods are often computationally very extensive and rounding errors are in many cases not negligible. As an example we will discuss the *LU* decomposition. On the other hand, many iterative methods are fast and rounding errors can be controlled easily. However, it is not guaranteed that an iterative procedure converges, even in cases where the system of equations is known to have unique solutions. Moreover, the result is an approximate solution. As an illustration for an iterative procedure we will discuss the GAUSS-SEIDEL method.

C.1 The *LU* Decomposition

The *LU* decomposition is essentially a numerical realization of GAUSSIAN elimination which is based on a fundamental property of linear systems of equations (C.2). This property states the system (C.2) to remain unchanged when a linear combination of rows is added to one particular row. This property is then employed in order to obtain a matrix in *triangular* form. It was demonstrated by DOOLITTLE and CROUT [4–6] that the GAUSSIAN elimination can be formulated as a decomposition of the matrix A into two matrices L and U, i.e.

$$A = LU, \tag{C.6}$$

where U is an *upper triangular* matrix and L is a *lower triangular* matrix. In particular, U is of the form

$$U = \begin{pmatrix} u_{11} & u_{12} & \dots & u_{1n} \\ 0 & u_{22} & \dots & u_{2n} \\ \vdots & & & \vdots \\ 0 & 0 & \dots & u_{nn} \end{pmatrix}, \tag{C.7}$$

and L is of the form

$$L = \begin{pmatrix} 1 & 0 & & \dots 0 \\ m_{21} & 1 & 0 & \dots 0 \\ m_{31} & m_{32} & 1 & \dots 0 \\ \vdots & & & \vdots \\ m_{n1} & m_{n2} & m_{n3} & \dots 1 \end{pmatrix}. \tag{C.8}$$

The factorization (C.6) is referred to as *LU decomposition*. The corresponding procedure can be easily identified by equating the elements in (C.6). One can show that the following operations yield the desired result: For $j = 1, 2, \dots, n$ one computes

$$u_{ij} = a_{ij} - \sum_{k=1}^{i-1} m_{ik} u_{kj} \qquad i = 1, 2, \dots, j, \tag{C.9}$$

$$m_{ij} = \frac{1}{u_{jj}} \left(a_{ij} - \sum_{k=1}^{j-1} m_{ik} u_{kj} \right) \quad i = j+1, j+2, \dots, n, \tag{C.10}$$

with the requirement that $u_{jj} \neq 0$. Note that in this notation we used the convention that the contribution of the sum is equal to zero if the upper boundary is less than the lower boundary. We rewrite Eq. (C.2) with the help of the *LU* decomposition (C.6)

$$Ax = LUx = b, \tag{C.11}$$

and by defining $y = Ux$, we have a system of equations for the variable y,

$$Ly = b. \tag{C.12}$$

Due to the particular form of L the system (C.12) is readily solved by *forward substitution*. We get the solution

$$y_i = b_i - \sum_{k=1}^{i-1} m_{ik} y_k, \qquad i = 1, 2, \dots, n. \tag{C.13}$$

The remaining equation reads

$$Ux = y, \tag{C.14}$$

which can solved by *backward substitution*:

$$x_i = \frac{1}{u_{ii}} \left(y_i - \sum_{k=i+1}^{n} u_{ik} x_k \right), \quad i = n, n-1, \dots, 1. \tag{C.15}$$

We note that this method can also be employed to invert the matrix A. The strategy is based on the relation

$$AX = I, \tag{C.16}$$

where $X = A^{-1}$ is to be determined and I is the n-dimensional identity. Equation (C.16) is equivalent to the following system of equations:

$$\begin{aligned} Ax_1 &= \begin{pmatrix} 1 \\ 0 \\ \vdots \\ 0 \end{pmatrix}, \\ Ax_2 &= \begin{pmatrix} 0 \\ 1 \\ 0 \\ \vdots \\ 0 \end{pmatrix}, \\ \vdots \quad & \quad \vdots \\ Ax_n &= \begin{pmatrix} 0 \\ \vdots \\ 0 \\ 1 \end{pmatrix}, \end{aligned} \tag{C.17}$$

where the vectors x_i are the rows of the unknown matrix X, i.e. $X = (x_1, x_2, \ldots, x_n)$. The n equations of (C.17) can be solved with the help of the LU decomposition.

Furthermore, one can easily calculate the determinant of A using the LU decomposition. We note that

$$\det(A) = \det(LU) = \det(L)\det(U) = \det(U), \tag{C.18}$$

since L and U are triangular matrices, the determinants are equal to the product of the diagonal elements, which yields $\det(L) = 1$. Hence we have

$$\det(A) = \det(U) = \prod_{i=1}^{n} u_{ii}. \tag{C.19}$$

In conclusion we remark that there are many specialized methods which have been designed particularly for matrices of specific forms, such as tridiagonal matrices, symmetric matrices, block-matrices, …. Such matrices commonly appear in physical applications, for instance, we remember that the matrix we encountered in Sect. 8.2 in the context of a finite difference approximation of boundary value problems, is tridiagonal. These specialized methods are usually the first choice if one has a matrix of such a specific form because they are much faster and more stable than methods developed for matrices of more general form. Since a full treatment of these methods is beyond the scope of this course, we refer the interested reader to books on numerical linear algebra [4, 5].

C.2 The Gauss-Seidel Method

The Gauss-Seidel method is an iterative procedure to approximate the solution of non-homogeneous systems of linear equations. The advantage of an iterative procedure, in contrast to a direct approach, is that its formulation is in general much simpler. However, one might have problems with the convergence of the method, even in cases where a solution exists and is unique. We note that the Gauss-Seidel method is of particular interest whenever one has to deal with *sparse* coefficient matrices. Let us define a *sparse matrix*: a matrix A is referred to as sparse, when the matrix is populated primarily by zeros. This requirement is not too restrictive since most of the matrices encountered in physical applications are indeed sparse. As an example we remember the matrices arising in the context of a finite difference approach to boundary value problems, Sect. 8.2.

Again, we use Eq. (C.1) as a starting point for our discussion. In order to allow a treatment with the help of the Gauss-Seidel method, we require that *all* diagonal elements of A are non-zero. We then solve each row of (C.1) for x_i. This yields the following hierarchy

$$\begin{aligned} x_1 &= -\frac{1}{a_{11}}\left(a_{12}x_2 + a_{13}x_3 + \cdots + a_{1n}x_n - f_1\right), \\ x_2 &= -\frac{1}{a_{22}}\left(a_{21}x_1 + a_{23}x_3 + \cdots + a_{2n}x_n - f_2\right), \\ \vdots\ &\ \ \vdots \\ x_n &= -\frac{1}{a_{nn}}\left(a_{n1}x_1 + a_{n2}x_2 + \cdots + a_{n,n-1}x_{n-1} - f_n\right), \end{aligned} \tag{C.20}$$

or in general for $i = 1, \ldots, n$

$$x_i = -\frac{1}{a_{ii}}\left(\sum_{\substack{j=1\\ j\neq i}}^{n} a_{ij}x_j - f_i\right). \tag{C.21}$$

We note that Eq. (C.21) can be rewritten as a matrix equation of the form

$$x = Cx + b, \tag{C.22}$$

where we defined the matrix $C = \{c_{ij}\}$ via

$$c_{ij} = \begin{cases} -\frac{a_{ij}}{a_{ii}} & i \neq j, \\ 0 & i = j, \end{cases} \tag{C.23}$$

and the vector $b = \{b_i\}$ as

$$b_i = \frac{f_i}{a_{ii}}. \tag{C.24}$$

We recognize that Eq. (C.21) can be transformed into an iterative form with the help of a trivial manipulation

$$x_i = x_i - \left[x_i + \frac{1}{a_{ii}} \left(\sum_{\substack{j=1 \\ j\neq i}}^{n} a_{ij} x_j - f_i \right) \right], \tag{C.25}$$

or

$$x_i^{(t+1)} = x_i^{(t)} - \Delta x_i^{(t)}, \tag{C.26}$$

where

$$\Delta x_i^{(t)} = x_i^{(t)} + \frac{1}{a_{ii}} \left(\sum_{j=1}^{i-1} a_{ij} x_j^{(t+1)} + \sum_{j=i+1}^{n} a_{ij} x_j^{(t)} - f_i \right). \tag{C.27}$$

Equation (C.26) in combination (C.27) produces a sequence of vectors

$$x^{(0)} \to x^{(1)} \to x^{(2)} \to \cdots \to x^{(m)}, \tag{C.28}$$

where $x^{(0)}$ is referred to as the initialization vector or trial vector. One can show that if this sequence converges, it approaches the exact solution x arbitrarily close, i.e.

$$\lim_{t\to\infty} x^{(t)} = x. \tag{C.29}$$

We remark that if we replace the terms $x_i^{(t+1)}$ on the right hand side of Eq. (C.27) with $x_i^{(t)}$ the method is referred to as the JACOBI method.

To terminate the GAUSS-SEIDEL method, we need an exit condition: One should terminate the iteration whenever

- The approximate solution $x^{(t)}$ obeys the required accuracy ε or $\tilde{\varepsilon}$, for instance

$$\max \left(|x_i^{(t)} - x_i^{(t-1)}| \right) \leq \varepsilon, \tag{C.30}$$

where ε is the absolute error, or

$$\max\left(\frac{|x_i^{(t)} - x_i^{(t-1)}|}{|x_i^{(t)}|}\right) \leq \tilde{\varepsilon}, \tag{C.31}$$

where $\tilde{\varepsilon}$ is the relative error.

- When a maximum number of iterations is reached. This condition may be interpreted as an emergency exit, which ensures that the iteration terminates even if the process is not convergent or has still not converged.

Let us discuss one final, however, crucial point of this appendix. In many cases the convergence of the GAUSS-SEIDEL method can be significantly improved by including a *relaxation parameter* ω to the iterative process. In this case the update routine (C.26) takes on the form

$$x_i^{(t+1)} = x_i^{(t)} - \omega \Delta x_i^{(t)}. \tag{C.32}$$

If the relaxation parameter ω obeys $\omega > 1$ one speaks of *over-relaxation*, if $\omega < 1$ of *under-relaxation* and if $\omega = 1$ the regular GAUSS-SEIDEL method is recovered. An appropriate choice of the relaxation parameter may fasten the convergence of the method significantly. The best result will certainly be obtained if the *ideal* value of ω, ω_i were known. Unfortunately, it is impossible to determine ω_i prior to the iteration in the general case. We remark the following properties:

- The method (C.32) is only convergent for $0 < \omega \leq 2$.
- If the matrix C is positive definite and $0 < \omega < 2$, the GAUSS-SEIDEL method converges for any choice of $x^{(0)}$ (OSTROWSKI-REICH theorem, [7]).
- In many cases, $1 \leq \omega_i \leq 2$. We note that this inequality holds only under particular restrictions for the matrix C [see Eq. (C.23)]. However, we note without going into detail, that these restrictions are almost always fulfilled when one is confronted with physical applications.
- If C is positive definite and tridiagonal, the ideal value ω_i can be calculated using

$$\omega_i = \frac{2}{1 + \sqrt{1 - \lambda^2}}, \tag{C.33}$$

where λ is the largest eigenvalue of C, Eq. (C.23).

- Since the calculation of λ is in many cases quite complex, one could employ the following idea: It is possible to prove that

$$\lim_{t\to\infty} \frac{|\Delta x^{(t+1)}|}{|\Delta x^{(t)}|} \to \lambda^2. \tag{C.34}$$

Hence, one may start with $\omega = 1$, perform t_0 $(20 < t_0 < 100)$ iterations and then approximate ω_i with the help of Eq. (C.33) and

$$\lambda^2 \approx \frac{|\Delta x^{(t_0)}|}{|\Delta x^{(t_0-1)}|}. \tag{C.35}$$

The iteration is then continued with the approximated value of ω_i until convergence is reached.

In conclusion we remark that numerous numerical libraries contain sophisticated routines to solve linear systems of equations. In many cases it is, thus, advisable to rely on such routines, in particular because they also provide various routines developed for specific matrices, as already discussed in Sect. C.1.

Appendix D
Basics of Probability Theory

D.1 Classical Definition

The classical probability $P(A)$ for an event A is defined by the number of favorable results n, divided by the number of possible results m,

$$P(A) = \frac{n}{m}. \tag{D.1}$$

For two events A and B we can deduce the following rules[1]

$$P(A \vee B) = P(A) + P(B) - P(A \wedge B), \tag{D.2a}$$

$$P(Z) = 0 \quad \text{impossible event; } Z \ldots \text{zero element}, \tag{D.2b}$$

$$P(I) = 1 \quad \text{certain event; } I \ldots \text{identity element}, \tag{D.2c}$$

$$0 \leq P(A) \leq 1, \tag{D.2d}$$

$$P(A|B) = \frac{P(A \wedge B)}{P(B)}, \tag{D.2e}$$

where $P(A|B)$ is the probability for the event A under the constraint that event B is true. Moreover, if $\overline{A}$ is the complementary event[2] to A we have

$$P(\overline{A}) = 1 - P(A). \tag{D.3}$$

[1] Here we use the symbols $\vee$ and $\wedge$ to denote the Boolean operators OR and AND, respectively.

[2] This means that $A \vee \overline{A} = I$ and $A \wedge \overline{A} = Z$.

B. A. Stickler and E. Schachinger, *Basic Concepts in Computational Physics*,
DOI: 10.1007/978-3-319-02435-6, © Springer International Publishing Switzerland 2014

The statistical definition of the probability for an event A reads

$$P(A) = \lim_{m\to\infty} \frac{n}{m}. \tag{D.4}$$

D.2 Random Variables and Moments

A random variable is a functional which assigns to an event ω a real number x from the set of possible outcomes Ω: $x = X(\omega)$.[3] Roughly speaking it is a variable whose value is assigned to the observation of some random process. The mean value of a discrete random variable X is defined by

$$\langle X\rangle = \sum_{\omega\in\Omega} X(\omega)P_\omega, \tag{D.5}$$

where P_ω is the probability for the event ω. For instance, in case of a dice-throw $X(\omega) \equiv n = 1, 2, \ldots, 6$.

In the following we regard discrete random variables, i.e. x can only take on discrete values. For a function of random variables $Y = f(X)$ we can write in general

$$\langle f(X)\rangle \equiv \langle f\rangle = \sum_i f(x_i)P_i. \tag{D.6}$$

Note that

$$\langle 1\rangle \equiv \sum_i P_i = 1. \tag{D.7}$$

Moments of order k are defined accordingly by

$$m_k := \left\langle X^k \right\rangle, \tag{D.8}$$

and central moments are defined as

$$\mu_k := \left\langle (\Delta X)^k \right\rangle = \left\langle (X - \langle X\rangle)^k \right\rangle. \tag{D.9}$$

Of particular interest is the second central moment, the *variance*:

$$\mathrm{var}\,(X) := \left\langle (X - \langle X\rangle)^2 \right\rangle = \left\langle X^2 \right\rangle - \langle X\rangle^2. \tag{D.10}$$

[3] A more exact formulation will follow in the course of this appendix.

The *standard deviation* σ is defined as the square root of the variance:

$$\sigma := \mathrm{std}(X) = \sqrt{\mathrm{var}\,(X)}. \tag{D.11}$$

For instance, for a discrete set of observations x_i where $i = 1, \ldots, N$ the sample mean value is given by

$$\overline{x} = \frac{1}{N}\sum_i x_i. \tag{D.12}$$

The error (standard deviation) of $\overline{x}$ (*standard error*) can be calculated from

$$\begin{aligned}\mathrm{var}\,(\overline{x}) &= \mathrm{var}\left(\frac{1}{N}\sum_i x_i\right)\\ &= \frac{1}{N^2}\sum_i \mathrm{var}\,(x_i)\\ &= \frac{1}{N^2}N\sigma^2\\ &= \frac{\sigma^2}{N},\end{aligned} \tag{D.13}$$

where we assumed that $\mathrm{cov}\left(x_i, x_j\right) = \mathrm{var}\,(x_i)\,\delta_{ij}$ [defined in Eq. (D.16)], i.e. the random variables are uncorrelated. Therefore,

$$\text{standard error} = \sigma_{\overline{x}} = \frac{\sigma}{\sqrt{N}}, \tag{D.14}$$

where σ is the standard deviation of the observations as defined above.

The above concept can be generalized to functions of multiple random variables. We only give two essential definitions, i.e. the definition of the mean value of such a function and the definition of the covariance, in the particular case of two random variables:

$$\langle f(X, Y)\rangle := \sum_{i,j} f(x_i, y_j)P_{ij}, \tag{D.15}$$

and

$$\mathrm{cov}\,(X, Y) := \langle (X - \langle X\rangle)(Y - \langle Y\rangle)\rangle = \langle XY\rangle - \langle X\rangle\,\langle Y\rangle\,. \tag{D.16}$$

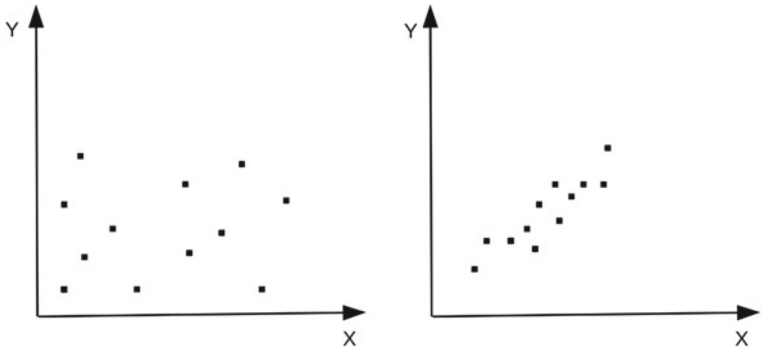

Fig. D.1 Uncorrelated (*left panel*) and positively correlated (*right panel*) variables X and Y

Note that

$$\operatorname{cov}(X,Y) = \begin{cases} >0 & \text{for } Y - \langle Y\rangle > 0 \Rightarrow X - \langle X\rangle > 0, \\ & \qquad \text{(positive linear correlation)} \\ <0 & \text{for } Y - \langle Y\rangle > 0 \Rightarrow X - \langle X\rangle < 0, \\ <0 & \text{for } X - \langle X\rangle > 0 \Rightarrow Y - \langle Y\rangle < 0, \\ & \qquad \text{(negative linear correlation)} \\ =0 & \text{no linear dependence between } X \text{ and } Y. \end{cases} \tag{D.17}$$

Random variables whose covariance is zero are called uncorrelated, see Fig. D.1.

D.3 Binomial Distribution and Limit Theorems

The binomial distribution is given by

$$P(k|n,p) = \binom{n}{k} p^k (1-p)^{n-k}, \tag{D.18}$$

where $\binom{n}{k}$ is the binomial coefficient

$$\binom{n}{k} = \frac{n!}{k!(n-k)!}. \tag{D.19}$$

According to STIRLING's approximation we have for large n

$$n! = n^{n+\frac{1}{2}} e^{-n} \sqrt{2\pi} \left[1 + \mathcal{O}(n^{-1})\right]. \tag{D.20}$$

As can easily be shown the mean value and the variance of the binomial distribution are given by

$$\langle k \rangle = np, \tag{D.21}$$

$$\mathrm{var}\,(k) = np(1-p). \tag{D.22}$$

The DE MOIVRE–LAPLACE theorem states that for $\sigma \gg 1$

$$P(k|n,p) \approx g(k|k_0,\sigma) = \frac{1}{\sqrt{2\pi\sigma^2}} \exp\left[-\frac{(k-k_0)^2}{2\sigma^2}\right], \tag{D.23}$$

where $k_0 = \langle k \rangle$ and $\sigma = \sqrt{\mathrm{var}\,(k)}$. Furthermore, we can deduce that

$$P(k = np|n,p) = \frac{1}{\sqrt{2\pi np(1-p)}} \longrightarrow 0, \tag{D.24}$$

for $n \to \infty$. BERNOULLI's law of large numbers follows in the limit $n \to \infty$:

$$P(|k/n - p| < \varepsilon|n,p) \to 1 \quad \forall\varepsilon > 0. \tag{D.25}$$

D.4 POISSON **Distribution and Counting Experiments**

In case that $np = \mu \equiv \text{const}$, i.e. the mean expectation value μ is independent of the number of experiments n, it follows that

$$\lim_{n\to\infty} P\left(k\middle|n, p = \frac{\mu}{n}\right) = \exp(-\mu)\frac{\mu^k}{k!} =: P(k|\mu). \tag{D.26}$$

The distribution $P(k|\mu)$ is named POISSON distribution. For the POISSON distribution we obtain

$$\langle k \rangle = \mu, \tag{D.27}$$

$$\mathrm{var}\,(k) = \mu. \tag{D.28}$$

It should be noted that counting experiments, as for instance radioactive decay, follow the Poisson statistics. Let t be a time interval in which we observe (in average) μ events. We now divide this time interval in n sub-intervals with $\Delta t = t/n$. If the events are assumed to be independent, the process follows a binomial distribution and we have $\mu = np$, which is equivalent to $p = \mu/n$. In case of radioactive decay we observe μ signals within one minute which are uniformly distributed over the time interval. If we now reduce the experiment to a duration of one second the probability of detecting a signal reduces consequently to $\mu/60$. Note that it is possible to approximate the binomial distribution $P(k|n, p)$ by $P(k|\mu)$ in the case that $p \ll 1$ but $np \ggg 1$. For large μ we can write

$$P(k|\mu) = \frac{1}{\sqrt{2\pi\sigma^2}} \exp\left[-\frac{(k-\mu)^2}{2\sigma^2}\right], \tag{D.29}$$

with

$$\sigma = \sqrt{\mu} \approx \sqrt{k}. \tag{D.30}$$

If μ is unknown (as in most experimentally relevant cases) one can approximate μ by

$$\mu = k \pm \sqrt{k}. \tag{D.31}$$

D.5 Continuous Variables

We define the *cumulative distribution function* (cdf), $F(x)$, of a continuous variable x by[4]

$$F(x) := P(X \leq x|\mathscr{B}), \tag{D.32}$$

where $\mathscr{B}$ is a generalized condition (*condition complex*). Moreover we define the *probability density function* (pdf), $p(x)$ by

$$p(x) = \frac{\mathrm{d}}{\mathrm{d}x} F(x). \tag{D.33}$$

It follows that

$$p(x)\mathrm{d}x = (F(x+\mathrm{d}x) - F(x)) \overset{!}{=} P(x \leq X \leq x + \mathrm{d}x|\mathscr{B}). \tag{D.34}$$

Hence,

$$F(x) = \int\limits_{-\infty}^{x} \mathrm{d}x' p(x'). \tag{D.35}$$

Note that the pdf is normalized, i.e.

$$\int \mathrm{d}x' p(x') = F(\infty) = P(X \leq \infty|\mathscr{B}) = 1, \tag{D.36}$$

and non-negative, i.e.

$$p(x) \geq 0. \tag{D.37}$$

[4] For convenience we use here the notation $F(x)$ for the cumulative distribution function in contrast to the notation $P(x)$ used throughout the second part of this book.

D.6 Bayes' Theorem

We regard a set of discrete events A_i under the generalized condition $\mathscr{B}$. Then we have the normalization condition

$$\sum_i P(A_i|\mathscr{B}) = 1, \tag{D.38}$$

and the marginalization rule

$$P(B|\mathscr{B}) = \sum_i P(B|A_i, \mathscr{B}) P(A_i|\mathscr{B}). \tag{D.39}$$

Bayes' theorem [8] for discrete variables follows from Eq. (D.2e) since $P(A \wedge B) = P(B \wedge A)$:

$$P(A|B, \mathscr{B}) = \frac{P(B|A, \mathscr{B}) P(A|\mathscr{B})}{P(B|\mathscr{B})}. \tag{D.40}$$

In case of continuous variables the above equations modify accordingly. The marginalization and Bayes' theorem for pdfs are given by

$$P(B|\mathscr{B}) = \int \mathrm{d}x P(B|x, \mathscr{B}) p(x|\mathscr{B}), \tag{D.41}$$

and

$$p(y|x, \mathscr{B}) = \frac{p(x|y, \mathscr{B}) p(y|\mathscr{B})}{p(x|\mathscr{B})}. \tag{D.42}$$

D.7 Normal Distribution

The normal distribution (Gauss distribution) is given by the pdf

$$p(x) = \mathscr{N}(x|x_0, \sigma) = \frac{1}{\sqrt{2\pi\sigma^2}} \exp\left[-\frac{(x - x_0)^2}{2\sigma^2}\right]. \tag{D.43}$$

The corresponding cdf is given by

$$F(x) = \frac{1}{\sqrt{2\pi\sigma^2}} \int_{-\infty}^{x} \mathrm{d}x' \exp\left[-\frac{(x' - x_0)^2}{2\sigma^2}\right] \tag{D.44}$$

$$= \Phi\left(\frac{x - x_0}{\sigma}\right) = \frac{1}{2} + \frac{1}{2}\mathrm{erf}\left(\frac{x - x_0}{\sqrt{2\sigma^2}}\right), \tag{D.45}$$

where $\Phi(x)$ is given by

$$\Phi(x) = \frac{1}{\sqrt{2\pi}} \int_{-\infty}^{x} \mathrm{d}x' e^{-x'^2/2}, \tag{D.46}$$

and $\mathrm{erf}(x)$ is the error function:

$$\mathrm{erf}(x) = \frac{2}{\sqrt{\pi}} \int_{0}^{x} \mathrm{d}x' e^{-x'^2}. \tag{D.47}$$

Furthermore, we obtain

$$\langle x \rangle = x_0, \tag{D.48}$$

$$\mathrm{var}(x) = \sigma^2. \tag{D.49}$$

D.8 Central Limit Theorem

Let S denote a random variable defined by

$$S = \sum_{i=1}^{N} c_i X_i, \tag{D.50}$$

where the X_i are independent and identically distributed random numbers with mean μ and variance σ^2 and

$$\lim_{N\to\infty} \frac{1}{N} \sum_{i=1}^{N} c_i^k = \text{const}, \quad \forall k \in \mathbb{Z}. \tag{D.51}$$

Then,

$$p(S|N, \mathscr{B}) \approx \mathscr{N}[S|\,\langle S \rangle\,, \mathrm{var}(S)], \tag{D.52}$$

with

$$\langle S \rangle = \mu \sum_{i=1}^{N} c_i, \tag{D.53}$$

and

$$\mathrm{var}(S) = \sigma^2 \sum_{i=1}^{N} c_i^2, \tag{D.54}$$

for large N. Note that the theorem of DE MOIVRE-LAPLACE is a special case of the central limit theorem, i.e. the X_i are binomial distributed.

D.9 Characteristic Function

The characteristic function $G(k)$ of a stochastic variable X is defined by

$$G(k) = \left\langle e^{ikX} \right\rangle = \int_I \mathrm{d}x e^{ikx} p(x), \tag{D.55}$$

where I denotes the range of the pdf $p(x)$. It follows that

$$G(0) = 1 \qquad \text{and} \qquad |G(k)| \leq 1. \tag{D.56}$$

Expanding Eq. (D.55) in a Taylor series with respect to k yields

$$G(k) = \sum_m \frac{(ik)^m}{m!} \int_I \mathrm{d}x x^m p(x) \equiv \sum_m \frac{(ik)^m}{m!} \left\langle X^m \right\rangle. \tag{D.57}$$

Hence, the characteristic function is a *moment generating function*.

D.10 KOLMOGOROV's Zero-One Law

In order to discuss KOLMOGOROV's zero-one law, we shall briefly put the concepts introduced above into a more systematic framework: Let A denote some particular event and $\{A_n\}$ a sequence of events. Then we define the probability space denoted by $(\Omega, \mathscr{A}, \mu)$ where Ω is the set of possible outcomes, $\mathscr{A}$ is a set of events which form a σ-algebra (also called σ-field). They fulfill

- $\emptyset \in \mathscr{A}$ and $\Omega \in \mathscr{A}$, (D.58a)

- if $A_1 \in \mathscr{A}$ and $A_2 \in \mathscr{A}$,

  then $A_1 \cup A_2 \in \mathscr{A}$, $A_1 \cap A_2 \in \mathscr{A}$ and $A_1 \setminus A_2 \in \mathscr{A}$, (D.58b)

- for a sequence $\{A_n\}$, $\cap_n A_n \in \mathscr{A}$ if $A_k \in \mathscr{A}\ \forall k$, (D.58c)

and μ is a measure $\mu : \Omega \to [0, 1]$, which obeys

- $\mu(\emptyset) = 0$, (D.59a)

- $\mu(A) = 1 - \mu(A^c)$, (D.59b)

- $\mu(\cup_n A_n) = \sum_n \mu(A_n)$ if $A_n \cap A_m = 0$ for all $n \neq m$. (D.59c)

From properties (D.58a) and (D.58b) we deduce that if $A \in \mathscr{A}$ then also $A^c = \Omega \setminus A \in \mathscr{A}$. Furthermore, we deduce from properties (D.59a) and (D.59b) that $\mu(\Omega) = 1$. $\mathscr{A}$ contains all possible subsets of Ω, i.e. all events we would like to consider. We note that the dimension of $\mathscr{A}$ is given by $\dim \mathscr{A} = 2^{\dim \Omega}$.

Let us give an illustrative example: We regard an ideal coin toss, where H denotes *heads* and T denotes *tails*. The set of possible outcomes Ω contains the two possible outcomes of the experiment, i.e. $\Omega = \{H, T\}$ (read: *heads or tails*). The σ-algebra $\mathscr{A}$ has dimension $2^2 = 4$ and contains all possible combinations. In particular we have $\mathscr{A} = \{\emptyset, \{H\}, \{T\}, \{H, T\}\}$. We clarify the notation $\emptyset$: neither heads nor tails, $\{H\}$: heads, $\{T\}$: tails, $\{H, T\}$: either heads or tails. The measure μ fulfills $\mu(\emptyset) = 0$, $\mu(\{H, T\}) = 1$, $\mu(\{H\}) = \mu(\{T\}) = 0.5$.

We consider a sequence of events $A_1, A_2, \ldots, A_n \subset \Omega$, denoted by $\{A_n\} \subset \Omega$. We note that we can form a σ-field from these events, by adding their complements A_i^c, intersections and unions [see properties (D.58a)–(D.58c)]. In particular, given $A \in \Omega$, we can define the σ-field $\sigma(A) = \{\emptyset, A, A^c, \Omega\}$.

We define the sequence of σ-fields

$$\mathscr{A}_i = \sigma(A_i, A_{i+1}, A_{i+2}, \ldots), \tag{D.60}$$

and note that $\mathscr{A}_1 \supset \mathscr{A}_2 \supset \mathscr{A}_3 \supset \ldots$, since, for instance, $\mathscr{A}_2 = \sigma(A_2, A_3, \ldots)$ contains all elements included in $\mathscr{A}_1 = \sigma(A_1, A_2, \ldots)$, except the elements associated with A_1.

Now the *tail σ-field $\mathscr{A}^*$* is defined as the intersection of all $\mathscr{A}_i$, $i = 1, \ldots, \infty$, i.e.

$$\mathscr{A}^* = \bigcap_{i=1}^{\infty} \mathscr{A}_i. \tag{D.61}$$

In an intuitive way we may state that the tail σ-field contains those events, which depend only on the limiting behavior of the sequence. These events are referred to as *tail events*. In terms of independent (not necessarily identically distributed) random variables X_n a typical example for a tail event might be the question whether or not the series

$$\xi = \sum_n X_n, \tag{D.62}$$

converges. Clearly, the answer to this question is independent of each finite subset of the sequence $\{X_n\}$. In contrast to that, the event that the series converges to a value $\xi > 1$ is not a tail event, since it depends on all elements of the sequence $\{X_n\}$, in particular, it is certainly not independent of the value X_1. A second example would be an infinite sequence of dice tosses. The event, that a sequence of n consecutive tosses occurs infinitely often is a tail event.

We are now in the position to give KOLMOGOROV's zero-one law: It states that any tail-event $\mathscr{T} \in \mathscr{A}^*$ occurs either with probability one or with probability zero, i.e. $\mu(\mathscr{T}) = 0$ or $\mu(\mathscr{T}) = 1$.

Let us briefly illustrate the meaning of this strong theorem by discussing the *dactylographic monkey*, as it was stated by BOREL: Suppose a monkey hits typewriter keys randomly forever, then it will eventually type every book in France's National Library. The truth of this statement is easily demonstrated with the help of KOLMOGORV's zero-one law: The probability that the monkey hits the correct typewriter keys at the first time it tries is very tiny, however, not necessarily equal to zero. Therefore, the probability that it hits the correct keys *some-when* cannot be zero and must be one according to KOLMOGORV's zero-one law.

D.11 The Correlation Coefficient

We shall briefly define and discuss the correlation coefficient due to its outstanding importance in mathematics and physics. Two random variables X and Y form a random vector $Z = (X, Y)$ which follows the pdf $p(Z) = p(X, Y)$ with the normalization

$$\int \mathrm{d}x \, \mathrm{d}y \, p(x, y) = 1. \tag{D.63}$$

The correlation coefficient r is now defined as

$$r = \frac{\operatorname{cov}(X, Y)}{\sqrt{\operatorname{var}(X) \operatorname{var}(Y)}}, \tag{D.64}$$

where $\operatorname{cov}(X, Y)$ is the covariance (D.16) of X and Y while $\operatorname{var}(\cdot)$ denotes the variance (D.10) of the respective argument. It follows from the CAUCHY-SCHWARZ inequality that $0 \le r^2 \le 1$ and, therefore, $-1 \le r \le 1$.[5]

The random variables X and Y are said to be the stronger correlated the bigger r^2 is because for statistical independent (uncorrelated) variables we have $p(x, y) = q_1(x)q_2(y)$, which includes $\operatorname{cov}(X, Y) = 0$, and, therefore, $r = 0$.

The definition of the correlation coefficient is usually motivated by the problem of linear regression. Suppose we have a set of data points Y associated with data points X. We would like to find a linear function $f(X) = a + bX$ which approximates the data points Y as good as possible. The problem may be stated as

[5] One defines the scalar product between random variables $(X, Y) = \operatorname{cov}(X, Y)$ and therefore $\|X\|^2 = (X, X) = \operatorname{var}(X)$. The CAUCHY-SCHWARZ inequality reads

$$|(X, Y)|^2 \le \| X \|^2 \| Y \|^2, \tag{D.65}$$

and therefore $0 \le r^2 \le 1$.

$$\left\langle [Y - f(X)]^2 \right\rangle = \left\langle (Y - a - bX)^2 \right\rangle \to \min, \tag{D.66}$$

where a and b are real constants. This is GAUSS's method of minimizing the square of errors. We have

$$\frac{\partial}{\partial a} \left\langle (Y - a - bX)^2 \right\rangle = -2 \left\langle Y - a - bX \right\rangle = 0, \tag{D.67}$$

and

$$\frac{\partial}{\partial b} \left\langle (Y - a - bX)^2 \right\rangle = -2 \left\langle (Y - a - bX)X \right\rangle = 0. \tag{D.68}$$

From Eq. (D.67) we have

$$a + b \left\langle X \right\rangle = \left\langle Y \right\rangle , \tag{D.69}$$

and from (D.68) we obtain

$$a \left\langle X \right\rangle + b \left\langle X^2 \right\rangle = \left\langle XY \right\rangle . \tag{D.70}$$

Equations (D.69) and (D.70) are readily solved for a and b and one obtains

$$a = \left\langle Y \right\rangle - b \left\langle X \right\rangle , \tag{D.71}$$

where

$$b = \frac{\left\langle XY \right\rangle - \left\langle X \right\rangle \left\langle Y \right\rangle}{\left\langle X^2 \right\rangle - \left\langle X \right\rangle^2} = \frac{\mathrm{cov}\,(X, Y)}{\mathrm{var}\,(X)}. \tag{D.72}$$

Hence, the solution to the problem is found to be

$$\begin{aligned} f(X) &= \left\langle Y \right\rangle - \frac{\mathrm{cov}\,(X, Y)}{\mathrm{var}\,(X)} (X - \left\langle X \right\rangle) \\ &= \left\langle Y \right\rangle - r \sqrt{\frac{\mathrm{var}\,(Y)}{\mathrm{var}\,(X)}} (X - \left\langle X \right\rangle). \end{aligned} \tag{D.73}$$

It follows immediately that the squared error is given by

$$\left\langle [y - F(x)]^2 \right\rangle = \mathrm{var}\,(Y)\,(1 - r^2). \tag{D.74}$$

Hence, we obtain the best result for $r = \pm 1$, i.e. the dependence is really linear. The worst result is obtained for $r = 0$.

D.12 Stable Distributions

A stable distribution is a distribution which reproduces itself. In particular, consider two random variables X_1 and X_2 which are independent copies of the random variable X, following the distribution p_X.[6]

Now p_X is referred to as a stable distribution if for arbitrary constants a and b the stochastic variable $aX_1 + bX_2$ has the same distribution as the stochastic variable $cX + d$ for some positive c and some $d \in \mathbb{R}$.

For this case one can write down the characteristic function analytically. We will give a special case, the so called *symmetric* Lévy *distributions*:

$$G_\alpha(k) = \exp\left(-\sigma |k|^\alpha\right) . \tag{D.75}$$

Here $\sigma > 0$ and $0 < \alpha \leq 2$. The pdf of such a distribution shows the asymptotic behavior

$$p_\alpha(x) \propto \frac{\alpha}{|x|^{1+\alpha}} \qquad |x| \to \infty. \tag{D.76}$$

From Eq. (D.75) we deduce that for $\alpha = 2$ one has the normal distribution. Moreover, we observe from Eq. (D.76) that the variance diverges for all $\alpha < 2$. However, the existence of the variance was the criterion for the validity of the central limit theorem formulated in Sect. D.8. We note that stable distributions reproduce themselves and are attractors for sums of independent identical distributed random variables. This is referred to as the *generalized central limit theorem*.

In conclusion we remark that for $\alpha = 1$ the Cauchy distribution results and note that stable distributions are also referred to as Lévy α-*stable distributions*.

[6] Independent copies of a random variable, are random variables, which are independent and follow the same distribution as the original random variable.

Appendix E
Phase Transitions

E.1 Some Basics

In many physical systems transitions between different phases are observed [9]. A different physical structure develops in these phases, such as ordered / disordered or magnetized / non-magnetized, etc. In many cases one can account those phase transitions to the variation of a macroscopic quantity (e.g. temperature, particle density, external fields, etc.). For instance, the phase transition from liquid to gaseous phase may be caused by an increase of the temperature to the boiling point. Furthermore, it is possible to define an *order parameter* φ. This parameter is usually zero in one phase and takes some definite value, $\varphi \neq 0$, in the other phase. It can be expressed as the first derivative of the free energy with respect to some external field. For instance, in case of the *ferromagnetic* transition, the magnetization plays the role of the *order parameter*.

From statistical mechanics [9] we know that in a canonical ensemble

$$P_r(T) = \frac{1}{Z} \exp\left[-\beta E_r\right], \tag{E.1}$$

is the probability for the micro-state r, where $\beta = 1/(k_B T)$ where k_B is the Boltzmann constant and T the temperature. In what follows we will leave out the arguments for the sake of a more compact notation. The canonical partition function Z is given by

$$Z = \sum_r \exp\left(-\beta E_r\right). \tag{E.2}$$

The free energy F is connected to Z by the relation

$$F = -\frac{1}{\beta} \ln Z. \tag{E.3}$$

B. A. Stickler and E. Schachinger, *Basic Concepts in Computational Physics*,
DOI: 10.1007/978-3-319-02435-6, © Springer International Publishing Switzerland 2014

REMINDER: the four thermodynamic potentials are the energy E, the free energy $F = E - TS$, the enthalpy $H = E + pV$, and the free enthalpy $G = E - TS + pV$, where S is the entropy, p the pressure, and V the volume. From the total derivatives one can deduce the *equations of state* and the MAXWELL relations.

We give the classification of phase transitions according to EHRENFEST:

First Order Phase Transition

If F is a continuous function of its variables at the transition point and its first derivative with respect to some thermodynamic variable is discontinuous we call it a *first order phase transition*. For instance, transitions from the liquid to the gaseous phase exhibit a first order phase transition because the density, which is the first derivative of the free energy with respect to the chemical potential, changes discontinuously at the boiling temperature $T = T_B$. We note the following characteristics of first order phase transitions:

1. The transition involves a *latent heat* ΔQ [for instance *latent heat of fusion* (melting or freezing)].
2. Both phases can coexist at the transition.
3. A metastable phase can be observed.

Second Order Phase Transition

In case of a second order phase transition, the first derivative of the free energy F stays continuous but the second derivative of F exhibits a discontinuity. For instance, in case of the *ferromagnetic phase transition* the magnetization (first derivative of F with respect to the external magnetic field B) changes continuously while the magnetic susceptibility χ (the second derivative of F with respect to B) is discontinuous at the CURIE temperature T_c.

Modern Classification

In the modern classification one identifies first order phase transitions by the occurrence of latent heat, i.e. the system absorbs or releases energy. Second order phase transitions (or *continuous* phase transitions) are characterized by a divergent susceptibility, an infinite correlation length, and/or a power law decay of correlations near criticality.

E.2 Landau Theory

We regard a second order phase transition with the order parameter φ [10]. Since we know that $\langle\varphi\rangle$ is continuous at $T = T_c$ we define φ in such a way that $\langle\varphi\rangle\,|_{T=T_c} = 0$. Furthermore, we have $\langle\varphi\rangle\,|_{T\geq T_c} = 0$ and $\langle\varphi\rangle\,|_{T<T_c} \neq 0$. We write the free energy as (the particular form is chosen in analogy to the theory of ferromagnetism):

$$F(T,h,\varphi) = F_0(T) + V\left[\frac{a(T-T_c)}{2}\varphi^2 + \frac{b}{4}\varphi^4 - h\varphi\right]. \tag{E.4}$$

Here, a and b are some constants and h denotes the external field. In equilibrium we have

$$\frac{\delta F}{\delta\varphi} = 0, \tag{E.5}$$

which results in

$$a(T-T_c)\varphi + b\varphi_0^3 = h. \tag{E.6}$$

For $h = 0$ and $T < T_c$ we obtain

$$\langle\varphi_0\rangle = \sqrt{\frac{a}{b}(T_c - T)} \sim (T_c - T)^{\gamma}, \tag{E.7}$$

where $\gamma = 1/2$ is called the *critical exponent*. For $T \geq T_c$ we have $\langle\varphi_0\rangle = 0$. We now regard a weak external field h. The order parameter will change

$$\varphi = \langle\varphi_0\rangle + \delta\varphi. \tag{E.8}$$

Again, we obtain

$$\frac{\delta F}{\delta\varphi} = a(T-T_c)(\langle\varphi_0\rangle + \delta\varphi) + b(\langle\varphi_0\rangle + \delta\varphi)^3 - h = 0. \tag{E.9}$$

Neglecting contributions of order $\mathscr{O}(\delta\varphi^2)$ yields for the susceptibility

$$\chi = \frac{\partial}{\partial h}\langle\varphi\rangle = \frac{\langle\delta\varphi\rangle}{h} \sim |T - T_c|^{\delta}, \tag{E.10}$$

where $\delta = -1$ is a second critical exponent. This is the Curie-Weiss law. Finally for $T = T_c$ we obtain from Eq. (E.6)

$$\varphi = \left(\frac{h}{b}\right)^{\frac{1}{3}} \sim h^{\frac{1}{\varepsilon}}, \tag{E.11}$$

with the third critical exponent ε. The LANDAU theory is a mean-field approximation since local fluctuations of the order parameter are neglected. Since fluctuations play a crucial role in phase transitions, the critical exponents obtained with LANDAU's approach deviate from experimental values.

However, the critical exponents are universal (property of *universality*), i.e. they depend only on the dimensionality and the symmetry of the interaction. This means, at the critical point the system is independent of its material-specific parameters.

Appendix F
Fractional Integrals and Derivatives in 1D

In this section we introduce briefly the common definitions and notations associated with fractional calculus in one dimension [11].

The RIEMANN–LIOUVILLE fractional integrals of order $\alpha \in \mathbb{C}$ $[\Re(\alpha) > 0]$, $I^{\alpha}_{a+}f(x)$ and $I^{\alpha}_{b-}f(x)$ on a finite interval $[a, b]$ on the real axis $\mathbb{R}$ are given by

$$I^{\alpha}_{a+}f(x) := \frac{1}{\Gamma(\alpha)} \int_a^x \mathrm{d}x' \, \frac{f(x')}{(x - x')^{1-\alpha}}, \quad \text{for} \quad (x > a, \; \Re(\alpha) > 0), \tag{F.1a}$$

$$I^{\alpha}_{b-}f(x) := \frac{1}{\Gamma(\alpha)} \int_x^b \mathrm{d}x' \, \frac{f(x')}{(x' - x)^{1-\alpha}}, \quad \text{for} \quad (x < b, \; \Re(\alpha) > 0), \tag{F.1b}$$

where $\Gamma(x)$ denotes the Gamma function, $\Re(\alpha)$ is the real part of α, and $f(x)$ is a sufficiently well behaved continuous, differentiable function for which the integrals in (F.1) exist. The corresponding RIEMANN-LIOUVILLE fractional derivatives $D^{\alpha}_{a+}f(x)$ and $D^{\alpha}_{b-}f(x)$ of order $\alpha \in \mathbb{C}$ $[\Re(\alpha) \geq 0]$ are defined by

$$\begin{aligned} D^{\alpha}_{a+}f(x) &:= \left(\frac{\mathrm{d}}{\mathrm{d}x}\right)^n (I^{n-\alpha}_{a+}f)(x) \\ &= \frac{1}{\Gamma(n-\alpha)} \left(\frac{\mathrm{d}}{\mathrm{d}x}\right)^n \int_a^x \mathrm{d}x' \, \frac{f(x')}{(x - x')^{\alpha-n+1}} \quad \text{for} \quad x > a, \end{aligned} \tag{F.2a}$$

and

$$\begin{aligned} D^{\alpha}_{b-}f(x) &:= \left(-\frac{\mathrm{d}}{\mathrm{d}x}\right)^n (I^{n-\alpha}_{b-}f)(x) \\ &= \frac{1}{\Gamma(n-\alpha)} \left(-\frac{\mathrm{d}}{\mathrm{d}x}\right)^n \int_x^b \mathrm{d}x' \, \frac{f(x')}{(x' - x)^{\alpha-n+1}} \quad \text{for} \quad x < b, \end{aligned} \tag{F.2b}$$

with $n = [\Re(\alpha)] + 1$. Here $[\Re(\alpha)]$ denotes the integer part of $\Re(\alpha)$. For $a \to -\infty$ and $b \to +\infty$ the RIEMANN-LIOUVILLE fractional integrals and derivatives are referred

B. A. Stickler and E. Schachinger, *Basic Concepts in Computational Physics*,
DOI: 10.1007/978-3-319-02435-6, © Springer International Publishing Switzerland 2014

to as WEYL fractional integrals and derivatives . In what follows, they will be denoted by $I^\alpha_\pm$ and $D^\alpha_\pm$, respectively.

If $\alpha \in \mathbb{C}$ $[\Re(\alpha) \geq 0]$ and $[a, b] \in \mathbb{R}$ is a finite interval, then the left- and right-sided CAPUTO fractional derivatives ${}^C\!D^\alpha_{a+}f(x)$ and ${}^C\!D^\alpha_{b-}f(x)$ are defined by

$$ {}^C\!D^\alpha_{a+}f(x) = D^\alpha_{a+}f(x) - \sum_{k=0}^{n-1} \frac{f^{(k)}(a)}{\Gamma(k-\alpha+1)}(x-a)^{k-\alpha}, \tag{F.3a} $$

and

$$ {}^C\!D^\alpha_{b-}f(x) = D^\alpha_{b-}f(x) - \sum_{k=0}^{n-1} \frac{(-1)^k f^{(k)}(b)}{\Gamma(k-\alpha+1)}(b-x)^{k-\alpha}, \tag{F.3b} $$

with

$$ n = \begin{cases} [\Re(\alpha)] + 1 & \alpha \notin \mathbb{N}, \\ \alpha & \alpha \in \mathbb{N}_0. \end{cases} \tag{F.3c} $$

This is, however, equivalent to

$$ \begin{aligned} {}^C\!D^\alpha_{a+}f(x) &= \frac{1}{\Gamma(n-\alpha)} \int_a^x \mathrm{d}x' \, \frac{f^{(n)}(x')}{(x-x')^{\alpha-n+1}} \\ &= (I^{n-\alpha}_{a+} D^n f)(x), \end{aligned} \tag{F.4a} $$

and

$$ \begin{aligned} {}^C\!D^\alpha_{b-}f(x) &= \frac{(-1)^n}{\Gamma(n-\alpha)} \int_x^b \mathrm{d}x' \, \frac{f^{(n)}(x')}{(x'-x)^{\alpha-n+1}} \\ &= (-1)^n (I^{n-\alpha}_{b-} D^n f)(x). \end{aligned} \tag{F.4b} $$

The symmetric fractional integrals $I^\alpha_{|x|}$ and derivatives $\mathscr{D}^\alpha_{|x|}$ are referred to as RIESZ fractional integrals or derivatives and are of the form

$$ I^\alpha_{|x|} = \frac{I^\alpha_+ + I^\alpha_-}{2\cos\left(\frac{\alpha\pi}{2}\right)}, \tag{F.5} $$

for $\alpha \in (0, 1)$ and

$$ \mathscr{D}^\alpha_{|x|} = \begin{cases} (-1)^{\frac{n}{2}} \frac{D^\alpha_+ + D^\alpha_-}{2\cos(\alpha\pi/2)} & \text{for} \quad n = [\Re(\alpha)] + 1 \equiv 2k, \ k \in \mathbb{N}_0, \\ \\ (-1)^{\frac{n-1}{2}} \frac{D^\alpha_+ - D^\alpha_-}{2\sin(\alpha\pi/2)} & \text{for} \quad n = [\Re(\alpha)] + 1 \equiv 2k+1, \ k \in \mathbb{N}_0. \end{cases} \tag{F.6} $$

Appendix G
Least Squares Fit

G.1 Motivation

In numerous physics applications a set of corresponding data points (x_k, y_k) was measured or calculated and a set of certain parameters $\{\alpha_j\}$ characterizing a function $f(x_k, \{\alpha_j\})$ is to be determined in such a way that

$$\chi^2 = \sum_k c_k \left[y_k - f(x_k, \{\alpha_j\})\right]^2 \to \text{min.} \tag{G.1}$$

This is referred to as a *least squares fit* problem. Here, $c_k \geq 0$ are weights, which indicate the relevance of a certain data point (x_k, y_k) for the fitting routine and $f(x, \{\alpha_j\})$ is referred to as the *model function*. Besides numerous applications in the context of experimentally obtained data points, we already came across such a problem in our discussion of data analysis in Chap. 19. Here it was of interest to determine the *experimental auto-correlation time* by fitting an exponential function to the measured auto-correlation coefficient $A(k)$ discussed in Sect. 19.3. Hence, we note that in many applications the parameters $\{\alpha_j\}$ can be associated with a physical property of interest.

We distinguish between two different cases: (i) the function $f(x_k, \{\alpha_j\})$ is a linear function of the parameters $\{\alpha_j\}$ and (ii) the function $f(x_k, \{\alpha_j\})$ is not linear in its parameters $\{\alpha_j\}$. It should be emphasized that in both cases the function does not need to be linear in x_k. In what follows we shall discuss linear as well as non-linear least squares fits. However, before proceeding some comments on the data points $\{y_k\}$ may be appropriate.

Suppose the points (x_k, y_k) stem from a measurement which has been repeated N-times. In this case for every value x_k we have N different values $\{y_k^j\}$ and we may use the arithmetic mean

$$\bar{y_k} = \frac{1}{N}\sum_j y_k^j, \tag{G.2}$$

B. A. Stickler and E. Schachinger, *Basic Concepts in Computational Physics*,
DOI: 10.1007/978-3-319-02435-6, © Springer International Publishing Switzerland 2014

in expression (G.1). We may also calculate the variance $\mathrm{var}\,(y_k)$ via[7]

$$\mathrm{var}\,(y_k) = \frac{1}{N}\sum_j (y_k^j - \bar{y_k})^2. \tag{G.3}$$

If we assume that the data points y_k^j follow a normal distribution with mean $\langle y_k \rangle$ and variance $\mathrm{var}\,(y_k)$ we may proceed in the following way: The weights c_k are chosen as

$$c_k = \frac{1}{\mathrm{var}\,(y_k)}. \tag{G.4}$$

The resulting fit parameters $\{\alpha_j\}$ are then regarded as mean values of parameters where the variances $\mathrm{var}\,(\alpha_i)$ as well as the covariances $\mathrm{cov}\,\left(\alpha_i, \alpha_j\right)$ can be obtained from the matrix

$$N_{ij} = \frac{1}{2}\frac{\partial^2 \chi^2}{\partial\alpha_i\partial\alpha_j}, \tag{G.5}$$

via inversion, i.e.

$$C = N^{-1}, \tag{G.6}$$

and

$$C_{ij} = \mathrm{cov}\,\left(\alpha_i, \alpha_j\right). \tag{G.7}$$

G.2 Linear Least Squares Fit

In this particular case we can write the model function $f(x_k, \{\alpha_j\})$ as

$$f(x_k, \{\alpha_j\}) = \sum_j \alpha_j \varphi_j(x_k), \tag{G.8}$$

where $\varphi_j(x_k)$ are linear independent basis functions, which do not have to be linear in x_k. The particular case of a *linear regression* of Appendix D.11 is included. Inserting (G.8) into (G.1) yields

$$\chi^2 = \sum_k c_k \left[y_k - \sum_j \alpha_j \varphi_j(x_k) \right]^2, \tag{G.9}$$

[7] In many cases one employs the *bias corrected variance* $\mathrm{var}\,(y_k)_B = \frac{N}{N-1}\mathrm{var}\,(y_k)$. For a detailed discussion of the bias corrected variance the interested reader is encouraged to consult a statistics textbook [12, 13].

which is supposed to tend to a minimum. Hence, we calculate

$$\frac{\partial \chi^2}{\partial \alpha_\ell} = -2 \sum_k c_k \varphi_\ell(x_k) \left[y_k - \sum_j \alpha_j \varphi_j(x_k) \right] \overset{!}{=} 0, \tag{G.10}$$

which yields

$$\sum_j \alpha_j \sum_k c_k \varphi_\ell(x_k) \varphi_j(x_k) = \sum_k c_k y_k \varphi_\ell(x_k), \tag{G.11}$$

for all ℓ. This equation may be rewritten as the linear equation

$$M\alpha = \beta, \tag{G.12}$$

where we introduced the vector $\alpha = (\alpha_1, \alpha_2, \ldots)^T$, the matrix M

$$M_{ij} = \sum_k c_k \varphi_i(x_k) \varphi_j(x_k), \tag{G.13}$$

and the vector β

$$\beta_i = \sum_k c_k y_k \varphi_i(x_k). \tag{G.14}$$

Equation (G.12) can, for instance, be solved with the help of the methods discussed in Appendix C. In the case of a linear least squares fit, it is also particularly simple to determine the covariances because we have

$$N_{ij} = \frac{1}{2} \frac{\partial^2 \chi^2}{\partial \alpha_i \partial \alpha_j} = M_{ij}. \tag{G.15}$$

G.3 Nonlinear Least Squares Fit

Before we discuss the most general case of a completely arbitrary function $f(x_k, \{\alpha_j\})$ we shall briefly mention that in most cases it is advantageous to directly linearize the function if possible. For instance, if the model function is an exponential function, it may be linearized by taking the data points $\ln(y_k)$ instead of y_k.

However, if this is not possible there are several methods how to solve the problem. If the function $f(x_k, \{\alpha_j\})$ and its derivatives with respect to the parameters α_j are known analytically, the Gauss-Newton method can be employed. We discuss this possibility in more detail in what follows. An alternative would be a deterministic optimization algorithm as they are introduced in Appendix H. If even this is not possible, methods discussed in Chap. 20, stochastic optimization, might be the obvious choice.

We describe now the GAUSS-NEWTON method which is essentially a generalization of the NEWTON method presented in Appendix B. The GAUSS-NEWTON method is a method developed to minimize the expression (G.1) iteratively, where the derivatives

$$\frac{\partial f(x_k, \{\alpha_j\})}{\partial \alpha_\ell}, \tag{G.16}$$

are assumed to be known analytically. In what follows the upper index on the parameters refers to the iteration index. One proceeds in the following steps:

1. Choose a set of initial values $\{\alpha_j^0\}$ for the iteration.
2. Linearize the function $f(x_l, \{\alpha_j^n\})$ and insert the result into Eq. (G.1), i.e.

$$\chi^2 \approx \sum_k c_k \left\{ y_k - f(x_k, \{\alpha_j^n\}) - \sum_\ell \left[\frac{\partial f(x_k, \{\alpha_j\})}{\partial \alpha_\ell} \right]_{\{\alpha_j\}=\{\alpha_j^n\}} (\alpha_\ell - \alpha_\ell^n) \right\}^2 . \tag{G.17}$$

For reasons of a more compact notation we introduce the abbreviations

$$\mathrm{d}f_{k,\ell}^n = \left[\frac{\partial f(x_k, \{\alpha_j\})}{\partial \alpha_\ell} \right]_{\{\alpha_j\}=\{\alpha_j^n\}}, \tag{G.18}$$

and

$$f_k^n = f(x_k, \{\alpha_j^n\}). \tag{G.19}$$

3. We solve

$$\frac{\partial \chi^2}{\partial \alpha_i} = -2 \sum_k c_k \mathrm{d}f_{k,i}^n \left[y_k - f_k - \sum_\ell \mathrm{d}f_{k,\ell}^n \, (\alpha_\ell - \alpha_\ell^n) \right] \overset{!}{=} 0, \tag{G.20}$$

for the parameters $\{\alpha_j\}$. Therefore, we define $\alpha = (\alpha_1, \alpha_2, \ldots)^T$,

$$\beta_i = \sum_k c_k (y_k - f_k^n) \mathrm{d}f_{k,i}^n \,, \tag{G.21}$$

as well as

$$M_{ij} = \sum_k c_k \mathrm{d}f_{k,i}^n \, \mathrm{d}f_{k,j}^n \,. \tag{G.22}$$

The resulting linear system of equations takes on the form

$$M(\alpha - \alpha^n) = \beta, \tag{G.23}$$

which is solved for $\Delta\alpha^n = \alpha - \alpha^n$. Please note that α^n denotes the value of α after n iterations. The next values are guessed according to

$$\alpha^{n+1} = \alpha^n + \Delta\alpha^n. \tag{G.24}$$

4. The iteration is terminated if for all parameters the desired accuracy was achieved. For instance, $|\alpha_j^{n+1} - \alpha_j^n| \leq \varepsilon$ can be used. Here ε is a small parameter. A criterion for the relative error can be formulated in analogue.

Some comments are in order: First of all we note that the calculation of the covariance matrix is more complicated in the nonlinear case because we also have to consider the second partial derivatives of the test function $f(x_k, \{\alpha_\ell\})$. However, if these can for some reason be neglected we obtain, again, that $N_{ij} = M_{ij}$, see Appendix G.2. Another, more serious problem is the fact that the GAUSS-NEWTON method suffers from severe instability problems. However, a possible solution was formulated by D. MARQUART [14], who suggested to multiply the diagonal elements of the matrix M with a factor $(1 + \lambda)$ where $\lambda > 0$. A detailed analysis shows that one can choose λ sufficiently large and in such a way that the value of χ_n^2 decreases monotonically, i.e. $\chi_{n+1}^2 \leq \chi_n^2$ for all n. However, an increase of λ decreases the convergence rate, i.e. more iterations are necessary in order to obtain the required accuracy. It is therefore desirable to choose λ values in such a way that the error is monotonically decreasing but that the convergence rate stays as large as possible. A possible strategy is to start with a given value of λ and to decrease it in every iteration step by a constant rate. However, if at some point the error χ^2 increases, i.e. $\chi_{n+1}^2 > \chi_n^2$ then λ has again to be increased.

Appendix H
Deterministic Optimization

H.1 Introduction

We use the term *deterministic optimization* to distinguish these particular optimization methods from the stochastic optimization methods discussed in Chap. 20. There are numerous different deterministic methods developed to find the minimum (or maximum) of a given function $f(x)$, where x can be a vector. Roughly speaking, we can distinguish between methods which require the knowledge of the Hessian,[8] methods which need gradients only, and methods which are based on function values only. For instance, if the gradient of a function is known analytically one may exploit NEWTON's method, as it was introduced in Appendix B. Note that such an approach requires the Hessian of the function $f(x)$.

In what follows we shall discuss in some detail two particular methods, namely the method of *steepest descent* and the method of *conjugate gradients*. Both methods require the knowledge of the gradient of the function, however, it may also be approximated with the help of finite differences (Chap. 2). A discussion of additional methods is beyond the scope of this book and the interested reader is referred to the available literature [15].

However, before discussing these two methods in more detail, let us briefly consider the quadratic problem, which can be solved analytically. In this case the function $f(x)$ can be written as

$$f(x) = \frac{1}{2}x^T Ax - b^T x + c, \tag{H.1}$$

where $x \in \mathbb{R}^N$, $A \in \mathbb{R}^{N\times N}$, $b \in \mathbb{R}^N$ and $c \in \mathbb{R}$ where we restrict the discussion to real valued functions for reasons of simplicity. We shall now demonstrate that for symmetric and positive definite matrices A, i.e. $A^T = A$ and $x^T Ax > 0$ for all $x \neq 0$, the minimum of $f(x)$ is given by $x = A^{-1}b$. The gradient of $f(x)$ is readily evaluated

[8] The Hessian, or HESSE matrix, $H \in \mathbb{R}^{N\times N}$ of a function $f(x)$, $x \in \mathbb{R}^N$ is the Jacobian of the Jacobian $J(x)$ of $f(x)$ defined in Eq. (B.8). Thus, it is the matrix of second order partial derivatives of a function. It describes the local curvature of a function of many variables.

B. A. Stickler and E. Schachinger, *Basic Concepts in Computational Physics*,
DOI: 10.1007/978-3-319-02435-6, © Springer International Publishing Switzerland 2014

to be[9]

$$\nabla f(x) = \frac{1}{2} A^T x + \frac{1}{2} A x - b, \tag{H.2}$$

which immediately yields the desired result,

$$Ax = b. \tag{H.3}$$

From the fact that we assumed A to be positive definite it follows that $x = A^{-1} b$ is a minimum. If A is not symmetric it is possible to solve the problem in a similar fashion by inverting the matrix $\left(A + A^T\right)/2$. In Appendix C we discussed some simple methods to solve the linear Eq. (H.3).

In what follows we will discuss methods which solve the minimization problem for some arbitrary function $f(x)$ iteratively by evaluating the gradient $\nabla f(x)$ at each iteration point x_n. This gradient is then employed to obtain the next guess x_{n+1} until convergence has been achieved.

H.2 Steepest Descent

The most simple gradient based method is *steepest descent*. It is based on the rather straight forward idea of moving in each iteration step into the opposite direction of the gradient, i.e. *downhill*. Hence, we may formulate it mathematically in the following way: Let x_n be the current position of our search for the minimum. Then we choose

$$x_{n+1} = x_n - \alpha_n \nabla f(x_n), \tag{H.4}$$

where the step-size in direction of the negative gradient, α_n, has to be determined in an additional step. The step-size should be chosen in such a way that we reach the line minimum in direction $\nabla f(x_n)$, i.e.

$$\frac{\mathrm{d}}{\mathrm{d}\alpha_n} f[x_{n+1}(\alpha_n)] = -\nabla f(x_{n+1}) \cdot \nabla f(x_n) \overset{!}{=} 0. \tag{H.5}$$

Hence, we observe that the search directions are orthogonal for an optimal choice of α_n. In practice α_n is estimated with the help of a separate minimization technique, such as bisection as it has already been used in our discussion of the shooting methods in Chap. 10.

[9] We remember from vector analysis that

$$\nabla_x \left(x^T A x\right) = \underbrace{\nabla_x \left(x^T A\right)}_{=A} x + \underbrace{\nabla_x \left(x^T A^T\right)}_{A^T} x = (A + A^T)x$$

where I is the identity.

We give an example in order to clarify the method and discuss its caveats: Suppose we want to find the global minimum of the function

$$f(x, y) = \cos(2x) + \sin(4y) + \exp(1.5x^2 + 0.7y^2) + 2x. \tag{H.6}$$

Its gradient is readily evaluated to be

$$\frac{\partial f(x, y)}{\partial x} = -2\sin(2x) + 3x\exp(1.5x^2 + 0.7y^2) + 2, \tag{H.7}$$

and

$$\frac{\partial f(x, y)}{\partial y} = 4\cos(4y) + 1.4y\exp(1.5x^2 + 0.7y^2). \tag{H.8}$$

We execute the algorithm in the following steps:

1. Choose some initial values x_0 and y_0.
2. Calculate the gradient $\nabla f(x_n, y_n)$.
3. Determine α_n in such a way that

$$f[x_{n+1}(\alpha_n), y_{n+1}(\alpha_n)] \rightarrow \min, \tag{H.9}$$

which is equivalent to

$$g(\alpha_n) := \nabla f[x_{n+1}(\alpha_n), y_{n+1}(\alpha_n)] \cdot \nabla f(x_n, y_n) = 0. \tag{H.10}$$

This is achieved by a bisection similar to the one employed in Sect. 10.3, i.e.

(a) Set $\alpha_n^a = 0$ and chose α_n^b arbitrary.
(b) Increase α_n^b until $g(\alpha_n^a)g(\alpha_n^b) < 0$.
(c) Define

$$\alpha_n^c = \frac{\alpha_n^a + \alpha_n^b}{2}, \tag{H.11}$$

and determine $g(\alpha_n^c)$.
(d) If $g(\alpha_n^a)g(\alpha_n^a) < 0$, set $\alpha_n^b = \alpha_n^c$ and return to step (c). Otherwise, set $\alpha_n^a = \alpha_n^c$ and return to step (c).
(e) The bisection is terminated if $|g(\alpha_n^a)| < \varepsilon$, some required accuracy.

4. Check whether $|f(x_{n+1}, y_{n+1}) - f(x_n, y_n)| \leq \eta$ with η some required accuracy.

The above algorithm was executed for the function $f(x, y)$ given by Eq. (H.6) for three different starting points, (0.8, −0.75), (0.8, 1.05), and (−1.05, 1.05). The function $f(x, y)$ as well as the iteration sequence towards the minimum for all three starting points is illustrated in Fig. H.1.

We note the following properties of the method: First of all it is a rather slow method due to the orthogonality of subsequent search directions. Moreover, as we observe from Fig. H.1, we can only find the local minimum closest to the starting

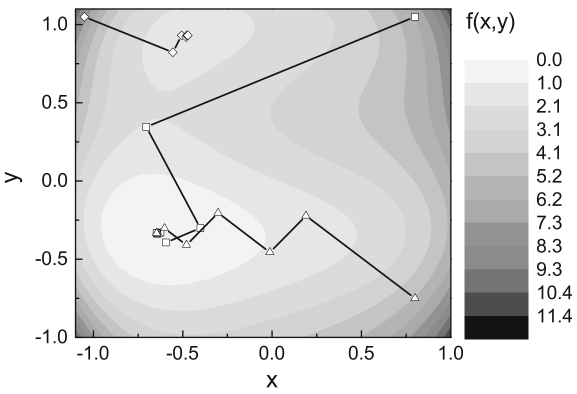

Fig. H.1 Iteration sequence of the method of steepest descent for three different starting points

point and not the global minimum of the function $f(x, y)$. The convergence rate is also highly affected by the choice of the initial position. More problems arise if the function $f(x, y)$ is not differentiable by analytic means because then the gradient has to be approximated by finite differences (Chap. 2). However, it is a very simple method which works in spaces of arbitrary dimension.

H.3 Conjugate Gradients

The method of *conjugate gradients* [15] is based on the definition of N orthogonal search directions $\{\psi_i\}$ in an N dimensional space. In contrast to steepest descent it is designed in such a way that we take only *one* step in each search direction, i.e. we are done after at most N steps, if the function $f(x)$ is of the quadratic form (H.1). In the more general case, however, it will take more steps but will, nevertheless, be much more efficient than the method of steepest descent. Let us formulate the method for a general function $f(x)$.

In what follows, $x \in \mathbb{R}^N$. We approximate the function $f(x)$ in the vicinity of the reference point x_n of the n-th iteration step up to second order and name the resulting function $\hat{f}(x)$, i.e.

$$\begin{aligned}\hat{f}_n(x) &:= f(x_n) + \nabla f(x_n) \cdot (x - x_n) + \frac{1}{2}(x - x_n) \cdot \left[\Delta f(x_n)(x - x_n)\right] \\ &\equiv f(x_n) - b_n^T(x - x_n) + \frac{1}{2}(x - x_n)^T A_n (x - x_n),\end{aligned} \tag{H.12}$$

where A_n denotes the Hessian[10] at position x_n and b_n is the negative gradient at x_n. In particular, for a quadratic function $f(x)$ we have the equality $\hat{f}(x) = f(x)$. We now

[10] Note that the Hessian is always symmetric for real valued $f(x)$ due to the symmetry of second order derivatives.

write the minimum of $f(x)$, $\hat{x}$, as a linear combination of search directions $\{\psi_i\}$ with coefficients λ_i and the initial point x_0:

$$\hat{x} = x_0 + \sum_{i=0}^{M} \lambda_i \psi_i. \tag{H.13}$$

Note that in the quadratic case (H.1) this sum will be restricted to $M = N - 1$. At each iteration instance we have the relation

$$x_{n+1} = x_n + \lambda_n \psi_n, \tag{H.14}$$

together with the goal

$$x_M \overset{!}{=} \hat{x}. \tag{H.15}$$

Let us define a couple of useful quantities. The deviation from the minimum at iteration step $n+1$, δ_{n+1}, is given by

$$\begin{aligned} \delta_{n+1} &= x_{n+1} - \hat{x} \\ &= x_n + \lambda_n \psi_n - \hat{x} \\ &= \delta_n + \lambda_n \psi_n. \end{aligned} \tag{H.16}$$

In a similar fashion we obtain the residual

$$\begin{aligned} r_{n+1} &:= -\nabla \hat{f}_n(x_{n+1}) \\ &= b_n - A_n(x_{n+1} - x_n) \\ &= b_n - \lambda_n A_n \psi_n, \end{aligned} \tag{H.17}$$

where we employed that

$$\frac{1}{2}\nabla\left[(x - x_n)^T A_n (x - x_n)\right] = A_n(x - x_n). \tag{H.18}$$

Finding the minimum of the quadratic approximation $\hat{f}(x)$ of $f(x)$ around x_n is equivalent to the condition

$$r_{n+1} = 0. \tag{H.19}$$

In particular, we have to find the product $\lambda_n \psi_n$ in such a way that $r_{n+1} = 0$. Of course, we could invert the Hessian A_n in order to obtain this result. However this would be too expensive from a computational point of view. The idea is to apply the *ideal* search strategy for quadratic functions to $\hat{f}_n(x)$ in order to obtain x_{n+1}. Hence, the method of conjugate gradients executes packages of N steps, where each package solves the quadratic problem around x_n, until the minimum of the original function

$f(x)$ has been found. Therefore, we have to generalize the relations (H.14), (H.16), and (H.17) for iterations within step n.

In particular, for every iteration step n we have

$$x_{n+1} = x_n + \sum_{\ell=0}^{N-1} \lambda_n^\ell \psi_n^\ell, \tag{H.20}$$

together with the definitions

$$x_n^{\ell+1} = x_n^\ell + \lambda_n^\ell \psi_n^\ell, \tag{H.21}$$

where $x_{n+1} \equiv x_n^N$. Furthermore, we define the deviation

$$\delta_n^{\ell+1} = x_n^{\ell+1} - x_{n+1} = \delta_n^\ell + \lambda_n^\ell \psi_n^\ell, \tag{H.22}$$

and the residual

$$\begin{aligned} r_n^{\ell+1} &= -\nabla \hat{f}_n(x_n^{\ell+1}) \\ &= b_n - A_n(x_n^{\ell+1} - x_n). \end{aligned} \tag{H.23}$$

In contrast to relation (H.17), Eq. (H.23) features the difference $(x_n^{\ell+1} - x_n)$ rather than $(x_{n+1} - x_n)$. We insert the recurrence (H.21) and obtain

$$\begin{aligned} r_n^{\ell+1} &= b_n - A_n(x_n^\ell - x_n) - \lambda_n^\ell A_n \psi_n^\ell \\ &= r_n^\ell - \lambda_n^\ell A_n \psi_n^\ell. \end{aligned} \tag{H.24}$$

Hence, in contrast to relation (H.17) Eq. (H.24) defines a recurrence relation. Again, we want to choose the search directions ψ_n^ℓ and the step length λ_n^ℓ in such a way that we find the minimum as quickly as possible. Suppose we already knew the search direction ψ_n^ℓ. The line minimum in this direction is then given by

$$\begin{aligned} \frac{\mathrm{d}}{\mathrm{d}\lambda_n^\ell} \hat{f}_n(x_n^{\ell+1}) &= \nabla \hat{f}(x_n^{\ell+1}) \cdot \psi_n^\ell \\ &= -r_n^{\ell+1} \cdot \psi_n^\ell \\ &= -(r_n^\ell - \lambda_n^\ell A_n \psi_n^\ell)^T \psi_n^\ell \\ &= -(r_n^\ell)^T \psi_n^\ell + \lambda_n^\ell (\psi_n^\ell)^T A_n \psi_n^\ell \\ &\overset{!}{=} 0, \end{aligned} \tag{H.25}$$

and we have

$$\lambda_n^\ell = \frac{(r_n^\ell)^T \psi_n^\ell}{(\psi_n^\ell)^T A_n \psi_n^\ell}. \tag{H.26}$$

Hence, the remaining unknown quantities in our algorithm are the search directions ψ_n^ℓ. So far, the only information we obtained is that the search direction ψ_n^ℓ is orthogonal to the residual $r_n^{\ell+1}$, see Eq. (H.25).

However, we also know that

$$\begin{aligned} 0 &= A_n \left(x_{n+1} - x_n\right) - b_n \\ &= A_n \sum_{\ell=0}^{N-1} \lambda_n^\ell \psi_n^\ell - b_n, \end{aligned} \tag{H.27}$$

and therefore

$$0 = \left(\psi_n^k\right)^T A_n \sum_{\ell=0}^{N-1} \lambda_n^\ell \psi_n^\ell - \left(\psi_n^k\right)^T b_n, \tag{H.28}$$

for arbitrary k. A sufficient condition to ensure the validity of relation (H.28) is to impose A_n*-orthogonality*, i.e. to demand that

$$\left\langle \psi_n^k \,\middle|\, \psi_n^\ell \right\rangle_{A_n} \equiv (\psi_n^k)^T A_n \psi_n^\ell = \delta_{k,\ell} \left\langle \psi_n^k \,\middle|\, \psi_n^k \right\rangle_{A_n}. \tag{H.29}$$

We note that $\langle \psi_n^k \mid \psi_n^\ell \rangle_A$ constitutes indeed a scalar product since A_n is positive definite in the neighborhood of a minimum.

Let us briefly demonstrate that the choice (H.29) fulfills Eq. (H.28). First of all we note that we obtain from Eq. (H.24)

$$r_n^{\ell+1} = b_n - \sum_{k=0}^{\ell} \lambda_n^k A_n \psi_n^k, \tag{H.30}$$

and, therefore, we get from Eq. (H.26) the coefficients λ_n^ℓ in the convenient form

$$\lambda_n^\ell = \frac{b_n^T \psi_n^\ell}{\langle \psi_n^\ell \mid \psi_n^\ell \rangle_{A_n}}. \tag{H.31}$$

Inserting the condition of orthogonality (H.29) into Eq. (H.28) gives

$$0 = \lambda_n^k \left\langle \psi_n^k \,\middle|\, \psi_n^k \right\rangle_{A_n} - \left(\psi_n^k\right)^T b_n, \tag{H.32}$$

which together with Eq. (H.31) proves the equality (H.28). Hence, the strategy is clear: We choose an initial direction ψ_n^0 and then construct the further directions in such a way that they fulfill A_n-orthogonality (H.29). Before discussing the construction of search directions in more detail we observe the following property:

$$(\psi_n^k)^T r_n^\ell = (\psi_n^k)^T b_n - \sum_{m=0}^{\ell-1} \lambda_n^m \Big\langle \psi_n^k \,\Big|\, \psi_n^m \Big\rangle_{A_n} = \begin{cases} (\psi_n^k)^T b_n & \text{for } k \geq \ell, \\ 0 & \text{else.} \end{cases} \tag{H.33}$$

This means that all search directions ψ_n^k for $k \leq \ell - 1$ are orthogonal to the residual r_n^ℓ, or in other words, all residuals r_n^ℓ are orthogonal (in the classical sense) to all previous search directions.

We shall now briefly outline the resulting update algorithm for search directions. Let $\{\varphi_n^\ell\}$ be a set of linear independent vectors that span our search space for $\hat{f}_n(x)$.[11] We write the search direction ψ_n^k as

$$\psi_n^k = \varphi_n^k + \sum_{\ell=0}^{k-1} \beta_n^{k\ell} \psi_n^\ell, \tag{H.34}$$

together with

$$\psi_n^0 = \varphi_n^0. \tag{H.35}$$

The expansion coefficients $\beta_n^{\ell k}$ can be determined recursively by imposing A_n-orthogonality for all $\ell < k$:

$$\begin{aligned} 0 &= \Big\langle \psi_n^k \,\Big|\, \psi_n^\ell \Big\rangle_{A_n} \\ &= \Big\langle \varphi_n^k \,\Big|\, \psi_n^\ell \Big\rangle_{A_n} + \sum_{m=0}^{k-1} \beta_n^{km} \Big\langle \psi_n^m \,\Big|\, \psi_n^\ell \Big\rangle_{A_n} \\ &= \Big\langle \varphi_n^k \,\Big|\, \psi_n^\ell \Big\rangle_{A_n} + \beta_n^{k\ell} \Big\langle \psi_n^\ell \,\Big|\, \psi_n^\ell \Big\rangle_{A_n}, \end{aligned} \tag{H.36}$$

and therefore

$$\beta_n^{k\ell} = -\frac{\langle \varphi_n^k \mid \psi_n^\ell \rangle_{A_n}}{\langle \psi_n^\ell \mid \psi_n^\ell \rangle_{A_n}}. \tag{H.37}$$

This procedure is known as the GRAM-SCHMIDT *conjugation*.

Now, the question arises how one should choose the basis vectors φ_n^ℓ and whether or not it is advantageous to choose the φ_n^ℓ as a function of n. A particularly clever choice is to take the residuals, i.e.

$$\varphi_n^\ell = r_n^\ell. \tag{H.38}$$

In this case we have for $\ell < k$

[11] In principle these linear independent vectors $\{\varphi_n^\ell\}$ do not need to depend on the index n, i.e. on the actual position x_n. However, we consider here the most general case as will become clear in what follows.

$$\begin{aligned}\beta_n^{k\ell} &= -\frac{\langle r_n^k \mid \psi_n^\ell\rangle_{A_n}}{\langle \psi_n^\ell \mid \psi_n^\ell\rangle_{A_n}} \\ &= -\frac{(r_n^k)^T A_n \psi_n^\ell}{\langle \psi_n^\ell \mid \psi_n^\ell\rangle_{A_n}} \\ &= -\frac{(r_n^k)^T}{\langle \psi_n^\ell \mid \psi_n^\ell\rangle_{A_n}}\left[\frac{r_n^\ell - r_n^{\ell+1}}{\lambda_n^\ell}\right],\end{aligned} \tag{H.39}$$

where we used recurrence (H.24). We now calculate with the help of Eq. (H.34)

$$(r_n^k)^T(r_n^\ell) = (r_n^k)^T\psi_n^\ell - (r_n^k)^T\sum_{m=0}^{\ell-1}\beta_n^{\ell m}\psi_n^m = 0, \tag{H.40}$$

for $\ell < k$ due to the orthogonality of the search direction and the residuals, see Eq. (H.33). Hence, we obtain for all $\ell < k$

$$\begin{aligned}\beta_n^{k\ell} &= \frac{1}{\lambda_n^{k-1}}\frac{(r_n^k)^T r_n^k \delta_{\ell+1,k}}{\left\langle \psi_n^{k-1} \,\middle|\, \psi_n^{k-1}\right\rangle_{A_n}} \\ &= \frac{(r_n^k)^T r_n^k}{(r_n^{k-1})^T r_n^{k-1}}\delta_{\ell,k-1}.\end{aligned} \tag{H.41}$$

Hence, the name *conjugated gradients*. We summarize the algorithm:

1. Choose an initial position x_0.
2. Determine the vector b_n and the matrix A_n for a given position x_n.
3. Perform the following N steps in order to calculate x_{n+1}:

(a) Set

$$\psi_n^0 = r_n^0 = b_n \quad \text{and} \quad \lambda_n^0 = \frac{b_n^T\psi_n^0}{\langle \psi_n^0 \mid \psi_n^0\rangle_{A_n}}, \tag{H.42}$$

as well as

$$x_{n+1} = x_n + \lambda_n^0\psi_n^0. \tag{H.43}$$

(b) Calculate for $k = 1, \ldots, N-1$ the residuals,

$$r_n^k = r_n^{k-1} - \lambda_n^{k-1}A_n\psi_n^{k-1}, \tag{H.44}$$

the new search directions

$$\psi_n^k = r_n^k + \frac{(r_n^k)^T r_n^k}{(r_n^{k-1})^T r_n^{k-1}}\psi_n^{k-1}, \tag{H.45}$$

the step lengths

$$\lambda_n^k = \frac{b_n^T \psi^k}{\langle \psi_n^k \mid \psi_n^k \rangle_{A_n}}, \tag{H.46}$$

and, finally, the modified positions

$$x_{n+1} = x_n + \lambda_n^k \psi_n^k. \tag{H.47}$$

4. If $|f(x_{n+1}) - f(x_n)| < \varepsilon$, with ε some required accuracy, terminate the iteration, otherwise return to step 2. In case of a convex function $f(x)$ terminate also after N steps.

Strictly speaking, this algorithm is only valid for convex functions because we note that one might get into trouble whenever a position is reached at which the Hessian is not positive definite. It is therefore desirable to exclude the Hessian from the algorithm. This can be achieved by an algorithm developed by Fletcher and Reeves [16]. Based on our pervious discussion the generalization is rather obvious: If we do not want to use the Hessian explicitly, we have to determine the step length λ_n^ℓ by minimizing $f(x_n^\ell + \lambda_n^\ell \psi_n^\ell)$ for a given search direction ψ_n^ℓ numerically. The residuals are then taken to be the exact gradient of the function $f(x_n^\ell)$ rather than of $\hat{f}_n(x_n^\ell)$. The next search direction ψ_n^{k+1} is then determined via

$$\psi_n^{k+1} = -\nabla f(x_n^{k+1}) + \frac{\|\nabla f(x_n^{k+1})\|^2}{\|\nabla f(x_n^k)\|^2} \psi_n^k. \tag{H.48}$$

Hence, we have the following algorithm (Fletcher-Reeves *algorithm*) :

1. Choose an initial position x_0.
2. Perform the following N steps in order to calculate x_{n+1}:
   (a) Set
   $$\psi_n^0 = -\nabla f(x_n). \tag{H.49}$$
   (b) Calculate for $k = 0, \dots, N-1$, λ_n^k by minimizing $f(x_n^k + \lambda_n^k \psi_n^k)$, the new position $x_n^{k+1} = x_n^k + \lambda_n^k \psi_n^k$ and the new search direction via
   $$\psi_n^k = -\nabla f(x_n^{k+1}) + \frac{\|\nabla f(x_n^{k+1})\|^2}{\|\nabla f(x_n^k)\|^2} \psi_n^k. \tag{H.50}$$
3. If $|f(x_{n+1}) - f(x_n)| < \varepsilon$, with ε some required accuracy, terminate the iteration, otherwise return to step 2.

The resulting sequence of steps towards the minimum for the same function and initial conditions as were used for Fig. H.1 is illustrated in Fig. H.2. In comparing

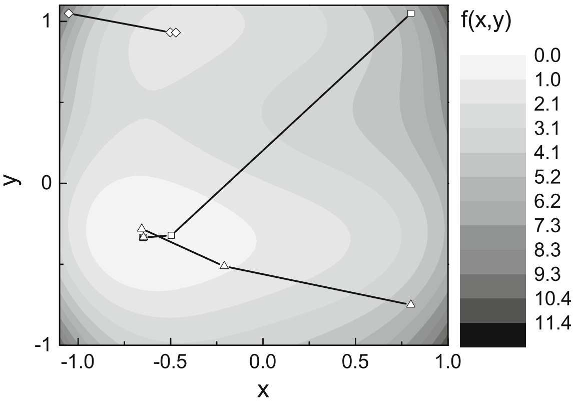

Fig. H.2 Iteration sequence of the method of conjugated gradients for three different starting points

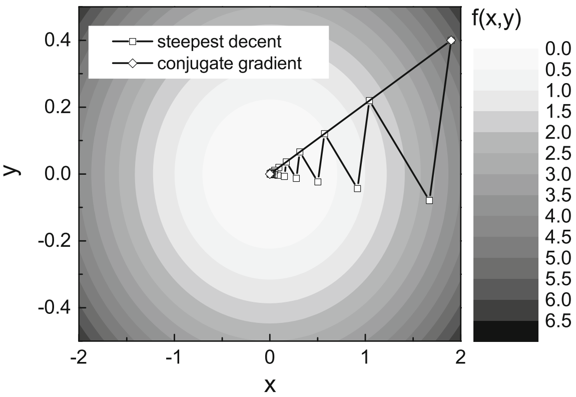

Fig. H.3 Comparison of the iteration sequence between the method of steepest descent and the method of conjugated gradients

Figures H.1 and H.2 we note immediately that the search strategy developed for the method of conjugate gradients superbly outperforms the search strategy of the method of steepest descent. In particular, if the ratio between the gradient in x and y direction is large, a strategy of orthogonal search directions is disadvantageous. This particular case is illustrated in Fig. H.3 for both, steepest descent and conjugate gradients. Here we investigate the convex function

$$f(x, y) = x^2 + 10y^2, \tag{H.51}$$

together with an initial position $(x_0, y_0) = (1.9, 0.4)$. The resulting sequence of points towards the minimum is illustrated in Fig. H.3. In the case of steepest descent the sequence approaches the minimum rather slowly since subsequent search directions have to be orthogonal to each other in the classical sense. The advantage of conjugate gradients is that A_n-orthonormality accelerates the convergence towards the minimum. In this example we reach it within two steps and a required absolute accuracy of $\eta = 10^{-7}$.

As a final remark we note that also the method of conjugate gradients will only find the *local minimum* closest to the initial position. Hence, the outcome of the method highly depends on the choice of x_0. Moreover, the calculation of the gradients may be very tedious and time-consuming from a numerical point of view.

References

1. Scheck, F.: Mechanics, 5th edn. Springer, Berlin (2010)
2. Jacques, I., Judd, C.: Numerical Analysis. Chapman and Hall, London (1987)
3. Burden, R.L., Faires, J.D.: Numerical Analysis. PWS-Kent Publishing Company, Boston (1993)
4. Westlake, J.R.: A Handbook of Numerical Matrix Inversion and Solution of Linear Equations. Wiley, New York (1968)
5. Stoer, J., Bulirsch, R.: Introduction to Numerical Analysis, 2nd edn. Springer, New York (1993)
6. Press, W.H., Teukolsky, S.A., Vetterling, W.T., Flannery, B.P.: Numerical Recipes in C++, 2nd edn. Cambridge University Press, Cambridge (2002)
7. Varga, R.S.: Matrix Iterative Analysis. 2nd edn. Springer Series in Computational Mathematics, vol. 27, Springer, New York (2000).
8. Lee, P.M.: Bayesian Statistics: An Introduction. Wiley, New York (2012)
9. Mandl, F.: Statistical Physics, 2nd edn. Wiley, New York (1988)
10. Landau, L.D., Lifshitz, E.M.: Course of Theoretical Physics, vol. 5: Statistical Physics, Pergamon Press, London (1963).
11. Kilbas, A.A., Srivastava, H.M., Trujillo, J.J.: Theory and Applications of Fractal Differential Equations. Elsevier, Amsterdam (2006)
12. Iversen, G.P., Gergen, I.: Statistics. Springer Undergraduate Textbooks in Statistics. Springer, Berlin (1997)
13. Keener, R.W.: Theoretical Statistics. Springer, New York (2010)
14. Marquart, D.: An algorithm for least-squares estimation of nonlinear parameters. J. Soc. Ind. Appl. Math. 11, 431–441 (1963). doi:10.1137/0111030.
15. Avriel, M.: Nonlinear Programming: Analysis and Methods. Dover Publications, New York (2003)
16. Fletcher, R., Reeves, C.M.: Function minimization by conjugate gradients. Comput. J. 7, 149–154 (1964). doi:10.1093/comjnl/7.2.149.

Index

A

Absolute error, *see* error
Adams–Bashford method, *see* integrator
Algorithm, 5
Anomalous diffusion, 267
Antiferromagnetism, 210
Auto-correlation function, 231
Auto-correlation time
  exponential, 293
  integrated, 292, 294
Auto-correlations, 291
Autonomous system, 89

B

Backward difference, 20, 31
Barometric formula, 109
Bayes' theorem, 337
Bernoulli's law of large numbers, 335
Binomial distribution, *see* probability density function
Boltzmann distribution, *see* probability density function
Boltzmann equation, 251
  collision integral, 251
  particle density, 252
Boundary conditions
  decoupled, 112
  Dirichlet conditions, 112, 150
  homogeneous, 112
  Neumann conditions, 112
  of first kind, 112
  of second kind, 112
  of third kind, 112
  periodic, 103, 116
  Sturm conditions, 112
Brownian motion, 171, 233
Butcher tableau, *see* integrator

C

Calculus
  mean value theorem, 199
Canonical partition function, 201, 205, 212
Caputo fractional derivative, 270, 271, 350
Cauchy distribution, *see* probability density function
Cdf, *see* cumulative distribution function
Central difference, 20
Central limit theorem, 181, 203, 339
  generalized, 343
Chaos
  attractor, 91
  deterministic, 12
  Lyapunov length, 91
  Lyapunov stability, 90
  Poincaré map, 91
  Poincaré section, 92
  theory, 12
Chapman–Kolmogorov equation, 234, 237, 242, 248, 249
χ^2 distribution, 181
Closed integration rule, 32
Cluster algorithm, 284
Computational cost, 12
Configuration space, 88, 315
Conjugate gradients, *see* deterministic optimization
Covariance, 333
Crank–Nicolson method, *see* integrator
Cumulative distribution function, 175, 185, 336

B. A. Stickler and E. Schachinger, *Basic Concepts in Computational Physics*,
DOI: 10.1007/978-3-319-02435-6, © Springer International Publishing Switzerland 2014

D
DE MOIVRE–LAPLACE theorem, 335, 339
Derivative
  finite difference, 147, 149, 157, 162, 264
    average μ, 22
    backward, 21, 23, 56, 100
    central, 21, 22, 57, 152, 161
    forward, 20, 23, 55
    operator technique, 22
    shift operator, 23
    three point approximation, 21
  fractional
    CAPUTO fractional derivative, 270, 271, 350
    RIEMANN–LIOUVILLE fractional derivative, 270, 349
    RIESZ fractional derivative, 271, 350
    WEYL fractional derivative, 350
  partial, 26
Detailed balance, 206, 239, 240, 244, 275, 277
Deterministic optimization, 357
  conjugate gradients, 360
    A_n-orthogonality, 363
    FLETCHER–REEVES algorithm, 366
    GRAM–SCHMIDT conjugation, 364
    line minimum, 362
    residual, 361
  Hessian matrix, 360
  steepest descent, 358
    convergence rate, 360
    line minimum, 358
Differential equation
  harmonic oscillator, 2
  LEGENDRE, 39
Diffusion equation, 123, 252, 262
  diffusion coefficient, 123, 252
  particle density, 123
DIRAC δ-distribution, 127, 201, 203
Distribution function, 171
Double pendulum
  chaotic, 87
  generalized momenta, 82
  HAMILTON equations of motion, 84
  HAMILTON function, 84
  kinetic energy, 82, 83
  LAGRANGE function, 81, 82
  POINCARÉ plot, 93
  potential energy, 82
  RUNGE–KUTTA algorithm, 85
  trajectories, 86

E
e-RK-4, 70, 71, 85
Eccentricity, 54
Effective potential, 52
Error
  absolute, 6
  algorithmic, 5
  input, 5
  measurement, 6
  methodological, 6, 8, 21, 77
  output, 5
  relative, 6
  rounding, 6
  standard, 333
  truncation, 4, 19, 21, 22, 25, 65, 66
Estimator, 219
  energy expectation value, 219
  error, 288
  internal energy, 219
EULER methods, 56, 58, 64, 67, 68, 74, 76
Exchange interaction, 209

F
FERRARI's method, 56
Ferromagnetism, 209, 210
FIBONACCI sequence, 176
Finite difference, 8, 17, 18, 30, 123
  backward, 20, 31
  central, 20
  forward, 20, 31
Finite difference derivative, *see* derivative
Finite volume effects, 103
FLETCHER–REEVES algorithm, *see* deterministic optimization
Floating-point form, 6
Fluctuation quantities, 213
FOKKER–PLANCK equation, 263
Forward difference, 20, 31
Fractal random walk, 270
  diffusion equation, 270
  fractal time random walk, 268
Fractional integral
  RIEMANN–LIOUVILLE fractional integral, 349
  RIESZ fractional integral, 350
  WEYL fractional integral, 350

G
GAUSS–SEIDL method, 327, 329
GAUSS distribution, *see* probability density function
GAUSS peak, 126

Gauss–Hermite quadrature, 43
Gauss–Legendre quadrature, 38
Gauss–Seidl method, 150
Gauss–Newton method, 353
Gaussian process, 233
Generalized diffusion model
  characteristic waiting time, 266
  jump length pdf, 265
  jump pdf, 265
  length variance, 266
  waiting time pdf, 265
Genetic algorithm, *see* stochastic optimization
Gibbs sampling, *see* Markov-chain Monte-Carlo sampling
Gravitational potential, 52
Grid-point, 18, 113, 124, 140, 150, 254
  distance between, 18, 113, 149, 160
  equally spaced, 18, 30, 149
  variable spaced, 18

H
Hamilton
  equations of motion, 73
  function, 73, 74, 303
Hamilton operator, *see* operator
Heat capacity, 213, 214, 280
Heat equation
  heat source/drain, 126
  homogeneous, 123
  inhomogeneous, 126
  stationary, one-dimensional, 123
  thermal diffusivity, 123
  time-dependent heat equation, *see* partial differential equation
Heisenberg model, 210
Hessian matrix, *see* deterministic optimization
Hill climbing, *see* stochastic optimization
Histogram technique, 179, 288, 295
Hit and miss integration, 199

I
Ill-conditioned, 9
  problems, 10
Implicit midpoint rule, 57
Importance sampling, 205, 275–277
Induced instability, 10
Integrable system, 89
Integration, *see* quadrature
Integrator
  Adams–Bashford method, 66
  backward Euler method, 64
  Butcher tableau, 69
  Crank–Nicolson method, 65
    algorithmic form, 68
  explicit Euler method, 56, 64, 67
    algoritmic form, 68
  explicit midpoint rule, 67
    algorithmic form, 68
  forward Euler method, 64
  implicit Euler method, 56, 64, 67
    algorithmic form, 68
  implicit midpoint rule, 57, 65, 68
  leap-frog method, 65, 101
  linear multi-step methods, 65, 66
  predictor–corrector method, 67
  Runge–Kutta method, 65, 67
    e-RK-4, 71, 85
    e-RK-4, algorithmic form, 70
    explicit, algorithmic form, 69
  simple integrators, 62
  Strömer–Verlet method, 65, 100
  symplectic integrators
    Euler method, 58, 74, 100
    flow of the system, 72
    Runge–Kutta method, 74
  velocity Verlet algorithm, 101
Inverse transformation method, 187, 205
Ising model, 205
  antiferromagnetism, 210
  expectation value
    energy, 213
    energy per particle, 216
  ferromagnetism, 209, 210
  Hamilton function, 210
  Hamilton operator, 211
    $\mathbb{Z}_2$ symmetry, 226
    one-dimensional chain, 212
  heat capacity, 213, 214
  magnetic susceptibility, 213, 214
  magnetization, 213, 219
  mean field approximation, 211
  molecular field, 211
  nearest neighbor interaction, 212
  numerics
    auto-correlation, 221
    cold start, 222
    cooling strategy, 224
    error on expectation values, 225
    hot start, 222
    initial configuration, 221
    lattice geometry, 220
    measurement, 223
    size effect, 224
    thermalization, 221, 223
    thermalization length, 221

  - phase transition, 217
  - spin correlation function, 217
  - thermodynamic limit, 217
  - transfer matrix, 215
    - eigenvalue, 216
  - two-dimensional solution, 217
- Isingmodel
  - exchange interaction, 209
  - paramagnetism, 209

J

- Jackknife averages, 290
- Jacobi determinant, 186
- Jacobi matrix, 73, 77, 322
- Jacobi method, 150, 328

K

- Kepler problem
  - absolute error, 55
  - central potential, 51
  - conservation
    - of angular momentum, 51
    - of energy, 51, 318
  - differential equation, 51
  - explicit Euler, 75
  - Hamilton equations of motion, 58, 74
  - Hamilton function, 57, 74
  - implicit Euler, 75
  - Lagrange equation, 317
  - Lagrange function, 315–317
  - pericenter velocity, 78
  - perihelion, 78
  - rotational invariance, 317
  - symplectic Euler, 76
  - translational invariance, 315
- Kolmogorov's zero-one law, 341

L

- L^2-norm, 132
- Lagrange polynomial, 36, 37, 67
- Landau theory, 347
- Landé factor, 211
- Langevin equation, *see* stochastic differential equation
- Laplace equation, *see* partial differential equation
- Law of large numbers, 200
- Leap-frog, *see* integrator and/or molecular dynamics
- Least squares fit, 351
  - linear, 352
  - model/test function, 351
  - nonlinear
    - Gauss–Newton method, 353
- Legendre polynomial, 39
  - normalization condition, 40
  - Rodrigues formula, 40
- Lennard–Jones potential, 98, 103
- Lévy flight, 267
  - diffusion equation, 268
  - fat-tailed jump length pdf, 268
  - jump length pdf, 268
- Lévy process, 232
- Linear equations, 113, 118, 162
  - Gauss–Seidel method, 327
    - relaxation parameter, 329
  - Gauss–Seidel method, 150
  - inhomogeneous, 115
  - Jacobi method, 150, 328
  - *LU* decomposition, 324
  - non-homogeneous, 323
  - sparse matrix, 327
  - tridiagonal matrix, 118, 124, 127, 162, 163, 326
- Linear multi-step methods, 65, 66
- Loop algorithm, 285
- *LU* decomposition, 324
- Lyapunov length, 91
- Lyapunov stability, 90

M

- Machine-number, 7
- Magnetic susceptibility, 213, 214, 280
- Magnetization, 213, 219, 281
- Marginalization rule, 190, 241, 337
- Markov process, 233
  - Chapman–Kolmogorov equation, 234, 237
  - detailed balance, 239, 240
  - equilibrium distribution function, 239
  - global balance, 239
  - Hamilton's equations of motion, 239
  - hierarchy of pdfs, 233
  - Markov property, 233
  - master equation, 237, 238
  - Poisson process, 236
    - transition probability, 236
    - waiting time, 236
  - precursor state, 233
  - time-homogeneous, 237
  - transition probability, 233
  - transition rate, 237
  - Wiener process, 235
    - transition probability, 235

- Markov-chain, 206, 241
  - absorbing state, 242
  - aperiodic state, 243, 254
  - Chapman–Kolmogorov equation, 242, 248, 249
  - closed set of states, 242
  - continuous state space, 247
  - continuous time, 247
  - detailed balance, 206, 244, 275, 277
  - equilibrium distribution, 243, 244
  - ergodic state, 243
  - irreducible, 242, 243
  - irreducible class, 242
  - Markov property, 241
  - null recurrent state, 242
  - periodic state, 243, 254
  - positive recurrent state, 242
  - recurrent state, 242
  - reversible, 244
  - stationary distribution, 243, 275
  - transient state, 242, 243
  - transition matrix, 241
  - transition probability, 277
- Markov-chain Monte-Carlo sampling
  - Gibbs sampling, 278
  - Metropolis algorithm, 205, 219, 275
    - acceptance probability, 206, 219, 278
    - asymmetric proposal probability, 278
    - correlations, 207
    - initialization, 207
    - thermalization, 207
  - Metropolis–Hastings algorithm, 276, 278, 304
  - slice sampling, 279
- Maxwell–Boltzmann distribution, 105
- Mean-value integration, *see* quadrature
- Methodological error, *see* error
- Metropolis algorithm, *see* Markov-chain Monte-Carlo sampling
- Metropolis–Hastings algorithm, *see* Markov-chain Monte-Carlo sampling
- Midpoint rules, 65, 67, 68
- Molecular dynamics, 97
  - barometric formula, 109
  - boundary conditions, 102
  - constant temperature, 104
  - external potential, 98
  - finite volume effects, 103
  - forces, 99
  - initial conditions, 105
  - leap-frog method, *see* intgrator
  - Lennard–Jones potential, 98
  - natural units, 106
  - Newton equations of motion, 97, 99
  - Strörmer–Verlet method, 100
  - system temperature, 104
  - thermal equilibrium, 105
  - time invariance, 102
  - total kinetic energy, 104
  - total velocity shift, 104
  - two-particle interaction, 98
  - velocity Verlet algorithm, 101
- Monte-Carlo integration, *see* quadrature

N

- NÉELtemperature, 209
- Newton method, 77, 321
- Newton–Cotes rules, 36
- Normal distribution, *see* probability density function
- Normalization condition, 119

O

- Open integration rule, 32
- Operator
  - expectation value, 133
  - Hamilton operator, 131, 160
  - Hermitian, 133
  - kinetic energy, 132
  - Laplace operator, 123
  - momentum, 132
  - position, 138
  - potential energy, 132
  - time-evolution operator, 160
- Operator technique, 22
- Ordinary differential equation, 51, 55
  - collocation point, 71
  - eigenvalue problem, 119, 132
  - explicit, 61, 62
  - homogeneous, 112
  - homogeneous boundary value problem, 119, 140
  - initial value problem, 61
  - integrators, *see* integrator
  - linear boundary value problem, 111
- Ornstein–Uhlenbeck process, 263
  - master equation, 263

P

- Paramagnetism, 209
- Partial differential equation
  - diffusion equation, *see* diffusion equation
  - elliptic, 147, 148

- hyperbolic, 147, 157
- LAPLACE equation
  - charge density, 148
- parabolic, 147, 151
- POISSON equation, 148
  - charge density, 148, 151
  - convergence condition, 151
  - dielectric function, 148
  - electric field, 148
  - electrostatic potential, 148
  - iterative solution, 150
- time-dependent heat equation, 151
  - CRANK–NICOLSON method, 153
  - explicit EULER method, 152, 155
  - implicit EULER method, 152, 154, 155
  - stability, 154
- time-dependent SCHRÖDINGER equation, *see* SCHRÖDINGER equation
- wave equation
  - explicit EULER method, 157
  - one-dimensional, 157

PAULI matrix, 211

Pdf, *see* probability density function, *see* stochastic process

Pendulum, 2
- period, 3

Phase space, 88

Phase transition
- critical exponent, 347
- CURIE - WEISS law, 347
- CURIE temperature, 209, 210, 346
- CURIE–WEISS law, 211
- first order, 346
- modern classification, 346
- NÉEL temperature, 210
- second order, 209, 346
  - LANDAU theory, 347
  - order parameter, 209, 347
- universality, 348

POINCARÉ map, 91

POINCARÉ section, 92

POISSON distribution, *see* probability density function

POISSON equation, *see* partial differential equation

POISSON process, 236

Poor person's assumption, 288

POTTS model, 279
- HAMILTON operator, 279
- heat capacity, 280
- magnetic susceptibility, 280
- magnetization, 281
- phase transition
  - first order, 282
  - histogram technique, 282
  - second order, 282

Predictor–corrector method, *see* integrator

Probability
- classical, 331
- conservation, 188
- correlation coefficient, 341
- event, 331
  - certain, 331
  - complimentary, 331
  - impossible, 331

Probability density function, 105, 174
- binomial distribution, 334
- BOLTZMANN distribution, 201, 205, 212, 219, 284, 295, 303, 307
- CAUCHY distribution, 307
- χ^2 distribution, 181
- composite pdf, 193
- exponential distribution, 195
- GAUSS distribution, 337
- LÉVY α-stable distributions, 343
- normal distribution, 186, 191, 203, 236, 264, 337
- piecewise defined, 193
- POISSON distribution, 236, 335
- stable distribution, 343
- TSALLIS distribution, 308

Q

Quadrature, 29
- backward rectangular rule, 31, 56, 64
- central rectangular rule, 32, 57, 64, 67, 101, 204
- closed integration rule, 32, 34
- elemental area, 31, 33
- forward rectangular rule, 31, 55, 64, 140
- GAUSS–HERMITE, 43
- GAUSS–LEGENDRE, 38
  - error, 42
  - grid-point, 40–42
  - weight, 40, 42
- improper integrals, 45
- integral transform, 46
- Monte-Carlo integration, 197, 204, 205, 219
  - approximation of π, 197
  - error, 204
  - expectation value, 200
  - hit and miss, 199
  - mean-value, 200
  - mean-value integration, 199

  - multiple integrals, 47
  - Newton–Cotes rules, 36
    - closed, 36
    - open, 37
  - open integration rule, 32
  - piecewise smooth integrand, 46
  - rectangular rule, 30, 32, 37
    - error, 31, 32
  - Rhomberg method, 37
  - Simpson rule, 35, 37
    - error, 38
    - three-eight rule, 36, 37
    - total error, 38
  - trapezoidal rule, 33, 37, 65
    - error, 34, 38
    - total error, 38

R

- Random number, 172
  - non-uniform distribution, 173, 185
  - pseudo, 174
  - real, 174
  - sequence, 173
    - correlation, 173, 178
    - moments, 173, 178
    - moments error, 178
  - uniform distribution, 173, 276
- Random number generator, 172
  - criteria, 174
  - Fibonacci, 176
    - lagged, 176
  - linear congruential, 175, 198
    - Park–Miller parameters, 175
    - shuffling, 176
  - Marsaglia–Zaman, 177
    - carry bit, 177
  - period, 174
  - quality
    - χ^2 test, 179
    - hypothesis test, 179
    - spectral test, 179
    - statistical tests, 178
  - seed, 175
  - shift register, 177
- Random sampling, *see* also Markov-chain Monte-Carlo sampling
  - direct method, 185
  - importance sampling, 205, 275–277
  - inverse transformation, 187, 205
  - n-sphere, 302
  - probability mixing, 193
  - rejection method, 190, 205
    - acceptance probability, 190
    - envelope, 190
    - histogram test, 193
  - simple sampling, 276
- Random variable, 171, 230, 332
  - central moments, 332
  - characteristic function, 339
  - mean value, 332
  - moments, 332
  - standard deviation, 333
  - uncorrelated, 334
  - variance, 332
- Random walk, 253
  - biased, 254
  - definition, 253
  - moments, 255
  - probability of first return, 258
  - recurrence, 257
  - recurrence probability, 258
  - transition rate, 254
  - unbiased, 254
  - variance, 256
- Randomness, 171
  - definition, 172
    - Chaitin, 173
  - event, 172
  - measurement, 172
  - probability, 172
- Rectangular rules, 31, 32, 55–57, 64, 67, 101, 140, 204
- Reflection principle, 257
- Regula falsi, 322
- Rejection method, 190, 193, 205
- Relative error, *see* error
- Rhomberg method, 37
- Riemann–Liouville fractional derivative, 270, 349
- Riemann–Liouville fractional integral, 349
- Riesz fractional derivative, 271, 350
- Riesz fractional integral, 350
- Rounding error, *see* error
- Runge–Kutta methods, 65, 67, 69, 70, 74

S

- Schrödinger equation
  - basis, 133
  - dimensionless variables, 135
  - eigenenergy, 132
  - eigenfunction, 132
  - Gauss wave packet, 165
  - stationary

    - one-dimensional, 120, 134
  - time-dependent, 160
    - Crank–Nicolson method, 161
    - explicit Euler method, 161
  - time-evolution operator, 160
  - total wave-function, 133
  - wave-function, 131
    - normalization, 134
- Series expansion
  - Lagrange polynomial, 36, 71
  - Legendre polynomials, 40
  - Taylor, 19, 23, 30, 32, 65, 68, 100, 101, 158, 237, 294
- Shooting method, 118
  - Numerov method, 120, 139, 141
- *σ* algebra, 339
- Simpson rule, 35, 37
- Simulated annealing, *see* stochastic optimization
- Slice sampling, *see* Markov-chain Monte-Carlo sampling
- Stability, 5, 9, 148
  - Courant–Friedrichs–Lewy condition, 148, 157
  - definition, 9
- Standard deviation, 333
- Standard error, *see* error
- Statistical bootstrap, 225, 290
- Steepest descent, *see* deterministic optimization
- Stirling approximation, 11, 258, 334
- Stochastic differential equation, 172, 263
  - random force, 263
- Stochastic matrix, 241
- Stochastic optimization
  - ant colony optimization, 313
  - cost function, 299
  - deluge algorithms, 312
  - genetic algorithm, 310
    - traveling salesperson problem, 311
  - grouping genetic algorithms, 313
  - hill climbing, 301
    - *N*-queens problem, 302
  - simulated annealing, 303
    - Aarts schedule, 307
    - acceptance probability, 305
    - fast, 307
    - generalized, 308
    - geometric cooling schedule, 306
    - initial temperature, 305
    - traveling salesperson problem, 308
  - threshold algorithms, 312
- Stochastic process
  - auto-correlation function, 231
  - auto-covariance function, 231
  - conditional pdf, 232
  - definition, 230
  - Gaussian process, 233
  - hierarchy of pdfs, 231
  - independent increments, 232
  - Lévy process, 232
  - moments, 230
  - pdf, 231
  - random variable, 230
    - realization, 230
  - random walk, 233
  - state space, 230
  - stationary increments, 232
  - stationary process, 232
  - time span, 230
  - time-homogeneous process, 232
  - transition probability, 232
  - Wiener process, 233
- Stochastic variable, *see* random variable
- Strömer–Verlet method, 65, 100
- Subtractive cancellation, 7, 19, 26
- Swendsen–Wang algorithm, 284
- Symplectic integrators, 57, 72, 74, 76
- Symplectic mapping, 73

T

- Taylor theorem, *see* series expansion
- Thermodynamic equilibrium, 207
- Thermodynamic expectation value, 205
- Time series plot, 288
- Time-dependent heat equation, *see* partial differential equation
- Trapezoidal rule, 33, 37, 65
- Traveling salesperson problem, 308, 311
- Truncation error, *see* error
- Two-body problem, *see* Kepler problem

V

- Variance, 138, 203, 332
- Velocity Verlet algorithm, 101
- Violation of energy conservation, 74, 77

W

- Wave equation, *see* partial differential equation
- Wave-function, *see* Schrödinger equation
- Weyl fractional derivative, 350
- Weyl fractional integral, 350
- White noise, 261
  - Gaussian, 261
- Wiener process, 233, 235, 259

continuous limit, 260
drift term, 261
independent increments, 260
self-similarity, 261
standard process, 260
WOLFF algorithm, 285